

JOURNAL OF THE MYANMAR ACADEMY OF ARTS AND SCIENCE



Geology

Vol. XIX, No.5A, January, 2023

Myanmar Academy of Arts and Science

Journal of the Myanmar Academy of Arts and Science

Vol. XIX, No.5A

Contents

Geology

<u>Sr. No.</u>	<u>Title</u>	<u>Page</u>
1	Ye Kyaw Thu , Geochemical Signatures of Gneiss Samples from Onzon, Thabeikkyin and Sagaing Areas: Implications for Protolith Composition, Source–Area Weathering and Depositional Tectonic Setting	1
2	Than Zaw , Petrography and Diagenesis Study of the Okhmintaung Formation Exposed in Chaung Zon Area, Pwintbyu Township, Magway Region	13
3	Win Lwin Thein , Lithofacies Analysis of Paleocene and Early Eocene Units of Sabadan Area, Mindon Township, Magway Region	25
4	Mya Moe Khaing , Petrogenesis of Metasedimentary Rocks in Bilin and Its Environs, Bilin Township, Mon State	35
5	Thidar Win , Erpentinization in the Mwetaung Ophiolite, Tiddim Township, Chin State	45
6	Aung Myo Zaw , Geophysical Approach to the Determination of Local Site Effect in Dagon Township, Yangon Region for Seismic Hazard	55
7	Paing Soe , Heavy Minerals Analysis of the Shwezetaung-Padan Coal Mine Area, Magway Region	67
8	Aung Ye Ko , Geochemical Characteristics of Gold Mineralization at Taung Ni Gold Prospect, Madaya Township, Mandalay Region, Myanmar	81
9	Myo Min Tun , Zeolites in Amygdaloidal Basalts from Tonngone Area, Tigyain Township, Sagaing Region, Myanmar	95
10	Zar Ni Swe , Economic Geology of the Hopang Area, ‘WA’ Self-Administered Division in the Northern Shan State, Myanmar	105
11	Tun Tun Min , Geochemical Investigation of Chromitites in Ultramafic Rocks of Taung-Pi-La Area, Kalay Township, Sagaing Region	115
12	Kyaw Khaing , Geochemical Analysis of Sandstone of Paunggyi Formation in the Akyiban Area, Tilin Township, Magway Region	127
13	May Thu Aung , Petrology and Petrogenesis of Metamorphic Rocks in Za Yat Kwin Area, Thabeikkyin Township, Mandalay Region	135
14	Wai Wai Lwin , Petrography and Diagenesis of the Kalaw Formation in the Tigyit Area, Shan State (South)	147
15	Hnin Min Soe , Protolith of Serpentinite Units at Yega-Inn and Kannbyu Areas Sagaing Region, Myanmar	157
16	Myo Thiri Sandar Aung , Petrogenesis of the Granitoids of Mokpalin-Kyauktanlay Quarries, Mon State Using Trace Element and Rare Earth Element Geochemistry	171
17	Htay Maung , Provenance and Depositional Processes Determination of Pondaung Formation Based on Heavy Mineral and Granulometric Analysis, Ti Gon- Ka Baing Area, Yinmarbin Township, Sagaing Region	181

<u>Sr. No.</u>	<u>Title</u>	<u>Page</u>
18	Moe Zat , Sedimentary Facies Analysis of Miocene Clastic Strata in Kalewa-Mawleik Area, Sagaing Region	191
19	Wint Wint Htun , Soil and Water Quality Analysis in Kyonpyaw Area, Patheingyi District, Ayeyarwady Region	207
20	Tin Aung Myint , Mineral Occurrences and Deposits Along Muse-Mandalay Proposed Railway Line	217
21	Ni Ni Win , Petrography of the Nyaung Bin Tha Area, Waingmaw Township, Kachin State	227
22	Khaing Khaing San , Study of the Stratigraphy of The Marine Reptile Fossil Bearing Limestone Unit in Lashio Area, Northern Shan State	239
23	Aung Kyaw Myat , Soil Deaggregation Along Yangon-Naypyidaw Highway Between Mile Post 10 and 40 in Myanmar	249
24	Tun Tun Win , Assessment of Seismic Soil Liquefaction Based on Shear Wave Velocity Using 2% and 10% Probabilities of PGA Values with Earthquake Magnitude-6.5 MW in Mandalay City	261
25	Wai Yan Lai Aung , The Existence of Hercynite in Metapelites from Mogoke Metamorphic Belt	271
26	Mi Mi Ko , Depositional Environment and Lithofacies Association of the Kangyigon Chaungshe Area, Nyaung U Township, Magway Region	281
27	Zin Maung Maung Thein , Perissodactyla from the Neogene Sediments of Myanmar	291
28	Zaw Lin Kyaw , Determination of Site Effects of Soil Condition on Spt Values for Ground Motion in Yangon Business City, Myanmar	301
29	Su Su Khine , Observation of Landforms of Granitic Rocks in Pa Nyit Beach in Launglon Township, Tanintharyi Region	313
30	Me Me Aung , Potential Landslides on Weathered Granitic Rocks Along the Myitkyina-Kanpetii Car Road, Kachin State	323
31	Than Than Thwe , Hydrocarbon Potential of Cretaceous Tethyan Realm in Myanmar	333
32	Teza Kyaw , Petrological Significance on Granitoid Rocks Exposed in Mya Yeik- Ta Yaw Gyin Area, Monywa-Salween Segment of Western Myanmar Arc	341
33	Tint Swe Myint , Tectonic Setting and Provenances of Pane Chaung Formation Exposed at the Eastern Part of Indo-Myanmar Range, West Myanmar	353
34	Naing Htun Lin , Evolution of Tide-Dominated Estuarine Facies System in the Oligocene Okhmintaung Formation of the Myasagaing-Shwemaungzun Area, the Minbu Sub-Basin, Central Myanmar	363
35	May Thet Aye , Petrography and Geochemistry of Calc-Silicate Rocks Exposed in Kantha-Aungtharya Area, Thabeikkyin Township, Mandalay Region	371
36	Khaing Myat Thwin , Reptilian Remains of Irrawaddy Formation in Yinseik Area, Magway Region	379

<u>Sr. No.</u>	<u>Title</u>	<u>Page</u>
37	Naw Chel Phaw , A Study on Evolution of Porosity in Sandstone Reservoirs of Okhmintaung Formation Between Ngape and Yenama Area, Magway Region	389
38	Tint Tint Tun Petrological Study of Metamorphic Rocks Exposed in Chaungzon Area, Chaungzon Township, Mon State	401
39	Khin Maung Hla , Deformation Characters Along the Sagaing Fault Zone Between Indaw and Singu Township, Central Myanmar	413
40	Hlaing Myo Nwe , Geochemical Properties of Laterite and Lateritization Processes in Hpa-an Township, Kayin State	423
41	Min Han Nyein , Chemical Analysis of the Groundwater in Mayangone Townshio, Yangon Region	433
42	Tin Myint Oo , A New Light on Development and Evolution of Mann Anticline East Flank of Salin Basin	443
43	Ko Yi Hla , Middle Shelf Zone Foraminiferas Occurred in the Sediments of Northern Part of the Andaman Sea	453

GEOCHEMICAL SIGNATURES OF GNEISS SAMPLES FROM ONZON, THABEIKKYIN AND SAGAING AREAS: IMPLICATIONS FOR PROTOLITH COMPOSITION, SOURCE–AREA WEATHERING AND DEPOSITIONAL TECTONIC SETTING

Ye Kyaw Thu¹ and Maw Maw Win²

Abstract

The Cenozoic Mogok metamorphic belt exposed at the western margin of the Shan-Thai Block consists of metaigneous and metasedimentary rocks with various granitoid intrusions. The common mineral assemblages of gneiss samples are characterized by garnet + biotite + plagioclase + K-feldspar + quartz with cordierite and sillimanite in some samples forming under upper amphibolite to granulite facies conditions. Geochemical data were used to evaluate the possible protolith composition, source–area weathering, provenance and tectonic setting of the gneiss samples. Sagaing samples are more enriched in Fe relative to Onzon and Thabeikkyin samples. Compared with average crustal content the samples show similar composition with depletion of CaO, Na₂O, P₂O₅, Sr and Nb and enrichment of Rb, Y and Th. Evidences from major and trace element concentrations, ratios and use of various diagrams point to the derivation of Onzon and SM2 unit samples from psammitic composition mainly greywacke and SM1 unit sample from pelitic compositions except for Thabeikkyin sample, which has felsic igneous protolith. In addition, Chemical Index of Alteration (CIA), Chemical Index of Weathering (CIW), Index of Compositional Variability (ICV) values and major element diagrams indicate that the source areas had undergone moderate to high degree of weathering. Based on the major and trace variation sediment deposition might have occurred at passive margin and active continental margin.

Keywords: geochemistry, protolith, source–area weathering, tectonic setting

Introduction

The compositions of the deep crustal metamorphic rocks are vital to decipher the lower crust and its protolith composition (Rudnick, 1992; Rollinson, 2012). Analyses of major, trace and rare earth elements concentration from metamorphosed rocks can reveal the details of protolith compositions, which cannot be determined in thin sections. The behavior of certain trace elements and products of their metamorphism can be considered as indicators of the continental crust composition, and the geochemical record of these rocks provides a key for understanding their evolution.

The Cenozoic Mogok metamorphic belt is sited at the western margin of the Shan-Thai Block and consists of metaigneous and metasedimentary rocks with various granitoid intrusions. These metamorphic rocks were regionally metamorphosed under medium- to high-grade amphibolite facies and localized granulite facies conditions, and has been estimated as Paleogene and younger in age (Bertrand et al., 1999, 2001; Barley et al., 2003; Mitchell et al., 2007; Searle et al., 2007; Yonemura et al., 2013; Maw Maw Win et al., 2016; Ye Kyaw Thu et al., 2016, 2017). Although, the Mogok metamorphic belt has been investigated by many previous studies, the geochemical signatures of the metasediments from the belt are very poorly constrained. The present study attempts to decipher the geochemical characteristics of gneiss samples from Onzon, Thabeikkyin and Sagaing areas in the middle segment of the Mogok metamorphic belt, and to place constraints on the composition and nature of the source rocks (provenance) and the tectonic setting for their deposition.

¹ Dr, Lecturer, Department of Geology, University of Magway

² Dr, Associate Professor, Department of Geology, Lashio University

Geology of the Onzon, Thabeikkyin and Sagaing Areas

Onzon and Thabeikkyin areas located 100 km north of the Mandalay region are dominated by high-grade paragneisses with various types of marbles and calc-silicate rocks (Fig. 1a). In the sampling area the marbles and calc-silicate rocks are well exposed and locally intruded by granitoid rocks. Major lithologies of the Onzon area include garnet–cordierite gneiss, garnet–biotite gneiss, and biotite gneiss. The gneiss samples contain the common mineral assemblage of garnet–biotite–plagioclase–K-feldspar–quartz with cordierite and sillimanite in some samples. In the Thabeikkyin area, the main rock type is highly weathered garnet–biotite gneiss, and show similar mineral assemblages as Onzon area. Ye Kyaw Thu et al. (2016, 2017) reported the pressure and temperature (P – T) conditions of 0.60–0.78 GPa/800–860 °C using a conventional geothermobarometers for the peak metamorphic stage from these areas.

In Sagaing area, the Mogok metamorphic rocks, which are locally named the Sagaing metamorphic rocks, are mainly composed of gneiss, marble, calc-silicate rock, schist, and amphibolite. The Mogok metamorphic rocks from the area are divided into Sagaing Metamorphic Unit 1 (SM1) and Sagaing Metamorphic Unit 2 (SM2), which are gneiss-dominant units that interleave layers of amphibolite and calc-silicate rock/marble, respectively (Fig. 1b). The SM samples are characterized by common mineral assemblages of garnet, biotite, plagioclase, K-feldspar, quartz, and graphite with sillimanite in some samples. The pressure and temperature (P – T) conditions were suggested 0.58–1.0 GPa/780–850 °C using a conventional geothermobarometers (Maw Maw Win et al., 2016).

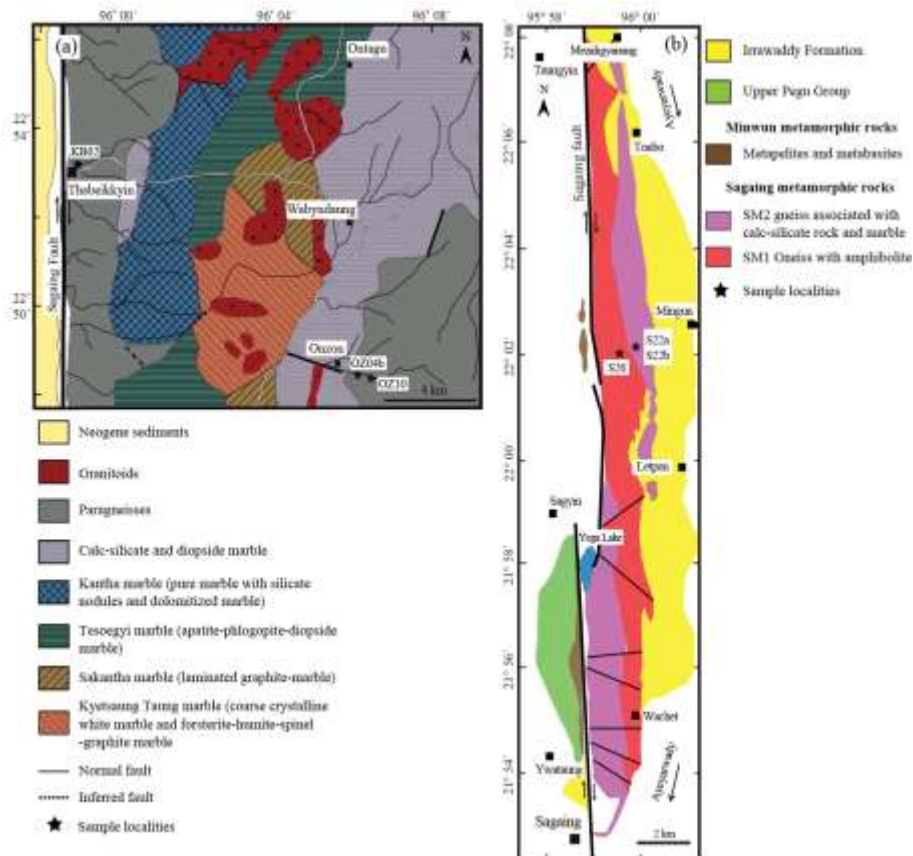


Figure 1 Geological map showing the major rock units of (a) Onzon and Thabeikkyin areas (after Myint Liwin Thein et al., 1990) and (b) Sagaing area (Maw Maw Win et al., 2016).

Petrography

The garnet–cordierite gneiss (OZ04b sample) and garnet–biotite gneisses (OZ10 sample) were collected from Onzon area (longitude 96° 06' 05"E, latitude 22° 48' 42"N; Fig. 1a), and the garnet-biotite gneiss (KB02 sample) were from Thabeikkyin area (longitude 95° 58' 59" E, latitude 22° 53' 18" N; Fig. 1a). S26 sample was collected from SM1 (95° 59' 18" E, 22° 02' 01" N; Fig. 1b), and S22a and S22b samples were from SM2 (95° 59' 57" E, 22° 02' 12" N; Fig. 1b). These samples were selected for detailed geochemical analysis, and OZ for OZ04b and OZ10 samples, KB for KB02 sample, SM1 for S26 sample and SM2 for S22a and b samples are here used for abbreviation. Abbreviations for minerals and end-members are after Whitney and Evans (2010).

All samples are characterized by garnet, biotite, plagioclase, K-feldspar, sillimanite and quartz with minor rutile, ilmenite, graphite and zircon with cordierite in OZ04b sample. Garnet grains occur as subhedral to anhedral porphyroblasts ranging in size from 2–5 mm in diameter (Fig. 2). Some garnets contain fine grains of sillimanite, cordierite, and quartz inclusions in OZ04b sample (Fig. 2a) and acicular sillimanite, biotite and quartz grains in OZ10, S26, S22a and b sample (Figs. 2c and d). Some garnet grains are partially replaced by secondary biotite and muscovite-rich aggregates along cracks. The cordierite in Sample OZ04b commonly contains symplectitic grains of quartz, rare spinel and biotite (Figs. 2a and b). Biotite grains occur as an inclusion phase in garnet and cordierite, as isolated phase in matrix and as intergrown phase with cordierite and quartz. Plagioclase and K-feldspar occur as primary phase in all samples (Fig. 2). In OZ04b and S26 samples, rutile occurs as isolated grain and intergrowth grains with ilmenite in the matrix (Fig. 2b). Spinel grains occur as symplectitic phase with cordierite in OZ04b sample (Fig. 2a). Prismatic sillimanite grains occur as matrix phase and inclusion in garnet (Fig. 2). Graphite, ilmenite, zircon, monazite and apatite occur as accessory phases in all samples.

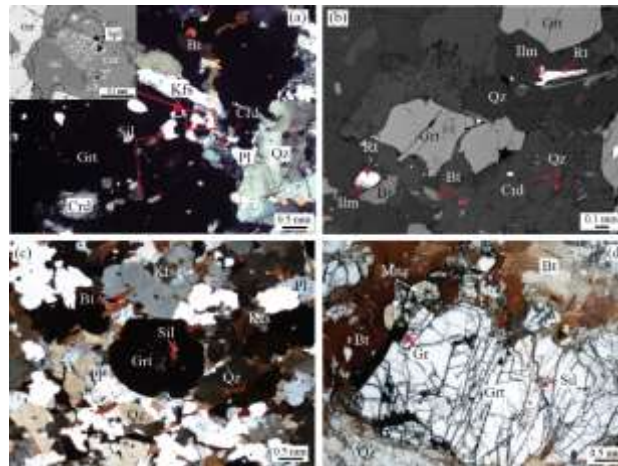


Figure 2 photomicrographs showing (a) garnet porphyroblast with inclusions of cordierite and sillimanite and symplectitic cordierite grain with spinel (OZ04b sample), (b) Back Scattered Electron (BSE) image of the symplectitic cordierite grain with quartz and biotite and intergrown rutile grain with ilmenite (OZ04b sample), (c) garnet grains with sillimanite inclusion (OZ10 sample) and (d) garnet grain and primary monazite (S26 sample).

Geochemistry

Analytical Procedures

Sample were made for the detailed study of the constituent mineral assemblages under polarizing microscope and were made powder and dried in the oven to dry out the water in the sample. Dried samples were weighed and placed in the microfurnace setting 950 °C for 5 hours. The glass beads were then prepared by fusing mixtures of powder samples and $\text{Li}_2\text{B}_4\text{O}_7$ in a weight ratio of 0.7:6.0. Whole-rock compositions used for the geochemical analysis were determined by an X-ray fluorescence spectrometer (XRF; Rigaku ZSX Primus II equipped with a Rh X-ray tube operated at 60 kV and 50 mA) at Nagoya University. Sedimentary and igneous rock reference samples issued by the Geological Survey of Japan (GSJ) were used for the calibration. Whole rock chemical analyses of studied samples are listed in table 1.

Table 1 Analysis of the major and trace elements of the analyzed samples

Sample	OZ04b	OZ10	KB01	S26	S22a	S22b
SiO ₂	69.99	73.91	64.51	51.73	67.45	62.58
TiO ₂	0.84	0.67	0.64	1.32	0.67	0.80
Al ₂ O ₃	12.38	11.06	16.35	18.61	12.58	14.90
Fe ₂ O ₃ *	6.33	5.38	5.78	13.19	7.91	7.93
MnO	0.09	0.09	0.14	0.19	0.14	0.11
MgO	3.48	2.62	2.05	5.51	3.17	3.28
CaO	1.34	1.03	2.46	2.33	1.46	1.45
Na ₂ O	1.76	1.99	2.64	1.42	1.46	1.15
K ₂ O	2.35	2.49	4.80	3.42	3.52	5.86
P ₂ O ₅	0.07	0.06	0.06	0.10	0.05	0.10
LOI	1.08	1.32	1.04	1.44	2.39	1.07
Total	99.71	100.62	100.47	99.26	100.80	99.23
Nb	13.1	1.08	4.30	57	31	33
Zr	279	191	178	272	279	232
Th	21	15.2	22.0	64.8	35.2	31.9
Y	38.2	23.9	29.0	77	58	48
Sr	88.6	52.6	251	181	305	158
Pb	13.7	10.0	27.1	33	22	40
Ba	358	621	1020	635	900	883
Rb	108	93.6	134	149	120	249
Cr	123	81.7	69.1	195	97	96
Ni	53.8	37.0	19.8	57	31	33
Zn	70.5	51.3	46.4	163	67	92
Co	19.8	29.5	28.4	30	17	19

* Fe₂O₃ as total Fe

Major, Transition and Trace Elements

The analyzed sample shows a range of SiO₂ (51.7 – 73.9 wt%), Al₂O₃ (11.1–18.6 wt%), MgO (2.1–5.5 wt%), Fe₂O₃ (5.4–13.2 wt%), CaO (1.0–2.5 wt%), Na₂O (1.2–2.6 wt%) and K₂O (2.3–5.9 wt%) (Table 1). X_{Fe} [= FeO/(FeO + MgO + MnO)] ranges from 0.64–0.66 for OZ samples, 0.73 for KB02 sample, 0.70 for S26 sample and 0.70–0.71 for SM2 samples and X_{Al} [= (Al₂O₃ – 3K₂O)/(Al₂O₃ – 3K₂O + FeO + MgO + MnO)] ranges from 0.31–1.25 for OZ sample, 0.20 for KB02 sample, 0.31 for S26 sample and 0.15 – 0.31 for SM2 samples. OZ samples are more enriched in SiO₂ (69.99 – 73.91 wt%). KB and SM samples are more enriched in Al₂O₃ and K₂O compared with OZ samples, and S26 sample shows high TiO₂ value (1.32 wt%). Figure 3 shows depletion in Al₂O₃ for OZ and SM2 samples but similar variation for KB and SM1 sample (Fig. 3a) compared with average shale and arenite composition. MgO are enriched in OZ and SM samples (Fig. 3b). Fe₂O₃ is enriched in SM samples, and OZ, and KB samples have similar variation (Fig. 3c). For Na and K, OZ and most SM samples show slight variation, and KB and S22b sample show enrichment (Fig. 3d).

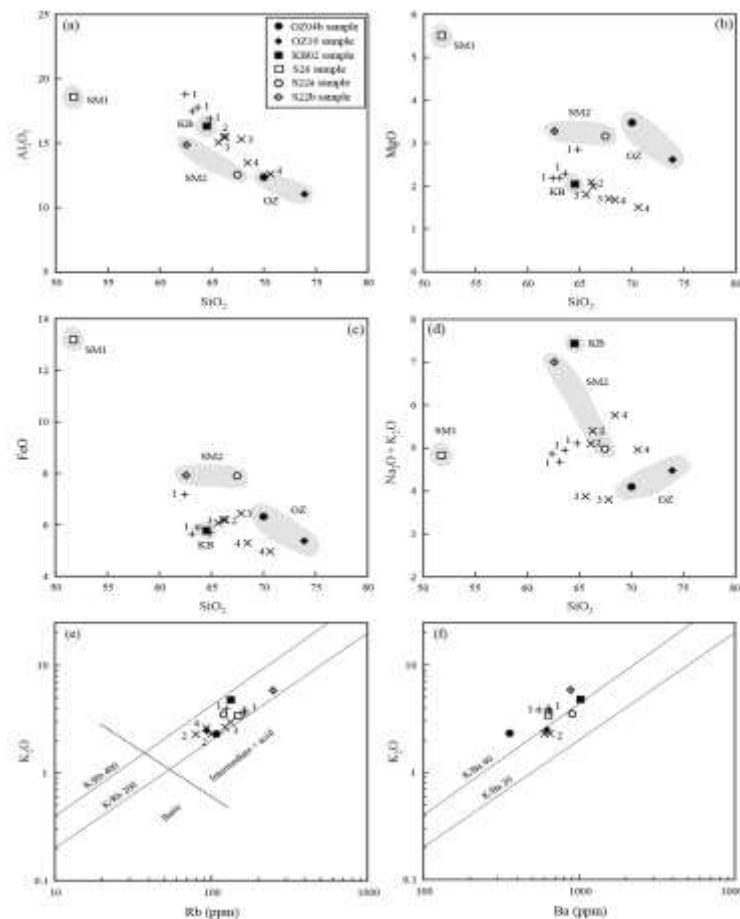


Figure 3 Geochemical variation diagrams for major and trace elements of the studied samples compared with average arenite and shale composition. 1 is average Proterozoic and Phanerozoic cratonic shale composition (Codie, 1993), Post–Archean Australian Shale (PAAS) (Taylor and McLennan, 1985 and McLennan 2001), and North American Shale Composition (NASC) (Gromet et al. 1984); 2 is average Paleozoic and Meso-Cenozoic greywacke composition (Codie, 1993); 3 is average lithic arenite (Argast and Donnelly, 1987) and 4 is feldspathic arenite (Argast and Donnelly, 1987). Boundary line between acid/intermediate and basic compositions in figure (e) is after Floyd and Leveridge (1987).

In figure 3e, the ranges in Rb concentration of S26 and S22a samples are nearly similar in composition with average shale and those of OZ samples are consistent with the greywacke composition. In KB sample the Rb range is near to that of the shale but deviate from it in Ba content (Fig. 3f). The K/Rb ratio for studied samples ranges from 217 to 294 ppm falling within normal field (K/Rb <300 ppm) except KB02 sample (360 ppm).

Spider diagram was made to identify the nature of protolith by normalizing all the analyzed elements to the upper continental crust (UCC) values of Rudnick and Gao (2003) (Fig. 4). The major and minor oxides have a similar composition relative to the UCC, but CaO, Na₂O and P₂O₅ show a slight depletion. Cr, Zn and Co contents show similar concentration to the UCC, and Ni show slight enrichment in OZ04b and S26 sample. For the large ion lithophile elements (LILE) Rb show enrichment for all samples but Sr is significantly depleted in OZ samples and Ba and Pb scatter around the UCC (Fig. 4). The concentration of the high field strength elements (HFSE) shows similar Zr contents, slight enrichment in Y and Th, and significant depletion in Nb, for OZ10 and KB02 samples. These concentrations are most likely to be controlled by the contents of the clay minerals and detrital accessories in the sedimentary protolith (Varga and Szakmány, 2004).

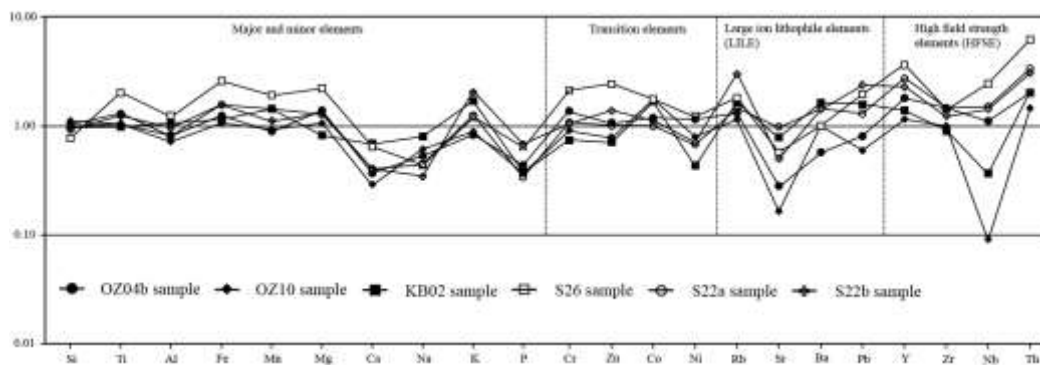


Figure 4 Bulk-rock composition of the analyzed samples plotted in an upper continental crust (UCC) normalized multi-element diagram. UCC data are from Rudnick and Gao (2003).

Discussion

Protolith Composition

The protolith of the studied samples was deduced based on geochemistry. Discriminant function, $DF = 10.44 - 0.21SiO_2 - 0.32Fe_2O_3$ (total Fe) $- 0.98 MgO + 0.55 CaO + 1.46 Na_2O + 0.54K_2O$ (Shaw 1972) can be deduced to determine whether the protolith is igneous or sedimentary in origin. Positive DF values are regarded as igneous parentage while negative values are of sedimentary origin. OZ and SM samples show negative DF values ranging from -4.55 to -5.14 suggesting a sedimentary origin. However, KB sample show positive DF value of 0.83 suggesting an igneous origin. In $\log(SiO_2/Al_2O_3)$ versus $\log(Fe_2O_3/K_2O)$ diagram of Herron, 1988 all sample fall within wacke field except S26 sample which fall in slightly Fe-rich shale (Fig. 5a). This is supported by the classification diagram of Wimmenauer (1984) and all samples fall within greywacke and arkose field except for SM1 sample which drop in shale field (Fig. 5b). In addition, the discrimination ratio of $100 \times TiO_2/Zr$ (wt.%/ppm), which are assumed to have a steady behaviour during metamorphism, is lower than 0.4 except S26 sample (0.48), which has shale protolith composition, and suggest to an input of psammitic material to the precursor sediment (Garcia et al., 1991). The Sr value of $53-89$ ppm (OZ samples), 251 ppm (KB sample) and $158-305$ ppm (SM samples) is consistent with the range of $20-360$ ppm (shale) and $100-400$ ppm (greywacke). K₂O and Ba are positively correlated (Fig. 3f) and K/Ba ratio of the samples ranges from $39-66$ ppm consistent with the range of average shale and greywacke.

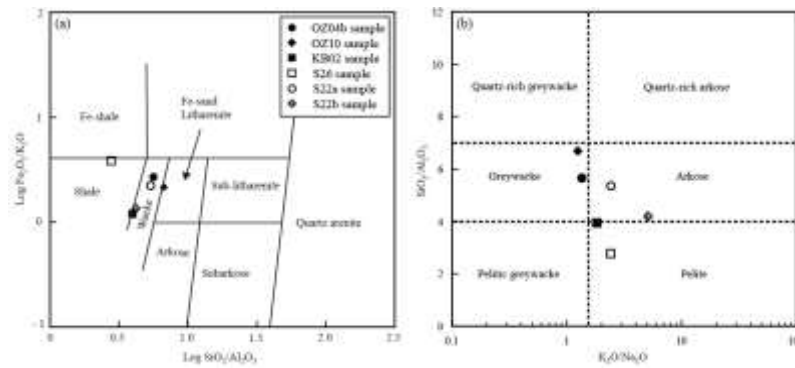


Figure 5 (a) $\log(\text{SiO}_2/\text{Al}_2\text{O}_3) - \log(\text{Fe}_2\text{O}_3/\text{K}_2\text{O})$ diagram (after Herron, 1988) and (b) $\text{K}_2\text{O}/\text{Na}_2\text{O}$ ratio and $\text{SiO}_2/\text{Al}_2\text{O}_3$ ratio diagram (after Wimmenauer, 1984).

The $\text{Al}_2\text{O}_3/\text{TiO}_2$ ratio of Girty et al. (1996) shows 26 for KB02 sample indicating a source with average andesitic to rhyodacitic composition. KB sample is rich in Al_2O_3 (16.35%), CaO (2.46%), Na_2O (2.64%) and K_2O (4.80%) and low SiO_2 (64.51%) and MgO (2.05%) (Table 1). In these respects, they are similar in composition to tonalite or granodiorite in major element composition. These features suggest that if the KB02 sample has igneous rather than sedimentary protolith, it is consistent with felsic igneous source rocks. In addition, Th/Co ratio (0.78 ppm) and Th/Cr ratio (0.32 ppm) of KB02 sample are consistent with the range of felsic source 0.04–3.25 ppm and 0.13–2.70 ppm, respectively (Cullers and Podkovyrov, 2000).

Based on the resulted geochemical data it is likely suggest that arenite associated with minor argillite composition of Early Paleozoic sequence of Shan Plateau (Maung Thein and Soe Win, 1970; Myint Lwin Thein et al., 1990; Myint Thein, 2014 pers. comm. in Maw Maw Win et al., 2016) or Mergui Group and older unexposed underlying rocks (Ridd and Watkinson, 2013) are primary contribution to the precursor sediments of the studied samples.

Source–Area Weathering

For each lithology the Chemical Index of Alteration CIA [= $\text{Al}_2\text{O}_3 / (\text{Al}_2\text{O}_3 + \text{CaO} + \text{Na}_2\text{O} + \text{K}_2\text{O}) \times 100$] (Nesbitt and Young, 1982) values vary as follows: OZ samples (67–69), KB sample (62), SM1 sample (72) and SM2 samples (64–66). The SM1 sample is compared to the average shale (CIA = 70–75, Taylor and McLennan, 1985). The Chemical Index of Weathering CIW [= $\text{Al}_2\text{O}_3 / (\text{Al}_2\text{O}_3 + \text{CaO} + \text{Na}_2\text{O}) \times 100$] (Harnois, 1988) value for OZ, KB, SM1 and SM2 samples are 79–80, 76, 83 and 81–85. This is supported by the Index of Compositional Variability ICV [= $(\text{Fe}_2\text{O}_3 + \text{K}_2\text{O} + \text{Na}_2\text{O} + \text{CaO} + \text{MgO} + \text{TiO}_2) / \text{Al}_2\text{O}_3$] (Cox et al., 1995) value ranging from 1.28–1.30 for OZ samples, 1.12 for KB sample, 1.46 for SM1 sample and 1.37–1.45 for SM2 sample. These ranges indicate that the precursor rocks in the source area had undergone moderate to high degrees of chemical weathering.

In the A–CN–K diagram ($\text{Al}_2\text{O}_3 - \text{CaO} + \text{Na}_2\text{O} - \text{K}_2\text{O}$), all samples are close to the boundary of plagioclase and alkali-feldspar except for SM1 sample, which is more Al rich indicating intense chemical weathering in the source region (Fig. 6a). In the A–CNK–FM diagram [$(\text{Al}_2\text{O}_3 - (\text{CaO} + \text{Na}_2\text{O} + \text{K}_2\text{O}) - (\text{Fe}_2\text{O}_3 + \text{MgO}))$], M1 value ($M1 = \text{FeO} + \text{MgO} + \text{Al}_2\text{O}_3 / \text{K}_2\text{O} + \text{Na}_2\text{O} + \text{CaO}$) range 2.44–5.21 and M2 value ($M2 = \text{Al}_2\text{O}_3 / \text{FeO} + \text{MgO}$) range 1.14–2.09 (Fig. 6b). This diagram shows the gradual chemical weathering trend. Fig. 6b shows that SM1 sample is plotted in the field A III and IV indicating intense weathered protolith and OZ and SM2 sample in field A III indicating a high weathering whereas KB02 sample show less weathered precursor rock.

Provenance and Tectonic Setting

The composition of major element or oxides was used to infer sedimentary provenance by the application of discriminant function analysis of Roser and Korsch (1988). In figure 7a, the samples are scattered in the quartzose sedimentary provenance field whereas KB02 sample is plotted in felsic igneous provenance field pointing to a major contribution of quartzose sedimentary rock to OZ and SM samples and felsic igneous materials to KB sample in their precursor sediments.

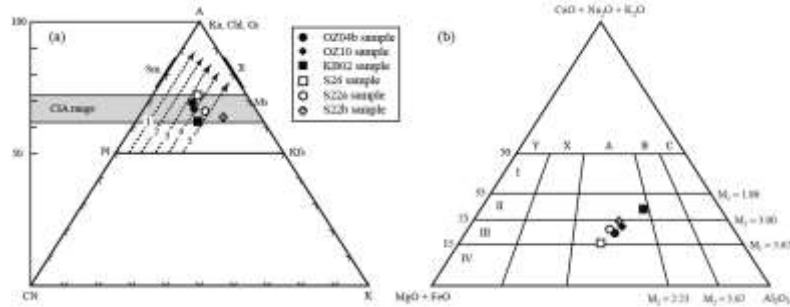


Figure 6 (a) A–CN–K diagram (after Nesbitt and Young, 1982) and (b) A–CNK–FM diagram for studied samples (after Englund and Jørgensen, 1973b). Weathering trends 1–5 are gabbro, tonalite, granodiorite, adamellite and granite (Fedo et al., 1997).

The present study was attempted to discriminate the tectonic setting based on the geochemical composition. The bivariate plot of logs K₂O/Na₂O against SiO₂/Al₂O₃ (Fig. 7b) and SiO₂ versus log K₂O/Na₂O (Fig. 7c) revealed that the samples are generally related to passive margin and active continental margin. Th–Co–Zr/10 tectonic discrimination diagram revealed that although some samples deviate from the distinctive setting, the source area is mostly of active continental margin (Fig. 7d).

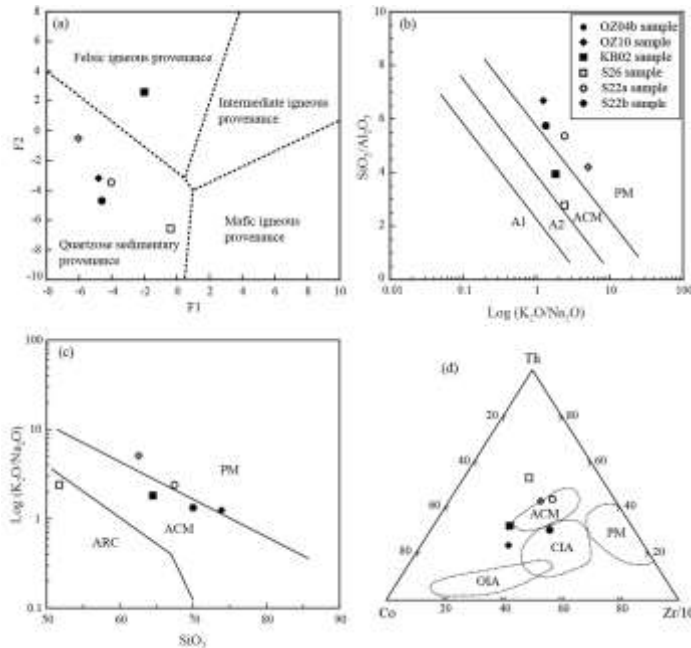


Figure 7 (a) Major element discriminant function diagram for studied samples (after Roser and Korsch, 1988), tectonic setting discrimination diagrams of (b) Log K₂O/Na₂O–SiO₂/Al₂O₃ (Maynard et al., 1982), (c) SiO₂–Log K₂O/Na₂O (Roser and Korsch, 1986), and (d) Th–Co–Zr/10 (Bhatia and Crook, 1986). A1 = arc setting; A2 = evolved arc setting; ACM = active continental margin; PM = passive margin; ARC = island arc margin; CIA = continental island arc; OIA = oceanic island arc.

Although some samples fall within a passive margin setting, it is likely that not all high-temperature rocks have such an origin. However, Searle et al. (1999; 2007) suggested that the western margin of Southeast Asia changed from a passive continental margin in the Permian with shallow, marine carbonate sedimentation, which continued throughout the Triassic and Lower Jurassic from the studies of Karakoram and Tibet, which was correlated in tectonic evolution with Mogok metamorphic belt. This was followed by an Andean-type convergent margin in Jurassic times, and magmatic activity during the India–Eurasian collision through Eocene–Miocene times. It is probable from the chemical compositions that the lithology and proportions of rock types vary and seem to record different tectonic settings and source area compositions, and certain tectonic settings do not necessarily generate rocks with distinct geochemical signatures (McLennan et al., 1990). More careful investigation of lithology followed by geochemical studies may still be needed to understand the metamorphism, protolith nature and tectonism of the Mogok metamorphic belt.

Conclusion

The Cenozoic Mogok metamorphic belt consists of metaigneous and metasedimentary rocks with various granitoid intrusions. The common mineral assemblages of gneiss samples are characterized by garnet + biotite + plagioclase + K-feldspar + quartz with cordierite and sillimanite in some samples. Based on the reported geothermobarometry the samples were formed under upper amphibolite to granulite facies conditions. Geochemical data were used to evaluate the possible protolith composition, source–area weathering, provenance and tectonic setting of the gneiss samples. Sagaing samples are more enriched in Fe compared with Onzon and Thabeikkyin samples. The major and minor oxides have a similar composition relative to the UCC with slight depletion of CaO, Na₂O and P₂O₅. Transition elements are comparable to average crustal content with slight enrichment of Ni. LILE elements scatter around with slight enrichment in Rb and marked depletion of Sr. HFSE elements show enrichment with marked Nb depletion. Evidences from major and trace element concentrations, ratios and use of various diagrams point to the derivation of Onzon samples and SM2 unit samples from psammitic composition mainly greywacke and SM1 unit sample from pelitic compositions except for Thabeikkyin sample, which has felsic igneous protolith. In addition, CIA, CIW and ICV values, and major element diagram have indicated the source areas had undergone moderate to high degree of weathering. Based on the major and trace element variation diagrams sediment deposition might have occurred at passive margin and active continental margin.

Acknowledgements

We would like to acknowledge late Dr. Myint Lwin Thein and his field party and also Dr. Myint Thein for allowing us to cite their unpublished field data of Onzon, Thabeikkyin and Sagaing areas. Thanks also due to petrology group of Nagoya University and colleagues at the Department of Geology, University of Magway for their comments and suggestions.

References

- Argast, S. and Donnelly, T.W., (1987) “The chemical discrimination of clastic sedimentary components.” *Journal of Sedimentary Petrology*, vol. 57, pp. 813–823.
- Barley, M.E., Pickard, A.L., Khin Zaw, Rak, P. and Doyle, M.G., (2003) “Jurassic to Miocene magmatism and metamorphism in the Mogok metamorphic belt and the India-Eurasia collision in Myanmar.” *Tectonics*, vol. 22, doi.10.1029/2002TC001398.
- Bertrand, G., Rangin, C., Maluski, H. and Bellon, H., (2001) “Diachronous cooling along the Mogok metamorphic belt (Shan Scarp, Myanmar); the trace of the northward migration of the Indian syntaxis.” *Journal of Asian Earth Sciences*, vol. 19, pp. 649–659.

- Bertrand, G., Rangin, C., Maluski, H., Tin Aung Han, Ohn Myint, Win Maw and San Lwin. (1999) "Cenozoic metamorphism along the Shan Scarp (Myanmar); evidences for ductile shear along the Sagaing Fault or the northward migration of the eastern Himalayan syntaxis?" *Geophysical Research Letters*, vol. 26, pp. 915-918.
- Bhatia, M.R. and Crook, K.A.W., (1986) "Trace element characteristics of graywackes and tectonic setting discrimination of sedimentary basins." *Contribution to Mineralogy and Petrology*, vol. 92, pp. 181-193.
- Condie, K.C., (1993) "Chemical composition and evolution of the upper continental crust: contrasting results from surface samples and shales." *Chemical Geology*, vol. 104, pp. 1-37.
- Cox, R., Lowe, D.R. (1995) "Compositional evolution of coarse elastic sediments in the south United States from 1.8 to 0.2 G.A. and implications for relationship between the development of crustal blocks and their sedimentary cover." *Journal of Sediment Research*, vol. 65, 477-494.
- Cullers, R.L., and Podkovyrov, V.N., (2000) "Geochemistry of the Mesoproterozoic Lakhanda shales in southeastern Yakutia, Russia: implications for mineralogical and provenance control, and recycling." *Precambrian Research*, vol. 104, pp. 77-93.
- Englund, J.O. and Jørgensen, P., (1973b) "A chemical classification system for argillaceous sediments and factors affecting their composition." *Geologiska Föreningens i Stockholm Förhandlingar*, vol. 95, pp. 87-97.
- Fedo, C.M., Young, G.M., Nesbitt, H.W., (1997) "Paleoclimate control on the composition of the Paleoproterozoic Serpent formation, Huronian Supergroup, Canada, a greenhouse to icehouse transition." *Precambrian Research*, vol. 86, pp. 201-223.
- Floyd, P.A., Leveridge, B.E., (1987) "Tectonic environment of the Devonian Gramscatho basin, south Cornwall: framework mode and geochemical evidence from turbiditic sandstones." *Journal of the Geological Society of London*, vol. 144, pp. 531-542.
- Garcia, D., Coelho, J., Perrin, M., (1991) "Fractionation between TiO₂ and Zr as a measure of sorting within shale and sandstone series (northern Portugal)." *European Journal of Mineralogy*, vol. 3, pp. 401-414.
- Girty, G.H., Ridge, D.L., Knaack, C., Johnson, D., Al-Riyami, R.K., (1996) "Provenance and depositional setting of Paleozoic chert and argillite, Sierra Nevada, California." *Journal of Sedimentary Research*, vol. 66, pp. 107-118.
- Gromet, L.P., Dymek, R.E., Haskin, L.A., Korotev, R.L., (1984) "The North American shale composite: its composition, major and trace element characteristics." *Geochimica et Cosmochimica Acta*, vol. 48, pp. 2469-2482.
- Harnois, L., (1988) "The CIW index - a new chemical index of weathering." *Sedimentary Geology*, vol. 55, pp. 319-322.
- Herron, M.M., (1988) "Geochemical classification of terrigenous sands and shales from core of log data." *Journal of Sedimentary Petrology*, vol. 58 (5), pp. 820-829.
- Maung Thein and Soe Win (1970) "The metamorphic petrology, structure and mineral resources of the Shantung-U-Thandawmywet Range, Kyaukse District." *Burma Science and Technology Journal*, vol. 3, pp. 487-514.
- Maw Maw Win, Enami, M. and Kato, T., (2016) "Metamorphic conditions and CHIME monazite ages of Late Eocene to Late Oligocene high-temperature Mogok metamorphic rocks in central Myanmar." *Journal of Asian Earth Sciences*, vol. 117, pp. 304-316.
- Maynard, J.B., Valloni, R., Yu, H., (1982) "Composition of modern deep sea sands from arc-related basins." *Geological Society of London, Special Publication*, vol. 10, pp. 551-561.
- McLennan, S.M., (2001) "Relationships between the trace element composition of sedimentary rocks and upper continental crust." *Geochemistry, Geophysics, Geosystems*, 2 (2000GC000109 (electronic publication).
- McLennan, S.M., Taylor, S.R., McCulloch, M.T., Maynard, J.B., (1990) "Geochemical and Nd-Sr isotopic composition of deep-sea turbidites: crustal evolution and plate tectonic associations." *Geochimica et Cosmochimica Acta*, vol. 54, pp. 2015-2050.
- Mitchell, A.H.G., Myint Thein Htay, Htun, K.M., Myint Naing Win, Thura Oo and Tin Hlaing (2007) "Rock relationships in the Mogok metamorphic belt, Tatkon to Mandalay, central Myanmar." *Journal of Asian Earth Sciences*, vol. 29, pp. 891-910.
- Myint Lwin Thein, Ohn Myint, Sun Kyi and Phone Nyunt Win (1990) "Geology and stratigraphy of the metamorphosed Early Paleozoic rocks of the Mogok-Thabeikkyin-Singu-Madaya Areas." Staff report, no. 98, pp. 24, Applied Geology Department, University of Yangon.

- Nesbitt, H. W. and Young, G. M., (1984) "Prediction of some weathering trends of plutonic and volcanic rocks based on thermodynamic and kinetic considerations." *Geochimica et Cosmochimica Acta*, vol. 48, pp. 1523–1534.
- Ridd, M.F., and Watkinson, I., (2013) "The Phuket-Slate Belt terrane: tectonic evolution and strike-slip emplacement of a major terrane on the Sundaland margin of Thailand and Myanmar." *Proceedings of the Geologists Association*, vol. 124, pp. 994-1010.
- Roser, B.P., Korsch, R.J., (1986) "Determination of tectonic setting of sandstone-mudstone suites using SiO₂ content and K₂O/Na₂O ratio." *Journal of Geology*, vol. 94, pp. 635-650.
- Roser, B.P., Korsch, R.J., (1988) "Provenance signatures of sandstone-mudstone suites determined using discriminant function analysis of major-element data." *Chemical Geology*, vol. 67, pp. 119–139.
- Rudnick, R.L., Gao, S., (2003) *The composition of the continental crust*. In: Rudnick, R.L. (Ed.), *The Crust*. Elsevier-Pergamon, Oxford, pp. 1–64.
- Searle, M.P., Khan, M.A., Fraser, J.E., and Gough, S.J., (1999) "The tectonic evolution of the Kohistan-Karakoram collision belt along the Karakoram Highway transect, north Pakistan." *Tectonics*, vol. 18, pp. 929-949.
- Searle, M.P., Noble, S.R., Cottle, J.M., Waters, D.J., Mitchell, A.H.G., Tin Hlaing and Horstwood, M.S.A., (2007) "Tectonic evolution of the Mogok metamorphic belt, Burma (Myanmar) constrained by U-T/Pb dating of metamorphic and magmatic rocks." *Tectonics*, vol. 26, TC3014.
- Shaw, D.M., (1956) "Geochemistry of Pelitic Rocks. Part III: Major Elements and General Geochemistry," *Geological Society of American Bulletin*, vol. 67, pp. 913–934.
- Shaw, D. M., (1972) "The origin of the Apsley gneiss, Ontario." *Canadian Journal of Earth Sciences*, vol. 9, pp.18–35.
- Taylor, S.R. and McLennan, S.M., (1985) *The Continental Crust: Its Composition and Evolution*. Blackwell Scientific Publishers, Oxford.
- Varga, A.R., Szakmány, G., (2004) "Geochemistry and provenance of the upper carboniferous sandstones from borehole diósvizsló-3 (Téseny Sandstone Formation, SW Hungary)." *Acta Mineralogica–Petrographica*, Szeged vol. 45/2, pp. 7–14.
- Whitney, D.L. and Evans, B.W., (2010) "Abbreviations for names of rock-forming minerals." *American Mineralogist*, vol. 95, pp. 185-187.
- Wimmenauer, W. (1984) "Das prävariskische Kristallin im Schwarzwald." *Fortschritte der Mineralogie*, 62 (Beiheft 2), pp. 69–86.
- Ye Kyaw Thu, Enami, M., Kato, T. and Tsuboi, M., (2017) "Granulite facies paragneisses from the middle segment of the Mogok metamorphic belt, central Myanmar." *Journal of Mineralogical and Petrological Sciences*, vol. 112, pp. 1–19.
- Ye Kyaw Thu, Maw Maw Win, Enami, M. and Tsuboi, M., (2016) "Ti-rich biotite in spinel and quartz-bearing paragneiss and related rocks from the Mogok metamorphic belt, central Myanmar." *Journal of Mineralogical and Petrological Sciences*, vol. 111, pp. 270–282.
- Yonemura, K., Osanai, Y., Nakano, N., Adachi, T., Charusiri, P. and Tun Naing Zaw, (2013) "EPMA U-Th-Pb monazite dating of metamorphic rocks from the Mogok Metamorphic Belt, central Myanmar." *Journal of Mineralogical and Petrological Sciences*, vol. 108, pp. 184-188.

PETROGRAPHY AND DIAGENESIS STUDY OF THE OKHMINTAUNG FORMATION EXPOSED IN CHAUNG ZON AREA, PWINTBYU TOWNSHIP, MAGWAY REGION

Than Zaw¹, Ye Kyaw Thu², Yin Yin Oo³

Abstract

The research area is located in Chaung Zon Village, Pwintbyu Township, Magway Region. Okhmintaung Formation is characterized by light grey, medium to coarse grained, thick bedded to massive type sandstones intercalated with thin-bedded mudstones and bluish grey shales are also occurred. The sandstones of the Okhmintaung Formation may be termed as “Sublitharenite”. Alteration of biotite to muscovite and oxidized biotite are more common in the Okhmintaung sandstone in the study area. The cementing material in the Okhmintaung sandstones are calcite and iron cements, glauconite, rutile and clay matrix. The common characteristics of late burial or phyllosilic stage are the alteration of clay mineral into micas and the development of well crystallized phyllosilicate minerals.

Keywords: Stratigraphy, Petrography, Nomenclature of sandstone, Diagenesis, Diagenesis stage.

Introduction

Location and size

The study area is located between north latitude 20° 12' 30" - 20° 16' 30" and east longitude 94° 25' 00" - 94° 28' 30". It is situated about 16 miles (25.75 km) west of the Pwintbyu Township. It falls in 2094/7 (84 L/7) and 2094/8 (84 L/8) referring to UTM topographic maps. Pathein-Monywa Highway is passing through the eastern part of the study area. The location map is shown in Figure (1-A).

Literature survey

The Tertiary rocks of Myanmar had been studied by geologists since 1869, but geological investigation has not yet completed. Theobald (1873) introduced the term “Pegu Group” and subdivided into two parts by an important unconformity which approximated the Oligocene-Miocene boundary and non-marine Plio-Pleistocene “Fossil Wood Group of the Irrawaddian”. The Minbu Basin of Central Cenozoic Belt, which includes the study area, was paid much attention by many geologists for primarily due to hydrocarbon prospects. As a result, the Tertiary rock units of Minbu Basin had been mapped and discussed by various geologists since 1800s and studied the stratigraphy, structure and oil prospects.

Aim and Objectives

- To prepare thin section for clastic rocks.
- To identify petrogenesis of sediments exposed in the study area by using the suitable advanced techniques possibly
- To take photograph all thin-sections and micro fossils

¹ Dr, Associate Professor, Department of Geology, Magway University, Myanmar

² Dr, Lecturer, Department of Geology, Magway University, Myanmar

³ Assistant Lecturer, Department of Geology, Magway University, Myanmar

Material and Methods

Suitable sandstone samples collected during field works are three dimensionally cut into thin sections and studied under a polarizing microscope. The detrital grains are identified by point counting on a slide and the modal composition is roughly estimated by comparing with percentage estimation charts of Folk *et al.*, 1970 in Tucker, 2001.

Tectonic Framework of study area in the Minbu Basin

The study area is situated in the Central Cenozoic Belt of Myanmar (Chibber, 1934; Tainsh, 1950; Maung Thein 1976, 2010, 2014) which constitutes one of the four geotectonic belts of Myanmar. The study area is located in northwestern part of the Minbu Basins.

According to the tectonic model of Maung Thein (1983), Minbu Basin, a part of Central Myanmar Belt is associated to be a fore-arc related basin. The study area generally encompasses a small segment of the Minbu Basin. It is composed mainly of Oligocene and Miocene sediments.

The study area comprising is surrounded by Central Volcanic Line and Pegu Yoma in the east, by the Western Ranges in the West, by the Chindwin Basin in the north and, by the Thayetmyo Sentaxis in the south respectively.

The eastern part is composed of Miocene stratigraphic sequence units and western part is Oligocene units. The study area is mainly composed of stratigraphic units from east to west; Irrawaddy Formation, Obogon Formation, Kyaukkok Formation, Pyawbye Formation, Okhmintaung Formation, Padaung Formation, and Shwezetaung Formation.

In the area, the Oligocene-Miocene succession is molassic in nature and generally dipping towards the east. The Miocene strata are constituted mainly of buff- coloured, fine- to medium-grained, thinly bedded sandstone intercalated with light gray to bluish gray shale, light gray to brown, medium- to coarse-grained, medium to thick bedded sandstone with minor gray shale and clay, bluish gray sandy clays with dispersed gypsum plates; concretionary bluish gray clays; intraformational conglomerate and subordinate sandstone.

The Oligocene rocks are buff to light greenish gray and compact, fine- to medium-grained, massive sandstone, dark bluish gray clay and mudstone with fine-grained, hard and compact sandstone, greenish gray, fine to medium-grained, massive sandstone, sandy shale and silty sand. The regional geologic setting of Chaung Zon area is shown in Figure (1-B).

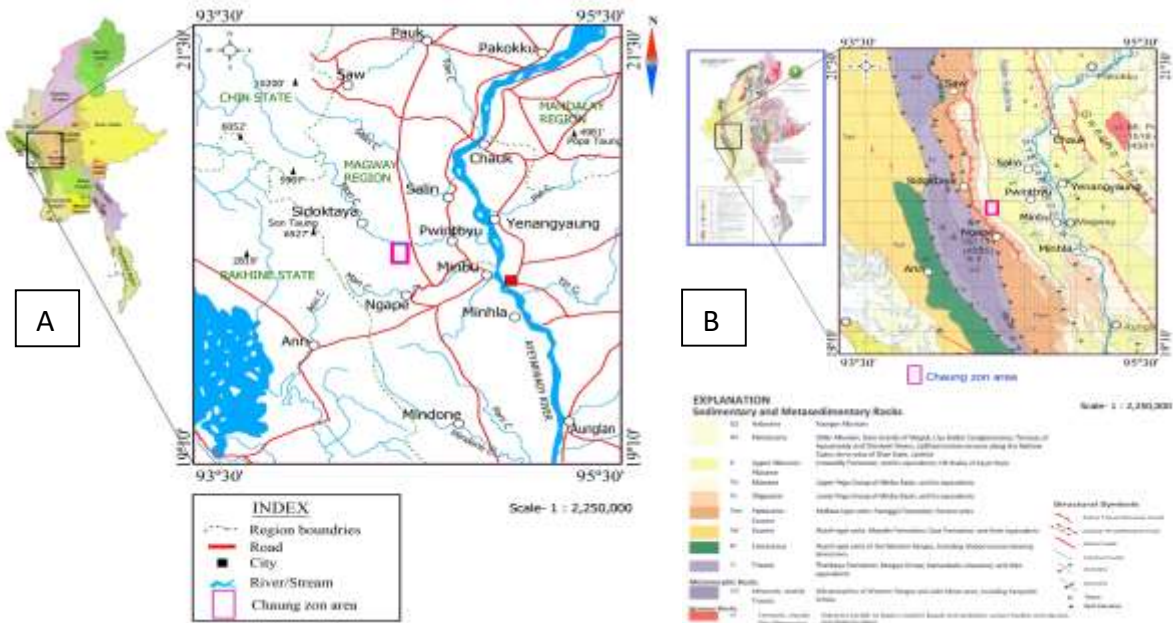


Figure 1(A) Location map of the Chaung Zon Area and (B) Regional geologic setting of the Chaung Zon area. (Source; Myanmar Geoscience Society, 2014)

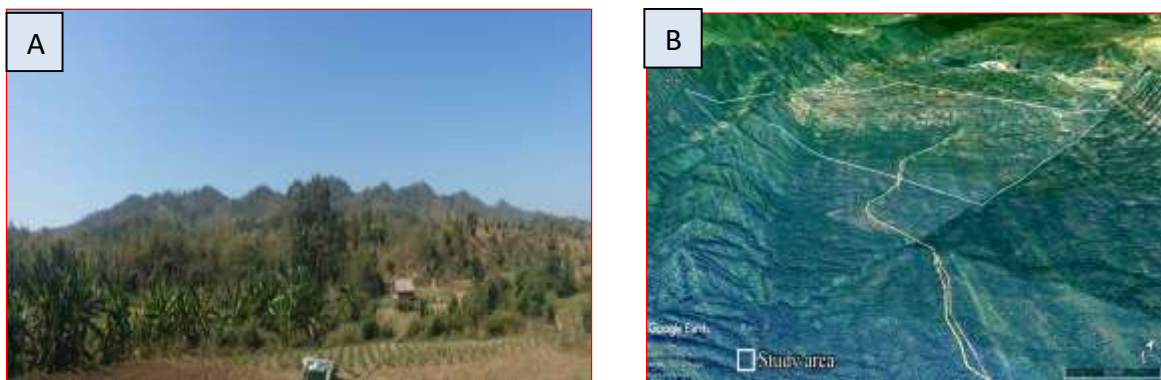


Figure 2 (A) Picturesque view of Kyunbotaung. (Facing to the North), (B) 3D landset image and topographic features of Chaung Zon area. (Source; Google Earth, 2017)

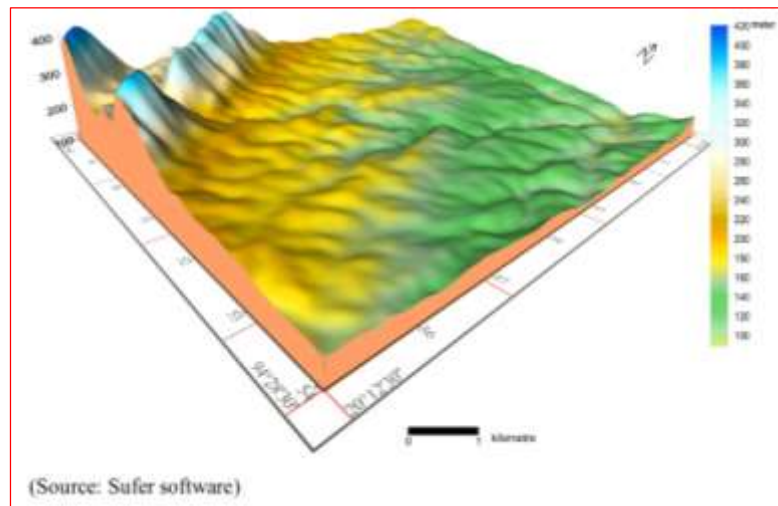


Figure 3 Evolution Development Map (EDM) of the study area.

Stratigraphy

General Statement

The study area, occupying a small segment of the western margin of the Inner-Myanmar Tertiary Basin, comprises mainly Oligocene-Miocene sediments deposited in marine to deltaic environments. The rocks sequence of the area in descending order are; Shwezetaw Formation (Early Oligocene), Padaung Formation (Early Oligocene), Okhmintaung Formation (Late Oligocene), Pyawbwe Formation (Early Miocene), Kyaukkok Formation (Middle Miocene), Obogon Formation (Late Miocene) and Irrawaddy Formation (Late Miocene to Pliocene). The author specialized the study of Okhmintaung Formation.

Okhmintaung Formation

The lower part of the Okhmintaung Formation is characterized by light grey, medium-to coarse-grained, thick-bedded to massive type sandstones intercalated with thin-bedded mudstones and bluish grey shales are also occurred. In the middle portion, dark grey-coloured, medium-to coarse-grained, thick-bedded sandstone intercalated with thinly mudstone is occurred. In the upper part, light grey, fine-to medium-grained, medium-to thick-bedded sandstones are found. Sand-balls or concretions and polyperthite concretions are also occurred in this upper part of lower portion. Shale partings are present in this sandstones bed.



Figure 4 The outcrop nature showing the Okhmintaung Formation, **a)** Light grey colored, medium-grained, thin to medium-bedded sandstones intercalated with 2-4 cm thick mud layer in the middle part (20° 15' 51" N - 94° 24' 38"E), **b)** Dark brown to yellowish brown colored, medium- to coarse-grained, thick- to massive sandstones exposed in the middle part (20° 15' 51" N - 94° 24' 38" E) and **c)** Hard and competent sandstones exposure with tabular and planar type cross bedding structures in the lower part (20° 15' 51" N - 94° 24' 38" E)

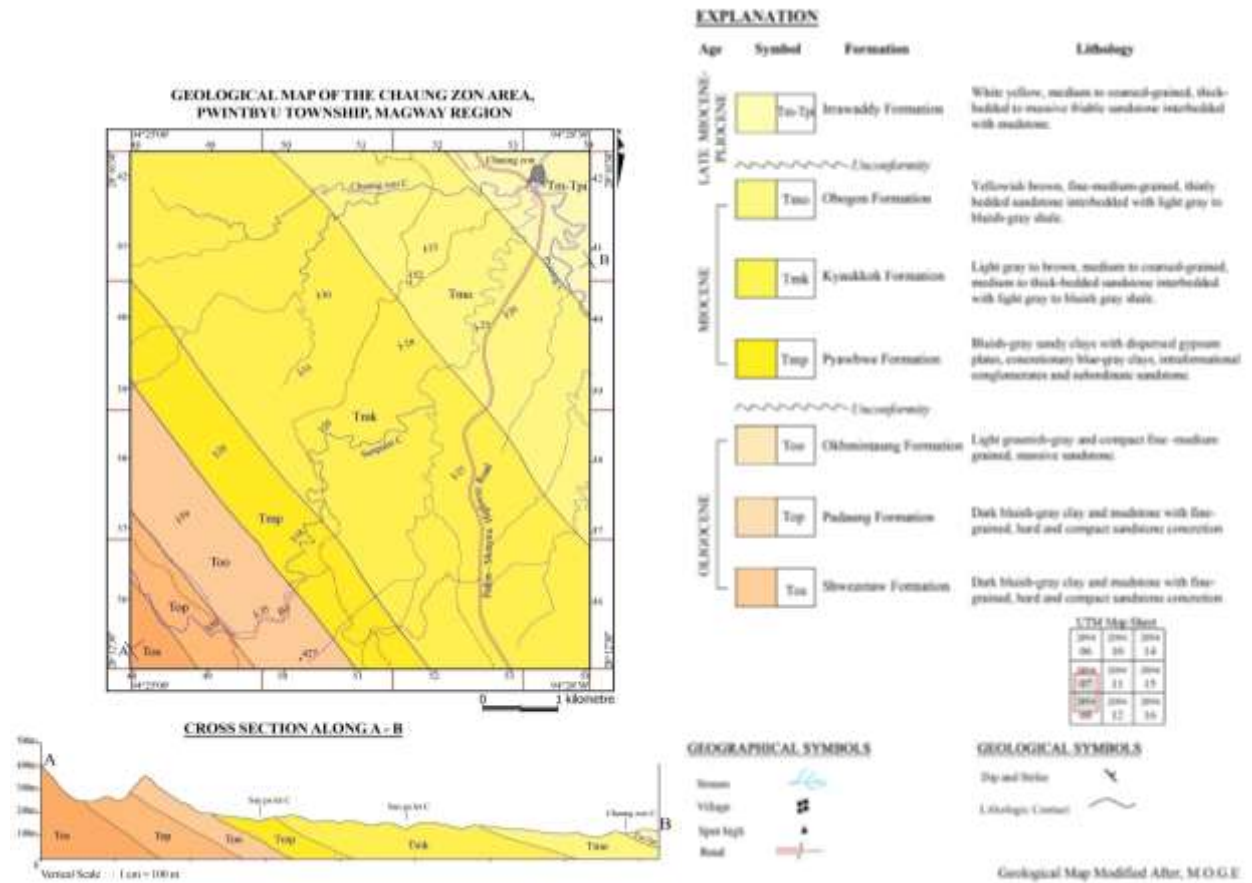


Figure 3 Geological map of the research area (Modified after MOGE)

Petrography

The percentage estimation of sandstones was shown in charts of Folk *et al.*, 1970 in Tucker, 2001 (Table 1). The sandstones are classified according to the simple classification of sandstone (after Pettijohn *et al.*, 1987 in Tucker, 2001). The sandstones of Okhmintaung Formation are composed of 55% to 72% detrital grains, 28% to 45% chemical cements and 2% to 5% of matrix. Detrital grains in these sandstones are generally moderately sorted and subangular to subrounded. The diameters of detrital grains are 0.1 mm to 2 mm.

Table 1 The detrital composition means of sandstones (in volume %) of Okhmintaung Formation of the study area. Quantitative models are recalculated from the data of thin slide.

Simple No.	Quartz	Feldspar	Rock Fragment	Total
Okh-1	60	18	22	100
Okh-2	66	14	20	100
Okh-3	60	20	20	100
Okh-4	72	14	14	100
Okh-5	70	10	20	100
Okh-6	72	10	18	100

Table 2 The detrital and cement composition of sandstones (in volume %) of Okhmintaung Formation.

Slide no	Qtz	Fel	Mica	Rx fg	Hev ml	Calcite cement	Iron cement	Mtx	Other detrital	Total
Okh-1	31	5	3	8	3	30	12	3	5	100
Okh-2	30	10	4	12	2	27	10	2	3	100
Okh-3	18	8	4	8	3	40	10	4	5	100
Okh-4	31	6	3	6	2	36	9	3	4	100
Okh-5	30	5	4	10	3	29	10	5	2	100
Okh-6	31	5	3	9	4	25	11	6	5	100

Quartz

Detrital quartz grains comprise 55% to 72% of total volume of the rock. Most are monocrystalline quartz grains which form subangular-to subrounded. Most of the monocrystalline quartz grains possess unit extinction where the whole crystal is extinguished uniformly under crossed polar. Some of the grain show undulated extinction where extinction is not uniform but sweeps across the crystal as it is rotated from 6° to 15°. Undulated extinction usually is a reflection of a stain in crystal lithic (Fig 5. a & c). Some crystals incorporated with mineral inclusion (Fig 6. a & b). They may be volcanic origin (Fig 5. a, c & 6. a). Polycrystalline quartz grains are straight boundaries represent up to 10% of total rock volume.

Most of quartz grains are monocrystalline represent up to 40% of total rock volume. When the boundaries between the crystals are sutured this is a characteristic of quartz from a metamorphic source. Composite quartz from igneous sources have straighter crystal boundaries. Some quartz grains are irregularly fractured.

Feldspar

Feldspar occupies 10% to 20% of the total detrital population. They are generally fresh and some are moderately weathered. Most of them are show angular, subangular to subrounded, and subsequent to elongated shape. Alkali feldspar are more common than calcic plagioclase, partly because they are more resistant to chemical weathering and partly because the ultimate source of many terrigenous rock is granite or gneiss, in which the feldspars are mainly the alkali variety. Orthoclase crystals usually break along the twin planes so that the simple Carlsbad twinning is rarely seen. Plagioclase can be identified by its polysynthetic and multiple twinning. Feldspars with overgrowth are found (Fig 7 b & d).

Rock fragments

The various rock fragments dominate a significant portion of the detrital grains averaging about 18% to 25% of the total volume. The various types of rock fragments are chert, clay, volcanic rock fragments are also observed in the sandstone of Okhmintaung Formation. The sedimentary rock fragments other than chert are relatively uncommon because they usually break down fairly easily into their components grains. Some large sandstone fragments, in which the component particles are all quartz, are clearly distinguishable even with PPL. Some metamorphic fragments formed elongated grains (Fig 5.d) which are classified as the slate fragments. The contrast with the composite quartz grains of igneous and metamorphic sources, where individual crystals are also found (Fig 6. b & 7. b). They are angular, subangular to subrounded and range in grain size from 0.5 mm to 1.5 mm and some are coated by iron cement.

Mica

Both biotite and muscovite comprise 4% to 10% of the detrital framework. Biotite and muscovite are well observed in Okhmintaung sandstones. Biotite flakes dominant. They show preferred orientation. Bifurcation of biotite mica and some biotite alter to glauconite in Okhmintaung sandstones (Fig 5.5 b). Biotite range in grain size about 0.15 mm to 0.2 mm in diameter. Some biotites are partly altered to chlorite, glauconite (Fig 5.4 b) and muscovite and iron oxide.

Heavy mineral

Heavy minerals comprise about 1% to 2% of the total rock volume. Heavy minerals grains composed of glauconite, magnetite, rutile, zircon, tourmaline and other opaque minerals. Glauconite grains are rounded to subrounded and range in size from 0.1mm to 0.3mm and most of heavy minerals are coated by calcite cement and iron cement.

Bioclasts

Biogenic fragments, both micro- and macro-fossils are present in the fossiliferous sandstones, especially, some samples no.5 and 6 of the Okhmintaung sandstones. They constituted more than 15 % the total rock volume of in this slide and include foraminifera, gastropods, bivalves and enchoids (Fig 7.c).

Cement and Matrix

In the Okhmintaung Formation, calcite cement constitutes about 25% to 40% and 3% to 10% iron cement of the total rock volume. The detrital fragments are firmly welded by calcite cement (Fig 5. c & d and 6. a, b, c & d and 7.a). Generally, the cement is filling of the pore spaces and some are voids remain. The boundaries of the calcite cement are showing sharp and straight characters, while some show curve to slightly sutured boundaries. Replacement of some silicate minerals by calcite cement is a common feature in this sandstone. Some detrital grain such as quartz, feldspar, and mica are markedly corroded and replaced by calcite. In this formation, iron oxide, hematite and clay matrix are also observed. The occurrence of the hematite cement as inclusion in the calcite cements and as scattered grains along the detrital grain boundaries. A few sandstones have a matrix of carbonate mud.

Nomenclature

Okhmintaung sandstone have less than 75% of quartz grains, feldspar comprise 10% to 20% and rock fragments 14% to 20% of the total detrital grains. When the sandstone composition is plotted in the triangular diagram of the Pettijohn *et al.*, (1987), all the sandstones of the Okhmintaung Formation may be termed as "Sublitharenite" seen in Figure (8).

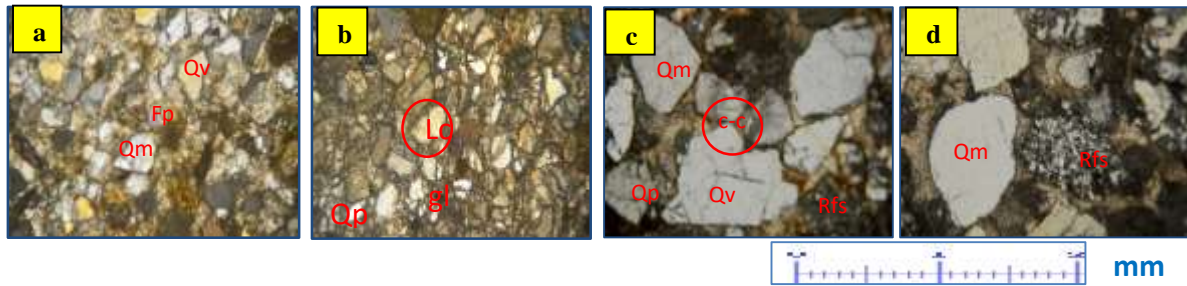


Figure 5 Photomicrographs of sandstones from Okhmintaung Formation. a) and b) Subangular to subrounded quartz grains (Qm, Qp & Qv), plagioclase feldspar (Fp), chert (cht) rock fragment (Rf) and glauconite (gl) which are single crystals, taken with plane-polarized and the matrix between sand grains contain iron oxide and calcite, c) and d) Quartz crystal may sometimes incorporate minerals inclusion and some volcanic quartz (Qv) show uniform or straight extinction and rounded by light brown matrix. Sedimentary rock fragments (Rfs) are found. Quartz grains are found in concave-convex contact, point contact and suture contact. Polycrystalline quartz (Qp) grains are large and rounded boundaries. Concave-convex (c-c) contact also occurred

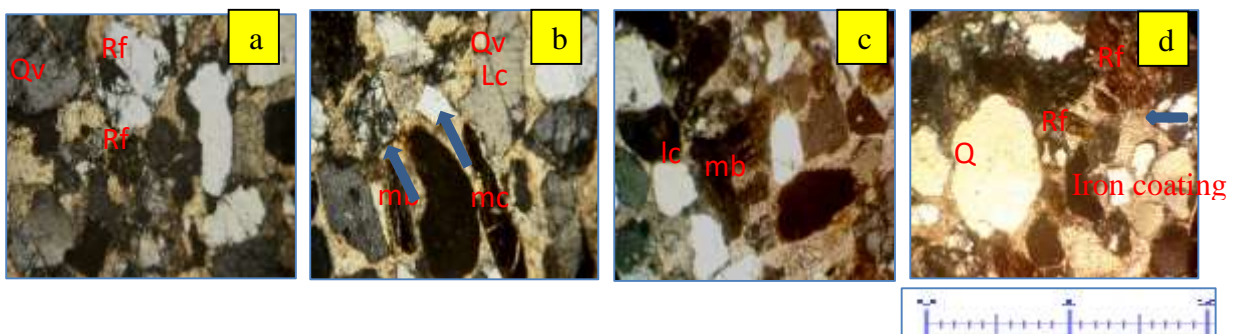


Figure 6 Photomicrographs of sandstones from Okhmintaung Formation. a) and b) Some metamorphic quartz (mQ) show cross-hatch fracture and straight boundaries and volcanic quartz grains (Qv) are long contact and tangential contact. Biotite micas (mb) are long and fracture features in this sandstones. The detrital grains in this sandstone are parallel orientation. c) and d) Quartz overgrowth (Qm) thin oxide and or thin oxide or clay coating between the grains and the overgrowth is visible (PPL). A single-crystal quartz grain with strongly undulate extinction; grain extinguishes completely with more than 5° of stage rotation (XN); volcanic rock fragments with small laths of plagioclase feldspar and a very finely crystalline matrix. Biotite micas (mb) and rock fragments (Rf) are coarse-grained metamorphic rocks often schistose.

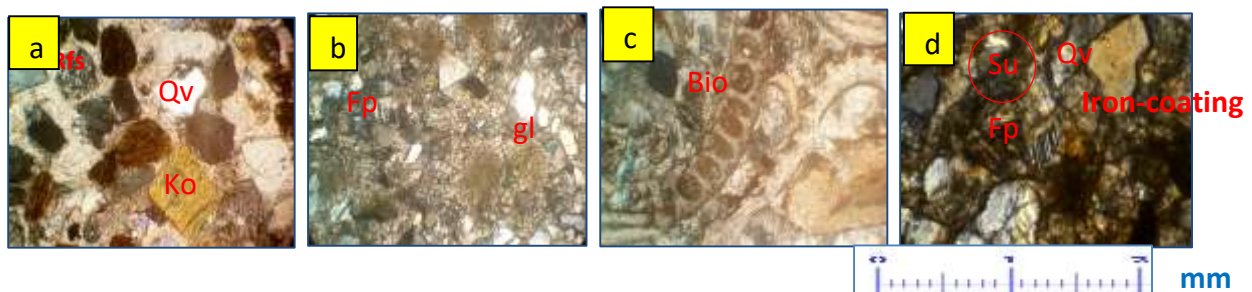


Figure 7 Photomicrographs of sandstones of Okhmintaung Formation. a) Quartz overgrowth (Qv) thin oxide and or clay coating between the grains and the overgrowth is visible (PPL). Sedimentary rock fragments (Rfs) source from sandstones. Orthoclase feldspars (Ko) are cloudy appearance due to alteration. b) & d) Partially dissolved feldspar grains and glauconite (gl) are occurred and overgrowth quartz grain crystal (Qv) also present. Fractured quartz with embayment indicating igneous derivatives. Plagioclase feldspars (Fp) are polysynthetic and multiple twinning. c) Foraminiferal occur in fossiliferous sandstones.

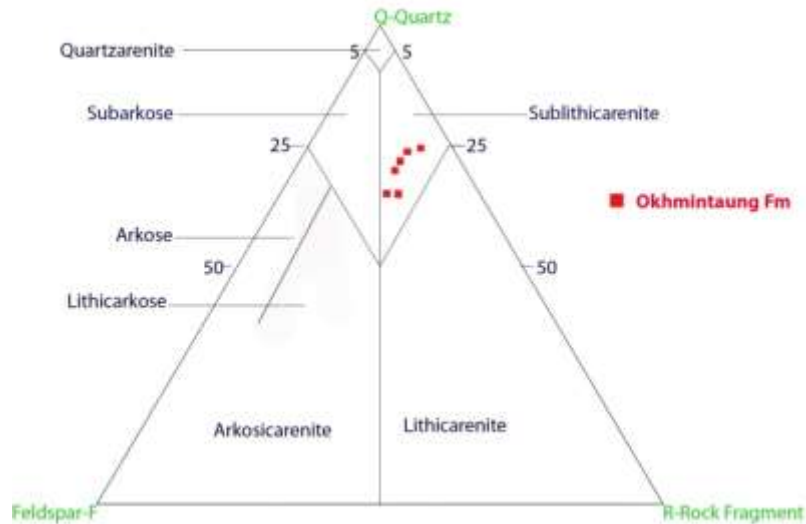


Figure 8 Compositional diagram of sandstone of Okhmintaung Formation (After Pettijohn et al., 1987)

Diagenesis of Okhmintaung Formation

Compaction: The first stage of diagenesis is the compaction of the sediment. It increases the density of the sediments. It occurs in all loose aggregate as the clasts rearrange themselves under moderate pressure. Pore-water in the voids between grains is expelled in the processes and compaction by repacking may reduce the volume of a body of sand by around 10% (Nichol, 2009). Before cementation compaction take place dominantly by mechanical processes, resulting slippage between individual grains reorientation and subsequences fractures of some grains.

Cementation: Quartz cement often occurs as overgrowth on the original quartz grains. Calcite cement is composed of 16% to 51% of the total rock volume. Calcite is soluble in surface water and therefore cemented sandstones often have their cement partially dissolved. Dissolution of calcite cement results in the secondary porosity. Iron oxide cement comprises 5% to 11% of total rock volume. Some iron oxides are the next common and may be cementing material in the sandstone.

Replacement: The process of practically simultaneous capillary solution and deposition by which as new mineral of partly or wholly differing chemical composition may grow in the body of an old mineral or mineral aggregates. In the study area, calcite cement is corroded and wedge apart to the detrital quartz and feldspar.

Authigenesis: Authigenesis is formed when new minerals are crystallized in the sediment or rock during diagenesis. These new minerals may be produced by reaction involving phase already present in the sediment, through precipitation of material introduced in the fluid phase, or a chemical reaction between primary sedimentary minerals and ions is introduced by the fluids. This process overlaps with weathering and cementation, usually involves recrystallization and may result in replacement.

Result and Discussion

1. Okhmintaung sandstone has less than 75% of quartz grains, feldspar comprise 10% to 20% and rock fragments 14% to 20% of the total detrital grains. When the sandstone composition is

plotted in the triangular diagram of the Pettijohn *et al.*, (1987), all the sandstones of the Okhmintaung Formation may be termed as “Sublithicarenite”.

2. **Redoxomorphic Stage:** This stage is characterized by all the reflection due to oxidation and reducing in the sediments during and immediately after burial. The reaction in this stage occurs along the sediment in which total iron content exceeds 3%. Alteration of biotite to muscovite and oxidized biotite are more common in the Okhmintaung sandstone in the study area.
3. **Locomorphic Stage:** During this stage, precipitation of mineral matter fill in the pore spaces and replacement of detrital mineral grains are significant. The cementing material in the Okhmintaung sandstones are calcite and iron cements, glauconite, rutile and clay matrix. Pore spaces between the detrital grains are also filled by silica cement.
4. **Phylломorphic Stage:** This stage is the last stage of diagenesis which involves authigenesis of some minerals. The common characteristics of late burial or phylломorphic stage are the alteration of clay mineral into micas and the development of well crystallized phyllosilicate minerals. Biogenic fragments, both micro- and macro-fossils are present in the fossiliferous sandstones, especially, some samples no.5 and 6 of the Okhmintaung sandstones.

Summery and Conclusion

The study area is located between north latitude 20° 12' 30" - 20° 16' 30" and east longitude 94° 25' 00" - 94° 28' 30". It is situated about 16 miles (25.75 km) west of the Pwintbyu Township. It falls in 2094/7 (84 L/7) and 2094/8 (84 L/8) referring to UTM topographic maps. The lower part of the Okhmintaung Formation is characterized by light grey, medium-to coarse-grained, thick-bedded to massive type sandstones intercalated with thin-bedded mudstones and bluish grey shales are also occurred. In the middle portion, dark grey-coloured, medium-to coarse-grained, thick-bedded sandstone intercalated with thinly mudstone is occurred. In the upper part, light grey, fine-to medium-grained, medium-to thick-bedded sandstones are found. Sand-balls or concretions and polyperthite concretions are also occurred in this upper part of lower portion, Shale partings are present in this sandstones bed.

Detrital quartz grains comprise 55% to 72% of total volume of the rock. Most are monocrystalline quartz grains which form subangular-to subrounded. Feldspar occupies 10% to 20% of the total detrital population. They are generally fresh and some are moderately weathered. The various rock fragments dominate a significant portion of the detrital grains averaging about 18% to 25% of the total volume. Both biotite and muscovite comprise 4% to 10% of the detrital framework. Biotite and muscovite are well observed in Okhmintaung sandstones. Heavy minerals grains composed of glauconite, magnetite, rutile, zircon, tourmaline and other opaque minerals. Calcite cement constitutes about 25% to 40% and 3% to 10% iron cement of the total rock volume. When the sandstone composition is plotted in the triangular diagram of the Pettijohn *et al.*, (1987), all the sandstones of the Okhmintaung Formation may be termed as “Sublithicarenite”.

The first stage of diagenesis is the compaction of the sediment. It increases the density of the sediments. It occurs in all loose aggregate as the clasts rearrange themselves under moderate pressure. Calcite is soluble in surface water and therefore cemented sandstones often have their cement partially dissolved. Dissolution of calcite cement results in the secondary porosity. The process of practically simultaneous capillary solution and deposition by which as new mineral of partly or wholly differing chemical composition may grow in the body of an old mineral or mineral aggregates. Authigenesis is formed when new minerals are crystallized in the sediment or rock during diagenesis. These new minerals may be produced by reaction involving phase already present in the sediment, through precipitation of material introduced in the fluid phase, or a chemical reaction between primary sedimentary minerals and ions is introduced by the fluids.

Redoxomorphic Stage is characterized by all the reflection due to oxidation and reducing in the sediments during and immediately after burial. The reaction in this stage occurs along the sediment in which total iron content exceeds 3%. During the **Locomorphic Stage**, precipitation of mineral matter fill in the pore spaces and replacement of detrital mineral grains are significant. **Phylломorphic Stage** is the last stage of diagenesis which involves authigenesis of some minerals. The common characteristics of late burial or phylломorphic stage are the alteration of clay mineral into micas and the development of well crystallized phyllosilicate minerals.

Acknowledgements

Firstly, I would like to thank my works of gratitude to Dr. Khin Maung Oo, Rector of Magway University, for his kind permission to carry out this research. I am also special thanks to Dr. Khin San, Professor and Head, and Dr. Myo Myint Zaw, Professor, Department of Geology, Magway University, for their valuable suggestions and guidance. Special thanks are also due to the teaching staffs, Geology Department, Magway University, for their help and suggestions. I would like to thanks local people of Mezale village and especially, U Aung Naing family for hospitality and helping me during my field work.

References

- Chhibber, H. L. (1934) “*Geology of Burm.*” Macmillan, London
- Dapples, E.C., (1992) “Stages of diagenesis in the development of Sandstones.” *Geological. Society of America. Bulletin*, vol.73, pp. 913–934.
- Dapples, E.C., (1967) *Diagenesis of Sandstones; developments in sedimentology*. 8th, Elsevier Publishing Company, Amsterdam.
- Folk, R. L., (1974) “*Petrology of Sedimentary Rocks.*” Austin, Texas, Hemphill, pp. 182.
- Folk, R. L., (1980) “*Petrology of Sedimentary Rocks.*” Austin, Texas, Hemphill, pp. 159.
- Krunbein, W.C. and Sloss, L.L., (1963) “*Stratigraphy and sedimentation.*” 2nd edition, Frceman & Co., San Francisco.
- Maung Maung, (1978) “*Stratigraphy and Sedimentation of the Myohta-Ngazun Area.*” Tada U and Ngazun Townships, Mandalay Arts and Science University. M. Sc Thesis (unpub) pp. 103.
- Maung Maung, (1994) “*Petrology of Shwezettaw-Kyauk-O-Ngape area, Ngape-Minbu Township, Magway Region.*” M. Sc Thesis (unpub). Geology Department, Mandalay University, pp. 154.
- Miall, A.D., (1984) “*Principles of Sedimentary Basin Analysis.*” New York, Springer, Verlag.
- Miall, A. D., (1995) Collision-related foreland basins. In: “*Tectonics of Sedimentary Basins*” (Eds Ingersoll, R.V. & Busby, C.J.). Blackwell Science, Oxford; PP. 393–424.
- Myint Thein, (1966) “*Stratigraphy and Structure of the Taungtalone Area.*” Mandalay Arts and Science University, unpub. M. Sc. Thesis.
- Myo Myint Zaw, (2011) “Petrology of the Molasse Sediments In Myinza — Hmwele Gangaw Township.” PhD Disseration.
- Nichols, G.J., (2009) “*Sedimentology and Stratigraphy.*” (2nd ed): John Wile & Sons, New York.
- Pitman, J. K, Price, L. C, Lefever, J. A., (2001) Diagenesis and Fracture Development in Bakken Fromation, Williston Basin; Implications for Reservoir Quality in the Middle Member. *US Geological Survey Professional paper*, pp. 1653.
- Peter, A.Schoole, (1979) A color illustrated guide to constituents, textures, cements and porosities of sandstones and association rocks, “*The American association of petroleum geologists*”, Tulsa, Oklahomma, U.S.A.
- Tucker, M.E., (1996) “*Sedimentary Rocks in the field.*” (2nd ed): John Wiley and Sons, Chictester, New Yourk., Brisban. Tosono. Singapore.
- Tucker, M.E., (2001) “*Sedimentary Petrology.*” (3rd ed). Blackwell Science Ltd., UK
- Thank Zaw Moe, (2017) “*Sedimentology Of The Neogene Sequences Exposed In Myothit Taungnyo Area.*” Magway and Mandalay Regions, PhD Disseration.
- Underwood, M.B. and Moore, G.F., (1995). Trenches and trench-slope basins. In: “*Tectonics of Sedimentary Basins*” (Eds Ingersoll, R.V. & Busby, C.J.). Blackwell Science, Oxford; pp179–220.

Internet Sources:

- <http://www.marinespecies.org/aphia.php?p=taxdetails&id=113445>
- <http://www.marinespecies.org/aphia.php?p=taxdetails&id=113445>
- <http://www.foraminifera.eu/globigerinoides.php>

LITHOFACIES ANALYSIS OF PALEOCENE AND EARLY EOCENE UNITS OF SABADAN AREA, MINDON TOWNSHIP, MAGWAY REGION

Win Lwin Thein¹, Paing Soe², Aye Ko³

Abstract

The study area, Sabadan area is located in the Mindon Township, Magway Region. It lies between latitude 19°07'00" to 19°11'10" and longitude 94°47' 20" to 94° 51' 40". The study area is situated between the Central Cenozoic Belt and Western Ranges. The eastern part of the area (to the east of the Kabaw Fault) occupies Paleocene to Eocene molasses type units of Paunggyi Formation, Laungshe Formation, Tilin Formation and Tabyin Formation. Among these, only two lithofacies are detail studied. Four lithofacies association can be established in the late Paleocene and early Eocene of Paunggyi and Laungshe Formations. They are (1) submarine fan Association, (2) Offshore Association (3) Shoreface Association (4) Delta front Association. The Paunggyi Formation shows at submarine fan environment, which include upper fan, middle fan and lower fan. The environment of Laungshe Formation is classified into three major group; offshore, shore face and delta front. There are four lithostratigraphic units are exposed in the Sabadan area, but only two lithostratigraphic units of the Paunggyi Formation and Laungshe Formation are detailed study.

Keywords: molasses, facies, lithostratigraphic unit

Introduction

The study area, Sabadan area, is situated between the Central Cenozoic Belt and Western Ranges bounded in the northeast by Minbu basin, in the west by Western Ranges, in the southeast by Pyay embayment. The Sabadan area occupies Paleocene to Eocene molasses type units and had been conducted by many workers as petrology, petrogenesis and other general geology. However, the detailed sedimentology studies including lithofacies analysis and their distinct depositional environments have still needed in the study area and the present study attempt to decipher the lithological characteristics and depositional environments mainly on Paunggyi and Laungshe (Paleogene) units.

Materials and Methods

After the field investigation, the observed data were plotted on the base map and geological map was drawn by using field data and lithologic evidences. And then, the paper was prepared step by step. The data collected in the field were firstly evaluated. On the basis of the recent field data and other literatures, the proper outlines were selected for the preparation of final dissertation. The measured data were applied for the establishment of stratigraphic succession and detailed logs. The lithofacies were classified according to the facies codes modified from (Miall, 1978-b in Walker, 1922) on the basis of grain size, primary sedimentary structures and lithologic signatures.

¹ Associate Professor, Department of Geology, University of Magway

² Dr, Associate Professor, Department of Geology, University of Magway

³ Lecturer, Department of Geology, University of Magway

1. Lithofacies Analysis of Paunggyi and Laungshe Formations

3.1. Lithofacies Characteristics

3.1.1 Facies A: matrix supported conglomerate (Cmc)

Description

This Facies occurs in the both Paunggyi Formation and Laungshe Formation (Fig. 3.a and b). In the Paunggyi Formation, matrix supported conglomerate are mostly occurs at the base. It is mainly composed quartz pebbles, sandstone fragment, clay pebbles and metamorphic rock fragment. The nature of the boundaries between contact unit are sharp. In the Middle part, thick bedded to massive conglomerate are occurred and small amount of conglomerate beds are also occurred at the upper part of the Paunggyi Formation. The Facies is associated with gritty sandstone of Facies C, sand-shale interbed sequence of Facies I and massive shale of Facies J.

In Laungshe Formation, matrix supported conglomerate facies (Gcm) is observed as the lower part. It is composed of quartz pebbles, sand clasts and sandstone fragments. The size of quartz pebbles and sand clasts range from 1mm to 2 cm in diameter and most of the quartz pebbles and sandstone clasts are subangular to subrounded and lacking graded nature.

3.1.2 Facies B: Sandstone with mud clasts (Smc)

Description

This Facies occurs in the lower and middle part of the Paunggyi Formation (Fig. 3.c). In the Lower part, thin to medium bedded, dark grey to grey colored, coarse grained sandstone are occurred.

This sandstone contains mud clasts which the size is 0.5 to 1 cm. Medium grained sandstone also occurred middle part of the Paunggyi Formation which they contain little amount of mud clast. The nature of the contact unit is gradational. This Facies is distributed in the lower part and middle part of the Laungshe Formation (Fig.3.d). It is mainly composed of light grey to grey colored, medium grained sandstone with mud clasts. The thickness of mud clast is 1cm to 3cm. Sandstone with mud clasts did not observed upper part of Laungshe Formation. The nature of the boundaries with underlying unit is gradational and upper unit is sharp.

This Facies is associated with matrix supported conglomerate of Facies A, gritty sandstone of Facies C and sandstone with asymmetrical wave ripple of Facies D.

3.1.3 Facies C: Gritty sandstone (Sg)

Description

The facies have thin to medium bedded, greenish grey to dark grey colored gritty sandstone occur at the upper part of the Paunggyi Formation (Fig. 3.e). Gritty sandstone contained mud clast. The contact between lower unit and upper unit are sharp. This Facies is associated bioturbated sandstone of Facies D and massive shale of Facies J.

This Facies is distributed in the lower part of the Laungshe Formation. It is composed of medium bedded, light grey to grey colored, gritty sandstone. Gritty sandstone is not observed at the middle and upper part of the Laungshe Formation. The contact between the lower unit and upper unit are gradational. This Facies is associated with matrix supported conglomerate of Facies A, sandstone with mud clasts of Facies B and sandstone with asymmetrical wave ripple of Facies D.

3.1.4 Facies D: bioturbated sandstone (Sb)

Description

This Facies is exposed at the both Paunggyi and Laungshe Formation(Fig. 3.f and 4.a). Bioturbated sandstone occur in the lower part of the Paunggyi Formation which is characterised by thin to medium bedded, grey colored, fine grained bioturbated sandstone. The nature of the boundaries contact with the lower unit is sharp and upper unit is gradational. This Facies is associated with gritty sandstone of Facies B and massive shale of Facies J.

Bioturbated sandstone is occur in the lower, middle and upper part of the Laungshe Formation composed of thin to medium bedded, greenish grey to grey colored sandstone with bioturbation. The contact between lower and upper units are sharp. This Facies is associated with sandstone with load cast of Facies E, sandstone with wavy bedding of Facies H and sand-shale interbed sequence of Facies I.

3.1.5 Facies E: Sandstone with Load Cast (Sl)

Description

This facies is distributed in the upper part of the Laungshe Formation (Fig. 4.b). This facies is mainly composed of light grey to grey colored, thin to medium- bedded sandstone with load casts.The upper boundary and lower boundary are gradational. This Facies is associated with bioturbated sandstone of Facies D, sandstone with wavy bedding of Facies H and sand-shale interbed sequence of Facies I.

3.1.6 Facies F: Sandstone with asymmetrical wave ripple (Sr)

Description

This Facies is distributed in the lower member of the Laungshe Formation (Fig. 4.c). It is mainly composed of dark grey to grey colored, fine to medium bedded, fine grained sandstone with asymmetrical ripple mark. The lower boundary and upper boundary are sharp. This Facies is associated with matrix supported conglomerate of Facies A, sandstone with mud clast of Facies B and gritty sandstone of Facies C.

3.1.7 Facies G: Horizontal laminated sandstone (Sh)

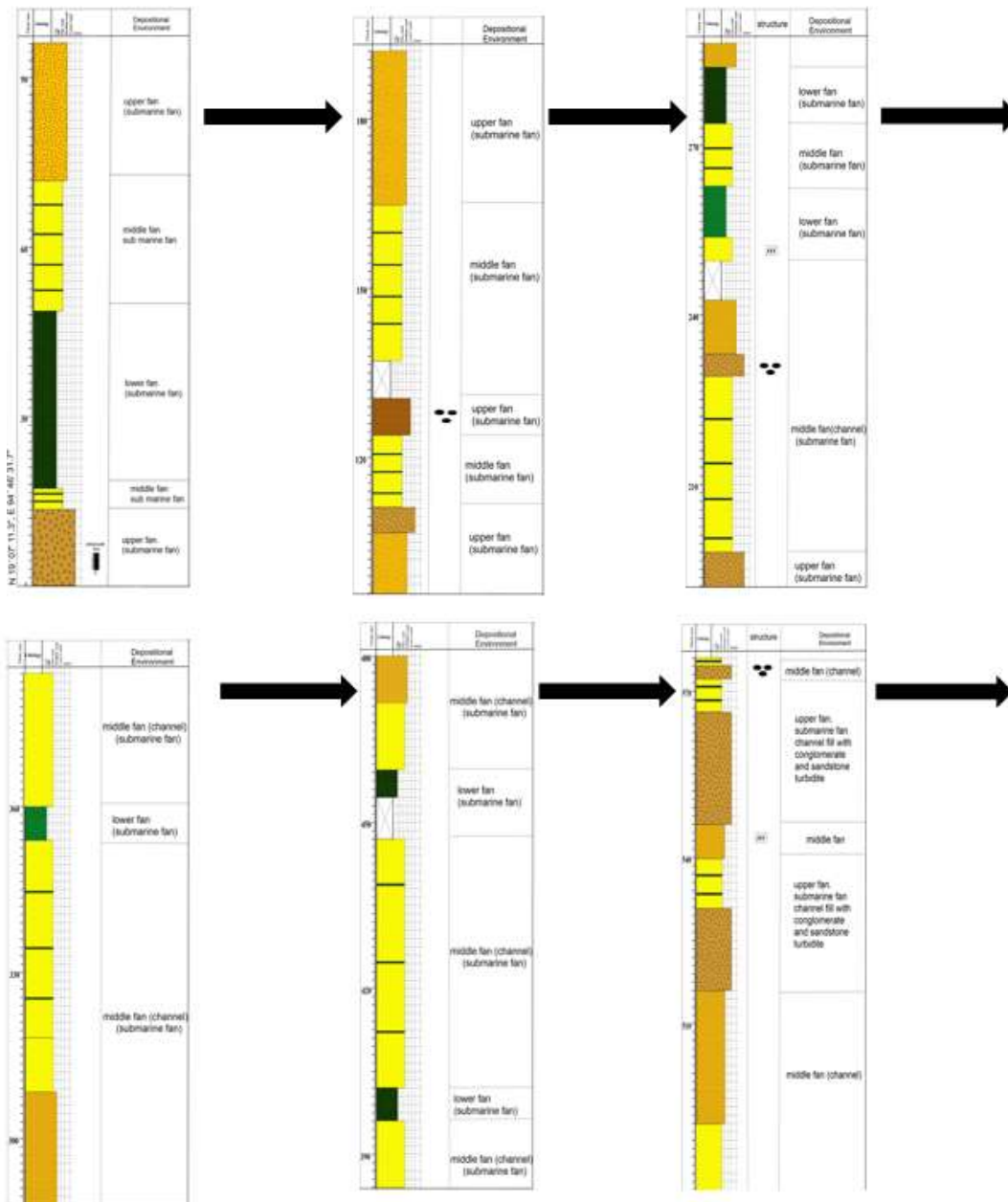
Description

This Facies is distributed in the upper part of the Laungshe Formation (Fig.4. d). It is composed of grey colored, fine grained horizontal laminated sandstone. The nature of boundary between upper and lower boundary is gradational. This Facies is associated with asymmetrical wave ripple of Facies F and sandstone with wavy bedding of Facies I.

3.1.8 Facies H: Sandstone with wavy bedding (Sw)

Description

This Facies is mostly distributed in the upper part of the Laungshe Formation (Fig. 4.e).It is composed of thin bedded, grey colored, fine grained sandstone with wavy bedding. The contact between lower unit and upper unit is gradational. This Facies is associated with bioturbated sandstone of Facies D, sandstone with load cast of Facies E and sand-shale interbed sequence of Facies I.



Vertical Scale

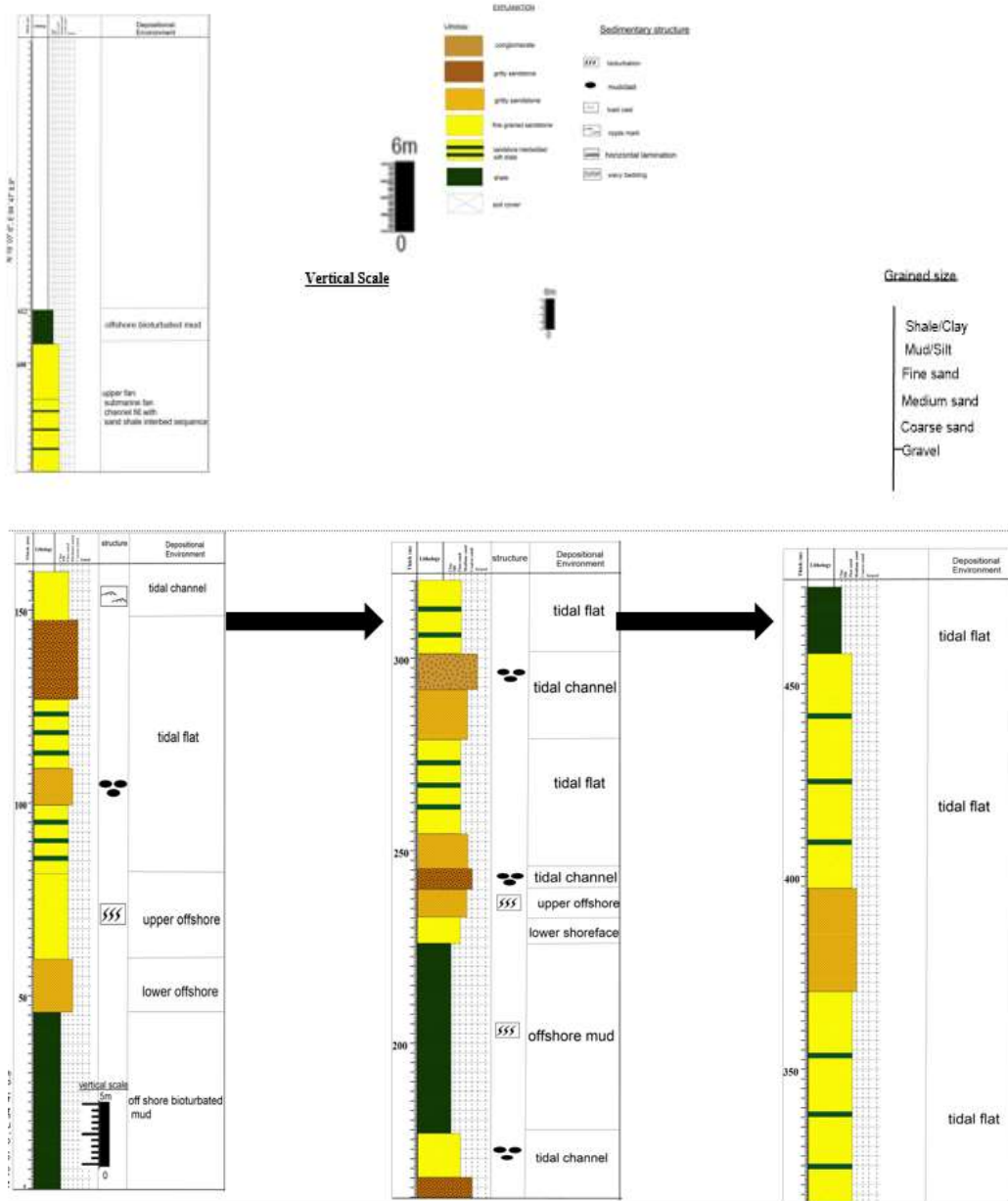


Figure 2 Detailed facies column of the Paunggyi and Laungshe Formations measured along the Shu Chaung sections in the Sabadan Area.

3.1.9 Facies I: Sand-shale interbed sequence (Fsh)

Description

This facies is widely distributed in the Paunggyi Formation and Laungshe Formation (Fig.4.f and 5.a). It is mainly composed of fine- grained, light grey colored sandstone and grey colored shale. This Facies is associated with bioturbated sandstone of Facies D, sandstone with load clast of Facies E and horizontal laminated sandstone of Facies G. The contact between the lower unit and upper unit are gradational.

3.1.10 Facies J: massive shale (Fm)

Description

The Facies are occurred at the both of Paunggyi and Laungshe Formation (Fig. 5. b). In the Paunggyi Formation, dark grey to black colored, thick bedded to massive shale are occurred and massive shale are also occurred at the Laungshe Formation. This Facies is associated with gritty sandstone of Facies C and bioturbated sandstone of Facies D. The contact of these two Facies is sharp contact.

3.2 Lithofacies Association

The combination of two or more facies, which were formed in a single depositional environment at the same time, is grouped into a facies association. A facies association can thus be used for more detailed interpretation of depositional environments. Lithofacies have been classified on the basis of sedimentary structures, lithology and fossils. Lithofacies associations were distinguished with respect to their lithology, facies successions and bed geometry. They are

1. Submarine fan lithofacies association
2. Offshore lithofacies association
3. Shore face lithofacies association and
4. Delta front lithofacies association

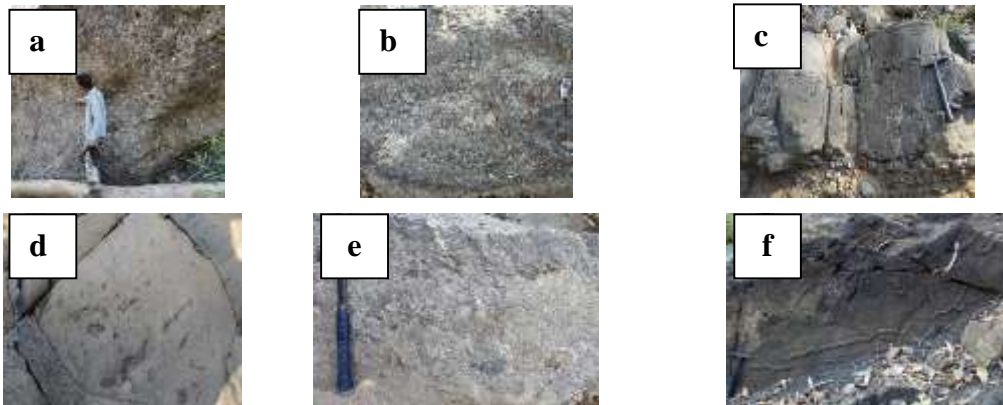


Figure 3 (a) Matrix supported conglomerate of Paunggyi Formation exposed at the Sabadan area (b) matrix supported conglomerate of Laungshe Formation exposed at the Sabadan area (c) thin to medium bedded, dark grey to grey colored, coarse grained sandstone with mud clast in Paunggyi Formation exposed at the Sabadan area (d) light grey to grey colored, medium grained sandstone with mud clasts in Laungshe Formation exposed at the Sabadan area (e) Greenish grey to dark grey colored gritty sandstone exposed at the Sabadan area (f) medium bedded, grey colored, fine grained bioturbated sandstone of Paunggyi Formation exposed at the Sabadan area.

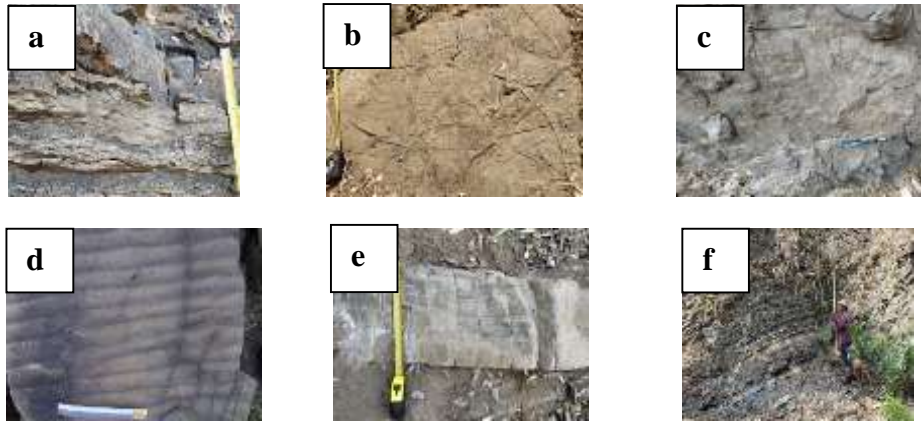


Figure 4 (a) thin to medium bedded, greenish grey to grey colored sandstone with bioturbation of Laungshe Formation exposed at the Sabadan area (b) Light grey to grey colored, thin to medium-bedded sandstone with load casts of Laungshe Formation exposed at the Sabadan area (c) Dark grey to grey colored, fine to medium bedded, fine grained sandstone with asymmetrical ripple marks exposed at the Sabadan area (d) Grey colored, fine grained horizontal laminated sandstone of Laungshe Formation exposed at the Sabadan area (e) Thin bedded, grey colored, fine grained sandstone with wavy bedding of Laungshe Formation exposed at the Sabadan area (f) Sand-shale interbedded sequence of Paunggyi Formation exposed at the Sabadan area.



Figure 5 (a) Sand-shale interbedded sequence of Laungshe Formation exposed at the Sabadan area (b) Dark grey to black colored, thick bedded to massive shale exposed at the Sabadan area.

3.3 Depositional environment of Paunggyi and Laungshe Formation

The Paunggyi Formation shows a submarine fan environment which includes upper fan, middle fan, and lower fan. In the channel of the upper fan is the area of deposition of conglomerate, in my study area, matrix supported conglomerate may be deposited as upper fan. Middle fan of submarine fan also shows a sequence that may be deposited as middle fan, and lower fan includes massive shale. So, the depositional environment of Paunggyi Formation may be deposited as a submarine fan environment (Fig. 6).

The environment of Laungshe Formation is classified into three major groups: offshore, shore face, and delta front. Offshore includes offshore bioturbated mud, lower offshore, and upper offshore. Upper offshore, muddy fine sand shows laminated sand and bioturbated sand. In the study area, gritty sandstone and bioturbated sandstone may be deposited in an offshore environment. Shoreface includes tidal channels and tidal flats. Tidal channels contribute an important part to the development of tidal flats. Subtidal zones are made up of channels and sand bar sediments. Bioturbation is very weak, as the rate of sedimentation is very high in the tidal channel. The tidal channel may show sandstone with asymmetrical wave ripple. The channel bottoms of the larger tidal channels are mostly sandy, matrix supported conglomerate, sandstone with mud clast, and gritty sandstone may serve as channel deposits.

Tidal flat develop along the gently dipping seacoasts with marked tidal rhythms, where enough sediment is available and strong wave action is not present. The tidal flat is located marginal parts of intertidal zone. Intertidal zone are located between the high and low water lines over a vertical range of usually 2 or 3 m, and up to 10 or 15 m, depending upon the tidal range. The primary sedimentary structures including mega-ripple, small scale cross bedding on the sand flat, wavy and lenticular bedding which were formed under tidal flat condition. Muddy tidal flat deposits rich in organic material may contain sandy sediments. Massive shale, horizontal laminated sandstone and sand-shale interbed sequence are character of delta front. Therefore, the depositional environment of Laungshe Formation can be defined as shoreface and delta front environment.

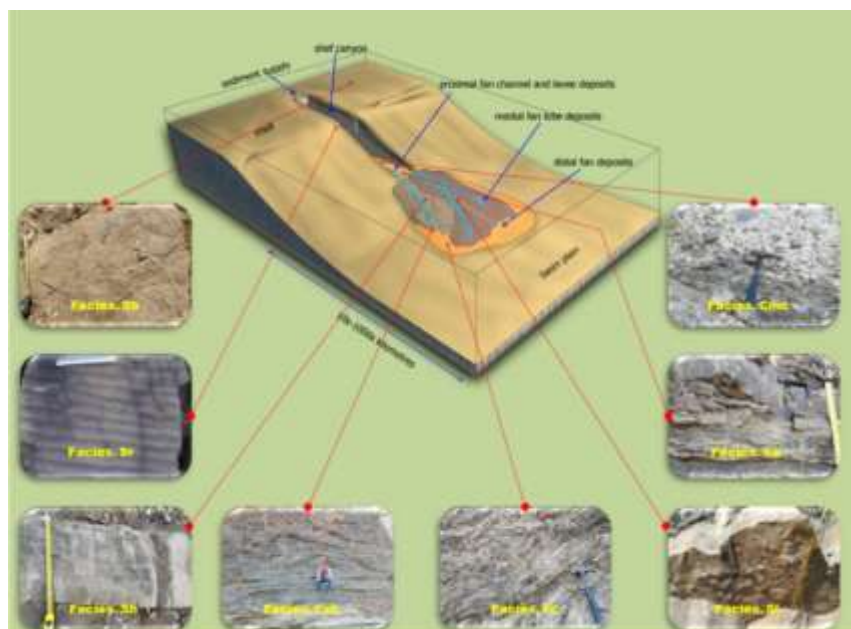


Figure 6 Depositional Environments model on a shelf, shelf canyon (channel) and submarine fan of the Sabadan area, Mindon Township

Conclusion

The study area, Sabadan area, is situated between the Central Cenozoic Belt and Western Ranges. It is bounded in the northeast by Minbu basin, in the west by Western Ranges, in the southeast by Pyay embayment. The eastern part of the area (to the east of the Kabaw Fault) occupies Paleocene to Eocene molasses type units of Paunggyi Formation, Laungshe Formation, Tilin Formation and Tabyin Formation. Among them, only two lithofacies representing the Paleocene and early Eocene units are studied in detail. Four lithofacies association, which were distinguished with respect to their lithology, facies successions and bed geometry can be established in the late Paleocene and early Eocene of Paunggyi and Laungshe Formations. They are (1) Submarine fan lithofacies association, (2) Offshore lithofacies association, (3) Shore face lithofacies association and (4) Delta front lithofacies association.

The Paunggyi Formation shows at submarine fan environment which include upper fan, middle fan and lower fan. In the channel of the upper fan is the area of deposition of conglomerate, in my study area, matrix supported conglomerate may be deposited as upper fan. Middle fan of submarine fan also shows sequence may be deposited as middle fan, and lower fan include massive shale.

The environment of Laungshe Formation is classified into three major group; offshore, shore face and delta front. Offshore include offshore bioturbated mud, lower offshore and upper

offshore. Upper offshore, muddy fine sand show laminated sand and bioturbated sand. In the study area, gritty sandstone and bioturbated sandstone may be deposited offshore environment. Shoreface includes tidal channel and tidal flat. Tidal channels contribute an important part to the development of tidal flat. Muddy tidal flat deposits rich in organic material may contain sandy sediments. Massive shale, horizontal laminated sandstone and sand-shale interbed sequence are character of delta front. Therefore, the depositional environment of Laungshe Formation can be defined as shoreface and delta front environment.

Acknowledgement

I would like to express gratitude to Dr. Paing Soe, Associate Professor and U Aye Ko, Lecturer, Department of Geology, University of Magway. Thanks are also due to people who helped during the field trip in Sabadan area, and colleagues of Department of Geology, University of Magway for their comments.

References

- Chibber, H.L. (1934) *The Geology of Burma*; Mac Millian, London. Compton, R.R., (1962): *Manual of Field Geology*. John Wiley & Sons, New York.
- Cotter, G. de P. (1912) The Pegu-Eocene Succession in the Minbu District near Ngape. *Rec, Memoirs of Geological Survey of India*, v.41, pt.4, p.221-239.
- Gadow, S., Reineck, H.E. (1969) Abländiger Sandtransport bei Sturmfluten. *Senckenbergiana marit.*
- Ingram, R. L. (1954) *Terminology for the thickness of stratification and parting units in Sedimentary rocks*, Geol. Soc. Am. Bull. Kyaw Win and ThitWai (1971) The Geology of the Arakan Chin Ranges. *Burma Research Cong. Rangoon*.
- Miall, A.D. (1984) *Principles of Sedimentary Basin Analysis*: New York, Springer, Verlag.
- Moore, R. C. (1949) *Sedimentary Facies in Geologist History*: Geological Society of America.
- Nichols, G. J. (2009) *Sedimentology and Stratigraphy*, 2nd edition, John Wiley & Sons, New York.
- Potter, P.E. (1959) Facies Model, Conference, *Science Geology*, vol. 71, pp. 41-471.
- Reading, H.G. (1996) *Sedimentary Environments and Facies*. 3rd edition. Oxford Blackwell Scientific Publications.
- Reineck, H.E. (1963 a) Sedimentgefüge im bereich der sudlichen Nordsee. *Abh. Senckenbergische naturforsch. Ges.*
- Reineck, H.E., Singh, I.B. (1967) Primary sedimentary structures in the recent sediments of the jade, North Sea. *Marine Geology*
- Reineck, H.E and Singh, I.B. (1980) *Depositional Sedimentary Environments* (2nd edition). Springer-Verlag. New York.
- Stoke, R.B. (2012) A Review on the Geology of Myanmar (Burma). *Journal of Southeast Asian Earth Sciences*.
- Stamp, L.D. (1922) Outline of the Tertiary Geology of Burma. *Geology Magazine*.
- Than Htut and SweMyint (2008) Biostratigraphic Correlation of the Well Sections in the Central Myanmar Basin. *Journal of Myanmar Geoscience Society*. vol.1, no.1.
- Theobald, W. (1873) The Geology of Pegu. *Memoirs of Geological Survey of India*, vol. 10, no 3.
- Tucker, M. E. (1982) A Facies Description of Sedimentary Rocks I. *Journal of Myanmar Geoscience Society*. V.1, no.1, pp 1-20.
- Thet Htar Su Wai (2015) Geology of the Kwin Gyi Area, Mindon Township, Magway Region. *Unpublised M.Sc. Thesis*, Department of Geology, Magway University.
- Walker, R.G. and James, N.P. (1992) *Facies Models: Response to Sea Level Change*. Geological association of Canada. Geological Association of Canada, St John's, Newfoundland.
- Walker, R.G. (1992) *Facies Models: Response to Sea Level Change* (Eds Walker, R.G. & James, N.P.). Geological Association of Canada, St Johns.

PETROGENESIS OF METASEDIMENTARY ROCKS IN BILIN AND ITS ENVIEONS, BILIN TOWNSHIP, MON STATE

Mya Moe Khaing¹, Khin Mg Hla², Hlaing Myo Nwe³,
Min Han Nyein⁴, Tint Tint Tun⁵

Abstract

According to field and petrological characters, the metasedimentary rocks of the study area consist of slate, phyllite intercalated with quartz mica schist and quartzite. The mineral assemblages of the Bilin area had been subjected to two types of metamorphism; regional metamorphism reinforced by local contact metamorphism. Regional metamorphism of pelitic rocks gave rise to the formation of slate and phyllite intercalated quartz mica schist. Generally, the grade of metamorphism increases gradually towards the west. The regional metamorphism was superimposed by contact metamorphism by the emplacement of igneous intrusion especially biotite granite and diorite intrusion. Furthermore, the presences of spotted phyllites are the indication of the existence of contact metamorphism. The grain size becomes coarser with increasing in grade of metamorphism such as in slate, phyllite and schist. According to the mineral assemblages, the regional metamorphism of the study area had taken place within the "Greenschist facies". Greenschist facies results from low temperature and pressure condition and the formation of some minerals indicate a temperature of approximately 250°C to 400°C and depth of about 2kb to 4kb. The metamorphic rocks of the study area belong to the Mergui Group. The metamorphism of the study area probably took place Post Carboniferous in age.

Keywords: mineral assemblages, contact and regional metamorphism, Greenschist facies

Introduction

The study area is situated about 170 km (106 miles) north-east of Yangon and about 96 km (60 miles) north-west of Mawlamyine in Mon State. It is lying between Latitude 17°12'45'' N to 17°21'45'' N and Longitude 97°09'00'' E to 17°14'45'' E in one inch topographic map No. 94G/3 and G/4. It extends about 8 kilometers from east to west and 14.4 kilometers from north to south. The total areal coverage is about 116.5 kilometers (45 square miles). The location map of the study area is shown in Fig (1).

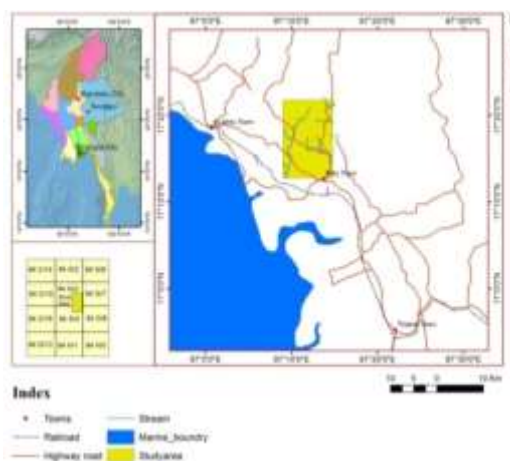


Figure 1 Location map of the study area

¹ Dr, Associate Professor, Department of Geology, Bago University

² Dr, Professor & Head, Department of Geology, Bago University

³ Dr, Associate Professor, Department of Geology, Bago University

⁴ Assistant Lecturer, Department of Geology, Bago University

⁵ Assistant Lecturer, Department of Geology, Bago University

Purpose of study

- To prepare a fairly detailed geological map of the assigned area
- To determine the nature of metamorphism of the study area
- To interpret the probable conditions of metamorphism in Bilin area

Method of Study

The preparation of thin sections was carried out 50 thin sections from metasedimentary rocks were made for identification and mineralogical studies. Detailed petrographic studies of metamorphic rocks were done and then based on the mineral assemblages of the metamorphic rocks, the metamorphic grade and P.T condition of this area is determined.

Regional Geologic Setting

The investigated area is situated in the Eastern Highland (Shan Tanintharyi Block), one of the tectonic provinces of Myanmar by Maung Thein (1976). It is located in Bilin Plain, which lies in the northern continuation of Thaninthayi granite belt, which is actually a part of western tin bearing batholiths known as western tin belt of South East Asia Tin Province (Mitchell, 1977 and Nyan Thin, 1984). Structurally, the study area is bounded by NNW-SSE trending two major fault systems. They are Three Pagoda fault and Papun fault. The main stream of the Bilin River flows north to south, especially at the eastern boundary of the study area. The Pleistocene alluvium covered the south-west and south-east of the area as lateritic terrain. The Regional Geological map of the study area is shown in Fig (2).

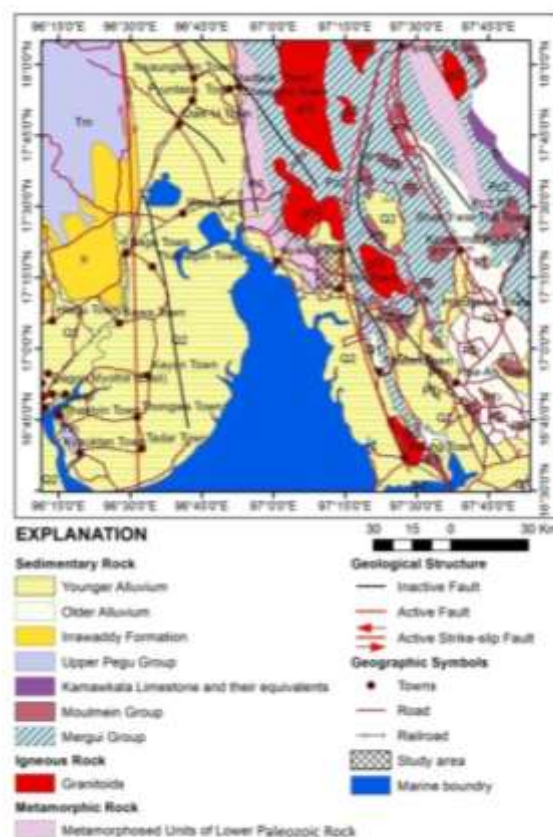


Figure 2 Regional Geological map of the study area (Myanmar Geosciences Society, 2014)

Rock Sequence of the study area

The study area is chiefly covered by igneous and metasedimentary rocks in Fig (3). Igneous rocks are well exposed in the northern, north-western and south-eastern parts and then metasedimentary rocks are cropped out in the central and western parts of the study area. In the study area, the major igneous rocks include biotite granite, biotite-muscovite granite, diorite, meladiorite, microdiorite, hornblendite, biotite microgranite, leucogranite and pyroxenite. Metasedimentary rocks consist of slate, phyllite intercalated with schist and quartzite.

Younger Alluvium	}	Holocene
Older Alluvium (laterite and lateritic soil)		
Igneous rocks		
Pegmatite, Dolerite, Lamprophyre (spessartite) Dykes		
Aplite, Quartzofeldspathic and Quartz Veins		
Leucogranite		
Biotite microgranite		
Biotite granite, Biotite-muscovite granite	}	Eocene
Diorite, Meladiorite, Hornblendite		
Pyroxenite		
Metasedimentary rocks		
Slate, Phyllite intercalated with Schist	}	Silurian-Carboniferous (Mergui Group)
Quartzite		

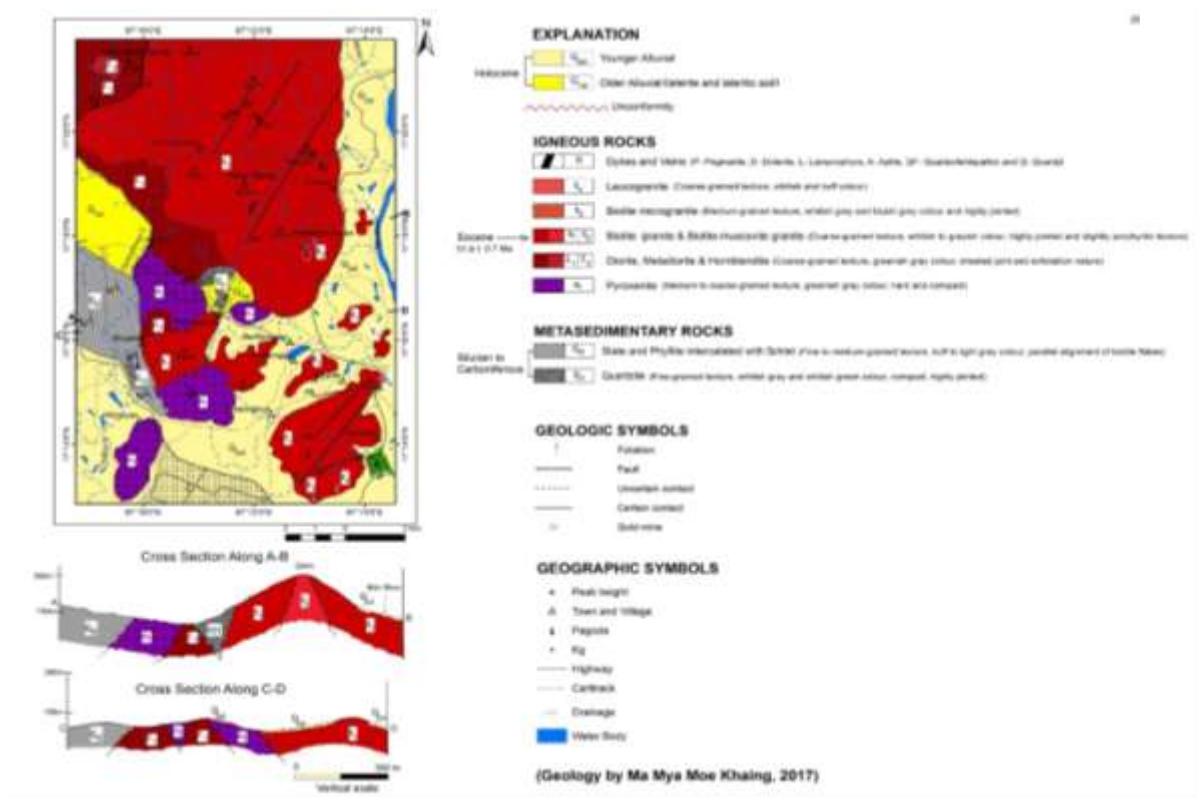


Figure 3 Geological Map of Bilin area and its environs

Results and Findings

Petrogenesis of Metasedimentary rocks

Metasedimentary rocks are divided into the following units, according to field and petrological characters. They are 1. Slate and phyllite intercalated with quartz mica schist
2. Quartzite

Slate is observed along the bullock track at Alugale village. It has very fine-grained texture. It is mainly composed of biotite, quartz, chlorite and muscovite, in Fig (3, A). Phyllite is well distributed at Alugale, Alugyi, Winpyan villages and Alontaung Pagoda. This unit consists of phyllite and quartz mica schist. Quartz vein are intruding into this units. Good exposures are observed along the bullock track of Alugale village. It has fine-grained, exhibits phyllitic texture. It is mainly composed of muscovite, quartz, chlorite, biotite, graphite and iron oxides, in Fig (3, A). Biotite and muscovite occurs as fibrous aggregates, in Fig (3, B). Quartz mica schist shows slightly foliated nature. The main constituent minerals in this rock are mica, quartz and feldspar, in Fig (3, C). Exposures can be observed along the bullock track at the Alugale village, and it is intercalated with phyllite. The common mica is biotite and it is yellowish brown in colour, mica shows alignment on weathered surface. It is generally weathered to the dark yellowish brown colour due to predominance of biotite and fresh colour is gray or yellowish gray. It has fine to medium-grained, schistose texture. Schistosity is shown by lepidoblastic mineral grains of mica. It is mainly composed of quartz, orthoclase, plagioclase, biotite and muscovite, in Fig (3, D). Crystallization of platy minerals under a directed stress results in a preferred orientation of the plates normal to the direction of maximum stress. The resulting foliation is one of the most prominent features of regional metamorphosed rocks. Quartzites are well exposed at the northern part of Paingdawe village and at the hillside of Alontaung Pagoda (117 m peak). It has fine-grained, sugary texture and compact. It is mainly composed of quartz, feldspar, mica and epidote, in Fig (3, E and F).

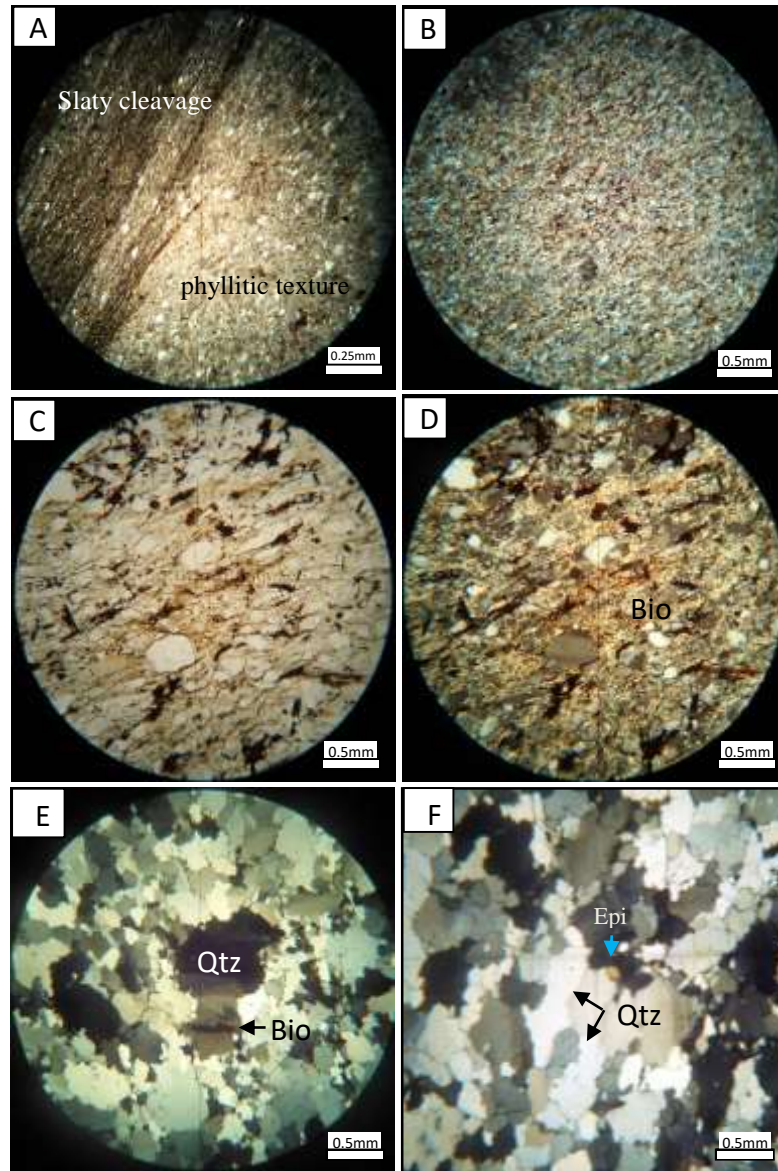


Figure 3 (A) Slaty cleavage and phyllitic texture (under PPL and between X.N, 10X)
 (B) Parallel orientation of fibrous aggregates mica in phyllite (between X.N, 4X)
 (C, D) Development of foliation (schistosity) by alignment of mica in quartz mica schist (under PPL and between X.N, 4X)
 (E) Undulose or wavy extinction of quartz and granoblastic texture in quartzite (between X.N, 4X)
 (F) Epidote crystal with elongated quartz in quartzite (between X.N, 4X)

Types of Metamorphism

The mineral assemblages of the Bilin area had been subjected to two types of metamorphism; regional metamorphism reinforced by local contact metamorphism. Regional metamorphism of pelitic rocks gave rise to the formation of slate and phyllite intercalated quartz mica schist. Generally, the grade of metamorphism increases gradually towards the west. The regional metamorphism was superimposed by contact metamorphism by the emplacement of igneous intrusion especially biotite granite and diorite intrusion. Furthermore, the presences of

spotted phyllites are the indication of the existence of contact metamorphism. Pelitic rocks such as clay, shale and mudstone were transformed into slate, phyllite and schist by the effect of regional metamorphism. They are characterized by strong schistosity which is defined by preferred orientation of mica flakes. The grain size becomes coarser with increasing in grade of metamorphism such as in slate, phyllite and schist. Quartzite in the study area can be regarded as being derived from quartz rich sandstone.

Mineral assemblages

The nomenclature, defining mineral assemblages and metamorphic facies classification made in the study area are based on Turner and Verhoogen (1960), Barth (1962), Hyndman (1972) and Winter (2013). On the basis of various mineral assemblages, low grade metamorphic mineral of chlorite is obvious that this rock had greenschist facies. Greenschist facies is regarded in the western and the central parts of the study area. Slate and phyllite intercalated quartz mica schist are cropped out at Alugale village. Epidote quartzite is exposed at the northern part of Paingdawe village.

The mineral assemblages recognized in slate unit are;

Biotite + quartz + chlorite + muscovite

The mineral assemblages recognized in phyllite unit are;

Biotite + quartz + chlorite + muscovite

Muscovite + quartz + chlorite + sericite

Biotite + quartz + kaoline

The mineral assemblages recognized in spotted phyllite unit are;

Biotite + quartz + muscovite + chlorite

The mineral assemblages recognized in schist unit are;

Biotite + quartz + orthoclase ± plagioclase

Biotite + muscovite + quartz + orthoclase + plagioclase

Biotite + muscovite + quartz + chlorite + orthoclase

The mineral assemblages recognized in quartzite unit are;

Quartz + epidote + plagioclase

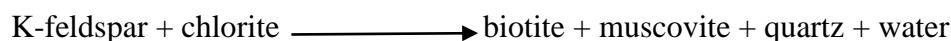
Quartz + orthoclase + muscovite + sericite

Quartz + orthoclase + microcline + muscovite

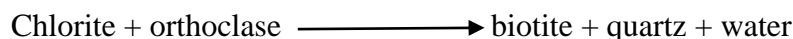
The above mentioned mineral assemblages were plotted on AKF diagram, in Fig (4). The mineral assemblages are used to define the metamorphic facies.

Regional metamorphism

According to the mineral assemblages, the regional metamorphism of the study area had taken place within the “**Greenschist facies**” (Turner, 1968) or low grade (Winkler, 1979). Biotite in phyllite in study area can be formed according to this reaction (Winkler, 1973).



Biotite is common in schist. With increasing metamorphism biotite become stable mineral. Biotite is formed from chlorite (Barth, 1962)



Contact metamorphism

Spotted phyllites are observed in the vicinity of Alugale village and are indicative of the resulting contact metamorphic effects. Spotted phyllites include biotite + quartz + muscovite+ chlorite. The spotted phyllites are found at the contact of some igneous rocks and adjacent metasedimentary rocks, in Fig (5).

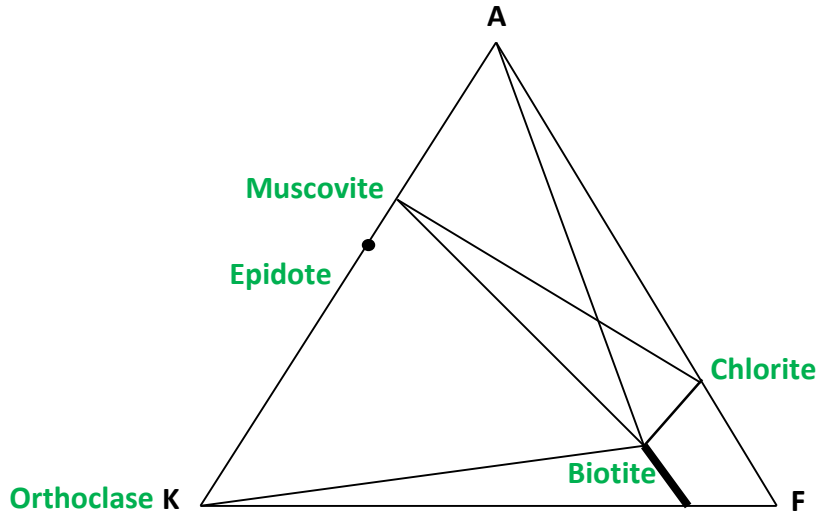


Figure 4 AKF diagram showing the mineral assemblages of Greenschist facies (after Turner and Verhoogen, 1960)

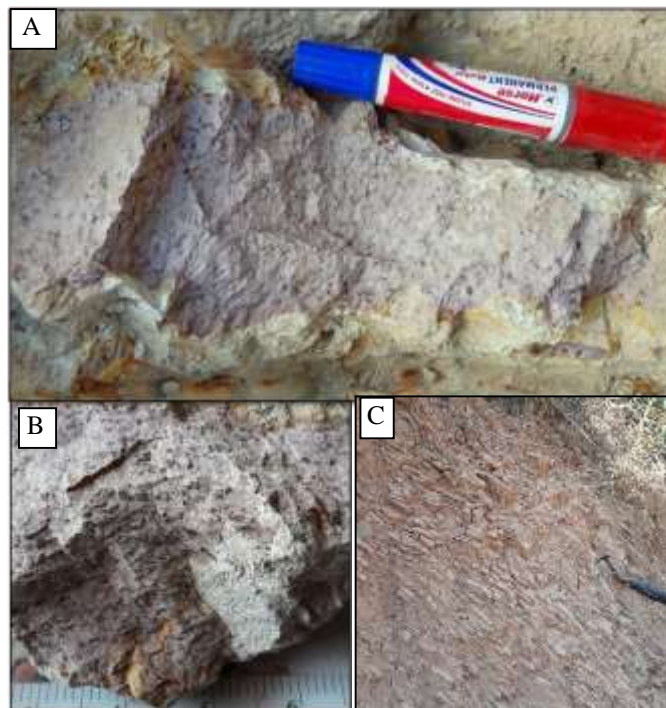


Figure 5 (A, B) Spotted phyllite exhibits spotted nature on fresh surface at Alugale village, facing 120° (Loc: N 17° 15' 36" E 97° 09' 35")
 (C) Spotted phyllite exposed at Alugale village, facing 150° (Loc: N 17° 15' 36" E 97° 09' 35")

Estimation of P-T Conditions

The estimation of P-T conditions for metamorphic mineral assemblages in the study area can be explained as follow:

Greenschist facies results from low temperature and pressure condition and the formation of some minerals indicate a temperature of approximately 250°C to 400°C and depth of about 2kb to 4kb (Winkler, 1979), in Fig (6).

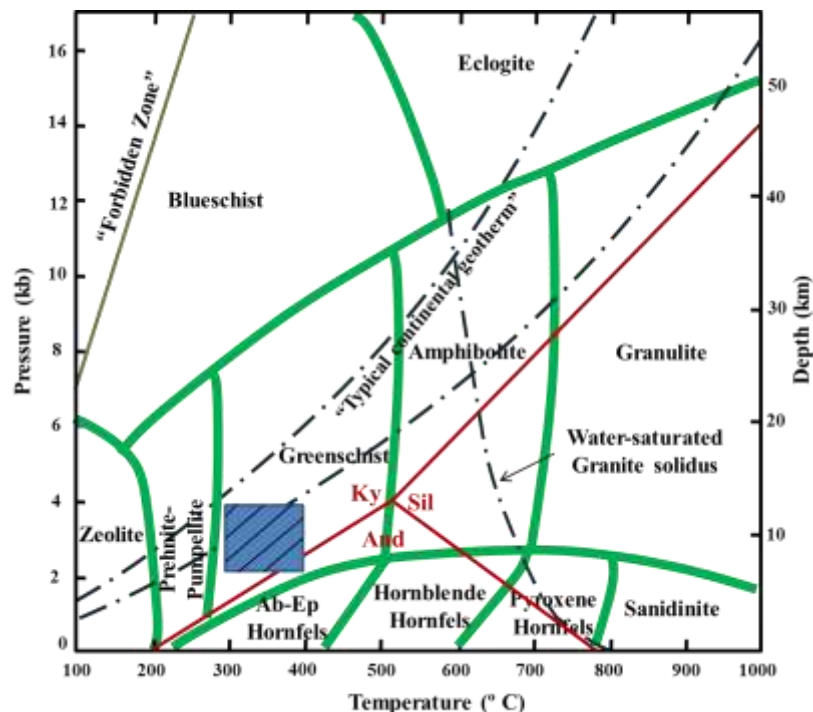


Figure 6 Temperature-pressure diagram showing the probable conditions of metamorphism (after Winter, 2013)

Age of metamorphism and metamorphic rocks

The metamorphic rocks of the study area belong to the Mergui Group. Its lower part has not been separated mapped yet. The lower part may be older in age, possibly Silurian to Carboniferous. Therefore, the metamorphism of the study area probably took place “Post Carboniferous” in age.

Conclusion and Discussion

Metasedimentary rocks consist of slate, phyllite intercalated with schist and quartzite. The mineral assemblages of the Bilin area had been subjected to two types of metamorphism; regional metamorphism reinforced by local contact metamorphism. Generally, the grade of metamorphism increases gradually towards the west. The regional metamorphism was superimposed by contact metamorphism by the emplacement of igneous intrusion especially biotite granite and diorite intrusion. Pelitic rocks such as clay, shale and mudstone were transformed into slate, phyllite and schist by the effect of regional metamorphism. They are characterized by strong foliation which is defined by preferred orientation of mica flakes. Quartzite in the study area can be regarded as being derived from quartz rich sandstone. Spotted phyllites are observed in the vicinity of Alugale village and are indicative of the resulting contact metamorphic effects. The spotted phyllites are found at the contact of some igneous rocks and adjacent metasedimentary rocks. On the basis of various

mineral assemblages, the regional metamorphism of the study area had taken place within the “Greenschist facies”. Greenschist facies results from low temperature and pressure condition and the formation of some minerals indicate a temperature of approximately 250°C to 400°C and depth of about 2kb to 4kb. The metamorphic rocks of the study area belong to the Mergui Group. The metamorphism of the study area probably took place Post Carboniferous in age.

Acknowledgements

I wish to express my gratitude to Professor U Hla Kyi, Part-Time Professor, Applied Geology Department, University of Yangon and Professor U Thein Win, Pro-Rector (Retired), West Yangon University for the continuous support of my study, patience, motivation, and immense knowledge. Their guidance helped me in all the time of research writing.

References

- Barth, T.F.W., (1962). *Theoretical Petrology*. (2nd ed) New York, John Wiley & Sons, Inc
- Hyndman. D.W., (1985). *Petrology of Igneous and Metamorphic rocks*, New York, Mc Graw-Hill. 2nd Edition, p.786.
- Hyndman.D.W., (1972). *Petrology of Igneous and Metamorphic rocks*, New York, And London McGraw-Hill.2nd Edition, p.526.
- MaungThein, (2014). *Geological map of Myanmar*, p.13
- Mitchell, A.H.G, (1977), *Tectonic setting for emplacement Southeast Asian Tin granite*, c/o UNDP, P.O.Box 650, Ragoon, Burma, Geol. Soc. Malaysia Bulletin 9, Nov. 1977;pp.123-140.
- Nyan Thin, U, (1984). *Some Aspect of Granitic Rocks of Tanasserim Division*, Unpublished paper.
- Turner.F.J.and Verhoogen, J., (1960). *Igneous and metamorphic rocks* 2nd ed., Mcgraw-hill book Co.inc., Newyork, p.694
- Turner.F.J., (1968). *Metamorphic Petrology, Mineralogical and field aspects*, MC GRAW- HILL BOOK COMPANY, p.403.
- Winkler,H.G.F and Sen, S.K., (1973). *Normenclature of granulites and other high grade metamorphic rocks*.Jb.Mineral.Mh.p.393-402.
- Winkler,H.G.F, (1979). *Petrogenesis of Metamorphic Rocks*, Springer-Verlag New York INC. p.348
- Winter.J.D., (2013). *An introduction to Igneous and Metamorphic Petrology*, Prentice Hall, New Jersey, p.697

SERPENTINIZATION IN THE MWETAUNG OPHIOLITE, TIDDIM TOWNSHIP, CHIN STATE

Thidar Win¹, Shwe Soe², Teza Kyaw³

Abstract

The study area is bounded by the latitude 23° 22' to 23° 30' N and the longitude 94° 00' to 94° 03' E, in one inch topographic map 84-I/3. It is located about 17 miles (27 km) NW of Kalemmyo, Sagaing Region and Tiddim Township of Northern Chin Hills. In this area, Mwetaung Hill lies prominently on the eastern flank of the northern Chin Hills. It conspicuously high hill protruding from the alluvial plain is wholly built up of ultramafic rocks tectonically bounded by the highly folded Pane Chaung Group to the west. The most ultramafic rocks of the study area are completely serpentinitized. Serpentinization is a widespread process in ophiolitic mantle. In study area serpentinites or serpentinitized ultramafic rocks are classified into three types of serpentinites: massive serpentinite, sheared serpentinite and cross-fibre serpentinite, based on their physical appearances and microscopic study. into type 1, type 5 and type 8. Degree of serpentinitization for the study area is early to advanced stage. Serpentine textures such as mesh texture, ribbon texture and bladed mat are found. Magnetite is present in minor amounts in all types of the rocks. Their nature and textures are important for the determination of the degree of serpentinitization. Serpentinites derived from ophiolite peridotites is probably equilibrated at low temperature below about 500°C. The time of serpentinitization in the study area is Early Cretaceous because it is related to the time of emplacement of the ultramafic body.

Keywords: Serpentinization, Ultramafic rocks, Mwetaung, Ophiolite

Introduction

Location, Accessibility and Physiography

The study area is bounded by the latitude 23° 22' to 23° 30' N and the longitude 94° 00' to 94° 03' E, in one inch topographic map 84-I/3. It is located about 17 miles (27 km) NW of Kalemmyo. The area lies prominently on the eastern flank of the northern Chin Hills, Sagaing Region and Tiddim Township of Northern Chin Hills. It is good accessible from Kalemmyo by car and motor cycle throughout the year. The location map of the area is shown in (Fig.1).

Regional Geologic Setting

Myanmar can be subdivided into six N-S trending major tectonic domains. From west to east are: (1) Rakhine Coastal Strip as an ensimatic foredeep, (2) Indoburman Ranges as an outer arc or forearc, (3) Western Innerburman Tertiary Basin as an interarc basin, (4) Central Volcanic Belt (Central Volcanic Line) as an inner magmatic volcanic arc, (5) Eastern Innerburman Tertiary Basin as backarc basin and (6) Shan-Taninthayi massif as ensialic Sinoburman Ranges (Bender, 1983, Khin Zaw, 1990). The Indoburman Ranges (Western Ranges) of Myanmar, consisting of the Naga Hills, Chin Hills and Rakhine Yoma, are underlain by thick, mildly deformed, slightly folded, and weakly metamorphosed (Fig. 2).

¹ Dr. Associate Professor, Department of Geology, Kalay University

² Lecturer, Department of Geology, Yadanabon University

³ Dr. Associate Professor, Department of Geology, Monywa University

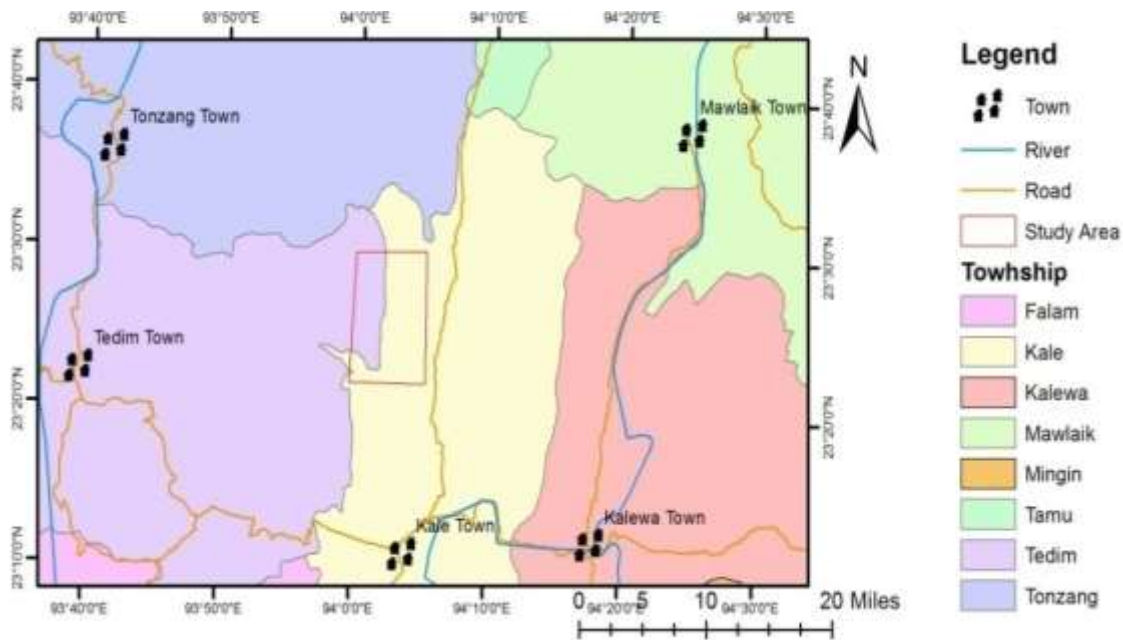


Figure 1 Location map of the study area

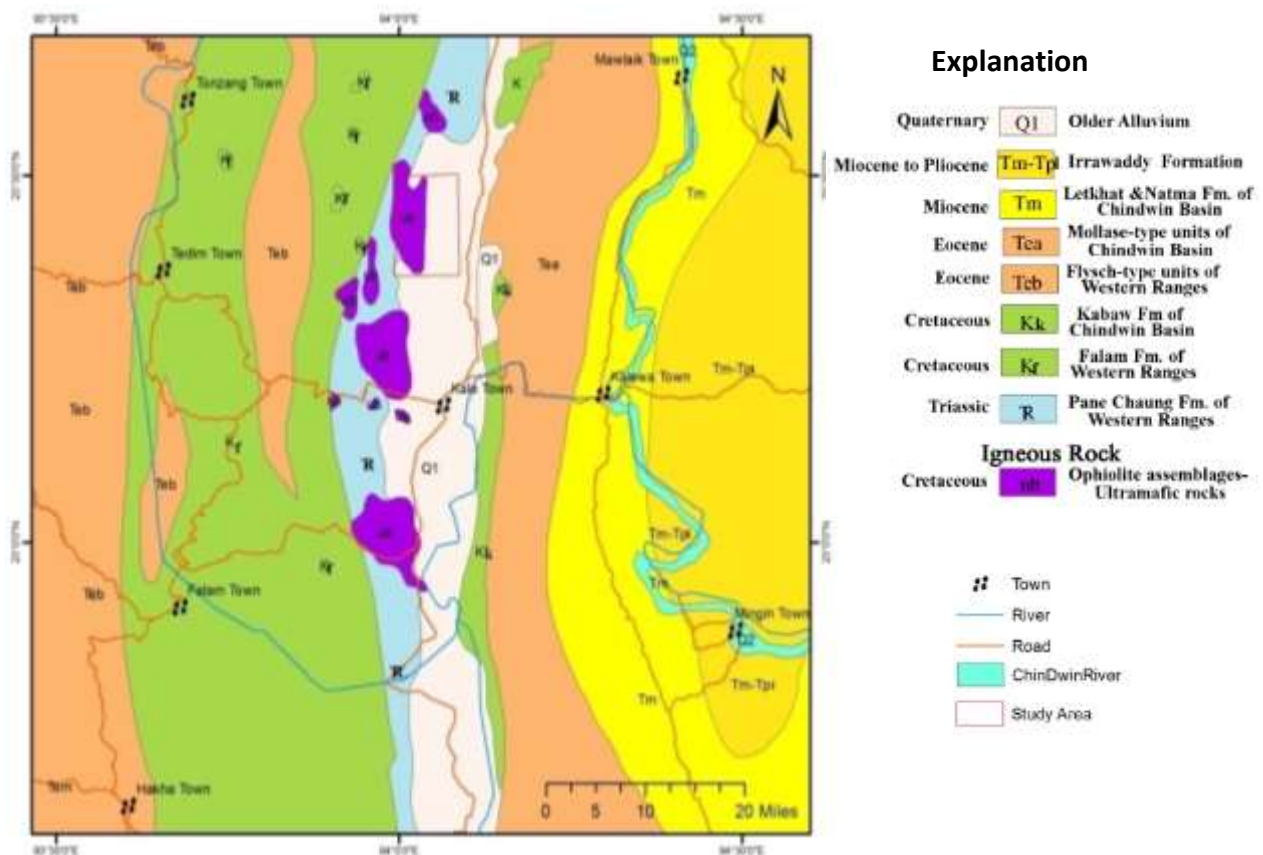


Figure 2 Regional Geological Map showing the study area (After Myanmar Geosciences Society: 2014)

The study area occupies the boundary between western margin of the Innerburman Tertiary Basin and at the foot of eastern Indoburman Ranges. According to Hutchison (1975), the study area lies in the main ophiolite belt of Naga Line. The area falls within the Western Ophiolite Belt of Myanmar (Hla Htay, 1985; Mitchell, 1993). It is suggested to be dismembered and incomplete

ophiolite belt, consisting of ultramafic rocks, pillow lava, basic dykes, spilite, radiolarian chert, small amounts of limestones Mwetaung hill of the study area lies prominently on the eastern flank of the northern Chin Hills.

Purpose and Method of study

This research is focus to describe detailed types of serpentinization, classified serpentinization processes, determination of the degree of serpentinization, described texture, and temperature of serpentinization of the study area. During the field period, the topographic map 84-I/3 is enlarged to a scale of four inches to one mile and used as base map to plot all the measured geological data. In the laboratory, the representative specimens collected from the field were prepared to more than (30) thin sections for mineralogical characterization of the various rock types were recorded by using field data and microscopic studies.

Serpentinization

1. Types of Serpentinites

The ultramafic rocks such as harzburgite, dunite and lherzolite in the study area were partially to completely serpentinized. Three types of serpentinites could be differentiated in the area according to their physical appearance and microscopic features. In the field, three main categories of serpentinites can be distinguished by their physical appearance, Thidar Win(2014). They are massive serpentinite, sheared serpentinite and cross-fibre serpentinite(Fig.3).

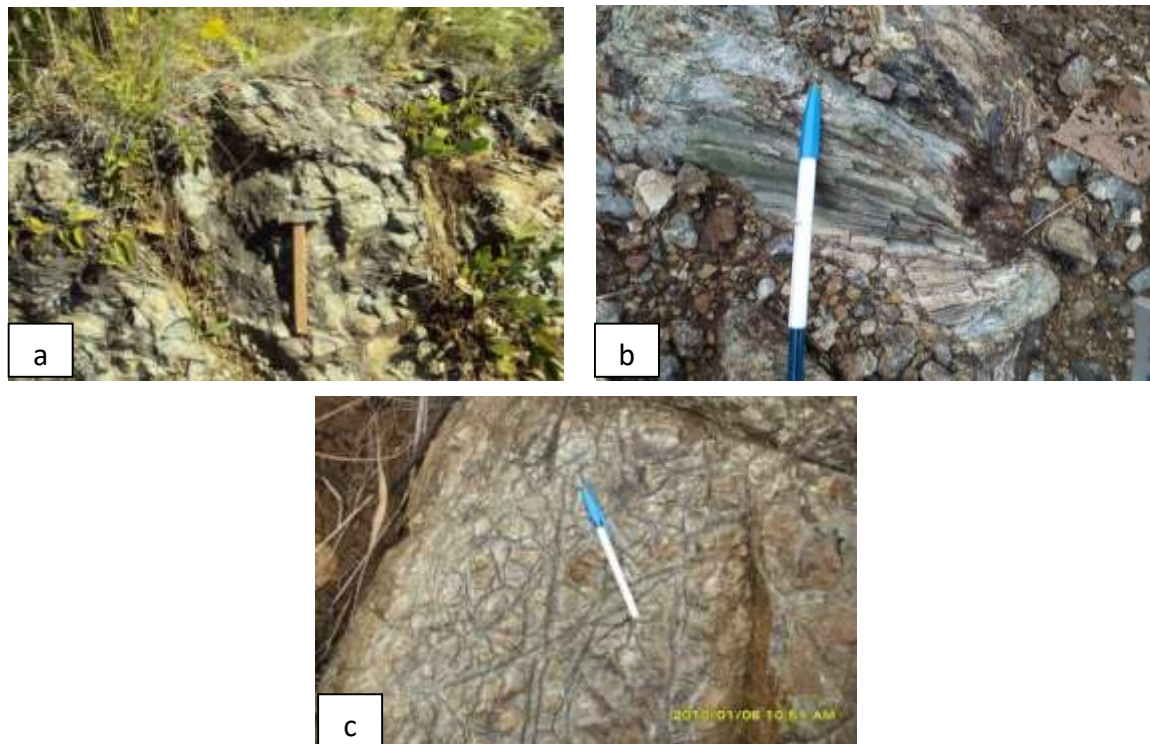


Figure 3 Exposures of various serpentinites (a) massive serpentinite, (b) sheared serpentinite and (c) cross-fibre serpentinite

Table 1 Eight types of serpentinization process (Wicks and Whittaker, 1977)

Type	Condition	Texture	Mineral	Regime	Remarks
Type 1.*	-Falling temperature (or constant) -Absence of substantial shearing -Nucleation of antigorite	Pseudomorph texture	Antigorite	A	Fracture-filling veins produced with this type will be composed of antigorite
Type 2.	-Falling temperature (or constant) -Presence of substantial shearing -Nucleation of antigorite		Antigorite	A	
Type 3.	-Falling temperature (or constant) -Absence of substantial shearing -No nucleation of antigorite	Pseudomorph texture	Lizardite Lizardite \pm brucite	B&C	Chrysotile does not usually occur in abundance in the pseudomorph, but may occur in veins along joint planes with or without lizardite and brucite
Type 4.	-Falling temperature -Presence of substantial shearing -No nucleation of antigorite	Foliated non-pseudomorph texture	Chrysotile \pm	B&C	With or without lizardite, and chrysotile \pm lizardite \pm brucite veins
Type 5.*	-Rising temperature -Absence of substantial shearing -No nucleation of antigorite	Recrystallization of pseudomorph texture, Nonpseudo mor-phic texture	Lizardite \pm brucite Chrysotile \pm Lizardite \pm brucite	B&C	Associated veins with similar in mineralogy.
Type 6.	-Rising temperature -Presence of substantial shearing -No nucleation of antigorite	Foliated non-pseudomorph texture	Chrysotile \pm Lizardite \pm brucite	B&C	Less frequently multi layered lizardite \pm brucite.
Type 7.	-Rising temperature -Absence of substantial shearing -Nucleation of antigorite	Recrystallization of type 3 texture, non-pseudo-morphic, crude pseudo-morphic, texture	Antigorite+_brucite	B, C & A	
Type 8.*	-Rising temperature -Presence of substantial shearing -Nucleation of antigorite	Foliated non-pseudomorph texture	Antigorite+_brucite	B, C & A	

* Types of serpentinization found in the study area

Following the work of Wicks and Whittaker, 1977, a possible model of serpentinization was described in Table (1). There are eight types of serpentinization process based on the conditions of temperatures, presence of substantial shear, and nucleation of antigorite. In accordance with the classification by Wicks and Whittaker (1977), type-1, type-5 and type-8 serpentinization process can be observed in the study area.

1.1 Massive serpentinite

This type is the most common serpentinite in the area. In this type, the chief mineral is antigorite, and lizardite and brucite occur as accessory minerals. Pseudomorphic texture (mesh texture) is predominant over non-pseudomorphic texture (interpenetrating texture). Locally, chrysotile is seen as veins by fracture filling. So, it is possibly matched with the type 1 of Wicks and Whittaker.

1.2 Sheared Serpentinite

This type is characterized by higher tectonic strain. So, shearing features are found in this type. The chief mineral is antigorite with lizardite, chrysotile and brucite in minor amounts. The type of serpentinization is possibly type 8 of Wicks and Whittaker (1977).

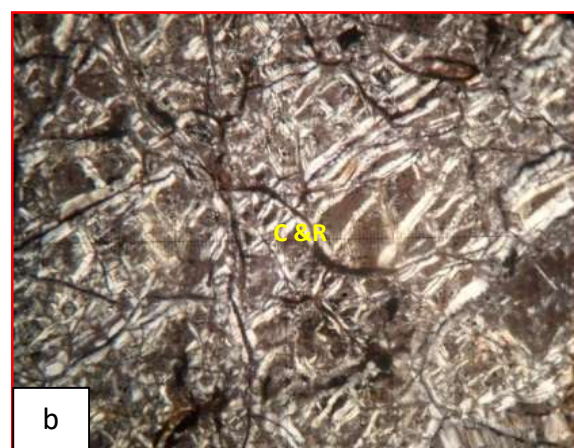
1.3 Cross-fibre Serpentinite

In this type, chrysotile, lizardite and magnetite in order of abundance are chief minerals. The texture is non-pseudomorphic, and dislocated chrysotile veinlets indicate post-deformation event. This type of serpentinization may be type 5.

2. Textures of serpentinization

Wicks and Whittaker (1977) defined three main serpentinite textures; (a) pseudomorphic, (b) non-pseudomorphic, and (c) intermediate texture. Maltaman (1978) also described serpentinite textures as mesh texture, ribbon texture and bladed mat. In the pseudomorphic texture, the original minerals of olivine and pyroxene crystals are observed as relicts. Non-pseudomorphic texture can be sub-divided into interpenetrating and interlocking texture. Interpenetrating texture is mainly composed of antigorite, and interlocking texture comprises grains of serpentine. In the early stage of serpentinization, the textures of the original peridotites are still preserved. In the last stage of serpentinization, olivine and orthopyroxene grains occur as rare relicts in the rock and veins.

Mesh texture consists of cores and cords in which the cores represent the centre of serpentinized olivines and the cords represent the serpentinized grain boundaries or fractures Fig. (4a,b). Hourglass texture, interpenetrating and interlocking, is also found in some thin sections (Fig.4c).



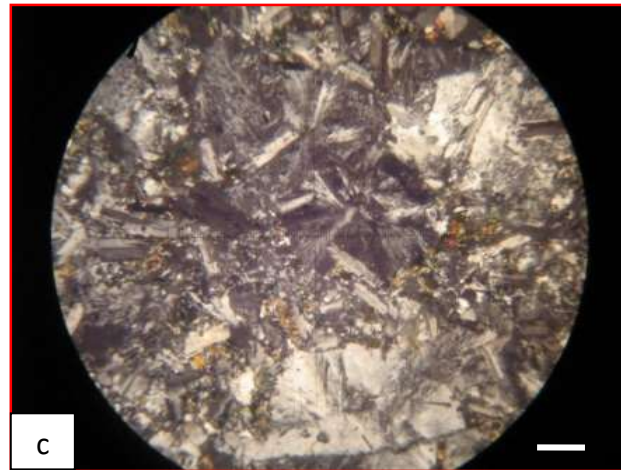
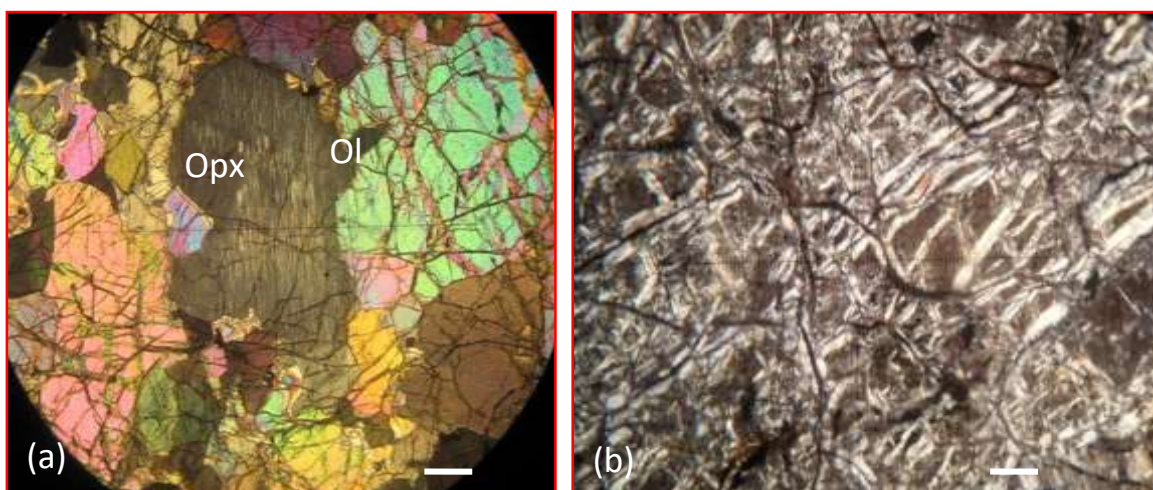


Figure 4 Serpentine textures, core (C) and ring (R) (a) outcrop view and (b) photomicrographic view. (c) Photomicrographs of hourglass texture in serpentinite.

3. Degree of Serpentinization

In massive serpentinite, the advanced stage is predominant, but the early stage is rare. In sheared serpentinite, early to advanced stage texture is common, whereas in cross-fibre serpentinite moderate and advanced stage textures are abundant. In the early stage of serpentinization, the textures of the original peridotites are still preserved. Relicts of olivine and orthopyroxene are visible in them (Fig. 5 a).

Most of the serpentines are cut by late-stage serpentine veins, with a high variety of morphologies and textures that imply different mechanisms and conditions of formation. Several fine thread-like serpentine veins and veinlets occur in criss-cross pattern. As the serpentinization progresses, relicts of olivine and pyroxene begin keeping only the skeletal remains of the minerals. Mesh textures (Fig. 5 b) and bastite textures appear in the rocks in place of pyroxene and olivine (Fig. 5 c). It is noted that magnetite is present in minor amounts in all types of ultramafic rocks. Their nature and textures are important for the determination of the degree of serpentinization. There is often a correlation between the distribution of magnetite and degree of serpentinization and the colour of the serpentinites (Wicks & Whittaker, 1977). During the early stage, magnetite formed as discrete fine-grains throughout the whole unit. When the degree of serpentinization is increased, magnetite is developed in mesh centre of concentrated small disseminated grains, and in the advanced stage, magnetite is present in large amounts and in granular form (Fig.5 d).



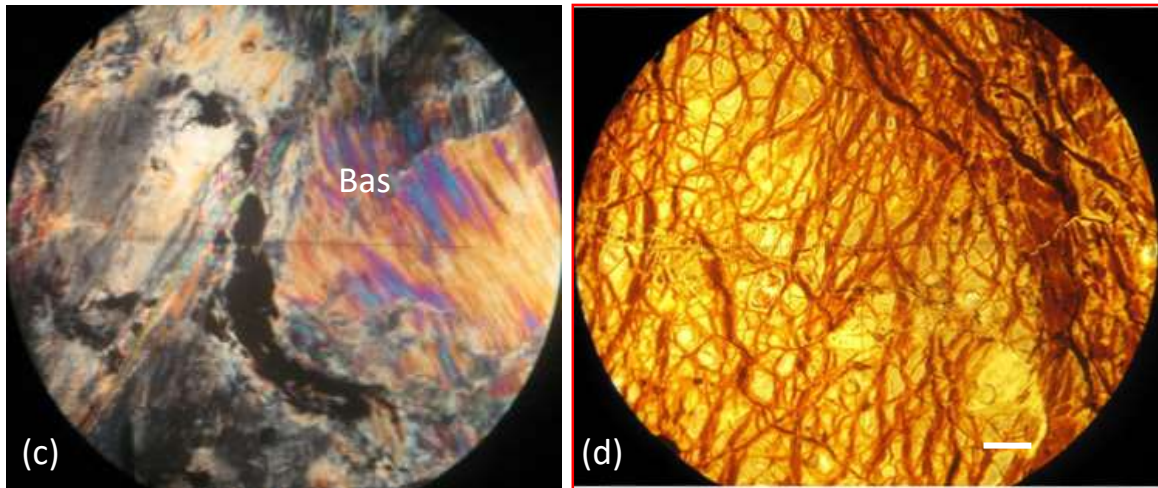


Figure 5 Photomicrographs showing the increasing degree of serpentinization in ultramafic rocks (Opx= orthopyroxene, Ol= olivine, Bas= bastite) (Scale bar is 1 mm).

4. Temperature of serpentinization

Serpentinites derived from ophiolite peridotites are probably formed by the hydration in the lithosphere at temperature below 500°C (Fig.6). Pyroxene deforms plastically at temperature higher >800°C than the upper temperature boundary of serpentinization 550°C. Thus, pyroxene foliations and lineations must have formed while the rock was still peridotite in the mantle and before serpentinization. Recognition of serpent species in ophiolite assemblages, therefore, can be of establishing P-T conditions during serpentinization. Serpentinization may have formed in a condition of low pressure and low temperature.

Serpentinite contains three main minerals; lizardite, chrysotile and antigorite with minor amounts of bastite, and brucite. Lizardite is stable at low temperature (50-300°C), and chrysotile is metastable (Evan, 2004). Antigorite may be stable at higher temperatures than lizardite and chrysotile.

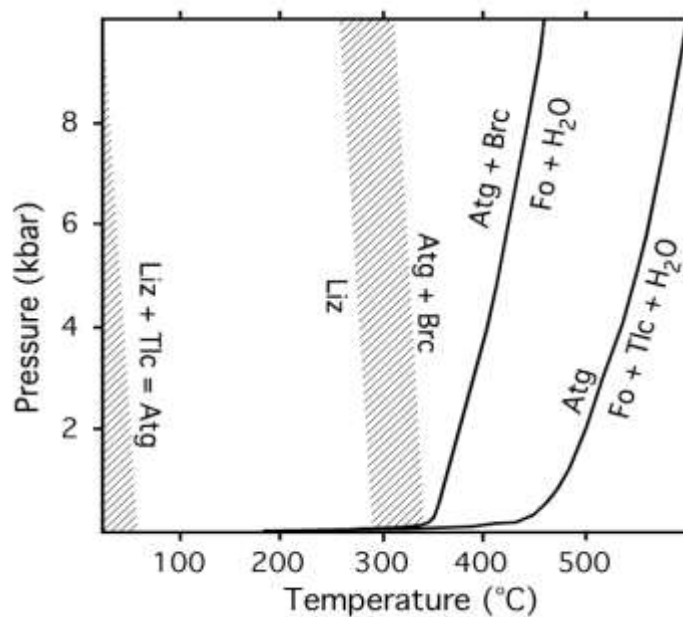


Figure 6 P-T diagram for serpentine minerals (modified from Evans, 2004). Shaded areas show uncertainty in location of reactions. Liz = lizardite, Tlc = talc, Atg = antigorite, Brc = brucite, Fo = forsterite.

5. Time of serpentization

Since no absolute age is obtained as yet, relative age, citing the views of previous observers and the field observations is to be considered. Chhibber (1934) early described the age of serpentine as Late Cretaceous to Early Eocene. This assumption is in agreement with the postulated age of Mitchell (1979)'s. According to the Chuan-Liu et.,al,(2016) they are studied the age of Myanmar Ophiolites including the Kalaymyo Ophiolite suggested that the Kalaymyo area of Mwetaung Ophiolite was formed during Early Cretaceous Therefore, the time of serpentization in the study area was probably during Early Cretaceous because it is related to the time of emplacement of the ultramafic body.

Conclusion

Mwetaung ultramafic body lies as the part of Indoburman Ranges and including in the Western Ophiolite Belt. Serpentine minerals are the weathering product of ultramafic igneous rocks. There are three types of serpentinites; massive, sheared and crossed fiber serpentinite. Three types of serpentine texture are pseudomorphous, non-pseudomorphous and serpentine veins texture. Pseudomorphous texture shows mesh texture and hourglass texture while non-pseudomorphous texture exhibit interpenetrating and interlocking texture. Magnetite is present in minor amounts in all types of the rocks. Their nature and textures are important for the determination of the degree of serpentization. Degree of serpentization for the study area is early to advanced stage. Serpentinites derived from ophiolite peridotites is probably equilibrated at low temperature below about 500°C. The time of serpentization in the study area is Early Cretaceous because it is related to the time of emplacement of the ultramafic body.

Acknowledgement

We wish express our thanks to Rector Dr Thar Htun Maung of Kalay University for providing necessary resources. I am greatly thankful to my supervisor Dr Min Aung, Rector (retired), for his valuable suggestion, great encouragement and interest.

References

- Bashir, E (2012). Study of Serpentinized Ultramafic Rocks of Bela Ophiolite, Balochistan, Pakistan, *Journal of Geography and Geology*, vol.4, p. 79-89.
- Bender, F., 1983. *Geology of Burma*. Borntraeger, Berlin. 293p.
- Chhibber, H. L., (1934) *Geology of Burma*, Macmillan, London, 538p.
- Evans, B.W., (2004). The serpentinite multisystem revisited: Chrysotile is metastable: *International Geology Review*, vol.46, p. 479-506.
- Hla Htay. (1985) Mineralogy and Petrology of the Webula Ultramafic body and Khwekha Metamorphics, Falam Township, Unpub, M Sc. (Thesis), Yangon University, p. 298.
- Hla Htay, (2008). The Geology and Serpentinization of Inkhraingbum-Myitson Area, Myitkyina Township, Kachin State, *Journal of Myanmar Academy of Arts and Science*, vol. VI, No. 5, p. 59-82, Universities Press, Yangon, Myanmar.
- Hutchison, C.S., (1975) Ophiolite in Southeast Asia, *Geological Society of America Bulletin*, vol.86, p. 797-806.
- Khin Zaw., (1990) Geological, petrological and geochemical characteristics of granitoid rocks in Burma: with special reference to the associated W-Sn mineralization and their tectonic setting in *Journal of Southeast Asian Earth Sciences*, vol. 4, No. 4, p. 293-335.
- Liu, C.Z., Chung, S.L., Wu, F.Y., Zhang, C., Xu, Y., Wang, J.G., Chen, Y., and Guo, S., (2016) Tethyan suturing in Southeast Asia: Zircon U-Pb and Hf-O isotopic constraints from Myanmar ophiolites. *Geology*,44: 311-314.

Maltaman, A.J., (1978) Serpentine textures in Anglesey, North Wales, United

Mitchell, A.H.G, (1979) Geology and Exploration Geochemistry of part of the Northern and Southern Chin hills and Arakan Yoma, Western Burma.

Mitchell, A.H.G., (1993) Cretaceous-Cenozoic tectonic events in the western Myanmar (Burma)-Assam Region.
Journal of the Geological Society of London. vol. 150, p. 1090-1102.

Thidar Win, (2014) Geology and Petrology of the Mwetaung-Yazagyo Area, Tiddim Township, Chin State, unpublished Ph.D dissertation, University of Mandalay

Wicks, F.J and Whittaker, E.J.W, (1977). Serpentine textures and serpentinization. *Can. Mineral*, vol.15, p. 459-488.

GEOPHYSICAL APPROACH TO THE DETERMINATION OF LOCAL SITE EFFECT IN DAGON TOWNSHIP, YANGON REGION FOR SEISMIC HAZARD

Aung Myo Zaw¹ & Tun Naing²

Abstract

Determination of local Site effect had carried out at 43 sites in Dagon Township, Yangon, Myanmar. Yangon area is located in moderate to high seismic prone area and high damage can be expected because the soil conditions in the city vary from alluvial soil to soft rock. The potential damage effects can be estimated on the basis of local soil effects. To determine the local soil conditions and its effects, analysis of the ratio of horizontal to vertical (H/V) spectra of microtremor was performed. The microtremor measurements were conducted by the SMAR-6A3P seismograph with LS-8800 data logger and GPS time composition at 200 Hz sampling rate. Finally, sediment thickness, shear wave velocity structures and potential soil amplification were determined. The potential frequency is ranging from 1.25Hz to 2.65Hz and the amplitude is ranging from 0.2 to 3.8. The potential soil thickness is ranging from 52 m to 106 m and average shear wave velocity of upper 30m depth, V_s^{30} , is ranging from 200 m⁻¹ to 540 m⁻¹ in general. Microtremors analysis show that southeastern and northwestern part of the Dagon Township is covered by thick and soft sediments (low frequency and high peak amplitude) while the central part of the Dagon Township is generally covered by thin and soft sediments (high frequency and high peak amplitude). These results can be used for urban seismic hazard assessments and risk mitigations in future.

Keywords: microtremors, spectral ratio, fundamental frequency, sediment thickness, shear wave velocity, site amplification

Introduction

Yangon is the capital city of Myanmar and this city has great density of the population, high concentration of residential buildings and public buildings, and a large number of old buildings in downtown Yangon. It had experienced several earthquakes in the past including Bago Earthquake with 7.3M on May 5 in 1930 because it is near to the Sagaing Fault. In addition to that, most of its townships are located in soft alluvial plain which is mainly composed of gravel, sand, silt and clay where strong ground motion and high amplification of local sediments can be expected. Nakamura (1989) proposed a method inferring site amplification factors to incident seismic shear waves using microtremor H/V ratio at a single site. This method is allowed detailed mapping of local site effects in an urban area without knowing precise subsurface geological and S-wave structure (Tun Naing et.al., 2013). According to this method, it is found that the microtremor H/V ratios coincide with amplification factors of near-surface structures to incident shear waves (Nakamura, 1989). The single station microtremor observation is measured about 20 (or) 30 minutes to determine horizontal to vertical Fourier amplitude spectral ratio from unknown sources. The sources of microtremor can be man-made or natural. Microtremors with frequencies above 1Hz are generally associated with man-made such as road traffic, trains, machinery while those below 1Hz are associated with natural phenomena such as wind, wave action and variations in atmospheric pressure.

Location and Size

Dagon Township is the major part of downtown area of Yangon as shown in Figure (1) and it has the population of 25,082 according to 2014 Myanmar Population and Housing Census.

¹ Dr. Lecturer, Department of Geology, Dagon University

² Dr. Professor & Head, Department of Engineering Geology, Yangon Technological University

The total area of Dagon Township is 4.92 km². This township has many historical buildings and cultural heritage as well.

Seismicity of Yangon

Yangon region can be regarded as a moderate seismic prone. It is tectonically bounded by Sagaing Fault in the east, West Bago Yoma fault in the north, and the Andaman rift zone in the south (Win Swe & Win Naing, 2008). The seismogenic Sagaing Fault is passing through about 40 km away from Yangon and it had experienced several earthquakes in the past. The most significant earthquake occurred around this region is the Bago earthquake of 5th May, 1930 with the magnitude of 7.3 M_w , as shown in Figure (2). This earthquake caused 500 casualties and large destruction in Bago while 50 casualties and some damages in Yangon.

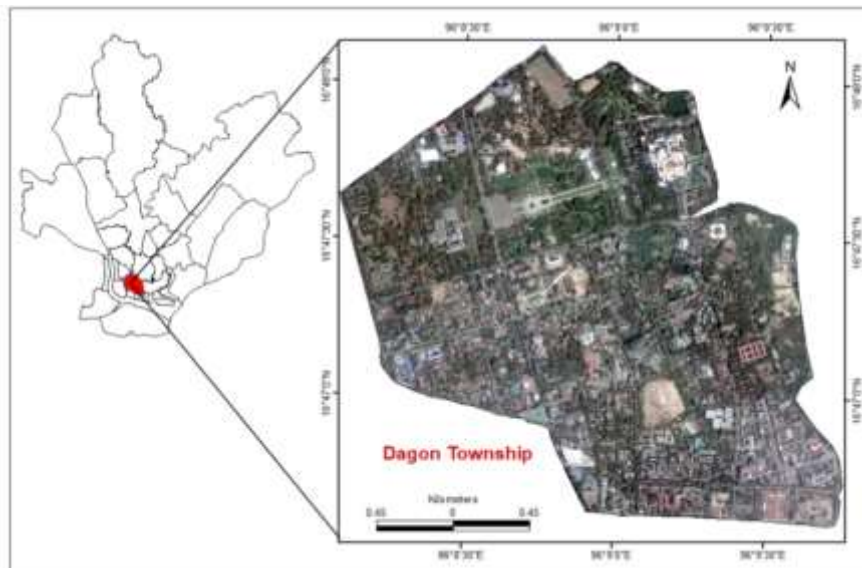


Figure 1 Location map of the study area

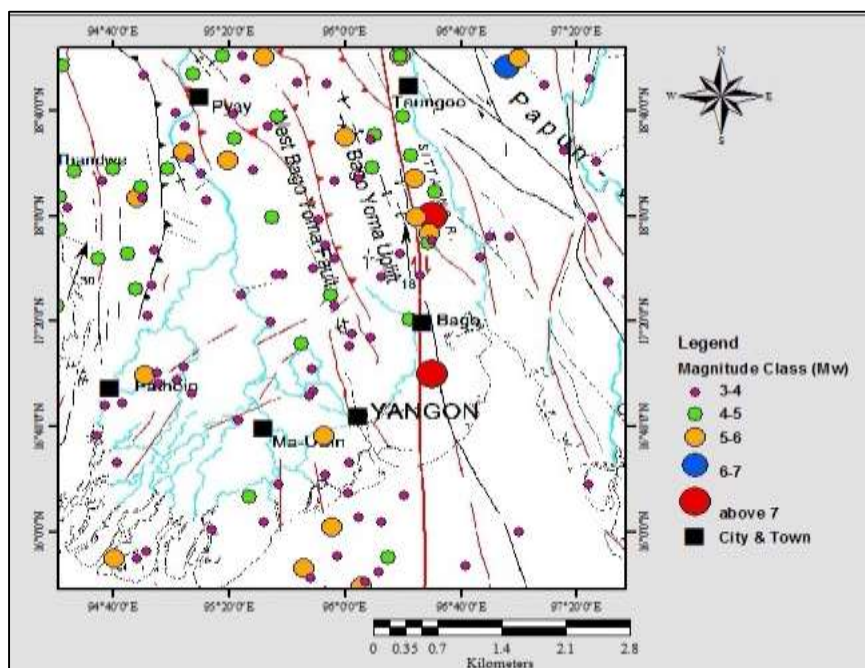


Figure 2 Seismic activities of Yangon area and its environs (ANSS catalog of 1900–2019 complement with MEC data)

Materials and Methods

The methodology mainly includes four portions: desk study, preliminary site investigation, detailed site investigation, and data analysis and processing. The desk study mainly includes literature reviews. The preliminary investigation performs initial site investigation. Detailed subsurface investigation program throughout the Dagon Township, including field measurements and laboratory tests are included in detailed investigation stage. Modeling analyses by using different software will be the main task in data analysis and processing. Figure (3) showing the scheme for the method of study of the whole research.

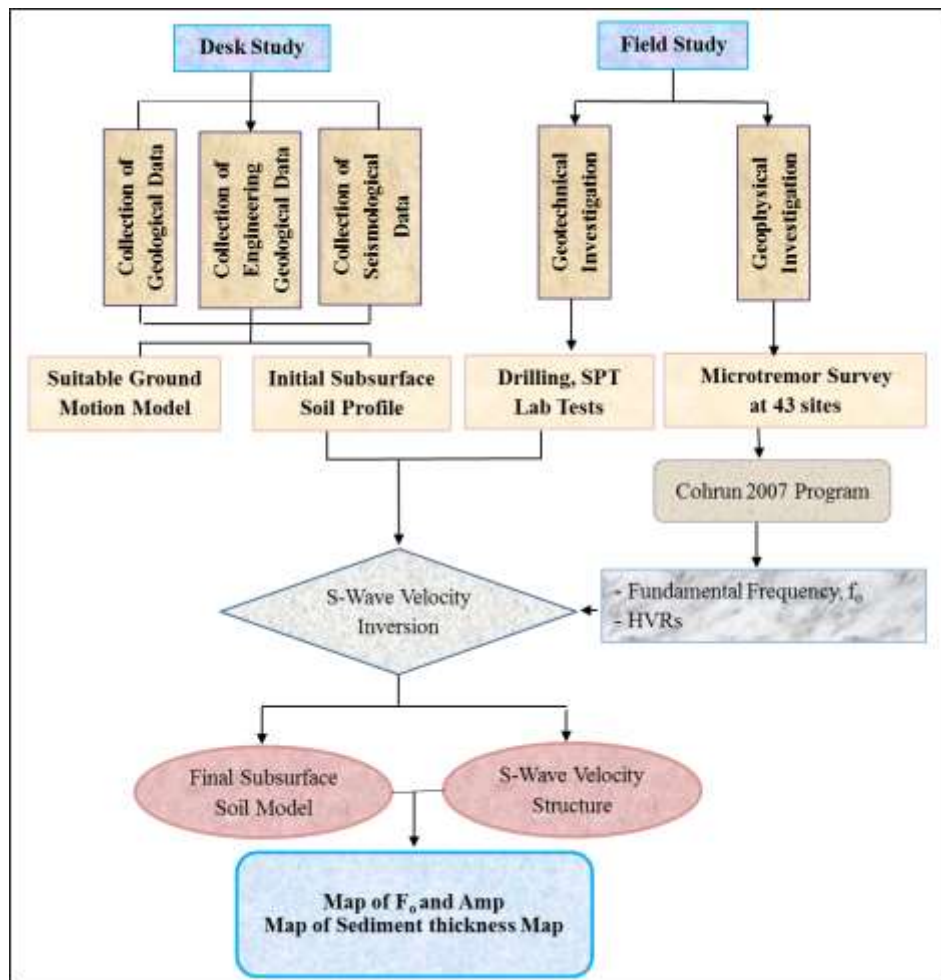


Figure 3 Scheme for the method of study of the whole research

Geophysical Measurement (Microtremor Survey)

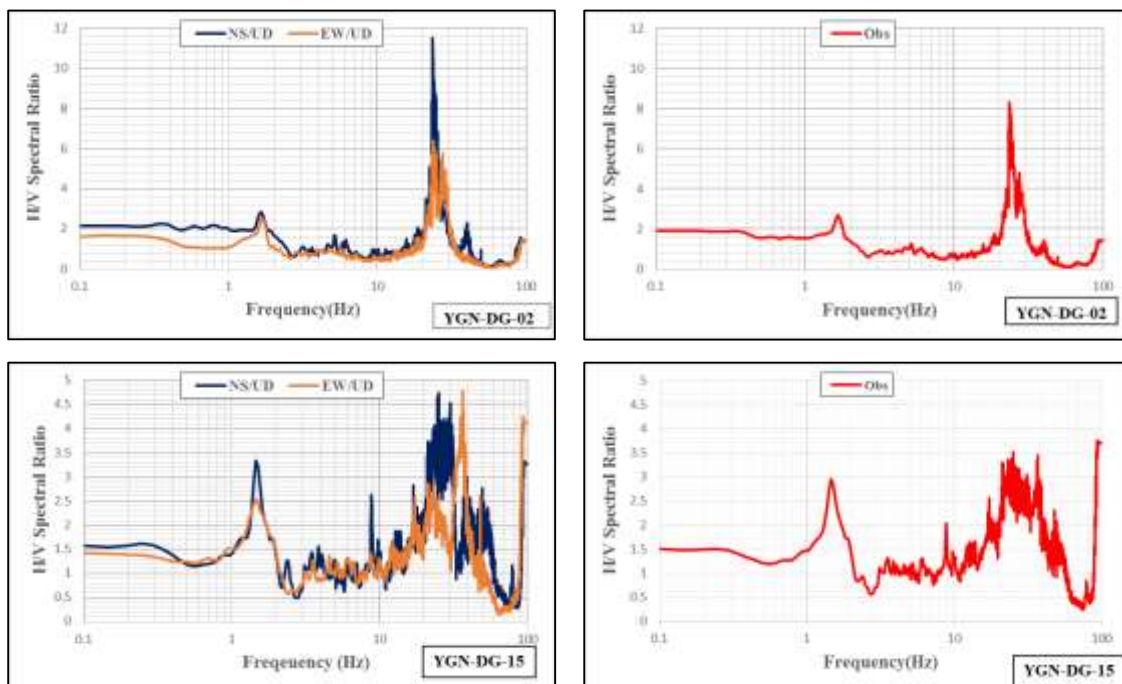
The microtremors, ambient seismic noises, generating low amplitude vibrations by natural disturbances have been used as a tool to estimate seismic response of underlying soil layers (Kanai and Tanaka, 1954). Based on the diffuse field theory (Sesma et.al., 2011), the microtremor H/V spectral ratios correspond to the square root of the ratio of the imaginary part of horizontal displacement for a horizontally applied unit harmonic load and the imaginary part of vertical displacement for a vertically applied unit load. The microtremor single station measurements had been conducted at 43 sites throughout the Dagon Township as shown in Figure (4). These measurements were conducted for 20 minutes at each site at the sampling rate of 200 Hz/s by using SMAR-6A3P seismometer shown in Figure(5).



Figure 4 Geophysical Measurement of the research area, (a).Locations of microtremor measurements in Dagon Township, Yangon, (b) SMAR-6A3P Microtremor Equipment and Microtremor Surveying

Determination of Microtremor (H/V)

The horizontal-to-vertical spectral ratio (HVRs) together with fundamental frequency of each site had been determined. HVRs of NS/UD and EW/UD were determined first and then the final observed microtremor spectrum has been determined by averaging the spectra of NS component and EW component (by averaging NS/UD, EW/UD) Figure (5). The observed microtremor HVRs show the two peaks; one at low frequency and one at high frequency. The peak at low frequency is related to deeper soil layers while the peak at high frequency is more related to shallow soil layers. The low peak amplitude suggests that the impedance contrasts between the underlying layers are small. And the high peak amplitude suggests that the impedance contrasts between the underlying layers are large.



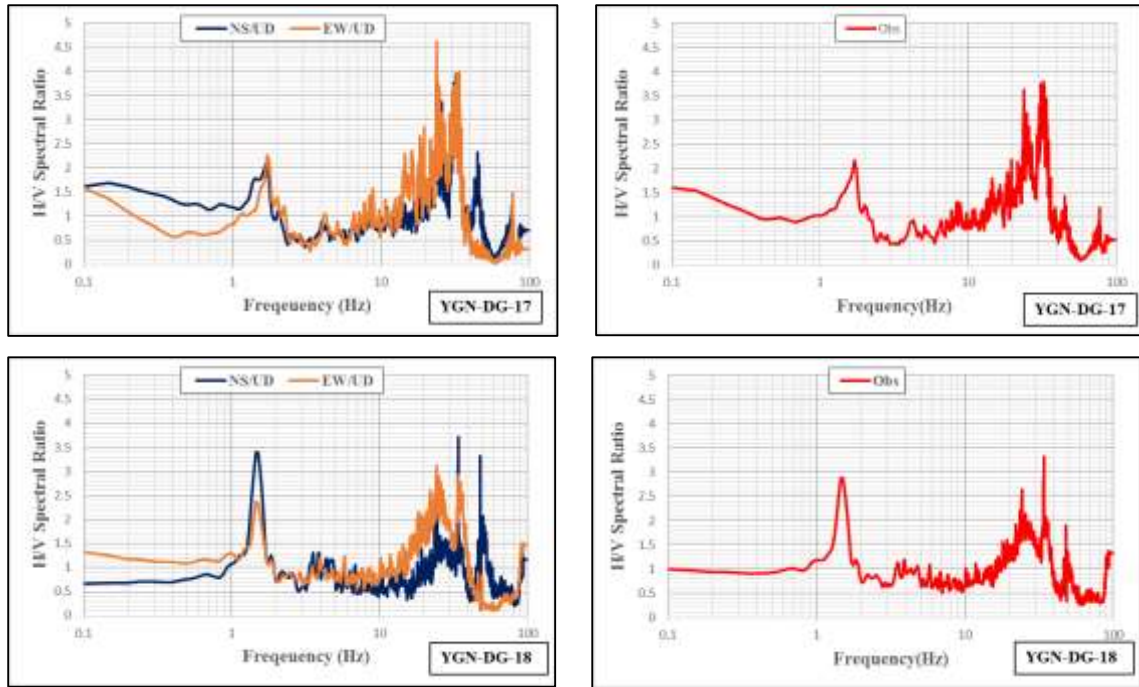


Figure 5 NS/UD, EW/UD and Observed Microtremor Spectra (Obs) of Some Selected Sites YGN-DG 2, 15, 17, 18 in Dagon Township; (YGN-DG-2) at the ancient church, corner of Pyihtaungsu Yeiktha street and Myoma Kaung street, (YGN-DG-15) at the corner of U Wisara Road and Shin Saw Pu Road, (YGN-DG-17) at the corner of Ahlone Road and Myoma Kyaung Road near the Pyihtaungsu Yeiktha, (YGN-DG-18) at the Dagon Park, junction between Shwedagon Pogoda Road and U Wisara Road.

Shear wave Velocity (S-wave) Inversion

The model 6-layer is used as an initial model and the S-wave velocity contrast between each layer in the model is not high because the amplitude of observed mean HVRs is low. Based on observed HVRs and calculated HVRs, the velocity and thickness of each layer in initial model is modified by the increase or decrease in percentage until observed the best fit in terms of peak amplitude and frequency. The horizontal to vertical ratio (HVRs) of observed microtremor is in red colour, theoretical or final one is in dark blue colour and green for initial model is shown in Figures (6) with the tables using by trial and error inversion process and final soil model. The elastic half spaces of the Tables represent the seismic bedrocks as shown in Table (1).

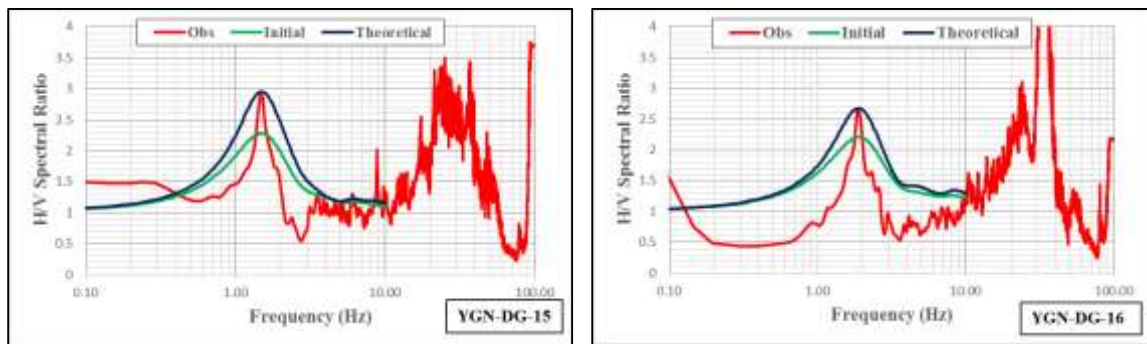


Figure 6 Initial, Modified Spectra and Observed H/V Spectra of Some Selected Sites (YGN-DG-15, 16) in Dagon Township, Yangon

Table 1 Initial and Modified Soil Model of YGN-DG-15 in Dagon Township

Layer	Thickness (m)		Vp*		Vs**		Unit Wt.	
	Initial	Modi	Initial	Modi	Initial	Modi	Initial	Modi
1	2	4	1502	1329	250	200	1.93	1.87
2	9	10	1536	1417	300	250	1.94	1.90
3	12	14	1633	1502	350	300	1.95	1.93
4	16	15	1695	1695	400	400	1.99	1.99
5	24	16	1957	1815	500	500	2.06	2.02
6	25	18	2091	1844	600	520	2.09	2.03
Elastic Half Space	88888	88888	2219	2219	800	800	2.12	2.12

* Primary Wave Velocity ** Shear Wave Velocity

Identification of Shear Wave Velocity (S-Wave) Structure

The shear wave velocity structure was constructed based on final modified soil model derived from inversion process of each site where microtremor measurement was conducted and identified S-wave velocity structure in some selected sites at Dagon Township. Shear wave velocity (V_s) is an essential parameter for evaluating the dynamic properties of soils. The S-wave velocity (V_s) structure of sedimentary deposits can control site dependent strong ground motions and resulting geotechnical problems and structural damage. The shear wave velocity structure of individual site was constructed based on final modified soil model from inversion process of each site where microtremor measurement was conducted as shown in Figure (7). In the Shear wave velocity profile, the blue line represents the S-wave velocity structure of initial model and the red line represents the S-wave velocity structures of modified of final one.

Determination of V_s^{30}

The most important parameter in the classification of the seismic design categories is the shear wave velocity of the topmost 30m of sediment depth, the V_s^{30} , and it had also been calculated based on the following equation (Borcherdt, 1970).

$$V_s^{30} = \frac{\sum_{i=1}^n d_i}{\sum_{i=1}^n d_i / v_{si}}$$

Where,

- d_i = thickness of i^{th} soil layer
- v_{si} = shear wave velocity in i^{th} soil layer
- n = number of soil layer

The Shear wave velocity structures are obtained together with subsurface soil layers, their thickness and unit weight at each site where microtremors measurement was conducted. The sediment thickness can be obtained after the trial and error inversions are being focused on fundamental peak of horizontal to vertical ratio (H/V).

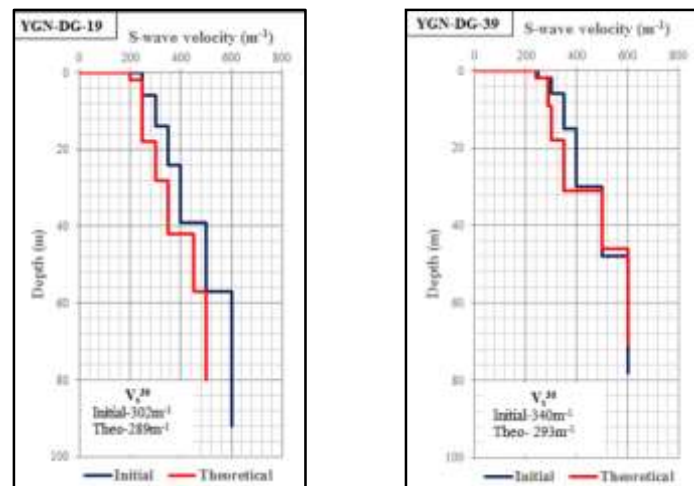


Figure 7 S-wave Velocity Structures of YGN-DG-19, 39 in Dagon Township

Results and Discussion

Based on fundamental peak, the peak amplitude of H/V and fundamental frequency of all measured sites in Dagon Township had been determined. These results show that the peak amplitude of H/V (potential soil amplification) are ranging from 0.2 to 3.8 as shown in Figure (8), while the fundamental frequencies are ranging from 1.25 Hz to 2.65 Hz as shown in Figure (9).

Peak Amplitude (Amp)

The peak amplitude of microtremor H/V is in five red coloured zones as shown in Figure(8): the first zone is between southern part of Pyay Road and southern part of Myoma Kyaung Road; the second zone is around B.E.H.S No (1) Dagon, Ahlanpya Pagoda Road; the third zone is near National Theater, U Wisara Road; the fourth zone is western part of Pyidaungzu Yeiktha street; and the fourth zone is northern part of Pyay Road, near Yangon Region Parliament which are remarkably higher than the other parts. It can be regarded that these zones are generally composed of softer sediments and higher amplification of ground motion can be expected during a future earthquake than other places. In the meantime, lowest amplitude is observed in Purple colored where the dense sediments and lower amplification of ground motion can be expected during a future earthquake.

Fundamental Frequency (Freq)

The Fundamental Frequency map as shown in Figure (9), the lowest fundamental frequency is in four purple colored zones: the first zone is around Ministry of Construction; the second zone is between Khay Pin Street and Taw win street; the third zone is around Alan Pya Pagoda; and the fourth zone is northern Part of Yangon Region Parliament. These zones can generally be regarded that the sediment in this zone is thicker than the other area. Meanwhile, the highest fundamental frequency is observed in red colored zone where the thinner sediment can be expected. The medium thick sediment can be observed in green colored zones.

Predominant Period

The predominant period is inversely proportional to fundamental frequency and it is one of the most important parameter. The buildings with similar or coincide natural period to predominant period of underlying soil layers will be suffered stronger shaking and likely to be serve damage during an earthquake. The predominant period of the short period appears on a very thick soft ground, because such ground consisted of plural layers and the influence of the uppermost layer is

remarkable. The predominant period on fresh rock, bed rock and sand hill, show very long period, but amplitude is always very small. In Figure (10), predominant period between 0.78-0.8 were noted that at the Min Ye Kyaw Zwa street. The period map shows how many stories should be constructed in this area because 0.1s is equal to the one-story structure as a rule of thumb.

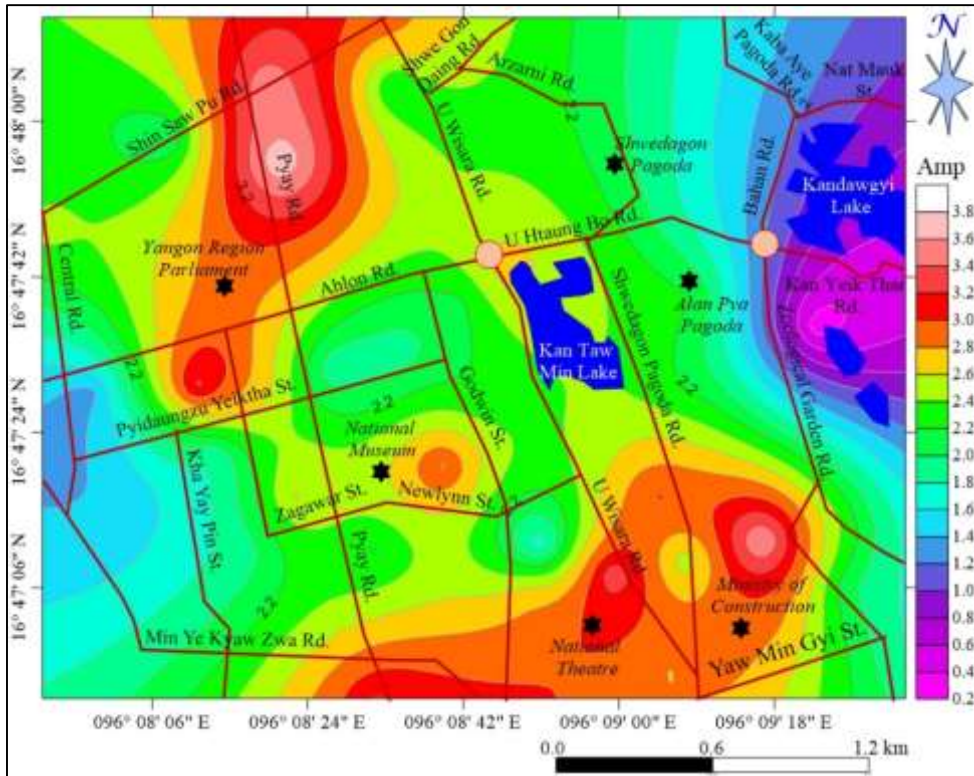


Figure 8 Peak Amplitude (Amplification) Map of Dagon Township in southern Yangon

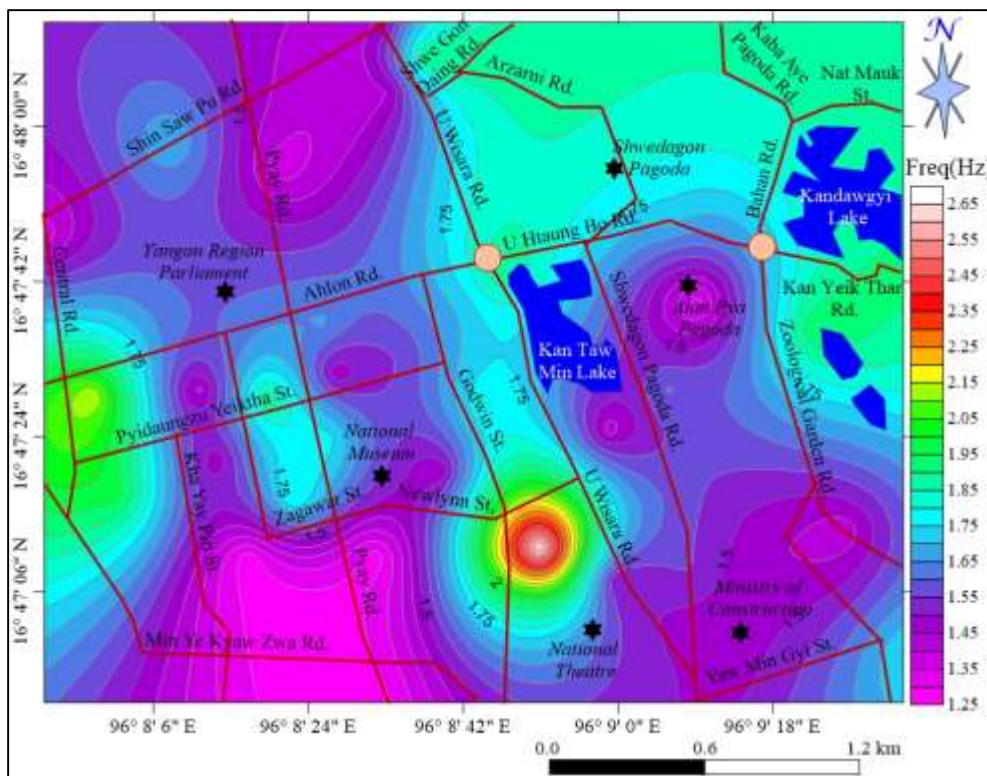


Figure 9 Fundamental Frequency Map of Dagon Township in southern Yangon

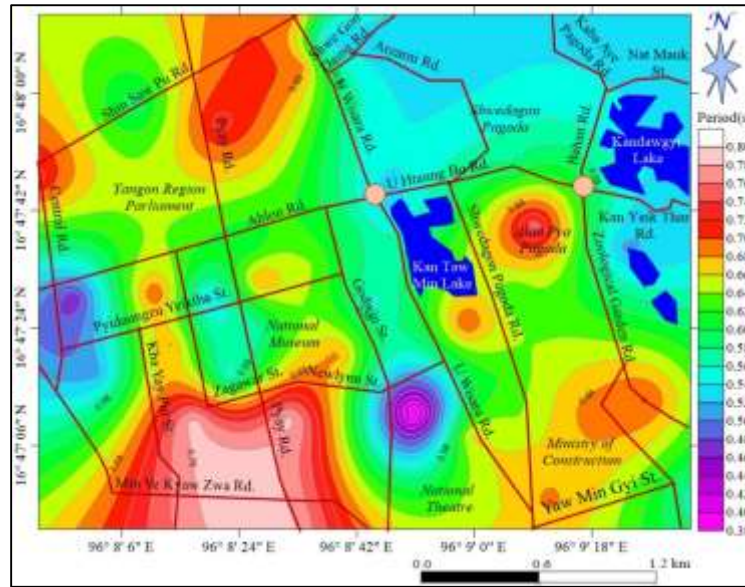


Figure 10 Predominant Period Map of Dagon Township in southern Yangon

Sediment Thickness

The shear wave velocity structures are obtained together with subsurface soil layers, their thickness and unit weight at each site where microtremors measurement was conducted. The sediment thickness can be obtained after the trial and error inversions are being focused on fundamental peak of horizontal to vertical ratio (H/V). In Figure (11), the thinner sediment zones (the purple color) are mainly observed in central portion of the Dagon Township, especially the area Road between U Wisara Road and Shwedagon Pagoda Road; around Yangon Region Parliament; U Htaung Bo Junction. These portions are not suitable for low rise building because the buildings can be fallen due to the equal frequency of underlying soil layers and buildings. The thicker sediment zones (the red color) are mainly observed the road between Pyay Road and Myoma Kyaung Street, Northwestern part of Dagon Township, near Shin saw Pu Road, and around the Alan Pya Pagoda. These portions are unsuitable for high rise building. In addition to the Dagon Township are mainly composed of medium thick sediment zone, these zone are sediment depth between 70m - 90m.

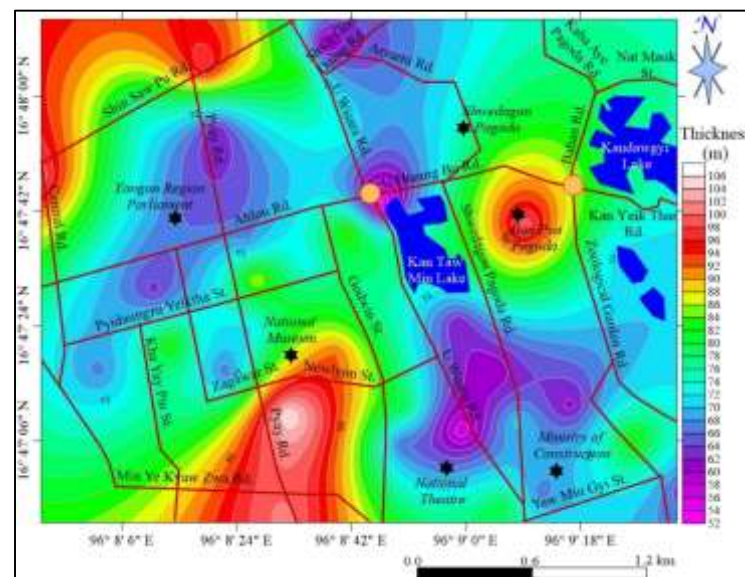


Figure 11 Soil Thickness Map of Dagon Township in Yangon

Average Shear Wave Velocity (V_s^{30})

The average shear wave velocity of upper 30 m depth (V_s^{30}) is calculated from velocity structure of final soil model and map of V_s^{30} is as shown in Figure (12). The purple colour represents the softer sediment zone (relatively low velocity) and the red colour represents the dense sediment zone (relatively high velocity). The lowest shear wave velocity zones (purple color) can be observed along the southern portion of the Dagon township; and northern portion of Pyay Road near Yangon Region Parliament and Pyidaungzu Yeiktha street, where the soft sediments are occupied. According to these results, the strong ground shaking can be expected including Yangon Region Parliament, National Theater and Ministry of Construction office compound. The highest shear wave velocity zones (red colour) can be observed in the eastern part and western part of Dagon Township where the dense sediments are occurred.

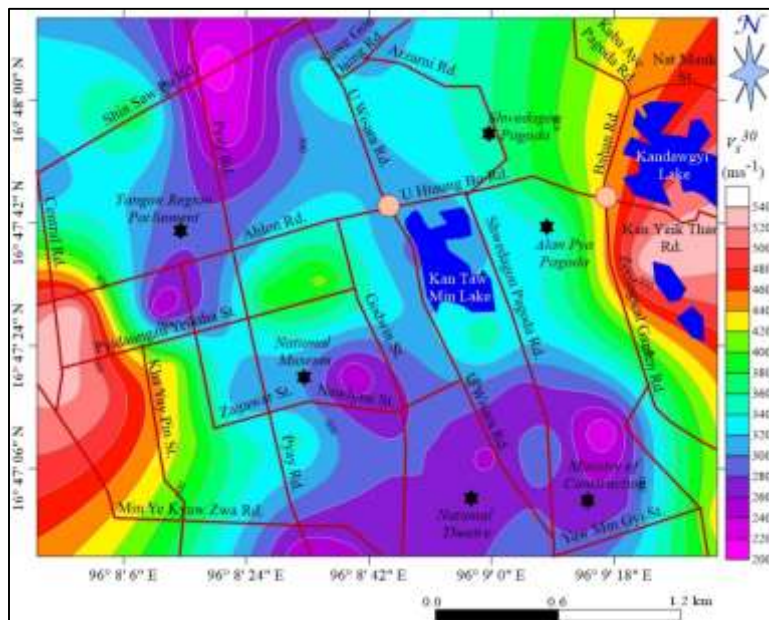


Figure 12 V_s^{30} Map of Dagon Township in Yangon

Concluding Remarks

This research mainly focused on the acquisition of ground information for future liquefaction hazard analysis in southern Yangon (Dagon, Mingalar Taung Nyunt, Ahlone, Lanmadaw, Latha, Kyauktada, Papedan, Botataung, Pazundaung Townships) where Dagon township is included. The microtremor survey had been applied as the main tool for research activities in the field and available secondary boring data were combined to microtremor data during the data processing and analysis. Based on results of overall research works, the following facts are concluded.

1. The fundamental frequency of underlying soil layers is ranging from 1.25 Hz to 2.65 Hz and the lowest frequency zone is encountered in most part of the Dagon Township especially and highest frequency zone in south-western part of U Wisara Road and moderate zones in the rest area.
2. The peak amplitude microtremor H/V ratio or potential soil amplification factor is between 0.2 and 3.8 in general and the places between southern part of Pyay Road and southern part of Myoma Kyaung Road; around B.E.H.S No (1) Dagon, Ahlanpya Pagoda Road; near National Theater, U Wisara Road; western part of Pyidaungzu Yeiktha street; and northern part of Pyay

Road, near Yangon Region Parliament can experience higher soil amplification effect during an earthquake than other parts.

3. The highest predominant period between 0.78-0.8 s were noted that the Min Ye Kyaw Zwa street.
4. Based on determined subsurface soil profiles and related engineering properties, it is revealed that the thickness of sediment is ranging from 52 m to 106 m, and relatively thicker sediment zones are observed in road between Pyay Road and around Alan Pya Pagoda. These portion are not suitable for high rise building.
5. The average shear wave velocity of upper 30m depth, V_s^{30} , is 200m^{-1} and 540m^{-1} in general. The lowest shear wave velocity zones; along the southern portion of the Dagon township; and northern portion of Pyay Road near Yangon Region Parliament and Pyidaungzu Yeiktha street, Yangon Region Parliament, National Theater and Ministry of Construction office compound, where strong ground shaking can be expected.

Acknowledgements

The authors thank the Ministry of Education, Department of Higher Education for the permission to carry out this research and financial support. I acknowledge Dr. Nu Nu Yee and Dr Nay Thwe Kyi, Pro-Rectors of Dagon University for their kind permission to submit this research paper. I would also like to express my sincere gratitude to Professor Dr. Kyi Kyi Maw, Head of Department of Geology, Dagon University for her encouragement, suggestions and Discussions.

References

- Borcherdt, R.D. (1970). Effect of local geology on ground motion near San Francisco Bay, *Bulletin of the Seismological Society of America*, Vol-60, no1:29-61pp.
- Bour M., Fouissac D., Dominique P., Martin C., (1998), On the use of microtremor recordings in seismic microzonation, *Soil Dynamic and Earthquarth Engineering*. Vol. 17, pp.465-474.
- Kanai, K and Tanaka, T. (1954). Measurement of the Microtremor. *Bulletin of Earthquake Research Institute*; Vol:32, 199-209pp.
- Nakamura, Y. (1989). A Method for Dynamic Characteristics Estimation of Subsurface Using Microtremor on the Ground Surface, *Quarterly Rep. Railway Tech. Res. Inst.*, Vol. 30
- Sánchez-Sesma, F.J., Rodríguez, M., Iturrarán-Viveros, U., Luzón, F., Campillo, M., Margerin, L., García-Jerez, A., Suárez, M., Santoyo, M. A., and Rodríguez-Castellanos, A. 2011. "A Theory for microtremor H/V Spectral ratio: Application for a layered medium." *Geophysical Journal International*, Vol. 186, pp 221-225
- Tun N., Hiroshi K., Shinichi M., Myo T., Chit T. M., Thazin H. T., Khin K. K. O., (2013). S-Wave Velocity Profiles Based on The HVRs in Bago, Myanmar for Seismic Hazard Mapping, *Earthquake Engineering, JAEE*, Vol.2, pp 45-55
- Win Swe. and Win Naing., (2008). Seismicity and major active faults of Myanmar, *Journal of the Myanmar Geosciences Society*, Vol.1, No.1, pp.1-20

HEAVY MINERALS ANALYSIS OF THE SHWEZETAW-PADAN COAL MINE AREA, MAGWAY REGION

Paing Soe^{1*}, Maung Maung²

Abstract

The Late Eocene coal-bearing Yaw Formation and Early Oligocene Shwezetaw Formation are exposed in the western part of the Salin sub-basin, Magway Region, records part of the forearc basin. At least twelve heavy mineral species are identified from the sandstones of Yaw and Shwezetaw formations. High maturity index of the middle part of the Shwezetaw Formation may indicate that these heavy minerals came from a long way or there was abundance of stable minerals in source area. Well-rounded grains of zircon, garnet, tourmaline, and rutile are derived from the pre-existing metasedimentary rocks and euhedral crystals were probably derived from acid igneous rocks. Rutile is widespread accessory mineral in metamorphic rocks and it is less significant in igneous rocks. Kyanite, sillimanite, staurolite and garnet were derived from high grade metamorphic rocks. The association of augite and magnetite may indicate basic igneous source. The most sediment in the Shwezetaw-Padan coal mine area were probably derived from recycled orogen including foreland uplift or subduction complex (Western Ranges), Central Igneous Line and mixed magmatic arc (Salingyi Uplift).

Keywords: Salin sub-basin, heavy mineral, source area, recycled orogen, subduction.

Introduction

Myanmar is situated between the northern end of the Sunda–Andaman arc and the eastern end of the India–Asia collision zone. Myanmar hosts abundant economically important resources, such as those of the gemstone-rich Mogok Metamorphic Belt, numerous metal ore deposits, and oil and gas reserves (e.g. Pivnik et al., 1998; Mitchell et al., 2007, andrey, 2006; Searle et al., 2007; Ridd and Racey, 2015b; Khin Zaw et al., 2017; Mitchell, 2017). The origin of the Central Basin remains unclear, and sub-basins within it are described by different authors in various ways including forearc, backarc, and pull- apart types (e.g. Mitchell, 1993; Pivnik et al., 1998; Bertrand and Rangin, 2003; Ridd and Racey, 2015b; Licht et al., 2018) (Gough et al., 2019). Myanmar's commercial onshore oil and gas fields occur in sub-basins of the Central Basin and Ridd and Racey (2015) identify the Salin Sub-basin. The Shwezetaw-Padan coal mine area is situated in the western margin of Salin Sub-basin. It is located between latitudes 19° 55' to 20° 10' North and longitudes 94° 30' to 94° 40' East (Figure.1). The eastern part of the coal mine area is low land and the western part of the study area is moderately rugged terrain. The Shwezetaw-Padan coal mine area can be reached from Yangon, Mandalay, Patheingyi, Monywa, Magway and Ann by car throughout the year.

Previous Work

The Lepper (1933) made the field works for a rock sequence of the Pegu Group in Minbu Basin. Chhibber (1934) studied the geology of Myanmar including the Minbu Basin. The geological, geophysical and seismic surveys of Myanmar Oil and Gas Enterprise, Ministry of Energy have been carried out in 1962, 1965, 1975, 1980, 1985 and 1990, respectively and have been mapped the present development structural map.

¹ Dr, Associate Professor, Department of Geology, University of Magway, Magway Region, Myanmar

² Dr, Principle, Myin Gyan Degree College, Mandalay Region, Myanmar

*Corresponding e-mail; paingsoe.geol@gmail.com

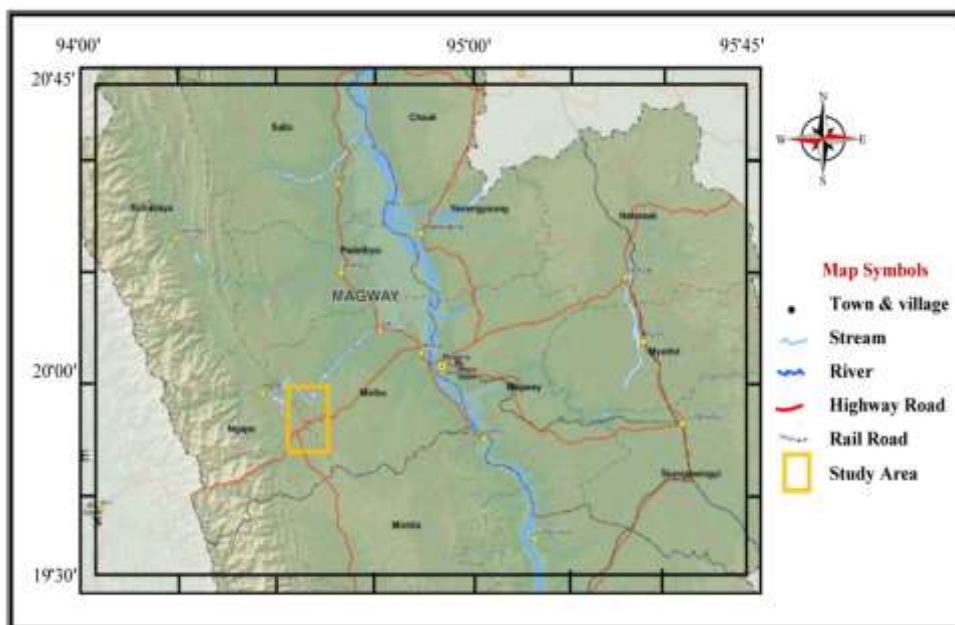


Figure 1 Location map of the Shwezetaw-Padan coal mine area, Magway Region.

Materials and Methods

The field work was carried out along the exposure of the Eocene to Oligocene rock units of the Shwezetaw-Padan coal mine area. Detail sections measurements were carried out along the stream sections and car road cuts section. These sections have been measured bed by bed, and loose and friable sandstone samples have been taken every few centimeters or tens of centimeters, depending on facies changes. The lithology, texture, sedimentary structures, fossil content and tectonic deformation were checked and recorded in note book during measurements. The preliminary action of loose and friable sandstone samples for heavy mineral analysis was carried out as follows:

The loose sands were dried in air or in an oven. The collected samples were weighted about 100 grams. The 100 grams of disaggregated sands were sieved for 15 minutes with Standard Sieve Shaker using B.S sieves spaced at one-phi interval. The individual sieved fractions were weighed. The separations of mineral were made from the 0.125mm size fractions following the technique suggested by Krumbein and Pettijohn (1938). In order to remove iron and carbonate coatings, the sand fractions (0.125mm) were boiled with oxalic acid ($C_2H_2O_4$) and then treated with dilute hydrochloric acid until dissolve liquid is clear. Then the sediments were dried in air or in an oven and later the heavy fraction was separated from the light minerals by using bromoform ($CHBr_3$) (specific gravity = 2.87) using a separatory funnel. The heavy minerals thus obtained were dried and separated by magnet into magnetic and non-magnetic fractions. The heavy mineral grains were mounted on a glass slice using Canada balsam. Thus heavy mineral slides have been obtained, following the procedure described by Krumbein and Pettijohn (1938). Then the heavy minerals were studied by using the petrographic microscope.

Identification of mineral type was based on optical characteristics such as color, pleochroism, absorption, relief, extinction, and birefringence; others are size, crystal form, and elongation. Therefore, 50-200 grains were counted in each slide with the size and roundness of each mineral note. The “ZTR” index which is a quantitative definition of mineral assemblage was calculated using the percentage of the combined zircon, tourmaline and rutile grains for each sample according to the formula below.

$$\text{ZTR index} = \frac{\text{Zircon + Tourmaline + Rutile}}{\text{Total No.of non-opaque heavy minerals}}$$

This formula is referred to as Hubert's (1962) scheme. The calculated index is expressed in percentage to ascertain the mineralogical maturity of the sediment. Accordingly, ZTR < 75% implies immature to submature sediments and ZTR > 75% indicates mineralogically matured sediments. ZTR Maturity index and individual percentage mineral of the Yaw Formation and Shwezetaw Formation sediments samples are shown in Table (3) and Figure(2).

Geological Setting and Stratigraphy

The Central Myanmar Basin (CMB) lies between the Indo-Burman Ranges (IBR) in the west and the Shan Plateau in the east Metcalfe (2011, 2013). The Central Myanmar Basin (CMB) is divided into the eastern (backarc) and the western (forearc) troughs particularly after the late Miocene when the Central Volcanic Line (CVL) became well established. The western trough of the CMB is further subdivided into a few sub-basin, namely (from north to south) the Hukaung, Chindwin, Minbu/Salin, Pyay and Irrawaddy sub-basins.

The Indo-Myanmar Ranges include regional metamorphic, volcanic, and Triassic to Eocene sedimentary rocks (Bender, 1983; Uddin and Lundberg, 1998; Allen et al., 2008; Mitchell et al., 2010; Steckler et al., 2016). The Kabaw Fault Zone marks the western edge of the Central Basin which is filled with Upper Cretaceous to Pleistocene terrestrial to marine sediments (Takai et al., 2001; Allen et al., 2008; Oo et al., 2015; Licht et al., 2016) and is subdivided by a north-south trending line of young volcanoes separating elongate so-called 'forearc' basins in the west from 'backarc' basins in the east (Ni et al., 1989; Pivnik et al., 1998; Maurin and Rangin, 2009; Licht et al., 2016; Mitchell, 2017). There are two ultramafic belts in the northeast (Tagaung-Myitkyina Belt) and the west (Mitchell et al., 2007; Searle et al., 2007; Mitchell et al., 2012; Sevastjanova et al., 2016).

The eastern margin of the Central Basin is the Shan Scarp, which includes the Jurassic to Cretaceous marine sediments of the Paunglaung-Mawchi Zone (Bertrand et al., 1999; Mitchell, 1989; Bertrand and Rangin, 2003; Searle et al., 2007; Sevastjanova et al., 2016). Further to the east there are Permo-Carboniferous rocks of the Slate Belt (Mitchell et al., 2007; Ridd and Watkinson, 2013), and highgrade metamorphic rocks of the Mogok Metamorphic Belt (Searle and Ba Than Haq, 1964; Barley et al., 2003; Searle et al., 2007), and the Shan Plateau, where there is a succession of Cambrian to Triassic siliciclastic, carbonate, and volcanic rocks (Mitchell, 1989; Bertrand and Rangin, 2003; Mitchell et al., 2012).

The present Shwezetaw-Padan coal mine area is situated a small segment of the western margin in Salin sub-basin, west of Magway and Minbu. The rocks of the coal mine area can be differentiated into four lithostratigraphic units of the formation rank are; (1) Pondaung Formation, (2) Yaw Formation, (3) Shwezetaw Formation and (4) Padaung Formation. Present research is friable sand samples for heavy minerals analysis from the Yaw and Shwezetaw formations.

The term "Yaw Formation" was renamed from "Yaw Shale" of Cotter (1912) by Aung Khin and Kyaw Win (1969). In the study area, Yaw Formation is well exposed nearly north south trending along the east of Padan village. Yaw Formation consists mainly of bluish grey to dark grey clays, thin- to thick-bedded sandstone, sand-shale interbeds, variegated clay and sub-bituminous coal seams. The lower contact with the underlying Pondaung Formation is gradational whereas its upper contact with the overlying Shwezetaw Formation is unconformable. Based on the fossil evidence, lithology and stratigraphic position indicated Late Eocene age for the Yaw Formation.

"Shwezetaw Sandstone" was first introduced by Cotter (1912) for a sequence of massive sandstone and siltstone. It was named after the Shwezetaw Pagoda Hill (20° 07' N, 94° 35' E). The same lithostratigraphic unit was described by Verderbung (1921) as "Shwezetaw Stage" in Maung Maung (1994). In 1969, Aung Khin and Kyaw Win critically reexamined the Tertiary succession in the type area and renamed "Shwezetaw Formation" on the basis of the regional facies pattern. Shwezetaw Formation consists of greenish gray to grayish-brown color, massive, compact, fine- to medium-grained, thin- to medium-bedded, calcareous and ripple marked, fossiliferous sandstones, sandy shale and silty sands. The upper part of the Shwezetaw Formation becomes argillaceous and grades into shales or clays of the Padaung Formation. Based on the fossil evidence, lithology and stratigraphic position indicated Early Oligocene age for the Shwezetaw Formation.

Heavy Mineral Analysis

Heavy mineral grains are present in concentration from 2.45 to 3.46 percent in terrigenous rocks. Heavy minerals are high-density accessory mineral constituents of siliciclastic sediments and they are found as the minor components in the sandstones. They are useful in evaluating diagenetic history as well as the pre-erosional weathering and tectonic history of source area (Tucker, 2001 and Lindholm, 1987). They were eroded from the source area and mechanical separating during transportation and deposition in the present research area. The heavy mineral grains (0.15 mm in diameter) were studied and they rarely exceed one per cent of the total rock volume. They are very resistant to chemical weathering and mechanical abrasion. The heavy minerals grains comprise about 1.2% and which have specific gravity ($> 2.89 \text{ g/cm}^3$). They contain both opaque and non-opaque detrital minerals. The heavy minerals are removed from more abundant light minerals by gravity separation in a high density liquid.

Description of Heavy Minerals Species

In the Shwezetaw-Padan coal mine area, the weights in percent of the heavy mineral grains are various. Non-magnetic heavy minerals are more common than the magnetic heavy minerals. In magnetic heavy minerals, opaque volume percentages are more than the non-opaque volume percentages. In non-magnetic heavy minerals, non-opaque volume percentages are more than opaque volume percentages. At least (12) heavy mineral species are identified from the sandstones of Yaw and Shwezetaw formations. ZTR Maturity index and individual percentage mineral of the Yaw Formation and Shwezetaw Formation sediments samples are shown in (Table 3). They are zircon, tourmaline, rutile, augite, garnet, hornblende, kyanite, sillimanite and staurolite and opaque minerals.

Description of Opaque, Magnetic Heavy Minerals

In the sandstones of Yaw Formation and Shwezetaw Formation, opaque, magnetic minerals are widely distributed which are magnetite, hematite and ilmenite.

Magnetite

Fe_3O_4 is the chemical composition of the magnetite and it forms in cubic system. Magnetite shows granular form and more pronounce, metallic luster than other. It is metallic grey to black in polarized light, and some alter to red hematite. Magnetite is very common in the study area. This oxide of iron is a member of the spinel group of minerals with the general formula R^{++} or R^{+++} , in which the divalent R^{++} is commonly Mg or Fe, less commonly Mn or Zn. The trivalent R^{+++} is Al, Fe or Cr in different cases.

Hematite

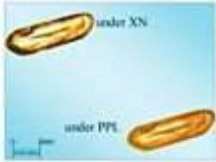
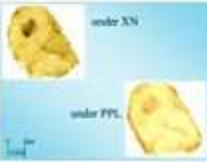
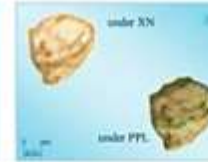
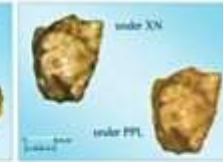
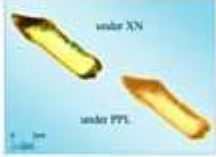
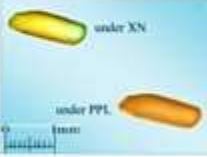
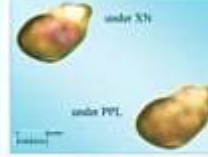
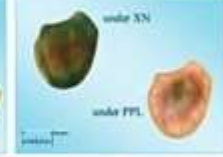
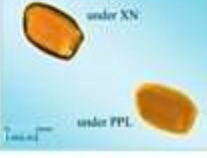
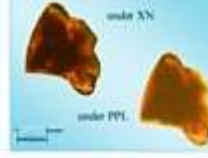
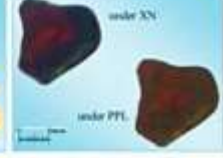
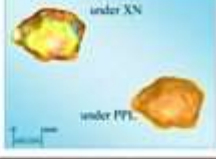
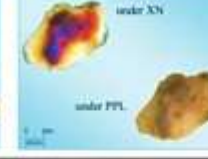
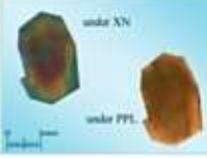
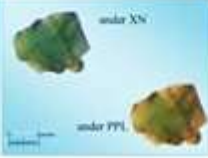
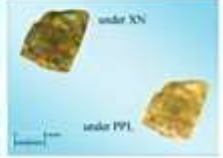
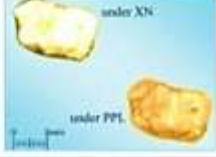
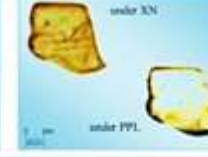
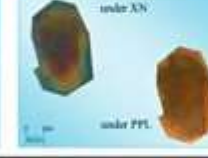
The chemical composition of hematite is Fe_2O_3 and it is formed in trigonal system. It may be opaque or translucent. It shows cheery red and black to deep color red. Beautifully crystalline specimens of hematite are well known object in mineral collectors, but it is disappointing material in rock sections, usually occurring only as minute grains or disseminated specks filling the role of pigment. Thus the bright red streaks and blotches in the Cornish serpentine consist of hematite. In these conditions, the hematite is bright red in thin section, but when more massive it may be black and opaque.

Table 1 Physical properties and provenance of the heavy minerals exposed in Shwezetaw-Padan coal mines Area

Minerals (Under XN)	G	H	Form	Colors	Luster	Miscellaneous	Provenance
 Zircon ($ZrSiO_4$)	4.6 – 4.7	7.5	Tetragonal, short prisms with pyramids; cleavage rare	Usually colorless, some particles are mauve, yellow to brown	Adamantine	Particles often show euhedral form with well-marked crystal faces; well-worn particles usually elongate, elliptical or globular; contain large mineral, liquid or gas inclusions; many particles show well-defined zoning; particles can survive many reworkings	Sialic to intermediate igneous rocks
 Tourmaline	3.0 – 3.3	7- 7.5	Hexagonal - rhombohedral; striated prismatic; cleavage lacking or poor	Yellow-brown, dark brown, indigo to black		Particles occur as elongate prisms, irregular fractured pieces and well rounded ovals; inclusions are common. Particles can survive many reworkings	Pneumatolytic rocks, pegmatites, schists, gneisses, marble
 Rutile (TiO_2)	4.24	6 – 6.5	Tetragonal, often striated	Yellow, reddish brown, red	Adamantine	Particles irregular, generally elongate, prismatic with rounded pyramidal ends common; inclusions abundant. Characterized by form, very high birefringence, high relief, deep color and striae	Sialic igneous and crystalline metamorphic rocks
 Augite (Pyroxene)	3.2- 3.4	5-6	Monoclinic; cleavage-perfect prismatic at about 90°	Pale brownish gray or pale grayish green	Vitreous	Particles usually elongate, worn cleavage fragments, sometimes with dentate ends; irregular or poorly rounded	Intermediate and basic igneous rocks
 Garnet	3.5 - 4.3	7	Isometric, dodecahedra, trapezohedra; fracture-conchoidal	Colorless, pale pink, orange, red, apricot-yellow, amber	Glassy	Characterized by color, conchoidal fracture, isotropism and high relief	Igneous and metamorphic rocks; high abundance indicates metamorphic
 Hornblende (Amphibole)	2.9- 3.5	5-6	Long, blade-like prisms; cleavage-two oblique	Dark brown and green to black;	Satiny, glassy, pearly	Particles elongate, prismatic, with longitudinal cleavage and marked diagonal cross-fractures; may occur as irregular fractured particles; hornblende often nearly opaque and appear translucent just on thin edges	Igneous and metamorphic rocks
 Kyanite Al_2SiO_5	3.6	5-7	Triclinic; bladed; cleavage – 2 at 90°	Usually colorless, rarely pale blue	Vitreous to pearly	Particles are elongate and of marked rectangular outline to short, moderately rounded and elliptical; carbonaceous inclusions common; particles may alter along edges to "mica"	Schists and gneisses
 Staurolite ($Fe,Mg)_2$, ($Al,Fe)_6O_6$ (SiO_4) ₃ , (O, OH) ₂	3.7	7 – 7.5	Orthorhombic; short prisms, cruciform twins	Yellow, gold, brown	When altered, dull to earthy; when fresh, resinous to vitreous	Particles irregular, somewhat platy with hackly to subconchoidal fractures; inclusions numerous; bright interference colors	Crystalline schists, slates and sometimes gneisses
 Sillimanite Al_2SiO_5	3. 23	6- 7	Orthorhombic; cleavage = one direction, perfect	Colorless	Vitreous	Particles irregular to short prismatic, split longitudinally and have striae parallel to length	Metamorphosed argillaceous rocks

G = Specific Gravity H = Hardness

Table 2 Heavy minerals of the Shwezetaw-Padan coal mines Area

1	Zircon ($ZrSiO_4$)				
2	Tourmaline				
3	Rutile (TiO_2)				
4	Augite (Pyroxene)				
5	Garnet				
6	Hornblende (Amphibole)				
7	Kyanite Al_2SiO_5				
8	Staurolite $(Fe,Mg)_2$, $(Al,Fe)_9O_6$ $(SiO_4)_4(O,OH)_2$				
9	Sillimanite Al_2SiO_4				

Ilmenite

It is formed in trigonal system and it has $FeO.TiO_2$ in chemical composition. Ilmenite shows orthorhombic forms and metallic luster. Its color is brownish to purplish black in reflected light.

Hardness of the ilmenite is 5-6 and specific gravity is 4.6- 4.9. These minerals are more common in lower part of the Shwezetaw Formation (Sample No. Ss- 1/26).

Description of Non-Opaque, Magnetic Heavy Minerals

Hornblende

Hornblende is characterized by its short or slender prisms, irregular or rectangular fragments, to long thin flakes. Some grains may be thick and massive, platy or bladed. Others are partially fibrous or are sometimes intergrowth with another amphibole, rarely with pyroxene phases. Hacksaw or dog tooth termination is commonly observed in the hornblende heavy grains. Hornblende is the most unstable minerals and exhibits the saw-teeth mark by intrastratal solution. Grains of volcanic origin are often euhedral and have terminations at one or both ends (Mange and Maurer, 1992). Characteristic hornblende colours are bluish green, brown green and brown. The dark-brown or reddish-brown varieties are less common. Colour zoning or patchy colour arrangements are frequent. They are present in a large variety of igneous and metasedimentary rocks. The forms and colours of hornblende grains in the Yaw and Shwezetaw formations are brown green and euhedral grains. The typical source of hornblende is acid, intermediate igneous rocks and their older metamorphic rocks.

Garnet

Garnets are abundant in the sandstone sample of the Yaw Formation in the study area. Garnets occurred as colorless, reddish brown to grey varieties with subangular to subrounded grains. Hardness of the garnet is 7 and specific gravity is 3.5 - 4.3. The particles of garnet vary from each other. It is the metastable mineral. The garnet is distinguished by high relief, uneven fracture and isotropism. Inclusions of quartz, iron ore, apatite, zircon, rutile, muscovite, biotite and graphite are common (Fig. 3.7.a - d). Throughout the formation, garnet mineral gradually decreases from older to younger formations. Some of the grains contain inclusions. Garnet is common in a variety of metamorphic rocks and is also present in plutonic igneous rocks, pegmatites, in ultramafic varieties and in some acid volcanics. In sediments, almandine is the most widespread garnet (Mange and Maurer, 1992).

Description of Non-Opaque, Non-Magnetic Heavy Minerals

Zircon

Zircon occurs throughout the stratigraphic succession without break. Zircon in the research area is colourless, yellow and grey (Table.1, 2). Zircon grain shape in the research area is euhedral, long prismatic with bi-prismatic terminations, but some grains are well-rounded. The morphological characteristics of zircon are determined by the physical and chemical conditions during growth. Some grains occur thick marginal zoning and contain gas, liquid and small euhedral inclusions.

Zircon is a remarkably widespread accessory mineral in rocks of crustal origin. It is particularly ubiquitous in silicic and intermediate igneous rocks. Zircon may reach high concentration in some beach sands and placers (Mange et al., 1992). The presence of rounded zircon in sandstone that contains few if any other heavy minerals is suggestive of sediment recycling or of an episode of intensive chemical leaching or mechanical abrasion. Evidence of heavy-mineral concentration of zircon may indicate that recycled sedimentary rocks terrane (provenance) type (Sam Boggs, 2009).

Tourmaline

Tourmaline is an abundant stable mineral of the research area. The size, shape and colour of tourmaline in the study area are variable. Tourmaline displays a wide range of colours and these are, in general, indications of composition. Iron-bearing tourmalines are very dark (almost opaque) or deep blue, but elbaïtes have light or deep blue (indicolite) and pink (rubellite) shades. Colour zoning is frequent and euhedral to subhedral and prismatic grains of tourmaline are occurred. Distribution of tourmaline is abundant in Upper sandstone member of the Shwezetaw Formation of the research area (Table.1, 2).

Tourmaline crystallizes in granites, granite pegmatites and in contact- or regionally metamorphosed rocks (Mange et al., 1992). Tourmalines are widespread in all types of detrital sediments and are ultrastable both mechanically and chemically.

Polycyclic tourmaline grains eroded from pre-existing siliciclastic deposits are well to very well-rounded and are associated with equally well-rounded zircons and rutiles (Mange and Maurer, 1992). Tourmaline is particularly resistant to both chemical decomposition and mechanical abrasion and, like quartz, can survive multiple recycling. Thus, the presence of tourmaline in sandstone that contains few if any other heavy minerals is suggestive of sediment recycling or of an episode of intensive chemical leaching or mechanical abrasion.

Rutile

It is a slightly common mineral in the rock samples of the Yaw Formation and more common in Shwezetaw Formation. Rutiles are subhedral to anhedral and subrounded to rounded grains. Rutile has color variation from grains and show deep blood red color in the center of the grain and a thick black hole surrounds the grain (Table.1, 2). Hardness of the rutile is 6 – 6.5 and specific gravity is 4.24. Rutiles can be distinguished from cassiterites by its very high relief and strong pleochroism. Well rounded rutiles indicate recycled sedimentary source rock (Mange and Maurer, 1992).

Rutile is a widespread accessory mineral in metamorphic rocks, particularly in schists, gneisses and amphibolites. Well-rounded rutiles indicate recycled sedimentary source rock (Mange and Maurer, 1992). Rutile is a common accessory mineral in high temperature and high pressure metamorphic and igneous rocks. Rutile is a non-silicate mineral occurring as a necessary constituent of igneous rocks and many granites, diorites and their metamorphic derivatives such as gneisses and amphibolites. Rutile is used as a source of titanium. Rutile is widespread accessory mineral in metamorphic rocks and it is less significant in igneous rocks.

Kyanite

Kyanite in the research area shows angular to bladed or prismatic forms. Most grains are colourless and some shows yellow to uneven colour distribution (Table.1, 2). Hardness of the kyanite is 5 - 7 and specific gravity is 3.6. The large extinction angle assists in distinguishing kyanite from sillimanite. Kyanite occurs in gneisses, granulites and pelitic schists which are generated by the regional metamorphism of mostly pelitic rocks. It is considered as an indicator of the metamorphic zone. It is resistant to acidic weathering (Grimm, 1973; Nickel, 1973 in Mange and Maurer, 1992) and is fairly stable in the diagenetic environment.

Sillimanite

Sillimanite in the study area shows long slender prisms, short stout prismatic fragments and fibrous form. Sometime, inclusions of spinel, biotite and zircon are often present. Prismatic grains are colourless and some appears with a pale green or pale brown hue and some of the crystals are

bent (Table.1, 2). Hardness of the sillimanite is 6 - 7 and specific gravity is 3.23. Extinction of the prisms and fibres is parallel. Staurolite, kyanite and andalusite in a heavy mineral suite may indicate the presence of sillimanite. Sillimanite crystallizes in high-temperature metamorphic rocks and occurs in sillimanite-cordierite gneisses and biotite-sillimanite hornfelses. It is also present in granulite facies rocks. High-grade regional metamorphism of pelitic rocks also produces sillimanite (Mange and Maurer, 1992).

Staurolite

Staurolite occurs throughout the stratigraphic horizons of the Yaw and Shwazetaw formations. It is characterized by irregular, angular, somewhat platy, often fractured grains which show poorly defined cleavage traces. Rarely, diamond-shaped basal sections are found. Inclusions of quartz and carbonaceous matter are common (Table.1, 2). It has bright yellowish colours in shades of pale yellow through golden yellow to dark yellowish-brown. Birefringence of staurolite is moderate and interference colours range from first-order grey or yellow in thin fragments to second-order orange, red and bluish-green in thicker specimens. Staurolite is one of the easily identifiable detrital minerals. Staurolite is almost exclusively a product of medium-grade regional metamorphism and it forms in mica schists, derived from argillaceous sediments, and less frequently in gneisses (Mange and Maurer, 1992).

Augite

Augite occurred in the study area is dominantly euhedral or subhedral and short or long slender prisms with terminations at one or both ends. Volcanic augites may show embayments or corrosion. Sometimes with conchoidal fractures or grooves on their surface. Compositional zoning is fairly common. They appear in various shades of green and sometimes brown or yellowish brown. It shows second and third order interference colors appeared as bright yellow, orange, red and blue concentric bands on rounded grains (Table.1, 2). Augite is wide spread in various ultramafic and intermediate igneous rock types and is particularly common in gabbros, dolerites, andesites and basalts, and also in some peridotite (Mange and Maurer, 1992).

Table 3 ZTR Maturity index and individual percentage minerals in sediments samples of the Yaw Formation and Shwazetaw Formation of Shwazetaw-Padan coal mine area

Sample No.	Z	T	R	Aug	Chl	G	H	Ky	Sill	St	Opaque	Non-opaque	Z+T+R	ZTR % index	
Yaw Formation	Tey- 2/12	15	9	8	6	3	6	6	-	9	4	20	66	32	48.5 %
	Tey- 6/13	18	5	12	11	10	2	11	3	5	5	16	82	35	42.7 %
	Tey- 7/13	12	7	4	2	1	6	2	3	8	15	25	60	23	38.3 %
Shwazetaw Formation	Ss- 1/26	17	6	7	6	6	3	6	4	3	4	22	62	30	48.4 %
	Ss- 13/21	21	15	7	5	5	-	5	5	3	4	12	70	43	61.4 %
	Ss- 16/21	19	12	8	5	-	3	5	3	-	3	24	58	39	67.2 %
Total	102	54	46	35	25	20	35	18	28	35	119	398	202	306.50 %	
%	25.6	13.6	11.6	8.8	6.3	5	8.8	4.5	7	8.8					51.08 %

Average ZTR % index = 51.08 %

Total Opaque = 119

Total Non-opaque = 398

Z- Zircon, T- Tourmaline, R- Rutile, Aug = Augite , Chl- Chlorite , G- Garnet, H = Hornblende, Ky = Kyanite, Sill-Sillimanite, St-Staurolite

Table 4 Percentage of Zircon, Tourmaline, Rutile, ZTR Maturity and Maturity index

Heavy Mineral Species	Yaw Formation			Shwezetaw Formation		
	Tey- 2/12 Lower	Tey-6/13 Middle	Tey-7/13 Upper	Ss-1/26 Lower	Ss-13/21 Middle	Ss-16/21 Upper
Zircon	15	18	12	17	21	19
Tourmaline	9	5	7	6	15	12
Rutile	8	12	4	7	7	8
ZTR maturity	32	35	23	30	43	39
Maturity index (ZTR/r)	0.47	0.54	0.30	0.43	0.75	0.64

(ZTR- zircon, tourmaline and rutile, r-rest of the other heavy minerals)



Figure 2 Variations in ZTR maturity index of the Yaw Formation and Shwezetaw Formation exposed in Padan-Minbu area {Maturity index is calculated by using the formula, RTZ/r (RTZ means rutile, tourmaline and zircon; r means the rest of the heavy mineral species)}. (After; Maria A. Mange and Heinz F. W. Maurer, 1992)

Results and Discussion

The purpose of the heavy mineral analysis is to examine the nature of source rocks and source area, made in transportation of detrital particles and prevailing condition during the sediment deposition. The study of heavy mineral distribution reveals the following characters:

In the Yaw and Shwezetaw formations, stable heavy minerals are abundant such as opaque, kyanite, sillimanite, tourmaline, rutiles and zircon. Euhedral and well-rounded grains of zircon, rutiles and tourmaline are associated together.

The maturity index of heavy mineral suites of Yaw Formation and Shwezetaw Formation are calculated using the formula of RTZ/r (Where R, T, Z represent rutile, tourmaline, and zircon respectively and "r" represents the rest of heavy mineral species). According to this relation, the maturity index of sample no. Tey-2/12, Tey-6/13, Tey-7/13 in Yaw sandstones is 0.47, 0.54, 0.30 and sample no. Ss-1/26, Ss-13/21, Ss-16/21 in Shwezetaw sandstones is 0.43, 0.75, 0.64 respectively, see Table (4).

In Yaw and Shwezetaw formations, abundant opaque grains, low density heavy mineral assemblages, a relatively high ZTR index, poor preservation, and moderate grain rounding indicate intense weathering in the source area and/or diagenetic dissolution of the unstable components.

Unstable grains such as hornblende grains are the more abundant in sample no. Tey-2/12, Tey-6/1 and Ss-1/26. The maturity index of heavy mineral suits is lowest in sample No. (Tey-7/13) but highest in sample No. (Ss-13/21) as shown in Table (4) and Figure (2). The unstable minerals have no resistant to weathering and diagenetic processes. But, the presence of such minerals indicates that the sediments were derived from the near source area rapidly or from the area which consisted of mass of such minerals. Higher maturity index may indicate that heavy minerals came from a long way or there was abundance of stable minerals in source area.

Heavy mineral association of well-rounded grains of zircon, garnet, tourmaline, and rutile shows that the sediments were derived from the pre-existing metasedimentary rocks. Euhedral grains may be from the primary source and the rounded grains may be from the older sedimentary units or the source was located at a long way.

Hacksaw or dog tooth termination is commonly observed in the hornblende heavy grains. There was influence of the intrastratal solution on the heavy minerals and may decrease the unstable minerals.

The heavy minerals obtained from all samples are generally similar in mineralogical aspects. Their percentage is slightly varied from each other. This appears to indicate that the provenance has remained unchanged.

According to ZTR % index (Table.3), the highest percentage of 25.6% is zircon and the second abundance percentage of 13.6 is tourmaline. Rutile comes next with 11.60% abundance. ZTR % index of the augite, hornblende and staurolite are equal amount and the lowest percentage of 5% is garnet. According to Hubert's formula (1962), total ZTR% index is 51.08 % (ZTR% index < 75%). The sediments of the study area implies immature to sub mature sediments.

Zircon is a remarkably widespread accessory mineral in rocks of crustal origin. Zircon and tourmaline are particularly resistant to both chemical decomposition and mechanical abrasion and, like quartz, can survive multiple recycling. Thus, the presence of abundant, rounded zircon and tourmaline in a sandstone that contains few if any other heavy minerals is suggestive of sediment recycling or of an episode of intensive chemical leaching or mechanical abrasion. Evidence of heavy-mineral concentration of zircon may indicate that recycled sedimentary rocks terrane (provenance) type (Sam Boggs, 2009).

Tourmaline occurs on granite pegmatites. It is usually brown in colour (sometimes greenish) or brownish yellow. Its shape is commonly euhedral. It is a common detrital heavy mineral in sedimentary rocks. So varieties of tourmaline are used gemstones.

Rutile is a common accessory mineral in high temperature and high pressure metamorphic and igneous rocks. Rutile is a non-silicate mineral occurring as a necessary constituent of igneous rocks and many granites, diorites and their metamorphic derivatives such as gneisses and amphibolites. Rutile is used as a source of titanium. Rutile is widespread accessory mineral in metamorphic rocks and it is less significant in igneous rocks.

Staurolite is one of the index minerals that are used to estimate the temperature, depth and pressure of which a rock undergoes metamorphism. Staurolite is a regional metamorphic mineral of intermediate high grade.

Sillimanites are produced by high-grade regional metamorphism of pelitic rocks. Tourmaline crystallizes in granites, granite pegmatites, in pneumatolitic veins and in contact or regional metamorphosed rocks.

Kyanite, sillimanite, staurolite and garnet were derived from high grade metamorphic rocks. The association of augite and magnetite may indicate basic igneous source.

According to R. C. Lindholm, 1987, euhedral crystal of zircon, tourmaline and hornblende of the study area were derived from acid igneous rocks. Hornblende (reddish brown variety) derived from basic igneous rocks. Moreover, garnet, hornblende (blue-green variety), kyanite and staurolite may indicate high grade metamorphic rocks. Rutile, rounded tourmaline and rounded zircon were derived from reworked sediments.

Provenance Study

Sandstone compositions are influenced by the character of the sedimentary provenance, the nature of the sedimentary processes within the depositional basin, and the kind of dispersal paths that link provenance to basin. The key relations between provenance and basin are governed by plate tectonics, which thus ultimately controls the distribution of different types of sandstones (Dickinson & Suczek, 1979).

Source Rock

On the basis of heavy minerals analysis, the common heavy minerals present in the Yaw and Shwezetaw sandstones are zircon, tourmaline, rutile, augite, garnet, hornblende, kyanite, opaque, sillimanite and staurolite. (Table 1-3). Provenance interpretations are made from the evidence of light minerals fraction (quartz, feldspar and rock fragments) and heavy mineral analysis.

1. According to Lindholm (1991), euhedral crystals of zircon and hornblende in the research area were probably derived from acid igneous rocks and blue green variety may indicate low to high-grade metamorphic rocks.
2. Heavy minerals such as zircon (both rounded and euhedral), tourmaline and rutile are present. According to Pettijohn (1957), such texture and composition of heavy minerals indicate recycled origin (pre-existing sedimentary rocks).

Source Area

Recycled orogens are uplifted and deformed supra-crustal rocks which formed mountain belts, volcanic and metasediments. From the above mention factors, the most of the sediments in the Shwezetaw-Padan coal mine area were probably derived from recycled orogen including foreland uplift or subduction complex (Western Ranges), Central Igneous Line and mixed magmatic arc (Salingyi Uplift).

Conclusion

The rocks units of the Shwezetaw-Padan coal mine area can be differentiated into four lithostratigraphic units of the formation rank are; (1) Pondaung Formation, (2) Yaw Formation, (3) Shwezetaw Formation and (4) Padaung Formation. (12) heavy mineral species are identified from the sandstones of Yaw and Shwezetaw formations.

Higher maturity index may indicate that heavy minerals came from a long way or there was abundance of stable minerals in source area. So, the sediments from the middle part of the Shwezetaw Formation are stable minerals and came from a long way. Well-rounded grains of zircon, garnet, tourmaline, and rutile are shown that the sediments were derived from the pre-existing metasedimentary rocks. Euhedral crystals of zircon and hornblende in the research area were probably derived from acid igneous rocks. Rutile is widespread accessory mineral in

metamorphic rocks and it is less significant in igneous rocks. Kyanite, sillimanite, staurolite and garnet were derived from high grade metamorphic rocks. The association of augite and magnetite may indicate basic igneous source.

From the above mention factors, it is reasonably concluded that most of the sediments in the Shwezeta-Padan coal mine area were probably derived from recycled orogen including foreland uplift or subduction complex (Western Ranges), Central Igneous Line and mixed magmatic arc (Salingyi Uplift).

Acknowledgements

First I would like to thank Dr Maung Maung, Principal of Myin Gyan Degree College for giving me a seed of research minded to me. And the persons I ought to thank are my parents and the teachers from kindergarten to University.

References

- A. D. Miall, (2000) Facies analysis: in *Principles of Sedimentary Basin Analysis*, Springer, Berlin, Germany, pp. 141-248.
- Aung Khin & Kyaw Win, (1969) "Geology and hydrocarbon prospects of the Burma Tertiary geosyncline". *Union of Burma Jour. Sci. & Tech*, vol.2, no.1, pp.52-73.
- C. R., Fielding, (1984) "A coal depositional model for the Durham Coal Measures of northeast England". *J.Geol. Soc., London*, 141, pp. 919-931.
- Dickinson, W.R. and Suczek, C.A., (1979) *Plate Tectonics and Sandstone compositions*: Am. Assoc. Petroleum Geologists, Bull. 63 (12), P.2164-2182. (in Maung Maung, 1994)
- Dickinson, W.R., (1985) *Interpreting provenance relations from detrital modes of sandstones*: G. G. Zuffa (Ed.), Provenance of Arenites, 333-361. D. Reidel Publishing Company.
- G. de. P., Cotter, (1912) "The Pegu-Eocene Succession in the Minbu District near Ngape". *Rec. Geol. Surv. India*, vol. 41, pt. 4, pp. 221-239.
- G. J. Nichols, (1999) *Sedimentology and Stratigraphy*, 1st edition, Blackwell Scientific Publications, Oxford, pp. 355.
- G.W., Lepper, (1933) "An outline of the geology of the oil-bearing regions of the Chindwin-Irrawaddy valley of Burma, and of Assam-Arakan". *World Petroleum Congress*, Paper No. 169.
- Garzanti, E., Doglioni, C., Vezzoli, G., and Ando, S., (2002). "Orogenic Belt and Orogenic Sediment Provenance: Laboratoria di Petrografiae Sedimentario, Lioartimento di ScienziGeotecnologic, Universita di Milano-Bicocca, Piaza della Scienza." 4, 20126 Milano, Italy.
- H. E. Reineck, and I. B. Singh, *Depositional Sedimentary Environments*, 2nd Edition, Springer, New York, 549pp, 1980.
- H. L., Chhibber, (1934) *The geology of Burma*. Macmillan London. Mac Millan.
- H.G., Reading, (1996) *Sedimentary Environments and Facies*. 3rd Edition. Oxford Blackwell Scientific Publications, pp. 154-228.
- I., Metcalfe, (2011) "Tectonic framework and Phanerozoic evolution of Sundaland". *Gondwana Res.* 19, 3-21.
- I., Metcalfe, (2013) "Gondwana dispersion and Asian accretion: tectonic and palaeogeographic evolution of eastern Tethys". *J. Asian Earth Sci.* 66, pp.1-33.
- J. M. Coleman, and, D. B. Prior, (1980) *Deltaic influences on shelfedge instability processes*. pp. 345-353. Springer-Verlag, Berlin, 9.4.1.
- Lepper, G.W., (1933) "An outline of the geology of the oil-bearing regions of the Chindwin-Irrawaddy valley of Burma, and of Assam-Arakan". *World Petroleum Congress*, Paper No. 169.
- Lindholm, R.C., (1991) *A Practical Approach to sedimentology*. CBS Publisher & Distributors.
- Maria A. Mange and Heinz F. W. Maurer, (1992) *Heavy minerals in colour*. Chapman and hall. London, pp. 230.

- Mitchell, A., (1993) "Cretaceous-Cenozoic tectonic events in the western Myanmar (Burma) – Assam region". J. Geol. Soc. 150, pp. 1089–1102.
- Mitchell, A., (2017) *Geological belts, plate boundaries, and mineral deposits in Myanmar*. Elsevier, Oxford
- Mitchell, A., (2017) *Geological belts, plate boundaries, and mineral deposits in Myanmar*. Elsevier, Oxford.
- Mitchell, A., Chung, S.-L., Oo, T., Lin, T.-H., Hung, C.-H., (2012) "Zircon U-Pb ages in Myanmar: Magmatic–metamorphic events and the closure of a neo-Tethys ocean" J.Asian Earth Sci. 56, pp. 1–23
- Mitchell, A., Chung, S.-L., Oo, T., Lin, T.-H., Hung, C.-H., (2012) "Zircon U-Pb ages in Myanmar: Magmatic–metamorphic events and the closure of a neo-Tethys ocean" J.Asian Earth Sci. 56, pp.1–23.
- Mitchell, A., Hlaing, T., Htay, N., (2010) "Indo-Myanmar Ranges in the tectonic framework of the Himalaya and Southeast Asia. Indo-Burman Ranges in the Tectonic Framework of the Himalaya and Southeast Asia". Geol. Soc. India, Memoir 75, pp. 3–24.
- Mitchell, A., Htay, M.T., Htun, K.M., Win, M.N., Oo, T., Hlaing, T., (2007) "Rock relationships in the Mogok metamorphic belt, Tatkon to Mandalay, central Myanmar". J. Asian Earth Sci. 29, pp. 891–910.
- Morley, C.K., Searle, M., (2017) "Regional tectonics, structure and evolution of the Andaman-Nicobar Islands from ophiolite formation and obduction to collision and back-arc spreading". In: Bandopadhyay, P.C., Carter, A. (Eds.), *The AndamanNicobar Accretionary Ridge Vol. 47*. Geological Society of London, Memoir,, pp.51–74.
- Pettijohn, F.J, (1957) *Sedimentary Rocks*, 3rd Edition, Harper and Row Press, New York: springer Verlag pp.618.
- Pivnik, D.A., Nahm, J., Tucker, R.S., Smith, G.O., Nyein, K., Nyunt, M., Maung, P.H., (1998) "Polyphase deformation in a fore-arc/back-arc basin, Salin subbasin, Myanmar (Burma)". Am. Assoc. Pet. Geol. Bull. 82, pp. 1837–1856.
- R .G.Walker, and N.P. James, (1992) *Facies Models: Geological association of Canada*. 157-218 pp. Geol. Ass. Canada, St John's, Newfoundland.
- Ridd, M.F., Racey, A., (2015a) "Introduction to the petroleum geology of Myanmar". Geol. Soc., Lond., Memoirs 45 (1), pp. 1–6.
- Ridd, M.F., Racey, A., (2015b) "Onshore petroleum geology of Myanmar: Central Burma Depression". Geolog. Soc. Lond., Memoir 45, pp. 21–50.
- Ridd, M.F., Racey, A., (2015b). "Onshore petroleum geology of Myanmar: Central Burma Depression". Geolog. Soc. Lond., Memoir 45, 21–50.
- Searle, M., Noble, S., Cottle, J., Waters, D., Mitchell, A., Hlaing, T., Horstwood, M., (2007) "Tectonic evolution of the Mogok metamorphic belt, Burma (Myanmar) constrained by U-Th-Pb dating of metamorphic and magmatic rocks". *Tectonics* 26, TC3014. <https://doi.org/10.1029/2006TC002083>
- T., Elliot, (1986) Delta. In; *Sedimewntary Environments and Facies* (Ed. Reading, H.G.). Blackwell Scientific Publications, Oxford; pp.113-154.
- Tsung Aung, (1980) Geological Map of Central Myanmar Basin, 1 inch to 4 miles scale, MOGE.
- Zaw, Khin, Swe, Win, Barber, A.J., Crow, M.J., Nwe, Yin Yin, (2017) "Introduction to the geology of Myanmar". In: In: Barber, A.J., Zaw, K., Crow, M.J. (Eds.), *Myanmar: Geology, Resources, and Tectonics Vol. 48*. Geological Society of London, Memoir, pp. 1–17.

GEOCHEMICAL CHARACTERISTICS OF GOLD MINERALIZATION AT TAUNG NI GOLD PROSPECT, MADAYA TOWNSHIP, MANDALAY REGION, MYANMAR

Aung Ye Ko¹, Day Wa Aung², Ohn Thwin³ and May Thwe Aye⁴

Abstract

Taung Ni gold prospect area is situated in Madaya Township, Mandalay Region, Myanmar. The host rocks, quartzite and phyllite were metamorphosed under greenschist facies conditions. Gold mineralization is mainly hosted by quartzite of Chaungmagyi Group which is deformed, jointed, brecciated and interbedded with phyllite. In its area, gold-bearing sulphide quartz veins and auriferous deformed/ remobilized quartz veins are found. In these two types of veins systems, Pearson statistical analyses confirm a significant correlation between SiO₂ and other major oxides as most strongly negative correlation indicates that the both quartz veins bearing gold are of hydrothermal origin. The Co and Ni contents in pyrite show Co>Ni and the average ratio for Co/Ni is 2.698. The gold fineness shows two ranges: (1) high fineness (826.2 - 881.3) and (2) low fineness (771 - 795). In sulphide bearing quartz vein (Early Stage), homogenization temperature can be measured and it ranges from 340°C to 403°C and melting temperature ranging from -1.7 to -2.0, salinity NaCl equiv. wt.% range from 3.01 to 3.53. In deformed quartz vein (Later Stage), the range of melting temperature is from -1.3 °C to -1.6 °C and salinity NaCl equiv. wt. % is from 2.31 to 2.83. Homogenization temperature is 320°C to 396°C.

Keywords – Taung Ni gold prospect, gold-bearing quartz veins, Co and Ni ratio, gold fineness, fluid inclusion microthermometry.

Introduction

Taung Ni area is situated in Madaya Township, Mandalay Region, Myanmar. It is located approximately 47 km to the northeast of Mandalay, and about 35 km northwest of Pyin-Oo-Lwin. It lies partly in Mogok Metamorphic Belt (MMB) and between the Sagaing Fault in the west and the Shan Scarp Fault in the east. The area occupies the western marginal zone of Shan Plateau and to the east of the Central Myanmar Basin. Location map of the study area is shown in Figure.1.

Aim and Methods of Study

The major purpose of this research is to elucidate significant anomalies, determine their relationships, use correlation analyses and assess mineralization zones so as to determine the origin of mineralization such as magmatic, hydrothermal, sedimentary or metamorphic. This research consists of two main stages, field work and laboratory work. During the field work, quartz veins samples and ore samples were collected from the quartz veins in the mineralization zone and the laboratory work consists of Atomic Absorption Spectrophotometry (AAS) and X-ray Fluorescence (XRF) methods, and ore microscopy, Scanning Electron Microscopy (SEM) - Energy-Dispersive X-ray Analyzer (EDX) analysis and Fluid inclusion microthermometry.

¹ Ph.D Candidate, Department of Geology, University of Yangon, Myanmar

² Dr, Professor & Head, Department of Geology, University of Yangon, Myanmar

³ Dr, Part-Time Professor, Department of Geology, University of Yangon, Myanmar

⁴ Dr, Professor, Department of Geology, University of Yangon, Myanmar

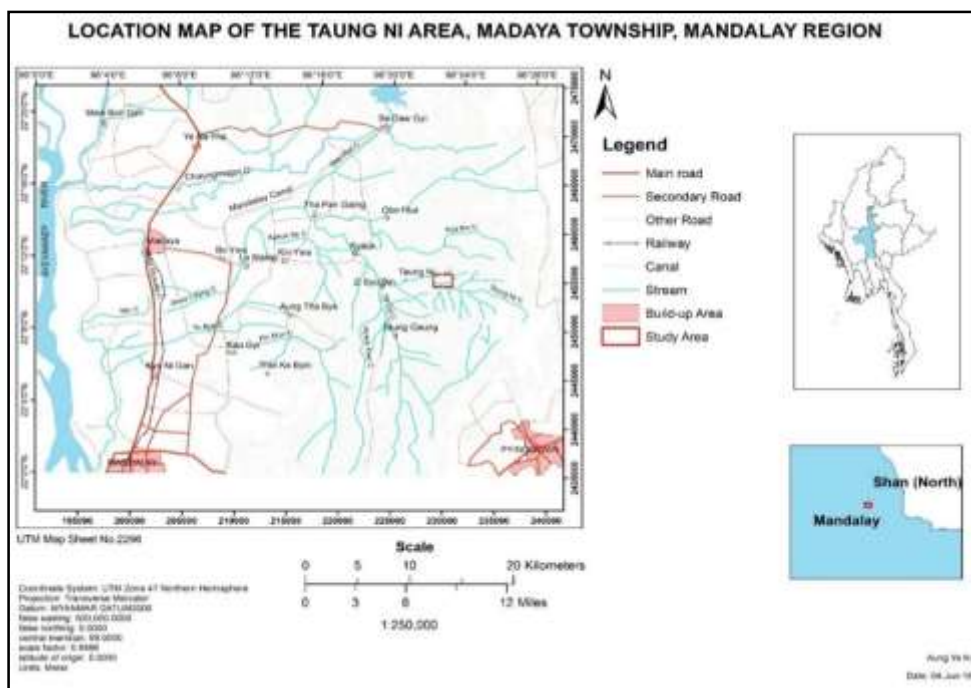


Figure1 Location Map of the Taung Gaung Area, Madaya Township, Mandalay Region

Deposit Geology

The study area, falling in the Shan-Thai Block, lies in the eastern margin of Mogok Metamorphic Belt (MMB) and between the Sagaing Fault in the west and the Shan Scarp Fault in the east. It occupies the western marginal zone of Shan Plateau to the east of the Central Myanmar Basin. The MMB consists of metamorphosed sedimentary sequences of Precambrian to Carboniferous age. Basement sediments are intruded by Jurassic to Tertiary age granitoids. Stratigraphic rock units include Mogok Group, Chaungmagyi Group, Panguyun Group, Naungkangyi Group and Upper Plateau Limestone.

The geology of the Taung Ni area is quite simple. There is only one stratigraphic rock units in this area. It is Upper Precambrian to Lower Cambrian age of Chaungmagyi Group, consisting of Mauk Kaw Quartzite and Kin Sandy Phyllite (Khin Maung Shwe, 1973) (Figure 2). On the basis of microscopic study and XRD results, quartzite and phyllite were composed of low-grade metamorphic minerals such as albite, quartz, chlorite, sericite, epidote, muscovite, actinolite, and biotite. Opaque minerals were often found as disseminations especially observed in phyllite with foliations resulting from the sub-parallel to parallel orientation of minerals such as chlorite or micas due to strong pressure conditions of metamorphism. Therefore, this rock type has been formed by low grade regional metamorphism. The common occurrence of chlorite and sericite suggest the low pressure and low temperature. It shows that this rock type is of the greenschist facies (Aung Ye Ko et al., 2018c).

The mineralization style of the study area is the designated vein type deposit hosted by quartzite of Chaungmagyi Group which is deformed, jointed and brecciated and interbedded with phyllite. The gold-bearing mineralized veins are mostly brecciated and crushed. The thickness of the auriferous quartz vein/ veinlets ranges from 1cm to 15cm which fill NE-SW and E-W structure lineaments of dilational fault zone. The main controlling factor is the regional structure that nearly trends NE-SW and possibly formed by the activity of Phayaung Taung Fault and cause the deformation like, shearing, brecciation favourable for mineralization. Gold is associated with pyrite, arsenopyrite, chalcopyrite, hematite, silver, gold, electrum, petzite, hessite and tellurobismuthite.

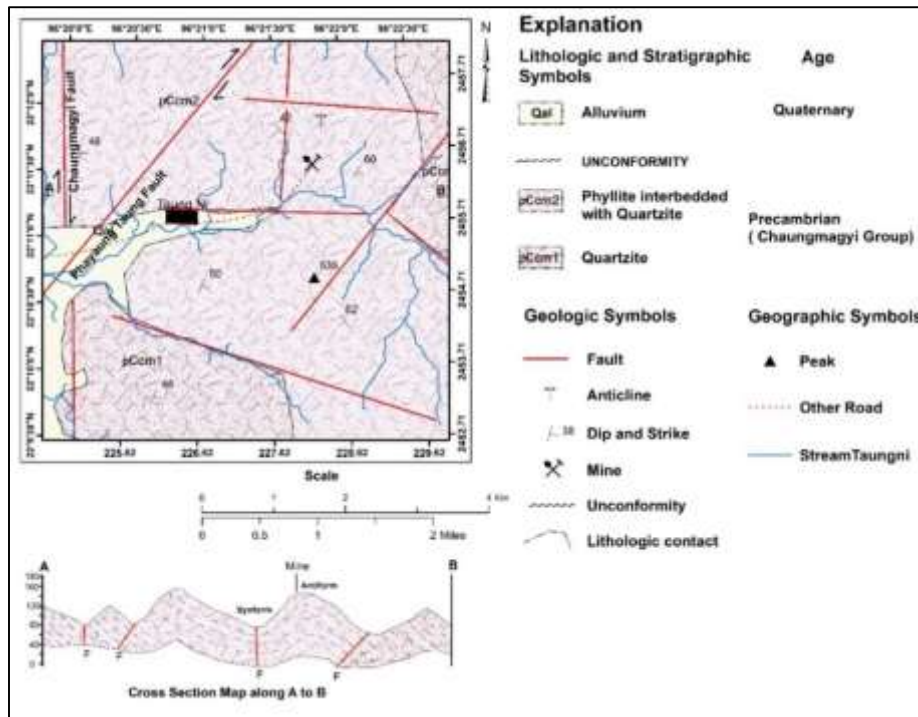


Figure 2 Geological Map of the Taung Ni Area and its environs, Madaya Township, Mandalay Region, Myanmar

Results and Discussion

Geochemistry of gold-bearing quartz veins

In Taung Ni area, two types of vein systems are found: (1) gold-bearing sulphide quartz veins and (2) auriferous deformed/remobilized quartz veins in strongly brecciated and oxidized zone (Figure. 3 & 4).

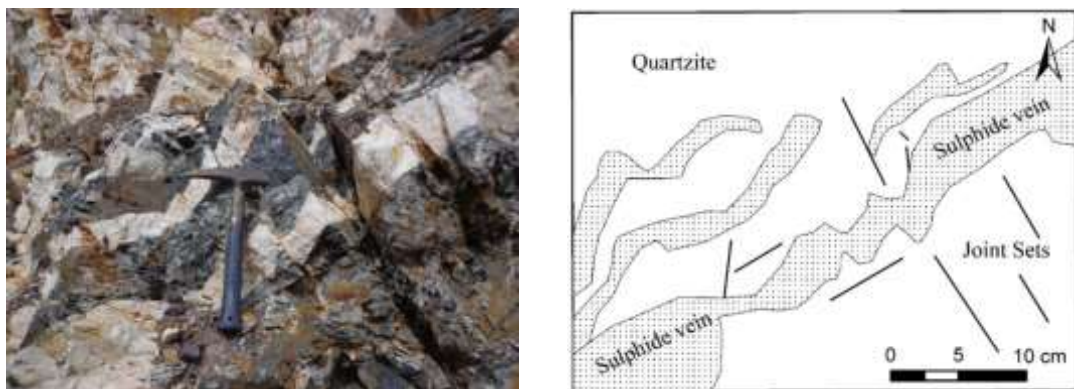


Figure 3 Individual vein system of sulphide quartz veins hosted in quartzite

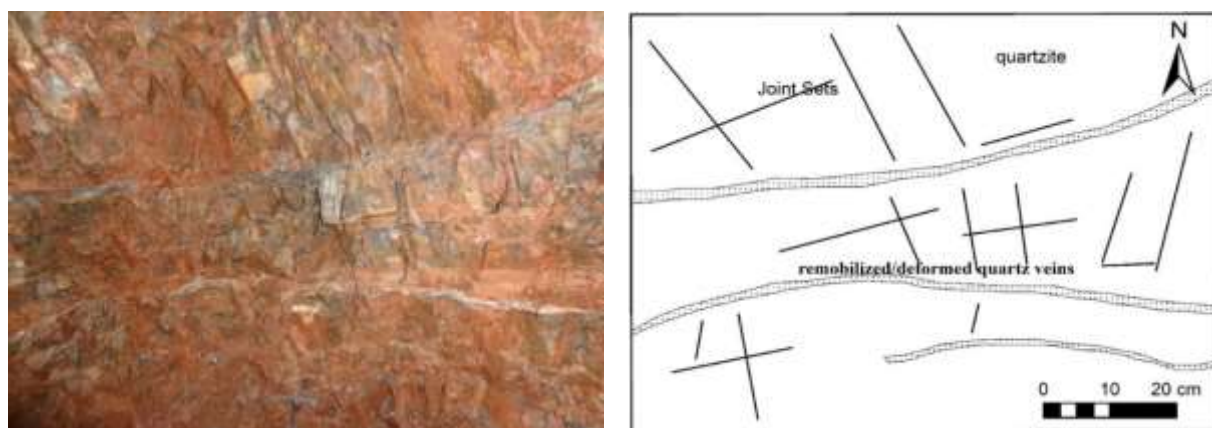


Figure 4 Individual vein system of deformed/remobilized quartz veins hosted in quartzite

In gold-bearing sulphide quartz veins, the whole rock geochemical composition of quartz vein with XRF method of analysis is shown in APPENDIX. The quartz veins are highly siliceous. The composition of SiO_2 varies from 89.81 to 99.68wt%, Al_2O_3 ranges from 0.05 to 2.23wt%, Fe_2O_3 is of the order of 0.07 to 6.26wt%, and MgO varies from 0.01to 1.23wt%, and the concentrations of other major oxides are very low.

Pearson statistical analyses confirm a strong negative correlation between SiO_2 and other major oxides (Table 1). The results indicate that the quartz veins were of hydrothermal origin. The Si-Al discrimination diagram is used to distinguish hydrothermal from sedimentary deposits (Peters, 1988). The ore samples in gold-bearing sulphide quartz veins are almost within the field of hydrothermal field (Figure 5).

The concentration of (Ni-Zn-Co) in quartz veins were plotted on ternary diagram which was used to differentiate between hydrothermal and sedimentary deposits (Figure 6). The data plotted indicate that the quartz veins bearing gold are of hydrothermal origin (Choi and Hariya, 1992).

The concentration of (Co+Ni+Cu+Zn)-Fe-Mn in quartz veins were plotted on ternary diagram which was used to differentiate between hydrothermal and sedimentary deposits (Figure 7). The data plotted indicate that the quartz veins bearing gold are of hydrothermal origin (Bonatti, Kraemer and Rydell, 1972c).

Table 1 Pearson correlation coefficient values of major oxides in gold-bearing sulphide quartz veins

Proximity Matrix										
Case	Matrix File Input									
	SiO_2	TiO_2	Al_2O_3	Fe_2O_3	MnO	MgO	CaO	Na_2O	K_2O	P_2O_5
SiO_2	1									
TiO_2	-0.506	1								
Al_2O_3	-0.48	0.196	1							
Fe_2O_3	-0.954	0.581	0.209	1						
MnO	-0.845	0.327	-0.035	0.933	1					
MgO	-0.526	0.146	0.932	0.276	0.031	1				
CaO	-0.486	0.29	0.913	0.257	-0.034	0.969	1			
Na_2O	-0.007	0.125	0.326	-0.089	-0.117	0.016	0.08	1		
K_2O	0.114	-0.25	-0.258	-0.064	0.08	-0.301	-0.43	-0.34	1	
P_2O_5	-0.897	0.082	0.443	0.81	0.802	0.557	0.44	-0.13	-0.04	1

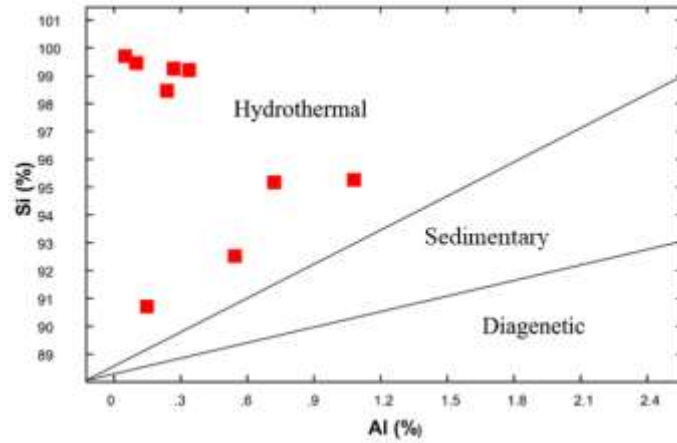


Figure 5 Si-Al discrimination diagram of gold-bearing sulphide quartz veins

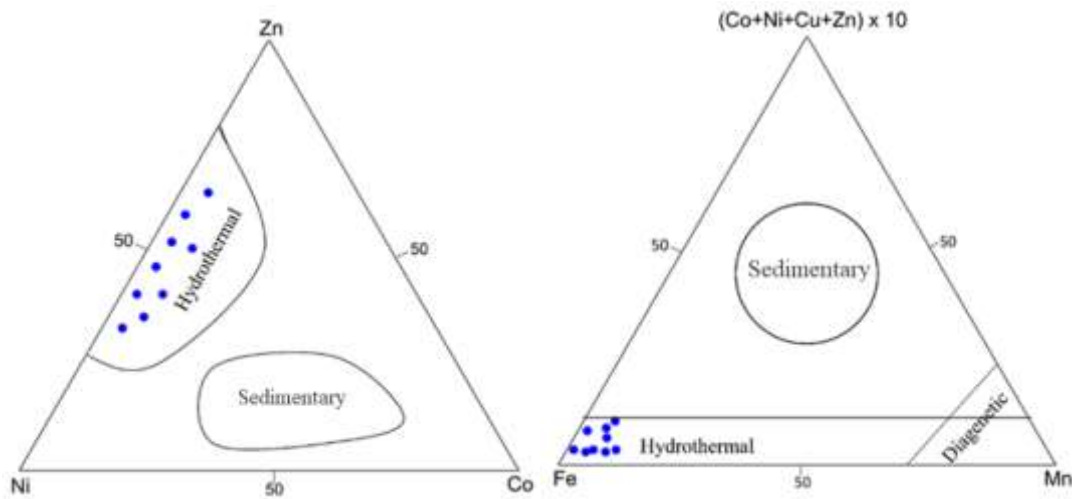


Figure 6 (Ni-Zn-Co) ternary plot of gold-bearing sulphide quartz veins

Figure 7 (Co+Ni+Cu+Zn)-Fe-Mn ternary plot of gold-bearing sulphide quartz veins

Au, Ag, As, Bi, Cu, Mo, Pb, S, Sb, Se and Te were analyzed by atomic absorption spectrometry (AAS). This method yields very high-quality data for these elements (Nurmi et al., 1991) with detection limits of 0.01ppm. The concentration of Au varies from 1.53 to 2.62 ppm, and the concentrations of associated elements in gold-bearing sulphide quartz veins are shown in Table 2. Pearson correlation coefficient values of Au and associated elements in gold-bearing sulphide quartz veins are shown in Table 3.

Table 2 The concentration of Au and associated elements in gold-bearing sulphide quartz veins

	Au (ppm)	Ag (ppm)	As (ppm)	Bi (ppm)	Cu	Mo	Pb	S	Sb	Se	Te
TNQS-1	1.53	2.1	6	2.1	3560	42	4	0.1	0.7	0.2	150
TNQS-2	1.75	1.3	3	1.97	2520	46	4	0.3	0.27	1.2	170
TNQS-3	2.62	4.8	8	4.29	5400	36	5	1.2	0.56	1.3	230
TNQS-4	2.59	4.5	7	3.36	5550	59	7	1.7	0.55	1.3	280
TNQS-5	1.57	2.2	3	2.1	3210	47	3	1.1	0.52	0.5	120
TNQS-6	1.65	1.2	4	1.81	4100	30	9	0.1	0.6	0.7	140
TNQS-7	1.8	2.8	6	1.3	3220	32	4	0.2	0.5	1.2	100

Table 3 Pearson correlation coefficient values of Au and associated elements in gold-bearing sulphide quartz veins

Proximity Matrix											
Case	Matrix File Input										
	Au	Ag	As	Bi	Cu	Mo	Pb	S	Sb	Se	Te
Au	1										
Ag	0.912	1									
As	0.786	0.911	1								
Bi	0.874	0.828	0.704	1							
Cu	0.857	0.826	0.818	0.832	1						
Mo	0.324	0.308	0.11	0.318	0.209	1					
Pb	0.278	0.043	0.136	0.195	0.567	-0.103	1				
S	0.759	0.78	0.506	0.746	0.686	0.684	0.085	1			
Sb	0.002	0.227	0.49	0.161	0.463	-0.185	0.321	0.009	1		
Se	0.738	0.543	0.363	0.408	0.362	0.113	0.106	0.407	-0.558	1	
Te	0.875	0.723	0.621	0.846	0.804	0.602	0.383	0.741	0.022	0.511	1

Ag, As, Bi, Cu, S, Se and Te are strongly correlated with Au (Table 3). These correlations show that the mineralization indicates the complex nature of hydrothermal system (Theodore et al., 1998). Although Mo, Pb and Sb are not closely associated with Au, Mo is moderately associated with Au, Ag, As, Bi, Cu, S, Se, Te, Pb and Sb are separate components. Bi, Te and Cu are strongly correlated with Au and Ag. As, Se and S are very well correlated with each other (Table 3). Analysis of the geological data from the gold-bearing sulphide quartz veins shows two distinct geological association: (1) Au, Ag, Bi, Te and Cu and (2) As, Se and S. Mo, Pb and Sb vary independent of each other and other associations.

In auriferous deformed/remobilized quartz veins, the whole rock geochemical composition of quartz vein was analyzed with XRF as shown in APPENDIX. The composition of SiO₂ varies from 83.78 to 96.58wt%, Al₂O₃ ranges from 1.6 to 9.15wt%, Fe₂O₃ is of the order of 0.65 to 3.49wt%, and MgO varies from 0.03 to 0.57wt%, and the concentrations of other major oxides are very low.

Pearson statistical analyses confirm a strong negative correlation between SiO₂ and other major oxides (Table 4). The results indicate that the quartz veins were of hydrothermal origin.

Fe and Mn are characteristically fractionated on precipitation from hydrothermal solution (Shah and Khan, 1999).

The Si-Al discrimination diagram is used to distinguish hydrothermal from sedimentary deposits (Peters, 1988). The ore samples in gold-bearing sulphide quartz veins are almost within the field of hydrothermal field (Figure 8).

The concentration of (Ni-Zn-Co) in quartz veins were plotted on ternary diagram which was used to differentiate between hydrothermal and sedimentary deposits (Figure 9). The data plotted indicate that the quartz veins bearing gold are of hydrothermal origin (Choi and Hariya, 1992).

The concentration of (Co+Ni+Cu+Zn)-Fe-Mn in quartz veins were plotted on ternary diagram which was used to differentiate between hydrothermal and sedimentary deposits (Figure 10). The data plotted indicate that the quartz veins bearing gold are of hydrothermal origin (Bonatti, Kraemer and Rydell, 1972c).

Table 4 Pearson correlation coefficient values of major oxides in auriferous deformed/remobilized quartz veins

Proximity Matrix										
Case	Matrix File Input									
	SiO2	TiO2	Al2O3	Fe2O3	MnO	MgO	CaO	Na2O	K2O	P2O5
SiO2	1									
TiO2	-0.804	1								
Al2O3	-0.86	0.985	1							
Fe2O3	-0.942	0.901	0.939	1						
MnO	-0.062	-0.3	-0.318	-0.205	1					
MgO	-0.671	0.206	0.256	0.514	0.405	1				
CaO	-0.468	-0.129	-0.047	0.209	0.689	0.86	1			
Na2O	-0.641	0.08	0.164	0.408	0.551	0.938	0.968	1		
K2O	-0.83	0.976	0.973	0.917	-0.212	0.223	-0.063	0.127	1	
P2O5	-0.418	0.497	0.55	0.351	-0.297	-0.055	-0.128	0.026	0.455	1

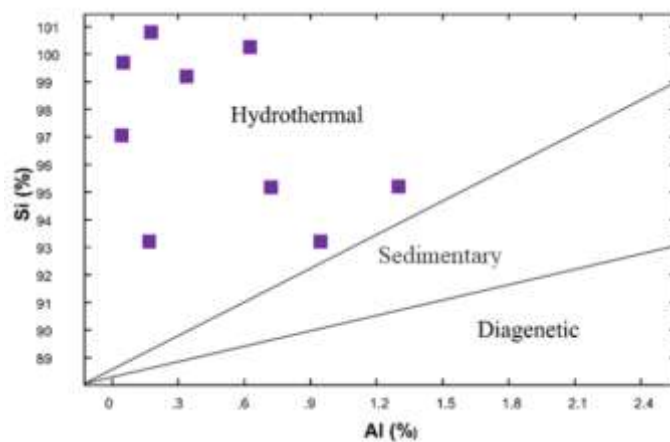


Figure 8 Si-Al discrimination diagram of auriferous deformed/ remobilized quartz veins

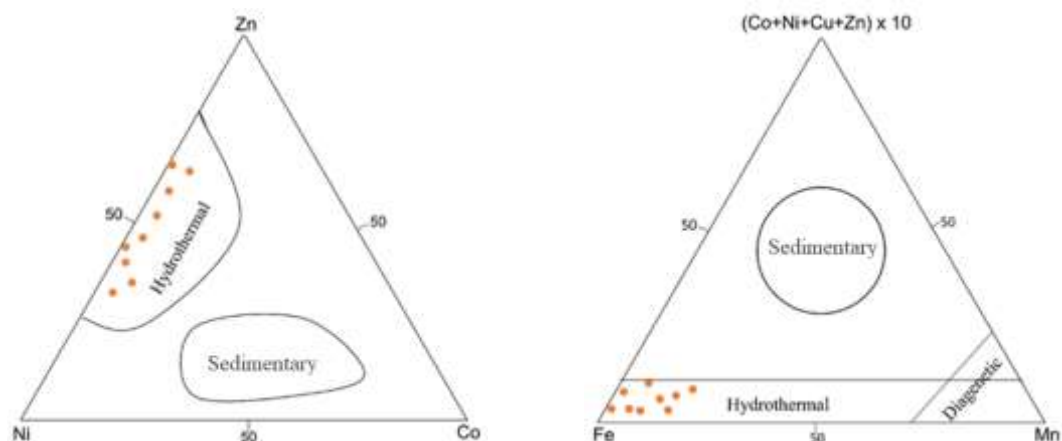


Figure 9 (Ni-Zn-Co) ternary plot of auriferous deformed/remobilized quartz veins **Figure 10** (Co+Ni+Cu+Zn)-Fe-Mn ternary plot of auriferous deformed/remobilized quartz veins

Au, Ag, Fe, Cu, Zn, As and Pb were analyzed by atomic absorption spectrometry (AAS). This method yields very high-quality data for these elements (Nurmi et al., 1991) with detection limits of 0.01ppm. The concentration of Au varies from 1.54 to 7.55 ppm, and the concentrations of associated elements in auriferous deformed/ remobilized quartz veins are shown in Table 5. Pearson correlation coefficient values of Au and associated elements in auriferous deformed/ remobilized quartz veins are shown in Table 6.

Table 5 The concentration of Au and associated elements in auriferous deformed/remobilized quartz veins

	Au	Ag	Fe	Cu	Zn	As	Pb
TNQD-1	7.01	8.77	154320	32500	10	10	5
TNQD-2	1.54	0	72800	17500	11	14	9
TNQD-3	4.72	1.1	29220	37021	17	9	0
TNQD-4	3.55	4.25	95940	22560	13	11	18
TNQD-5	2.12	0.37	56700	21250	20	3	0
TNQD-6	2.15	0	32090	24472	30	12	0
TNQD-7	4.51	7.81	73170	36880	23	5	12
TNQD-8	1.61	0.085	47970	16770	15	8	0
TNQD-9	7.55	5.56	166200	31330	19	3	0

Table 6 Pearson correlation coefficient values of Au and associated elements in auriferous deformed/ remobilized quartz veins

Proximity Matrix							
Case	Matrix File Input						
	Au	Ag	Fe	Cu	Zn	As	Pb
Au	1						
Ag	0.826	1					
Fe	0.802	0.743	1				
Cu	0.711	0.653	0.251	1			
Zn	-0.228	-0.194	-0.415	0.19	1		
As	-0.262	-0.276	-0.247	-0.325	-0.274	1	
Pb	-0.03	0.406	0.177	-0.014	-0.335	0.319	1

Ag, Fe and Cu are strongly correlated with Au. As and Pb are moderately correlated with each other (Table 6). Analysis of the geological data from the auriferous deformed/ remobilized quartz veins shows two distinct geological associations: (1) Au, Ag, Fe and Cu and (2) Pb and As, and Zn is not correlated with other elements.

Minor Elements in Pyrite

The Co and Ni ratio in pyrite appears to have been used to distinguish magmatic, hydrothermal and sedimentary origins of pyrites in ore deposition (Loftus-Hills and Solomon, 1967; Braliala et al., 1979; Bajwah et al., 1987; Brill, 1989). The Co/Ni ratio for magmatic pyrites is greater than 5 in most cases, and in some greater than 10 (Braliala et al., 1979; Bajwah et al., 1987). The Co and Ni contents and the Co/Ni ratios in hydrothermal pyrites vary greatly; the Co and Ni contents can reach up to 1000ppm, and the Co/Ni ratios are generally greater than 1 and can show much variation. Sedimentary pyrites are generally characterized by low contents of Co and Ni and a Co/Ni ratio <1. Generally, Co contents, which are less than 100ppm, are less than Ni contents (Chen et al., 1987).

Xuexin (1984) mentioned a statistically significant difference among sedimentary, hydrothermal (replacement veins), and massive sulphide pyrites (Table 7). According to his study, the massive sulphide pyrites are characterized by a Co:Ni ratio between 5 and 50; hydrothermal pyrites by a variable Co:Ni ratio (often less than 5); and sedimentary pyrites by a much lower Co:Ni ratio (typically < 1). Pyrite from sulphide ore deposits generally contains appreciable amounts of cobalt and has Co > Ni.

Table 7 Geometric means of cobalt (Co) and nickel (Ni) contents (in ppm) and Co:Ni ratios of sediment, hydrothermal, and massive sulphide pyrite minerals (Xuexin, 1984)

No.	Type of Pyrite	Co	Ni	Co:Ni
1	Sedimentary	41	65	0.8
2	Volcano-Hydrothermal, Metamorphosed and Skarn-Hydrothermal	141	121	2-3
3	Volcanogenic Massive Sulphide	486	56	3.5

According to Carstens (1942), pyrite of sedimentary origin is characterized by containing less than 100 ppm cobalt and Co < Ni, whereas pyrite of hydrothermal origin has 400-2400 ppm cobalt and Co > Ni. Pyrite from high-temperature deposits is generally high in cobalt, but noted exceptions and considered that the effect of temperature was slight. Pyrite of high-temperature and hydrothermal sulphide deposits has only a slightly higher average nickel content than pyrite of sedimentary origin and the ranges of concentration overlap. Hawley (1952) found that Ni content was a little higher in high-temperature samples.

In the study area, 20 pyrite minerals were detected by SEM-EDX to know the elemental composition. The Co and Ni contents of ore-bearing pyrites from the Taung Ni gold prospect range from 0.33-0.78wt% and 0.13-0.36wt%, respectively. Average contents of Co and Ni are 0.526wt% and 0.195wt%, respectively. (Table 8). Average content of Co (0.526 wt.%) is higher than Ni content (0.195 wt.%) and it shows that their origin may be of hydrothermal origin. Average ratio for Co/Ni is 2.698. It indicates that pyrites from Taung Ni gold prospect area may be formed under the hydrothermal conditions.

Table 8 SEM-EDX analyses of element composition (wt.%) of pyrite minerals. Element composition (normalized wt.%) of pyrite minerals

No.	Samples	Fe(wt%)	S(wt%)	Co(wt%)	Ni(wt%)	Co/Ni
1	TNP-1	43.23	55.65	0.78	0.36	2.166667
2	TNP-2	45.89	53.36	0.55	0.2	2.75
3	TNP-3	45.02	54.3	0.53	0.15	3.533333
4	TNP-4	45.25	54.23	0.39	0.13	3
5	TNP-5	43.21	55.91	0.65	0.23	2.826087
6	TNP-7	44.78	54.74	0.33	0.15	2.2
7	TNP-9	43.56	55.74	0.5	0.2	2.5
8	TNP-10	45.23	54.15	0.48	0.14	3.428571
	Average			0.52625	0.195	2.69872

Gold Fineness

Gold occurs generally in the native state and is the most abundant of all the gold minerals. It usually occurs associated with a little quantity of silver. The silver content of gold is commonly given as fineness (Gold Fineness- 1000 Au/Au+Ag) (Fisher, 1945). Fisher (1950) concluded that fineness used with other criteria furnishes a sensitive and reliable guide to the relative temperature of ore formation, at least within the epithermal and the upper part of the mesothermal range of temperatures. The fineness of epithermal gold is from 500 to 700. Near the bottom of the epithermal zone (corresponding to the leptothermal zone of Graton, 1933), the fineness is about 700 and may be as much as 800. The fineness of mesothermal gold varies from 750 to 900, with 850-870 being common. The fineness of hypothermal gold is always greater than 800. Fineness of 900 or more results from oxidation under conditions favouring the removal of silver. According to Morrison et al. (1991) the major deposit classes are characterized by the overall average range of deposits and total range of gold fineness values as follows: Archaean 700±1000 (780±1000); slate belt 920(800±1000); plutonic 825 (650±970); porphyry 700±1000 (650±1000); volcanogenic 650±850 (520±870); epithermal 440±1000 (0±1000). The major deposit classes are characterized by the overall average or range of averages and total range of gold fineness (After Fisher, 1950 and Morrison et al., 1991) (Table 9).

Gold fineness was calculated in the study area, based on the result of SEM-EDX analysis. Gold fineness of SEM-EDX analysis of electrum grains is shown in Table.10. It ranges from 771.2 to 795 with average gold fineness of 779.14. Gold fineness of SEM-EDX analysis of gold grains is shown in Table.11. It ranges from 826.2 to 881.3 with average gold fineness of 851.94.

The gold fineness showed two ranges: (1) high fineness (826.2 - 881.3) and (2) low fineness (771 - 795). It suggests that Au was remobilized and recrystallized during later stages.

Table 9 Overall average, range of averages and range of fineness for major deposit lasses (After Fisher, 1950 and Morrison et al., 1991)

Deposit Types	Overall Average /Range of Averages	Total Range
Archean	940	780 ± 1000
Plutonic	825	650 ± 970
Porphyry	700 ± 1000	650 ± 1000
Volcanogenic	650 ± 850	520 ± 870
Slate belt	920	800 ± 1000
Hypothermal		925
Mesothermal	850 ± 870	750 ± 900
Epithermal	440 ± 1000	0 ± 1000

Table 10 Gold Fineness of SEM-EDX analysis of electrum grains

No.	Element	Au (wt%)	Ag (wt%)	Gold Fineness	Remark
1	Grain 1	77.12	22.88	771.2	Electrum
2	Grain 2	77.84	22.16	778.4	Electrum
3	Grain 3	79.5	20.5	795	Electrum
4	Grain 4	76.91	23.09	769	Electrum
5	Grain 5	78.2	21.8	782	Electrum
Average		77.914	22.086	779.14	

Table 11 Gold Fineness of SEM-EDX analysis of gold grains

No.	Element	Au (wt%)	Ag (wt%)	Gold Fineness	Remark
1	Grain 1	82.62	17.38	826.2	Gold
2	Grain 2	85.32	14.68	853.2	Gold
3	Grain 3	85.05	14.95	850.5	Gold
4	Grain 4	87.5	12.5	875	Gold
5	Grain 5	84.03	15.97	840.3	Gold
6	Grain 6	82.86	17.14	828.6	Gold
7	Grain 7	84.19	15.81	841.9	Gold
8	Grain 8	83.62	16.38	836.2	Gold
9	Grain 9	84.18	15.82	841.8	Gold
10	Grain 10	88.13	11.87	881.3	Gold
11	Grain 11	87.1	12.9	871	Gold
12	Grain 12	87.73	12.27	877.3	Gold
Average		85.19	14.81	851.94	

Fluid Inclusion Geochemistry

In the study area, based on the number of phases present at room temperature (Shepherd et al., 1985) and their microthermometric features, two fluid inclusion types were recognized: Type I monophasic aqueous inclusions (L=Liquid), and Type II two-phase (L=Liquid+V=Vapour) aqueous inclusions. Type II is more abundant of the two inclusion types.

Monophasic aqueous inclusions (Type I) of fluid inclusions occur in both quartz veins and are characterized by single phase (liquid or gas) at room temperature. Aqueous two-phase fluid inclusions (Type II) are also seen in both gold-bearing sulphide quartz veins, and deformed quartz veins by a vapour bubble in an aqueous liquid at room temperature with transparency and low relief.

In sulphide-bearing veins (Early Stage), both ice melting and homogenization temperature can be measured and it ranges from 340°C to 403°C and melting temperature ranges from -1.7 to -2.0 (NaCl equiv. wt.% range from 3.01 to 3.53).

In deformed quartz vein (Later Stage), it also has bi-phase inclusions, homogenization temperature can be measured, the range of melting temperature is from -1.3 °C to -1.6 °C and salinity NaCl equiv. wt. % is from 2.31 to 2.83. Homogenization temperature is 320°C to 396°C.

From fluid inclusion data of mineralized quartz veins, it can be deduced that there are two different mineralization phases marked by difference of homogenization temperature and salinity. Fluid inclusion microthermometry data of selected samples is shown in Table 12. Temperature-salinity diagram for various types of ore deposits (Wilkinson, 2001) is shown in Figure 11.

Table 12 Fluid inclusion microthermometry data of selected samples

Sample ID	Host Rock	Host Mineral	Inclusion Type	No. of Inclusion	Homogenization Tem, Range (°C)	Ice Melting Tem (°C)	Salinity (wt% NaCl)	Remarks
PYT-1	quartzite	quartz	L-V	11	340-403	-1.7 to -2	3.01 to 3.53	Sulphide quartz vein (Early Stage)
PYT-2	quartzite	quartz	L-V	10	320-396	-1.3 to -1.6	2.31 to 2.83	Deformed quartz vein (Later Stage)

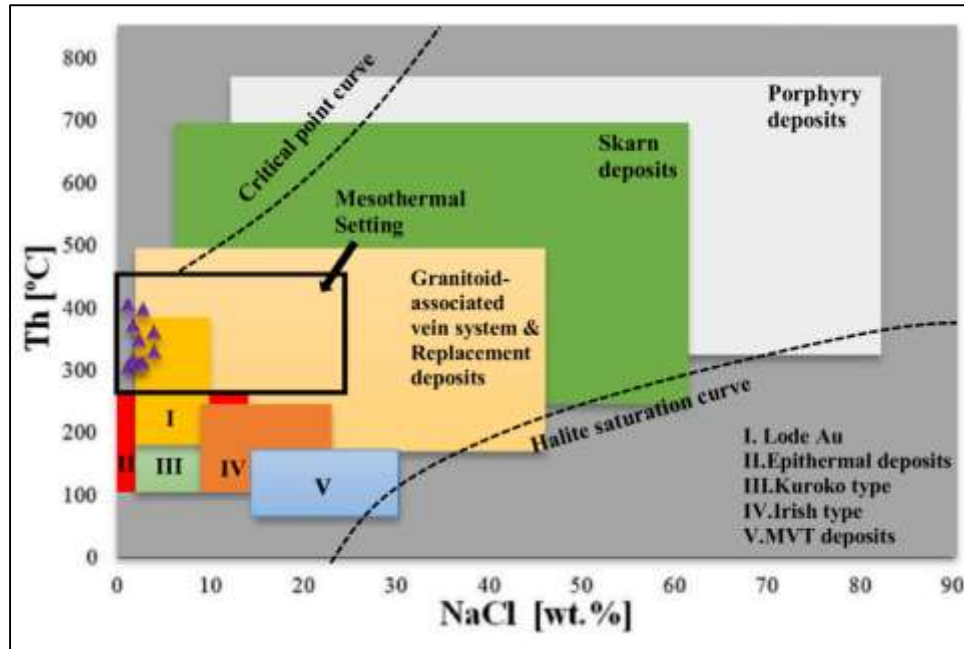


Figure 11 Temperature-salinity diagram for various types of ore deposits (Wilkinson, 2001)

Conclusion

At Taung Ni gold prospect, two types of veins system are found: (1) gold-bearing sulphide quartz vein and (2) auriferous deformed/remobilized quartz vein in strongly brecciated and oxidized zone. In both types of quartz veins, Pearson statistical analyses confirm a strong negative correlation between SiO_2 and other major oxides. The results indicate that the quartz veins were of hydrothermal origin. In both types of quartz veins, the Si-Al discrimination diagram, (Ni-Zn-Co) ternary plot and (Co+Ni+Cu+Zn)-Fe-Mn ternary plot indicate that the quartz veins bearing gold are of hydrothermal origin. In gold-bearing sulphide quartz veins, Ag, As, Bi, Cu, S, Se and Te are strongly correlated with Au. These correlations show that the mineralization indicates the complex nature of hydrothermal system. In auriferous deformed/ remobilized quartz veins, Ag, Fe and Cu are strongly correlated with Au. In the study area, the Co and Ni contents in pyrite show $\text{Co} > \text{Ni}$ and the average ratio for Co/Ni is 2.698. It indicates that pyrites from Taung Ni gold prospect area may be formed under the hydrothermal conditions. The gold fineness shows two ranges: (1) high fineness (826.2 - 881.3) and (2) low fineness (771 - 795). It suggests that Au was remobilized and recrystallized during late stages. Gold mineralization in veins shows two generations as indicated by gold fineness probably suggesting multiple gold depositions. Gold fineness indicates that the Taung Ni gold prospect was formed with the mesothermal setting. From fluid inclusion data of mineralized quartz veins, it can be recognized that there are two different mineralization phases marked by difference of homogenization temperature and salinity. In sulphide bearing vein (Early Stage), homogenization temperature can be measured and it ranges from 340°C to 403°C and melting temperature ranging from -1.7 to -2.0 , salinity NaCl equiv. wt.% range from 3.01 to 3.53. In deformed quartz vein (Later Stage), it also has bi- phase inclusions, the range of melting temperature is from -1.3°C to -1.6°C and salinity NaCl equiv. wt. % is from 2.31 to 2.83. Homogenization temperature is 320 to 396°C . Therefore, it suggests that the Taung Ni gold prospect is considered to be consistent with mesothermal setting.

Acknowledgements

I am deeply grateful to U Than Htay, Deputy Director General (Retired), Department of Geological Survey and Mineral Exploration, Ministry of Mines for his critical reading and improvement of the manuscript.

References

- Aung Ye Ko, Day Wa Aung and Ohn Thwin, (2018c) "Petrography and Mineralogical, Geochemical Investigations of Metamorphic Rocks in Taung Ni Area, Madaya Township, Mandalay Region". *Universities Research Journal 2018, Vol. 11, No.11. University of Yangon, Myanmar.* P 203-224.
- Bajwah, Z.U., Seccombe, P. K., & Offier, R., (1987) "Trace element distribution, Co: Ni ratios and genesis of the Big Cadia iron-copper deposit, New South Wales, Australia". *Mineralium Deposita*, 22(4), 292-300.
- Bonatti, E., Kraemer T., and Rydell H.S., (1972c) "Classification and genesis of submarine iron - manganese deposits. In Ferromanganese Deposits on the Ocean Floor". *IDOE, Columbia University, New York*, pp.149-166.
- Bralia, A., Sabatini, G. & Troja, F., (1979) "A revaluation of the Co/Ni ratio in pyrite as geochemical tool in ore genesis problems: evidences from southern Tuscany pyritic deposits". *Mineralium Deposita*, 14(3), 353-374.
- Brill., B. A., (1989) "Trace element contents and partitioning of elements in ore minerals from the CSA Cu-Pb-Zn deposit, Australia". *Canadian Mineralogist*, 27(2), 263-274.
- Carstens, C.W. (1942) "Uber den Co-Ni-Gehalt norwegischer Schwefelkies-vorkommen: Kgl". *Norske Videnskabs, Selgkabs, Forh.* 15: 165–168.
- Chen, G. Y., (1987) "Genetic mineralogy and prospecting mineralogy". *Chongqing Publishing House, Chongqing*, 874pp.
- Choi, J.M., and Hariya Y., (1992) "Geochemical study of manganese oxide deposits in the Setana area, south western Hokkaido, Japan". *Mining Geology*, 42, 165-173.
- Fisher, N. H., (1945) *The fineness of gold, with special reference to the Morobe gold field*: Econ. Geology, v. 40, p. 449-495 and 537-563.
- Fisher, N. H., (1950) "Application of gold fineness to the search for ore": *Australasian Inst. Mining and Metallurgy Proc.* 156-157, p. 185-190.
- Graton, L. C., (1933) "The depth-zones in ore deposition": *Econ Geology*, v. 28, p. 513- 555.
- Hawley, J.E., (1952) "Spectrographic studies of pyrite in some Eastern Canadian mines", *Economic Geology* 47: 260–304.
- Khin Maung Shwe., 1973. *The Geology of Sedaw-Taung Gaung Area, Mandalay District*. M.Sc Thesis, Department of Geology, University of Mandalay (Unpublished)
- Loftus-Hills, G. & Solomon, M., (1967) "Cobalt, nickel and selenium in sulphides as indicators of ore genesis". *Mineralium Deposita*, 2(3), 228-242.
- Morrison, G.W., Rose, W.J., and Jaireth, S., (1991) "Geological and geochemical controls on the silver content (fineness) of gold in gold- silver deposits". *Ore Geology Reviews*, Vol.6: pp. 333-364.
- Nurmi, P. A., Lestinen, P. & Niskavaara, H. (1991) Geochemical characteristics of mesothermal gold deposits in the Fennoscandian Shield, and a comparison with selected Canadian and Australian deposits. Geological Survey of Finland, Bulletin 351. 101 p.
- Peters, T., (1988) "Geochemistry of manganese - bearing cherts associated with Alpine ophiolites and the Hawasina formations in Oman," *Marine Geology*, vol. 84, no. 3-4, pp. 229–238, 1988.
- Shah, M.T., and Khan A., (1999) "Geochemistry and origin of Mn-deposits in the Waziristan ophiolite complex, north Waziristan, Pakistan". *Mineralium Deposita*. P.697-704.
- Theodore, T.G., Bornhorst, Pekka A., (1998) "Nurmi and Olavi Kontoniemi Geochemistry of gold and associated elements in the Paleoproterozoic Osikonmaki gold deposit, southeastern Finland". *Geological Survey of Finland, Special Paper* 25.81 - 90.
- Wilkinson, J.J., (2001) Fluid inclusions in hydrothermal ore deposits. *Lithos* 55: 229–272.
- Xuexin, S., (1984) "Minor Elements and Ore Genesis of the Fankou Lead-Zinc Deposit, China". *Mineral Deposita* 19: 95 104.

ZEOLITES IN AMYGDALOIDAL BASALTS FROM TONGGE AREA, TIGYAING TOWNSHIP, SAGAING REGION, MYANMAR

Myo Min Tun¹, Thet Tun², Thet Naing³

Abstract

Tongge basaltic field is situated 100 km north of Mandalay in Tigyaing Township, Sagaing Region of Myanmar. It is regarded as an intraplate Quaternary basaltic field and located to the north of well-known Singu-Kabwet basaltic lava field of Central Myanmar. In this study, zeolites filling in the amygdaloids of the olivine basalts from Tongge area have been reported and studied by field observation, transmitted light microscopy and X-ray diffraction analysis. The zeolite group minerals are identified as natrolite, phillipsite, mordenite, laumontite, analcime, and epistilbite. Non-zeolite mineral phases in the amygdaloidal infillings are recognized as smectite, quartz (as amorphous silica), and carbonates. Zeolites and associated minerals are interpreted to be developed possibly as a consequence of late-stage hydrothermal circulation. Moderately to weakly alkaline hydrothermal solutions are responsible for the formation of zeolites in the basalts. Due to the occurrence of different zeolite minerals, it can be deduced that a change in fluid composition occurred as temperature dropped during their formation.

Keywords: Tongge basalt, Amygdaloidal, zeolites, hydrothermal, alkaline

Introduction

Zeolites are crystalline, microporous, hydrous alumina-silicates of alkaline or alkaline earth metals. Framework structure of zeolites consists of [SKO] and [AlO] tetrahedra, which corner-share to form open structures. Such tetrahedra are linked to each other by sharing every O with adjacent tetrahedron to form interconnected cages and channels containing mobile water molecules and alkali and/or alkaline earth cations (Breck, 1974; Barrer, 1982; Gottardi and Galli, 1985; Szoztak, 1998). Zeolites form at low pressures, temperatures, and alkaline pH in the presence of H₂O and possess channels and voids in their structures.

Natural zeolites occur in the rocks of different mineralogical and chemical composition, age and geological environments. They are developed during aqueous fluids reaction with rocks in a variety of geological environments (Breck, 1974; Gottardi and Galli, 1985). Their formation and distribution depend on three main factors (Bargar & Keith, 1995; Chipera and Apps, 2001; Sheppard and Hay, 2001; Utada, 2001); (a) the composition of host rocks, (b) variation in temperature and pressure and (c) the chemistry of pore water. Two main origins were recognized (Iijima, 1980; Gottardi & Galli, 1985; Hay & Sheppard, 2001): (1) those formed under diagenesis to very low-grade metamorphism, resulted from leaching of glass-containing volcanic lavas and tufts by alkaline aqueous solution and (2) those of hydrothermal genesis. Zeolites occurring in volcanic terrains are developed either during burial metamorphism (Neuhoff et al., 1999), hydrothermal alteration (Walker, 1960) or diagenetic processes influenced by the high heat flow in the active geothermal systems (Weisenberger and Selbekk, 2008).

Zeolites are widely used in several applications such as catalysts, adsorbents and ion exchangers (Breck, 1974; Booker et al, 1996; Dixit and Prasada, 1998; Misaelides, 2011; Loiola et al., 2012). Previous studies reported the occurrences of zeolites in late stage pegmatite veins (Orlandi and Scortecchi, 1985, in hydrothermal ore veins (Deer et al., 2004), as alteration products along fault planes (Vincent and Ehlig, 1988), in hydrothermal fractures and veins of granites and

¹ Associate Professor, Department of Geology, Kyaukse University, Kyaukse, Myanmar

² Professor and Head, Department of Geology, Kyaukse University, Kyaukse, Myanmar

³ Professor and Head, Department of Geology, Patheingyi University, Patheingyi, Myanmar

gneisses (Weisenberger and Bucher, 2010, and in hydrothermal alteration of epithermal high-sulfidation system (Tun et al., 2017).

Tonngge basaltic field is situated 100 km north of Mandalay in Tigyaing Township, Sagaing Region, Myanmar (Figure 1) and is regarded as an intraplate Quaternary basaltic field (Tun et al., 2019). It is located to the north of well-known Singu-Kwbwet basaltic lava field of central Myanmar. This study reports natural zeolites filling in the amygdales of intraplate alkali olivine basalts from Tonngge area and investigates the mineralogical characteristics of zeolites and other associated minerals.

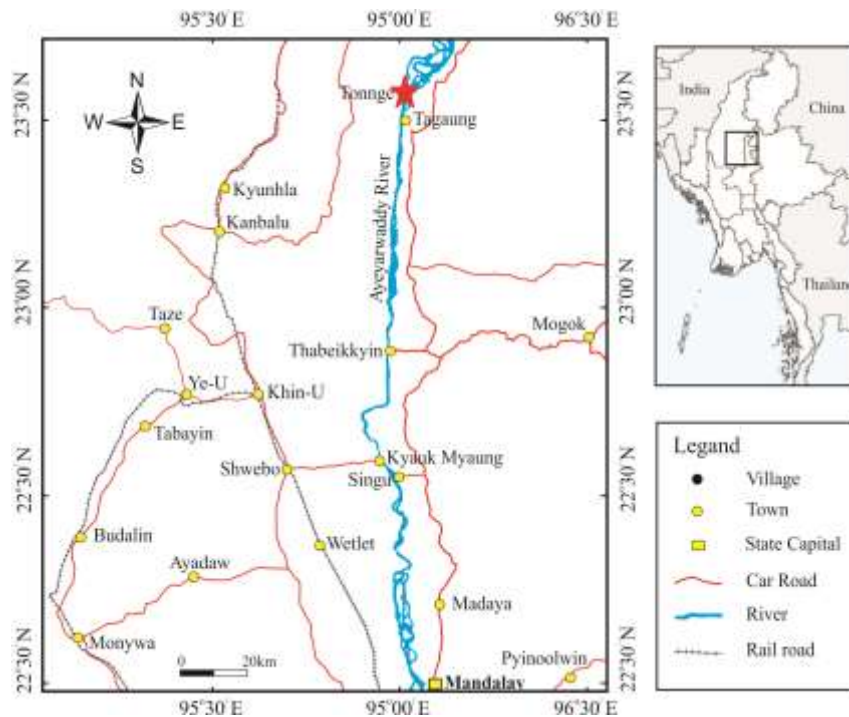


Figure 1 Location map of the Tonngge area, Tigyaing Township, Sagaing Region, Myanmar.

Geology of the Tonngge Area

Basaltic field in the Tonngge area is roughly circular in outline (Figure 2) and consisting of basaltic lava flows. Eruption seems to be occurred from a central vent in the northeastern part of the Tonge Hill and further spread out horizontally to the south-southwest direction. The lavas rest unconformably upon the clastic sediments of Irrawaddy Formation (Upper Miocene-Pliocene). Thus, the age of the basaltic lava field is considered to be post-Pliocene.

The lava flows has an average thickness of less than 5 m (Figure 3a). The fresh surface of the basalts is bluish to dark grey in color (Figure 3b). Their surfaces are often coated by reddish brown iron oxides. The flows are characterized by vesicular nature (Figure 3c) in the upper part whereas columnar in the lower section (Figure 3d). Vertical columns are 4- to 6-sided and 0.3 to 0.5 m across in diameter. Prismatic jointing is common. Dyke-like intrusion is observed in the central-eastern part. In this area, basaltic lava exhibits vesiculation features containing abundant amygdaloidal infillings.

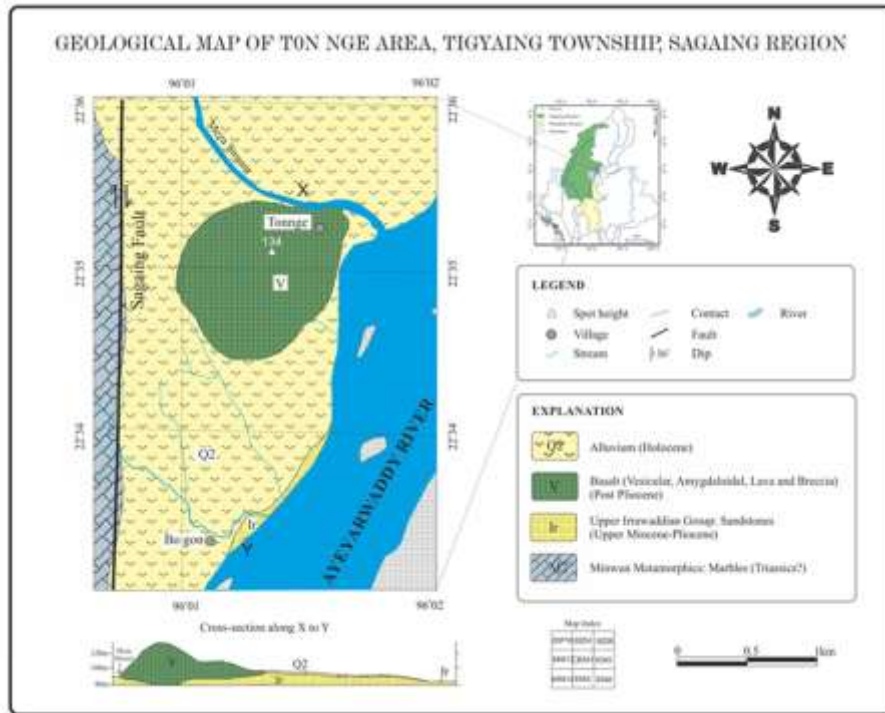


Figure 2 Geological Map of the Tonngé area, Tigyaing Township, Sagaing Region (after Theingi, 2018 and Tun et al, 2019).



Figure 3 Nature of exposure of Tonngé basalts (a) Basaltic lava flow in the western part of the area (b) An exposure of dark grey olivine basalt at the quarry in the central portion of the research area (c) Vesicular basalt in the southern part of the Tonngé area (d) Basalt column in the southeastern part of the study area.

Materials and Methods

Geological fieldworks primarily focusing on the collection of representative samples of natural zeolites-bearing basalts from the Tonngge area have been made. Samples containing zeolites and other secondary minerals filling in amygdales were taken from rock exposures in the quarries. Petrographical and microscopic studies were carried out for the identification of mineral species from the collected samples. A transmitted light polarizing microscope was used to examine the optical properties of zeolites. X-Ray Diffraction (XRD) patterns of zeolites were recorded with a Rigaku RINT-2100 Diffractometer using Cu-K α radiation at 40 kV and 20 mA. Count data were gathered from 2°- 65° two theta ranges operated at 2°/minute scanning rate. Mineral identification used the powder diffraction file (PDF-2) of International Centre for Diffraction Data. Nomenclature used for the description of the zeolite group minerals follows that of Combs et al. (1998).

Results and Discussion

Field Occurrences of Zeolites

A good exposure of zeolite occurrence was observed in a quarry located to the west of Tonngge village. In this locality, zeolites occur in amygdales or cavities of the amygdaloidal olivine basalts. The olivine basalts that usually show a reddish brown weathering surface (Figure 4a, 4b & 4d). Fresh olivine basalts are bluish to dark gray with zeolites developed as void-filling (Figure 4a). Figure 2 shows macroscopic characteristics of zeolites commonly observed in the field. The occurrence and distribution of zeolites and other secondary associated minerals in the amygdales of the basalts are non-uniform and discontinuous in nature. Zeolites generally occur as minerals outlining the cavities and sometimes they completely fill them. They are perfectly rounded (Fig. 4a), elliptical (Fig. 4b and 4d) and irregular in shape (Fig. 4c), and their sizes range from 1–10 cm in diameter (Fig. 4a to 4d).

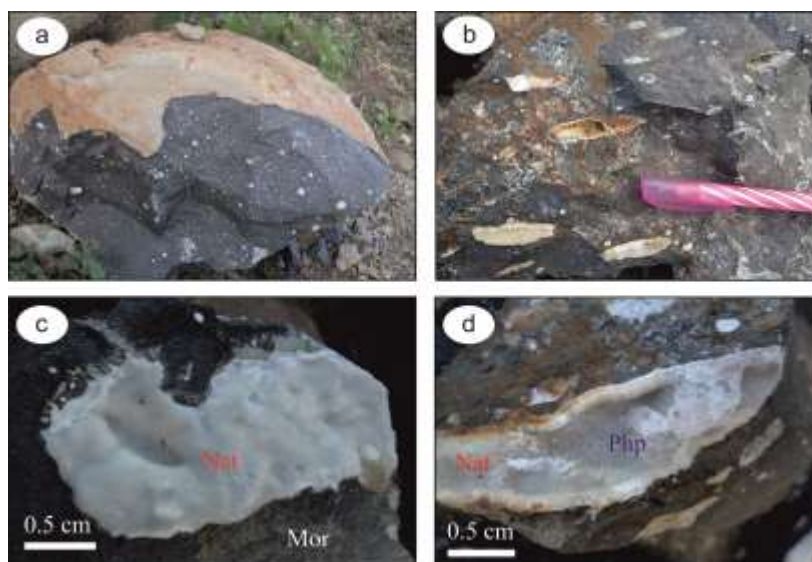


Figure 4 Outcrops nature of zeolite infillings in Tonngge basalt (a) small and rounded amygdales filled by zeolites (b) elongated cavities filled by zeolites and other secondary minerals in the amygdaloidal basalt (c) Large irregular void filled by zeolites (natrolite and mordenite) (d) Large and elongate cavity filled by zeolites (natrolite and phillipsite). Ntr-Natrolite; Mor-Mordenite; Php-Phillipsite.

Vesicles are developed when dissolved gases are escaped during the ascent of lava as a result of pressure drop, forming gas bubbles and leaving the cavities in the upper part of the lava flow. Those vesicles are filled with secondary minerals due to near-surface circulation of meteoric water. Some large amygdales are observed (Figure 4c). Veins development is not observed. Druzy amygdales, having a partial filling, exhibit various types of zeolite minerals. A fibrous zeolite phases displaying a silky luster occupy the outer cavity wall whilst a fibrous interior or granular zeolite phases having a glassy luster occur as an interior padding. Zeolytic phases and other associated minerals such as calcite and smectite in the amygdaloidal basalts were considered to be deposited sequentially from the outer wall to the center of amygdales. The spatial distribution of zeolites is likely to be controlled by the chemistry of host rock, its porosity, and local hydrological and hydrothermal conditions.

Petrography

The basalts from Tonngge area are porphyritic, holocrystalline and consist mainly of phenocrysts of olivine, plagioclase \pm clinopyroxene (Figure 5a and 5b). Olivine is the dominant mineral in the studied samples. The groundmass is intergranular and consists predominantly of plagioclase microlites with subordinate olivine, clinopyroxene, and opaque minerals (titanomagnetite and ilmenite). Parallel and sub-parallel arrangement of plagioclase microlites developing trachytic texture (Figure 5a) is commonly observed in the basalt samples. Glomeroporphyritic texture (Figure 5b) is also observed in the basalt sample by the clustered olivine phenocrysts in the fine-grained plagioclase laths. Absence of quartz and presence of fairly abundant olivine suggest the rocks as alkali olivine basalts.

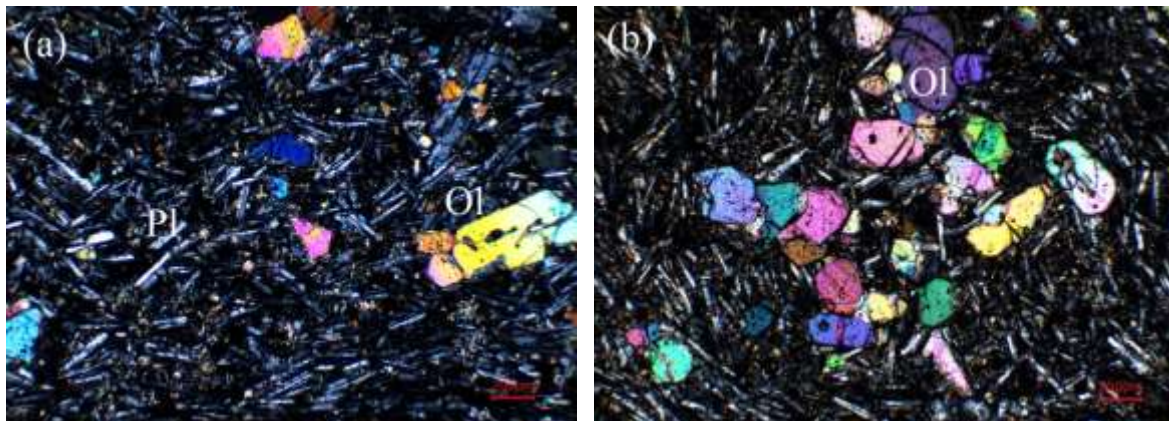


Figure 5 (a) Phenocrysts and microphenocrysts of olivine set in the trachytic plagioclase microlites (b) Glomeroporphyritic texture showing a cluster of olivine phenocrysts enclosed by fine-grained groundmass of plagioclase, olivine and pyroxene. Ol-Olivine; Pl-Plagioclase.

Zeolites are white with silky luster and show a predominance of fibrous aggregates, acicular and radial aggregates (Fig.6a-6d). Most zeolites are relatively coarse-grained and easily identifiable. However, they sometimes occur as fine-grained aggregates and are identified by petrographic microscopy and XRD analyses. Figure 4 illustrates the main microscopic features of the zeolites and associated mineral phases. The common zeolite mineral is natrolite and others include phillipsite, mordenite, laumontite, analcime and epistilbite.

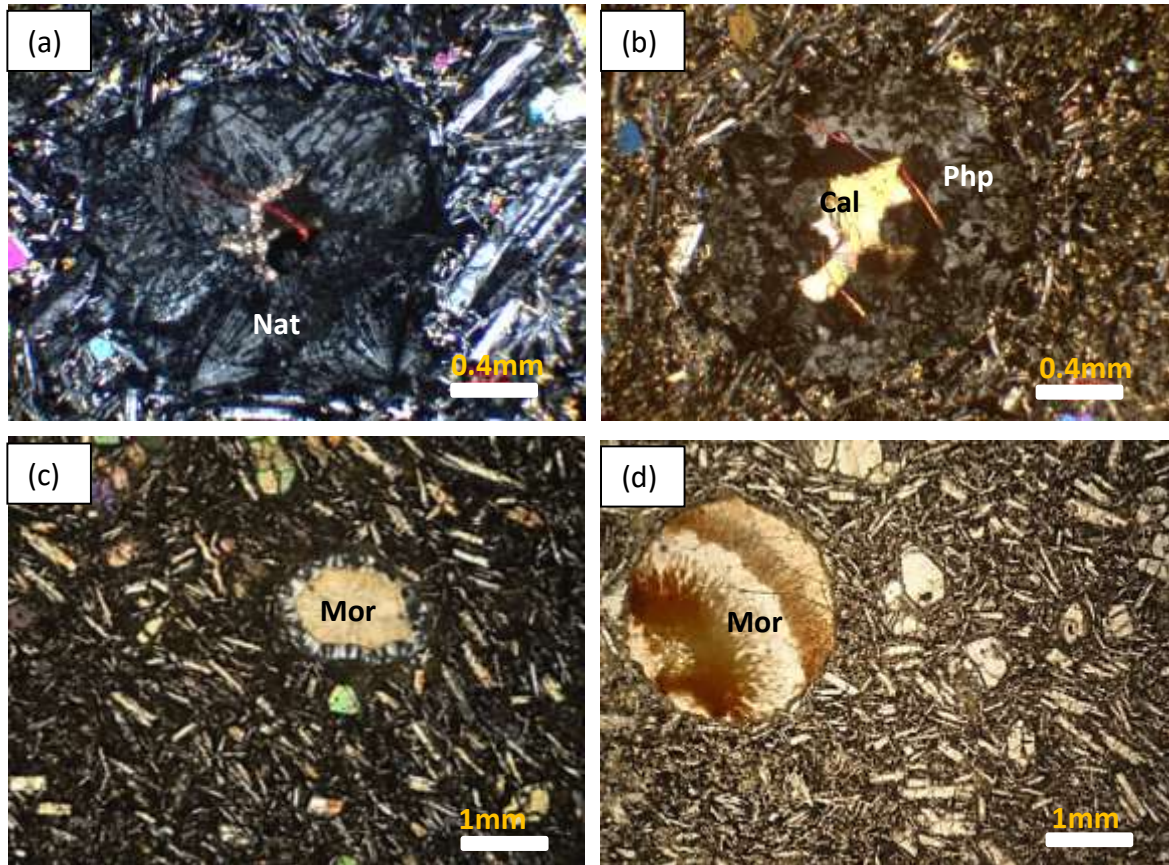


Figure 6 Photomicrographs of zeolites in amygdaloidal basalt of the Tonngne area in thin-section (a and b) fan-shape zeolite (natrolite) enclosing calcite in the cavity of olivine basalt (under XN) (c) Mordenite enclosed by other radial aggregate zeolite in the ellipsoidal amygdale (under XN). (c) Radial and fibrous zeolite (mordenite) completely filling the perfectly rounded cavity in olivine basalt (under PPL). Mineral abbreviations as in Figure 4.

X-Ray Diffraction Analysis

Qualitative XRD analysis enables the identification of the mineral species of zeolite. Figure 7 and Figure 8 illustrate representative zeolites diffraction patterns and associated phases. XRD analysis identifies the zeolite species, including natrolite, as the dominant phase of zeolite, followed by laumontite, phillipsite, analcime, epistilbite and mordenite. Other secondary mineral associated with zeolite was smectite.

Results from the X-Ray Diffraction analysis (Figure 7 and 8) indicate that laumontite has the characteristic peaks having the d-spacings of 9.42Å, 4.16Å and 3.03Å. Phillipsite has characteristic peaks with d-spacings of 7.20 to 7.23 Å, 5.07 Å and 4.16Å. Natrolite is identified in the X-Ray diffractograms by the diffraction peaks with basal spacing of 6.55 Å, 5.89 Å, 4.69 Å, 4.60 Å, and 4.36 Å. Analcime has characteristic peaks with d-spacings of 5.63Å, 3.44Å and 2.93Å. The presence of epistilbite was evident by the XRD pattern exhibiting d-spacings of 3.91Å and 3.76Å. Mordenite is identified by its characteristic diffraction peak with basal spacing of 3.22Å in the X-Ray diffractograms.

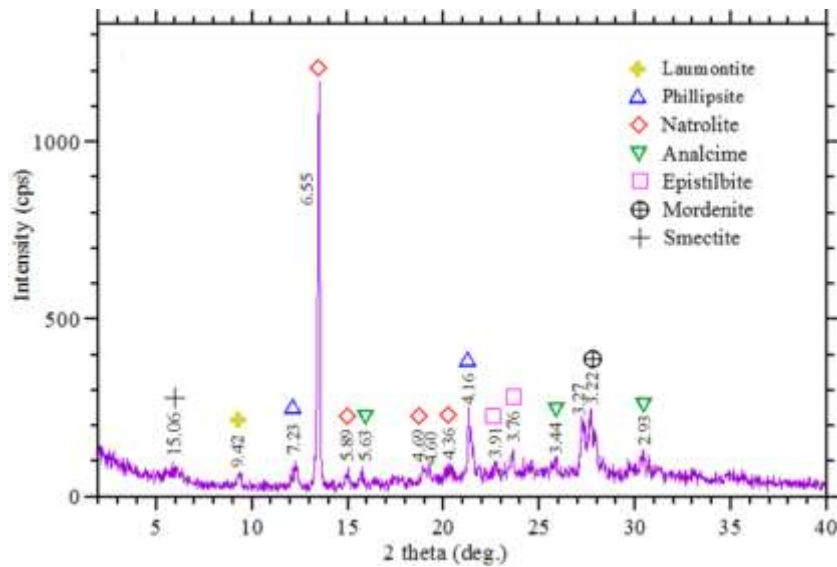


Figure 7 Diffraction pattern of zeolite mineral assemblage and associated phase in amygdaloidal basalt of Tonngge area. It shows an assemblage of natrolite, phillipsite, mordenite, laumontite, analcime and epistilbite. The main zeolytic phases are natrolite, phillipsite and mordenite. Non-zeolite mineral is nontronite.

In addition to zeolite minerals, the XRD pattern also shows the presence of a certain amount of nontronite (smectite) as non-zeolite mineral having its main diffraction peak occurring at 15.06 or 15.06 Å (Figure 7 and 8), provides an evidence for the alteration of pre-existing minerals. Several zeolytic phases were identified in this study which could be organized into five structural groups according to Meier's classification (1968). The heulandite group was represented by laumontite and mordenite. Clinoptilolite group was represented by epistilbite. The analcime group is represented by analcime. The natrolite group was made up of natrolite. Phillipsite belongs to the phillipsite group.

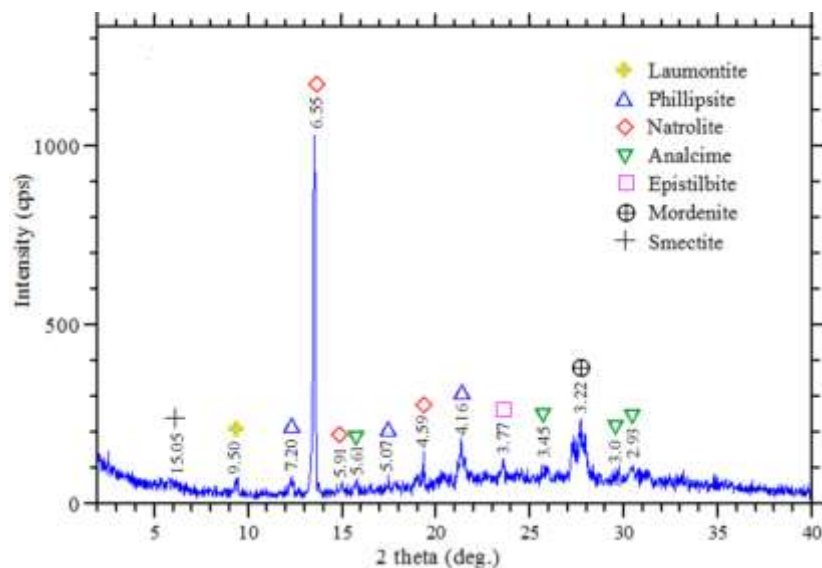


Figure 8 Diffraction pattern of zeolite mineral assemblage and associated phase in amygdaloidal basalt of Tonngge area. It shows an assemblage of natrolite, phillipsite, mordenite, laumontite, analcime and epistilbite. The main zeolytic phases are natrolite, phillipsite and mordenite. Non-zeolite mineral is nontronite.

Formation of Zeolites

Tongge basalt is particularly well-known for its characteristic intraplate character and amygdaloidal texture. The distribution of zeolites in the basalt has been controlled by a combination of factors such as temperature, pressure, hot aqueous fluid circulation and rock's chemical composition (Walker, 1960). The zeolites and associated secondary minerals were deposited from the outer wall to the center of amygdales in the basalts.

Chemical elements necessary for the formation of these mineral phases were released directly as a result of hydrothermal devitrification. Zeolites were probably formed from fluids, which penetrated the vesicles and fractures, but the origin of the fluid remains unknown and yet to be studied. No sequential zoning of zeolites was observed in this study. Non-zeolite and smectite group mineral nontronite was probably formed by basalt devitrification as a result of hydration, although ferromagnesian mineral phases in the basalts may also have been responsible for its formation. Hence, the existence of nontronite along with very well-developed zeolite crystals such as analcime, and phillipsite indicated that nontronite was deposited prior to fibrous zeolites, and suggest low temperature (<100 °C) hydrothermal alteration (Deer et al., 2004).

Phillipsite formation is usually triggered by host basalt low-temperature hydrothermal alteration (~ 90 °C). Ca- and K-rich fluids changed their composition as the temperature decreased (Chipera and Apps, 2001). Depletion of these elements in the fluid during phillipsite formation promoted the introduction of Na-rich zeolites such as calc-sodic analcime, chabazite and natrolite (Cochemé et al., 1994), at lower temperatures (Chipera and Apps, 2001). It was experimentally confirmed that chabazite is stable up to 100 °C, whereas analcime is stable in the temperature range between 100 and 200 °C (Hay and Sheppard, 2001). Chipera and Apps (2001) stated that decreased in Si activity reduced the analcime stability field and promoted natrolite development after analcime and chabazite. This suggested that zeolites formed in the edges of basalt cavities are at higher temperature and lower Si activity during the early stage of crystallization, whereas zeolite species in the central cavity were developed under lower temperature condition and are more aluminous in composition.

Formation of laumontite and stilbite could be attributed to the nature of the hydrothermal fluids associated with pluton emplacement, which were more likely enriched in elements such as Ca, Ba, and Sr produced by a late event, taking into account that they usually appear to be developed as filling fractures in basalts.

Conclusions and Recommendation

Formation of zeolites and associated secondary minerals filling amygdales in basaltic rocks from Tongge area has been documented in this study. Zeolites deposited in vesicles were the result of a hydrothermal process, having a variety of species and this was due to reduced Si activity in the fluid. The variable amounts of silica, alumina and alkali and alkaline-earth cations required for zeolite formation could be resulted either from primary igneous fenocrystal dissolution or the plagioclase alteration reaction that release calcium in the rock matrix. Due to the occurrence of different zeolite minerals, it can be deduced that a change in fluid composition occurred as temperature dropped. Secondary mineral smectite represented the first crystallized species lining the outer part of the cavities. Na-rich zeolites such as analcime, and phillipsite were the first zeolites that became crystallized, followed by acicular-fibrous natrolite and Ca-rich zeolites. The Si activity decreased during alteration and temperature increased to 200 °C thereby allowing analcime formation followed by that of natrolite. Laumontite and stilbite formation could be attributed to the presence of Ca, Ba, and Sr-rich hydrothermal fluids produced by a late event.

It is strongly recommended that SEM-EDS or EPMA analysis of zeolites should be carried out in order to identify the chemical composition of each mineral species, and to interpret the chemical variation among them. It would help understand the sequence of mineral deposition, origin and evolution of these zeolite group minerals in the amygdaloidal olivine basalts of Tongge area.

Acknowledgements

The authors would like to give special thanks to Dr Aung Khin Myint, Rector of Kyaukse University, for his permission to carry out this research. We want to extend our thanks to Dr Su Su Win, Pro-rector of Kyaukse University for her kind support for the present work. We would like to acknowledge the Head of the Tongge Village, Tigyain Township (Sagaing Region) for his kind support during field investigation in the research area.

References

- Bargar, K.E. and Keith, T.E.C. (1995) Calcium zeolites in rhyolitic drill cores from Yellowstone national park, Wyoming. In D.W. Minga, F.A. Mumpton (eds), "Natural Zeolites," International Committee on Natural Zeolites, *Brockport*, New York, pp. 69-86.
- Barrer, R. M. (1982) Hydrothermal chemistry of zeolites," *Academic Press*, New York, 360p.
- Booker, N. A. Cooney, E.L. Priestley, A.J. (1996) Ammonia removal from sewage using natural Australian zeolite," *Water Sci Technol*, Vol. 34, pp. 17-24.
- Breck, D.W. (1974) Zeolite Molecular Sieves: Structure, Chemistry and Use, *John Wiley*, New York, 313p.
- Chipera, S.J. and Apps, J.A. (2001) Geochemical stability of natural zeolites" In: D.L. Bish, D. W. Ming (eds), "Natural Zeolites: Occurrence, Properties, Applications," *Reviews in Mineralogy and Geochemistry*, Mineralogical Society of America, Vol. 45, pp. 117-161.
- Cochemé, J., Aguirre, L., Bevins, R. and Robinson, D. (1994) Zeolitization processes in basic lavas of the Baucarit Formation, Northwestern Mexico, *Rev Soc Geol Chile*, Vol. 21, pp. 217-231.
- Coombs, D.S., Alberti, A., Armbruster, T., Artioli, G., Colella, C., Galli, E., Grice, J.D., Liebau, F., Mandarino, J.A., Minato, H., Nickel, E.H., Passaglia, E., Peacor, D.R., Quartieri, S., Rinaldi, R., Ross, M., Sheppard, R.A., Tillmanns, E. and Vezzalini, G. (1998) Recommended nomenclature for zeolite minerals: Report of the Subcommittee on Zeolites of the Mineralogical Association, Commission on New Minerals and Mineral Names, *European Journal of Mineralogy*, Vol. 10, pp. 1037-1081.
- Deer, W.A., Howie, R.A., Wise, W.S., and Zussman, J. (2004) *An Introduction to Rock-Forming Minerals*," Longmans, The Geological Society, London, 696p.
- Dixit, L. and Prasada, T.S.R. (1998) New approach to acid catalysis and hydrocarbon - zeolite interactions," *Stud Surf Sci Catal*, Vol. 113, pp. 313-319.
- Gottardi, G. and Galli, E. (1985) Natural Zeolites. *Springer-Verlag*, Berlin, Germany, 409p.
- Hay, R. and Sheppard, R. (2001) Occurrence of zeolites in sedimentary rocks: An overview" In: D.L. Bish, D.W. Ming (eds), "Natural Zeolites: Occurrence, Properties, Applications," *Reviews in Mineralogy and Geochemistry*, Mineralogical Society of America and the Geochemical Society, Vol. 45, pp. 217-234.
- Iijima, A. (1980) Geology of natural zeolites and zeolitic rocks. *Pure and Applied Chemistry*, Vol. 52, pp. 2115-2130.
- Loiola, A.R., Andrade, J.C.R.A., Sasaki, J.M., and da Silva, L.R.D. (2012) Structural analysis of zeolite NaA synthesized by a cost-effective hydrothermal method using kaolin and its use as water softener," *J Coll Int Sci*, Vol. 367, pp. 34-39.
- Meier, W.M. (1968) Zeolite structures In: R Szostak (eds), "Molecular Sieves," *Blackie Academic and Professional*, London, pp. 10-27.
- Misaelides, P. (2011) Application of natural zeolites in environmental remediation: A short review," *Micropor. Mesopor. Mat.*, Vol. 144, pp. 15-18.
- Neuhoff, P.S. Fridriksson, T. Arnórsson, S. (1999) Porosity evolution and mineral paragenesis during low-grade metamorphism of basaltic lavas at Teigarhorn, Eastern Iceland," *Am J Sci*, Vol. 299, pp. 467-501.

- Orlandi, P. and Scortecchi, P.B. (1985) Minerals of the Elba pegmatites, *Mineral Rec*, Vol. 16, pp. 353-364.
- Szoztak, R. (1998) Molecular sieves, *Blackie Academic and Professional*, London, 359p.
- Sheppard, R.A. and Hay, R.L. (2001) Formation of zeolites in open hydrologic systems” In D.L. Bish, D.W. Ming (eds) “Natural Zeolites: Occurrence, Properties, Applications,” *Reviews in Mineralogy and Geochemistry*, Mineralogical Society of America and the Geochemical Society, Vol. 45, pp. 261-276.
- Theingi, M. (2018) Petrology and Tectonic Significance of Basaltic Rocks from Tonngge Area, Sagaing Region. MSc Thesis (unpublished), University of Mandalay, Mandalay, Myanmar.
- Tun, M.M., Yonezu, K., and Watanabe, K. (2017) Laumontite Mineralization in the Cijulang High-Sulfidation Epithermal Deposit, West Java, Indonesia,” *In the Proceedings of International Symposium on Earth Science and Technology*, Japan, pp.690-693.
- Tun, M. M., Theingi, M., Khaing, S.Y., Naing, T., Sann, Z.O. and Thin, A.K. (2019) Petrology and Geochemistry of Basalts from Tonngge Area, Tigyaing Township, Sagaing Region, Myanmar, *Open Journal of Geology*, 2019, Vol. 9, No.9, pp. 516-526.
- Utada, M. (2001) Zeolites in hydrothermally altered rocks In D.L. Bish and D.W. Ming (eds). “Natural zeolites: Occurrence, Properties, Applications,” *Reviews in Mineralogy and Geochemistry*, Mineralogical Society of America and the Geochemical Society, Vol. 45, pp. 305-319.
- Vincent, M.W. and Ehlig, P.L. (1988) Laumontite mineralization in rocks exposed north of San Andreas Fault at Cajon Pass, southern California, *Geophys. Res. Let.*, Vol. 15, pp. 977-980.
- Walker, G.P.L. (1960) Zeolite zones and dike distribution in relation to the structure of the basalts of eastern Iceland, *J Geol* , Vol. 68, pp. 515-528..
- Weisenberger, T. and Selbekk, R.S. (2008) Multi-stage zeolite facies mineralization in the Hvalfjörður area, Iceland,” *Int. J. Earth Sci.*, Vol. 98, pp. 985- 999.
- Weisenberger, T. and Bucher, K. (2010) Zeolites in fissures of granites and gneisses of the Central Alps,” *J Metam Geol*, Vol. 28, pp. 825-847.

ECONOMIC GEOLOGY OF THE HOPANG AREA, ‘WA’ SELF-ADMINISTERED DIVISION IN THE NORTHERN SHAN STATE, MYANMAR

Zar Ni Swe¹, Si Si Mar², Ali Akbar Khan³, Myo Min³

Abstract

The investigated area is situated in Hopang Township, “Wa” Self-Administered Division in northern Shan State, Myanmar. This area is mainly composed of various lithologic units ranging in age from Precambrian to Mesozoic. Precambrian units are mostly metasedimentary rocks and Paleozoic to Mesozoic units are carbonate and clastic sedimentary rocks. A number of known lead-zinc mines within the Shan Plateau lie in a broad NE-SW orientated belt extending from the Shan Scarp in the west up to the Chinese border in the east. Hopang area is economically important because the sizeable Pb-Zn-Cu mineral deposits are well developed at Hpalin mine. The carbonate-hosted Pb-Zn-Cu veins are observed as fissure filling and cavity filling types occurred along the northeast-southwest striking fault. The major ore minerals such as pyrite, chalcopyrite, sphalerite and galena are associated with the lesser amount of azurite, malachite, chalcocite, bornite, arsenopyrite, chrysocolla and laurionite. Limestone, dolomite and porphyritic biotite granite are mostly abundant and they are used for industrial materials, construction materials and decorative stone.

Keywords: Hopang, Shan Plateau, Hpalin mine, industrial materials, construction materials

Introduction

Location of the study area

The study area is situated in the Hopang Township, ‘Wa’ Self-Administered Division in the northern Shan State. It is located about 156 km NE of Lashio Township. This area lies between the North Latitude 23° 19' 00" to 23° 26' 30" and East Longitude 98° 42' 30" to 98° 48' 00" in UTM map sheet No.2398 (11and15). It covers about 48 square miles. Lashio-Chinshwehaw Highway passes through the northern part of the Hopang Area. The location map of the study area is shown in (Fig.1).

The present study area is economically important because the sizeable Pb-Zn-Cu mineral deposits are well developed at Hpalin mine. Industrial raw materials, such as limestone and dolomite are present extensively in the study area.

¹ Associate Professor, Department of Geology, Shwebo University

² Lecturer, Department of Geology, Kyaukse University

³ Professor (Retd.), Department of Geology, University of Mandalay

³ Professor, Department of Geology, University of Mandalay

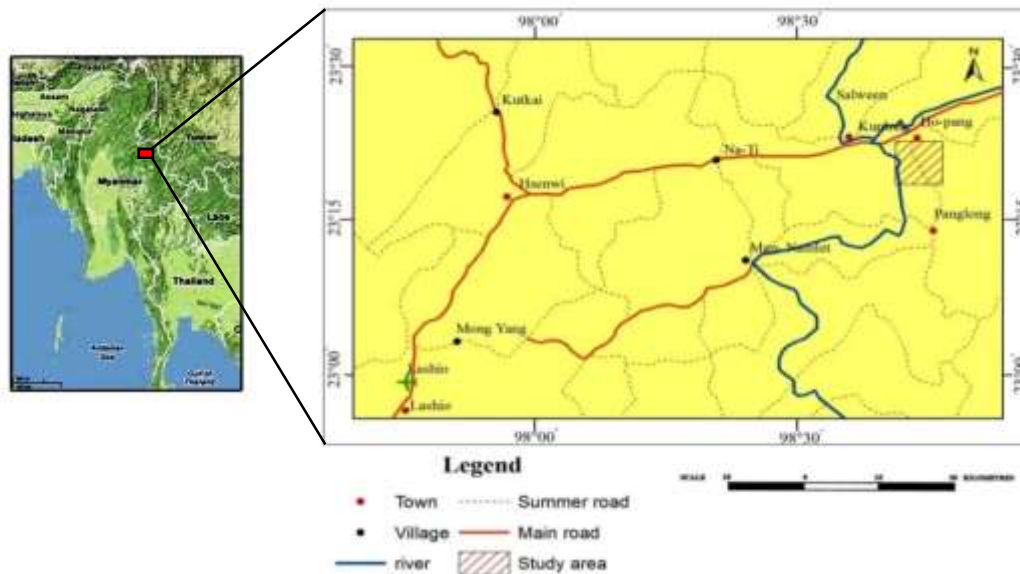


Figure 1 Location map of the Hopang Area, Northern Shan State.

General Geology of the Hopang Area

The study area lies in the Shan-Tanintharyi Block (Mg Thein, 2014). It is situated in the Shan Plateau (Eastern Highlands) which is generally trending NNE-SSW direction. The Shan Plateau largely comprises a series of Ordovician-Triassic dominantly carbonate rocks overlying the Precambrian metasedimentary rocks of the Chaung Magyi Group, the Cambrian Panyun Formation and associated Bawdwin Volcanics (Mitchell et al., 1977). Major lineament identified from satellite image of the area is Momeik Fault, trends approximately ENE-WSW in direction. Moreover, the area lies between the Momeik Fault (Nanting) in the north and Lashio Fault in the south.

The Hopang area is mainly composed of various lithologic units ranging in age from pre-Paleozoic to Mesozoic sediments which are shown in geological map of the Hopang area (Fig.2). They are the Precambrian Chaungmagyi Group (La Touche, 1913) near Nan-pi and Pan-kauk Villages, Cambrian Panyun Formation (Brown, 1917) near the Hsup-kun village, Ordovician Sitha Formation (Ko Ko Gyi, 1991) near the Har-phyat village, Silurian Nyaungbaw Formation (I.G.C.P, 1980) Narzayet-Pangmong car-road, Plateau Limestone (La Touche, 1913; Aye Ko Aung, 2012) Hen-na Village and car-road between Hopang to Hpa-lin mine and Nwabangyi Dolomite Formation (Garson et al., 1976) car road between Hopang to Chushwe, near Naung-san and Hpa-kyut Villages, and Late Jurassic Hsipaw Red Bed (Brunnschweiler, 1970) Naung-hate, Na-za-yet villages and road cut section from Ma-hwe to Hwai-pon. Good exposures can be observed along the road cutting side. The porphyritic biotite granite boulders are well exposed along the streams section and eastern part of Thanlwin River (Mitchell, 1977) along the Hpa-lin and Chu-shwe, Tong-ma-ka Village, Nam-leng Chaung, Nam-hkan Chaung, Mong-kun Chaung, and near the Hsup-kun Village. Some metamorphosed limestones are well observed near the Hpa-lin mine and Pan-kauk Village.

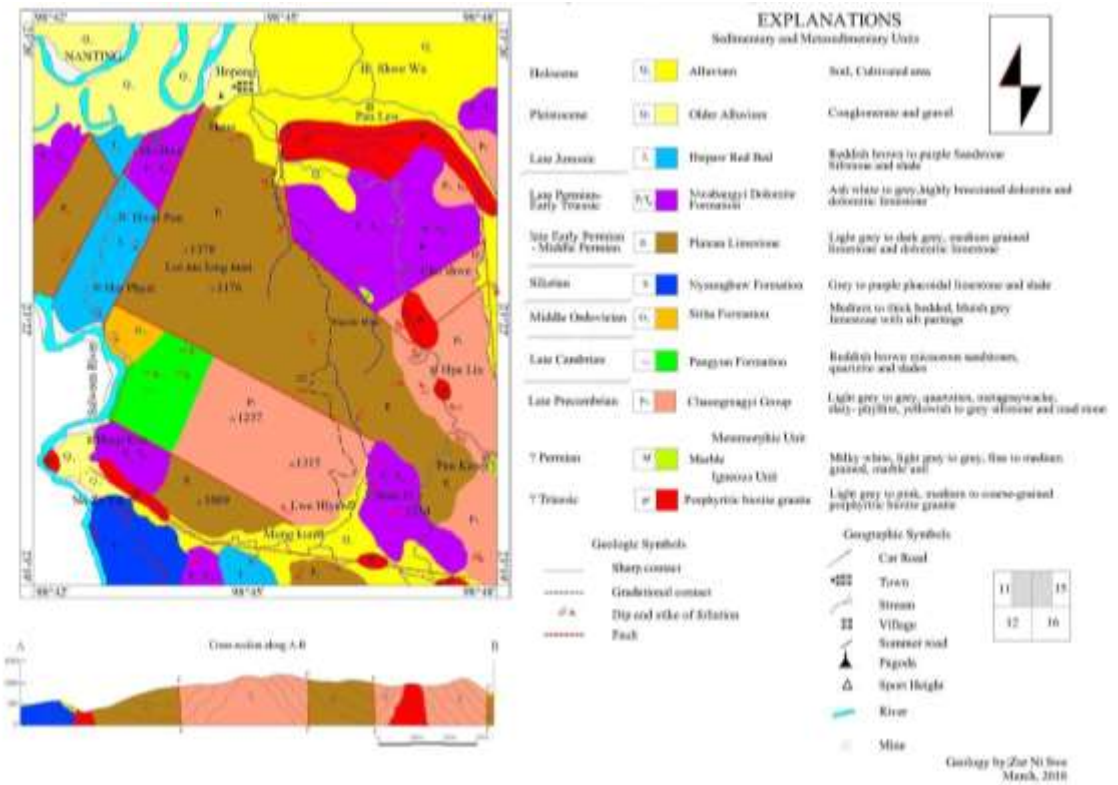


Figure 2 Geological map of the Hopang area, Northern Shan State.

Mineral Resources

A number of known lead-zinc mines within the Shan Plateau lie in a broad NE-SW orientated belt extending from the Shan Scarp in the west up to the Chinese border in the east (Gardiner et al., 2016) (Fig. 3A). The carbonate-hosted lead-zinc-copper veins are observed as fissure filling and cavity filling types. The hydrothermal solution enters the fractures and it does dissolve the country rocks.

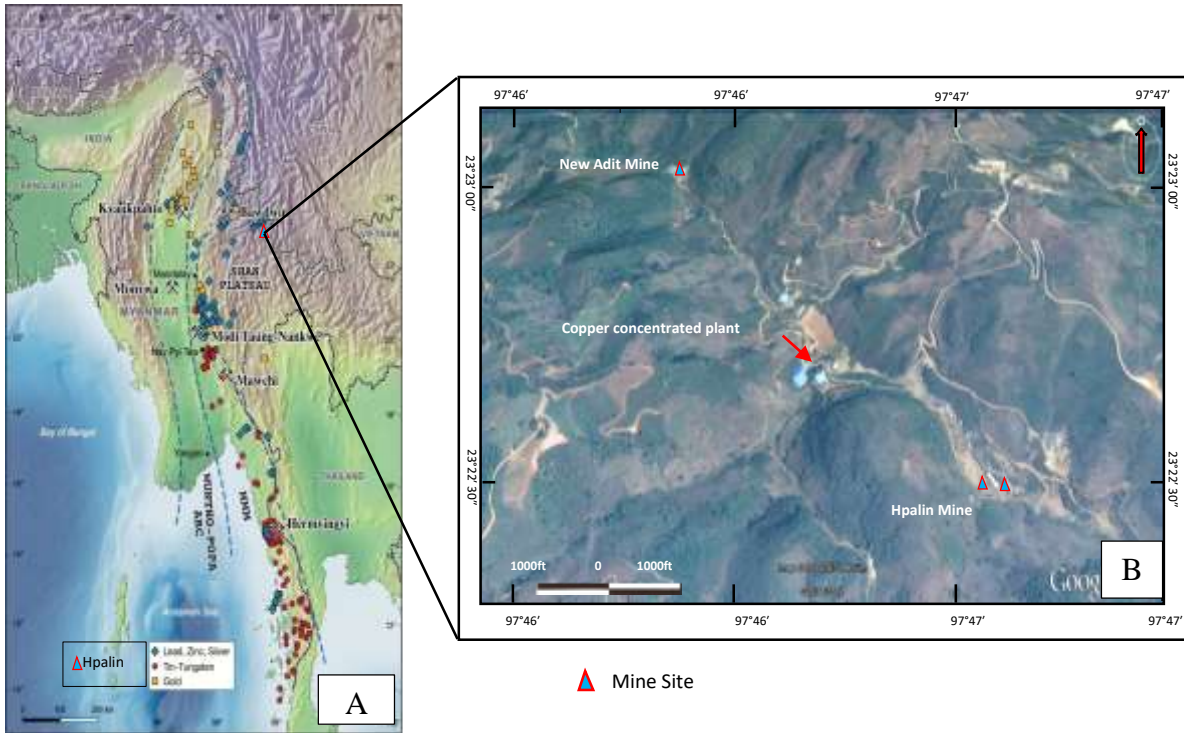


Figure 3 (A) Map showing locations of primary lead-zinc, tin-tungsten and gold deposits and working in Myanmar. (After Gardiner et.al, 2016)
 (B) Location of Hpalin mine site, at Wa area. (Source: Google Earth)

Hopang area has been famously known as Hpalin lead-zinc-copper mine since British colonial time and until recently very limited production has been done (Fig.3B). Available descriptions indicate dominantly limestone host rocks, with reference to old workings and slag dumps suggesting a reasonably long history of mining to the British colonial era or before, and noted grades ranging from around (1-10) % Pb or Zn, up to (40, 50, 80) % Pb or Zn (with Fe grades noted also, occasionally). The mineralization consists of galena, sphalerite, chalcopryite, pyrite and magnetite (Fig.4) and (Fig.5).



Figure 4 Observation of ore minerals extracted from Hpalin mine during Unity E&R field trip.



Figure 5 High-grade copper ore minerals exposed near the Hpalin mine during Unity E&R field trip.

Hpalin Mine

Hpalin mine (N 23° 22' 42.0", E 98° 46' 43.3") is located at 12 km from the border of mainland China and stands at the elevation of the 884 m in the northern Shan State (Fig.6). This area lies between the two principal cross-faults (Momeik and Mongkun) and most of mineralization zones are contacting with granite and marble (or) limestone.



Figure 6 Main production of lead-zinc-copper ore minerals working at Hpalin adit mine in 2014 (N 23° 22' 31.0", E 98° 46' 58.4")

In general, lead-zinc-copper mineralized zone occurred along the northeast- southwest striking fault. The lead-zinc-copper mineralization in study area has been controlled by regional structure. The igneous activity manifested in the east of the area must have been the source of the silica and subsequent sulfide which were brought into the fractures and cavities caused by faulting. They are found as stringers, veinlets, lenticular and banded nature. The mineralization occur Permian Plateau Limestone which consists of light grey to grey, thick-bedded to massive carbonates. The major ore minerals such as pyrite, chalcopyrite, sphalerite and galena are associated with the lesser amount of azurite, malachite, chalcocite, bornite, arsenopyrite chrysocolla and laurionite (Fig.7). Subsequent oxidation and near-surface alterations resulted in some iron oxide in the upper part. From the surface to the depth 100 m, mineralized zone is striking nearly north-south direction and dipping 60° east in direction. The width of the mineralized zone is about 20- 30 m and the length of strike is about 100-150 m. At the deeper level of the mine, the mineralized zone is hard and compact.

A few years ago, Chinese Company was producing high-grade copper and also builds copper concentrated plant (Fig.8). Recently, all operations were shut down as Chinese company cheated on their partners.

Rock Resources

In the study area, limestone, dolomite and porphyritic biotite granite are mostly abundant and they are used for industrial materials, construction materials and decorative stone.

Plateau Limestone

Plateau Limestone is exposed in the middle part and south western part of the study area. The calcitic limestone is more resistant to weathering and most of the ridges are commonly occupied by very steep hill sides with irregular surface topography (Fig.9). Good exposures can be observed near the Hen-na Village and between the car-road from Hopang to Hpa-lin mine (Fig.10).

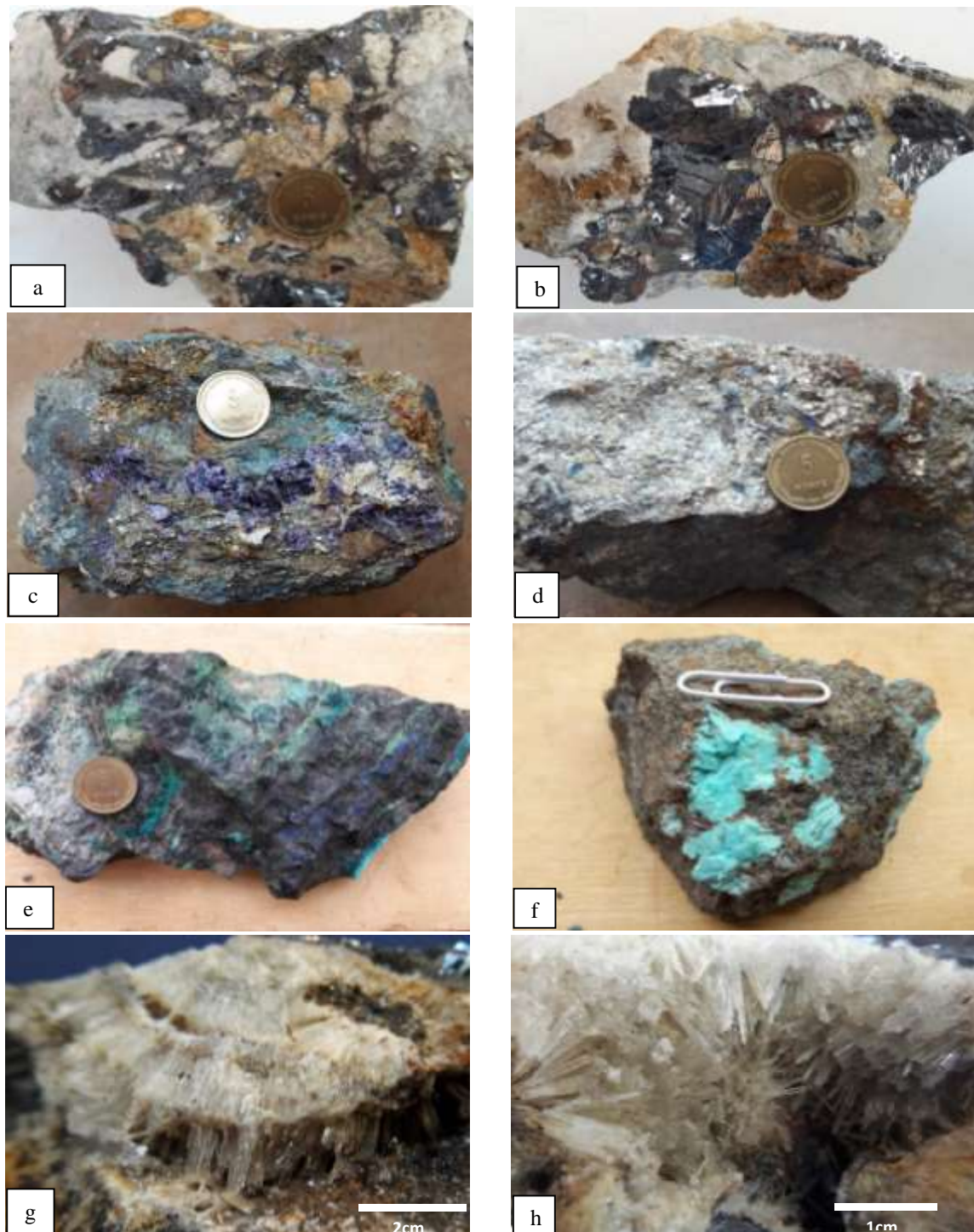


Figure 7 Ore samples collected from Hpalin mine.

(a-b) Very coarse euhedral galena crystals (c-d) High-grade copper sulfide ore (e) Secondary copper minerals of malachite (pale green) and azurite (blue) (f) Chrysocolla (copper silicate) mineral (g-h) Fibrous and acicular form of laurionite crystals.

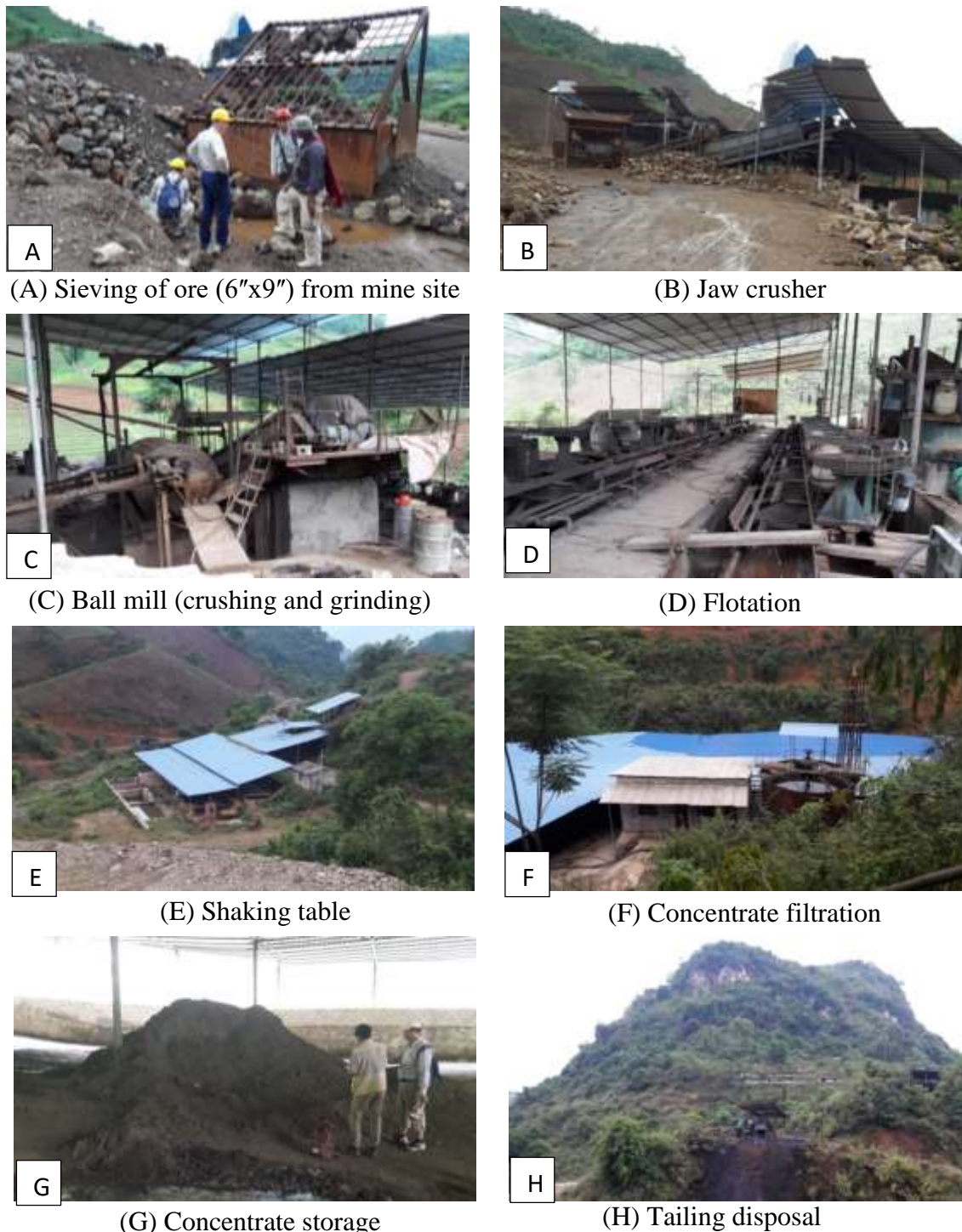


Figure 8 Photographs showing the process of copper concentrated plant that production for lead-zinc-copper ore minerals at Hpalin mine.

Nwabangyi Dolomite Formation

This formation is well exposed in north eastern part and central part of the study area. This unit is occupied by scanty vegetation and display low-lying, rolling knolls. In many places, this unit is covered either by a thick residual terra-rossa soil or by grass. The dolomites have a characteristically shattered appearance on fresh and weathered surfaces. Good exposures can be observed at the car road section between Hopang to Chushwe Village (Fig.11) and near the hydroelectric power (Fig.12).



Figure 9 Outcrop nature of Plateau Limestone near the Hen-na Village.



Figure 10 Thick-bedded to massive, light grey Plateau Limestone unit exposed near Hopang.



Figure 11 Highly brecciated Nwabangyi Dolomite Formation exposed along the car road section



Figure 12 Light grey to grey, medium to thick bedded, highly brecciated dolomite.

Porphyritic biotite granite

The granite intrusive bodies are extensively found along the streams section (Fig.13). In the eastern part of the Thanlwin River, various sizes of rounded granite boulders are also well observed near the Hsup-kun Village (Fig.14).



Figure 13 The spheroidal weathering of granite boulder exposed on Nam-leng Chaung.



Figure 14 The smooth surface and well-rounded granite boulders exposed in the eastern bank of Thanlwin River.

Findings and Discussion

The important minerals, such as copper, lead, and zinc are found at Hpalin mine. Copper is primarily used for electrical applications because it is an excellent conductor of electricity. An important use of lead is in batteries; among its many other applications and is used in paints and ceramics. The zinc coating on steel cans keeps the cans from rusting and zinc is also used in the manufacture of brass and other alloys.

Limestone and dolomite are used as fluxing materials in iron and steel industry. Limestone is used in cement factory, paper mill, agricultural dressing and water purification. Lime is mainly consumed in building trade, but it is applicable in the chemical industries and is an important fertilizer. The various sizes of angular pebbles and conglomerate are applied as paving-stone of floor slab, table, chair, vase, paper-weight, etc., and also used in building houses and walls. Light to pink colour porphyritic biotite granite is used for flagstone (Fig.15). Phacoidal limestone of Nyaungbaw Formation and white marble unit can be used as a decorative stone. Highly brecciated dolomite or dolomitic limestones used as construction and building materials. The broken pieces of limestones are used as road ballast, construction and building materials (Fig. 16). Gravels and sand from Thanlwin River are used as construction material and road materials.



Figure 15 Photograph shows the making of flagstones, cut off from the decorative stones.



Figure 16 Construction materials are produced from Plateau Limestone at quarry site.

Therefore, the economic potential of Hopang area is very interesting and the local Company has planned to exploit the ore from this mine with Unity (Energy & Resources) Australia Company.

Conclusion

Hopang area is located in the Shan Plateau which is generally trending NNE-SSW direction. This area largely comprises the Precambrian Chaung Magyi Group, Panyun Formation, Sitha Formation, Nyaungbaw Formation, Plateau Limestone, Nwabangyi Dolomite Formation and Hsipaw Red Bed. The porphyritic biotite granite and some metamorphosed limestone are observed near the Hpa-lin mine. The famously known Hpalin lead-zinc-copper mine since British colonial time and until recently very limited production has been done and noted grades ranging from around (1-10) % Pb or Zn, up to (40, 50, 80)% Pb or Zn (with Fe). The major ore minerals such as pyrite, chalcopyrite, sphalerite and galena are associated with other sulfide minerals. In the study area, limestone, dolomite and porphyritic biotite granite are mostly abundant and they are used for industrial materials, construction materials and decorative stone.

Acknowledgements

The authors are deeply thankful to Dr Than Than Nu, Professor and Head of Geology Department, University of Mandalay, for her kind permission to carry out field works in this area. We also thank to Professor Dr Khin Khin Lin, Head of geology Department, Shwebo University for her guidance and valuable suggestions. The authors also acknowledge to U Aung Soe Min (WSAD), Pan-Khun Company, for willing help, arrangement for field trip and giving facilities during the field investigation. Special thanks are due to U Khin Maung Si, Director (Retd.) D.G.S.E, Chief Geologist, Unity Energy and Resources Co.Ltd, Managing Director, High Land Hopang Resources, for encouragement and help during this field work.

References

- Aye Ko Aung (2012). The Paleozoic Stratigraphy of Shan Plateau, Myanmar-An Updated Version. *Journal of the Myanmar Geosciences Society, Special Volume 5(1)*: 1-73.
- Brown, J.C., and Sondhi, V.P., (1933). The geology of the country between Kalaw and Tounggyi, Southern Shan State: *Rec. Geol. Surv. India*, vol.67, pt.2.
- Brunnschweiler, R.O., (1970). Contributions to the post-Silurian geology of Burma. *Geological Society of Australia*, v.17, pp.59-79.
- Gardiner, N.J., Roob, L.J., and Searle, M.P., (2016). The Metallogenic Provinces of Myanmar, *Applied Earth Science*, 123:1, 25-38p.
- Garson, M.S., Amos, B.J. and Mitchell, A.H.G., (1976). The geology of the area around Nyaungga and Ye-ngan, southern Shan State, Burma; *Overseas Men, Inst. Geol. Sci.* No.2: pp.19-30
- I.G.C.P (Burmese National Committee), (1980). Stratigraphic Committee field excursion in the Maymyo-Yadanatheingi-Hsipaw and Bawdwin areas. Field Excursion No.7, 1-29.
- Ko Ko Gyi, (1991) Geology and Mineral Resources of the Kywenadauk-Okhpho Area, Pyinoolwin Township, M.Sc. Thesis (unpublished), Geol. Dept., Mandalay University.
- La Touche, T.H.D. (1913). Geology of the northern Shan State. *Memoirs of the Geological Survey of India 39(2)*: 1-379.
- Maung Thein (2014). Geological Map of Myanmar: Compiled and updated by Myanmar Geosciences Society, Explanatory Brochure, 34p.
- Mitchell, A.H.G., Marshall, T.R., Skinner, A.C., Baker, M.D., Amos, B.J., and Bateson, J.H. (1977). Geology and exploration geochemistry of the Yadanatheingi and Kyaukme-Longtawkno areas, northern Shan State, Burma. *Overseas Geol. Miner. Res.*, 51: 35.

GEOCHEMICAL INVESTIGATION OF CHROMITITES IN ULTRAMAFIC ROCKS OF TAUNG-PI-LA AREA, KALAY TOWNSHIP, SAGAING REGION

Tun Tun Min¹, Tint Swe Myint², Zam Khan Mang³

Abstract

Taung-Pi-La Area is situated about 3.84 miles (6.22 kilometers) west of Kalemmyo, Sagaing Region. The principal rock types of the Taung-Pi-La Area include harzburgite, dunite and serpentinites which are formed during Late Jurassic to Early Cretaceous. Exposures of pyroxenite were observed in the research area. Seven chromitites occurred in the Taung-Pi-La ultramafic rocks. Chromitite are massive, nodular and disseminate types displaying pull-apart, cataclastic, net and clot textures. Among the chromite grains, the interstitial silicate of olivine, orthopyroxene and serpentine are found. X-ray diffraction (XRD) of chromitites of the Taung-Pi-La Area shows magnesiochromite ($MgCr_2O_4$) type. Chromitite composition is characterized by Cr_2O_3 ranging from 27.10 to 59.43 wt.%, Al_2O_3 from 7.36 to 26.60 wt.%, MgO 8.27 to 26.80 wt.%, and FeO ranges from 4.37 to 14.66 wt.%. The maximum Fe_2O_3 content is 2.45 wt% and TiO_2 is always below 0.18 wt%, as typical for podiform chromitites and ophiolitic chromitites. The high-Cr chromitites are typically hosted in highly depleted harzburgites. In the TiO_2 vs. Cr_2O_3 , $Mg\#[Mg/(Mg+Fe^{2+})]$ versus $Cr\#[Cr/(Cr+Al)]$ and TiO_2 vs. Fe^{2+}/Mg diagrams, most of the chromitites belongs to the podiform chromitites. The trivalent ion plot ($Cr-Al-Fe^{3+}$) and Al_2O_3 vs Cr_2O_3 of chromitite compositions show that chromitites are derived from mantle source. According to the TiO_2 and Al_2O_3 diagram, chromitites of the Taung-Pi-La Area are formed in the supra-subduction zone (SSZ).

Keywords: pull-apart and cataclastic textures, magnesiochromite, podiform chromitites, supra-subduction zone

Introduction

The research area is situated about 3.84 miles (6.22 kilometers) west of Kalemmyo, Sagaing Region. The area is bounded by N latitude $23^\circ 11'$ to $23^\circ 12' 10''$ and E longitude $93^\circ 58' 30''$ to $94^\circ 00' 30''$. It lies in UTM map sheet No.2393 16 and 2394 04 composite. It extends about 1.36 miles (2.18 kilometers) from north to south and 2.12 miles (3.40 kilometers) from east to west, covers 2.88 square miles (7.41 square kilometers). The location map of the research area is shown in Fig. (1). S of the Bhopi Vum the WNW-SSE trending hill of Taung-Pi-La is situated within the alluvial plain. The aeromagnetic map shows a direct connection with the Bhopi Vum. The topography of this area is generally low-lying in the eastern part, but it is higher and fairly rugged in the middle part. It is the dismembered incomplete ophiolite belt with nickel and chromite mineralization. The purpose of this study is to outline the geochemistry of chromitites and associated ultramafic rocks, and also to give some constraints on the petrogenesis of chromitites in this area.

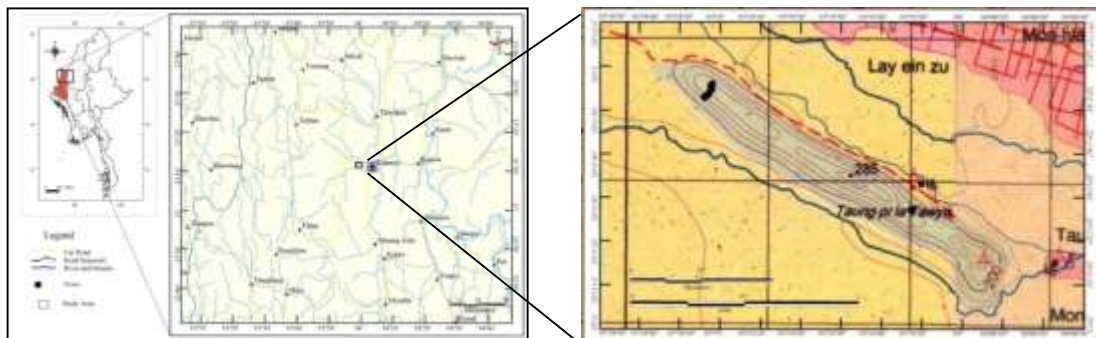


Figure 1 Location map of the research area.

¹ Dr, Associate Professor, Department of Geology, Shwebo University

² Dr, Associate Professor, Department of Geology, Kalay University

³ Assistant Lecturer, Department of Geology, Kalay University

Materials and Methods

Identification of textural relationships of chromitites was investigated microscopically on polished thin sections under reflected light ore microscope. Six representative chromitite samples collected from the research area have been selected and analyzed by X-ray fluorescences (XRF), X-ray Analytical Microscope (XGT 5200, HORIBA Scientific) and X-ray diffraction (XRD) at Mandalay University Research Center and Department of Research and Innovation (Naypyidaw).

General Geology

The Kalemio ophiolite outcrops at the eastern margin of the Indo-Burma Range and consists of huge ultramafic massifs (Mwe Taung, Bhopi Vum and Webula) as well as small ultramafic massifs (Taung-Pi-La) but little mafic rocks. The principal rock types of the Taung-Pi-La Area include harzburgite, dunite, serpentinite and pyroxenite. Podiform chromitite (massive, nodular and disseminate) are observed in the research area. Chlorite schist are rare occur. Pyroxenites and chlorite schist are not mappable. Mitchell *et al.*, 2015 argued that the ophiolites are best explained by the Late Jurassic or Early Cretaceous (ca.end-Jurassic) continental collision on a Medial Myanmar Suture Zone, prior to development of the west-facing Popa-Loimye arc system to the west. The geological map of the research area is shown in Fig. (2).

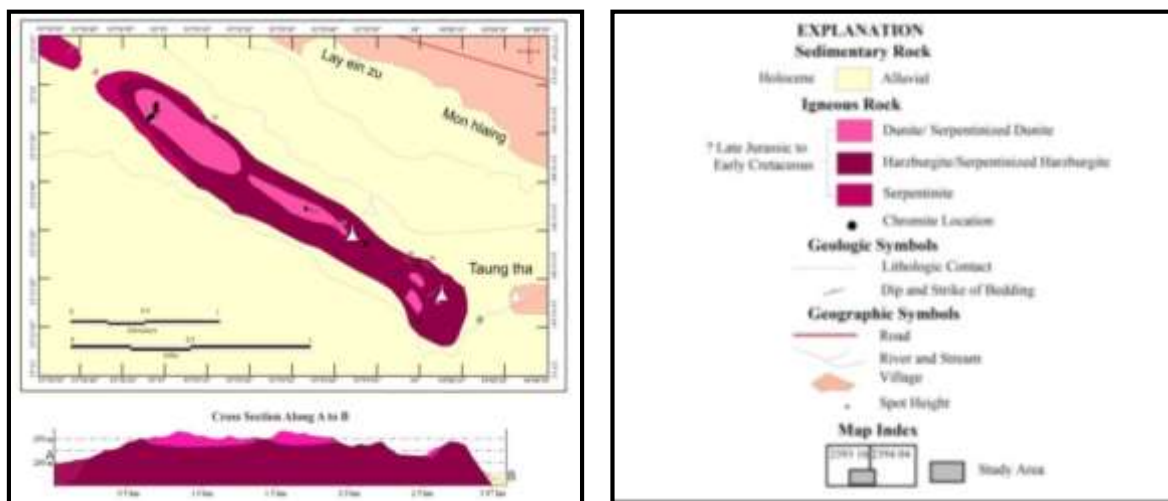


Figure 2 Geological map of the research area (Tun Tun Min *et al.*, 2019).

Occurrences and Types of Chromitites

Seven chromitites were collected in the Taung-Pi-La Area (Fig. 2). The chromitites bodies are typically lens shaped, although many occur as tabular like bodies (Fig. 3A), but some occur as veins and stringers in dunite (Fig.3B).The chromite mineralization is concentrated along the western part of Taung-Pi-La. The boundaries of the chromitite pods with enclosing dunite are generally sharp (Fig.3C). Chromitites of the research area display massive, nodular (Fig. 3D) and disseminated types.

Petrography of Chromitites

Chromitites in the research area are composed of coarse-grained aggregates of chromite and silicate minerals (as in matrix). The chromite grains are subhedral to euhedral in shape and vary in size from 0.03 to 1 mm. It shows black colour with brownish and yellow tinge under ore microscope. The matrix is composed of olivine and serpentine group of minerals plus minor

chlorite. Most of the chromite grains showed pull-apart and cataclastic texture (Fig.4A). In massive ores, the small interstitial chromite grains are found to be rounded and corroded (Fig.4B). Segregation of finer subhedral grains in the interspaces of coarsely granular chromite mosaic was described as clot texture by Mukherjee (1969) (Fig.4C). Chromites intercumulus chromite grains are joined together to form net-texture (Fig.3D).

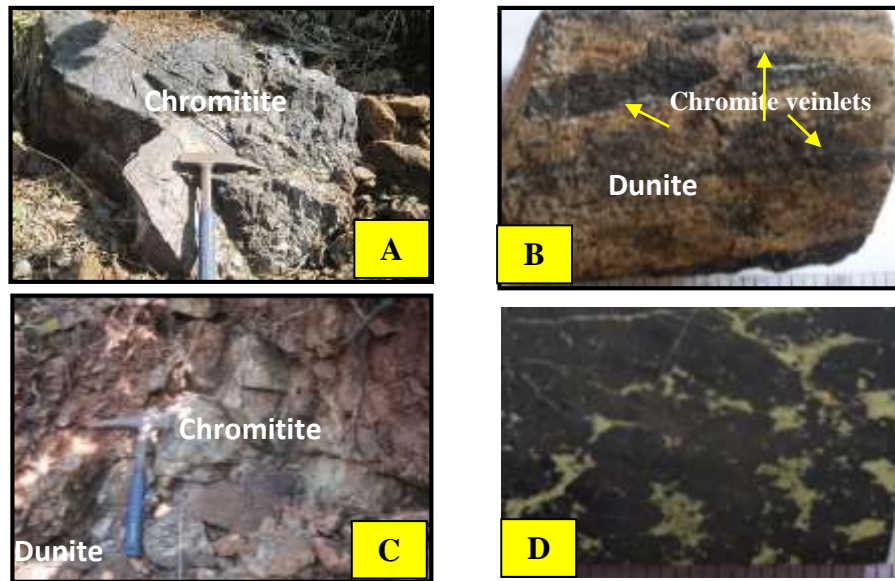


Figure 3 Types of chromitites of Taung-Pi-La. (A) Massive chromitite. (Loc: N 23° 11' 54.72" and E 93° 58' 57.82"). (B) Chromite veinlets occur in dunite of the research area. (C) Field photograph of chromitite enveloped dunite in Taung-Pi-La ultramafic body. (D) Nodular chromitite show net textured chromites.

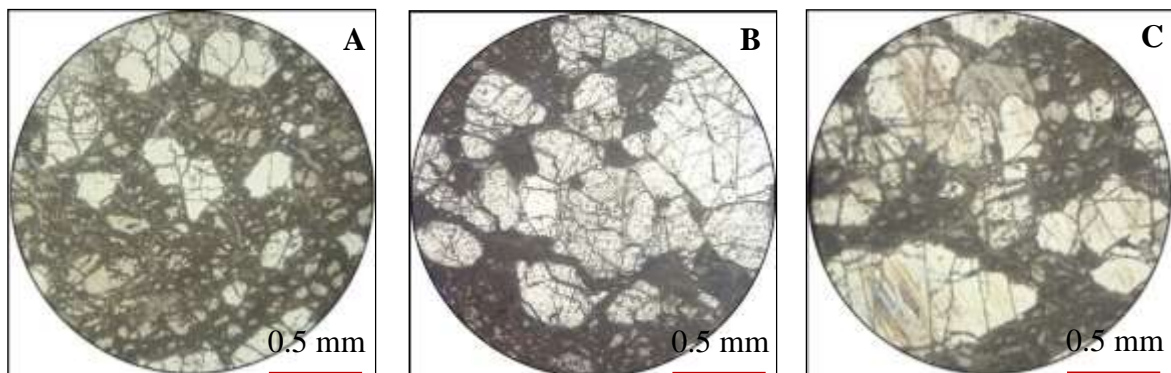


Figure 4 Textures of chromitites. (A) cataclastic textured chromites. (B) Resorbed grains of chromite. (C) Clot texture of chromite (under ore microscope).

Results

Geochemistry of Chromitites

The results of XRF analyses of chromitite were presented in Table 1. Chromitite composition is characterized by Cr₂O₃ ranging from 27.10 to 59.43 wt.%, Al₂O₃ from 7.36 to 26.60 wt.%, MgO 8.27 to 26.80 wt.%, and FeO ranges from 4.37 to 14.66 wt.%. X-ray powder diffraction (XRD) analysis indicates that the studied chromitites are of magnesiochromite

(MgCr₂O₄) (Fig. 5A). In the Mg# vs. Cr# diagram (Dick and Bullen 1984) (Fig. 5B), most of the chromitites belongs to the magnesiocromite type except one sample.

Table 1 Chemical data of chromitites of Taung-Pi-La Area.

ore	Massive chromitites			Nodular chromitites		
	Samp: No.	1	2	3	4	5
SiO ₂	11.70	11.10	12.20	22.60	20.6	3.63
TiO ₂	0.17	0.15	0.14	0.13	0.15	0.18
Al ₂ O ₃	26.10	26.60	25.50	18.20	17.80	7.36
Fe ₂ O ₃	2.37	2.45	2.43	2.11	2.08	6.98
FeO	4.98	5.15	5.11	4.42	4.37	14.66
Cr ₂ O ₃	29.40	30.70	29.60	27.10	27.50	59.43
MgO	24.20	22.80	24.60	24.30	26.80	8.27
CaO	0.32	1.14	0.35	1.26	0.76	0.00
Na ₂ O	0.58	0.00	0.00	0.00	0.00	0.00
K ₂ O	0.06	0.07	0.06	0.00	0.06	0.00
NiO	0.08	0.08	0.08	0.09	0.09	0.19
V ₂ O ₅	0.08	0.06	0.08	0.05	0.05	0.00
Co ₂ O ₃	0.02	0.02	0.02	0.02	0.00	0.00
ZnO	0.02	0.03	0.02	0.02	0.023	0.11
WO ₃	0.05	0.05	0.03	0.02	0.00	0.00
Total	100	100	100	100	100	101
Si	5.50	5.20	5.70	11.00	9.60	1.70
Mg	15.00	14.00	15.00	15.00	16.00	5.00
Al	6.90	7.00	6.70	4.80	4.70	1.90
Cr	10.00	11.00	10.00	9.30	9.40	20.00
Fe ²⁺	3.87	4.00	3.97	3.44	3.40	11.4
Ti	0.10	0.10	0.10	0.10	0.10	0.10
Ni	0.10	0.10	0.10	0.10	0.10	0.10
Mg/(Mg+Fe ²⁺)	0.77	0.75	0.77	0.79	0.81	0.28
Cr/(Cr+Al)	0.60	0.60	0.60	0.66	0.67	0.91

Under XGT microscopic study, aerial analysis of X-ray mapping of Mg, Si, Fe, Al, Ti, Cr, Mn, Ni, Pm, Zn and Bi in nodular chromitites are shown in Fig (6). FeO, Cr₂O₃ and Al₂O₃ content of the massive chromitites have higher composition than nodular chromitites. Massive chromitites contain lower SiO₂ than nodular chromitites. Mg, Fe and Si in nodular chromitites contain mostly indicates that olivine or serpentine (Fig 6).

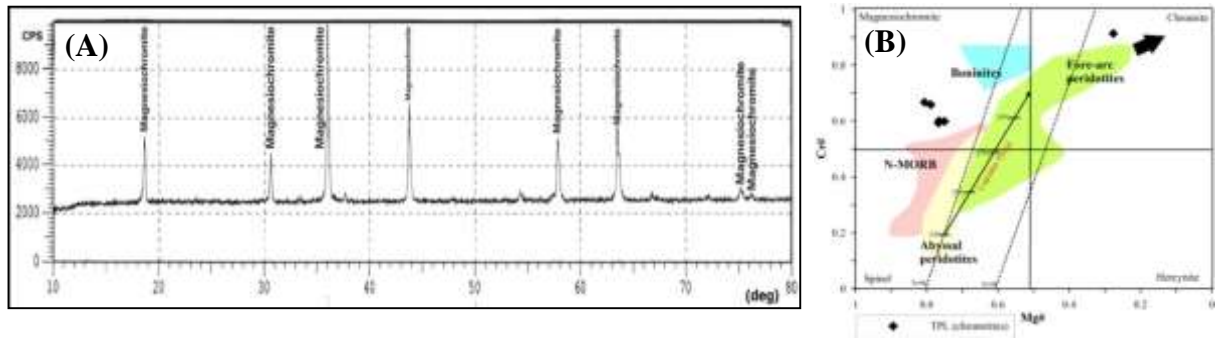


Figure 5 (A) X-ray diffractograms of chromitite from the research area. (B) Chromitites from the Taung-Pi-La Area plotted on the Cr# [Cr/(Cr + Al)] versus Mg# [Mg/(Mg + Fe²⁺)] diagram. Fields are collected from Dick and Bullen, 1984.

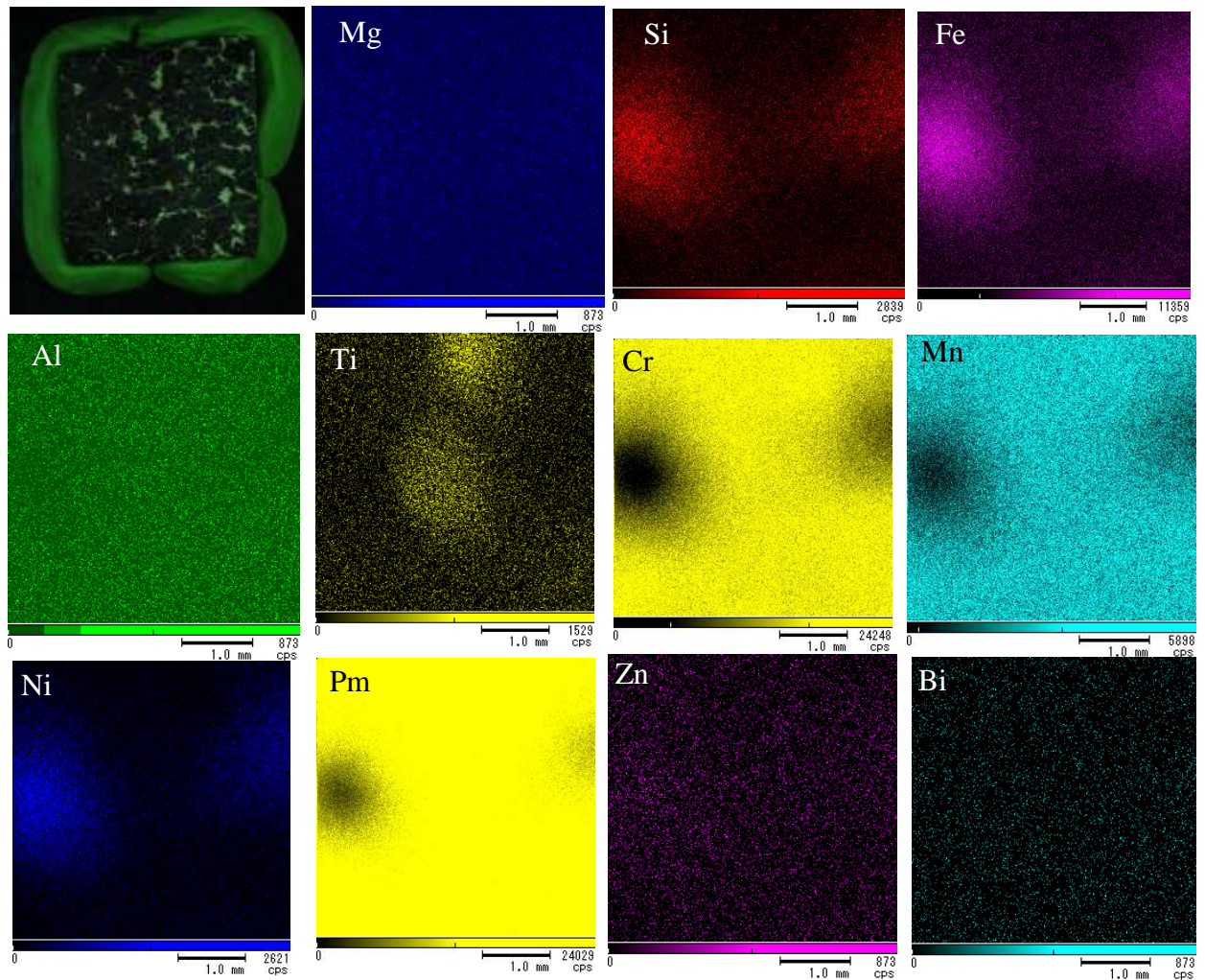


Figure 6 X-ray maps of the elements Mg, Si, Fe, Al, Ti, Cr, Mn, Ni, Pm, Zn and Bi of nodular chromitite sample under X-ray analytical microscope.

Chromitites from Taung-Pi-La Area show a wide range of composition, with Cr-numbers varying from 0.60 to 0.91 and Mg numbers (0.28-0.81) (Table 1). In the chromitites, FeO contents of chromitites are negatively correlated with MgO (Fig. 7B), whereas Cr₂O₃ contents are negatively correlated with MgO (Fig. 7D). The Al₂O₃ (7.36-26.60 wt.%) abundance in podiform chromitite depends on the melt of peridotite composition which is a function of pressure, temperature and the degree of partial melting (Kamentesky *et al.*, 2001).

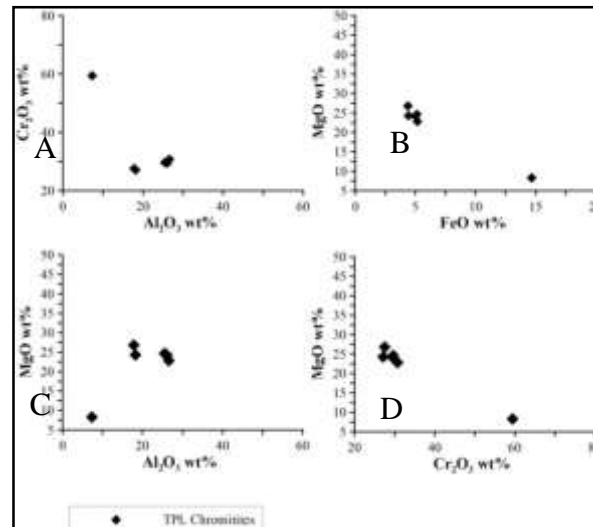


Figure 7 (A-D) Interelemental relationships of chromitites from Taung-Pi-La Area.

The samples studied in this work yield Cr₂O₃ contents of (27.10 - 59.43 wt.%), with a correspondingly high Cr# [Cr/(Cr + Al) atomic ratio; 0.6-0.9] and Mg# [(Mg/Mg+ Fe²⁺) atomic ratio; 0.28-0.81] the studied samples are plotted in the high Cr type (Fig.8). In the Cr# vs. Ti and Cr# vs. Ni diagrams, these samples are displayed to belong to Cr-rich chromitites (Fig.9).

High Cr-rich chromitites (Cr#> 0.6) might have formed initial liquid after higher degree of partial melting. In the diagram Cr#[Cr/(Cr+Al)] versus Mg#[Mg/(Mg+Fe²⁺)], the composition of these chromitites plotted in or near the field of podiform (ophiolite) chromitites (Fig. 10A). Nickel content (0.08-0.19 wt %) of chromitites in ophiolites are similar to those of chromitites in typical podiform chromitites (Ahmed, 1984). In the Cr# vs. TiO₂ discriminant diagrams (Barnes and Roeder, 2001), chromitites from the Taung-Pi-La Area are displayed at the ophiolitic chromitites (Fig. 10B). In Cr-Al- Fe³⁺ (atomic element) ternary diagram (Proenza *et al.*,2007), the studied samples overlaps the compositional field for typical podiform (ophiolitic) chromitites (Fig.11A). In Cr# vs. Fe₂O₃ diagram, high-Cr chromitites plotted in the podiform chromitites fields (Fig.11B).

The compositional characteristics of the Taung-Pi-La chromitites, i.e. Cr, Al, Mg, Fe³⁺ and Ti concentrations, are in accordance with those from typical podiform chromitites hosted in the mantle section of ophiolites. In the TiO₂ vs. Cr₂O₃ diagram (Fig.12A), most of the chromitite samples belong to the podiform chromitites. The maximum Fe₂O₃ content is 2.45 wt% and TiO₂ is always below 0.18 wt%, as typical for podiform chromitites and ophiolitic chromitites. The low TiO₂ contents of studied samples (0.13-0.17 wt %) also indicate its characteristics as podiform chromitites.

In the Fe²⁺/Mg vs. TiO₂ diagram (Fig.12B), chromitites are situated at the podiform chromitites field. The chromitites have a low Fe/Mg ratio indicating low Fe/Mg ratio of the magma from which they have crystallized. Fe-Mg exchange temperatures (Ballhaus *et al.*, 1991) of chromite from massive chromitite and olivine from coexisting silicate mantle dunite or harzburgite are between 915 and 1200°C, which suggest magmatic origin of chromite.

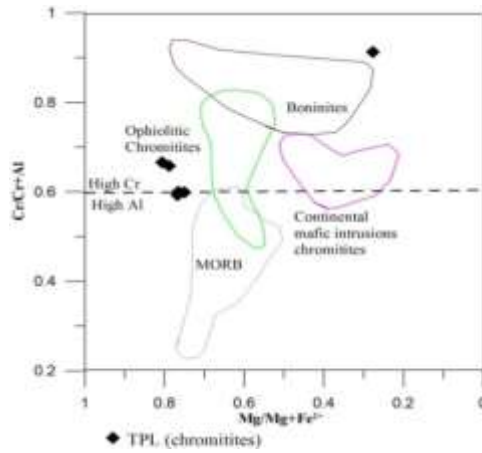


Figure 8 Cr# [(Cr/Cr + Al) atomic ratio] versus Mg# [(Mg/Mg+ Fe²⁺) atomic ratio] of chromitites. (Field from Proenza *et al.*, 2007).

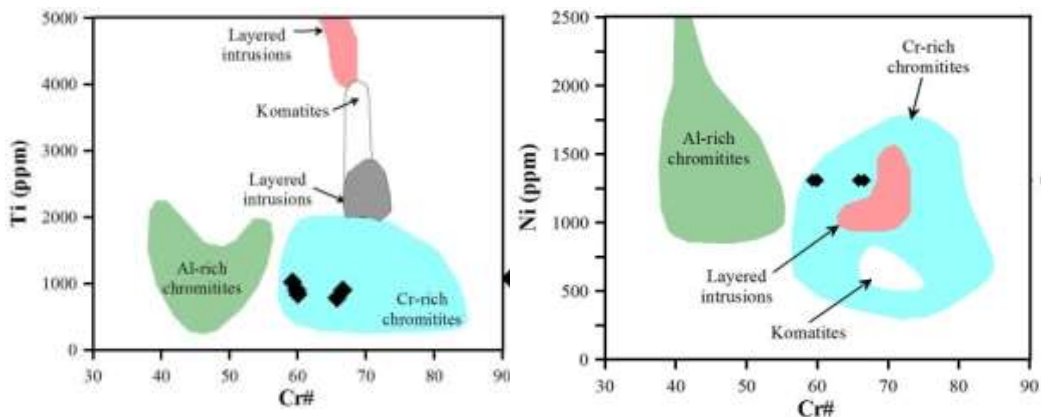


Figure 9 Compositional variations of Cr# vs. Ti and Ni of the chromitites. Data sources for the high-Al and high-Cr ophiolitic chromitites are collected from Zhou *et al.*, 2014.

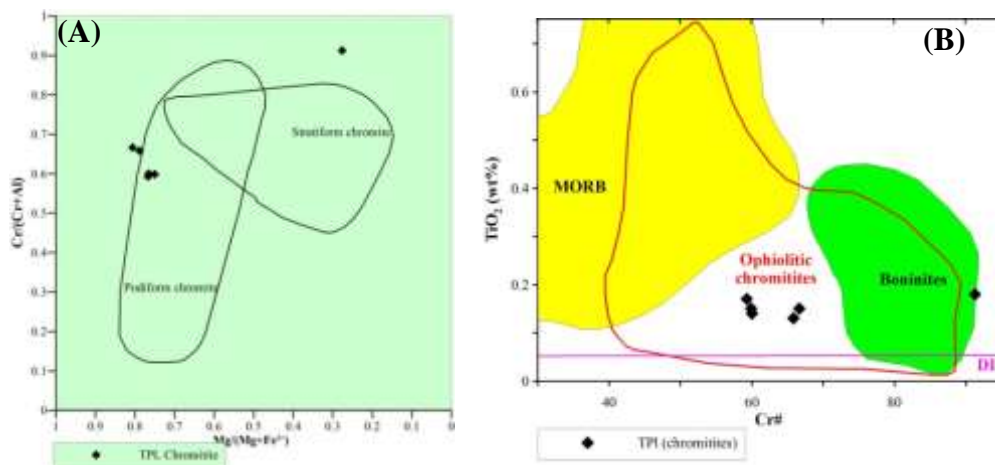


Figure 10 (A) Chromitites are plotted on the Cr# [Cr/Cr+Al] versus Mg# [Mg/Mg+ Fe²⁺] diagram. Compositional fields of podiform and stratiform chromitites are collected from Leblanc and Nicolas (1992) and Irvine (1967) (in Mirza, T.A, 2008), respectively. (B) Composition of chromitites from the research area are plotted on the Cr# vs. TiO₂ (wt%) diagram. Compositional fields are from Barnes and Roeder (2001).

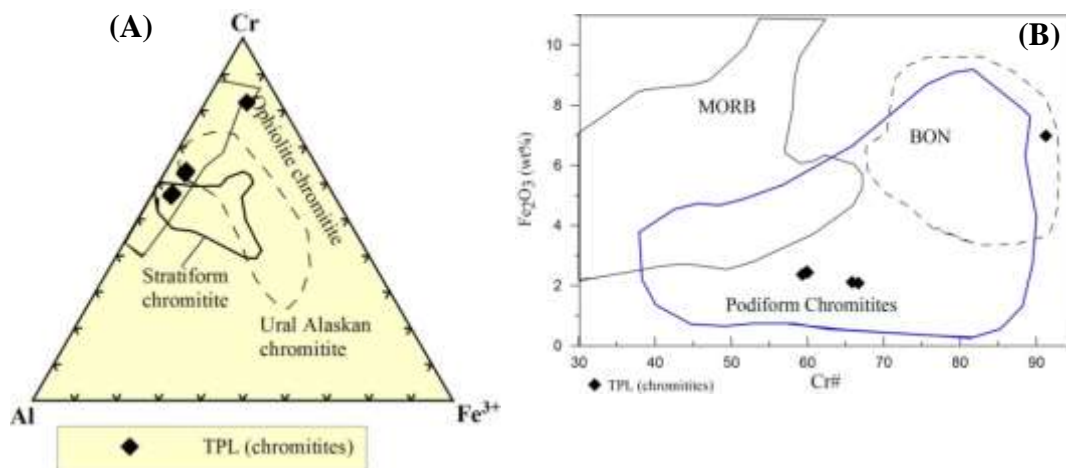


Figure 11 (A) Cr-Al- Fe³⁺ (atomic element) ternary diagram. Data sources for chromitites of different tectonic settings are from Proenza *et al.*, 2007. (B) Fe₂O₃ vs. Cr# for chromitites from the Taung-Pi-La. The field of podiform chromitites is compiled from Dare (2008).

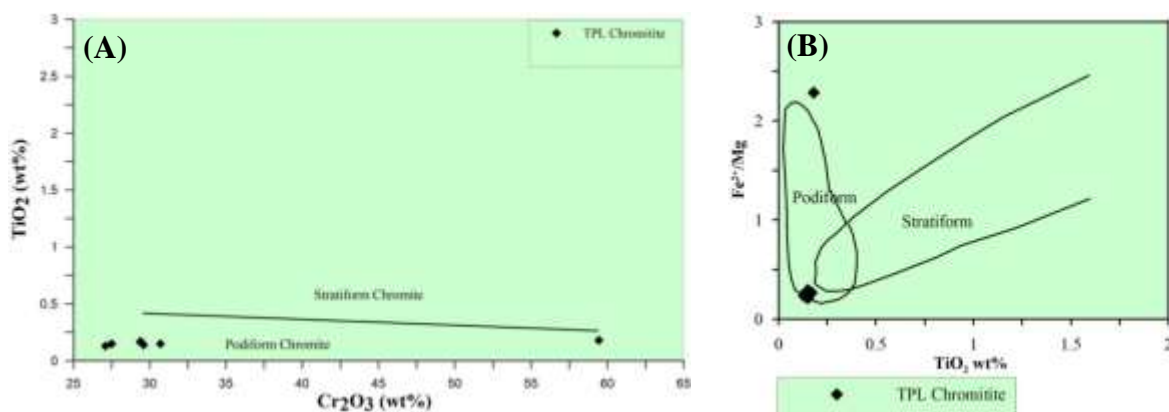


Figure 12 (A) Chemical compositions of chromitites compared with stratiform and podiform chromitites on TiO₂ wt% vs Cr₂O₃ wt% diagram. Fields are from Musallam *et al.* (1981) and Arai *et al.* (2004) (in Mirza, T.A, 2008). (B) Chromitites of the studied area are plotted in the Fe²⁺/Mg vs. TiO₂ podiform and stratiform chromitite diagram.

Petrogenesis of Chromitites

Such chromitites hosted in depleted peridotites, crystallized from mantle melts (Coleman, 1977). Chromitites commonly have dunite envelopes grading outward into harzburgite which were explained by additional partial melting of harzburgite (Thayer, 1963). Chromitites and adjacent peridotites should yield insights into the melt-rock interaction process and the mechanism of chromitite formation in the upper mantle. The podiform chromitite is usually associated with dunite; it occurs as pod-like bodies with dunite envelopes of mantle origin (Nicolas, 1989). The trivalent ion plot (Cr-Al- Fe³⁺) and Cr₂O₃ vs Al₂O₃ of chromitite compositions show their mantle origin (Fig.12A &12B). The TiO₂ and Al₂O₃ contents of chromitite from genetically- related peridotite, dunite and chromitite samples aids the interpretation of the tectonic setting in which they formed. On the tectonic discrimination diagrams, chromitites of the Taung-Pi-La Area are plotted in the supra-subduction zone (SSZ) field (Fig. 12C).

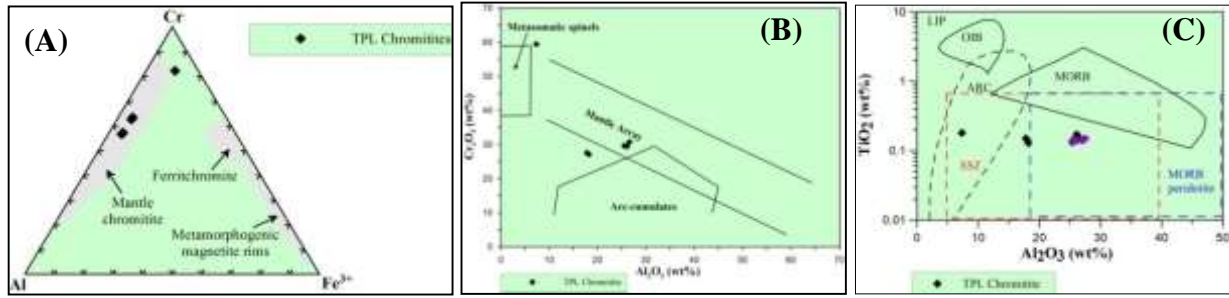


Figure 13 (A) Trivalent ion plot (Cr-Al-Fe³⁺) of chromitite compositions. Mantle chromitite, Ferrichromite and metamorphogenic magnetite field (Arai and Yurimoto, 1994) are shown for comparison. (B) Cr₂O₃ versus Al₂O₃ plot of the chromitite of the present study. Fields are collected from Franz and Wirth (2000). (C) Plot of TiO₂ versus Al₂O₃ in chromitite from Taung-Pi-La ophiolite complex. Fields are after Kamenetsky *et al.* (2001). SSZ; Supra-subduction zone; LIP, large igneous province; MORB, mid-ocean ridge basalt; OIB, ocean island basalt. ARC = arc related volcanic rocks.

Moreover, a diagram of TiO₂ versus Fe₂O₃ indicates that almost all samples from Taung-Pi-La plot within the field of SSZ ophiolites (Fig. 13A). The podiform chromitite must have formed under the uppermost mantle conditions in SSZ environments. Chromitites fall within a boninitic affinity (Fig. 13B). Chromites with high Cr# (>70) are commonly found in boninitic lavas and these are thought to have formed in SSZ environments. Podiform chromitites formed from hydrous boninitic magmas in a SSZ environment (Zhou *et al.*, 1996).

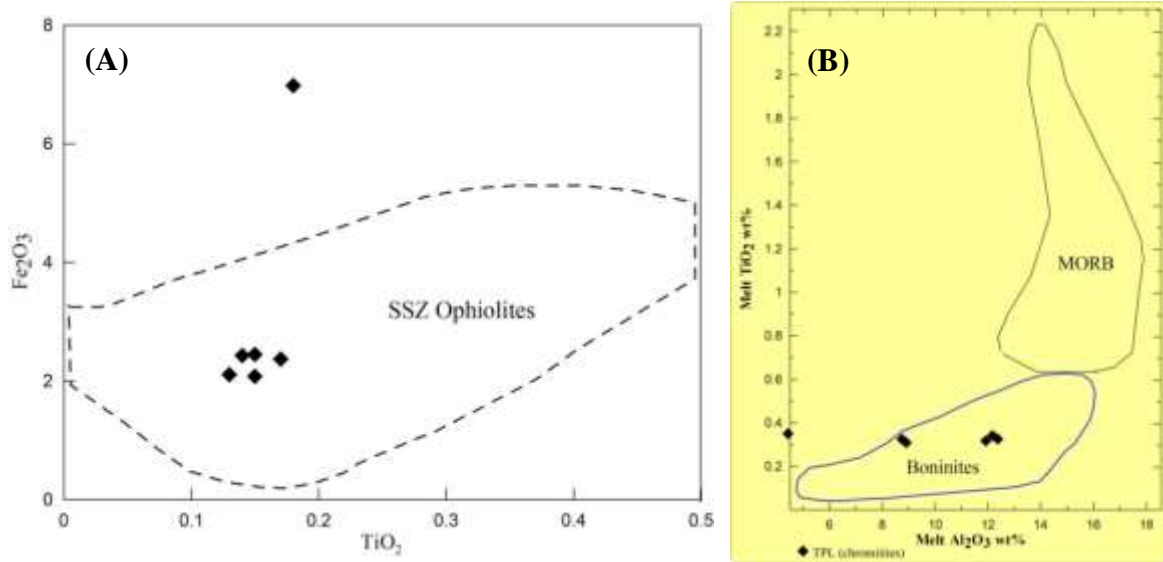


Figure 14 (A) Plots of TiO₂ vs. Fe₂O₃ of chromitites of the study area (fields after Bridges *et al.* 1995). (B) Composition of the parental melt in equilibrium with the studied chromitite in terms of TiO₂ versus Al₂O₃ (wt.%). Data sources for chromian spinel of different tectonic settings are from Pagé and Barnes (2009).

$$\ln (\text{wt \% Al}_2\text{O}_3 \text{ in melt}) = 0.41322 \times (\ln (\text{wt \% Al}_2\text{O}_3 \text{ in chromitite})) + 1.38529.$$

$$\ln (\text{wt \% TiO}_2 \text{ in melt}) = 0.82574 \times (\ln (\text{wt \% TiO}_2 \text{ in chromitite})) + 0.20203.$$

Conclusion

Podiform chromitites in Taung-Pi-La are enclosed in dunite which, in turn, is surrounded by harzburgite. Chromitites are presented by massive, nodular and disseminate types displaying pull-apart, cataclastic, net and clot textures. Among the chromite grains, the interstitial silicate of olivine, orthopyroxene, serpentine and chlorite are found. X-ray diffraction (XRD) of chromitites shows pattern of magnesiochromite (MgCr_2O_4). The TiO_2 vs. Cr_2O_3 diagram, $\text{Cr}\#[\text{Cr}/(\text{Cr}+\text{Al})]$ versus $\text{Mg}\#[\text{Mg}/(\text{Mg}+\text{Fe}^{2+})]$ and TiO_2 vs. Fe^{2+}/Mg diagram indicate that most of the chromitite samples belongs to the podiform chromitites. The high-Cr chromitites ($\text{Cr}\# > 0.6$) are typically hosted in highly depleted harzburgites and formed initial liquid after higher degree of partial melting. The trivalent ion plot ($\text{Cr}-\text{Al}-\text{Fe}^{3+}$) and Cr_2O_3 vs Al_2O_3 of chromitite compositions show their mantle origin. According to tectonic discrimination diagram, Taung-Pi-La chromitites must be generated from hydrous boninitic magmas in a SSZ environment. Chromitites and adjacent peridotites should yield insights into the melt-rock interaction process.

Acknowledgements

We express our thanks to Dr. Win Swe (Rector, Shwebo University) and Dr. Myo Myo, (Pro-rector, Shwebo University) for their kind permission and encouragement to carry out our research work. We are so grateful to Professor Dr. Khin Khin Lin, Head of Department of Geology, Shwebo University, for her invaluable suggestions and constructive comments. We would like to express our thanks to Dr. Zaw Win, Professor, Department of Geology, Shwebo University, for his close supervision and invaluable encouragements throughout this work.

References

- Ahmed, Z. (1984) "Stratigraphic and textural variations in the chromitic competition of the ophiolitic Sakhakot-Qila complex, Pakistan." *Economic Geology*. Vol.79, 1334-1359.
- Arai, S, and Yurimoto, H. (1994) "Podiform chromitites of the Tari-Misaka ultramafic complex, southwest Japan, as mantle-melt interaction products." *Economic Geology*. Vol.89, pp.1279-1288.
- Ballhaus, C., Berry, R.F., Green, D.H. (1991) "High pressure experimental calibration on the olivine-orthopyroxene-spinel oxygen geobarometer: implications for the oxidation state of the upper mantle." *Contributions to Mineralogy and Petrology*, 107, 27-40.
- Barnes, S.J., Roeder, P.L. (2001) "The range of spinel compositions in terrestrial mafic and ultramafic rocks" *J. Petrol.* 42, 2279-2302.
- Bonatti, E., and Michael, P.J. (1989) "Mantle peridotites from continental rifts to ocean basins to subduction zones". *Earth planet Sci. Lett.*, Vol.91, pp.297- 311.
- Bridges, J.C., Prichard, H.M., Meireles, C.A., 1995. Podiform chromitite-bearing ultrabasic rocks from the Braganca massif, northern Portugal: fragments of island arc mantle? *Geological Magazine* 132, 39-49.
- Coleman, R. G.(1977). *Ophiolite: Ancient Oceanic Lithosphere?* Springer, Berlin, Heidelberg, New York, 229p.
- Dare, S.A.S., Pearce, J.A., McDonald, I., and Styles M.T. (2008) Tectonic discrimination of peridotites using fO₂-Cr# and Ga-Ti-Fe^{III} systematics in chrome-spinel: *Chemical Geology*, v. 261, p. 199-216.
- Dick, H.J.B. and Bullen, T. (1984) "Chromium spinel as a petrogenetic indicator in abyssal and alpine-type peridotites and spatially associated lavas". *Contributions to Mineralogy and Petrology*, 86, 54-76.
- Franz, L. and Wirth, R. (2000). "Spinel inclusions in olivine of peridotite xenoliths from TUBAF seamount (Bismark Archipelago/Papua New Guinea): evidence for thermal and tectonic evolution of the oceanic lithospheric." *Contrib Mineral. Petrol.*, v.140, pp.283-295.
- Kamenetsky, V.S., Crawford, A.J., Meffre, S. (2001) "Factors controlling chemistry of magmatic spinel: an empirical study of associated olivine, Cr-spinel and melt inclusions from primitive rocks." *Journal of Petrology*, 42, 655-671.
- Mitchell, A.H.G., Myint Thein Htay and Kyaw Min Htun. (2015) "The Medial Myanmar Suture Zone and the Western Myanmar-Mogok foreland". *Journal of the Myanmar Geosciences Society* vol.6, no.1, 73-88.

- Mirza, T.A. (2008) *Petrogenesis of the Mawat ophiolite complex and the associated chromitite, Kurdistan Region, NE Iraq*. Ph.D. Thesis.
- Nicolas, A. (1989) "Structure of ophiolite and dynamic of oceanic lithosphere." Kluwer Academic press.
- Pagé, P.; Barnes, S.-J. (2009) Using trace elements in chromites to constrain the origin of podiform chromitites in the Thetford Mines ophiolite, Québec, Canada. *Econ. Geol.* 2009, 104, 997-1018.
- Proenza, J.; Zaccarini, F.; Lewis, J.; Longo, F.; Garuti, G. (2007) Chromian spinel composition and the platinum-group minerals of the PGE-rich Loma Peguera chromitites, Loma Caribeperidotites, Dominican Republic. *Can.Mineral*45, 631–648.
- Thayer, T.P. (1963) Geologic features of podiform chromite deposits in OECD seminar on "Methods of Prospecting for chromite", Athens, pp.135-148.
- Tun Tun Min and Immanuel. (2019) "Petrology of the Ophiolite Suite in Taung-Pi-La Hill, Kalay Township, Sagaing Region." *Proceeding of 12th NCSE, YTU*, P.176-180.
- Zhou, M.-F., Robinson, P.T., Malpas, J., and Li, Z., 1996, Podiform chromitites in the Luobusa ophiolite (southern Tibet): Implications for melt-rock interaction and chromite segregation in the upper mantle: *Journal of Petrology*, v. 37, p. 3–21.
- Zhou, M.-F., Robinson, P.T., Su, B.X., Gao, J.F., Li, J.W., Yang, J.S., Malpas, J. (2014) "Compositions of chromite, associated minerals, and parental magmas of podiform chromite deposits: the role of slab contamination of asthenospheric melts in suprasubduction zone environments." *Gondwana Res.* 26 (1), 262–283.

GEOCHEMICAL ANALYSIS OF SANDSTONE OF PAUNGGYI FORMATION IN THE AKYIBAN AREA, TILIN TOWNSHIP, MAGWAY REGION

Kyaw Khaing¹, Day Wa Aung², La Won Htike³

Abstract

The present study mainly focuses on the Geochemistry of Clastic sedimentary rock mainly on the sandstones of Paleocene. Paunggyi Formation exposed in the northernmost part of the Minbu Basin, Tilin, Magway region. The study attempts to constrain their source rocks, palaeo-weathering and tectonic setting of the provenance. The study area mainly consists of Tertiary Clastic Sedimentary rocks. Selected samples from the research area were analyzed using X-ray Fluorescence (XRF) for major oxides and some trace elements to know the chemical composition of sandstone and to classify the sandstone. Lithologically, the Paunggyi Formation is mainly composed of buff to grey, medium bedded sandstone, compact to friable thick bedded to massive gritty sandstone and conglomerate. By the XRF analysis, sandstones of the Paunggyi Formation fell within the litharenite zone. The analysis also points out that most of the sandstones are Fe-sand composition. By the discriminant diagram the Paunggyi sandstones samples indicating the mafic igneous and intermediate igneous provenances. Moreover, sandstones of the Paunggyi Formation were deposited in the active continental margin shifted to the downward of the oceanic island arc field. Additionally, the average CIA and CIW values of Paunggyi sandstones indicate very low degree of chemical weathering might have taken place in the source area.

Keywords: Litharenite, Mafic igneous provenance, Active continental margin

Introduction

The research area, northernmost part of the Minbu Basin, is located at 16 km east of Tilin, Magwe region. It lies between latitudes 21° 36' N and 21° 44' N and longitudes 94° 09' E and 94° 17' E in UTM-No 2194-02 and 2194-06. The location map of the study area is shown in figure (1). Tilin is easily accessible from Pakokku by car. The western part of the study area can be easily accessible by car from Pakokku to Tilin throughout the year but the eastern part of the study area is less accessible in rainy season.

The research area is a mountainous and forested region and the ranges are running north-south direction. Because of the sandstone dominant and shale dominant formation, this area shows ridge and valley topography. The whole area is occupied by thick soil cover and cultivation is good. The study area is swampy during rainy season. It lies between Pondaung range and the eastern flank of the Chin hill. Three dimensional map of the study area is shown in figure (2).

¹ Lecturer, Department of Geology, Pyay University

² Professor and Head, Department of Geology, University of Yangon

³ Assistance Lecturer, Department of Geology, Pakokku University

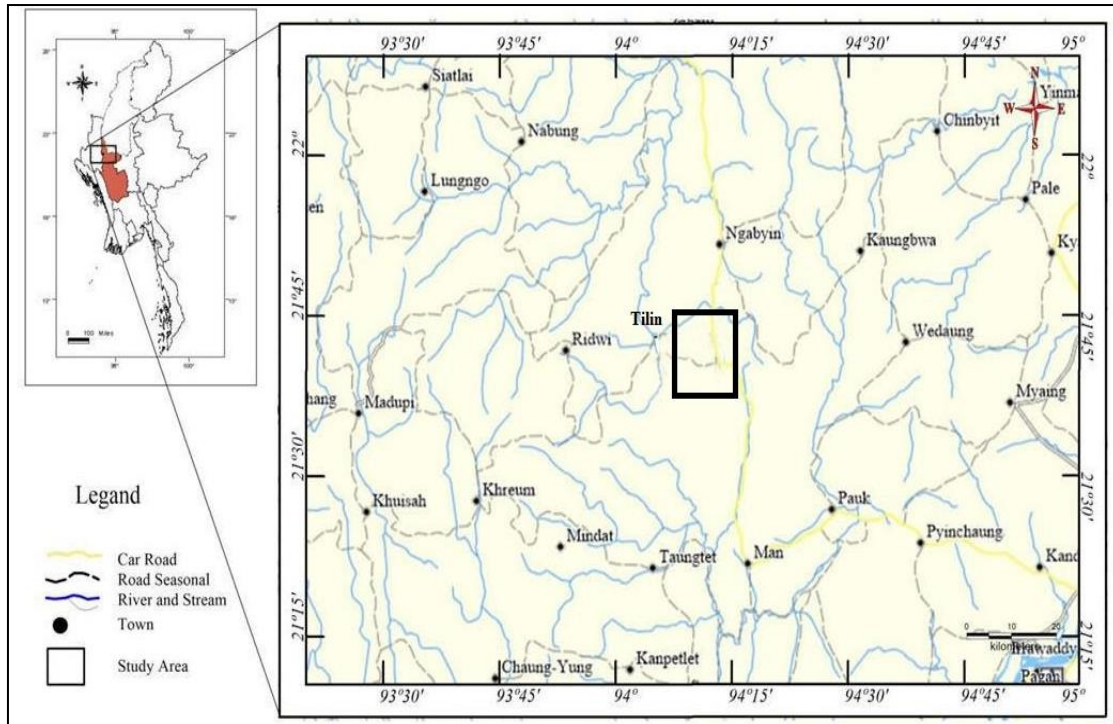


Figure 1 Location map of the study Area

Methodology

The X-ray Fluorescence (XRF) analysis conducted to know the chemical composition of sandstone and to classify the sandstone. The samples collected in the field were performed chemical analysis as X-ray Fluorescence. This method is most widely used analysis techniques in the application of quantitative major element analysis, minor and trace element analysis (Hutchison, 1974). Selected samples from the research area were analyzed using X-ray Fluorescence (XRF) for major oxides and some trace elements. In this research, X-ray Fluorescence (XRF) analyses were be done to interpret the chemical classification and weathering of the clastic sediments.

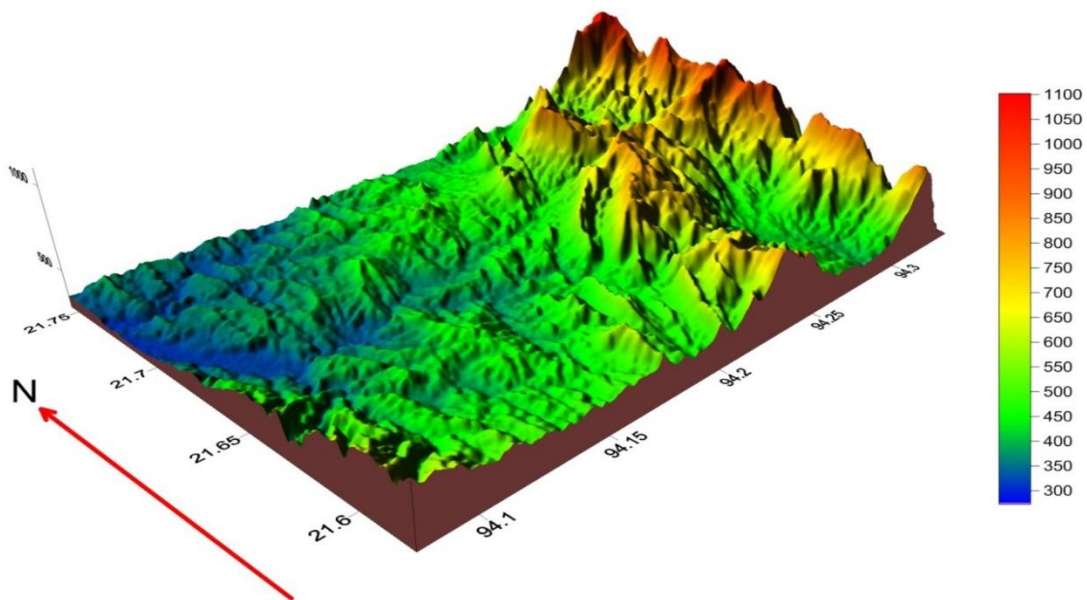


Figure 2 3D Map of the Ale ban Area, Tilin Township

Geochemical Analysis of Sandstone

Geochemical data are useful in the analysis of provenance studies, tectonic setting of basin, weathering, transport and erosion of sediments, depositional and diagenetic processes (Rollison, 1993). In geochemical analysis, the mineralogical and chemical composition of clastic sedimentary rocks are controlled by various factors, including (1) the composition of their source rocks, (2) environmental parameters influencing the weathering of source rocks (e.g., temperature, rainfall and topography), (3) duration of weathering, (4) transportation mechanism of clastic material from source region to depositor, (5) depositional environment and (6) post-depositional processes (e.g., diagenesis and metamorphism).

The present study examines the geochemistry of sandstones including Paunggyi Formations attempts to constrain their source rocks, palaeoweathering and tectonic setting of the provenance. Owing to limitations of analytical facilities, the present work is based on chemical analyses data of major elements of the investigated sandstones of the study area. The geochemical composition (Wt %) of Paunggyi sandstones are shown in the Table (1).

Table 1 Chemical Composition of Paunggyi Sandstone

Element	Pg-1	Pg-70	Pg-91	Pg-140	Pg-152	Pg-170	Pg-183	Pg-195	Pg-234	Pg-227	Pg-70
SiO ₂	36.83	55.63	51.46	52.33	54.28	53.3	44.97	35.76	41.43	38.51	55.63
Al ₂ O ₃	10.63	14.78	12.57	12.41	14.64	15.56	12.11	10.03	9.024	11.82	14.78
Fe ₂ O ₃	4.378	5.692	2.647	3.312	6.375	8.369	3.301	6.432	3.279	3.979	5.692
Na ₂ O	2.07	2.98	2.77	2.72	2.87	2.86	2.1	1.37	1.64	2.32	2.98
K ₂ O	1.01	0.815	1.54	1.26	1.02	0.859	1.31	1.01	1.03	0.831	0.815
SO ₃	0.05	0.048	0.048	0.043	0.041	0.039	0.053	0.053	0.065	0.0647	0.048
TiO ₂	0.547	0.723	0.412	0.606	0.701	0.922	0.797	0.633	0.489	0.987	0.723
CaO	18	0.833	10.28	8.139	3.482	1.11	14.67	18.27	14.84	17.23	0.833
MnO	0.632	0.0446	0.194	0.266	0.11	0.148	0.359	0.324	0.295	0.532	0.0446
Cr ₂ O ₃	0.023	0.0341	0.0264	0.021	0.0391	0.0439	0.0547	0.026	0.023	0.031	0.0341
SrO	0.0466	0.0084	0.0335	0.0351	0.0263	0.0092	0.043	0.0486	0.0536	0.0403	0.0084
P ₂ O ₅	0.0873	0.073	0.062	0.065	0.0106	0.056	0.0756	0.131	0.047	0.129	0.073
ZrO ₂	0.013	0.0143	0.0107	0.0133	0.016	0.0205	0.0125	0.015	0.009	0.0139	0.0143
CuO	0	0	0	0	0	0	0	0	0	0	0
Rb ₂ O	0	0	0.003	0	0	0	0	0	0	0	0
ZnO	0.0106	0.0085	0.007	0.0092	0.0129	0.0111	0.0095	0.0117	0.0089	0.0127	0.0085
NiO	0	0	0	0	0.008	0.007	0	0	0	0	0
FeO	0	0	0	0	0	0	0	0	0	0	0
MgO	0.817	1.23	0.543	0.527	1.04	1.38	0.026	0.745	0.597	0.705	1.23

Geochemical classification of sandstones

The composition of sandstone can be got from XRF analysis. To conduct XRF analysis, 10 sandstone samples were taken from the selected layer of sandstones from Paunggyi Formation.

Sandstones are classified and named variously based on their chemical composition. In the present study, sandstones were classified according to the scheme proposed by Pettijohn *et al.* (1972) and Herron (1988). Although Pettijohn *et al.* (1972) classified the sandstones based on the bivariates log (Na₂O/K₂O) versus log (SiO₂/Al₂O₃) diagram. Herron (1988) proposed the bivariate log (Fe₂O₃/K₂O) versus log (SiO₂/Al₂O₃) diagram. Herron also examined the importance of the major oxide variables and classified the clastic rocks mainly as Fe-sands with little portions on the wacke zone. The results of log ratio are plotted on the diagrams of sandstone classification. The geochemical classification diagrams of Pettijohn *et al.*, (1972) (figure-3) pointed that Paunggyi sandstones fell within the litharenite zone. However five samples of Paunggyi sandstone are greywacke. Herron (1988) also pointed out Paunggyi sandstones are Fe-sand except four samples of sandstone (figure 4).

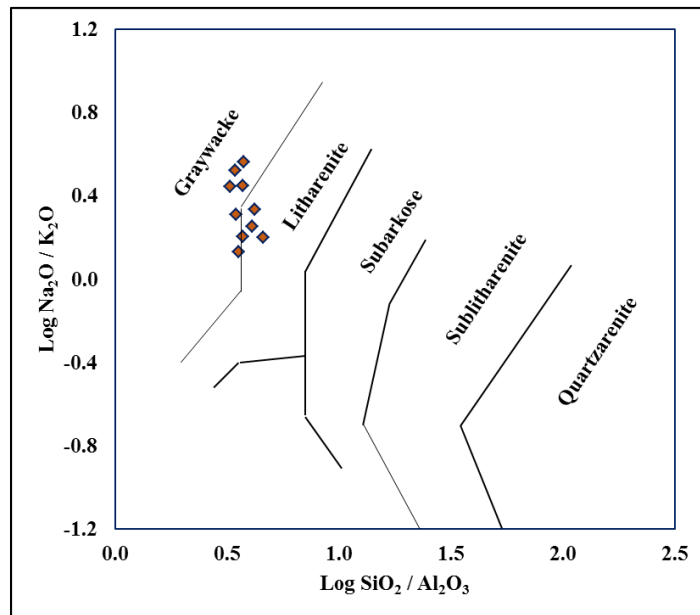


Figure 3 Chemical classification diagram of Pettijohn *et al.* (1972) of Paunggyi sandstones

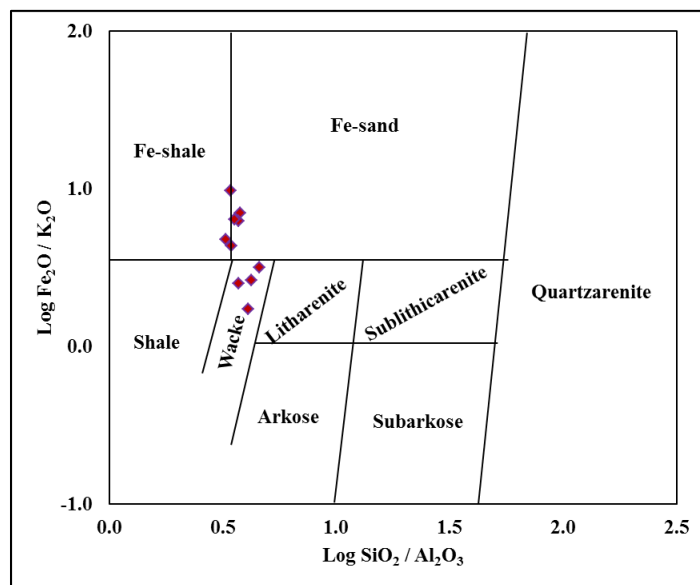


Figure 4 Chemical classification diagram of Herron (1988) of Paunggyi sandstones

Source rock lithology and tectonic provenance

In the published literature several major-, trace-, rare-earth element-based discrimination diagram are proposed to decipher the source rock of the siliciclastic sedimentary rocks (eg., Taylor and McLennan, 1985; Roser and Korsch, 1988; McLennan *et al.*, 1993; Condie, 1993; Gu *et al.*, 2002; Cingolani *et al.*, 2003). In order to use major element of provenance interpretations we considered the discriminant functions of Roser and Korsch (1988), which use Al₂O₃, TiO₂, Fe₂O₃, MgO, CaO, Na₂O and K₂O contents as variables. In the discriminant diagram (figure-5), the Paunggyi sandstones samples plot in the field of mafic igneous and intermediate igneous provenances. The Al₂O₃ and TiO₂ contents of the siliciclastic sedimentary rocks are considered as significant indicators of their provenance. During weathering of source rocks, Al and Ti remain essentially immobile, owing to solubility of their oxides and hydroxides in low temperature aqueous solutions (e.g., Stumm and Morgan, 1981; Yamamoto *et al.*, 1986; Sugitani *et al.*, 1996). It is well known that in normal igneous rocks Al resides mostly in feldspars and Ti in mafic minerals (e.g., olivine, pyroxene, hornblende, biotite, ilmenite).

According to the petrographically, the sandstone of this area comprises various lithic fragments such as quartz and volcanic rock fragments which are relatively abundant in Paunggyi sandstone (figure- 6 and 7).

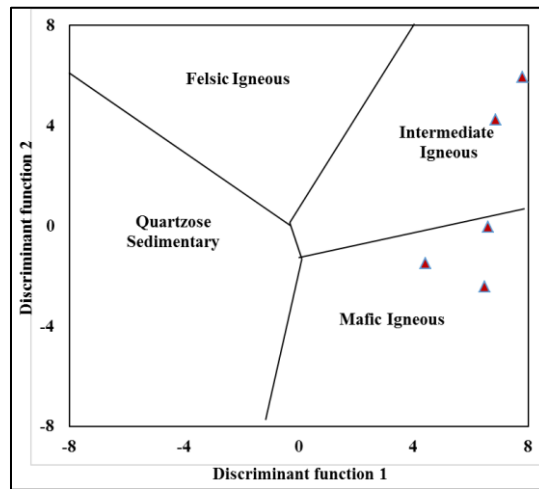


Figure 5 Discriminant function diagram for the provenance signation of the Paunggyi sandstones using major elements, Roser and Korsch (1988)



Figure 6 Volcanic rock fragment and frame work grain cemented with calcite cement and later fill iron cement in the Paunggyi Sandstone under X.N

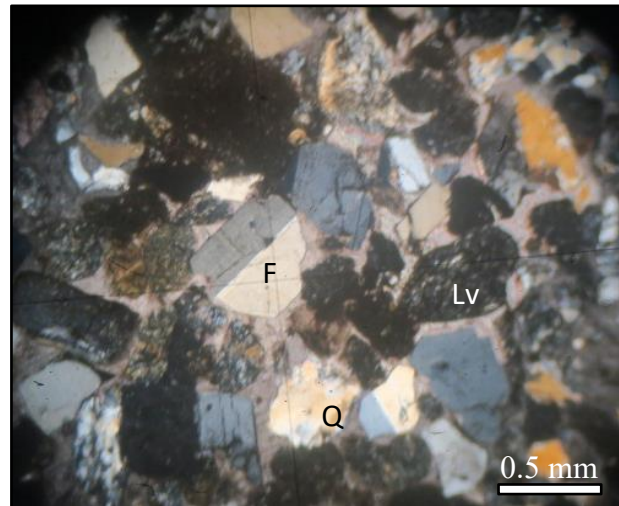


Figure 7 Photomicrograph showing monocrystalline quartz (Qm), feldspar (F), volcanic fragment in the Paunggyi sandstone under X.N

Several studies have shown that the chemical composition of siliciclastic sedimentary rocks are significantly controlled by plate tectonic settings of their provenances and depositional basins, and as a result, the siliciclastic rocks from different tectonic settings possess terrain-specific geochemical signatures (Bhatia, 1983; Bhatia and Crook, 1986; Roser and Korsch, 1986). Among the various tectonic setting discrimination diagrams, the major element-based discrimination diagrams of Bhatia (1983) and Roser and Korsch (1986) are widely used. In the discrimination diagram of Bhatia (1983) and Roser and Korsch (1986) the bivariate, including discriminant functions, are based on immobile and variable mobile major elements, including Na_2O and K_2O .

In the present study, the discrimination diagrams proposed by Bhatia (1983) used to discuss the tectonic setting by the major element geochemistry of sandstone samples. The Paunggyi sandstones were deposited in the active continental margin (figure 8c). However, in the diagrams of Bhatia 1983 (figure 8a and b), some of the Paunggyi sandstones are shifted to the downward of the oceanic island arc field because of TiO_2 composition is low.

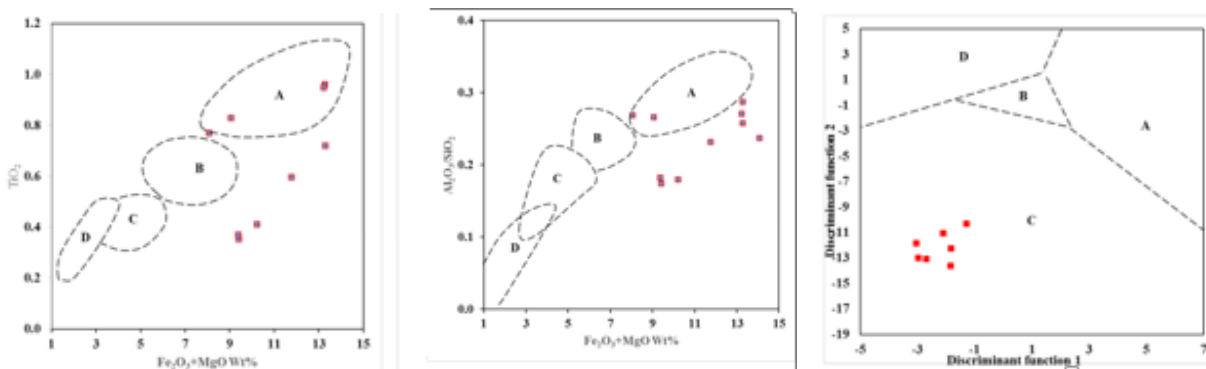


Figure 8 Plot of the major element composition of the Paunggyi sandstone on the tectonic setting discrimination diagrams of Bhatia (1983). a: $\text{Fe}_2\text{O}_3 + \text{MgO}$ vs TiO_2 ; b: $\text{Fe}_2\text{O}_3 + \text{MgO}$ vs $\text{Al}_2\text{O}_3/\text{SiO}_2$; c: discrimination diagram. A: Oceanic island arc, B: Continental island arc, C: Active continental margin, D: Passive margin.

Geochemical weathering of source area

Intensity of chemical weathering of source rocks is controlled mainly by source rock composition, duration of weathering, climatic and rates of tectonic uplift of source region. About 75% of the labile materials of the upper crust is composed of feldspars and volcanic glass and chemical weathering of these materials ultimately results in the formation of clay minerals (e.g., Nesbitt and Young, 1982, 1989; Taylor and McLennan, 1985). During chemical weathering Ca, Na and K are largely removed from source rocks.

The degree of source rock weathering is quantified variously. A few indices of weathering have been proposed based on molecular proportion of mobiles and immobiles element oxides (Na₂O, CaO, K₂O and Al₂O₃). Among the known indices of weathering/alteration the Chemical index of Alteration (CIA; Nesbitt and Young, 1982) is well established as a method of quantifying the degree of source weathering. Source weathering and elemental redistribution during diagenesis also can be assessed using Chemical Index of weathering (CIW; Harnois, 1988). The weathering effects can be evaluate in terms of the molecular percentage of the oxide components, using the formulae of chemical index of weathering (CIW= [Al₂O₃/ Al₂O₃+ CaO + Na₂O] x 100); (Harois, 1988) and chemical index of alteration (CIA= [Al₂O₃/ Al₂O₃+ CaO + Na₂O + K₂O] x 100); (Nesbitt and Young, 1982). The CIA and CIW are interpreted in similar way with values of 50 for unweathering upper continental crust and roughly 100 for highly weathered materials, with complete removal of alkali and alkaline-earth elements (McLennan, 1993). Low CIA values (i.e. 50 or less) also might reflect cool and/or arid conditions (Fedo *et al*, 1995).

According to CIA values, the Paunggyi sandstone of the degree of source weathering varies from 34 to 79% (average= 47%). CIW values suggest the degree of source weathering in the range from 23 to 82% (average= 52%). Average CIA and CIW values indicate very low degree of source weathering.

Mobility of elements during the progress of chemical weathering of source material and post-depositional chemical modifications of the sandstones can be evaluated by plotting the molar proportions of Al₂O₃, Na₂O+ CaO and K₂O in A-CN-K ternary disgram (Nesbitt and Young, 1982). Weathering trends might be predicated to be parallel to the A-CN join towards the composition of Al₂O₃ and Na and Ca are removed by chemical weathering of plagioclase feldspars. The average values of Paunggyi sandstones indicate extreme degree of chemical weathering (figure-9)

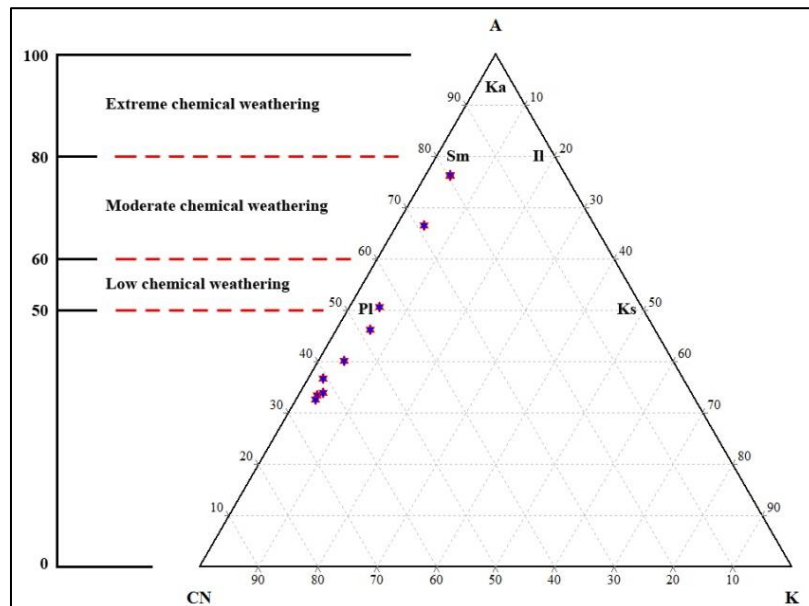


Figure 9 A-CN-K ternary Paunggyi sandstone of weathering diagram A= Al₂O₃; CN= (CaO+Na₂O); K=K₂O (Nesbitt and Young, 1982)

Conclusion

The research area, northernmost part of the Minbu Basin, is located at 16 km east of Tilin, Magwe region. It lies between latitudes 21° 36' N and 21° 44' N and longitudes 94° 09' E and 94° 17' E in UTM-No 2194-02 and 2194-06. The present study examines the geochemistry of sandstones including Paunggyi formations attempts to constrain their source rocks, palaeoweathering and tectonic setting of the provenance. Paunggyi sandstones fell within the litharenite zone. However five sample of Paunggyi sandstone is greywacke. The Paunggyi sandstone samples plot in the field of mafic igneous and intermediate igneous provenances. The Paunggyi sandstones were deposited in the active continental margin. The average CIA and CIW values of Paunggyi sandstones indicate very low degree of chemical weathering.

Acknowledgement

We would like to express our gratitude to Dr Kyi Kyi Swe, Professor and Head, Pyay University, for her permission and departmental facilitates and Dr Thida Oo, Professor, Department of Geology, Pyay University. we are greatly thankful to Dr Day Wa Aung, Professor and Head, University of Yangon, for his guidance and invaluable suggestions. Finally, we wish to thank to all teachers in Geology Department, Pyay University, for their help and encouragement throughout this research work.

References

- Bhatia, M. R., (1983), Plate tectonics and geochemical composition of sandstones: *Journal of Geology*, 91, 611-627.
- Bhatia, M. R., Crook, K. A. W., (1986), Trace element characteristics of greywackes and tectonic setting discrimination of sedimentary basins: *Contributions to mineralogy and Petrology*, 92, 181-193.
- Cingolani, C.A., Manassero, M. and Abre, P. (2003) Composition, provenance and tectonic setting of Ordovician siliciclastic rocks in the San Rafael Block: Southern extension of the Precordillera crustal fragment, Argentina. *Jour. South Amer. Earth Sci. Rev.*, v.16, pp.91-106.
- Condie, K.C. (1993) Chemical composition and evolution of the upper continental crust: contrasting results from surface samples and shales. *Chem. Geol.*, v.104, pp.1-37.
- Fedo, C. M., Nesbitt, H. W., & Young, G. M., (1995), Unraveling the effects of potassium metasomatics in sedimentary rocks and paleosols, with implication for paleoweathering conditions and provenance, *Geology*, 23, p.921-924.
- Gu, X.X., Liu, J.M., Zheng, M.H., Tang, I.H. and Qi, L. (2002) Provenance and Tectonic Setting of the Proterozoic Turbidites in Hunan, South China: Geochemical evidence. *Jour. Sed. Res.*, v.72(3), pp.392-407.
- Harnois, L., (1988), The CIW index: A new chemical index of weathering: *Sedimentary Geology*, 55, 319-322.
- Herron, M. M., (1988), Geochemical classification of terrigenous sands and shales from core or log data: *Journal of sedimentary Petrology*, 58, 820-829.
- Hutchison, C. S., (1974), Laboratory Hand Book of Petrographic Techniques.
- McLennan, S. M., (1993), Weathering and global denudation: *The journal of Geology*, 101, 295-303.
- Nesbitt, H. W., Young, G. M., (1982), Early Proterozoic climates and plate motions inferred from major element chemistry of lutites: *Nature*, 299, 715-717.
- Pettijhon, F. J., Potter, P. E., Siever, R., (1972), *Sand and Sandstone*: New York, Springer-verlag.
- Roser, B. P., Korsch, R. J., (1986), Determination of tectonic setting of sandstone-mudstone suites using SiO₂ content and K₂O/ Na₂O ratio: *Journal of Geology*, 94, 635-650.
- Roser, B. P., Korsch, R. J., (1988), Provenance signatures of sandstone-mudstone suites determined using discriminant function analysis of major-element data: *Chemical geology*, 67, 119-139.
- Stumm, W. and Morgan, J.J. (1981) Aquatic chemistry: A prologue emphasizing chemical equilibria in natural waters. John Wiley and Sons, New York, 780p.
- Sugitani, K., Horiuchi, Y., Adachi, M. and Sugisaki, R. (1996) Anomalously low Al₂O₃/TiO₂ values for Archean cherts from the Pilbara Block, Western Australia-possible evidence for extensive chemical weathering on the early earth. *Precambrian Res.*, v.80, pp.49-76.
- Taylor, A. S., McLennan, S. M., (1985), the continental crust: its composition and evolution: Oxford, Blackwell, 312 p.
- Yamamoto, K., Sugisaki, R. and Arai, F. (1986) Chemical aspects of alteration of acidic tuffs and their application to siliceous deposits. *Chem. Geol.*, v.55, pp.61-76.

PETROLOGY AND PETROGENESIS OF METAMORPHIC ROCKS IN ZAYAT KWIN AREA, THABEIKKYIN TOWNSHIP, MANDALAY REGION

May Thu Aung ¹, Tun Naing Zaw ², Toe Toe Win Kyi ³

Abstract

The study area is situated in southern part of Thabeikkyin Township, Mandalay Regions. The study area is located in UTM map No 2296 01. The study area falls within the Mogok Metamorphic Belt, mainly composed of metamorphic rocks and igneous rock. The study area comprises gneiss, marble and garnet – diopside - calc – silicate rock. In gneiss unit includes biotite - gneiss and marble units includes graphite marble, phlogopite – diopside marble and grossularite - diopside marble. Garnet – diopside - calc – silicate rock is composed of calcite, quartz, feldspar (orthoclase, plagioclase), diopside, sphene, garnet, zircon and opaque minerals. Most of the calcite twin bands are giving tapering twin and its showing first order to upper higher order. These calcite twins are gradationally change small to large twins and change the colour because of due to the effect of deformation. According to the mineral assemblages, regional metamorphism (amphibolites facies) is recognized in the study area. The grade of the metamorphism in the study area is medium to high grade metamorphism.

Keywords: Mogok Metamorphic Belt, tapering twin, amphibolites facies

Introduction

The study area is located in the eastern part of Thabeikkyin Township and the northern part of Singu Township in Mandalay Region. It is situated between latitude 22° 25' to 22° 30' and longitude 96° 99' to 96° 04' and in UTM map number 2296 01. Transport and communication to the study area is easily accessible. This area is readily accessible as the car road connecting Mandalay- Mogok and Mandalay – Thabeikkyin passes through it. Location map of the study area is shown in Figure. 1. Topographically, the eastern part of the study area is mountainous terrain and western marginal area is flat – lying topography and they are trending nearly N – S in direction. In the research area, the main stream flows from east to west. They are locally named as Kyet Saung Taung Chaung and On Zon Chaung. The drainage pattern of the study area is coarse dendritic pattern. Drainage pattern of the study area is shown in Figure. 2.

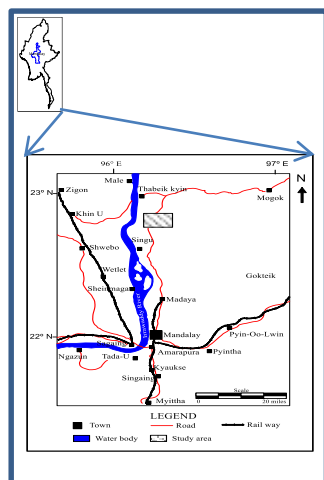


Figure 1 Location map of the study area

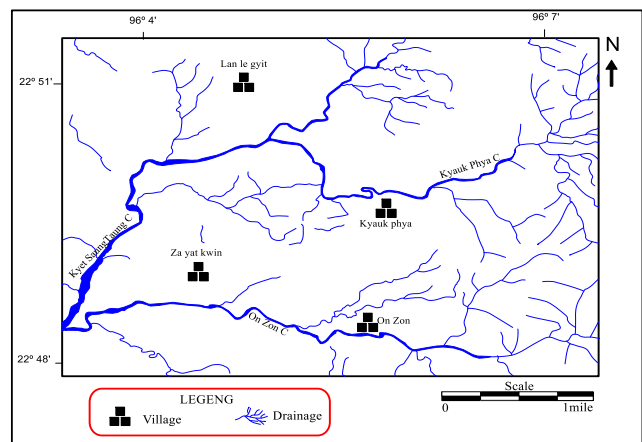


Figure 2 Drainage pattern of the study area

¹ Assistant Lecturer, Department of Geology, Loikaw University

² Dr., Associate Professor, Department of Geology, University of Yangon

³ Dr., Professor and Head, Department of Geology, Loikaw University

Regional Geologic Setting

The present area lies in the Mogok Belt of Searle and Haq (1964), and occupies a part of the western margin of eastern highlands. The Mogok Belt is a narrow zone (about 10 – 15 miles wide) of regionally metamorphosed rocks, extending southwest from Mogok through Kyaukse to Thazi and Yamethin. The regional geologic setting of the study area is shown in Figure.3. The study area is located about 91.2 km to the SW of the well known Mogok stone track and the same structural trends passing through both areas can readily be seen on landsat images. The mineralogy and rock type of the present area are rather similar to those of the Mogok area. The western margin of the study area is the Cenozoic rocks of the Central Burma Belt separated from the rocks of the Mogok series by the well known Sagaing fault.

The outpouring of basaltic lava through this fault has resulted in the formation of the Singu lava plateau in the south – western part of near the study area. The metamorphic rocks of the area extend father north and brought in contact with the rocks of the Upper Irrawaddy Province (of Bender, 1991) along the Momeik fault. Father east beyond the study area marble, gneiss, calc – silicate and granitic igneous rocks are exposed (One million scale, Geological Map of Burma, 1977).

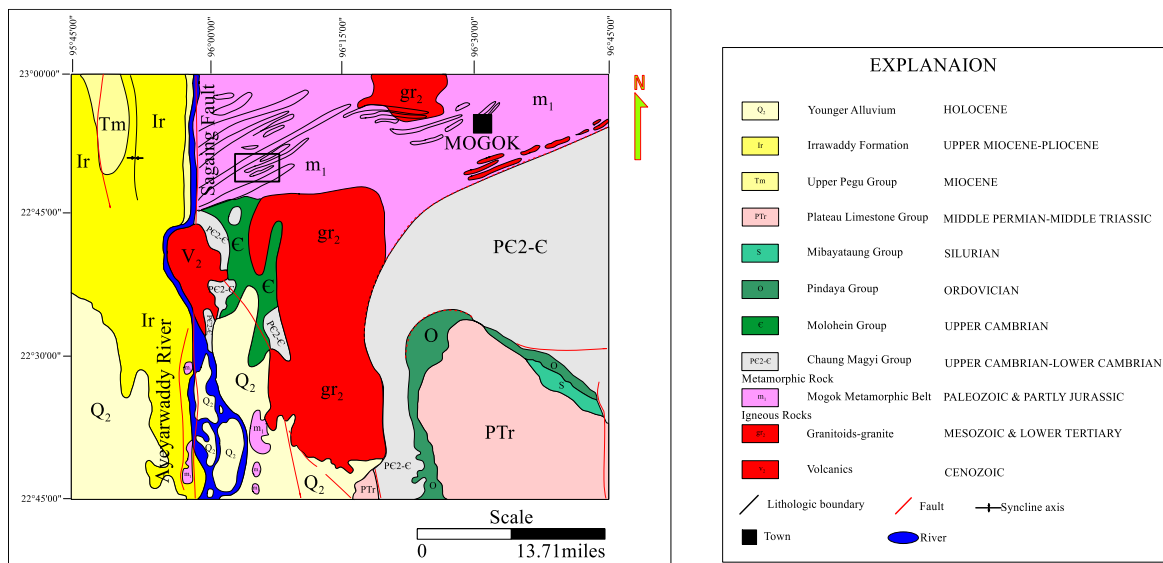


Figure 3 Regional Geological Map of the study area (from One million scale, Geological Map of Burma, 1977)

Metamorphic Rocks of the Study Area

This area is mainly composed of high – grade metamorphic rocks of the Mogok Metamorphic Belt. Exposures can be found in the Kyet Saung Taung in phlogopite - diopside marble and graphite marble. Phlogopite – diopside marble can occur in the On Zon Chaung. In the eastern part of the study area occur as grossularite - diopside marble. The biotite - gneiss unit occurs in near the Za Yat Kwin village and this unit is highly weathered. The garnet – diopside - calc - silicate rocks mostly occurs in the north eastern part of the study area and a few occurs in the Kyet Saung Taung and at the end of the Za Yat Kwin Village.

Rock Unit

Possible Age

Alluvium

Quaternary

Unconformity

~~~~~

**Metamorphic rocks**

|                                           |   |                            |
|-------------------------------------------|---|----------------------------|
| Biotite - gneiss                          | } | Late Paleozoic to Mesozoic |
| Garnet – diopside - calc - silicate rocks |   |                            |
| Graphite marble                           |   |                            |
| Phlogopite – diopside marble              |   |                            |
| Grossularite - diopside marble            |   |                            |

**Petrography**

The research area is mainly composed of the medium to high grade metamorphic rocks. Especially, types of marble, biotite - gneiss and garnet – diopside - calc – silicate rocks are well exposed in the study area.

**Biotite gneiss**

**Megascopic studies**

This unit is occur in the between Za Yat Kwin village and Kyet Saung Taung. It is highly weathered and red colour on weathered surface and grey colour on fresh surface, Figure. (4). It is medium – grained, gneissose texture and banded of felsic (quartz, feldspar) and mafic (biotite) minerals.

**Microscopic studies**

Biotite - gneiss shows medium - grained and gneissose texture, figure. (5). It is composed of the alkali feldspar, plagioclase, quartz, biotite, muscovite and apatite, sphene, zircon and opaque are accessories minerals.

Alkali feldspars are orthoclase, string perthite and myrmekite. Orthoclase occurs as subhedral form of simple twin. String perthite and myrmekite are also occurs in the biotite gneiss, figure. (6). Plagioclase feldspar is also found in this unit. Plagioclase feldspar occurs as polysynthetic twinning.

Quartz usually occurs as anhedral grains with suture boundaries and shows undulose extinction, figure. (7). Biotite is found as subhedral form. Muscovite is also occur subhedral prismatic crystals. Euhedral form of sphene and it shows very high relief. Zircon and apatite are displays subhedral to euhedral form and opaque are accessories minerals in this unit.



**Figure 4** Jointed nature of biotite gneiss in near the Za Yat Kwin village (Loc; N 22°49' 47.79", E 96°5'11.61", Facing - 80°)

**Figure 5** Gneissose texture of the biotite - gneiss (Bet.XN, 4X)

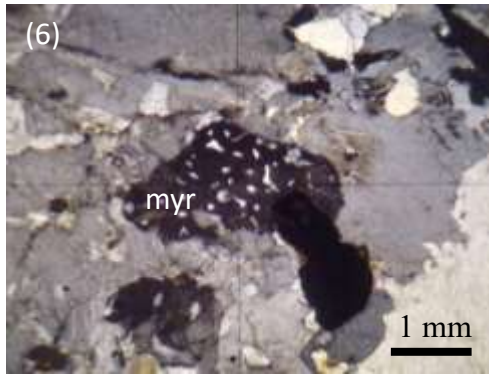


**Figure 6** Myrmekite occur in the biotite – gneiss (Bet.XN, 4X)

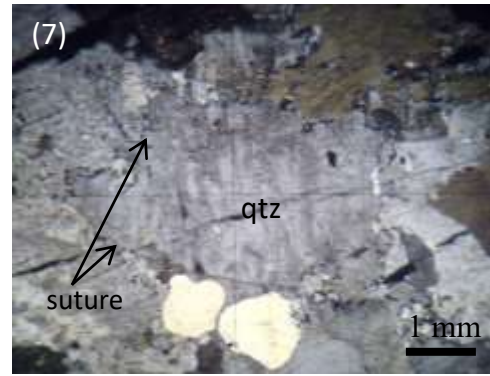


**Figure 7** Suture contacts of quartz grains in the biotite - gneiss (Bet.XN, 4X)

### Garnet – diopside - calc - silicate rock

#### Megascopic Studies

Garnet – diopside - calc – silicate rocks is well exposed in Za Yat Kwin village and northeastern part of the study area. It is dark green colour on weathered surface and fresh surface is gray, figure. (8).

#### Microscopic Studies

It has coarse – grained, granoblastic texture, figure. (9). It is comprises calcite, quartz, feldspar (orthoclase and plagioclase), diopside, sphene, garnet (grossularite), zircon and opaque minerals. Calcite shows anhedral form and rhombohedral cleavages. This calcite twin bands are bent and sometimes showing tapering twins because due to the effect of strain, figure. (10, 11, 12). Quartz usually occurs as anhedral grains and undulose extinction.

Feldspars are found as orthoclase and plagioclase. Anhedral orthoclase is showing untwined nature. Plagioclase displays polysynthetic twinning. Diopside form as anhedral and short prismatic crystal. The size of the diopside is 0.2 mm to 1.5 mm in diameter. Garnet (grossularite) occurs as anhedral grains with crack, figure. (13). Sphene display subhedral to euhedral forms. Euhedral zircon occurs in garnet – diopside - calc – silicate rock and opaque minerals are occurred in this unit.



**Figure 8** Drag Fold in garnet – diopside - calc – silicate rock at Za Yat Kwin village (Loc; N 22° 49' 38.36", E 96° 4' 53.29", Facing – 260°)

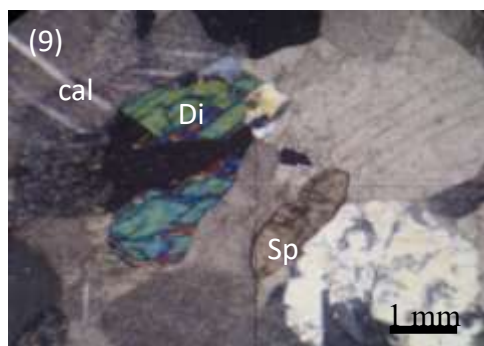


**Figure 9** Granoblastic texture of garnet – diopside - calc – silicate rock (Bet.XN, 4X)

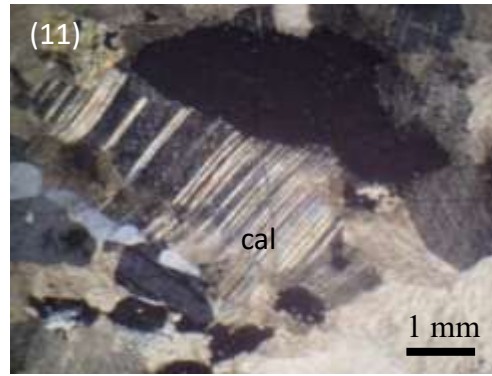
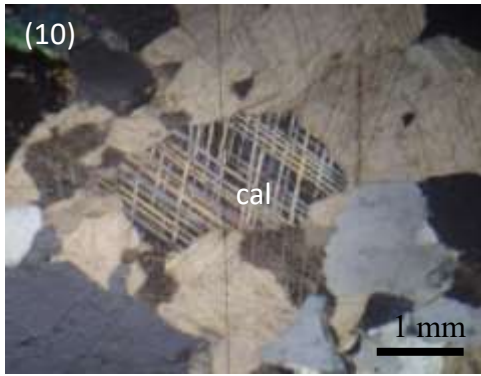


**Figure 10** Thick patchy twin calcite in garnet – diopside - calc – silicate rock (Bet. XN, 4X)

**Figure 11** Thick twins calcite in garnet – diopside - calc - silicate rock (Bet. XN, 4X)

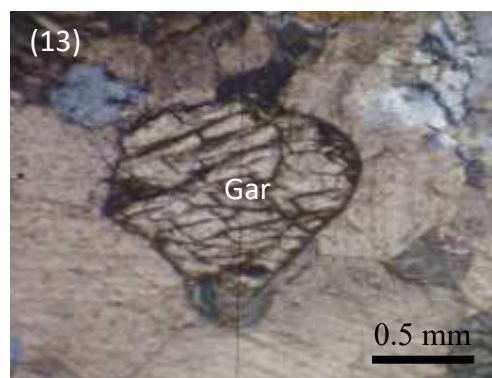
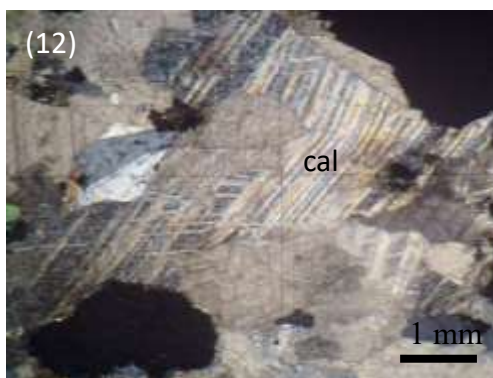


**Figure 12** Curve deformation of calcite twins in garnet–diopside -calc- ilicate rock (Bet. XN, 4X)

**Figure 13** Rounded garnet (grossularite) in garnet – diopside - calc - silicate rock (Bet.XN, 10X)

### **Graphite marble**

#### **Megascopic studies**

Graphite marble occurs in the Kyet Saung Taung near the Za Yat Kwin village, figure. (14). Graphite marble is commonly grey colour on weathered surface and whitish colour on fresh surface. This unit is medium to coarse grained and it fairly hard and compact.

#### **Microscopic studies**

Graphite marble is coarse – grained and granoblastic texture, figure. (15). It is mainly composed of calcite and some graphite. Accessories minerals are diopside, apatite, zircon and opaque minerals. Calcite displays anhedral grains and distinct rhombohedral cleavages, figure. (16). Graphite occurs as dark and opaque. Diopside shows subhedral short prismatic form. Apatite is found as six – sided form, figure. (17). Euhedral zircon and opaque are occurs in graphite marble.

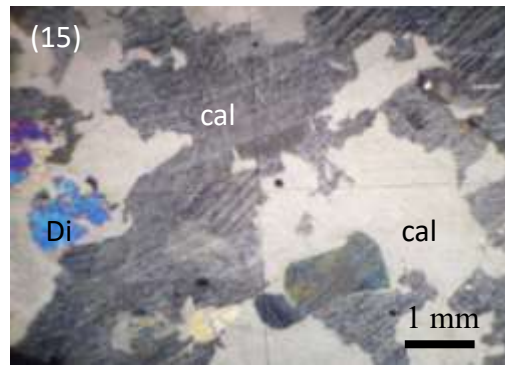


**Figure 14** Exposures nature of graphite marble at Kyat Saung Taung near the Za Yat Kwin village (Loc; N 22° 50' 05.30", E 96° 4' 34.81", Facing – 300°)

**Figure 15** Granoblastic texture of graphite marble (Bet.XN, 4X)

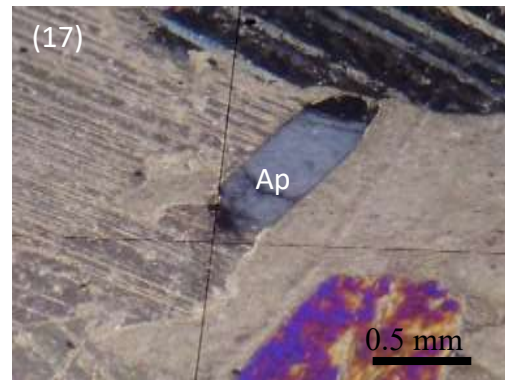
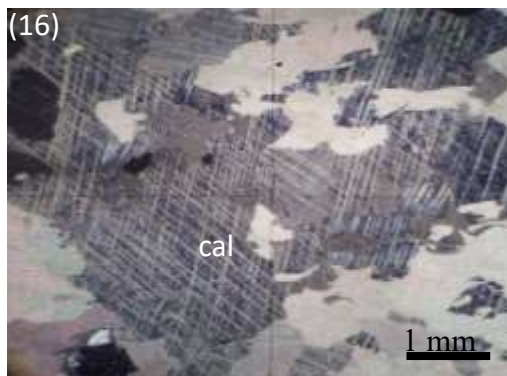


**Figure 16** Thin twin rhombohedral cleavages of calcite in graphite marble (Bet.XN, 4X)

**Figure 17** Subhedral to euhedral form apatite in graphite marble (Bet.XN, 10X)

### Phlogopite – diopside marble

#### Megascopic studies

Phlogopite – diopside marble are occurs in the Kyet Saung Taung near the Za Yat Kwin village and the On Zon Chaung, figure. (18). This unit is medium to coarse – grained, massive nature. Dark green colour on weather surface and whitish colour on fresh surface.

#### Microscopic studies

It is coarse – grained, granoblastic texture and mainly composed of calcite, diopside, forsterite, phlogopite, quartz, garnet (grossularite) and accessory minerals are apatite, opaque, zircon, spinel and sphene. Calcite is found as coarse – grained, anhedral crystals. The size varies from 1mm to greater than 4 mm in diameter. Calcite shows rhombohedral cleavages and some calcite twin bands are bent because of deformation, figure. (19, 20, 21, 22).

Diopside shows subhedral form and it sometime distinct two sets of cleavages. Some diopside show polysynthetic twin. The size of diopside is 0.5mm to greater than 4 mm in diameter. Forsterite shows subhedral crystals, figure. (23). It is giving parallel extinction. Phlogopite shows subhedral or tabular form, figure. (24) and grain size varies from 0.5 mm to 2.5 mm in diameter. Phlogopite display one set of cleavage and parallel extinction. Garnet (grossularite) display subhedral grains with fractures and cracks.

Sphene shows spindle – shaped and subhedral form. Euhedral zircon occurs in phlogopite - diopside marble, Figure. (25). Quartz usually occurs as anhedral grains. But subhedral form of quartz can occur in this unit. It is showing wavy extinction. Subhedral form apatite and opaque are common in phlogopite - diopside marble. Spinel occurs as euhedral three to four sided and it shows isotropic between cross nicols.

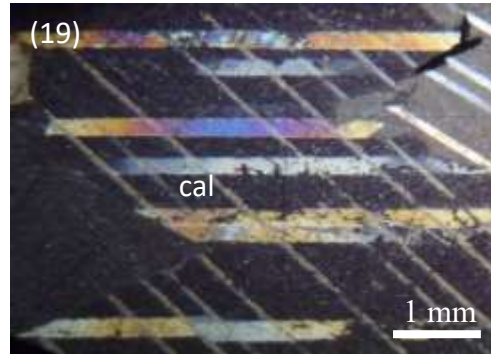


**Figure 18** Good exposures of phlogopite – diopside marble at On Zon Chaung (Loc; N 22° 48' 44.68", E 96° 5' 50.21", Facing - 270°)

**Figure 19** Thick twins of calcite in phlogopite – diopside marble (Bet.XN, 4X)

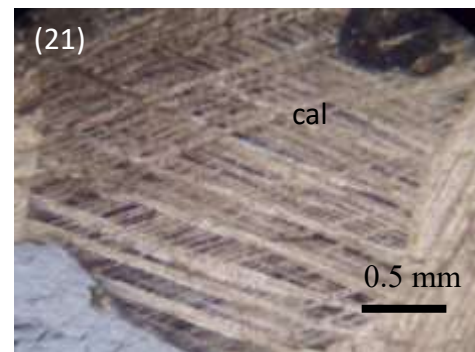
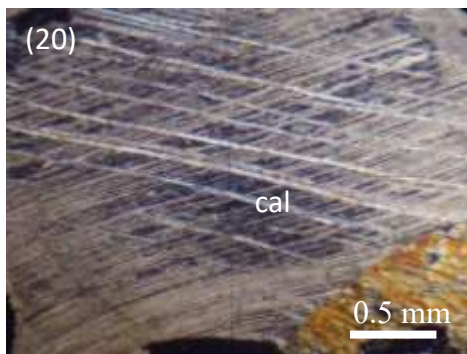


**Figure 20** Thin twins and tapering of calcite in phlogopite – diopside marble (Bet.XN, 10X)

**Figure 21** Thin to thick twins calcite in phlogopite – diopside marble (Bet.XN, 10X)

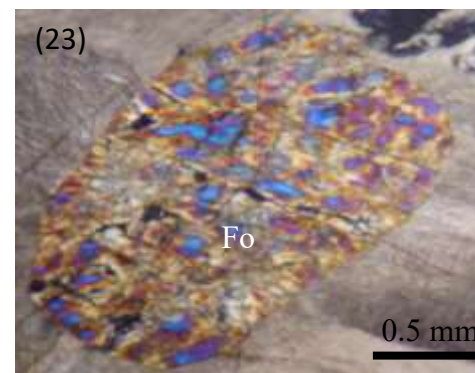
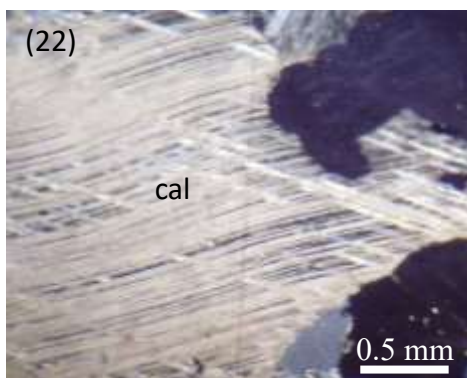


**Figure 22** Curve deformation calcite twins in phlogopite – diopside marble (Bet.XN, 10X)

**Figure 23** Forsterite in phlogopite - diopside marble (Bet.XN, 10X)

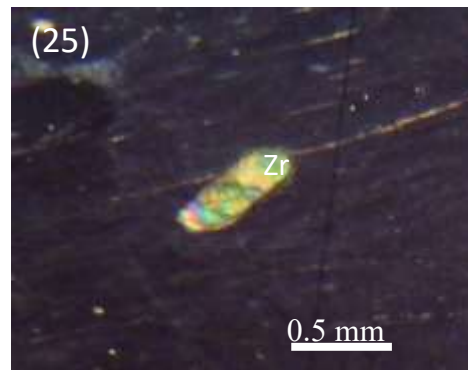
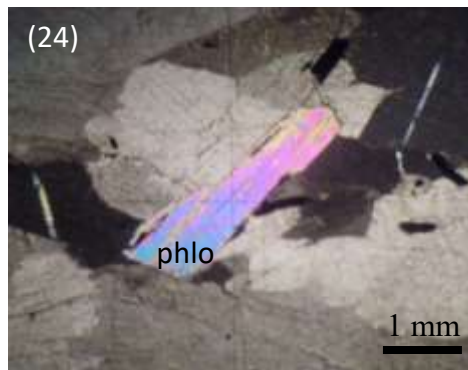


**Figure 24** Sheets form of phlogopite in phlogopite – diopside marble (Bet.XN, 4X)

**Figure 25** Euhedral form zircon in phlogopite – diopside marble (Bet.XN, 10X)

### Grossularite - diopside marble

#### Megascope studies

Near the Kyauk Phya village occurs grossularite - diopside marble figure. (26). This unit is occurs in the southeastern part of the study area near the Kyauk Phya village. It is gray colour on weather surface and whitish colour on fresh surface. Grossular - diopside marble and pure white marble are closely related.

#### Microscopic studies

Grossularite - diopside marble is coarse – grained, granoblastic texture. It is mainly composed of calcite, garnet (grossularite), diopside, phlogopite, forsterite, muscovite and opaque are accessories minerals.

Calcite has two sets of rhombohedral cleavages and occur tapering twin in the calcite. Most of the calcite twins bands are show first order to upper higher order. And then, most of the twin bands are strain of the deformation, figure. (27, 28). Garnet (grossularite) show subhedral to euhedral (six sided) form. All of the garnet (grossularite) minerals are show anomalous extinction because due to the deformation, figure. (29). Muscovite is occurs in the garnet diopside marble. Phlogopite show subhedral form and the size of phlogopite is 0.5 mm to 1.5 mm in diameter. Forstrite show subhedral crystals. Forsterite is showing parallel extinction. Diopside show subhedral form and it alteration occur in the garnet diopside marble. Opaque is occurs in the accessory mineral in this unit.



**Figure 26** Outcrop nature of grossularite - diopside marble near the Kyauk Phya village (Loc; N 22° 49' 31.62", E 96° 5' 47.15", Facing – 290°)

**Figure 27** Due to the deformation of calcite twin bands are curved in the grossularite – diopside marble (Bet.X.N, 4X)

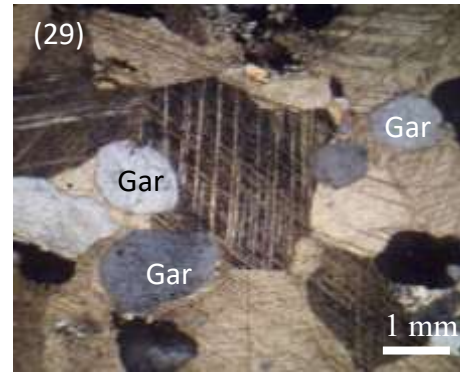
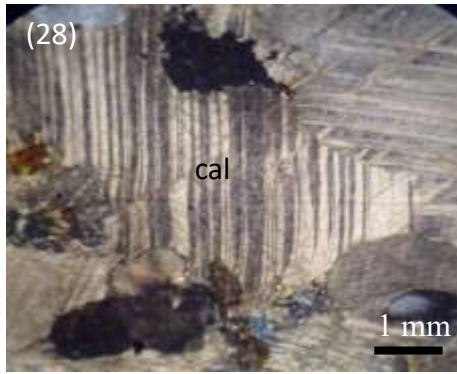


**Figure 28** Tapering twin in grossularite - diopside marble (Bet.X.N, 4X)

**Figure 29** Garnet is showing anomalous extinction in the grossularite - diopside marble (Bet.X.N, 4X)

### Petrogenesis

#### Mineral Assemblages and Metamorphic Facies

For the classification, nomenclature and defining mineral assemblages, thin section cut from various metamorphic rock types were studied for the mineral association. The mineral assemblages recognized in facies and rock types indicate that the metamorphic rocks of the area belong to the amphibolites facies. The following mineral assemblages are recognized in the study area.

Mineral assemblage recognized in biotite - gneiss is;

1. Orthoclase + quartz + plagioclase + biotite

Mineral assemblage recognized in garnet – diopside - calc – silicate rock is;

2. Calcite + quartz + orthoclase + plagioclase + diopside + garnet (grossularite)

Mineral assemblages recognized in marbles are;

3. Calcite + graphite + diopside
4. Calcite + diopside + phlogopite + forsterite + quartz + garnet (grossularite)
5. Calcite + diopside
6. Calcite + diopside + phlogopite + forsterite + garnet (grossularite) + muscovite

The above mineral assemblages were plotted on ACF and AKF diagrams are shown in figure.30, 31, 32 and 33.

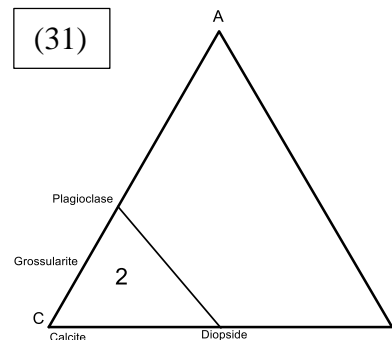
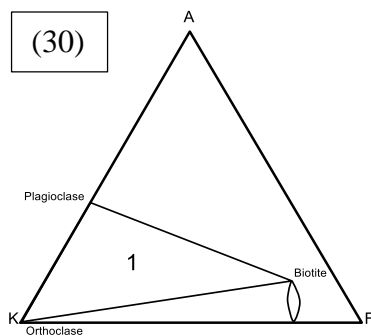


**Figure 30** AKF diagram showing the mineral assemblages of Amphibolite Facies (after Turner and Verhoogen, 1960)

**Figure 31** ACF diagram showing the mineral assemblages of Amphibolite Facies (after Turner, 1981)

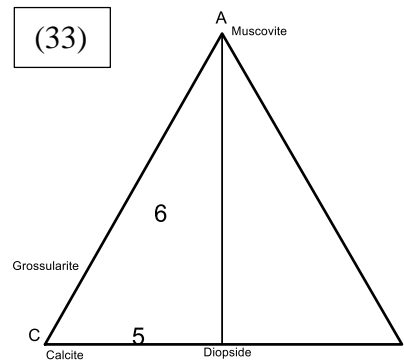
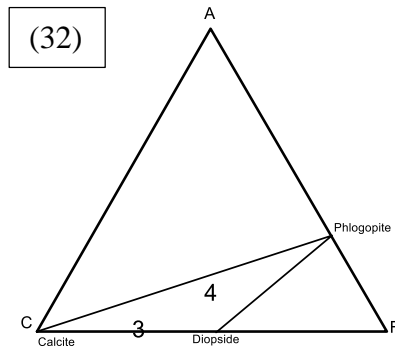


**Figure 32** ACF diagram showing the mineral assemblages of Amphibolite Facies (after Turner and Verhoogen, 1960)

**Figure 33** ACF diagram showing the mineral assemblages of Amphibolite Facies (after Askola, 1939)

### Types of Metamorphism

The mineral assemblages are found in the area indicate that the study area had been subjected to regional metamorphism. Regional metamorphism is the most wide spread and the grade of metamorphic facies is Amphibolite Facies. The index minerals of amphibolite facies such as diopside and forsterite are occurred in the study area. Therefore, it can be indicated that the rocks of the study area belong to the upper amphibolites facies.

According to the modern classification of the facies series (Miyashiro, 1980) the medium to high grade regional metamorphism of this area belong to the medium pressure. The occurrence of diopside from at about 600°C and  $P_f = 5$  kbars (Winkler, 1979). In the study area, the occurrence of grossularite from 600°C at 2 kbars (Winkler, 1979). The formation of forsterite takes place at 700°C and  $P_f = 5$  kbars (Winkler, 1979).

### Metamorphic Grade

Twin morphology in calcite appears to be strongly temperature dependant and has been proposed as a geothermometer (Burkhard, 1993). The number and volume of twins in calcite has been proposed as a microgauge for different stress (Jamison and Spang, 1976, Laurent et. al 1990). According to the petrographic analysis of the calcite twins in marble units, metamorphic grade of the study area increase to the south, Figure. 34.

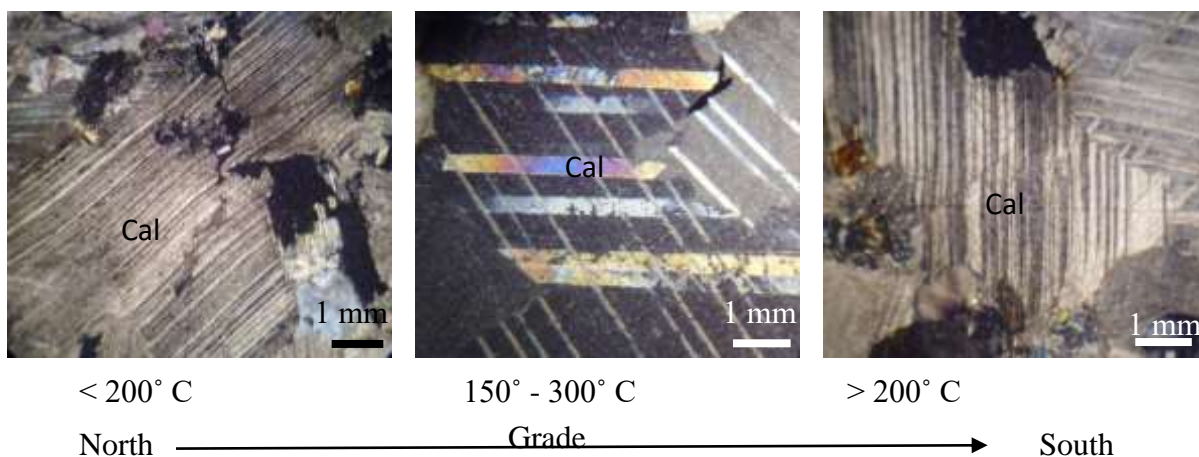
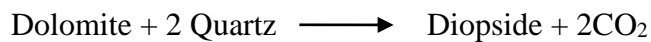


**Figure 34** Appearance of calcite twins with increasing temperature reproduced (Burkhard, 1993)

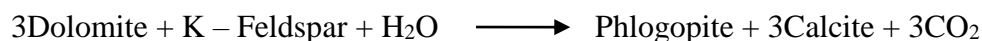
### Regional Metamorphism

According to the mineral assemblages the regional metamorphism of the study area had taken place in the "Amphibolite Facies" (Turner and Verhoogen, 1960 and Askola, 1939). The following mineral reactions are significant in the formation and paragenesis of some minerals.

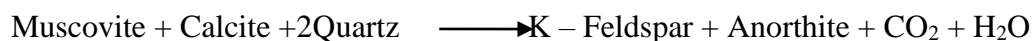
1. Diopside is found in types of marble. Diopside can be formed from the following equation, (Winkler, 1979).



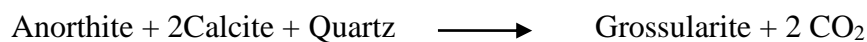
2. Phlogopite is found in types of marble. Phlogopite can be obtained from the following equation, (Winkler, 1979).



3. K - Feldspar can be obtained from the following equation;



4. The equation for garnet (grossularite) is the following equation;



5. The presence of forsterite may have been due to the following reaction (Winkler, 1979)



### Origin of Metamorphic Rock

Biotite - gneiss has been derived from pelitic rocks. Calc - silicate rock and types of marble are have been derived from the siliceous dolomitic limestone and calcareous rocks.

### Summary and conclusion

The study area is falls within the UTM map number 2296 01 and located in the eastern part of Thabeikkyin Township and the northern part of Singu Township in Mandalay Region. The present study area lies within the Mogok Metamorphic Belt, lying between Sagaing Fault and Shan Scarp Fault. The metamorphic rocks such as biotite - gneiss, grossularite - diopside marble, phlogopite - diopside marble, graphite marble and garnet - diopside - calc - silicate rocks. Biotite - gneiss is well exposed in the central part of the study area near the Za Yat Kwin village.

Marbles are widely distributed in the study area. Especially, marbles are can be found in the Kyet Saung Taung. Garnet - diopside - calc - silicate rocks is well exposed in the Za Yat Kwin village and northeastern part of the study area. Regional metamorphism (amphibolites facies) is recognized in the study area. The grade of the metamorphism in the study area is medium to high grade metamorphism.

## **Acknowledgements**

I am greatly indebted to Professor Dr. Toe Toe Win Kyi, (Head of Geology Department, Loikaw University), Dr. Tun Naing Zaw, (Associate Professor, University of Yangon) for the encouragement to do this research area. The author is deeply grateful to U Soe Lwin (Ministry of Mine), U Win Htike Oo (Ministry of Mine) for his valuable idea and suggestions during my research. Finally, my deepest thanks are due to my family for their encouragements in carrying out my research.

## **References**

- Alling, H.L., (1932). Perthites, *Journal of the Mineralogical Society of America*, Vol.17, No.2, p. 43-65.
- Burkhard, M. (1993). Calcite twins, their geometry, appearance and significance as stress – strain markers and indicators of tectonic regime: a review. *J. Struct. Geol.* 15, 357 – 368.
- Chhibber, H.L., (1934). *Geology of Burma*, MacMillan and Co-Ltd, London.
- Jamison, W.R., Spang, J.H., (1976) Use of calcite twin lamellae to infer differential stress. *Geol Soc Am* 87.868 – 872.
- Kerr, P. F, PH.D. (1942). *Optical Mineralogy*, Mc Graw-hill Book Company, INC, New York and London.
- Rocker. Mason, 1977 (), *Petrology of the Metamorphic Rocks*.
- Searle and Ba Than Haq, *The Mogok Belt of Burma and its relationship to the Himalayan Orogeny*.
- Soe Thura Tun, Maung Thein, Nyunt Htay and Kyaing Sein, (2014). *Myanmar Geoscience Society*.
- Turner, F.J, and J.Verhoogen, 1960. *Igneous and Metamorphic Petrology*. Mcgraw-hill Book Co. Inc. New York.
- Turner, F.J, and J., Verhoogen, (1962) *Metamorphic Reactions and Metamorphic Facies*. *Mem. Geol.Soc.America*.
- Williams, H. F. J Turner and C.M. Guilbert, (1982). *Petrography: an Introduction to the study of Rocks in Thin Section*. W. H. Freeman Company, New York.
- Winkler, H.E, G (1919), *Petrogenesis of metamorphic Rocks*, 5<sup>th</sup> ed, New York & Berlin.
- Winter. J. D., (2013.) *An introduction to Igneous and Metamorphic Petrology*, Prentice Hall, New Jersey, p.697.

## **PETROGRAPHY AND DIAGENESIS OF THE KALAW FORMATION IN THE TIGYIT AREA, SHAN STATE (SOUTH)**

Wai Wai Lwin<sup>1\*</sup>, Day Wa Aung<sup>2</sup>, Kyaw Khaing<sup>3</sup>

### **Abstract**

The aim of this paper are to classify the sandstones of Kalaw Formation and to describe diagenesis of these sandstones of the Tigyit area. The research area lies in Tigyit area, Shan State (South) and its situated in the tectonic province of Shan-Tanintharyi Block of Myanmar. The study area is mainly composed of Mesozoic to Cenozoic clastic sediments and subordinate amount of Paleozoic to Mesozoic age of carbonate rocks. Petrographic studies of the selected sandstone samples collected from the Kalaw Formation were carried out in detail. The sandstones of Kalaw Formation have less than 75 percent of detrital framework and 25 percent matrix. The detrital grains are composed of quartz, feldspar, mica, various kinds of rock fragments and very little heavy minerals. Medium-grained sandstones of Kalaw Formation fall in “Litharenites” and fine-grained sandstones of Kalaw Formation fall in the field of “Arkose”. Generally, three processes of diagenesis are observed in the sandstones. These are; compaction, cementation and authigenesis.

**Keywords:** *diagenesis, detrital grains, litharenite, arkose, authigenesis*

### **Introduction**

The study area lies along the highway from Aungban to Loikaw in the Pinlaung Township, Shan State (South) and its fall in the tectonic province of Shan-Tanintharyi Block or in the Eastern Highlands of Myanmar. The location map of the study area is shown in Figure 1. It is mainly composed of Mesozoic to Cenozoic clastic sediments and subordinate amount of Paleozoic to Mesozoic carbonate rocks. The sedimentary rocks are of Late Permian to Early Triassic of Nwabangyi Dolomite Formation, Middle Triassic of Natteik Formation, Jurassic of Loi-an Group, Cretaceous of Kalaw Formation and Pliocene of Hsi-khip Formation. The regional geologic setting of the study area is shown in Figure 2. The present study area divides the Kalaw Formation into three different members: Lower conglomerate-sandstone member, Middle sandstone-shale member, and Upper conglomerate member.

Lower conglomerate-sandstone member is mainly composed of thick-bedded to massive, polyolithic conglomerates, and this member is widely distributed at the Myatheintan taung Figure 3. Middle sandstone- shale member is mainly composed of thin to medium-bedded red sandstone interbedded with thin, soft and friable red siltstone Figure 4. Upper conglomerate member is chiefly made up of very massive, hard, dark purplish conglomerate intercalated with minor red siltstone, and reddish sandstone and these member is well exposed at the Myatheintan range, and Tayoktaung Figure 5.

---

<sup>1\*</sup> Lecturer, Department of Geology, Myeik University ( wailwin.wai02@gmail.com)

<sup>2</sup> Professor and Head, Department of Geology, University of Yangon

<sup>3</sup> Lecturer, Department of Geology, Pyay University





**Figure 5** Massive, hard, dark purplish conglomerate occurring in the upper member of Kalaw Formation (N. 20°26' 12.1" and E. 96°43' 35.8")

**Petrography and Diagenesis of the Kalaw Formation**

Six representative samples were collected from the Kalaw Formation in the Tigyt area. Petrographic studies of the selected sandstone samples collected from the Kalaw Formation were carried out in detail. Modal composition of the various grain types present was estimated by comparing the percentage estimation comparison charts, and the classification scheme of Pettijohn et al. (1987) was used in this petrographic study.

**Sandstone**

The sandstones of Kalaw Formation have less than 75 percent of detrital framework and 25 percent matrix. The detrital grains are composed of quartz, feldspar, mica, various kinds of rock fragments and very little heavy minerals. The maximum diameter of grains ranges from 0.2 mm to 0.5 mm and minimum diameter of grains, 0.05mm to 0.1 mm. Most grains are angular to subrounded and they generally have moderately to well sorted nature. As the grain contacts are tangential to concavo-convex, the sandstones of the Kalaw Formation have grain-supported frameworks. Detrital grains are set in calcite and hematite cements. Mineral composition and detrital percentages of these sandstones are shown in Table 1, 2 and Figure 6.

**Table 1 Mineral composition of the sandstones of Kalaw Formation**

| Sample No.           | KRB-1                            | KRB-2 | KRB-3 | KRB-4 | KRB-5 | KRB-6 |
|----------------------|----------------------------------|-------|-------|-------|-------|-------|
|                      | Composition in volume percentage |       |       |       |       |       |
| <b>Quartz</b>        | 60                               | 45    | 53    | 48    | 47    | 35    |
| <b>Feldspar</b>      | 7                                | 8     | 8     | 32    | 29    | 38    |
| <b>Rock Fragment</b> | 25                               | 32    | 30    | 7     | 8     | 5     |
| <b>Mica</b>          | 2                                | 3     | 3     | 3     | 4     | 13    |
| <b>Heavy Mineral</b> | 1                                | 2     | 1     | 2     | 2     | -     |
| <b>Matrix</b>        | 3                                | 7     | 3     | 6     | 6     | 6     |
| <b>Cement</b>        | 2                                | 3     | 2     | 2     | 4     | 3     |

**Table 2 Detrital percentage of the sandstone of Kalaw Formation**

| Sample No.           | KRB-1                           | KRB-2 | KRB-3 | KRB-4 | KRB-5 | KRB-6 |
|----------------------|---------------------------------|-------|-------|-------|-------|-------|
|                      | Essential Framework in volume % |       |       |       |       |       |
| <b>Quartz</b>        | 65                              | 53    | 58    | 55    | 56    | 45    |
| <b>Feldspar</b>      | 8                               | 9     | 9     | 37    | 35    | 49    |
| <b>Rock Fragment</b> | 27                              | 38    | 33    | 8     | 9     | 6     |

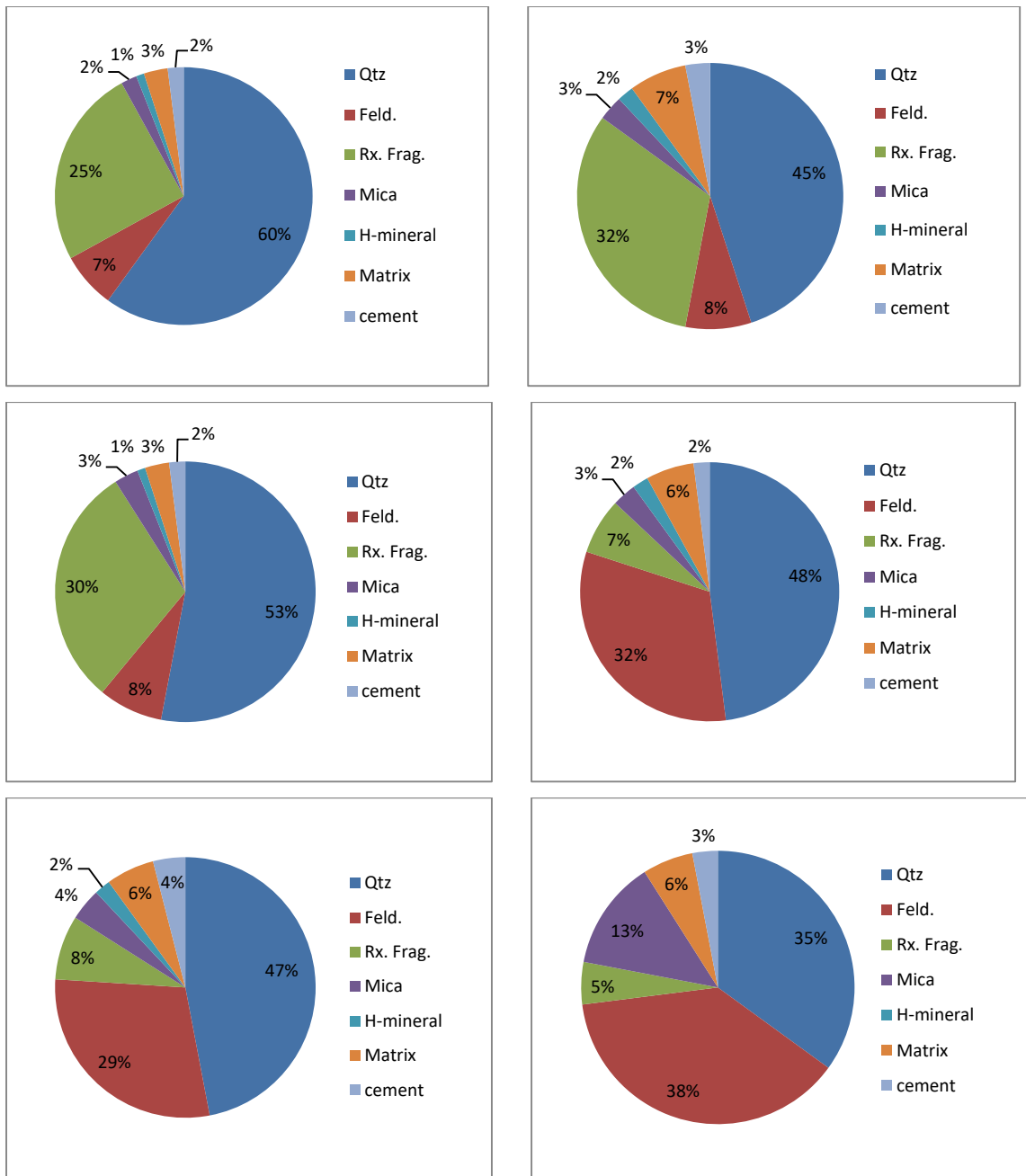


**Figure 6** Modal composition of sandstones of Kalaw Formation exposed at the study area

**Detrital Fraction**

Quartz is the most abundant mineral in these sandstones and it comprises 45 to 65 percent of the total grains. Most of the quartz grains are mono-crystalline. They show undulatory extinction and some have minute inclusions. Some of the quartz grains are corroded by the cement and are often fractured. Nearly two thirds of the total quartz grains are of igneous origin and the rest are derived from metamorphic rocks.

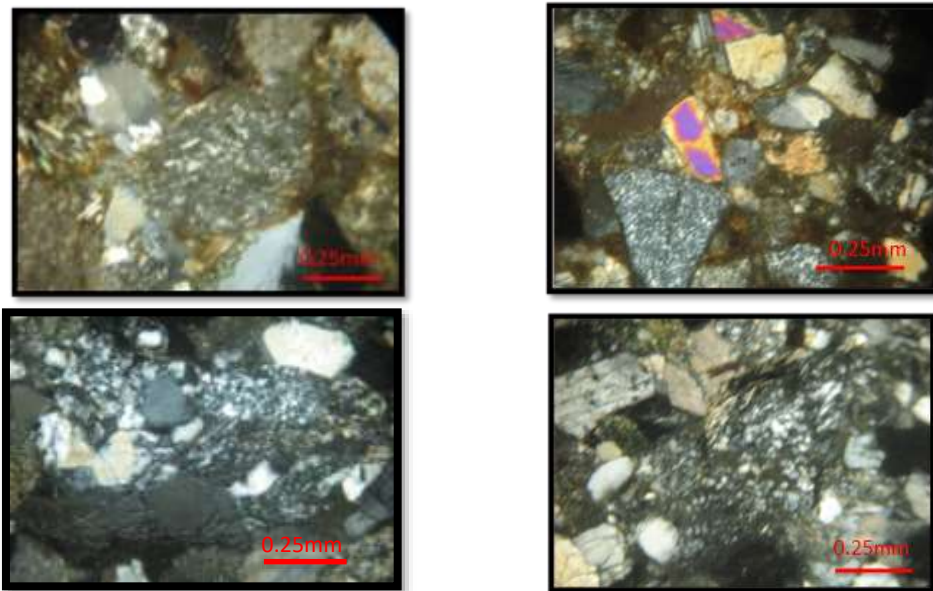
Feldspar comprises less than 10 percent of the total fractions in medium-grained sandstones, but in the finer sandstones of Kalaw Formation it reaches over 45 percent. of the different types of feldspar, potash feldspars, chiefly orthoclase, are more common than the plagioclase. Nearly all of the orthoclase shows a dull or cloudy nature and some grains include the

bright specks formed by sericitization process. Some plagioclase feldspars show polysynthetic twin.

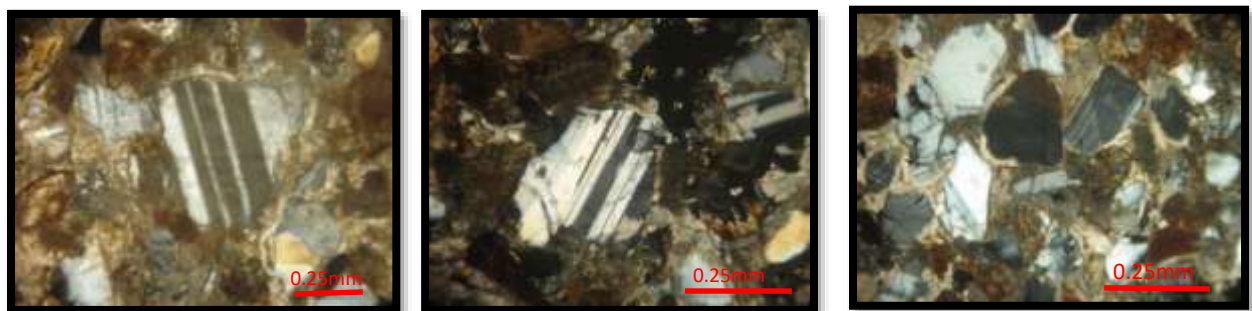
Lithic fragments are common in medium-grained sandstones comprising greater than 25 percent of the total detrital fraction, but fine-grained sandstones contain less than 10 percent. The most common lithic fragments are fine-grained sedimentary rocks such as siltstone, limestone, chert, and meta-sedimentary rock, quartzite. Stable fragments of detrital chert and quartzite grains are more abundant than the other unstable rock fragments of the siltstone. The rock fragments are generally oxidized and pigmented by hematite cement. Mostly muscovite comprises 3 to 7 percent of the framework. Bending and contorting of muscovite due to the introduction of hematite and calcite cements are frequently observed. Less than 3 percent of the detrital fraction is composed of heavy mineral grains of hematite, magnetite and hornblende.

### Nomenclature

Medium-grained of sandstones contain quartz is less than 75%, feldspar is less than 10%, and rock fragments is greater than 25%. Thus, these sandstones fall in “Litharenites” (according to Pettijohn, 1987) Figure 7. Fine-grained textures of sandstones consists of less than 75% of quartz, greater than 25% of feldspar, and less than 10% of rock fragments. So, these sandstones are fall into “Arkose” according to Pettijohn (1987), Figure 8.



**Figure 7** Photomicrographs showing litharenite of Kalaw Formation (Under XN)



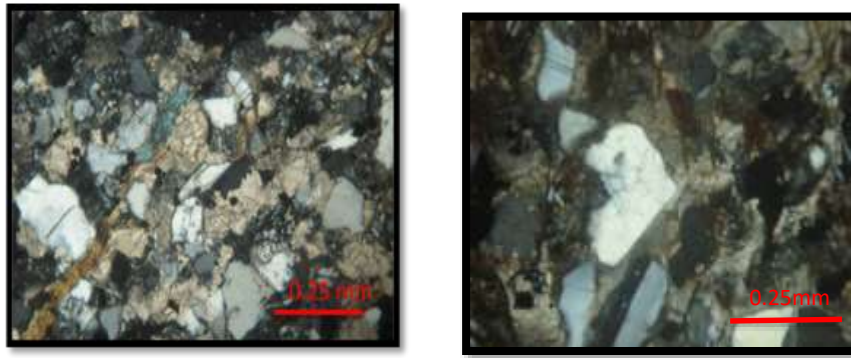


**Figure 8** Photomicrographs showing euhedral form of plagioclase feldspar in arkosic sandstone of Kalaw Formation (Between XN)

In a simple quartz-feldspar-rock fragments plot, the sandstones of the Loi-an Group were derived from the craton interior and a recycled orogeny and the sandstones of Kalaw Formation may derived from transitional continental and a recycled orogeny as shown in Figure 9 & 10.

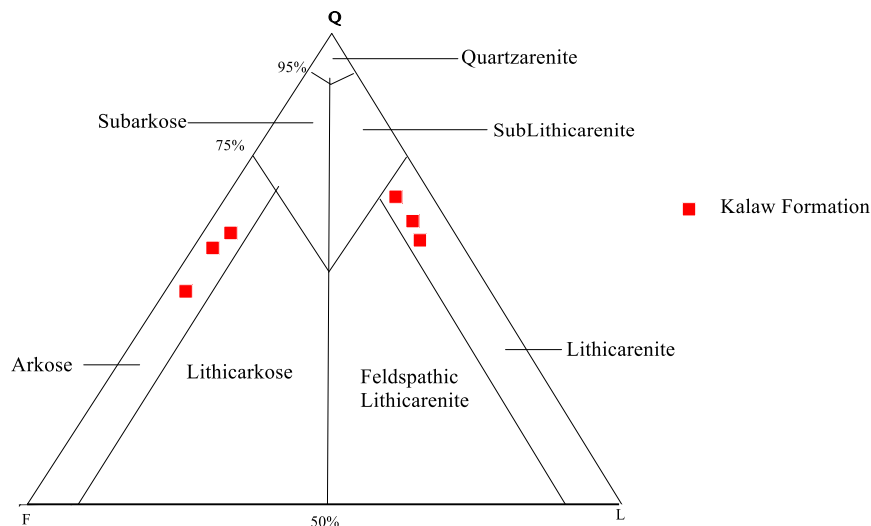


**Figure 9** QFL triangular plots of the sandstones of Loi-an and Kalaw Formation (based on Pettijohn, 1987)

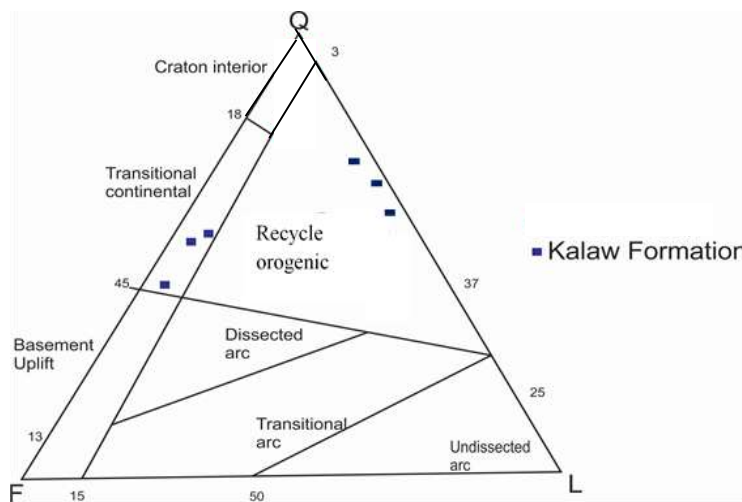


**Figure 10** QFL triangular plots showing the provenances of the sandstones of Loi-an Group and Kalaw Formation of the study area (After Dickinson, 1985)

## Diagenesis of the Kalaw Formation

Diagenesis has been divided into two stages in the study area (Kalaw Formation) such as early diagenesis, for processes taking place from deposition and into the shallow-burial realms, and late diagenesis for those processes affecting the sediments at deeper levels and on uplift. Generally, three processes of diagenesis are observed in the sandstones. These are (1) Compaction, (2) Cementation, and (3) Authigenesis.

### Compaction

The sandstones of the study area were subjected to intense mechanical and chemical compaction during burial. The grain boundaries appear to be a prominent and diagnostic feature of deeply buried sandstone and are also an indicator of compaction and geothermal gradient (Taylor, 1950 in Arif *et al.*, 2009). During compaction framework grains are sliding past each other and packed into a tighter configuration. Some of the monocrystalline quartz grains display intensive fracturing, and large detrital micas are commonly bent around more resistant grains by the forces of compaction Figure 11 (A). Corrosion of detrital grains such as quartz and feldspar are common in the study area Figure 11 (B).

### Cementation

The chemically precipitated material, which forms cement, is an important constituent of sandstones (Pettijohn, 1975 in Arif *et al.*, 2009). Iron oxide cement are the most common in Figure 12.

### Authigenesis

Authigenesis is the process by which new mineral is formed within an enclosing sediments or sedimentary rock during or after deposition by replacement or recrystallization or by secondary enlargement of quartz overgrowth. The most valid source of silica for overgrowth is probably that generated by pressure dissolution of detrital quartz grains during compaction on burial (Turner, 1980 in Arif *et al.*, 2009) or by infiltration of silica bearing pore fluids from adjacent areas. Sandstones with high content of volcanic rock fragments and feldspars are subjected too much alteration during diagenesis (Tucker, 2001). The minerals which are usually affected by alteration are feldspars. In the sandstones from the study area, partially coated Iron oxide rim around the detrital grains in the Kalaw Formation Figure 13 A & B, feldspar is altered to sericite and clay minerals Figure 14 A & B.

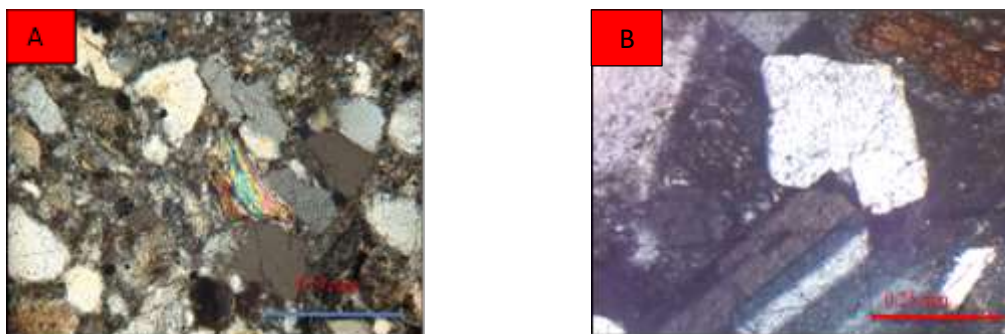


**Figure 11** Photomicrographs showing (A) bent and contorted muscovite flake due to effect of compaction in the sandstones of the Kalaw Formation (Between XN), (B) quartz grain corrosion nature in the sandstones of the Kalaw Foramtion (Between XN)

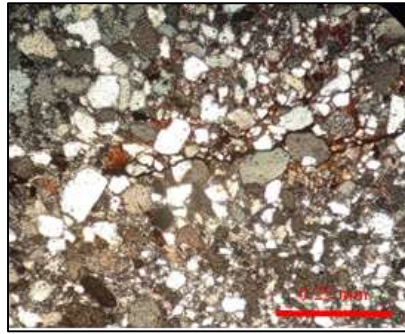


**Figure 12** Photomicrograph showing iron oxide cement in the Kalaw Formation (Between XN)

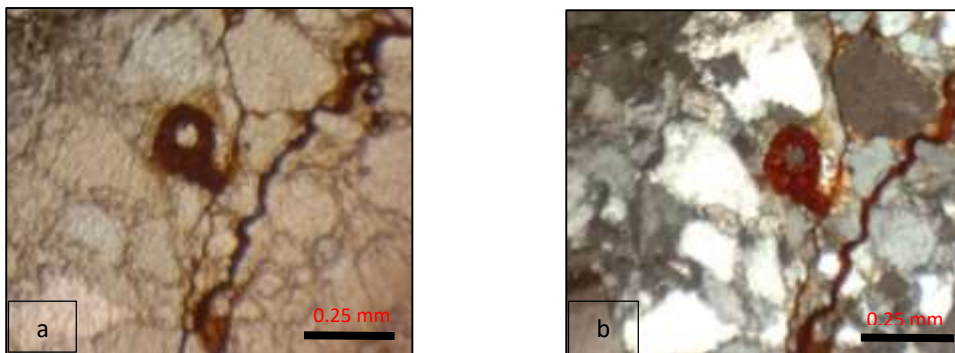


**Figure 13** Photomicrograph showing partially coated Iron oxide rim around the detrital grains in the Kalaw Formation (a) PPL, (b) X.N

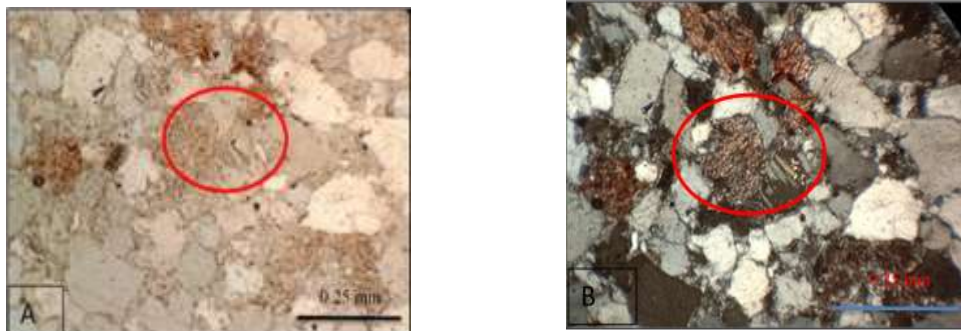


**Figure 14** Photomicrograph showing alteration of plagioclase feldspar to clay mineral in the Kalaw Formation (A) PPL, (B) X.N

### Paragenetic Diagenesis of Clastic Rocks

In the initial stage, iron oxide cementation occurs around the quartz and feldspar grains, and calcite cementation and silica cementation also appears in the detrital grains. Compaction involved dewatering and closer packing of grains. Some compaction through overburden pressure results in bending of non-resistant grains such as mica. Compaction is the main mechanical event, and began shortly after deposition with a limited amount of grains. Authigenic minerals can be formed at the early stage. Paragenetic diagenesis of clastic rocks of the study area as shown in Figure 15.

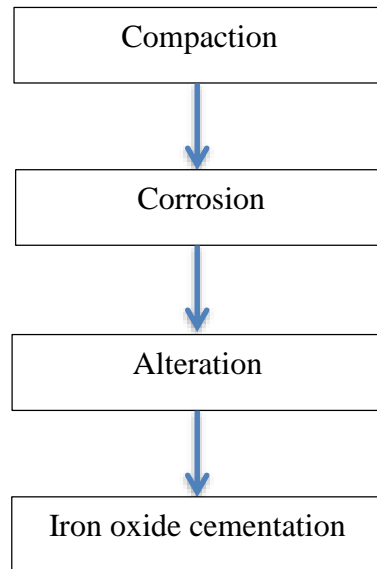


**Figure 15** Paragenetic Diagenesis of the Kalaw Formation of the Tigyit area

### Conclusion

The study area lies along the highway from Aungban to Loikaw in the Pinlaung Township, Shan State (south) and falls in the tectonic province of Shan-Tanintharyi Block or in the Eastern Highlands of Myanmar. Petrographic studies of the selected sandstone samples collected from the Kalaw Formation were carried out in detail. The sandstones of Kalaw Formation fall in “Litharenites” and “Arkose”. Three processes of diagenesis are observed in the sandstones of Kalaw Formation. These are Compaction, Cementation, and Authigenesis.

### Acknowledgements

I wish to express my special thanks to Dr. Day Wa Aung, Professor & Head, Department of Geology, and University of Yangon, Dr. Soe Moe Lwin, Professor & Head, Department of Geology, and Myeik University and Dr. Win Min Oo, Professor, Department of Geology, Myeik University for their advices, comments and great encouragements.

### References

- Amos, B.J., (1975). Stratigraphy of some of the Upper Paleozoic and Mesozoic carbonate rocks of the Eastern Highlands, Burma: *Newsl. Stratigraphy*, V.4, p.47-70.
- Aung Win Swe, (2010). Geology of the Southern Part of the Kalaw-Pinlaung Basin, Southern Shan State, Upb. *PhD Dissertation*, Department of Geology, University of Mandalay, (Unpublished), p107.
- Ba Thaw, DGSE, (1989). *Coal Exploration in Hsi-hkip Area, Pinlaung Township, Southern Shan State*
- Bender, F., (1983). *Geology of Burma*, Gebruder Brontraeger, Berlin, p. 293.
- Bertrand, G., Rangin, (2003). Tectonic of the Western Margin of the Shan Plateau (Cetral Myanmar): Implication for the India-Indochina Oblique Convergence Since the Oligocene. *Journal of Asian Earth Sciences*, vol. 21 (2003), p. 1139-1157.
- Dickinson, W.R., (1985): Interpreting provenance relationship from detrital modes of sandstones: In Zuffa, G.G., (ed.); *Provenance of Arenites*, Dordrecht, NATO ASI Series, C 148, D. Reidel Publishing Company, Dordrecht p. 333-363.
- Dickinson, W. R., Suczek, C. A., (1979), Plate tectonics and sandstone compositions: *American Association of Petroleum Geologist*, 63, 2164-2182.

- Garson, M.S., A.H.G., Mitchell and B.J., Amos, (1976). Geology of the area around Neyaungga and Ye-ngan, southern Shan State, Burma. *Overseas Mem. Inst. Geol. Sci.* No.2, 72p. Galloway, W. E., 1975, Process framework for describing the morphologic and stratigraphic evolution of deltaic depositional systems. In: *Deltas* (Ed. M. L. Broussard), pp. 87-98. Houston Geological Society.
- Krumbein, W. C. and Pettijohn, F. J., (1938), *Manual of sedimentary Petrography*, Appleton Century- Crofts, New York, 549p.
- Nichols, G. J., (1999), *Sedimentology and Stratigraphy*, 1st edition, *Blackwell Scientific Publications*, Oxford, 355pp
- Nichols, G. J., (2009), *Sedimentology and Stratigraphy*, 2nd edition, *Blackwell Scientific Publications*, Oxford, 419pp

## **PROTOLITH OF SERPENTINITE UNITS AT YEGA-INN AND KANNBYU AREAS SAGAING REGION, MYANMAR**

Hnin Min Soe\*

### **Abstract**

The study area is situated along the Sagaing Fault between the Kannbyu and Yega-Inn areas. The main objective of this study is to emphasize the serpentinite unit of ophiolite suite (Central Ophiolite Belt) along the Sagaing Fault and to discuss their protolith that is related to fault activity. The Sagaing Fault is located at the continental plate boundary between the Myanmar Plate and Sundaland Plate. It is an active fault that causes seismic damage in the major cities of Myanmar. Small outcrop of serpentinites are found in the Kannbyu area and massive bolder in the Yega-Inn (lake) area. They occurred along this fault, and examined the highly sheared serpentinite bodies in the Kannbyu and Yega-Inn areas by the Electron probe micro-analyzer (EPMA). Rock samples from these areas have not been yet up to now by EPMA laboratory analyzed method especially serpentinite units that have not been done in Myanmar. Sheared serpentinites and related rocks: such as talc and chlorite-bearing rocks, show the foliation is defined by alignments of small rock fragments. Sporadically serpentinite units in this area are completely serpentinitized, weathered, the morphology and chemistry of their spinels, coupled with micro-texture, indicate that the protolith of these serpentinites are mainly harzburgite and dunite and these units are cut by gabbroic veins in places. Chrome spinel samples showed the variable in chemical composition range of fore-arc peridotites, and they are similar to those in the mantle section of nearby ophiolites. Antigorite serpentine mineral is the main phase of the studied samples. No shape preferred orientation of the antigorite is present, indicating that the serpentinitization occurred at ~ 500 °C under relatively static conditions. Locally, these serpentinites were deformed and it is probably due to the activity of the Sagaing Fault, resulting in the formation of serpentinite schist. Serpentinitized peridotite and related minerals such as talc and saponite in the research area is probably linked to variations in the activity of the Sagaing Fault.

**Keywords:** Protolith of serpentinites, Chemical variations of spinels, Sagaing Fault activity,

### **Introduction**

The study areas: The Kannbyu and Yega-Inn along the Sagaing Fault is prone to earthquakes because it lies along the continental plate boundary between the Burma Plate and Sundaland Plate (Win Swe, 1981). The Sagaing Fault is the dextral strike-slip fault that acts as a part of a 3700 km long oblique subduction at the Sunda Trench, and it has a slip rate of 10~23 mm/year (Maurin et al., 2010; Vigny, 2003; Wang et al., 2011). The Greater Indian continent against the southeastern Asian collision caused the clockwise rotation of the subduction zone, which resulted in strike-slip faulting. Understanding of the factors controlling the pattern of seismicity along the Sagaing Fault is therefore very important for seismic risk mitigation in the major cities of the Myanmar (Fig. 1). About the magnitude (7.0 – 7.5) of earthquakes with have been produced by this fault, causing severe damages (Maurin et al., 2010; Hurukawa and Maung, 2011; Wang, 2014; Wang et al., 2011). Isolated serpentinite bodies are found intruding all the rock types along the northern part of the Sagaing Fault, especially Kannbyu and Yega-inn areas, and they are part of the Central Ophiolite Belt (Hla Htay et al., 2017). Some rocks and serpentinite units containing similarly ductile minerals are commonly believed to be the cause of the creep and low strength of the San Andreas Fault, California, USA, which is another example of a long strike-slip fault, which extends roughly 1,200 km along the tectonic boundary between the Pacific and North American Plates (Moore and Rymer, 2007; Lockner et al., 2011). The main objective of this study was to know about the protoliths of serpentinites along the Sagaing Fault and to discuss the fault activity by analyzing rock samples with the aid of EPMA method.

---

\* Dr, Professor, Department of Geology, Kyaukse University, Mandalay Region, Myanmar

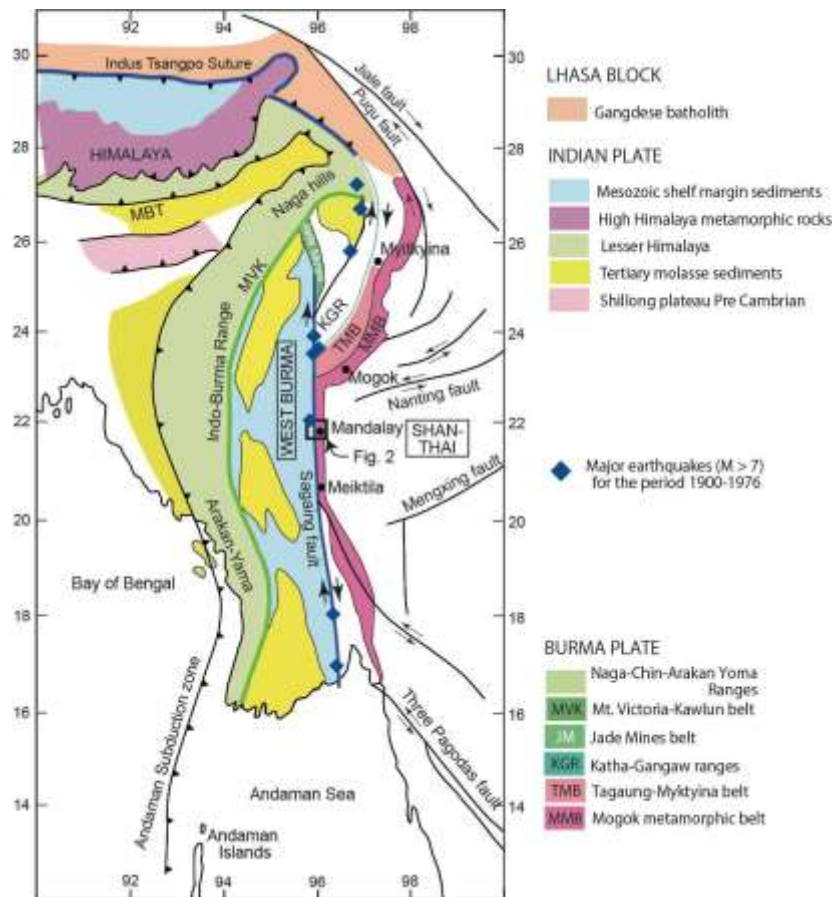


**Figure 1** Showed the geological and tectonic map around the Sagaing Fault (after Searle et al., 2007) can see the hypocenter of previous earthquakes with magnitude  $\geq 7.0$  for the period of 1900-1976 (after Sloan et al., 2017).

## 1.1 Background geology of the study areas

The study area is covered by sedimentary rocks, but metamorphic rocks of the Mogok Metamorphic Belt (MMB) occurred on the eastern side of the central part of the Sagaing Fault. Serpentinite units along the Sagaing Fault area are member of ophiolite suite especially in the Kannbyu and Yega-Inn areas, Sagaing region. Geological maps of the study areas are shown in (Fig.2).

### 1.1.1 Sagaing, Minwun and Kannbyu Areas

There is the Sagaing ridge of fairly high hills trending NNW-SSE with east dips of moderate to high angle in the east and the Minwun ridge of rolling hills with eastwards subvertical dips in the west. **They** are parallel and separated by a narrow straight valley that turns out to be the Sagaing Fault valley. The Sagaing Metamorphics from bottom to top are hornblende gneiss unit, marble unit and marble-gneiss interbedded unit. Hornblende gneiss unit consists of hornblende gneiss, biotite-hornblende gneiss, amphibolite and hornblendite. Pegmatite and quartzofeldspathic veins cut a crossed the gneisses in some places. Marble unit contains forsterite-phlogopite marble, diopside marble, and calc-silicate rocks. The grade of the Sagaing Metamorphic is ranging from amphibolite to granulite facies. Due to the radiometric dating of a phlogopite mineral by Ar-Ar method, their age of metamorphism is possibly 21 Ma (Early Miocene) (Bertrand *et al.* 1996) and the age of the Sagaing Metamorphic is Proterozoic to Late Paleozoic (Myint Thein *et al.* 2017). Carbonates and shale formed in a shallow, warm sea were the protoliths of these metamorphic

rocks. Sagaing Metamorphic can be correlated with Ordovician units which were exposed in the Shan State.

**The Minwun** Metamorphics occupy a narrow linear belt and it consists of garnet muscovite schist, kyanite muscovite schist, actinolite schist and talc chlorite schist. At Yega-Inn (lake) area serpentinite bodies are found as patches in all rock types. Slightly metamorphosed limestones (mylonitized limestones) with orbitolinid were exposed as blocks and interleaved with the greenschist units (Myint Thein 2009) in this area. Carbonate rocks, mud rocks and basic igneous rocks were the protoliths of the Minwun Metamorphic and the grade of metamorphism in the study area is from greenschist to amphibolite facies according to Kan Saw (1973). The Minwun Metamorphics is Middle to Late Triassic in age after Myint Thein (2017).

**The Kannbyu** area is located along the Sagaing Fault zone and it is the northern continuation of the Sagaing area. Two-third of that area is covered by sedimentary and metamorphic rocks with an ophiolite suite of the Central Ophiolite Belt (COB). Igneous rocks in this area are pyroxenite, serpentized peridotite, serpentinites, dolerite, plagiogranite and pillow basalt. Small serpentinite bodies are intruding all the rock types except the Pleistocene terrace deposits of the study area. They are closed association with greywacke, bedded red chert and siliceous limestones. According to the occurrence of colonial rugosa corals in limestone unit, the age of this is probably Permian to Lower Triassic (Than Htut Lwin, 2008).

The Male Formation is at the Kannbyu area consists of interbedded gritty fine-grained sandstone, siltstone and locally variegated shale with leaf fossils. Due to the U – Pb dating method for the detrital zircon from this formation is about 48 Ma (Eocene) (Myint Thein, 2017). The Minwun Metamorphics rocks are overlying by a sedimentary stratum which is assigned to the Upper Pegu Group (Miocene) (Maung Maung 1982; Myint Thein et al. 1982). Outcrops of sandstone unit in the Irrawaddy Formation occurred as a narrow linear belt between the Sagaing Metamorphic rocks and the Ayeyarwady River. The Irrawaddy Formation consists of fluvial deposits (upper part) and fanglomerate unit (lower part) in which vertebrate fossils assemblages are found (Myint Thein 2017). Terrace deposits are widespread along the Ayeyarwady River. Due to above finding vertebrate fossils; the probable age of this unit is Middle to Upper Pleistocene (Than Htut Lwin, 2008). Alluvial deposits covered in the study area especially along the valley of the Sagaing Fault.

### 1.1.2 Central Ophiolite Belt (COB)

The study area lies in the Central Ophiolite Belt (COB) and it is located in the northern part of the Myanmar which is also between the Western and Eastern Inner-Burma Tertiary Basins (Hla Htay et al., 2017). It extends from the Putao area of Kachin State in the north, through the Phakant-Tawmaw and to the Sagaing-Minwun ranges in the south and terminates at central part of the Myanmar. There are four ophiolite occurrences so far from south to north, the Minwun range, Kyaukpahto area, Indawgyi area and Phakant-Tawmaw area.

According to Hla Htay et al., (2017) the Central Ophiolite Belt (COB) is dismembered incomplete ophiolite composing of peridotite and serpentinites. The mafic cumulate part of ophiolite sequence at the Indawgyi area, however the mafic sheet dyke complex is almost missing. As metamorphic fabric, the Katha Metamorphics (Triassic), greenschist can be observed in the south, the amphibolites schist present at the Indawgyi area in the middle and Glaucophene schist at jade mine area in the north. The metamorphism increases from south to north. The associated sedimentary rocks are mostly greywacke, argillite, chert of the Ngapyawdaw Chaung Formation in the Kyaukpahto and Minwun areas, and molassic sedimentary rocks just covered the Indawgyi and jade mine areas. Jade mines are present in the north of this belt particularly the Phakant-

Tawmaw area. Small amount of chromite, magnetite, gold and platinum group minerals (PGM) are found in this belt.

## Sample Interpretation

### 2.1 Serpentinite unit

In the study area, serpentinite is a member of ophiolite suite which lies in the Central Ophiolite Belt (COB). Serpentinite outcrops along the Sagaing Fault are irregular bodies sporadically exposed at the Kannbyu and Yega-Inn (lake) areas (Fig.3). They are green to dark green in both on fresh and weathered surface and a characteristic soapy appearance is common in light green or dark green serpentinite exposures. Microscopically, serpentine minerals can be divided into three such as lizardite, antigorite and chrysotile and relict olivine, magnetite and chromite occurred as accessories minerals. Pseudomorphic, non-pseudomorphic and serpentine veins are three types of serpentine textures under microscope. Lizardite is abundant in pseudomorphic texture and more antigorite found in non-pseudomorphic texture. Chrysotile occurred as veins serpentine. Among them non-pseudomorphic texture is common in antigorite serpentine. Antigorite found as anhedral grains or aggregates of lamellar flakes in most thin section study (Fig.11).

In the Yega-Inn area, the fault traces steps to the right in a relay on the east side of the lake (Fig.4). Some parts of the serpentinites are extensively sheared (Fig.5), and serpentinite-related rocks, such as talc and/or chlorite-bearing rocks are also observed. Greywacke (Fig.6), chert (Fig.7), limestone (Fig.8), and gabbroic (Fig. 9) rocks are observed around the outcrops of serpentinite and these rocks are interpreted to represent a dismembered ophiolitic suite (Hla Htay et al., 2017). A foliation defined by the alignments of small rock fragments and minerals in the sheared serpentinite strikes nearly N-S trends and dips to the east (Fig.5). Carbonate veins are common in the Kannbyu area (Fig.10). Specimens collected relatively from massive blocks in the sheared zones, including three serpentinitized blocks (samples KC, KE and KF) from the Kannbyu area, and three serpentinitized blocks (samples YK, YL and YP) from the Yega-Inn area.

The presumed primary silicate minerals of the original ultramafic rocks, such as olivine and pyroxenes are absent from the study samples due to serpentinitization and weathering. The main serpentine phase in the study samples was confirmed to be aggregates of lamellar flakes antigorite (Fig.11) by Raman micro-spectrometry at Kanazawa University, Japan. Although it is difficult to know the primary structure before serpentinitization, aggregates of magnetite is sometimes aligned in sub-millimeter-sized and they probably represent the lamellae of pyroxene (bastite-like texture) (Figs.12a and 12b). The antigorite is light green to colorless and show no shape-preferred orientation in most samples (Figs. 12a and 12b), but sample KC shows a slight shape-preferred orientation of antigorite in the form of an anastomosing network (Figs. 12c and 12d). Weathered olivine was also observed in sample KC (Figs 12e and 12f). A dusty serpentine with yellowish interference color occurs rarely in veinlets and/or networks (Figs. 12a and 12b). Sample YK exhibits dusty-colored fine-grained mineral networks of tremolite and chlorite with an alignment that is parallel to the anastomosing network of antigorite (Figs 12g and 12h). Grains of spinels are partly to completely altered, but they have retained their original shape (Fig.13a). The spinels are subhedral to vermicular texture involving magnetite along their rims (Fig.13b-f).

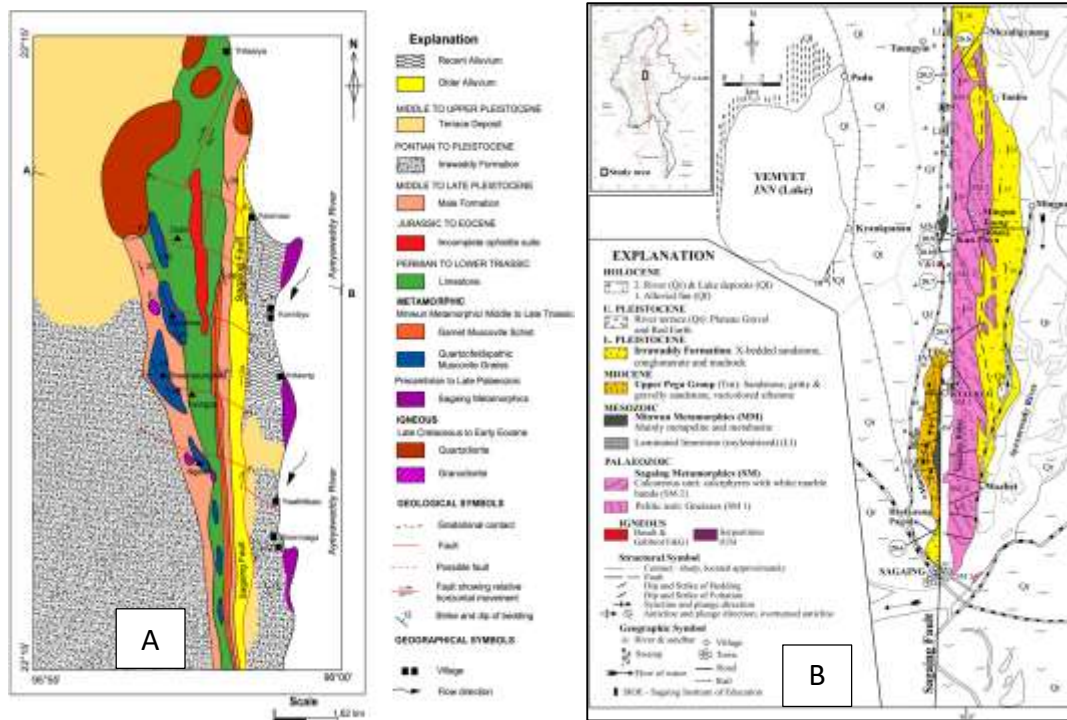


**Figure 2 (A & B)** Geological map of the Kannbyu and Yega-Inn areas, Sagaing Region. (A) after Hla Htay et.al, (2017) and (B) Myint Thein (2017).



(source: Google).

**Figure 3** Location of serpentinite outcrops at Kannbyu and Yega-Inn areas

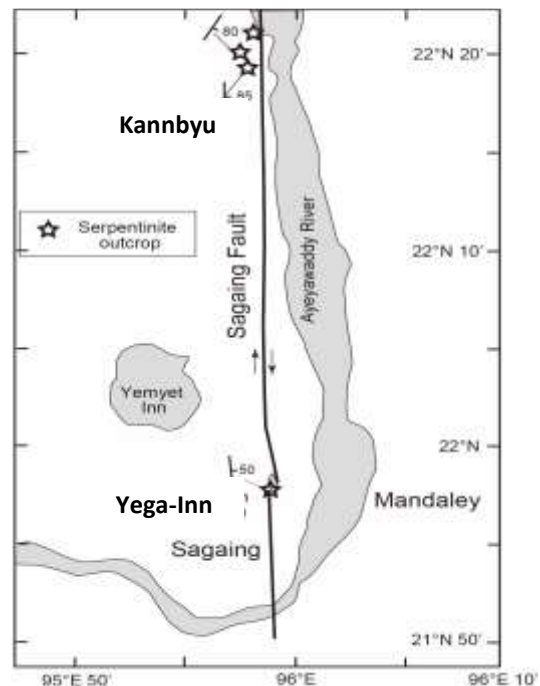


**Figure 4** Locality of serpentinite outcrops showing direction of sheared plane.



**Figure 5** Exposures of serpentinite schists at the Kannbyu area and the Yega-Inn areas.



**Figure 6** Well joint sets in greywacke unit exposed at Kannbyu area.



**Figure 7** Highly brecciated nature of chert unit outcrop at Kannbyu area.



**Figure 8** Massive type limestone unit exposed at Kannbyu area.



**Figure 9** Bold massive unit of gabbro exposed at Kannbyu area.

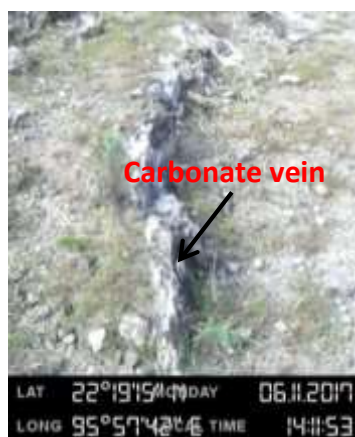


**Figure 10** N-S trending carbonate vein near serpentinite unit at Kannbyu area.

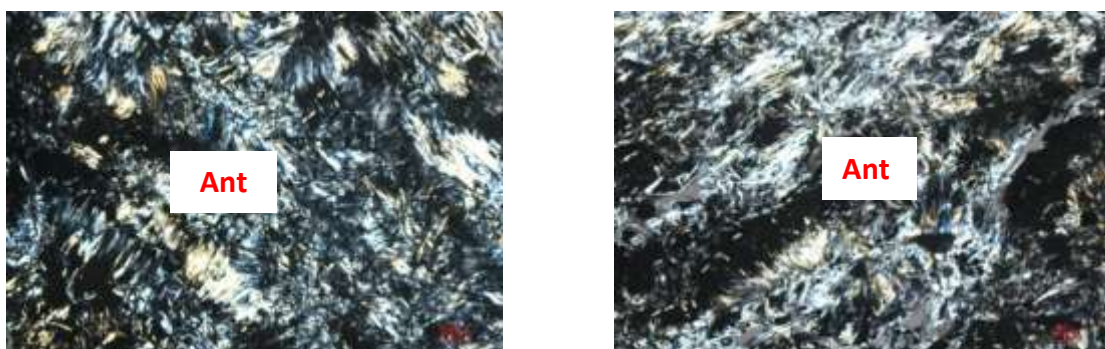


**Figure 11** Photomicrographs showing the non-pseudomorphic texture of antigorite (Ant) in serpentinite unit at Kannbyu area.

## Chemical Analysis of Serpentine Minerals

### 3.1. Analytical method

The study of major-element compositions of minerals in the research area were decided using an electron probe micro-analyzer (EPMA) (JEOL JXA-8800 Superprobe, JEOL) at Kanazawa University, Japan. The analytical data were performed with an accelerating voltage of 20 kV and beam current of 20 nA. A beam diameter of 3  $\mu\text{m}$  was applied to all analytical points. Natural and synthetic mineral standards provided by JEOL were applied for data reduction, using ZAF corrections of JEOL software. In-house mineral standards (chromian spinel, olivine, diopside and Potash feldspar) were analyzed repeatedly to check daily data quality on a daily basis. The measured concentrations of all elements in these in-house minerals are consistent with the averaged values from long-term analyses and are within the standard deviation. Data precision, confirmed by multiple analyses of single points of standard minerals prepared in-house, was better than 5% and 10% relative standard deviation from the averaged values for elements with contents  $>0.5$  wt% and  $<0.5$  wt%, respectively. The major element compositions of analyzed minerals are listed in Table 1-3.

### 3. 2. Analytical results

The  $\text{Al}_2\text{O}_3$  content of serpentines varies from  $<0.02$  to 3.4 wt% (Table-1). The NiO content of the serpentine is usually  $<0.3$  wt%, but for the dusty serpentine it is  $>0.6$  wt% (up to 1.5 wt%) (Table-1). The XMg (=  $\text{Mg}/(\text{Mg} + \text{Fe total})$  atomic ratio) values of serpentine ranges from 0.96 to 0.99 for sample KF (one analysis for sample SC gave a similar composition), and 0.92 to 0.95 for samples YK, YL and YP, respectively (Table-1). The values of Mg# (=  $\text{Mg} / (\text{Mg} + \text{Fe}_{2+})$  atomic

ratio) and Cr# ( $= \text{Cr} / (\text{Cr} + \text{Al})$  atomic ratio) in the spinel cores are respectively 0.353 - 0.413 and 0.798 - 0.818 for sample KC, 0.460 - 0.587 and 0.681 - 0.695 for sample KE and 0.372 - 0.555 and 0.777 - 0.803 for sample KF (Fig.14). The chrome spinel in samples YK, YL and YP are generally having high contents of  $\text{Fe}^{3+}$ , even in the core of grains (i.e., ferritchromite, Cr-magnetite and magnetite (Fig.14). The cores of chrome spinels in sample KC, KE and KF have low contents of  $\text{Fe}^{3+}$  [ $\text{YFe}^{3+} < 0.1$ , where  $\text{YFe}^{3+} = \text{Fe}^{3+} / (\text{Fe}^{3+} + \text{Al} + \text{Cr})$  atomic ratio, and they have ferritchromite and Cr-magnetite rims. The  $\text{TiO}_2$  contents of the core of chrome spinel in samples KC, KE and KF are  $< 0.05$  wt%. The Cr-magnetite in sample YK has a higher  $\text{TiO}_2$  content (up to 1.2 wt%) than in the other samples (Table-2). Amphibole in sample YK is tremolite (Table-3).

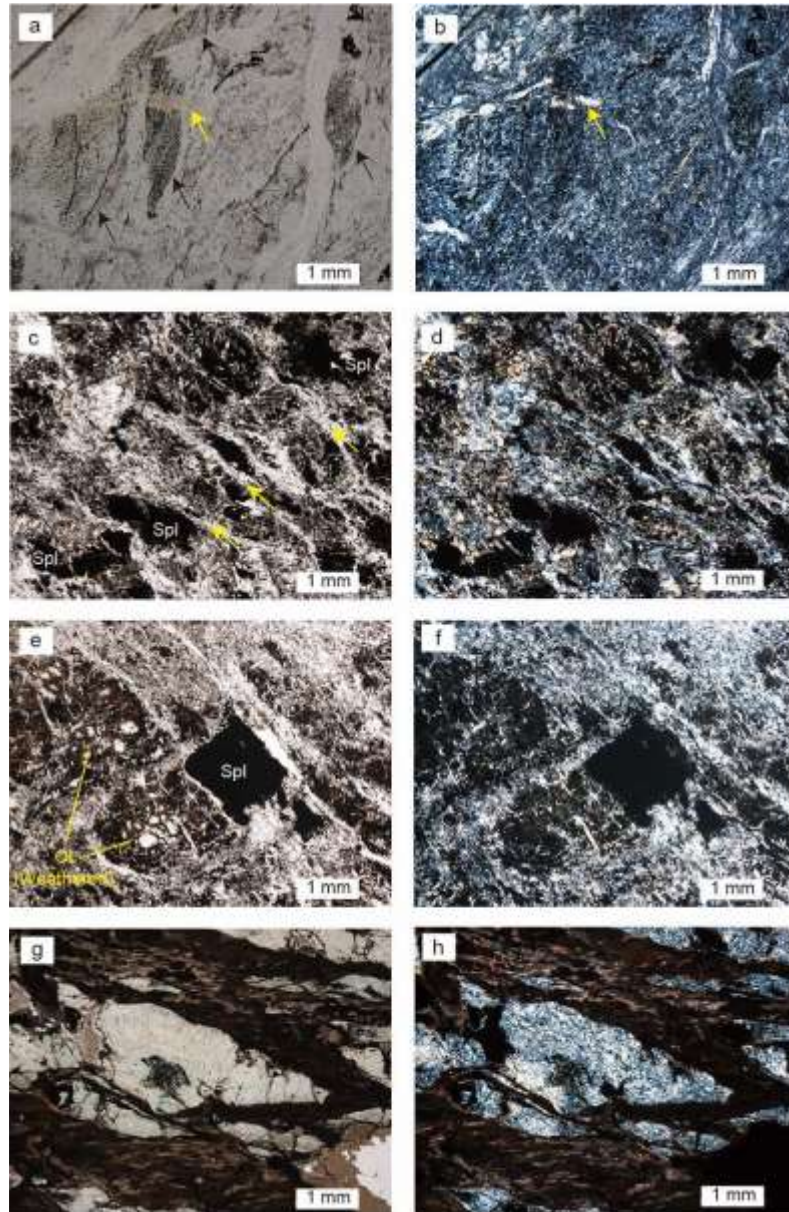


**Figure 12** Photomicrographs of the studied serpentinite blocks. (a) Magnetite aggregates (black arrows) in antigorite matrix. Dusty serpentine veinlet is also observed (yellow arrow), between P.P.L (b) under X.N. (c) Antigorite network parallel to the direction of antigorite elongation (yellow arrows) between P.P.L (d) under X.N (e) Weathered olivine in antigorite matrix, between P.P.L (f) under X.N. (g) Chlorite-tremolite network (dark-colored) in antigorite matrix, between P.P.L (h) under X.N.

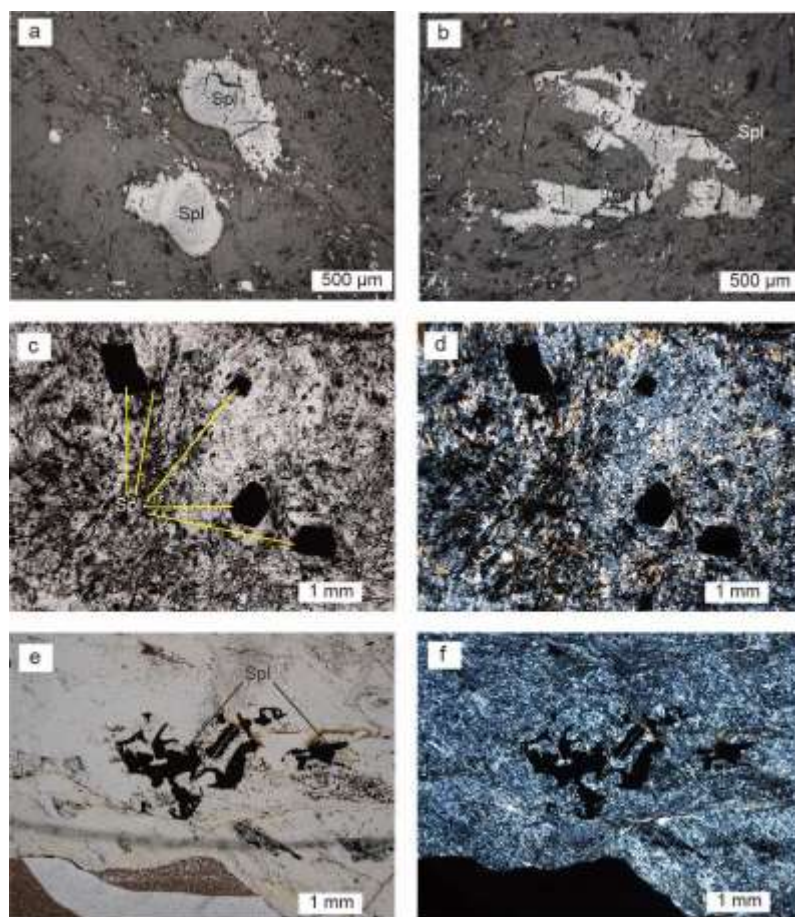


**Figure 13** Photomicrographs showing occurrence and shape of chrome spinels. Reflected light image of subhedral chrome spinel (a) vermicular chrome spinel, (b) showing zoning, (c) Euhedral to subhedral shaped chrome spinel between P.P.L (d) under X.N. (e) Vermicular-shaped spinel between P.P.L (f) under X.N.

**Table 1 Representative Olivine compositions (Serpentine composition)**

| Locality                       | Kannbyu |        |        |        |        |        |
|--------------------------------|---------|--------|--------|--------|--------|--------|
|                                | KF      | KF     | KF     | KF     | KF     | KF     |
| Area                           | 1       | 1      | 1      | 2      | 2      | 3      |
| Note                           |         | Blade  | brown  | blade  |        | Blade  |
| SiO <sub>2</sub>               | 44.30   | 45.60  | 45.90  | 44.80  | 45.40  | 44.60  |
| TiO <sub>2</sub>               | <0.04   | <0.04  | <0.04  | <0.04  | <0.04  | <0.04  |
| Al <sub>2</sub> O <sub>3</sub> | 1.73    | 0.03   | < 0.03 | 1.31   | <0.03  | 1.43   |
| Cr <sub>2</sub> O <sub>3</sub> | 0.79    | 0.05   | 0.05   | 0.18   | <0.05  | 0.08   |
| FeO                            | 1.61    | 1.80   | 0.84   | 2.42   | 0.54   | 2.62   |
| MnO                            | <0.05   | < 0.05 | < 0.05 | < 0.05 | < 0.05 | < 0.05 |
| MgO                            | 38      | 40.10  | 41.20  | 39.30  | 39.80  | 38.70  |
| CaO                            | <0.03   | <0.03  | <0.03  | <0.03  | <0.03  | <0.03  |
| Na <sub>2</sub> O              | <0.03   | <0.03  | <0.03  | <0.03  | <0.03  | <0.03  |
| K <sub>2</sub> O               | <0.03   | <0.03  | <0.03  | <0.03  | <0.03  | <0.03  |
| NiO                            | 0.13    | 0.28   | 0.15   | 0.15   | 0.22   | 0.16   |
| Total                          | 87.80   | 88.20  | 88.10  | 88.30  | 86.10  | 87.90  |
| Mg                             | 0.98    | 0.96   | 0.98   | 0.97   | 0.99   | 0.96   |

**Note:** Mg# = Mg/(Mg + Fe) atomic ratio

**Table 2 Representative chrome spinel compositions (Serpentine composition)**

| Locality                                                                                                                                                                     | Kannbyu |        |        |        |        |        |
|------------------------------------------------------------------------------------------------------------------------------------------------------------------------------|---------|--------|--------|--------|--------|--------|
|                                                                                                                                                                              | KC      | KC     | KC     | KC     | KE     | KE     |
| Area                                                                                                                                                                         | 1       | 1      | 3      | 7      | 1      | 1      |
| Note                                                                                                                                                                         | Core    | Rim    | Core   | Core   | Core   | Core   |
| SiO <sub>2</sub>                                                                                                                                                             | < 0.03  | 0.27   | < 0.03 | < 0.04 | < 0.03 | < 0.03 |
| TiO <sub>2</sub>                                                                                                                                                             | < 0.04  | < 0.04 | < 0.04 | < 0.04 | < 0.04 | < 0.04 |
| Al <sub>2</sub> O <sub>3</sub>                                                                                                                                               | 8.77    | 0.00   | 9.27   | 9.82   | 16.26  | 15.55  |
| Cr <sub>2</sub> O <sub>3</sub>                                                                                                                                               | 58.30   | 0.30   | 57.50  | 57.60  | 51.60  | 52.70  |
| FeO                                                                                                                                                                          | 23.70   | 87.60  | 22.80  | 23.80  | 21.50  | 16.70  |
| MnO                                                                                                                                                                          | 0.76    | 0.29   | 0.73   | 0.56   | 0.70   | 0.92   |
| MgO                                                                                                                                                                          | 8.17    | 2.46   | 7.98   | 6.92   | 9.46   | 11.47  |
| NiO                                                                                                                                                                          | 0.02    | 1.55   | 0.04   | 0.03   | 0.05   | 0.02   |
| Total                                                                                                                                                                        | 99.50   | 92.30  | 98.40  | 98.80  | 99.60  | 97.50  |
| XMg                                                                                                                                                                          | 0.41    | 0.14   | 0.41   | 0.35   | 0.46   | 0.55   |
| Cr                                                                                                                                                                           | 0.82    | 1.00   | 0.81   | 0.79   | 0.68   | 0.68   |
| YCr                                                                                                                                                                          | 0.77    | 0.03   | 0.76   | 0.78   | 0.66   | 0.67   |
| YAl                                                                                                                                                                          | 0.18    | 0.00   | 0.19   | 0.17   | 0.32   | 0.31   |
| YFe <sup>3+</sup>                                                                                                                                                            | 0.04    | 0.98   | 0.04   | 0.02   | 0.02   | 0.01   |
| <b>Note:</b> Fe <sup>3+</sup> was calculated based on stoichiometry. XMg = Mg/(Mg + Fe <sup>2+</sup> ), Cr# = Cr/(Cr + Al),<br>YCr = Cr/(Cr Table-2-serpentine composition). |         |        |        |        |        |        |

**Table 3 Representative amphibole compositions.**

| Locality                                     | Yega-Inn |        |        |        |
|----------------------------------------------|----------|--------|--------|--------|
|                                              | YK       | YK     | YK     | YK     |
| Area                                         | 1        | 1      | 2      | 2      |
| Note                                         | brown    |        | brown  |        |
| SiO <sub>2</sub>                             | 57.90    | 57.90  | 57.60  | 58.50  |
| TiO <sub>2</sub>                             | 0.05     | < 0.04 | < 0.04 | < 0.04 |
| Al <sub>2</sub> O <sub>3</sub>               | 0.08     | 0.10   | 0.12   | 0.06   |
| Cr <sub>2</sub> O <sub>3</sub>               | < 0.05   | < 0.05 | < 0.05 | < 0.05 |
| FeO                                          | 3.02     | 4.09   | 4.05   | 2.76   |
| MnO                                          | 0.09     | 0.00   | 0.11   | 0.08   |
| MgO                                          | 22.60    | 21.9   | 22.10  | 23.00  |
| CaO                                          | 12.90    | 12.70  | 12.40  | 12.90  |
| Na <sub>2</sub> O                            | < 0.03   | 0.05   | < 0.03 | 0.06   |
| K <sub>2</sub> O                             | 0.03     | 0.03   | 0.04   | < 0.03 |
| NiO                                          | 0.08     | 0.10   | 0.13   | 0.10   |
| Total                                        | 96.80    | 97.00  | 96.50  | 97.40  |
| XMg                                          | 0.93     | 0.91   | 0.91   | 0.94   |
| <b>Note:</b> XMg = Mg/(Mg + Fe) atomic ratio |          |        |        |        |

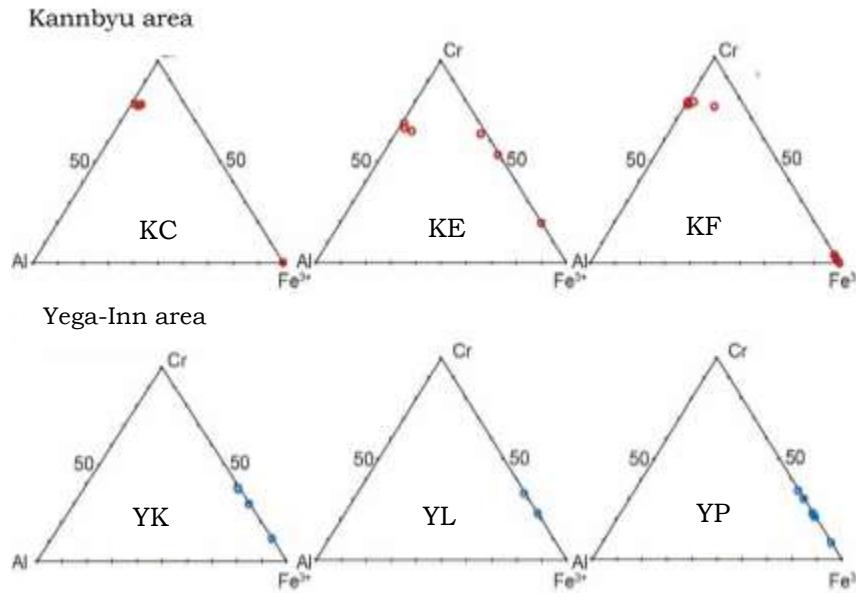


**Figure 14** Trivariant cation ratio of chrome spinel groups in serpentinites from the Kannbyu area (samples KC, KE and KF) and the Yega-Inn area (samples YK, YL and YP).

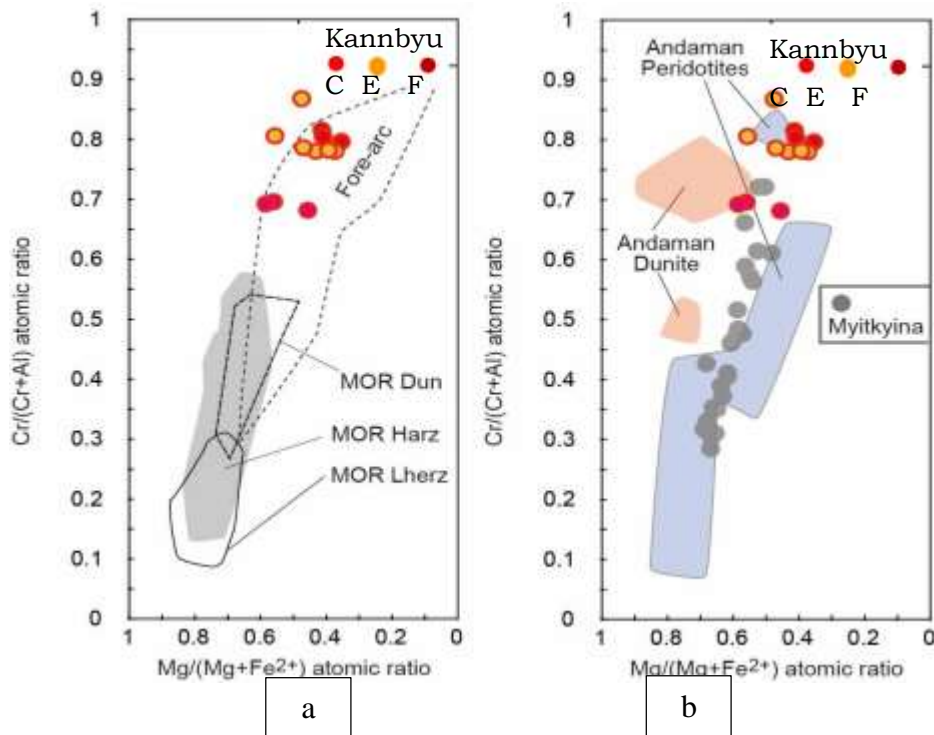


**Figure 15** Relationships between XMg (= Mg/(Mg + Fe<sup>2+</sup>) atomic ratio) and Cr# (= Cr/(Cr + Al) atomic ratio) of the less altered spinels with < 0.1 YFe<sup>3+</sup> (= Fe<sup>3+</sup>/(Fe<sup>3+</sup> + Al + Cr) atomic ratio) from the Kannbyu area. (a) Comparison between the studied samples and the compositional ranges of mid-ocean ridge-related abyssal peridotites and fore-arc peridotites (broken line). Data are from Warren (2016) for mid-ocean ridge abyssal peridotites, and Ishii et al. (1992) and Parkinson and Pearce (1999) for fore-arc peridotites, respectively. (b) Comparison between the studied samples and chrome spinels from the mantle section of the Andaman ophiolite (Ghosh et al., 2013) and the Myitkyina ophiolite (spinel peridotites from Liu et al., 2016).

## Discussions

### 4.1. Protolith of the serpentinite

Although the studied serpentinites are highly serpentized, spinel morphology indicates the protolith of chrome spinel peridotite (Matsumoto and Arai, 2005). The samples with bastite-like texture (Figs. 12a and 12b) and vermicular to anhedral shaped chrome spinel (Fig. 13) indicates that the protoliths were pyroxene-bearing peridotites. The less altered spinel cores in these samples are characterized by high values of Cr# and low contents of TiO<sub>2</sub>. We concluded, therefore, that the protolith of the studied serpentines was mainly a residual harzburgite that formed after a high degree of partial melting. Sample KF contains chrome spinel with subhedral to euhedral shape (Figs. 13c and 13d) and no bastite-like textures, and its protolith was probably dunite. The chrome spinels in sample KF are also characterized by high values of Cr#. Sample YK is characterized by the presence of tremolite-chlorite networks, and some of the Cr-magnetites show high TiO<sub>2</sub> contents, indicating a local enrichment of TiO<sub>2</sub> related to the network formation. The tremolite-chlorite networks (Figs. 12g and 12h), coupled with high contents of TiO<sub>2</sub> in the chrome spinels, indicate that the protolith of sample YK was a peridotite with gabbroic veins, with the veins now replaced by tremolite and chlorite.

### 4.2. Serpentinites Origin

The chemical compositions of the less altered spinel grains in the studied samples do not much those of chrome spinels in abyssal peridotites from a mid-ocean ridge setting, but they are similar to those of chrome spinels in fore-arc peridotites (Fig. 15a). Antigorite is generally interpreted to be stable under higher-temperature conditions (~500°C) than lizardite/crysotile, and mantle wedge peridotites are likely to be affected by hydration under the conditions at which antigorite is stable (e.g., Peacock and Hyndman, 1999; Mizukami et al., 2014). Peridotites with high Cr# spinel have been reported from the mantle section of ophiolites located regionally close to the present study area (e.g., the Myitkyina ophiolites: Liu et al., 2016; the Andaman ophiolite: Ghosh et al., 2017) (Fig. 15b). The highly refractory harzburgites ( $\pm$  dunite) in these ophiolites are interpreted as arc-related magmatic modifications of the mantle. Serpentinized peridotites in the Jade Mines Belt are antigorite serpentinite (Shi et al., 2005 MM), and they are mainly harzburgite, dunite and wehrlite (Searle et al., 2017).

## Conclusions

The study samples were collected from massive outcrops in highly sheared zone, along the Sagaing Fault. These outcrops do not usually show preferred orientation of antigorite. Peridotite unit of the Jade Mines Belts and ultramafic rocks (peridotites) and nearby ophiolites of the study area are not clear, it is expected that serpentization of ophiolitic mantle materials was initiated under static conditions prior to shearing along the Sagaing Fault, and that the serpentinites were then exhumed to the surface, probably as a result of movement on the fault. One of the important factors controlling fault behavior is the presence of weak materials such as serpentinite (e.g., Moore and Rymer, 2007), and studies of the San Andreas Fault revealed that serpentine-related minerals such as talc and saponite exist along the fault and their sliding behavior might cause fault creep (Moore and Rymer, 2007; Lockner et al., 2011). It is clear, therefore, that further investigation of the relationships between the activity of the Sagaing Fault and local geology is required for a better understanding of further seismic risk along this fault zone in Myanmar. This research is also emphatically meant to stimulate the interest of the future workers for improving the current findings with better expositions.

## Acknowledgement

Firstly, I am deeply thankful to Faculty of Geosciences and Civil Engineering, Kanazawa University, Japan, for permission to analyze the samples in EPMA analytical method in the lab there, this lab work is supported by JST (Japan Science Technology) Japan- Asia Youth Exchange short term program in 2018.

## References

- Bertrand, G., Rangin, C., Maluski, H., Bellon, H. & Giac Party, (1996). Diachronous cooling along the Mogok Metamorphic Belt (Shan Scarp, Myanmar): the trace of northward migration of the Indian syntaxis. *Journal of Asian Earth Sciences*, 19, 649–659.
- Curray, J.R., (2005). Tectonics and history of the Andaman Sea region 25. <https://doi.org/10.1016/j.jseaes.2004.09.001>.
- Ghosh, B., Morishita, T., Bhatta, K., (2013). Significance of chromian spinels from the mantle sequence of the Andaman Ophiolite, India: Paleogeodynamic implications. *Lithos* 164–167, 86–96. <https://doi.org/10.1016/j.lithos.2012.08.004>
- Ghosh, B., Bandyopadhyay, D., Morishita, T., (2017). Andaman–Nicobar Ophiolites, India: origin, evolution and emplacement. *Geol. Soc. London, Mem.* 47, 95–110. <https://doi.org/10.1144/M47.7>
- Hla Htay, Khin Zaw, Than Than Oo, (2017). The mafic–ultramafic (ophiolitic) rocks of Myanmar. *Geol. Soc. London, Mem.* 48, 117–141. <https://doi.org/10.1144/M48.6>
- Hurukawa, N., Maung, P.M., (2011). Two seismic gaps on the Sagaing Fault, Myanmar, derived from relocation of historical earthquakes since 1918 38, 1–5. <https://doi.org/10.1029/2010GL046099>.
- Ishii, T., Robinson, P.T., Maekawa, H., Fiske, L., (1992). Petrological studies of peridotites from serpentinite diapiric seamounts in the Izu-Ogasawara-Mariana fore arc, ODP Leg 125. In: Fryer, P., Pearce, J.A., Stokking, L.B., et al. (Eds.), *Proceedings of the Ocean Drilling Program, Scientific Results, 125*, College Station, Texas (Ocean Drilling Program), 445–485.
- Kan Saw (1973). *Geology of the Northern Mingun-Kabwet area*. MSc thesis, Mandalay University.
- Le Dain, A.Y., Tapponnier, P., Molnar, P., (1984). Active faulting and tectonics of Burma and surrounding regions. *J. Geophys. Res.* 89, 453. <https://doi.org/10.1029/JB089iB01p00453>.
- Liu, C., Zhang, C., Xu, Y., Wang, J., Chen, Y., Guo, S., Wu, F., Sein, K., (2016). Petrology and geochemistry of mantle peridotites from the Kalaymyo and Myitkyina ophiolites (Myanmar): Implications for tectonic settings. *Lithos* 264, 495–508. <https://doi.org/10.1016/j.lithos.2016.09.013>.
- Lockner, D.A., Morrow, C., Moore, D., Hickman, S., (2011). Low strength of deep San Andreas fault gouge from SAFOD core. *Nature* 472, 82–86. <https://doi.org/10.1038/nature09927>.
- Matsumoto, I., Arai, S., (2001). Morphological and chemical variations of chromian spinel in dunite-harzburgite complexes from the Sangun zone (SW Japan): implications for mantle /melt reaction and chromitite formation processes. *Mineral Petrol.* 73, 305–323. <https://doi.org/10.1007/s007100170004>
- Maung Maung (1982). The geology of Kyaukta area. Paper presented at the Natural Science Research Congress, 21 June 1982, Rangoon.
- Maurin, T., Masson, F., Rangin, C., Min, U.T., Collard, P., (2010). First global positioning system results in northern Myanmar: Constant and localized slip rate along the Sagaing fault. *Geology* 205 38, 591–594. <https://doi.org/10.1130/G30872.1>.
- Mizukami, T., Yokoyama, H., Hiramatsu, Y., Arai, S., Kawahara, H., Nagaya, T., Wallis, S.R., (2014). Two types of antigorite serpentinite controlling heterogeneous slow-slip behaviours of slab mantle interface. *Earth Planet. Sci. Lett.* 401, 148–158. <https://doi.org/10.1016/j.epsl.2014.06.009>.
- Moore, D.E., Rymer, M.J., (2007). Talc-bearing serpentinite and the creeping section of the San Andreas fault. *Nature* 448, 795–797. <https://doi.org/10.1038/nature06064>.
- Myint Thein, Kyaw Tint & Kan Saw (1982). *Geology of the eastern margin of the Central Burma Belt between Sagaing and Tagaung*. Research Titles, Geoscience Group. Policy Directing Committee on Research Projects, Burma, 259–303.
- Myint Thein (2009). Age, petrography and deformation of Laminated Limestone Unit the west side of the Sagaing Fault, Sagaing Division. Abstract presented at the Research Seminar, Myanmar Geosciences Society, 28 November 2009, Yangon.
- Myint Thein (2017). Current tectonic activity along the Sagaing Fault, Myanmar indicated by alluvial fans. In: Barber, A.J., Khin Zaw & Crow, M.J. (eds) *Myanmar: Geology, Resources and Tectonics*. Geological Society, London, *Memoirs*, 48, 443–452, <https://doi.org/10.1144/M48.20>

- Parkinson, I.A.N.J., Pearce, J.A., (1998). Peridotites from the Izu – Bonin – Mariana Forearc (ODPLeg 125): Evidence for Mantle Melting and Melt – Mantle Interaction in a Supra-Subduction Zone Setting 39, 1577–1618. <https://doi.org/10.1093/etroj/39.9.1577>.
- Peacock, S.M., Hyndman, R.D., (1999). Hydrous minerals in the mantle wedge and the maximum depth of subduction thrust earthquakes. *Geophys. Res. Lett.* 26,2517–2520. <https://doi.org/10.1029/1999GL900558>.
- Searle, M.P., Noble, S.R., Cottle, J.M., Waters, D.J., Mitchell, A.H.G., Hlaing, T., Horstwood, M.S.A., (2007). Tectonic evolution of the Mogok metamorphic belt, Burma (Myanmar) constrained by U-Th-Pb dating of metamorphic and magmatic rocks. *Tectonics* 26, n/a-n/a. <https://doi.org/10.1029/2006TC002083>.
- Shi, G.H., Stöckhert, B., Cui, W.Y., (2005.) Kosmochlor and chromian jadeite aggregates from the Myanmar jadeite area. *Mineral. Mag.* 69, 1059–1075. <https://doi.org/10.1180/0026461056960308>.
- Sloan, R.A., Elliott, J.R., Searle, M.P., Morley, C.K., (2017). Active tectonics of Myanmar and the Andaman Sea. *Geol. Soc. Mem.* 48, 19–52. <https://doi.org/10.1144/M48.2>
- Soe Thura Tun, Watkinson, I.M., (2017). The Sagaing Fault, Myanmar. *Geol. Soc. London, Mem.* 48, 413–441. <https://doi.org/10.1144/M48.19>.
- Than Htut Lwin (2008.) *Geology and gold mineralization in Sheinmagar area, Wetle Township, Sagaing Division*. PhD thesis, Department of Geology, University of Yangon.
- Vigny, C., (2003). Present-day crustal deformation around Sagaing Fault, Myanmar. *J. Geophys. Res.* 108. <https://doi.org/10.1029/2002jb001999>.
- Wang, Y., 2014 (). Active tectonic and earthquake Myanmar region. *J. Geophys. Res. Solid Earth* 3576–3822. <https://doi.org/10.1002/2013JB010762>.
- Wang, Y., Sieh, K., Aung, T., Min, S., Khaing, S.N., Tun, S.T., (2011). Earthquakes and slip rate of the southern Sagaing fault: Insights from an offset ancient fort wall, lower Burma (Myanmar). *Geophys. J. Int.* 185, 49–64. <https://doi.org/10.1111/j.1365-246X.2010.04918.x>.
- Warren, J.M., (2016). Global variations in abyssal peridotite compositions. *Lithos.* <https://doi.org/10.1016/j.lithos.2015.12.023>.
- Win Swe (1981). A major strike-slip fault in Burma. *Contributions to Burmese Geology*. Department of Geological Survey and Exploration, February 1981, Myanmar, 63–72.

## **PETROGENESIS OF THE GRANITOIDS OF MOKPALIN-KYAUKTANLAY QUARRIES, MON STATE USING TRACE ELEMENT AND RARE EARTH ELEMENT GEOCHEMISTRY**

Myo Thiri Sandar Aung<sup>1</sup>, Mi New Ni Aung<sup>2</sup>, Su Myat Aung<sup>2</sup>,  
War War Kyaw<sup>2</sup>, Aye Pyae Phy<sup>3</sup>

### **Abstract**

The Mokpalin-Kyauktanlay area occurs in the southern part of Mogok Metamorphic belt and belongs to the central granitoid belts of Myanmar. The trace elements and rare earth elements geochemistry data are used for the formation of granitoids of the study area. Geochemically, the whole rock of silica ratios varies from 64.55 to 75.31%, Al<sub>2</sub>O<sub>3</sub>, Fe<sub>2</sub>O<sub>3t</sub>, CaO, MgO ranges from 14.02-17.85%, 1.00-7.87%, 1.16-6.81 and, 0.24-3.24%. The varying ratios of the incompatible elements of Rb/Sr ratios (0.1-0.5), Ba/Sr ratios (0.4-2.9), and Ba/Rb ratios (4-16.3) in granitoids. The granitoid rocks have enrichment in the Light Rare-Earth Elements (LREE) and depletion in Heavy Rare-Earth Elements (HREE) and with negative europium anomalies and they come from the same origin. The age of quartz diorite was about 90.8±0.8 Ma (Mitchell et al. (2012). Tectonically they fall volcanic arc granite fields and were products of volcanic arc magmatism. These granitoids were generated from the partial melting of the shallow crust.

**Keywords:** Granitoids; Volcanic arc granite; Calc-alkaline; Magma mixing

### **Introduction**

The Mokpalin-Kyauktanlay area is mainly composed of igneous rocks. In the middle part of the area, it is composed of Mergui Group. Eastern part of the area has porphyritic biotite granites. Fresh samples of rock are only exposed in quarries. Most of the study areas are covered by lateritic soil and vegetation. The study area has more than twenty quarries. The quarries have made up of granitic and dioritic rocks. In Mokepalin Quarry no-1 is located at the side of the Eastern part of Yangon-Mawlamyine Highway line (Fig.1). The size of the quarry is about 1300' from East to West. The major rock units are diorite and granodiorite. Some are micromeladiorite and microdiorite. Several of dykes and veins are occurred as aplite, pegmatite, rhyolite, dacite porphyry, lamprophyre, quartzofeldspathic and quartz veins injected into the country rocks of the quarry no-1. Xenoliths and enclaves are observed in granitic and dioritic rocks. In Mokepalin Quarry no-2, located at the flank of the western part of the Yangon-Mawlamyine Highway line. The wide of the quarry is about 1500' from East to West. The wholly of the quarry no-2 is dominantly composed of diorite. In Kyauktanlay and Kann-ni Quarries, they are located in the western part of the area, most are more than 1000' wide. The quarries have mainly composed of granitic rocks. Lamprophyre and epidote veins are intruded in it. Many workers have been studied in this area. So the present study detailed on igneous intrusion, petrogenesis, trace elements and rare earth elements of the granitoid rocks.

---

<sup>1</sup> Dr, Associate Professor, Department of Geology, Myeik University

<sup>2</sup> Assistant Lecturer, Department of Geology, Myeik University

<sup>3</sup> Demonstrator, Department of Geology, Myeik University

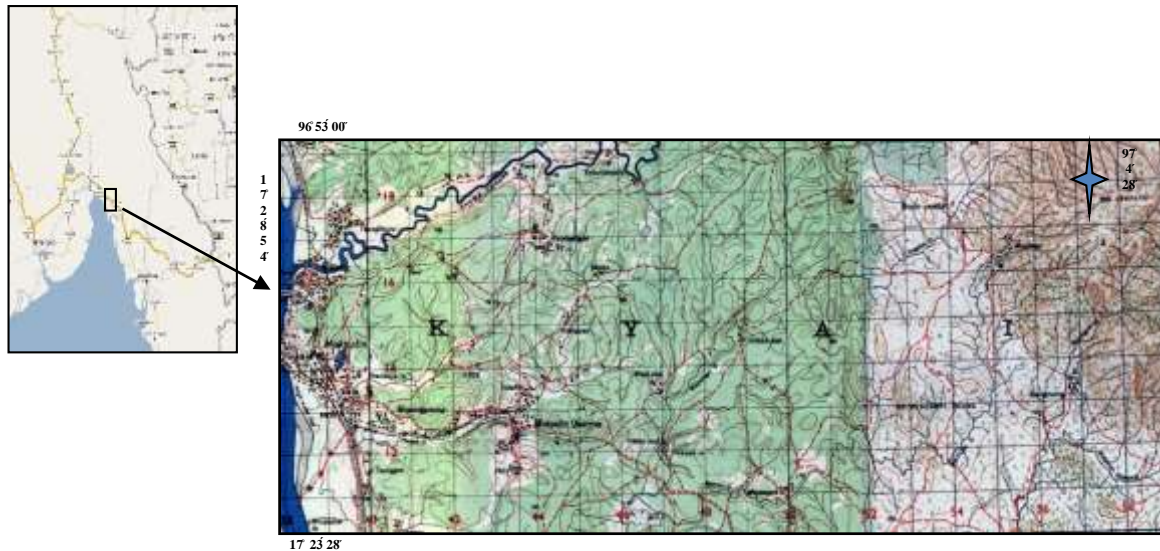


**Figure 1** Location map of the Mokpalin-Kanni-Kyauktanlay area.

### **Regional Geology and Study Area**

The general regional geologic setting southern part of Mogok Metamorphic belt and within Slate belt (Fig.2). It consists of rhyolitic tuff, meta-sedimentary rocks, probably of Carboniferous age close to the Mesozoic granite of Chhibber (1926). The Western granite belt of South East Asia and this belt are associated with eastward subduction of the Oceanic Indian plate (Pitcher, 1962). The study area lies in the northern part of western Tin Belt of South East Asia Tin province (Mitchell, 1977 and Nyan Thin, 1984) and lies within part of the Mogok Belt (Searle and Haq, 1964). Maung Thein (1983), regarded the central granitoid belt of Burma were developed in the tectonic setting of subduction related magmatic arc. The area belongs to the central granitoid belts of Myanmar (Khin Zaw, 1990). The area is structurally bounded by two major faults which are the Papun Fault system in the north and the Three Pagoda Fault in the south. The Sagaing fault was 1000Km to south and lies west of Mogok Metamorphic belt.

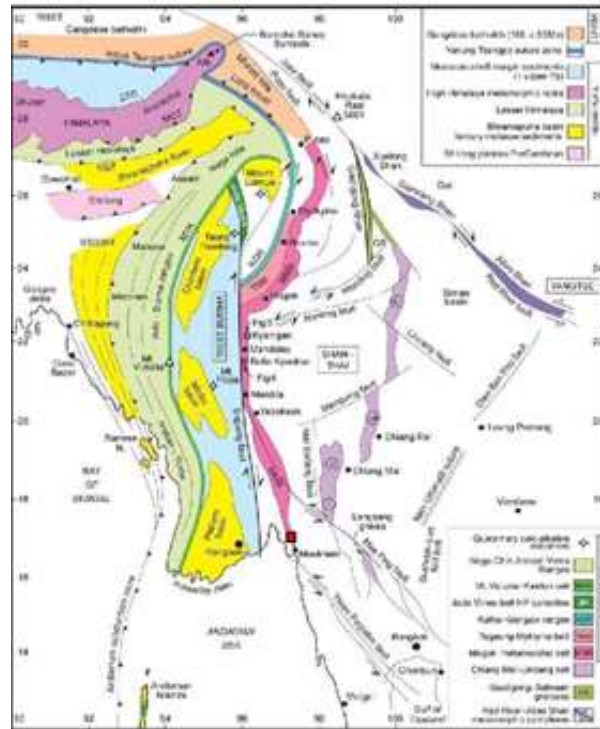


**Figure 2** Geological map of SE Asia, Myanmar and the Andaman sea region north to southern Tibet, showing the major suture zones , faults, and terrain boundaries (Searle *et al.*, 2007).

### Materials and Methods

Eight representative samples were sent to ALS laboratory of Geological Survey of Japan, AIST and the Acme analytical laboratories of Vancouver-Canada. In this study, most relevant methods available to determine contents of major, trace, and rare earth elements of the lamprophyres were applied for major and trace elements analysis were carried out using techniques of X-ray fluorescence spectrometry (XRF), inductively coupled plasma-mass spectrometry and inductively coupled plasma-atomic emission spectrometry. The analyzed data are presented in Table-1. Standard C.I.P.W norms and C.I.P.W norm with biotite and hornblende are calculated according to the rules of Hutchison, 1975. Triangular plots of some analyses results were carried out by Tridraw 2.6 software. For tectonic discrimination diagrams (Pearce *et al.*, 1984), differentiation index diagram, major oxides and trace elements variation diagrams, ternary diagrams, binary diagrams and triangular plots diagrams were drawn by using SPSS-16 software, GCD kit 3.0, Tri-draw software and Microsoft excel.

### Field Study and Petrography of Granite

Representative samples were collected from several locations throughout the Mokpalin, Kanni and Kyauktanlay quarries. Granodiorite and diorite are coarse-grained, and displays light grey on fresh and dark grey on weathered surfaces. It is widespread in occurrence and wherever exposed these are in sharp contact and gradational contact. In addition, thin veins of quartz and epidote sometimes occur and some joint faces coated with pyrites are noticeable. At Kanni quarries, highly weathered on top and fresh rocks beneath are observable. In some places, bands of dark and light-colored minerals in the form of stratification of intrusions are encountered. The

reverse xenoliths (i.e the inclusion of granodiorite in diorite) suggest a short time span between each intrusion (Fig.3-a).

Near the sharp contacts with diorite the xenoliths are mostly angular to surrounded in form indicating that these xenoliths were derived not afar from the plutons (Fig.3-b). Magma mixing and assimilation of felsic and mafic magma, in Mokpalin quarry is peculiar (Fig.4). Petrographically, the granodiorite and quartz diorite contain mainly plagioclase, quartz, biotite, hornblende, alkali feldspar and opaque minerals and apatite as accessory (Fig.5).

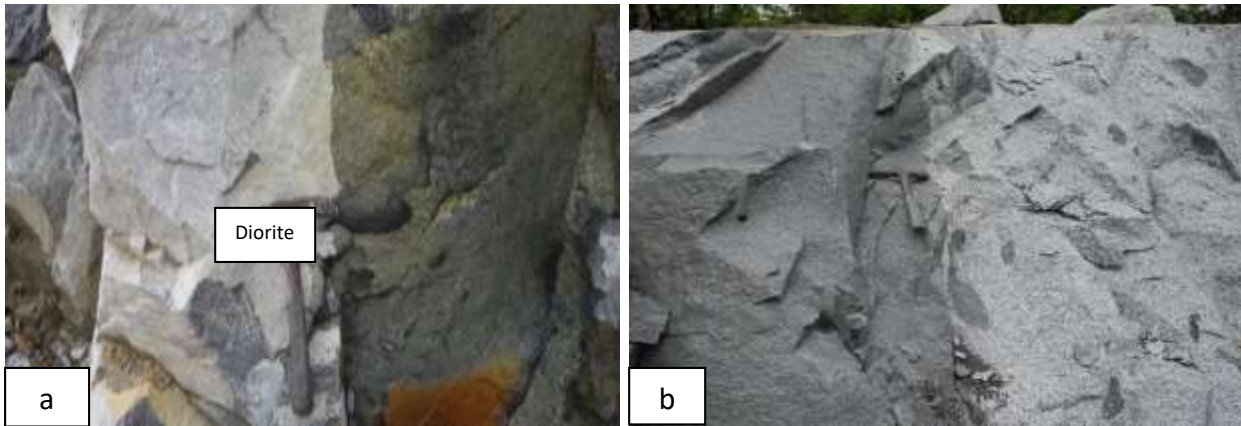


**Figure 3** Field photo shows (a) Diorite xenoliths observed in granodiorite (left). A sharp contact occurred between granodiorite and diorite at Kanni quarry. (b) small, medium and large-size microgranular mafic enclaves are sub-angular to surrounded in granodiorite at eastern part of the area.



**Figure 4** Assimilation of diorite and granitic magma, at Mokpalin quarry.

The granodiorites are medium to coarse-grained in texture and it is made up of quartz (20-30 vol-%), K-feldspar (25-30 vol-%), plagioclase (40-45 vol-%), biotite (2-10 vol-%) and amphibole (2-5 vol-%). Plagioclase is fractured and bent, suggesting plastic flow and crystal breakage during crystallization. Fractured crystals later were filled by recrystallized quartz. Mafic enclave show hornblende replaced by biotite mineral. Quartz exhibits undulatory extinction. K-feldspar crystals are subhedral in form containing small inclusions of amphibole and apatite grains. In QAP trilinear diagram (after Streckeisen, 1973) falls in the granodiorite field (Fig.6).

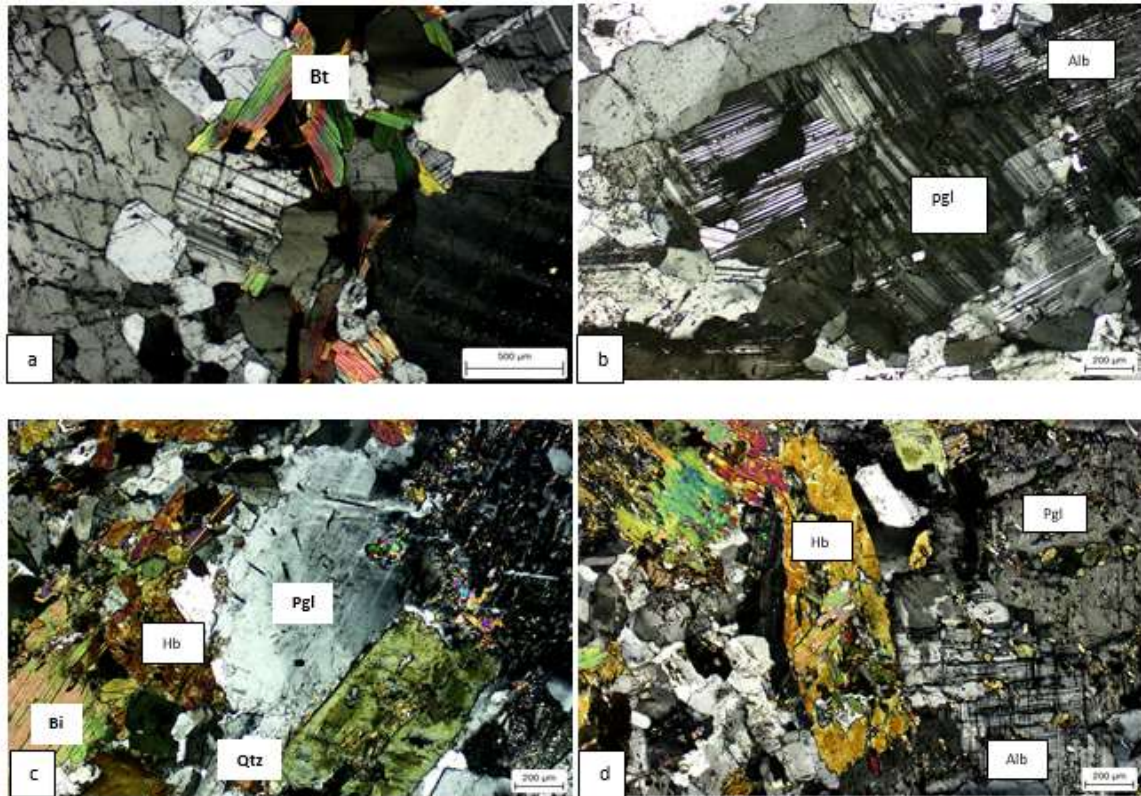


**Figure 5** Photomicrographs of the igneous rocks of study area (a) Strong pleochroism of biotite (b) Bent plagioclase contact at right angle with albite in granodiorite (c) Quartz diorite consists of plagioclase, amphibole, biotite and quartz (d) Mafic enclave shows hornblende replaced by biotites with sieve texture between XN, at Mokpalin Quarry-1. Abbreviations: Hb = amphibole; Pgl = plagioclase; Bi = biotite; Alb = albite; Qtz = quartz.

### Whole Rock Chemistry of Granitoids Rocks

The granitoids and quartz diorite are silica-rich, with  $\text{SiO}_2 = 55.93\text{--}75.91$  wt. %. They have high contents of alkalis, with  $\text{K}_2\text{O} = 1.5\text{--}8.6$  wt.%,  $\text{Na}_2\text{O} = 3.6\text{--}4.0$  wt.%,  $\text{Al}_2\text{O}_3 = 11.9\text{--}15.8$  wt.%,  $\text{FeO}$  (total Fe) =  $1.0\text{--}3.0$  wt.%,  $\text{MnO} = 0.0\text{--}0.1$  wt.%,  $\text{MgO} = 0.1\text{--}1.2$  wt.%,  $\text{TiO}_2 = 0.0\text{--}0.3$  wt.%, and  $\text{P}_2\text{O}_5 = 0.0\text{--}0.2$  wt.% (Table-1). The granitoid rocks in the study area fall in the calc-alkaline and partially tholeiitic field (Fig. 7-a). A/NK (molecular  $\text{Al}_2\text{O}_3/\text{Na}_2\text{O} + \text{K}_2\text{O}$ ) vs A/CNK (molecular  $\text{Al}_2\text{O}_3/\text{CaO} + \text{K}_2\text{O} + \text{Na}_2\text{O}$ ) diagram (Fig. 7-a) showing the subalkaline and metaluminous of peraluminous character of igneous rock of the study area (after Shand 1943). In RB-Ba-Sr diagram (Fig. 8-a) with the field corresponding to I-normal granite, II-anomalous granite, III-strongly differentiated granite, IV-granodiorite, V-diorite based diagram after El Bouseily *et al.*, (1975), they fall granodiorite and diorite field. The positions of the data points in the Q-Ab-Or ternary diagram (Fig. 8-b) indicate that the pluton crystallized at a water pressure between 0.5 kb and 1 kb.

On  $\text{SiO}_2\text{--K}_2\text{O}$  diagram, the entire rocks within in the medium to partially high-K calc-alkaline series field (Fig. 9-a). The chondrite-normalized REE patterns of the Mokpalin-Kyauktanlay granites (Fig. 9-b) show light REE enrichment with low  $\text{La}_n/\text{Yb}_n$  (6.51–8.53) and moderately negative Eu anomalies (0.33–0.90). The differences between individual granitoid patterns are relatively slight, but most of all patterns are nearly similar. Rb, Ba, Th, Nb and K increase consistently from diorite to granodiorite to granite consistent with fractional crystallization. The steeper slopes could reflect lower degree of partial melting in calc-alkaline

magma. Slightly negative Eu anomalies ( $Eu/Eu^* = 0.88-1.06$ ) and  $(La/Yb)_N = 7.7-15.3$  show slightly fractionated. In  $Fe_2O_3$ -MgO diagram (After Zorpi et al,1989) all the granitoid show partial melting and magma mixing (Fig.10-a). Geotectonically, according to Pearce et.al (1984) diagrams they fall in the field of volcanic arc granite field (VAG) (Fig.10-b).

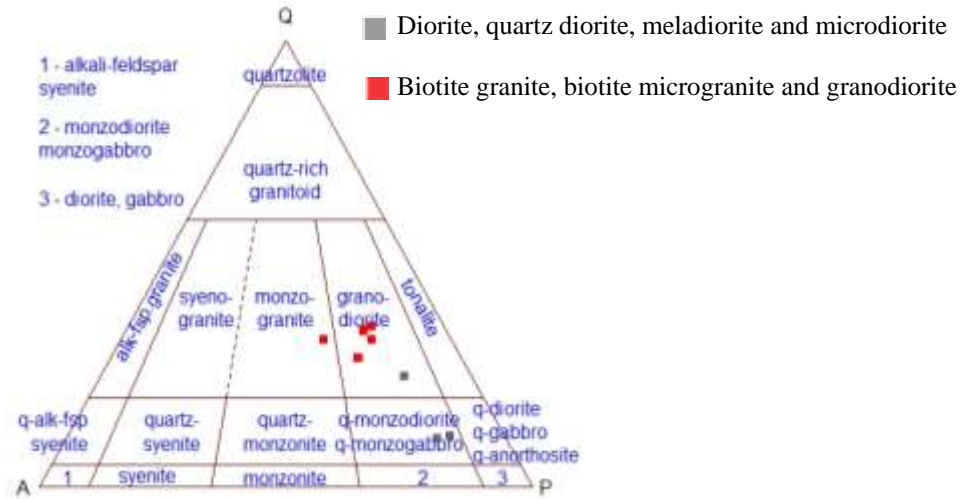


**Figure 6** QAP plot for the studied granitoids (fields are after Streckeisen, 1973).(Q= Quartz, A= Alkali feldspar and P= Plagioclase).

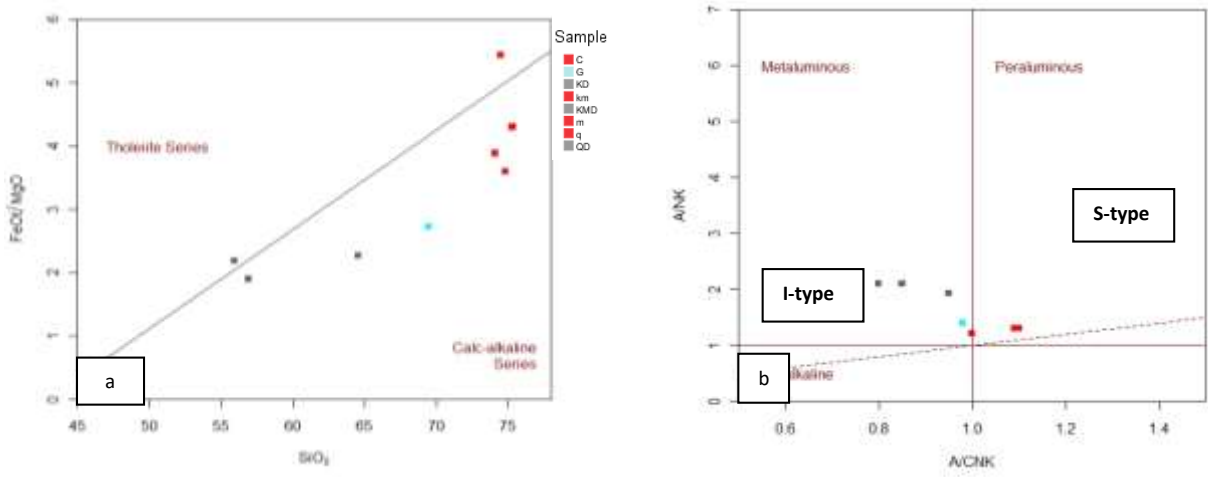


**Figure 7** (a)  $FeO/MgO$  vs  $SiO_2$  diagram subdividing the subalkaline magma series to Tholeiitic and Calc-alkaline series (After Miyashiro 1974). (b)  $A/NK$  (molecular  $Al_2O_3 / Na_2O + K_2O$ ) vs  $A/CNK$  (molecular  $Al_2O_3 / CaO + K_2O + Na_2O$ ) diagram showing the subalkaline and metaluminous of peraluminous character of igneous rock of the study area (after Shand 1943).

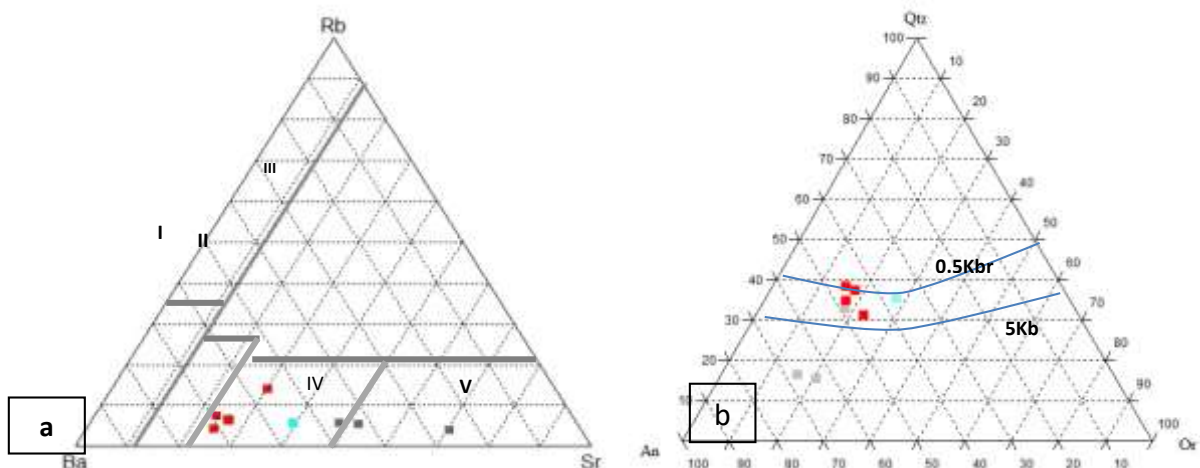


**Figure 8** (a) RB-Ba-Sr diagram with the field corresponding to I-normal granite, II- anomalous granite, III-strongly differentiated granite, IV-granodiorite, V-diorite based diagram after El Bouseily *et al.*, (1975). (b) Normative data plot of the granitic rocks of the study area showing that most of the granitic rocks were formed below 0.5kb of water vapour pressure, after Tuttle and Bowen (1958).

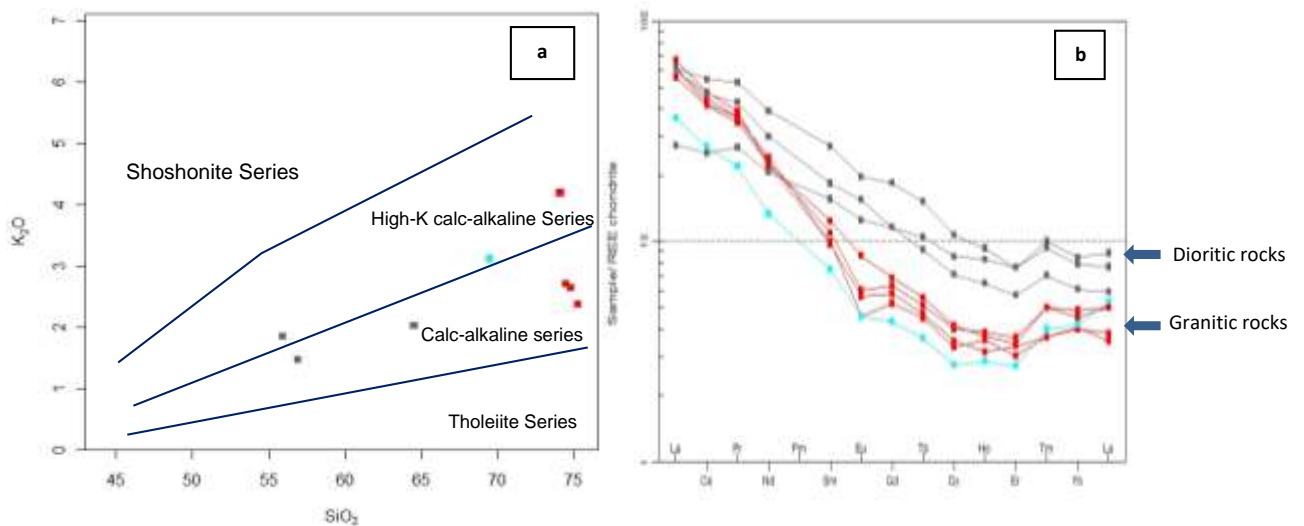


**Figure 9** (a) Plots of wt%. K<sub>2</sub>O versus wt%. SiO<sub>2</sub> for lamprophyres from Mokepalin-Kanniarea (after Peccerillo and Taylor 1976). (b) Chondrite-normalized REE diagram for granitoid rocks from the Mokepalin-Kanni area, normalizing values from (Nakamura 1974).

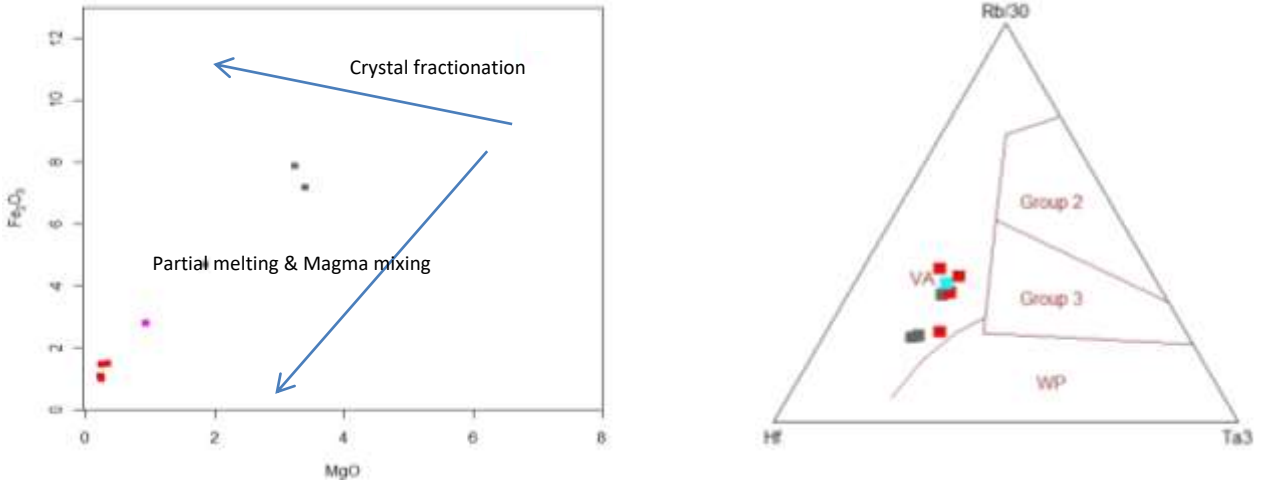


**Figure 10** (a) Fe<sub>2</sub>O<sub>3t</sub>- MgO diagram (After Zorpi et al, 1989). (b) Plot of igneous rocks on geotectonic classification of volcanic arc granite (Pearce *et al.* 1984).

**Table 1** Representative selected whole-rock analysis for major and trace element from granitoid rocks.

| Rock type<br>Sample            | Tholeiitic |       | Calc-alkaline |       |       |       |       |       |
|--------------------------------|------------|-------|---------------|-------|-------|-------|-------|-------|
|                                | KD         | QD    | KMD           | m     | C     | km    | G     | q     |
| SiO <sub>2</sub>               | 64.55      | 56.90 | 55.93         | 74.5  | 74.8  | 74.12 | 69.46 | 75.31 |
| TiO <sub>2</sub>               | 0.521      | 0.783 | 1.046         | 0.1   | 0.13  | 0.147 | 0.029 | 0.109 |
| Al <sub>2</sub> O <sub>3</sub> | 16.45      | 17.85 | 17.85         | 14.02 | 13.78 | 13.67 | 15.21 | 14.02 |
| Fe <sub>2</sub> O <sub>3</sub> | 4.69       | 7.18  | 7.87          | 1.45  | 1     | 1.48  | 2.8   | 1.08  |
| MnO                            | 0.09       | 0.12  | 0.12          | 0.07  | 0.04  | 0.06  | 0.07  | 0.03  |
| MgO                            | 1.857      | 3.402 | 3.24          | 0.24  | 0.25  | 0.343 | 0.926 | 0.226 |
| CaO                            | 4.785      | 6.805 | 6.566         | 1.16  | 1.37  | 1.412 | 2.711 | 1.189 |
| Na <sub>2</sub> O              | 3.85       | 4.26  | 4.04          | 4.79  | 5.13  | 3.92  | 4.36  | 4.91  |
| K <sub>2</sub> O               | 2.02       | 1.46  | 1.85          | 2.7   | 2.63  | 4.18  | 3.11  | 2.37  |
| P <sub>2</sub> O <sub>5</sub>  | 0.13       | 0.29  | 0.23          | 0.06  | 0.06  | 0.07  | 0.12  | 0.06  |
| LOI                            | 0.45       | 0.54  | 0.49          | 0.73  | 0.5   | 0.1   | 0.22  | 0.27  |
| Total                          | 99.40      | 99.58 | 99.23         | 99.82 | 99.69 | 99.50 | 99.27 | 99.57 |
| A/CNK                          | 0.95       | 0.85  | 0.86          | 1.1   | 1     | 1     | 0.98  | 1.1   |
| Ba                             | 388        | 267   | 385           | 558   | 560   | 413   | 759   | 667   |
| Ce                             | 21.8       | 40.4  | 47.1          | 36.5  | 38.6  | 23.2  | 35.9  | 41.2  |
| Cs                             | 1.07       | 2.48  | 1.57          | 1.2   | 1     | 2.81  | 3.04  | 0.78  |
| Dy                             | 2.93       | 2.42  | 3.66          | 1.21  | 1.13  | 0.94  | 1.42  | 1.37  |
| Er                             | 1.71       | 1.28  | 1.71          | 0.75  | 0.68  | 0.61  | 0.77  | 0.81  |
| Eu                             | 0.96       | 1.19  | 1.51          | 0.43  | 0.35  | 0.35  | 0.66  | 0.46  |
| Ga                             | 17.6       | 20.8  | 21.9          | 13.5  | 12    | 15.9  | 17.8  | 15.5  |
| Gd                             | 3.2        | 3.2   | 5.1           | 1.6   | 1.4   | 1.2   | 1.9   | 1.7   |
| Hf                             | 4.2        | 2.1   | 4.6           | 2.3   | 2.5   | 4     | 3.2   | 3.4   |
| Ho                             | 0.58       | 0.45  | 0.65          | 0.22  | 0.25  | 0.20  | 0.26  | 0.27  |
| La                             | 9          | 20    | 20.4          | 20    | 20.4  | 12    | 18.4  | 22    |
| Lu                             | 0.3        | 0.2   | 0.3           | 0.13  | 0.12  | 0.18  | 0.17  | 0.17  |
| Nb                             | 4.4        | 4     | 6.6           | 5     | 5.6   | 5.2   | 4.8   | 5.6   |
| Nd                             | 13         | 18.9  | 24.7          | 14.2  | 15.2  | 8.4   | 14    | 14.4  |
| Pr                             | 3          | 4.8   | 5.9           | 4.1   | 4.1   | 2.5   | 3.9   | 4.4   |
| Rb                             | 47         | 42    | 49            | 60    | 53    | 103   | 78    | 41    |
| Sm                             | 3.16       | 3.72  | 5.48          | 1.96  | 2.01  | 1.51  | 2.51  | 2.22  |

| Rock type<br>Sample                | Tholeiitic |       | Calc-alkaline |       |       |        |       |        |
|------------------------------------|------------|-------|---------------|-------|-------|--------|-------|--------|
|                                    | KD         | QD    | KMD           | m     | C     | km     | G     | q      |
| Sr                                 | 408        | 739   | 475           | 192   | 221   | 225    | 545   | 233    |
| Ta                                 | 0.5        | 0.3   | 0.5           | 0.4   | 0.4   | 0.5    | 0.5   | 0.5    |
| Eu/Eu*                             | 0.93       | 1.06  | 0.88          | 0.75  | 0.63  | 0.8    | 0.93  | 0.72   |
| Tb                                 | 0.49       | 0.43  | 0.71          | 0.22  | 0.21  | 0.17   | 0.26  | 0.24   |
| Th                                 | 4.63       | 6.38  | 4.93          | 5     | 4.9   | 12.9   | 8.56  | 5.7    |
| Ti                                 | <0.5       | <0.5  | <0.5          | 0.1   | <0.1  | 0.5    | <0.5  | <0.5   |
| Tm                                 | 0.3        | 0.2   | 0.3           | 0.11  | 0.11  | 0.12   | 0.15  | 0.15   |
| U                                  | 1.54       | 1.74  | 1.91          | 1.1   | 1     | 3.17   | 3.25  | 1.21   |
| V                                  | 99         | 181   | 199           | <8    | <8    | 22     | 48    | <5     |
| W                                  | <1         | 1     | <1            | 1.3   | 4.2   | <1     | <1    | 1      |
| Y                                  | 16.8       | 12.7  | 18.5          | 7.5   | 7.4   | 6.5    | 8.1   | 9.7    |
| Yb                                 | 1.86       | 1.33  | 1.73          | 0.88  | 0.89  | 0.92   | 0.99  | 1.07   |
| Zr                                 | 127        | 63    | 138           | 76.9  | 82.7  | 103    | 100   | 92     |
| Rb/Sr                              | 0.1        | 0.1   | 0.1           | 0.3   | 0.2   | 0.5    | 0.1   | 0.2    |
| Ba/Sr                              | 0.9        | 0.4   | 0.8           | 2.9   | 2.5   | 1.8    | 1.4   | 2.9    |
| Th/U                               | 3          | 3.7   | 2.6           | 4.5   | 4.9   | 4      | 2.6   | 4.7    |
| K <sub>2</sub> O/Na <sub>2</sub> O | 0.5        | 0.3   | 0.5           | 0.6   | 0.5   | 1.1    | 0.7   | 0.5    |
| ΣREE                               | 131.5      | 62.44 | 114.82        | 72.78 | 66.66 | 101.28 | 51.25 | 214.46 |

## Discussion and Conclusion

According to their geochemical composition these granitoids are occupied with metaluminous and slightly peraluminous character. They are high SiO<sub>2</sub>, Na<sub>2</sub>O+K<sub>2</sub>O, calc-alkaline to partially tholeiitic series. Major and trace element data of the Mokpalin-Kyauktanlay granitoids are typical of fractionated, crustal contaminated (e.g., low Mg#, and negative Nb and Ti anomalies). Field evidence, major and trace elements chemistry data of the diorite and granitic rocks may come from a partial melting and mixing of felsic and mafic magma. The trace element supports that a variable degree of partial melting. Their tectonic setting belongs to volcanic arc granite field.

## Acknowledgements

The author thanks to the Journal of Myanmar Academy of Arts and Science for editing on my research. Special acknowledge to Dr. Ni Ni Oo, Acting Rector of the Myeik University, and Dr. Soe Moe Lwin (Professor and Head of Department of Geology, Myeik University) for their permission to carry out this research. Finally, she also sincerely gratitude to Dr. Khin Zaw, University of Tasmania, Australia who provided valuable helps XRF data during the preparation of this manuscript.

## References

- Chhibber, H.L., (1926) Hornblende lamprophyres and associated rocks of Mokpalin Quarries, Thaton District: *Jour. Burma. Soc.* V.xvi,p. 167-168.
- El Bouseily. A.m., and AA. El Sokyary, (1975). The relation between Rb, Ba and Sr in granitic rocks, *Chem Geol* 16,p 207-209.
- Hutchison, C.S., (1975). Ophiolite in Southeast Asia. Geological Society of America Bulletin, 86, 797–806. Khin Zaw, 1990. Geological, petrological and geochemical characteristics of granitoid rocks in Burma with special reference to the associated W-Sn mineralization and their tectonic setting. *Jour. Of Southeast Asian Earth Sciences*, v.4. no.4. p.293-335.
- Maung Thein, (1983). *The geological evolution of Burma*, Department of Geology, Mandalay University, Mandalay, Burma, (Unpublish), 89p.

- Mitchell, A.H.G., Chung, S.-L., Thura Oo, Lin, T.-H. & Hung, C.-H. (2012). Zircon U–Pb ages in Myanmar: magmatic–metamorphic events and the closure of a neo-Tethys ocean? *Journal of Asian Earth Sciences*, 56, 1–23.
- Miyashiro, A. (1974). Volcanic rock series in island arcs and active continental margins. *Am. Sci.* 274, 321-55.
- Nakamura, N., (1974,) Determination of REE, Ba, Fe, Mg, Na and K in carbonaceous and ordinary chondrites, *Geochimica et Cosmochimica Acta*, vol. 38, no.5, p.757-775
- Nyan Thin, (1984). *Some aspects of granitic rocks of Tenasserian Division, Department of Geology, Rangoon University, Rangoon, Burma (Unpublished)*, 125p.
- Peccerillo, A & Taylor, SR, (1976). Geochemistry of Eocene Calc-alkaline volcanic rocks from the Kastamonu area, Northern Turkey. *Contributions to Mineralogy and Petrology*. 58: p. 63-81.
- Pearce, J.A., Harris, N.W., Trindle, A.G., (1984.) Trace element discrimination diagrams for the tectonic interpretation of granitic rocks. *Journal of Petrology* 25. P.956-983.
- Pitcher, W.S., (1962). Granite type and Tectonic Environment, *Mountain Building Process*, p- 19-37.
- Searle, D.L., and Haq, B.T., (1964, 2007). The Mogok Belt of Burma and its relation to the Himalayan Orogeny. 22<sup>nd</sup>. *Intern. Geol. Congress. India* (in press).
- Shand, S. J. (1943). *Eruptive Rocks. Their Genesis, Composition, Classification, and Their Relation to Ore-Deposits with a Chapter on Meteorite*. New York: John Wiley & Sons.
- Streckeisen, A.L. (1973). Plutonic rocks Classification and nomenclature recommended by IUGS sub commission of systematic of igneous rocks. *Geotimes*, 18, pp.26-30.
- Tuttle, O.F., and N. L., Bowen (1958): Origin of granite in the light of experimental studies in the system NaAlSi<sub>3</sub>O<sub>8</sub>-KAlSi<sub>3</sub>O<sub>8</sub>-SiO<sub>2</sub>-H<sub>2</sub>O, *Geol. Soc. Am. Mem*, 74.
- Zorpi MJ, Coulon C, Orsini JB, Cocirta C (1989) Magma mingling, zoning and emplacement in calc-alkaline granitoid plutons. *Tectonophysics* 157:315–329



## Stratigraphy

### General Statement

The research area is mainly composed Pondaung Formation, Yaw Formation, Letkat Formation and Natma Formation that were deposited during Eocene to Middle Miocene age (Fig-3). The present research is documented in the provenance and depositional environment based on heavy mineral analysis and granulometric analysis.

### Pondaung Formation

The term “Pondaung Formation” was firstly introduced by Cotter (1938) for the sandstone that occurred along with the Pondaung Range in the western part of the Pakokku District. This formation well crops out in the western part of the Ka Byu, Paung Wa, near the Tha Lauk, Kyat Ywa, Win Gon, Nyaung Bin Le, along the Pindaung Gyi hill, Pindaung Lay hill and Sin Don Chung, Shwe Bon Tha Chung.

This Formation is characterized by thick-bedded to massive, light greenish grey, hard and compact, cross-stratified and medium-to coarse-grained sandstones intercalated with light grey shale, siltstone (Fig-4). The greenish-grey, chocolate brown, purple color shale and clay have commonly occurred in the lower part of the study area (Fig-5). The upper portion is composed of thick-bedded to massive, reddish-brown and purple, fine-to medium-grained sandstones that are interbedded with silty mudstone and pebble sandstone (Fig-6). Moreover, the sub-angular or sub-rounded pebble of igneous, metamorphic and fossil woods are also observed (Fig-7). According to the previous works of Pondaung Primate Expedition Team (Aye Ko Aung. *et al.*, 1998) as assigned as Late Eocene age.

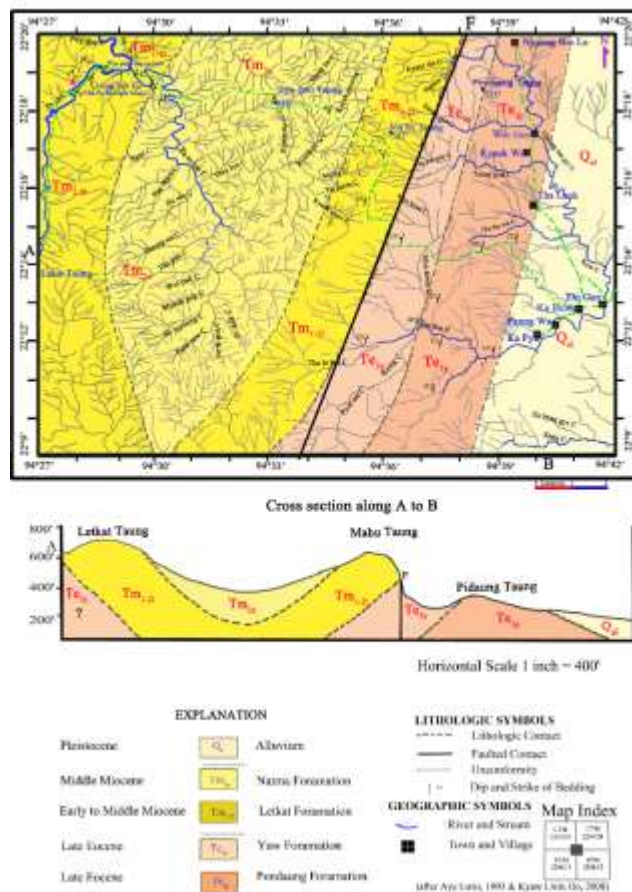


Figure 3 Geological map of the Research Area



**Figure 4** Thick-bedded to massive, light grey, hard and compact sandstones intercalated with shale of the Pondaung Formation (22°11'30"N, 94°37'29"E)



**Figure 5** Variegated clay of the Pondaung Formation (22°11'27"N, 94°36'48"E)



**Figure 6** Sub-rounded to rounded gritty-pebbly sandstones of the Pondaung Formation (22°13'05" N, 94°40'E)



**Figure 7** Silicified fossil woods fragment of the Pondaung Formation (22°12'36"N, 94°36'17"E)

### Systematic Description of Heavy Minerals

The heavy mineral analysis is one of the most important and widely used techniques in the determination of provenance studies (Pettijohn. *et al.*, 1975). The heavy minerals are those accessories that have a specific gravity greater than 2.89. There are two groups of heavy minerals in the Pondaung Formation: rutile, zircon, tourmaline, garnet, staurolite, epidote, chlorite, sillimanite, augite, diopside, hypersthene and olivine as a transparent group, and other minerals as an opaque group.

#### Transparent Heavy Minerals

##### (a) Ultra Stable Heavy Minerals

**Rutile** is found as prismatic, sub-angular to sub-rounded grains and rounded. Rutile can be identified by its high relief, red or brown to yellowish-orange color (Fig. 8), blood red, dark brown color, pleochroism from yellow to reddish-brown that contains about 7% of total heavy minerals (Fig. 21). The rounded grains are derived from reworked sediments source whereas the prismatic or platy forms are derived from mafic igneous rocks and high temperature-pressure metamorphic minerals of granulite and eclogite facies (Kerr, 1959; Pettijohn, 1975).

**Zircon** is characterized by its colorless, pale yellow or pale pink colors and high relief, but a few grains exhibit purple and light pink color. It is also found as prismatic, rounded, sub-rounded, elongated euhedral to subhedral with pyramidal endings (Fig. 9). The prismatic, sub-rounded,

elongated can be derived from metamorphic and acidic igneous source rocks whereas the rounded grains are abundant in reworked sediment (Kerr, 1959; Pettijohn, 1975). Some of the zircon grains show inclusions and overgrowths. The percentage of zircon is 9 % of the total heavy mineral grains (Fig. 21). The geological significance of zircon has been greatly emphasized because of its high stability and as a provenance indicator (Pettijohn, 1975).

**Tourmaline** is prismatic, rounded, sub-angular to sub-rounded, elongated, blue, pink, light brown, greenish-brown and yellowish-brown (Fig. 10). Grains show moderate to strongly pleochroic from light brown to dark brown, yellow to light brown and light green to dark green that contains about 8 % of total heavy minerals (Fig. 21). The tourmaline is derived from metamorphic and igneous source rocks but the rounded grains are derived from reworked sediment source (Kerr, 1959; Pettijohn 1975).

### (b) Metastable Heavy Minerals

**Garnet** is characterized by sub-rounded, angular and sub-angular in outline and pale brown to dark brown color that is isotropic (Fig. 11). The reliefs are very high and contain iron inclusions containing 5% of the total heavy minerals (Fig. 22). In sediments, almandine is the most widespread garnet (Mange and Maurer, 1992). Garnet is derived from dynamothermal metamorphic source and igneous source rocks (Kerr, 1959; Folk, 1957, Pettijohn, 1975).

**Staurolite** is sub-angular in outline and usually light yellow to straw yellow in color and pleochroic from yellow to pale yellow in color with sub-rounded, euhedral and platy, often fractured grains (Fig. 12). It constitutes 4% of the total heavy fraction (Fig. 22). Staurolite is a product of medium-grade regional metamorphism (Mange and Maurer, 1992).

**Epidote** is shown the short prismatic euhedral grain to subhedral grain, subrounded form, pistachio green to yellowish-green colors, sub-angular grains with high relief and weak pleochroism (Fig. 13). The percentage varies by 5 % of the total heavy minerals (Fig. 22). It has multiple sources including metamorphic and igneous rocks (Kerr, 1959), dynamothermal metamorphic rocks (Pettijohn, 1978). It is the index mineral of the albite-actinolite-epidote-chlorite zones of the green schist-facies regional metamorphism (Asideu *et al.*, 2000).

**Chlorite** occurs as irregular to sub-rounded grains, oval or irregular shape. The mineral is pale greenish-brown and greenish-grey in color and possesses high relief (Fig. 14). It shows various shades of green, sometimes in a patchy arrangement with an average of 6% (Fig. 22). Chlorite is a low-grade metamorphic rock, which is most common in the greenschist facies. Weathering courses can also produce chlorite as well as authigenically during diagenesis produce in sedimentary rocks (Pettijohn, 1975). In igneous rocks, it can also be generated by the hydrothermal alteration of ferromagnesian minerals (Mange and Maurer, 1992).

**Sillimanite** is show needle, fibrous or elongated, prismatic or irregular shape grains and colorless showing one set of cleavage with high relief and refractive index. The sillimanite contains 5% of the total heavy minerals (Fig. 22). It shows straight extinction, second and third-order interference colors with yellow, green and pink (Fig-15). Sillimanite occurs in high grade metamorphosed rocks (Pettijohn, 1975).

### (c) Unstable Heavy Minerals

**Augite** is characterized by pale brownish, pale greenish with sub-angular to sub-rounded and subhedral prismatic grains (Fig. 16). Most of the grains are highly altered. The interference color of augite is strong with an average of about 15% of the total heavy minerals (Fig. 23). The typical source for augite is a basic igneous rock of gabbro, dolerite and basalt. The typical source for augite is intermediate and mafic igneous rock (Pettijohn, 1975 and Lindholm, 1985).

**Diopside** is mostly sub-angular to sub-rounded, colorless to pale green color, birefringence is moderate to strong and interference colors are first to second order pink, yellow and bluish green (Fig. 17). Some grains may exhibit bright interference color bands, monoclinic systems and high relief. The populations of diopside are 14 % of the total heavy mineral grains (Fig. 23). Diopside is common metamorphic rocks and mafic igneous rocks (Pettijohn, 1975 and Lindholm, 1985).

**Hypersthene** occurs pale green to pale pink, brown to green color and has faint pleochroism and parallel extinction. It is a subhedral to anhedral forms, subrounded to irregular shape (Fig. 18). The grains are mostly thin prismatic form with having one set of cleavage. It constitutes 5% of the total heavy mineral grains (Fig. 23). Hypersthene is common in both extrusive and intrusive basic to intermediate igneous rocks (Pettijohn, 1975 and Lindholm, 1985).

**Olivine** is found in the orthorhombic system as colorless, reddish-brown to light greenish, elongated subrounded grains with traverse fracture (Fig. 19). The pleochroism is weak yellow to orange-yellow. The interference color is high. The population of olivine is 6 % of the total heavy mineral grains (Fig. 23). This mineral was probably derived from the basic and ultrabasic igneous rocks according to Pettijohn, 1975 and Lindholm, 1985.

**The opaque minerals**

These minerals are magnetite, chromite and hematite. The opaque minerals are identified the black color as magnetite, dark color with purplish as chromite and reddish-brown as hematite according to Kerr (1959) and Pettijohn (1975) (Fig. 20). The grains are sub-rounded and irregular in shape and size with broken surfaces. The opaque minerals contain about 10% of the total heavy minerals. The opaque minerals are derived from mafic igneous rocks.

According to the result of the character and percent of the heavy minerals (Fig. 21, 22, 23 & 24), the Pondaung Formation can be derived from igneous rocks that are substantial contributions to the metamorphic and sedimentary rocks in the research area.



**Figure 8** Ultra stable of the Rutile Minerals



**Figure 9** Ultra stable of the Zircon Minerals



**Figure 10** Ultra stable of the Tourmaline Minerals



**Figure 11** Meta stable of the Garnet Minerals

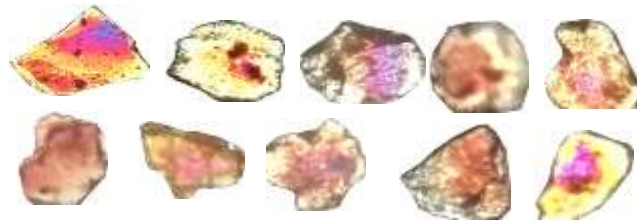


**Figure 12** Meta stable of the Staurolite Minerals



**Figure 13** Meta stable of the Epidote Minerals



**Figure 14** Meta stable of the Chlorite Minerals



**Figure 15** Meta stable of the Sillimanite Minerals

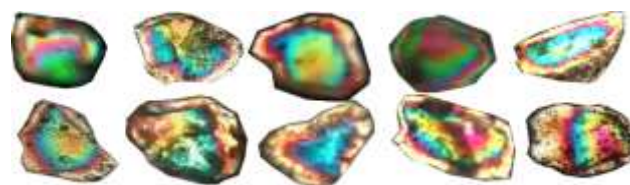


**Figure 16** Unstable of the Augite Minerals

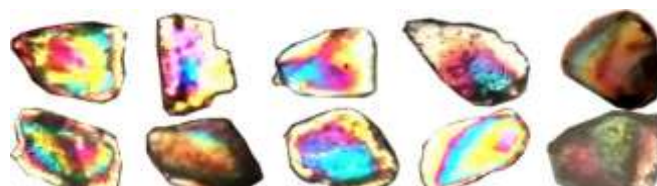


**Figure 17** Unstable of the Diopside Minerals



**Figure 18** Unstable of the Hypersthene Minerals



**Figure 19** Unstable of the Olivine Minerals



**Figure 20** Opaque Minerals

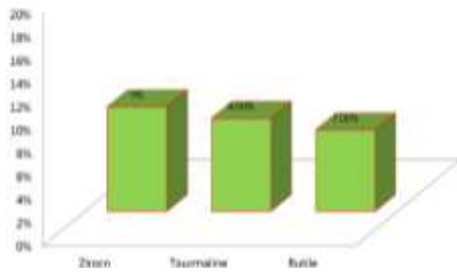


**Figure 21** Ultra stable Heavy Minerals

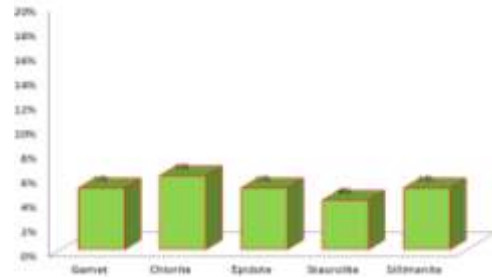


**Figure 22** Meta stable Heavy Minerals

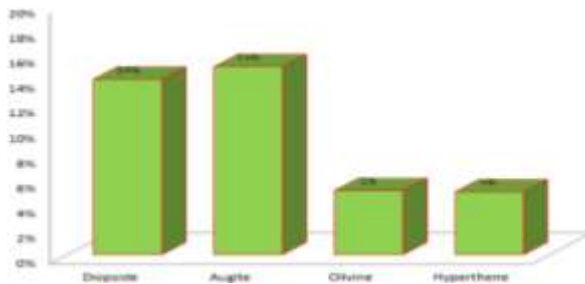


**Figure 23** Unstable Heavy Minerals

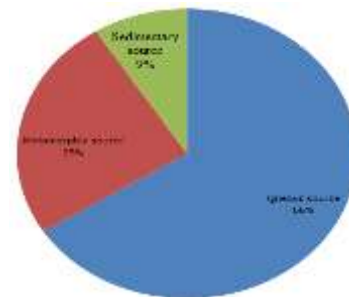


**Figure 24** The percent of the heavy minerals in the Pondaung Formation

### Granulometric Analysis

The six loose sand samples were collected from the present area. The 100 grams of sands were sieved for a period of 10 minutes. Sand samples were obtained by the straight sieving method in the study area.

**Graphic and Statistical Calculation**

The graphic mean size of the sediments indicates the average size of the sediments which is influenced by the source of supply, environment and average kinetic energy of the depositing agent (Sahu,1694). The following formula proposed by Folk and Ward, 1957 represents the graphic mean size;

$$\begin{aligned} \text{Medium } M_d &= \phi 50 \\ \text{Mean } M_z &= \frac{\phi 16 + \phi 50 + \phi 84}{3} \\ \text{Sorting } \delta_1 &= \frac{\phi 84 - \phi 16}{4} + \frac{\phi 95 - \phi 5}{6.6} \\ \text{Skewness } Sk_1 &= \frac{\phi 16 + \phi 84 - 2\phi 50}{2(\phi 84 - \phi 16)} + \frac{\phi 5 + \phi 95 - 2\phi 50}{2(\phi 95 - \phi 5)} \\ \text{Kurtosis } K_G &= \frac{\phi 95 - \phi 5}{2.44(\phi 75 - \phi 25)} \end{aligned}$$

The histogram plots are dominantly unimodal with a main peak around the 3Ø (Fig. 25). The unimodal nature of the Pondaung sediments also implies that sediments were carried by different modes of transportation.

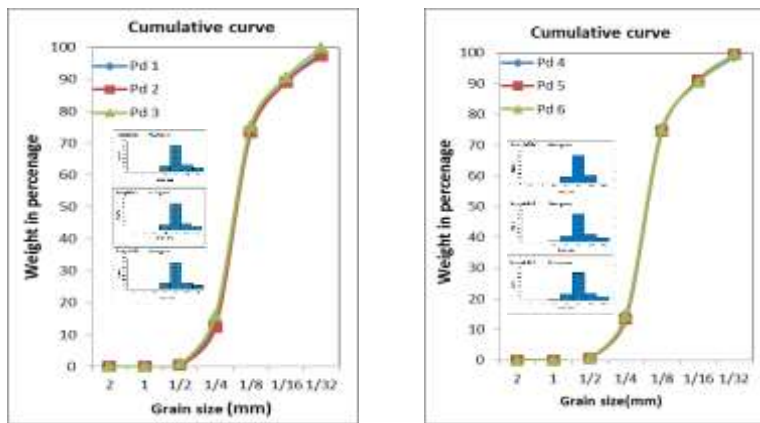


**Figure 25** Representative histograms and cumulative curves of size frequency distribution of the Pondaung Formation

Mode is the highest midpoint of the abundant class interval on a histogram. Median diameter is the 50% measure of the cumulative curve, the median range from 1.1 Ø to 1.2 Ø average sizes. The mean value of the analyzed sediments ranges from 1.4 Ø to 1.5 Ø respectively. The sorting value range from 0.8 Ø to 0.9 Ø; moderately to poorly sorted. The sorting results due to medium-energy (Folk and Ward, 1957) fluctuation of the depositing agent. Moreover, sorting nature does not reflect long transportation. The skewness value ranges from 0.1 Ø to 0.3 Ø. In the positively skewed; when both median and mean are shifted toward finer grains size, the coarser of the population shows better sorting than the finer of the population (Folk and Ward, 1957). The sand usually positive skewed, since much silt and clay is not removed by the current, but trapped between large grains. The kurtosis value is more than 1 Ø (1 Ø to 1.2 Ø), it is leptokurtic to mesokurtic indicates better sorting in the central portion of the size curve. According to Folk and Ward (1957), these sediments are the medium energy condition of the deposition.

**Visher Curve**

The composition of grain size curves and the interpretation of the separate population are aided by the use of log probability plots (Visher, 1969). The saltation population of the sandstones is nearly 2.5 to 2.75Ø and then sliding or rolling population generally is absent in the Pondaung formation. The break in the saltation populations ranges from about 60% to near 75%. Visher curve or log-probability curve of the Pondaung sediment samples show the presence of straight

lines were drawn to obtain two segments population which were demonstrated by coarse truncation and fine truncation in the study area (Fig. 26). According to Visher (1969), the samples of the Pondaung Formation could be deposited in the fluvial dominated deltaic environment.

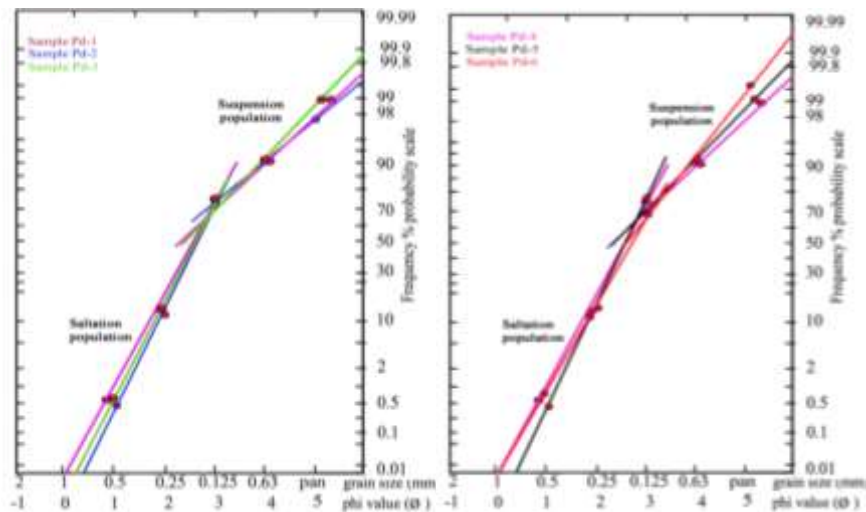


**Figure 26** Log-probability grain size of the Pondaung Formation

### Discussion and Interpretation

The Chindwin Basin including the present area was deposited shallow marine environment to a fluvial environment from Cretaceous to Neogene time. Thus, various approaches were made to interpret the provenance and depositional environments. The mineral such as zircon is important to interpret the provenance due to high durability in weathering and diagenetic processes during the sedimentation cycle (Wang *et al.*, 2014; Najman *et al.*, 2020).

The detrital heavy minerals identified from Pondaung Formation are rutile, zircon, tourmaline as ultra-stable, garnet, staurolite, epidote, chlorite, sillimanite as metastable; augite, diopside, hypersthene, olivine as unstable, and magnetite, chromite and hematite as opaque. The dominant and abundant heavy minerals are zircon, and the morphology is also platy form. Moreover, the proportions of heavy minerals from igneous are greater than the metamorphic and sedimentary rocks. Besides, detrital zircons of Eocene Formations from Chindwin Basin are mostly euhedral and have elongated to stout prismatic habits, indicating that they crystallized from magmas (Wang *et al.*, 2014; Najman *et al.*, 2020). Thus, the provenance of Pondaung Formation can be interpreted as Wuntho-Popa arc.

The facies associations of Pondaung Formation signify of the deposition in a fluvio-deltaic environment condition (Aung Naing Soe, *et al.*, 2002). The sediments of Pondaung Formation are interpreted as moderately to poorly sorted, the positive skewed and leptokurtic to mesokurtic kurtosis and then two straight segments that indicate the medium- to high-energy condition. This dynamic condition of Pondaung Formation was dominated by the fluvial dominated deltaic environment. Tectonically, all the sediments in the study area were derived mainly from the northern portion of the Western Granitoid Belt, especially Wuntho Massif and Salingyi Uplift, and Mogok Metamorphic Belt in Northern Myanmar. Now, the provenance of the Chindwin Basin was well derived from the WPA during Eocene time based on the isotope data of detrital zircon (Wang *et al.*, 2014; Najman *et al.*, 2020). It can be concluded that the Pondaung Formation was deposited in medium to high-energy fluvial deltaic environment derived from the igneous provenance of WPA.

## Acknowledgments

We are thankful to Dr.Thura Oo, Rector, Monywa University, for his help to carry out this research. We would like to thank to Dr. Than Than Win, Dr. Tun Min and Dr. Khin Nwe Aye, Pro-Rector, Monywa University, for their constructed comment and suggestion this paper. We would like to thank Professor Dr. Zaw Myint Ni, Head and Department of Geology, Monywa University, for his kind permission to submit this project paper. We would like to deeply acknowledge to Professor Dr. Myat Khaing, Department of Geology, Monywa University, for his critical reading of this manuscript, advice and suggestions concerning this research.

## References

- Asiedu, D. K., Suzuki, S. and Shibata, T., (2000). *Provenance of Sandstone From the Wakion subgroup of the Lower Cretaceous kanamon Group, Northern Kyushu, Japan*. The Island arc, Vol.9.p.128-144.
- Aung Naing Soe, Myitta, Soe Thura Tun, Aye Ko Aung, Tin Thein, Bernard Marandat, Stephane Ducrocq, Jean-Jacques Jaejer., (2002). Sedimentary facies of the late Middle Eocene Pondaung Formation (central Myanmar) and the paleoenvironments of its anthropoid primates. *Comptes Rendus Palevol*, p.1:153-160.
- Aye Ko Aung., (1998). Stratigraphic, age and sedimentology of the primate bearing Pondaung Formation, *Fossil Expedition Team Report*.
- Aye Lwin., (1993). The sedimentology of the sandstones of the Mahudaung area, Kani and Mingin Townships. *M.Sc Theiss, unpub*. University of Mandalay.
- Bender, F., (1983). *Geology of Burma*. Gebruder Bortrager, Berlin.p.293
- Cotter, G. de. P., (1912) Pegu-Eocene succession in the Minbu District near Ngape, Rec. *Geol. Surv., India*. Vol.41. Eocene sandstones in the southern Chindwin Basin, Maynamar: implications for the unroofing history of the Cretaceous-Eocene magmatic arc. *J. Asian Earth Science*. p.107, 172–194.
- Folk, R.L., and Ward, W. C., (1957). Brazos river bar: a study in the significance of grain size parameters. *Sedimentary Petrology*.
- Kerr, P. F., (1959). *Optical Mineralogy*, 3<sup>rd</sup> Edition, McGraw-Hill Book Company Inc., New York.
- Kyaw Lwin Oo., (2008). Sedimentology of Ecoene-Miocene Clastic strata in the southern Chindwin Basin, Myanmar. *Ph.D Thesis, unpub*. University of Yangon.
- Lindholm. RC., (1985). *A Pracrical Approach to Sedimentology*. London, Allen and Unwin. London.p.154-176.
- Mange, M. A & Maurer H. F. W., (1992). *Heavy Minerals in Colour*, Chapman & Hall, London.
- Najman.Y., Sobel. E., Millar. I., Stockli. D., Govin. G., Lisker. F., Garzanti. E., Limonta. M. Vezzoli. G., Copley. A., Zhang.P., Szymanski.E., Kahn.A., (2020). The exhumation of the Indo-Burman Ranges, Myanmar, *Earth and Planetary Science Letter* 530, p.1-14.
- Pettijohn, F. J., (1975). *Sedimentary Rocks*. 3<sup>rd</sup> edition. Harper and Raw Press, New York.
- Robinson, R. A. J., (2014.) Racey. C. A., Parrish. R. R., Horstwood. M. S. A., Oo, N. W., Bird, M. I. Thein, M., Walters, A. S., Oliver, G. J. H.
- Sahu. B. K., (1964). Depositional mechanism from the size analysis of clastic sediment. *Journal of sedimentary petrology*, 34(1), p.73-83.
- Visher, G. S., (1969). Grain-size Distribution and Sedimentary Processes. *Journal of Sedimentary Petrology*, vol. 39, no.3, p.1074-1106.
- Wang, J. C., Wu, F. Y., Tan, X. C., Liu, C. Z., (2014). Magmatic evolution of the Western Myanmar Arc documented by U-Pb and Hf isotopes in detrital zircon, *Tectonophysics*, p.97-105.

## **SEDIMENTARY FACIES ANALYSIS OF MIOCENE CLASTIC STRATA IN KALEWA-MAWLEIK AREA, SAGAING REGION**

Moe Zat<sup>1</sup>, Kyi Kyi Maw<sup>2</sup>, Yi Lar Tun<sup>3</sup>, Zaw Htaik<sup>4</sup> and Aye Aye Min<sup>4</sup>

### **Abstract**

The present study would offer the Sedimentary Facies of Miocene clastic sedimentary rock units of Letkat Formation (Early Miocene), Natma Formation (Middle Miocene) and Shwethamin Formation (Late Miocene) exposed in the southwestern Chindwin Basin, situated in Kalewa-Mawleik Townships, Sagaing Region. The study is mainly focus on outcrop-based sedimentary facies analysis. Eight lithofacies of Letkat Formation such as Trough cross-stratified sandstone (St) with basal erosional surface facies (Se) and lags (F.1), Pebbly gritty sandstone facies (Gm) (F.2), Sand-mud interlayer facies (Fl) (F.3), Thinly laminated fine sandstone facies (Sl) (F.4), Planar cross-stratified sandstone facies (Sp) (F.5), Horizontal to low-angle stratified sandstone facies (Sh) (F.6), Massive, variegated silty clay facies with fine-grained sandstone facies (Fsc) (F.7) and Bluish grey silty shale with silt and sand lens facies (Fsc) (F.8), five lithofacies of Natma Formation such as Massive nodular clay with fine-grained sandstone facies (Fsc) (F.1), Medium to thick-bedded, coarse-grained to gritty trough-cross bedded sandstone (Gt) with basal erosional surface (Se) facies (F.2), Planar cross-stratified sandstone facies (Sp) (F.3), Thinly bedded siltstone or silty fine sandstone and shale facies (Fl) (F.4) and Massive, variegated silty clay facies (Fm) (F.5) and six lithofacies of Shwethamin Formation such as Gritty to pebbly sandstone facies (Gm) (F.1), Trough cross-bedded sandstone facies (St) (F.2), Planar cross-bedded sandstone facies (Sp) (F.3), Horizontal laminated sandstone facies (Sh) (F.4), Thinly laminated fine sandstone and siltstone facies (Fl) (F.5) and Massive, variegated silty clay facies (Fm) (F.6) were deposited in braided river environment. For more environmentally specific, individual facies is needed to combine together into facies associations to define environment. At least five lithofacies association can be established in the Miocene sequence of the research area which are Sandy Fluvial Channel Facies Association (CH), Sand Bar Facies Association (SB), Gravel Bar Facies Association (GB), Overbank Fines Facies Association (OF) and Laminated Sand Sheet Facies Association (LS).

**Keywords:** Facies, Letkat Formation, Natma Formation, Shwethamin Formation

### **Introduction**

#### **1.1 Location and Physiography**

The research area, southern part of Chindwin Basin is situated in Kalewa-Mawleik Township lays in topographic map no. 84 I/6, I/7 and I/8.

On the basis of landform characteristics, the research area forms as strike ridges and valley intervening between the two ridges-forming units (Figure.1).

#### **Aims and Objectives**

The present project will attempt to carry out sedimentary facies of Miocene clastic strata in Kalewa-Mawlaik area.

#### **Materials and Methods**

1. Field investigation was conducted mainly responsible for the detailed sedimentological measurements Miocene Formations.

---

<sup>1</sup> Dr, Associate Professor, Department of Geology, Dagon University

<sup>2</sup> Dr, Professor and Head, Department of Geology, Dagon University

<sup>3</sup> Lecturer, Department of Geology, Dagon University

<sup>4</sup> Demonstrators, Department of Geology, Dagon University

2. Analysis outcrop-based sedimentary facies of rock units recognizing the evolution of the depositional system.

**Previous Work**

Aung Khin and Kyaw Win (1968, 1969); MOGE (1977), Than Htut and Chit Saing (2003) outlined the paleontology and stratigraphy of Eocene to Pleistocene units of Chindwin Basin.

In 1972, Dr Win Swe, U C. Thacpaw, Daw Nay Thaung Thaung and U Kyaw Nyunt also studied “Geology of Part of the Chindwin Basin of the Central Belt, Burma”.

**Regional Geologic Setting**

The research area is situated in the western part of the Southern Chindwin Basin which is a part of the Central Myanmar Tertiary Basin lying between the Western Ranges (Indoburman Ranges) in the west and Wuntho Igneous Massif in the east.

Regionally, the research area is mainly composed of clastic sedimentary rocks with a general trend of nearly N-S direction. In this area, Miocene rocks of Letkat, Natma and Shwethamin Formations are mostly cropped out along the middle part which is overlain unconformably by Late Eocene clastic sedimentary rocks of Yaw Formation and conformably by Miocene-Pliocene clastic sedimentary rocks of Irrawaddy Formation.

In the Miocene Formations, the rocks are distributed especially along the ridges of Kalewa-Mawlaik and some are along the stream section and the car-road section. The regional geology of the southern Chindwin Basin and its environs is shown in (Figure. 2).

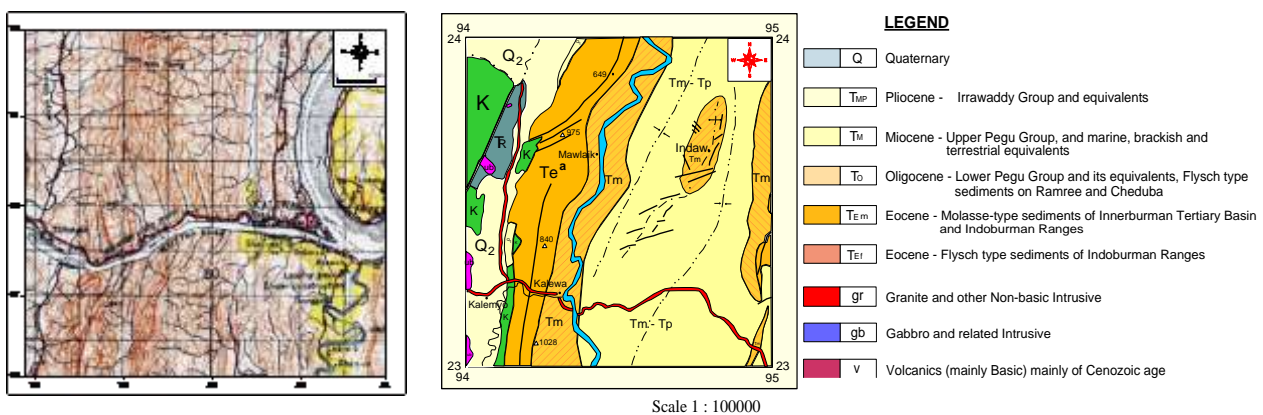


**Figure 1** Location and Physiographic feature of the research area **Figure 2** Regional geologic setting of the study area (From Geological Map of Myanmar, 1977)

**Stratigraphy**

**General Statement**

The study area, western part of the southern Chindwin Basin is underlain by thick succession of Plaeogene-Neogene clastic sedimentary strata. The exposed rock units are Letkat Formation (Early Miocene), Natma Formation (Middle Miocene) and Shwethamin Formation (Late Miocene). The stratigraphic succession is shown in Table (1).

## Sedimentary Facies Analysis of Miocene Formations

### Sedimentary Facies Analysis of Letkat Formation (Early Miocene)

#### 1. Trough cross-stratified sandstone (St) with basal erosional surface (Se) facies

##### Description

The lower part of the Letkat Formation is commonly started with very thick to massive, large scale trough cross-bedded fine to medium grained sandstones with sharp, deep and broad basal erosion surfaces scoring into the underlying Yaw Formation (Figure.3). This facies consists of fine to medium-grained, medium-bedded, light gray colored sandstones with mud drapes and clasts. Small to large-scale trough cross-beddings and mud clasts are the dominant sedimentary structures.

**Table 1 Stratigraphic Sequences of the Western Part of Southern Chindwin Kalewa Area**

| Age           | Stratigraphic Units  | Dominant Lithology                                     | Maximum Thickness (m) | Depositional System |
|---------------|----------------------|--------------------------------------------------------|-----------------------|---------------------|
| Late Miocene  | Shwethamin Formation | Sand, minor silty shale                                | 200                   | Fluvial system      |
| Early Miocene | Natma Formation      | Shale, silty shale, minor sand                         | 340                   | Fluvial system      |
| Early Miocene | Letkat Formation     | Sand, subordinate pebble-conglomerate, minor silt/clay | ?                     | Fluvial system      |

##### Interpretation

Very large-scale trough cross-bedded sandstones free from mud drapes in their foreset stratifications and the occurrence of intraformational mud clasts are commonly found in the basal part of the fluvial channels. The erosional base with clasts and detrital coal clasts-supported conglomeratic sandstones can be regarded as channel floor and basal deposits (Miall, 1987). Mud clasts present at the base of the trough cross-bedded sandstone reveal as the basal portion of a sandy fluvial channel.

Therefore, this facies pointed out that it had deposited in the distributary channel of fluvial environment.

#### 2. Pebbly gritty sandstone facies (Gm)

##### Description

This facies is mainly composed of medium to gritty, medium to thick bedded, light grey to yellowish grey colored pebbly gritty sandstones. Low angle cross-beddings are common in the gritty sandstone. Pebbles are scattered through the sand (Figure.4) and more typically at the top of the bed. Mostly, pebbles are more or less parallel to the large scale low angle cross-bedding.

##### Interpretation

Mostly, the pebbles are deposited in prograding gravelly and sandy distributary channels (Casshyap and Aslam, 1990). Low angle cross-beddings are produced by migration of bars with low channelward dipping slopes (Reineck and Singh, 1980). Clast-support rounded conglomerates

found in association with lithofacies; St and Sh suggest gravel bedforms or gravel bars of a high gradient, proximal bed-load braided river deposits (Reading, 1996).

Therefore, this facies can be interpreted as bars or channel lag deposit of the braided river.

### **3. Sand-mud interlayer facies (F1)**

#### **Description**

This facies is mainly composed of fine to medium-grained, thin to medium-bedded, light gray to gray colored sandstones and bluish gray colored shale. Parallel lamination, interlayering of sand-shale and small scale cross-lamination are the dominant sedimentary structures (Figure.5). Approximate sand-shale ratio is 3:2 in average.

#### **Interpretation**

The interlaying of sand-shale and the small scales cross-stratification indicate that the flow velocity generally fluctuated and were lower than those flow responsible for deposition of sand (Wood and Hopkins, 1989). In high-energy tidal environments, mud settles during slack water time, at high and low tide stands, when the current inverts its direction and its strength becomes insufficient to transport sand (Ricci Lucchi, 1995).

Therefore, the above listed documentation pointed out that the sand–mud interlayer facies had deposited in the overbank or waning flood deposit of fluvial channel.

### **4. Thinly laminated fine sandstone facies (F1)**

#### **Description**

This facies is mainly composed of thin to medium bedded, thinly parallel and wavy laminated fine sandstones with very thin carbonaceous laminations and minor ripple cross-laminations (Figure.6). Some place is scoured by a broad and shallow sandy minor channel with coal fragments as a basal lag.

#### **Interpretation**

Laminae in the shallow marine environments are produced by seasonal fluctuations in sediment supply or periodic stirring of the bottom by wave action (Blatt et al., 1980). Thinly laminated fine sandstone beds overlying thick unit of laminated shale represent the characteristic of a crevasse splay sandstone as well as carbonaceous silt and mud of interdistributary bay sediment deposited in delta plain environment (Coleman & Prior, 1980; Allen, 1987).

Therefore, this facies was deposited crevasse splay or planar bed flow (lower and upper flow regime) of fluvial channel.

### **5. Planar cross-stratified sandstone facies (Sp)**

#### **Description**

This facies is mainly composed of medium to thick-bedded, fine to medium-grained, sandstones with single sets of medium to large-scale planar-tabular cross-stratifications (Fig.6). Foresets are straight with sharp, angular lower contacts with inclined angle at 15° -30°.

#### **Interpretation**

Planar cross-bedding is commonly found in migrating straight crested subaqueous dunes of the active fluvial river channel (Miall, 1987). Large-scale single sets of planar cross-bedding also represent cross channel bars and associated with planar or horizontally stratified sandstone facies (Sh) suggesting sand flat accretion (Cant & Walker, 1978).

Therefore, this facies can be interpreted to have been deposited under transverse bars or dunes (lower flow regime) of fluvial river channel.

## **6. Horizontal to low-angle stratified sandstone facies (Sh)**

### **Description**

This facies is mainly composed fine to medium-grained, light grey to yellowish grey colored sandstones with horizontal to low-angle thinly parallel and wavy laminated fine sandstones with very thin carbonaceous laminations (Figure.7). Laminations are horizontal or have low dip angle ( $<10^\circ$ ) with parting lineation or plane bed stratification.

### **Interpretation**

Laminae in the shallow marine environments are produced by seasonal fluctuations in sediment supply or periodic stirring of the bottom by wave action (Blatt et al., 1980). Low-angle cross-bedding (angle of dip  $5^\circ$ - $10^\circ$ ) is very common in the ephemeral stream deposits and can be considered as a characteristic bedding of shallow or ephemeral stream deposits (Picard and High, 1973). Thick sequence of this facies also represents poorly channelized laminated sand sheet deposits (Miall, 1985).

Therefore, this facies can be interpreted to have been deposited under planar bed flow (lower and upper flow regime) or anti-dunes of fluvial environment.

## **7. Massive, variegated silty clay facies (Fm)**

### **Description**

This facies is characterized by massive, buff color clay and brownish, purplish to reddish mottled colors of massive variegated clays with calche nodules (Figure.8). The thickness varies from 5m to 40m. In this facies, silicified wood fragments are common. It is well developed in the upper portion of Letkat Formation.

### **Interpretation**

Fine-grained sediments are deposited as overbank material during flood stages of the river, on the flood plain, in bays, swamps, marshes and crevasse splays. The variegated clay with calche nodules, closely linked to the fluvial depositional system, has long been regarded as fluvial paleosols. It is a characteristic pedogenic feature of alluvial soil derived from the shallow burial early diagenetic alteration of fluvial flood plain deposits under semi-arid condition (Bowen & Kraus, 1993).

The presence of calche nodules suggest that the sediment was deposited in swampy deposits at basin margin.

## **8. Bluish grey silty shale with silt and sand lens facies (Fsc)**

### **Description**

This facies is mainly composed of gray and yellowish grey colored thick-bedded shales with subordinated amount of silt and sand lens (Fig.9). The discontinuous sand lenses with micro cross-lamination and coal clasts are notably observed, intercalated in thick bedded clay unit.

### **Interpretation**

Thick-bedded shales were probably deposited by suspension in low energy environment and disperse over wide area by the basinal processes (Reading, 1996). Organic content and the

association with dull coal, indicate an extremely low rate of sedimentation and an anoxic environment of deposition. Micro cross-laminated and fairly persistence thin sand layers are characterized by storm surged current (Reineck and Singh, 1980). The silty, parallel and lenticular laminations occurred in this shale facies indicate the depositional site near to the delta front.

Therefore, these facies can be deposited when the transgression took place in the depositional site, where there again have a deeper environment.

## **Sedimentary Facies Analysis of Natma Formation (Middle Miocene)**

### **1. Massive silty nodular clay with fine-grained sandstone facies (Fsc)**

#### **Description**

This facies is mainly composed of whitish gray colored thick-bedded shales with subordinated amount of silt and sand bands. The discontinuous sand lenses with micro cross-lamination, nodule silty shale (Figure.10) and coal clasts are notably observed, intercalated in thick bedded clay unit.

#### **Interpretation**

Clay particles are therefore present as suspended load in most currents of water and air and are only deposited when the flow ceases (Trucker, 1988). Thick-bedded shales were probably deposited by suspension in low energy environment and disperse over wide area by the basinal processes (Reading, 1996). The nodular shale is a result of dehydration process. Organic content and the association with dull coal, indicate an extremely low rate of sedimentation and an anoxic environment of deposition.

Therefore, these facies can be deposited when the transgression took place in the depositional site, where there again have a deeper environment.

### **2. Medium to thick-bedded, coarse-grained to gritty trough-cross bedded sandstone (Gt) with basal erosional surface (Se) facies**

#### **Description**

This facies is mainly composed of buff color, medium to thick-bedded, coarse-grained to gritty, medium to large-scale trough cross-bedded sandstone with sharp, deep and broad basal erosion surfaces scoring into the underlying silty shale. It consists of pebble-size mud clasts, coal clast and medium to large-scale cross-bedding (Figure.11). They are set in red ferruginous matrix.

#### **Interpretation**

The coarser and poorly sorted sediments than the adjoining deposits indicated that the deposition took place as channels fills where the various kinds of cross-beddings can be occurred. The deepest portions of the channles are floored either by a coarse lag deposit or by large sand waves (Hubbard, 1971 Oertel, 1973; Kumar and Sanders, 1974). Gravels may occur in cross bedded units representing bar deposits in gravelly braided rivers or as gravel lags, thin layers of coarse debris lying on the erosional scours at the bottoms of the river channels.

Therefore, this facies can be interpreted as bar/channel lag deposit of the braided river.

### **3. Planar cross-stratified sandstone facies (Sp)**

#### **Description**

This facies is mainly composed of medium to thick-bedded, medium-grained, sandstones with single sets of medium scale planar-tabular cross-stratifications. Foresets are straight with sharp, angular lower contacts with inclined angle at 15° -30° (Figure.12).

#### **Interpretation**

Planar cross-bedding is commonly found in migrating straight crested subaqueous dunes of the active fluvial river channel (Miall, 1987). Large-scale single sets of planar cross-bedding also represent cross channel bars and associated with planar or horizontally stratified sandstone facies (Sh) suggesting sand flat accretion (Cant & Walker, 1978).

Therefore, this facies can be interpreted to have been deposited under transverse bars or dunes (lower flow regime) of fluvial river channel.

### **4. Horizontal to low-angle stratified sandstone facies (Sh-Sl)**

#### **Description**

This facies is mainly composed fine to medium-grained, light grey to yellowish grey colored sandstones with horizontal to low-angle thinly parallel and wavy laminated fine sandstones with very thin carbonaceous laminations. Laminations are horizontal or have low dip angle (<10°) with parting lamination or plane bed stratification (Fig. 13).

#### **Interpretation**

Low-angle cross-bedding (angle of dip <10°) is very common in the ephemeral stream deposits and can be considered as a characteristic bedding of shallow or ephemeral stream deposits (Picard and High, 1973). In fluvial channel, these stratifications can be observed in wash-out dunes, anti-dunes, and commonly found in laminated sand sheets (Miall, 1978).

Therefore, this facies can be interpreted to have been deposited under planar bed flow (lower and upper flow regime) or anti-dunes of fluvial environment.

### **5. Thinly bedded siltstone or silty fine sandstone and shale facies (Fsc)**

#### **Description**

This facies is mainly composed of bluish grey color, brecciated shale, and variegated shale and interbedded with siltstone or silty fine sandstone and plant debris intercalation (Fig.14). The siltstones are yellowish white color and small to medium scale horizontal scale low-angle laminations are occurred in them. The sandstones are whitish grey color and very fine-grained.

#### **Interpretation**

Very fine sand and silt with clay and plant debris intercalations represent subaqueous levee deposits (Reineck and Singh, 1980). The sandstone beds with sharp or loaded bases were rapidly emplaced probably during periods of high fluvial discharge (Wood and Hopkins, 1989). The general sharp base nature of the shale beds indicate that deposition of mud from suspension may have occurred predominantly during periods of interflood quiescence rather than the waning flood stage.

In this facies, very fine sand and silt with clay and plant debris intercalations represent subaqueous levee deposits (Reineck and Singh, 1980).

## **6. Massive, variegated silty clay facies (Fm)**

### **Description**

The variegated clays are observed as the multicolor of mottled ash gray to greenish grey in chocolate brown to reddish brown matrix of sandy and silty clay with disseminated small carbonate nodules (Figure.15). In this facies, silicified wood fragments are common. It is well developed in the middle portion of Natma Formation.

### **Interpretation**

Fine-grained sediments are deposited as overbank material during flood stages of the river, on the flood plain, in bays, swamps, marshes and crevasse splays. The variegated clays are interpreted as semi-arid floodplain paleosols formed during lower water table at relative base-level fall or indicating that the rate of basin subsidence was less than the rate of deposition.

Therefore, extensive occurrence of paleosol formation in the upper part of Natma Formation may reflect prolonged exposed floodplains of non-depositional in a mixed-load meandering river system under semi-arid climate.

## **Sedimentary Facies Analysis of Shwethamin Formation (Late Miocene)**

### **1. Gritty to pebbly sandstone facies (Gm)**

#### **Description**

This facies is mainly composed of medium to gritty, medium to thick bedded, light grey to yellowish grey colored pebbly gritty sandstones with erosional base (Fig.16). Pebbles are scattered through the sand and more typically at the top of the bed. Wood fragments are also occurred in the basal part of this formation.

#### **Interpretation**

Gravels are more abundant and comprise main deposits of channels and bars (Tucker, 2003). Mostly, the pebbles are deposited in prograding gravelly and sandy distributary channels (Casshyap and Aslam, 1990). The erosional base with mud clasts and detrital coal clasts-supported conglomeratic sandstones can be regarded as channel floor and basal lag deposits (Miall, 1978).

Therefore, this facies is a characteristic of the channel lag deposit of the braided river formed during high stage of river with turbulence and erosive current.

### **2. Trough cross-bedded sandstone facies (St)**

#### **Description**

This facies consists of medium-grained, medium to thick-bedded, light gray colored sandstones with mud drapes and clasts. Small to large-scale trough cross-beddings (Figure.17) and mud clasts are the dominant sedimentary structures. The paleocurrent direction measured from cross-bedding is  $190^\circ$ .

#### **Interpretation**

The small scale cross-laminated fine to medium-grained sandstones is the lower flow regime structures of sandy fluvial channel and they are found as (Miall, 1972; Reading, 1996). Very large-scale trough cross-bedded sandstones free from mud drapes in their foreset stratifications and the occurrence of intraformational mud clasts are commonly found in the basal part of the fluvial channels. Wavy or erosive base upon which the present of mud drapes and clasts

is the deposition taken place in a channel area where the basal erosion can occur (Reineck and Singh, 1980).

Therefore, this facies pointed out that it had deposited in dunes of a fluvial channel.

### **3. Planar cross-bedded sandstone facies (St)**

#### **Description**

This facies is characterized by medium to thick-bedded, medium to coarse-grained sandstones with single sets of large scale planar cross-stratifications (Figure.18). In some outcrops, pebbles and grains are arranged in cross-beds.

#### **Interpretation**

Planar cross-bedding is commonly found in migrating straight crested subaqueous dunes of the active fluvial river channel (Miall, 1987). Large scale single sets of planar cross-bedding also represent cross channel bars and associated with planar or horizontally stratified sandstone (Sh) suggesting sand flat accretion (Reineck and Singh, 1980).

Therefore, this facies can be interpreted to have been deposited under transverse bars or dunes (lower flow regime) of fluvial river channel.

### **4. Horizontally laminated sandstone facies (Sh)**

#### **Description**

This facies is characterized by thick-bedded to massive, fine to medium-grained, light grey to buff color sandstone (Figure.19). Horizontal laminations with parting lineation or plane bed stratifications are found in this facies. It is vertically associated with trough cross-bedded sandstone facies (St).

#### **Interpretation**

Low-angle cross-bedding (angle of dip  $5^{\circ}$ - $10^{\circ}$ ) is very common in the ephemeral stream deposits and can be considered as a characteristic bedding of shallow or ephemeral stream deposits (Picard and High, 1973). In fluvial channel, these stratifications can be observed in wash-out dunes, anti-dunes, and commonly found in laminated sand sheets (Miall, 1978).

Therefore, this facies can be interpreted to have been deposited under shallow, high-energy (upper flow regime) flow conditions during which sediments was aggraded vertically.

### **5. Thinly laminated fine sandstone and siltstone (Fl)**

#### **Description**

This facies is mainly composed yellowish grey colored fine-grained and buff colored siltstone with thinly lamination (Figure.20). Mica and carbonaceous matters are present in laminations. Some place is scoured by a broad and shallow sandy minor channel with coal fragments as a basal lag.

#### **Interpretation**

Thick sequence of this facies also represents poorly channelized laminated sand sheet deposits (Miall, 1985). Thinly laminated fine sandstones and siltstones represent the characteristic of crevasse splay sandstone. Sharp base with fining upward and thinly laminated fine sandstone beds overlying thick unit of laminated shale represent the characteristic of a crevasse splay

sandstone as well as carbonaceous silt and mud of interdistributary bay sediment deposited in delta plain environment (Coleman & Prior, 1980; Allen, 1987).

Therefore, this facies was deposited in crevasse splay of delta plain environment.

## **6. Massive silty clay facies (Fm)**

### **Description**

This facies is characterized by massive, grey to buff color clay and brownish, purplish to reddish mottled colors of massive variegated clays (Figure.21). In this facies, silicified wood fragments and load cast nature are common. It is well developed in the upper portion of Natma Formation.

### **Interpretation**

The variegated clays are interpreted as semi-arid floodplain paleosols formed during lower water table at relative base-level fall or indicating that the rate of basin subsidence was less than the rate of deposition. When a mud is deposited in water it has a high water content which is lost as the sediment compacts and cements into a mudrock.

So, this facies is interpreted as swampy deposits at basin margin and interdistributary bay deposits on delta plain (Coleman and Gagliano, 1965).

## **Lithofacies Association of Miocene Formations**

### **1. Sandy Fluvial Channel Facies Association (CH)**

This lithofacies association is characterized by the lithofacies Se, St, Sp, Sh, Sr and the minor or subordinate facies (Fsc, Fl and Fm) of waning flood and overbank fines. It usually starts at the base with erosional concave-up, crude cross-bedded, gritty to pebbly sandstones (lithofacies Se) and associated lag deposits of Letkat, Natma and Shwethamin Formations. It is overlain by medium to large-scale trough cross-bedded coarse sandstone (St) with thickness vary from 1m to 5m gradually upward decrease in grain size and scale of primary structures; Sp, Sh, Sr in descending order. The upper part again overlain by the fine facies, Fsc, and Fm show the overall fining upward facies trend. In the lower part of the formations, this facies association is always found in association with sandy and gravelly bedforms (SB and minor SG). The middle part of the formations show thin facies associations of CH and thick LS. The upper part of the formations is mainly composed of thin CH which is intercalated within the thick overbank-floodplain fines (OF).

This facies association is commonly found in associated with sandbars and minor gravel bars in the lower part suggesting the coarse grained bedload braided river system. It gradually passes upward to the mixed-load meandering river systems in the upper of the formation (Miall, 1985).

### **2. Sand Bar Facies Association (SB)**

It is mainly comprised of Sp, Sh-Sl, St, Se and the subordinate facies of Sr, Fl and Fm. This facies association is significantly decreased upward in their scale and population throughout the vertical sequence of the Letkat and Shwethamin Formations. It is commonly associated with CH, GB and OF facies association.

This facies association can be interpreted as fluvial sandbars of varying types of the channel-fill complexes (e.g., dunes and transverse bars) and it also represents the crevasse channels and splay deposits (Miall, 1985).

The middle part of the formation is mainly dominated with thick multi-storey SB mainly composed of the coarse grained and large-scale co-sets of Sp, Sh-Sl, and St, Se lithofacies found in association with CH and minor GB suggesting a proximal braided river channel with sandy braided bars; transverse bars and downstream accretion sand bars (Cant & Walker, 1978; Reineck & Singh, 1980). The occurrence of bars more than 10m thick and large sand waves or sand-flats indicate that the river channels were large and had an extensive catchment area (MacCarthy, 1990). The scale of the sandbars decrease upwards in the sequence also reflect the overall upward fining fluvial system which could have resulted from and increased subsidence rate in the basin (Blair, 1986) and associated increased in relative sea-level as well as a reduction in sediment supply from the source areas.

### **3. Gravel Bar Facies Association (GB)**

The facies association GB (gravelly bars and bedforms) is commonly found in association with the facies association (SB) sand bedforms) and CH (sandy braided river channels) interbedded in the lower part of Letkat Formation. Pebbly gritty sandstones with varying proportion of gravels (granule to pebble sizes) are included in this facies association. Associations of massive or crudely bedded, pebble-clast-supported conglomerates (Gm and Gp with subordinate lithofacies; Gt, St, Sp) are interpreted as gravel has deposited in a low sinuosity gravelly braided river (Miall, 1978; MacCarthy, 1990).

In the downstream or the middle reaches of braided rivers, gravel beds grade into the small babbles and sand beds. In the lower, more active channels, bar gravel dominate, whereas sands and pebbly sands are common at higher topographic elevation (South Saskatchewan). As a result of downstream and laterally migrating sand and gravel bars, planar and trough cross-bedding are dominant.

### **4. Overbank fines Facies Association (OF)**

The overbank fine (OF) lithofacies associations represents natural levees, inter-fluvial overbank, flood plains and fluvial-floodplain paleosols in the facies analysis of the Fluvial Letkat, Natma and Shwethamin Formations. It is mainly composed of mudstone and siltstone lithofacies and found in association with minor interbeds of fine sand lithofacies; Sl, Sh, Sr. Carbonaceous matters and carbonate nodules or calche nodules are frequently observed.

This facies association is rarely observed in the lower part, subordinately occurred in the middle part, and well developed in the upper portion of the Letkat Formation. In the upper part of the formation, OF is interbedded with the lithofacies associations; SB of crevasse splays sands, SL of laminated sand sheets, and CH of sandy channels (Fig. 73).

OF in the lower part is dominated with light greenish grey mudstone/siltstone facies with carbonaceous matters and carbonized fossil-wood fragments. Whereas in the upper part is characterized by brownish, purplish to reddish mottled colours of thick variegated clays with desiccation cracks, calche nodules, and silicified wood fragments suggesting that the closer to the top of profile, the nearer to surface condition and thereby the more intensive the soil formation process (Kraus and Brown, 1985). The variegated clay of the upper part is interpreted as semi-arid floodplain paleosols formed during lower water table at relative base-level fall or indicting that the rate of basin subsidence was less than the rate of deposition.

### **5. Laminated Sand Sheet Facies Association (LS)**

This facies association is mainly composed horizontal to low angle cross-stratified sandstone facies Sh-Sl with minor lithofacies of Sp, St and Sr. It is best developed in the middle

and the upper part of the Letkat Formation commonly associated with the lithofacies associations; CH and OF.

In the middle of the formation, thick cyclic sequences of LS (10-15m) associated with shallower and broad sandy fluvial channel elements (CH) are interpreted to have deposited under shallow, high energy poorly channelized sheet deposits occurring as channel fill or bar tops (North and Taylor, 1996). The upper part of the formation contains the interbedded sequences of LS and OF suggesting flash-flood or generally unconfined sheet flood deposits, i.e., crevasses sand sheets deposition into the flood plains during highest stage of river (Miall, 1985).



**Figure 3** Photograph showing large scale trough cross-bedding showing that downcurrent truncation of cross bed set confined active large scale fluvial channel

**Figure 4** Photograph showing pebbles, conglomerates and coal scatter embedded in Lower Letkat Sandstone point out that bar/channel lag deposit of braided river

**Figure 5** Photograph showing sand-mud interlayering nature; light color representing sand beds with sharp or loaded bases which were rapidly emplaced, probably during periods of high fluvial discharge



**Figure 6** Photograph showing a fluvial sequence developed on a sharp channeled base little fining upward trend and may contain a scour surface (arrow) indicating that it is an amalgamated sandbody

**Figure 7** Photograph showing thick-bedded truncated set of medium to large-scale planar cross-stratified sandstone (Sp) of the lower part of Letkat Formation

**Figure 8** Photograph showing thick-bedded, low-angle ( $<10^\circ$ ) stratified medium-grained sandstone body which representing high energy (upper flow regime) condition



**Figure 9** Photograph showing variegated clays with caliche nodules indicating that the non-deposition in mix-load meandering river system under semi-arid climate

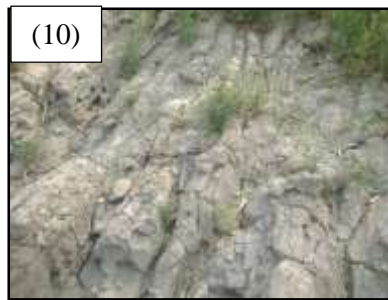


**Figure 10** Photograph showing thick bedded bluish grey silty shale resting between trough cross-bedded sandstone of Letkat Formation pointing out the transgression took place in the depositional site



**Figure 11** Photograph showing thick bedded nature of bluish grey shale with a few isolated cobbles in Natma Formation indicating flood sequence from braided river



**Figure 12** Photograph showing pebbly gritty sandstone laying the silty grey shale which is pointing out the protruding in a gravelly braided river



**Figure 13** Photograph showing medium planar cross-stratified, fine to medium-grained sandstone deposited in the lower flow regime found in fluvial channel

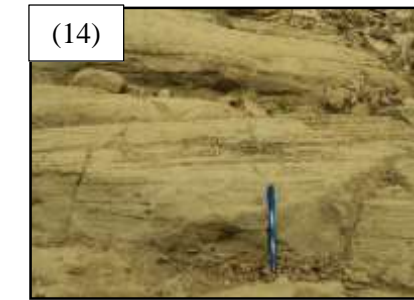


**Figure 14** Photograph showing horizontal to low-angle (<math><10^\circ</math>) stratified medium-grained sandstone body which representing high energy (upper flow regime) condition



**Figure 15** Photograph showing the variegated clay with caliche nodule, which is a characteristic of fluvial deposition system as paleosols



**Figure 16** Photograph showing silicified wood fragments in the basal part of gritty sandstone indication channel lag deposit



**Figure 17** Photograph showing large-scale trough cross-bedding point out the down current truncation of cross-bed set confined active large scale fluvial channel



**Figure 18** Photograph showing medium to thick-bedded, medium to coarse-grained sandstones with single sets of large scale planar cross-stratifications in Shwethamin sandstone

**Figure 19** Photograph showing medium-bedded horizontal to low-angle stratified medium-grained sandstone overlying the trough cross-bedded sandstone indicating the fluvial channel environment

**Figure 20** Photograph showing parallel continuous laminated fines sandstone indicating the waning floods deposits

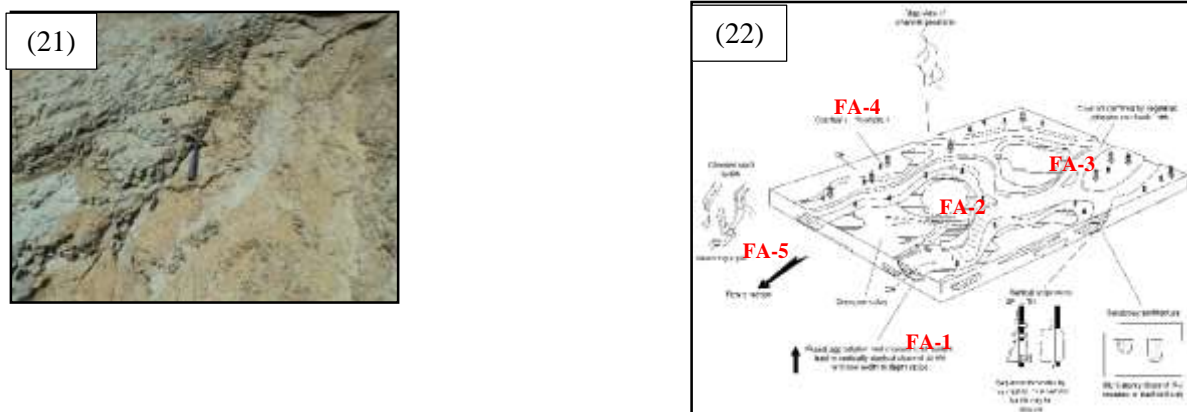


**Figure 21** Photograph showing thick-bedded variegated silty shale with numerous caliche nodules representing the characteristics pedogenic features of the semi-arid climate

**Figure 22** Generalized lithofacies association in braided river model of Letkat Formation of the study area

This predominance of this facies association over the others is one of the most outstanding features used to distinguish the ephemeral-fluvial river deposits of semi-arid region from the perennial river deposits of humid-region and it is also a characteristic of an aggrading fluvial river system (North and Taylor, 1996) developed during initial relative base-level rise.

## Conclusions

The present study would offer the sedimentological outcrop-based sedimentary facies analysis of the clastic sedimentary rock units of Letkat Formation, Natma Formation and Shwethamin (Late Eocene) exposed in the southwestern Chindwin Basin, situated in Kalewa-Mawleik Townships, Magway Region.

During Early Miocene, Letkat Formation was deposited in a fluvial-river system of the lowstand systems tract deposits (LST) deeply incised into the underlying Yaw Formation during relative sea-level fall, also be regarded as an incised fluvial channel-fill (IVF). The fluvial sequence of the lower part Letkat Formation is characterized by high bed-load gravelly and sandy, multi-

story sand bodies of braided channel-complexes with general lack of the overbank fines. The middle part of the formation is constructed with the shallow and broad amalgamated sandy channels with thick laminated sheets (LS) probably deposited as a result of unconfined sheet flooding. The upper part is becoming dominated with thick overbank-floodplains fines (OF) interbedded with the isolated major channels, minor channels or crevasse channels, and thin crevasse splays or laminated sand sheets. The lower part Natma Formation is becoming dominated with thick overbank-floodplains fines (OF) interbedded with the isolated major channels, minor channels or crevasse channels, and thin crevasse splays or laminated sand sheets in the fluvial system. The upward change in sand-body architectures within the sequence and lateral interconnected and amalgamated channel and meander belt systems with poorly preserved floodplain deposits. The lower part of Shwethamin Formation is characterized by high bedload gravelly and sandy, multi-story sand bodies of braided channel-complexes. The middle part is constructed with the shallow and broad amalgamated sandy channels whereas the upper part is dominated with thick overbank-floodplains fines.

### **Acknowledgements**

We wish to express our sincere gratitude to Dr. U Win Naing, Rector of Dagon University, Dr. Daw Nu Nu Yi and Dr. Daw Nay Thwe Kyi, Pro-Rectors of the Dagon University for their permission of this research work.

### **References**

- Anderton, R. (1985)**, Clastic facies models and facies analysis. In: *Sedimentology: Recent Developments and Applied Aspects* (Ed. by P.J. Brenchley and B.P.J. Williams), pp.31-47. Spce. Publ. Geol. Soc. London, 18-25.
- Miall, A.D., (1977)**, "Analysis of Fluvial Depositional System", American Association of Petroleum Geologists, Fall Education Conference (1981).
- Reineck, H.E. and Singh, J.B. (1980)**, *Depositional Sedimentary Environments*: Springer-Verlag, N.Y.
- Win Swe, U.C. Thacpaw, Daw Nay Thaung Thaung and U Kyaw Nyut, (1972)**, *Geology of Part of the Chindwin Basin of the Central Belt, Burma*.

## **SOIL AND WATER QUALITY ANALYSIS IN KYONPYAW AREA, PATHEIN DISTRICT, AYEYARWADY REGION**

Wint Wint Htun<sup>1</sup> and Saw Zar Chi<sup>2</sup>

### **Abstract**

The study area is bordered to the north by the Laymyethnar Township, to the south by the Kyaungkong Township, to the west by the Yae kyi Township and to the east by the Danupyu Township, Pathein District, Ayeyarwady Region. The study area consists of Myawaddy, Tayza, Aung San and Panlong Wards. The area is covered by alluvial deposit and underlain by Tertiary deposits of Irrawaddy Formation. This research has been accomplished to analysis on the soil and water quality. Seven soil samples were collected from four wards and analyzed for Arsenic, Copper, Lead, Zinc, Potassium, Manganese, Sodium, Calcium, Magnesium and Cadmium. Those were examined by Atomic Absorption Spectrometry (AAS) in the Geochemistry Laboratory of the Applied Geology Department, Yangon. Some parts of the study area, Copper, Lead and Zinc in the soil results are higher than the permissible limits of WHO standard. Eleven water samples were collected from surface and groundwater. Surface water samples are collected by water sampler, depth value was tested by HONDEX PS-7-LCD SOUNDER. Multiparameters (Multi probe), Single Probe, Hand-Held Refractometer instruments were also used in the surface and groundwater quality. Physio-chemical of pH, E.C, TDS, ORP, TH, TA, DO, Salinity, Temp, Turbidity, Mg<sup>++</sup>, Ca<sup>++</sup>, Fe<sup>++</sup>, Ca(HCO<sub>3</sub>)<sub>2</sub>, CL<sup>-</sup>, SO<sub>4</sub><sup>-</sup> were also analyzed at the Soil Examination Laboratory of Department of Fisheries, Ministry of Livestock and Laboratory, Thaketa Township, Yangon. According to the water quality analysis; temperature, calcium and iron are higher than WHO standard. Analyzed by the digital arsenator, arsenic in Panglong is higher than the WHO standard.

**Keywords:** *soil quality, surface and groundwater*

### **Introduction**

The study area lies in the western part of the Ayeyarwady Delta. The topography of the study area generally slopes gently downward from northwest to southeast, and is particularly low lying and flat especially around Darka Chaung and Ahtaung Chaung. The map index of the study area is 85 O/3 of one inch topographic map. It is the most highly populated town in Kyonpyaw Township, Pathein District, Ayeyarwady Region. Darka Chaung is flowing through Myawaddy Ward from the north and Panglong Ward to the south. It is essential for transported services to other places (Figure. 1).

---

<sup>1</sup> Associate Professor, Department of Geology, Pathein University

<sup>2</sup> MSc, Department of Geology, Hinthada University

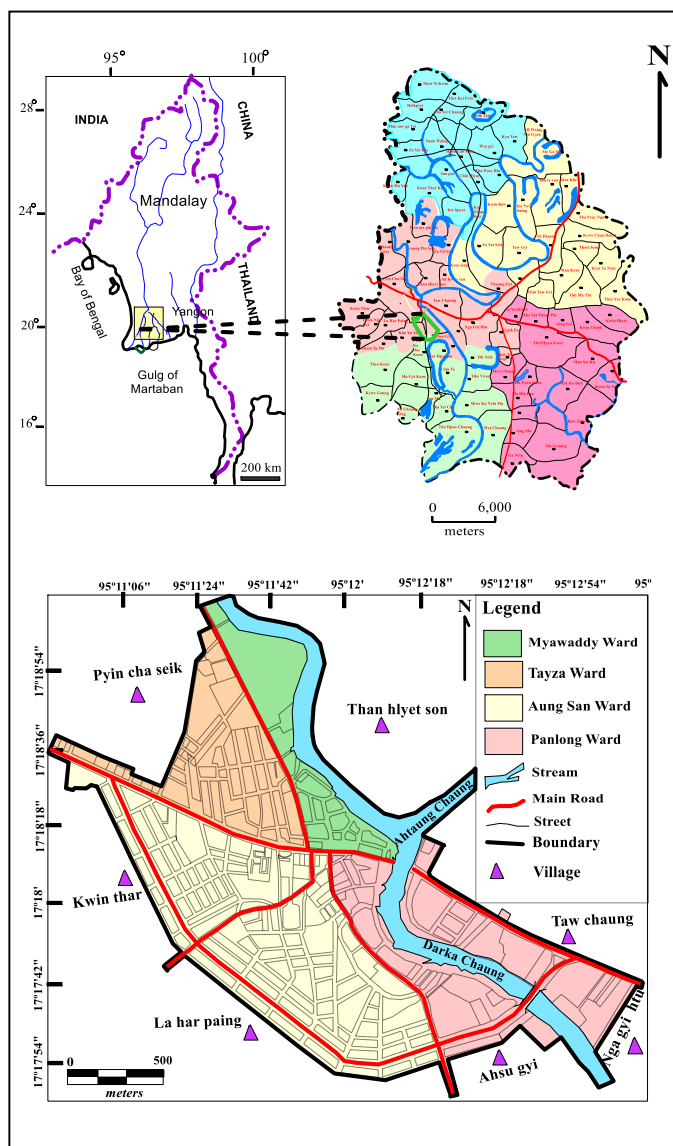


Figure 1 Location map of the study area

### Materials and Methods

Soil samples were collected by random collection method in December 2013 and in January 2014 in the Kyonpyaw. These samples were collected with an improvised with hand auger to a depth of 0.3 - 0.6 meter. Seven samples were randomly taken from different spots and homogenized. The all samples were analyzed for total concentrations of Arsenic, Copper, Lead, Zinc, Potassium, Manganese, Sodium, Calcium, Magnesium and Cadmium by Absorption Spectrometry (AAS) in the Geochemistry Laboratory, Applied Geology Department, Yangon.

Four surface water samples were collected from the Darka Chaung and depth value was tested by HONDEX PS-7-LCD SOUNDER. Water samples of well information were obtained from Water Resources Utilization Department (WRUD, 2013), Pathein. Seven groundwater samples were collected from Tayza, Aung San and Than Hlyet Sun village. Physio-chemical analyses of groundwater samples were made at the Soil Examination Laboratory of Department of Fisheries, Ministry of Livestock and Laboratory, Thaketa Township, Yangon. Multiparameters (Multi probe), Single Probe, Hand-Held Refractometer, HONDEX Ps-7- LCD DIGITAL SOUNDER and water sampler devices were well examined for surface and groundwater quality with help of Resource and Environment Myanmar Ltd. Yangon.

### Regional Geology

Kyonpyaw Town is situated at the southern part of Central Lowland and southwestern part of Myanmar. It is situated at the southernmost part of the Bago Yoma. That is mainly covered by the Tertiary and Quaternary Rock sequences. Precambrian meta-sediments and crystalline rocks from the western part of Sino-Burma Ranges are bounded to the East. At that part, Mesozoic to Cenozoic intrusive and extrusive rocks is associated with the Shan Boundary Fault. To the west, Eocene Flysch sediments of Indoburman Ranges are also exposed, respectively. In the northwestern part of the area, west of Hinthada, the Indoburman Flysch type sediments are covered associated with the small serpentinite bodies. This Flysch belt runs southward to the CoCo and Andaman Islands. Their regional geology and evidence of Eocene fauna indicate that the Flysch of this part is regarded as Eocene age (Dr Win Swe, 2012). Eastern foothills of the Western Ranges, are exposed with the North South trending features. Next Miocene Molasses facies, correlative with the Upper Pegu Group of Minbu Basin, are also exposed from the northern part of this region to the south. At the eastern side of these Miocene belts, fluvial sands, gravels and shales of late-Miocene-Pliocene age are exposed in a narrow belt that is a distinctive unit with the mammalian fauna and referred to as the Irrawaddy Formation. The whole part of the study area and its environs are mainly covered by the Quaternary Alluvial, (Figure 2) which is bordered on the south by the Gulf of Mataban. The geological successions of the Ayeyarwady Division are as shown in Table (1).

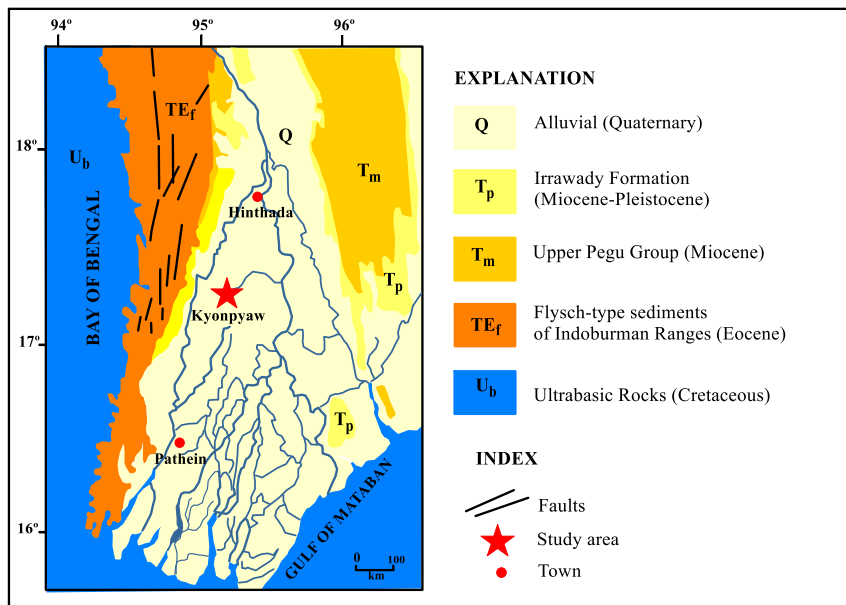


**Figure 2** Regional geological map of the study area and southern part of the Western Ranges (After Bender, 1983)

**Table (1) Geological succession of the Ayeyarwady Division**

| AGE                    | UNIT                                                                 |
|------------------------|----------------------------------------------------------------------|
| QUATERNARY             | Alluvial terrace and landslide deposits                              |
| UPPER MIOCENE-PLIOCENE | Irrawaddy Formation                                                  |
| MIOCENE                | Miocene strata (Upper Pegu Group)                                    |
| EOCENE                 | Eocene strata of molasses facies several formation of Western Ranges |
| EOCENE-CRETACEOUS      | Indoburman flysch of Western Ranges                                  |
| Igneous rock           |                                                                      |
| CRETACEOUS             | Dislocated Ultramafic rocks                                          |

### Results

#### Soil quality in Kyonpyaw Town

All of the soil samples were collected by random collection from different locations of the study area, (Figure 3).

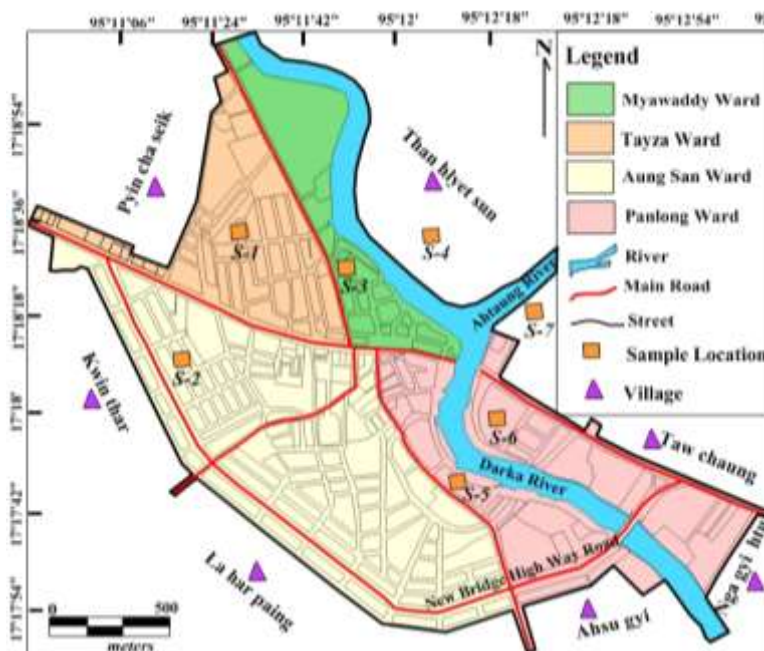


**Figure 3** Location of sampling sites for soil

Sample no.1 (S-1) soil was accounted in the east of Tayza Ward. This soil is occurred yellowish brown colored, medium-high plasticity, transportation soil. S-2 soil was accounted in the Nyaung Pin Thar Street (1), Aung San Ward. This soil is occurred yellowish-brown to bluish gray; clay portion is very high plasticity, silty clay and transportation soil. S-3 soil was accounted in the Ohwe tau street, Myawaddy Ward. This soil is occurred bluish gray colored, medium-high plasticity, transportation soil. S-4 soil was accounted in the Than Hlyet sun area. This soil is occurred yellowish brown, medium-high plasticity and transportation soil. S-5 was accounted in

the Pagoda Street, Panglong (1) Ward. This soil is occurred grayish colored, medium plasticity and transportation soil. S-6 was randomly accounted in the Kwittit Street, Panglong (4) Ward. This soil is occurred grayish colored, medium to high plasticity and transportation soil. Arsenic amount is not detected in this soil. S-7 was accounted in the Thirimingalar Street, Panlong (4) Ward near the Ahtaung Chaung. This soil is occurred reddish brown colored, medium plasticity and transportation soil.

**Comparison with WHO standard and soil quality of Kyonpyaw**

The seven soil results of the study area and comparison of the sample parameters with the World Health Origination (WHO) described in Table (2).

**Table 2 Comparative study for soil quality analysis of Kyonpyaw and WHO standard**

| Sample no | As | Cu * | Pb *  | Zn *  | Mn *  | Na * | K * | Ca * | Mg * | Cd *  | Cr *  | Fe * |
|-----------|----|------|-------|-------|-------|------|-----|------|------|-------|-------|------|
| WHO       |    | 20   | 10    | 50    | 50    | -    | -   | 200  | -    | 0.5   | 100   | 1000 |
| S-1       | ND | ND   | 0.004 | 0.015 | 0.009 | -    | -   | -    | -    | 0.08  | 0.018 | 5850 |
| S-2       | ND | ND   | 0.004 | 0.017 | 0.008 | -    | -   | -    | -    | 0.09  | 0.017 | 6100 |
| S-3       | ND | 95   | 115   | 75    | 17    | 20   | 25  | 15   | 18   | 0.007 | -     | -    |
| S-4       | ND | 105  | 130   | 80    | 18    | 18   | 30  | 20   | 15   | 0.006 | -     | -    |
| S-5       | ND | 100  | 120   | 85    | 20    | 30   | 25  | 18   | 19   | 0.005 | -     | -    |
| S-6       | ND | 95   | 115   | 80    | 21    | 25   | 22  | 20   | 20   | 0.006 | -     | -    |
| S-7       | ND | 105  | 120   | 75    | 19    | 20   | 18  | 23   | 18   | 0.07  | -     | -    |

(\*) = ppm, ND-not detected

According to the soil quality analysis, the levels of Copper, Lead and Zinc are higher than WHO standard in Myawaddy Ward, Panlong (1) Ward, Panglong (2) Ward, Than Hlyet Sun Area and Taw Chaung village. S-1 in Tayza Ward and S-2 in Aung San Ward are higher level of Iron than WHO standard.

**Water quality in Kyonpyaw Town**

In the Darka Chaung, four surface water samples are collected by water sampler and depth value was tested by HONDEX PS-7-LCD SOUNDER. Depend on the measurement of the depth, the maximum depth value is 5.5 m in the Darka Chaung and minimum depth value is 2.3 m in the Ahtaung Chaung. Table 3 described the surface water sample location and its characteristics.

**Table 3 Surface water sample locations and its characteristics SW-surface water**

| No. | Sample no. | Location                           | Time/Date           | Sources | Uses                                                                                            |
|-----|------------|------------------------------------|---------------------|---------|-------------------------------------------------------------------------------------------------|
| 1.  | SW-1       | N17° 18' 25.4":<br>E 95° 11' 50.8" | 1:00PM/<br>6.12.13  | River   | Drinking,<br>Irrigation,<br>Industrial,<br>Agricultural,<br>Domestics and<br>other<br>purposes. |
| 2.  | SW-2       | N17° 18' 10.6":<br>E 95° 12' 13.0" | 1:35PM/<br>16.12.13 | River   |                                                                                                 |
| 3.  | SW-3       | N17° 17' 49.5":<br>E 95° 12' 2.2"  | 2:05PM/<br>16.12.13 | River   |                                                                                                 |
| 4.  | SW-4       | N17° 17' 41.4":<br>E 95° 12' 23.2" | 1:55PM/<br>16.12.13 | River   |                                                                                                 |

Groundwater samples of GWKP-1 was collected at the Tayza Ward of Bogyok Street, GWKP-2 was collected at the Pauktauk Shweywar Street. GWKP-3 was collected at the Nyaungpinthar Street, Aung San Ward. In the Panglong (4) Ward, GWKP-4 was collected from Kaya Street, GWKP-4B was from the Saik Kyaik Thit Street, GWKP-6 was from the Kaya street, GWKP-5 was collected from the Than Hlyet Son village. Physio-chemical analyses of all surface water and groundwater samples were made at the Soil Examination Laboratory of Department of Fisheries, Ministry of Livestock and Laboratory, Thaketa Township, Yangon. Location of groundwater collected areas is shown in (Figure 4).

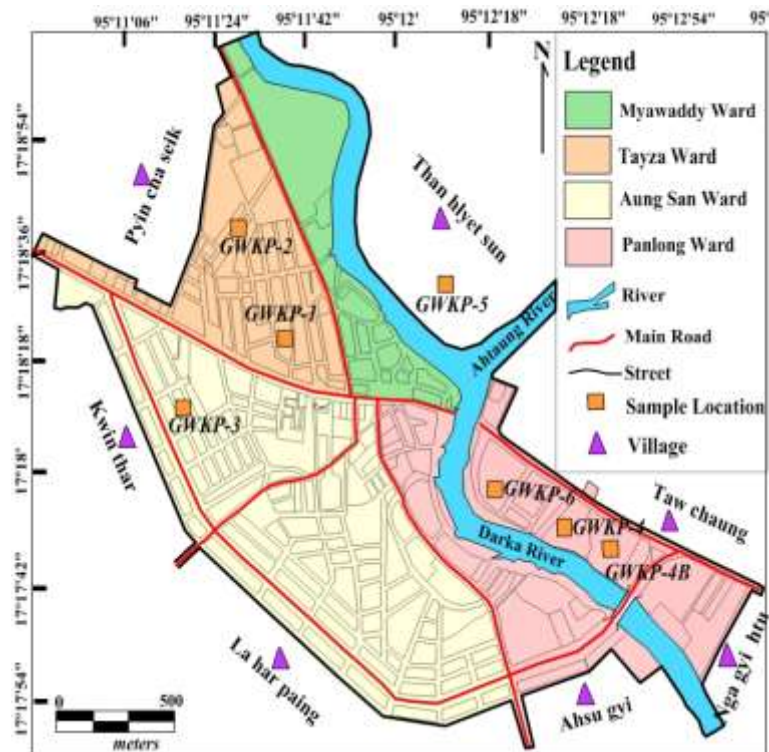


**Figure 4** Location of groundwater collected areas in Kyonpyaw Town

In the study area, high temperature rate was occurred in the SW-1 and GWKP-5, low temperature rate in SW-2 and GWKP-3. Some results of the water samples were considerably appearance as turbidities. pH value is higher than permissible limit in SW-4 and GWKP-1, 2, 3, and less than in SW-1. Electrical Conductivity (EC) was tested by the Multiparameters. SW-2 showed maximum EC value and SW-3 showed minimum value. TDS value of all surface water showed not more than 99 ppm. TDS and TH of the groundwater are not more than 300 ppm. High quality of ORP value found in SW-3 and low quality in SW-1. Surface and groundwater of DO both are not more than 7 ppm. High level of Calcium hardness found in SW-1. Distribution of Calcium hardness is shown in Figure 5a and 5b. Sulphate and Chloride value of both water sources within permissible limit.

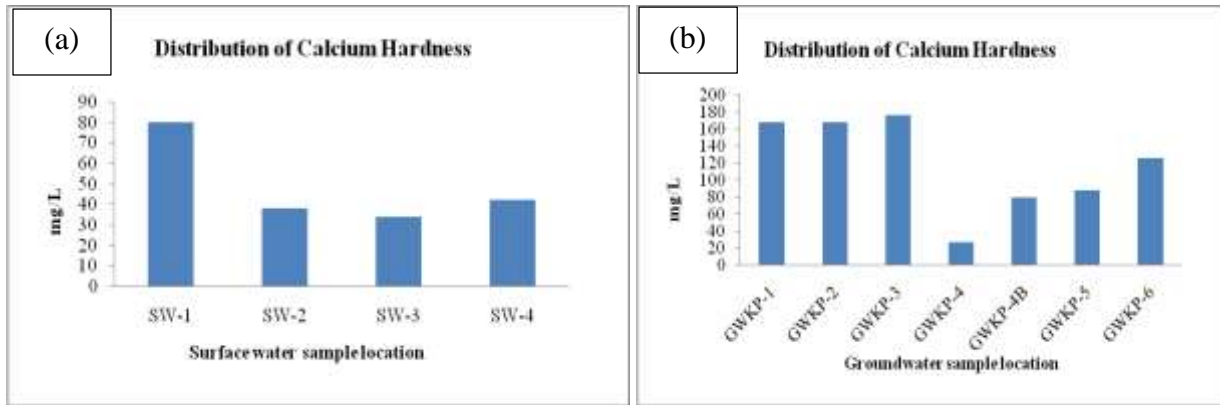


**Figure 5** (a) and (b) Distribution of Calcium hardness in surface and groundwater

### Arsenic concentration in Kyonpyaw and its Environs

Depend on the arsenic concentration measurement, Panlong 4 ward area in arsenic level is higher than WHO standard.

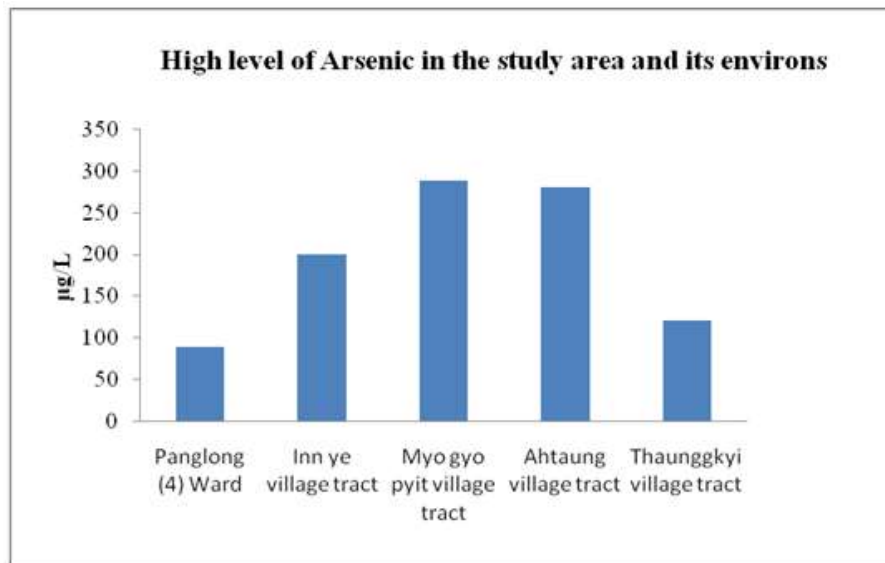


**Figure 6** Arsenic concentration in Kyonpyaw and its environs

### Discussion and Conclusion

In the study area, Darka Chaung is flowing through Myawaddy Ward from the north and Panglong Ward to the south. The study area extends about 7.2 km from north to south and 2.72 km from east to west. The whole part of the study area and its environs are mainly covered by the Quaternary Alluvial. Depend upon the soil quality analysis showed levels of Copper, Lead and Zinc are higher than WHO standard in Myawaddy Ward, Panlong (1) Ward, Panlong (2) Ward, Than Hlyet Sun Area and Taw Chaung village. The higher level of Iron, found more than WHO standard, in S-1 and S-2. The result of water quality, GWKP-1 to GWKP-6 and SW-1 to SW-4 of temperature are more higher limit than WHO standard. Calcium contents of GWKP-1 to GWKP-3, GWKP-4B, GWKP-5 and GWKP-6 are higher than WHO standard. Iron contents of GWKP-4 and GWKP-4B are higher limit than WHO standard. By analyzed with Digital Arsenator, Panglong (4) Quarter is more arsenic level than WHO standards.

Depend on the literature surveyed, Copper can also enter in the environment through waste dumps, domestic waste water, combustion of fossil fuels and wastes, wood production, phosphate fertilizer production. Copper is often found near mines, industrial settings, landfills and waste disposal. Zinc comes from human activities and Leads comes from industrial wastewater. Copper, Lead and Zinc compounds form the largest treat to human health.

According to field surveyed, waste disposal sites of Kyonpyaw, are located in Aung San Ward and Myawaddy Ward. It is suggested to consider selected proper disposal sites in the town and using proper waste disposal system. Also need and control of soil pollution.

The following steps have been suggested to control soil pollution.

- (a) Reducing chemical fertilizer and pesticide use.
- (b) Reusing of materials
- (c) Recycling and recovery of materials
- (d) Reforesting
- (e) Solid waste treatment
- (f) Storage of hazardous waste

The present research to reveals the relationship between geology, soil quality and water quality as well.

Municipal water supply system of Kyonpyaw Town is located only in Myawaddy Ward. All wards depend largely on dug wells, tube wells, hand-dug wells and some depends on lakes. The underlying water bearing layer is limited in amount in Aung San Ward and some parts of Tayza Ward. So, this town needs to supply of water from government and careful using our private wells.

Kyonpyaw Town is located in alluvial plain of Ayeyarwady Delta and as Laymyethnar Township, the Kyaungkong Township, the Hinthada Township has a record of high Arsenic level. Arsenic usually contaminates especially at the old Ayeyarwady River channel deposit. Most studies indicated that Arsenic is free at the well depth of 250 feet. If there is the case, one should consider to extraction the groundwater from deep tube well, rather than from the shallow ones.

### **Acknowledgements**

The author is grateful to Professor Dr Si Si Hla Bu, Rector, Pathein University, for her valuable advices and kind permission in preparation this work. The author would like to express the most heartfelt gratitude to Dr Than Htun, Pro-Rector of Pathein University for his valuable suggestions. The author also would like to express her sincere thanks to Professor Dr Thet Naing, Head of Department of Geology, Pathein University for his encouragement to present this paper. The author is thankful to Resource & Environment Myanmar Co., Ltd. (REM), Bahan Township, Yangon, for providing me the necessary instruments and information to complete this research. And special thanks to Ma Saw Zar Chi, MSc student, Hinthada University, for support me the necessary things for this research.

## References

- Aleinmar Htwe, (2002). **Environmental Potential Map of Yangon Area**. Unpublished M.Sc. Thesis, Department of Geology, Yangon Technological University.
- Fletcher, G. Driscoll., (1986). **Groundwater and Wells**, Johnson Division, St.Paul, Minnesota, 1089 pp.
- Maung Maung, (1996). **Urban Geology of Western Yangon area**. Unpublished M.Sc. Thesis, Department of Geology, University of Yangon.
- Maung Thin, Dr., (1996). Note on the Environmental geology of Yangon new urban extension area. Unpublished Country Paper, ESCAP, Bangkok.
- Tin Htay Mu, (2005). **Analysis of Potentials for Degradation of Groundwater Quality at the Confluence of the Hlaing and Pan Hlaing Rivers**. Unpublished PhD Thesis, Department of Engineering Geology, Yangon Technological University.
- Tin Maung Nyunt, (1994). **Urban water supply and sanitation in Myanmar**. Unpublished Research Paper, Department of Applied Geology.
- Tuinhof A., C. Dumars, S. Foster, K. Kemper, H. Gardunio, and M. Nanni, Sustainable Groundwater Management Concepts and Tools, Briefing Note1, World Bank, [www.worldbank.org/gwmate](http://www.worldbank.org/gwmate)
- Water Resources Utilization Department, (2007). **Chemical analysis data of water samples from Yangon area**.
- Water Resources Utilization Department, (1992). **Tube well inventory of Yangon area**.
- William and Mary Ann Cunningham, (2002). **Principles of Environmental Science Inquiry and Applications. International Edition**, Mc Graw Hill Inc., University of Minnesota, 418p.
- Win Naing, (2009). **Evaluation of Irrawaddy Aquifer in Yangon Area**, Unpublished PhD Thesis, Department of Geology, University of Yangon.
- Weight T.R., and Nebel J.B., (2002). **Environmental Science toward a Sustainable Future 2th Edition, USA**. 415p.
- Win Naing, (1972). **The Hydrogeology of Greater Rangoon Area**. Unpublished M.Sc Thesis, Department of Geology, Rangoon University.
- Win Naing, (1996). **Urban Geology of Eastern Yangon area**. Unpublished, M.Sc Thesis, Department of Geology, Yangon University
- Xavier Coello R. and S. Remigio Galarraga, (2007). **Groundwater vulnerability assessment**, Ecuador, [www.oas.org/usde/publication](http://www.oas.org/usde/publication).
- Ministry of Agriculture and Irrigation, (2005). **The Inter-Ministry Task Force on Water Resources**.
- Tokyo Engineering Consultants Co.LTD. and NJS Consultants Co.LTD., (2001). **The study on improvement of water supply system in Yangon City in the Union of Myanmar**, JICA Interim Report.

## **MINERAL OCCURRENCES AND DEPOSITS ALONG MUSE-MANDALAY PROPOSED RAILWAY LINE**

Tin Aung Myint<sup>1</sup> & Mi Mi Ko<sup>2</sup>

### **Abstract**

Myanmar, the second largest country in Southeast Asia, occupies geologically and tectonically a key position. A railway line connecting from Muse and Mandalay has been proposed to construct and the paper is written about all known deposits and occurrences typically exposed along and around the proposed Muse-Mandalay railway line. There would be lead-zinc-silver, antimony, gold that could be expected in it. Coal and phosphorous deposits might also be found as well. As mineral deposits are trending approximately N-S direction, those could be probably found during construction of the line crossing that trend. It should be needed to officially inform local and central government if some deposits occur during construction. Legal enforcement should act to give penalty for those people who carry away it from the line or make mineral dressing in situ.

**Keywords:** Muse-Mandalay railway line, mineral deposits and occurrences,

### **Introduction**

Myanmar, the second largest country in Southeast Asia, occupies geologically and tectonically a key position located in the northeast corner of the Indian Ocean. Tectonically Myanmar has collided with the Indian continent in the Naga Hills and is juxtaposed with the eastern end of the India-Asia collision zone and Himalayas to the east. It is found that Myanmar has a several number of world-class metallic mineral deposits, including copper, nickel, tin and tungsten, offshore and onshore reserves of oil and gas, and an abundance of gemstones especially ruby, sapphire and jade, etc. The paper is written about the mineral occurrences and deposits along Muse-Mandalay Railway Project.

For several decades, China has also been planning to build the China-Myanmar Economic Corridor (CMEC) to have access to the Indian Ocean. Consequently, a railway line connecting from Muse and Mandalay has been proposed. So, Muse is a significant and key border town in Myanmar on the China-Myanmar border. The proposed project is also a part of eastern corridor extension of the railway projects (Fig. 2) being undertaken in Yunnan Province of China, especially the construction of the Darui railway (short for Dali-Ruili railway) (Source: News from CGTN).

---

<sup>1</sup> Professor, Department of Geology, University of Mandalay

<sup>2</sup> Associate Professor, Department of Geology, Yadanabon University



(Source: Internet)

**Figure 1** Economic corridors in Greater Mekong Sub-region.

### Method of Study

Detailed geological study of the area, classification of rock units and the ore occurrences and deposits were carried out during the course of field study. Detailed geological data on dip and strike of the lithologic units, attitude of joints and other structural elements were measured and recorded. Tape-and-compass method and bore hole data are employed to determine the thickness of iron ore deposits, the nature of deposit types and the exposed rock units in the study area. The representative ore and rock samples were taken from each bore-hole and test-pit. The collected samples were analyzed by using PXRF. Photographs and sketches were taken for some significant features.

### Result

#### Mineral deposits along and around the Muse-Mandalay Railway line

#### Lead-Zinc-Silver Deposits

#### *Mohochang Prospect (Latitude 23° 25' N, Longitude 97° 30' E)*

The Mohochang mine (Figs.1&2) is located 25 miles northeast of Bawdwin/ Namtu and the old workings are centered around Mohochaung. At present there are no existing roads to the area but during the dry season the present trails can be converted into mule tracks (Soe Win, 2016). The Mohochang mines are in an area of rugged terrain, the Mohochang Peak reaching an elevation of 6439 feet can be viewed from Namtu. It is far from railway line.

The Chaung Magyi Group is of great importance in the Mohochang area in that it contains horizons in which the main lead-zinc mineralization occurs. They comprise the oldest rocks in the area. The white sandstone occurs along the contact of the Chaung Magyi rocks with the overlying Pangyun Formation. Pb-Zn mineralization is confined to this horizon (having an average of 43% Pb). The Tawnpeng granite (a biotite granite) lies along the northwest margin of the area and it intrudes the Chaung Magyi rocks. The main faults strikes N-S, NNW-SSE and E-W.

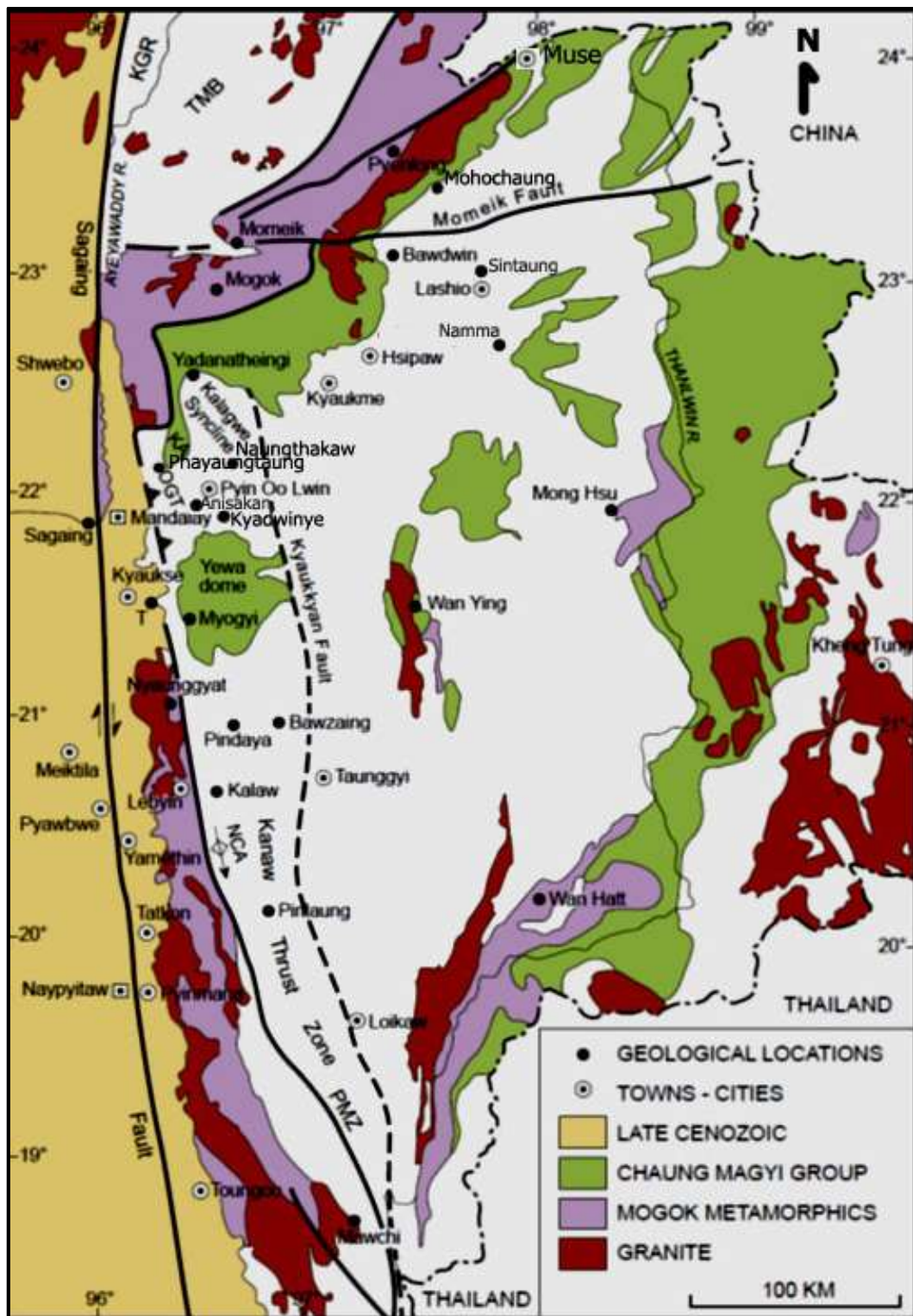


**Figure 2** Map of part of Shan Plateau showing mineral and gemstone locations described in text. (Modified from Mitchell, 2018)



and flow of solutions. Deposition took place along fractures in the magnesian limestone. It is 50 feet thick near the village of Kong Namlek and its general strike is NE-SW with a 25-35 degrees dip to NW.

***Bawdwin Mine (23° 6'23.57"N & 97°17'52.62"E)***

The Bawdwin mine (Figs.1&2) in Myanmar has been one of the world ranking lead mine before the World War II. This mine is situated about 8 miles west of Namtu and 60 miles from the border with the peoples' Republic of China. This mine is also far from railway line. According to the historical records, the Chinese first extracted silver from this area in 1912. Bawdwin stands at an elevation of more than 3000 feet above sea level. The terrain is rugged and devoid of vegetation, thought to be result of deforestation of crude smelting operations by the early Chinese artisanal mining. The main drainage is the Nam Panyun river that flows through the mine camp.

The oldest rocks belong to the Chaung Magyi Group of Pre-Cambrian age comprising slate, phyllites, greywackes and schists exposed to the west of the Bawdwin mine and Panyun Formation of Cambrian age overlying unconformably on the Chaung Magyi Group form the main host to mineralization.

The Tawnpeng granite occupies an extensive area especially west and northwest of Bawdwin and intrusive into the Chaung Magyi metasediments. The Loi Mi quartz porphyry occurs as a small stock and as sills and irregular masses along the Bawdwin ore zone. The Bawdwin lead zinc silver ore deposit consists of three sulphide high grade Pb-Zn ore and small pyrite-chalcopyrite ore body. The mineralization is approximately 2.5km in length and about 140 m wide within fault zone. At Bawdwin three main lodes are known. The Shan Lode in the north, the Chinaman the central lode and Meingtha in the south.

**Table 1 Three main lode exposed in Bawdwin mine.**

| <b>Name</b>   | <b>Max. Length</b> | <b>Max. Vert Dimension</b> | <b>Avg. Width</b> |
|---------------|--------------------|----------------------------|-------------------|
| Shan Lode     | 380m               | 350m                       | 6m                |
| Chinaman Lode | 400m               | 350m                       | 42m               |
| Meingtha Lode | 550m               | 450m                       | 6m                |

The ore reserve given by the Bawdwin in 1982-83 is 142877 tons (with 7.73%Pb, 3.45%Zn and 4.8602Ag) by underground mining, 105402 tons (with 5.98%Pb, 0.99%Zn) by open-cast mining.

***Yadanatheingi Mine (22°34'35.26"N, 96°29'43.54"E)***

The Pb ores of Yadanatheingi is located about 50 miles NE of Pyinoolwin (Figs. 1 & 2). Yadanatheingi is in the northeastern limb of the regional southeast-plunging Kalagway Syncline some 100km southwest of and along strike from the Bawdwin mine. A high Ag content of the ores is a noteworthy feature of this mine. It is mined from a shear zone about 30 feet thick which cuts across the Chaung Magyi Group in an NW-SE direction. Some similarity between the geological setting of Yadanatheingi and that of Bawdwin is suggested by the presence at Yadaatheingi of mineralized structures extending from the Chaung Magyi into quartzites of the Cambrian Panyun Formation (Mitchell, 2018).

The ore is found as fissure veins and stockworks and the Pb content is about 5-10%. In 1974-75, the mine produced 1600 tons of lead concentrate containing 50% Pb and 1% Zn (Bender,

1983). In 1986-87, 1322 tons of lead concentrate was produced. After privatization the Yadantheingi mine (about 1207000 tons of Pb) is operated by the Lin Pyae Mining Co., which is extracting the remnants from old deposits. Apparently no efforts have been made to search for ore extensions laterally or at depth.

## **Barite Deposits**

### ***Anisakan Barite deposits***

The barite deposits in the vicinity of Anisakan area (Figs. 1 & 2) are located at Peinnegon, Taunggyun, Indon-ye, Sitha, Dattaw, Bayaw and Byingyi. Barite occurs along fissures and fractures trending NNW-SSE to nearly N-S, in the Ordovician limestones and siltstones. The veins dipping steeply 50 to 90 degrees and their thickness vary from a few feet to more than 20 feet. The proved reserve amounts to about 213,000 tons with 97% barite, and the probable reserve amounts over 400,000 tons.

## **Iron Ore Deposits**

### ***Kyadwinye (21°53'39.64"N, 96°30'58.67"E)***

It is located on the eastern limb of a major anticline (Kyaingtaung anticline) (Fig. 3) whose anticlinal crest is located about six miles to the west. Iron ore occurs entirely in Maymyo Formation of Devonian age. Kyadwinye deposits contain high iron content (50%-60% Fe).

Moreover, numerous small scale iron occurrences which are economically unfeasible are found throughout the area. In Kyadwinye mine, (Figs. 1&2) the iron deposit occurs on the Main hill (Foot wall) (3498') and mine site in lower hill (Hanging Wall) separated by Kyadwinye normal fault. The area coverage is about 6725640 square feet (624811.9 sq.m.). The thickness of iron deposit on the Main hill is only 12.8' (4m) thick. However, at the mine, the iron ore deposit is much thicker, reaching up to 70' (22m) in thickness. The deposit is sedimentary in origin and the hematite and limonite ores occur in the cavities and depressions of the underlying. Plateau Limestone (Maymyo Dolomite). Field investigation shows that the mine is situated on the down thrown side of the fault (Tin Aung Myint, 2002).

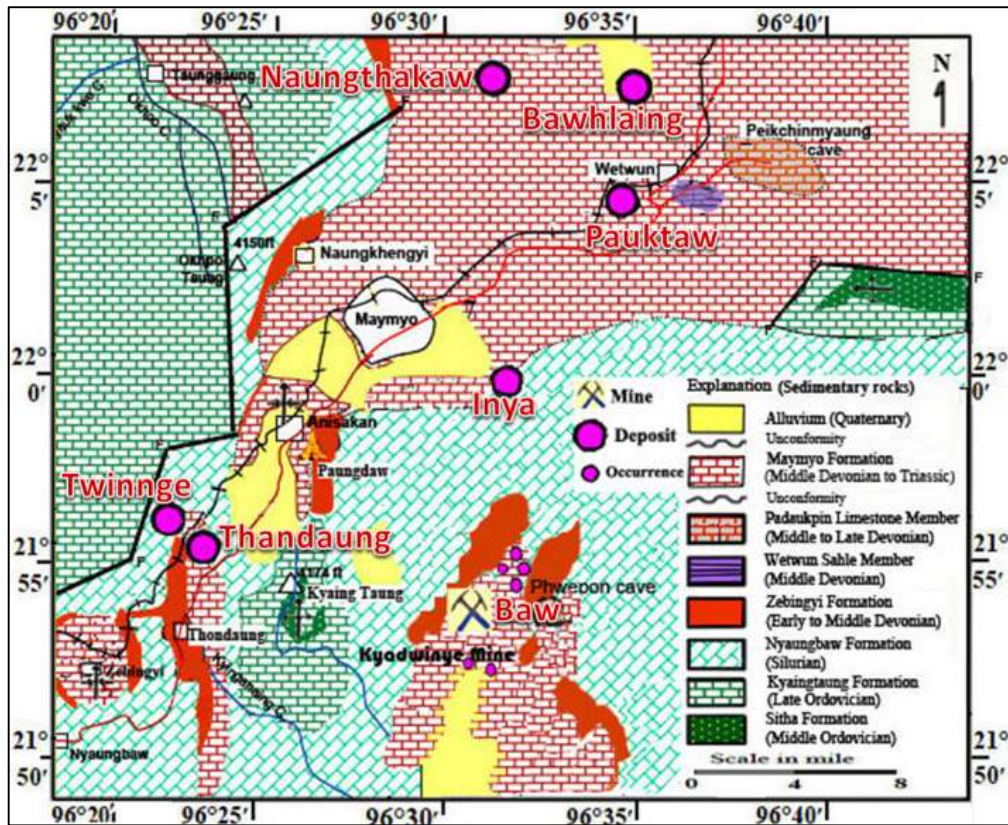


**Figure 3** Geology map of Pyinoolwin area including iron localities. (Tin Aung Myint, 2014)

In Kyadwinye, the iron ore deposit comprises limonite and hematite with minor amount of pyrite and magnetite found in dolomite and sandstone of Maymyo Formation. The bore-hole data indicates gradual increase of limonite content with depth. The surface of the ground shows scattered light brown ferruginous gravel and larger pieces of iron ores. Iron ore occurs in different forms: as boulders, nodular masses, gravels or floats. The biggest one is reaching up to 15 cubic meters (530cubic feet). The ore is trucked to the No.1 Iron and Steel Plant at Aniskan located about 16 km west of Pyinoolwin. The plant produces pig iron, steel billet, rounded bars and steel grinding balls (Soe Win, 1994). Although Krupp and BGD (1961-62) gave a reserve of 3 million tons, the estimated iron ore reserve is less than 2 million tons with average iron content of 58.5% (Tin Aung Myint & Mi Mi Ko, 2004).

**Inya (22° 0'57.77"N, 96°32'53.19"E):**

It is located 9 km SE of Pyin Oo Lwin (Fig.3). Brecciated limonitic ore occurs in dolomitic limestones. 4.5 million tons with an average Fe content of 35.2 %, Ti O<sub>2</sub> content of 1.5 %. The deposit although favorable for open cast mining, the ore is difficult to dress (intergrowth of hematite ore / laterite / bauxite). The Fe content is generally low and high TiO<sub>2</sub> content renders the ore difficult to smelt.

**Pauktaw (22° 4'46.78"N, 96°35'13.07"E):**

It lies close to the Mandalay- Lashio railway old line, 4 miles SW of Wetwin railway station (Fig.3). It is a small excavation worked in 1920 and 1921 by the Burma Corporation. 1,700 tons of ore, with an average iron content of 56- 57 %, have been removed from this working. The analysis of pisolitic materials contains 25.2 % Fe, 19.0 % Al<sub>2</sub> O<sub>3</sub>, 6.2 % MgO, and 10 % Si O<sub>2</sub> (Soe Win, 1994).

***Naungthakaw (22°8'47.03"N, 96°31'45.46"E):***

It lies about 6 miles to the NW of Pauktaw (Figs. 1, 2 & 3). Workable hematite ore vary from thin bands of few inches to thick ones of several feet thick. The deposit is covering the area of about 8 sq. miles. It is of residual type in Plateau Limestone. The iron content is 56 % Fe. This was mined by the Burma Corporation Ltd, in pre-war years with an annual production between 35,000 and 40,000 tons. The deposit is very close to the proposed railway line (Tin Aung Myint et al., 2019a).

**Gold Deposit*****Phayaung Taung Gold Mine (22° 7'39.79"N, 96°16'36.97"E)***

It is situated about 32 km northeast of Mandalay (Figs. 1 & 2). It is located at the junction of Slate Belt, eastern part of Mogok Metamorphic Belt and Shan Plateau bounded by two dextral strike-slip faults, namely the Sagaing fault (W) and the Shan scarp fault (E). The stratigraphic units exposed in the area are Chaung Magyi Group (CMG). Mineralization is commonly formed in quartzite (aks Maukkaw Quartzite) and mica schists. Phayaung Taung fault plays an important role to form large concentration of fluid flows. The Phayaung Taung gold mineralization is characterized by the gold bearing quartz with variable comb and ribbon textures. Ore mineral assemblage includes gold, chalcopyrite, pyrite, hematite, malachite and azurite. The Kin sandy phyllite of CMG, mica schists, garnet-staurolite schist of MMB at Baw Taung area and Maukkaw quartzite of the CMG are potential hosts for gold mineralization (Tin Aung Myint et al., 2019b). It has done already 12 drill holes and the estimated reserve is about 3.23Mt @ 4.78 g t<sup>-1</sup> Au. Now the mine is operated by Htawaya mining company (DGSE, 2013).

**Coal Occurrences**

The occurrences of coal measure along the railway line is mainly Tertiary coal-bearing layers occurred in Muse (?) and Lashio Basin (Figs. 1 & 2). Here, it is mainly emphasized on the coal occurrences around Lashio. Sintaung (23° 0'16.45"N, 97°45'9.18"E) near Lashio is very close to the line. It is an open pit mining of approximately 120m (L) x 72 m (W), with the thickness of 0.5-7m dipping 20°N. Other occurrences are found at Namma (22°39'14.71"N, 97°45'27.61"E) which is an old open coal mines and there are also some underground mines to the E of area. It has about 1600m (L) x 100m (W) with the thickness of 3-15m (including 3 layers), dipping 30°-60° NW. Since it is found as layers in Tertiary sediments, the age could be Late Miocene-Pliocene.

**Conclusion and Suggestion**

All known deposits and occurrences mentioned here are typically exposed along and around the proposed Muse-Mandalay railway line. But some exposed the line between Nanhphka-Muse are missing because of insurgent area and difficulty to do field works. Consequently there is also missing some geological information for that area. According to the existing geological records and possible structural trends, there would be lead-zinc-silver, antimony, gold that could be expected in it. Coal and phosphorous deposits might also be found as well. Some deposits are a little far from the proposed railway line. Why mentioned here is that mineral deposits are trending approximately N-S direction and those could be probably found during construction of the line such as tunneling, bridge, station and railway line etc.. For example, although Phayaung taung gold is far from the construction, gold occurrences are sporadically found along the western margin of Shan scarp, trending N-S direction. For Yadanatheingi lead-zinc-silver deposit, similar deposits and occurrences could be estimated in Pyin Oo Lwin, Naungcho and Kyaume as regional structural trending passing in these areas. Similarly, deposits at Bawdwin mine and Mohochaung mine, they

might also be extended more or less into Hsipaw, Lasho, Kutkai and Nam Hpatkar areas. For those reason, those deposits are plotted on the map as well.

Suggestion here is that if some precious mineral deposits or occurrences found along the line, it is needed to officially inform the authorized person from government and local community as well. Those communities should do monitoring work and help the construction railway project for mutual benefit. Legal enforcement should act to give penalty for those people who carry away it from the line or make mineral dressing in situ.

### Acknowledgements

We acknowledge Rector and Director General Dr Thein Win, Pro-rectors Dr Kathy Tin, Dr Mi Mi Gyi and Professor Dr Than Than Nu, Head of Geology Department, University of Mandalay for their encouragement and permission to accept this paper. Special thanks are extended to all members of the journal of the Myanmar Academy of Arts and Sciences for allowing us to publish the paper in journal. Thanks are also due to responsible personnel from government offices and villagers in the area for their hospitality and willing help during field trip.

### References

- Bender, F., (1983). *Geology of Burma*. Gebrudre Borntraegon., Berlin, 292 p.
- DGSE (2013). The Database on Mineral Occurrences of Myanmar. Unpublished Report for Department of Geological Survey and Mineral Exploration, Myanmar.
- Krupp & B.G.D., (1961-62). *Iron Ore Deposit at Kyadwinye*. Unpublished report.
- Mitchell, A.,H.,G., (2018) *Geological Belts, Plate Boundaries, and Mineral Deposits in Myanmar*, Elsevier, ISBN: 978-0-12-803382-1. 509p
- Soe Win, (1994). Iron Ore in Myanmar. Unpublished Report.
- Soe Win., (2016). Economic geology of the carbonate- hosted lead–zinc-deposits of the Loi Hsiang Trend, Nongcho Township, Northern Shan State. Ph.D. Thesis (Unpublished), Department of geology, Mandalay University. 145p.
- Tin Aung Myint, (2002). A Genetic Study on the Iron Ore Deposits at Kyadwinye Mine and Its Environs, Pyin-Oo-Lwin Township, Myanmar. Master of Research (Unpublished), Department of Geology, University of Mandalay.
- Tin Aung Myint, (2014) Combined geology map between Mandalay and Pyinn Oo Lwin area.
- Tin Aung Myint (2020) Overview on the Geology of the High Speed Railway Line between Mandalay and Lashio Section, *Mandalay University Research Journal*. Vol.11, No.5 2020.p-124-133.
- Tin Aung Myint, Hein Min Zaw & Than Than Nu (2019b) Comparative study on mineral prospect of Phayaung Taung and Baw Taung, Patheingyi Township, Mandalay Region, *Mandalay University Research Journal*. Vol. 10, No.5. p-249-259
- Tin Aung Myint & Mi Mi Ko, (2004). Occurrences of iron ores in Myanmar, research paper read at 4<sup>th</sup>. *Anniversary of Yandanabon University Opening*. Conference Hall, Yandanabon University, Mandalay City, Myanmar
- Tin Aung Myint & Mi Mi Ko (2020) Origin of iron ore deposits in Maymyo Formation exposed around Baw willage, Pyinoolwin Township, Mandalay Region, Myanmar. *Journal of the Myanmar Academy of Art and Sciences*, Vol. XVIII, No.5A, July, 2020. P-139-148.
- Tin Aung Myint, Mi Mi Ko & Khin Pyone (2019a) Types and origins of Iron Ore deposits and occurrence around Pyin Oo Lwin Mandalay Region, Myanmar, *1st, MISCC International Conference Proceedings*, p- 35-40.

## **PETROGRAPHY OF THE NYAUNG BIN THA AREA, WAINGMAW TOWNSHIP, KACHIN STATE**

Ni Ni Win<sup>1</sup>

### **Abstract**

The study area is situated in 27 Kilometers northeast of Myitkyina. The Nyaung Bin Tha area is built up of plutonic and volcanic units. The plutonic rocks exposed in the study area are peridotites, gabbro, granodiorite, and dolerite. The volcanic and volcanoclastic rocks include basalt, andesite, dacite, rhyolite and volcanic tuff. Almost all plutonic rocks are medium- to coarse-grained, and exhibit hypidiomorphic granular texture. Porphyritic textures, perthitic texture and myrmekitic textures are also recognized in these rocks. Ocellar texture is also observed in the samples taken from dolerite dyke. Plagioclase feldspar shows conspicuous zoning and twinning. Pyroxenes, in gabbro, occur as phenocrysts and display sector-zoned and each sector show oscillatory zoning. In basalt it shows resorbed and embayed texture, coroner or keleptic rim. Chloritization, seritization, epidotization and serpentization are common hydrothermal alteration occurred in the study area.

**Keywords:** Petrography, Hypidiomorphic granular, Porphyritic, Zoning and Twinning

### **Introduction**

The study area is situated in Waingmaw Township, Myitkyina District, Kachin State. It is located about 27 Kilometers northeast of Myitkyina. This area is bounded by north Latitude 25° 30' to 25° 35' 30" and East longitude 97° 30' to 97° 35'. This area falls in the UTM map sheet of 2597-10. It extends about 4.6 km long and 4.3 km wide. It covers approximately 20 square kilometer of fairly rugged terrain. It can be easily reached by car or motorcycle from Myitkyina. Location map of the study area is shown in figure (1).

### **Purposes of research work**

Previous workers researched regionally on geology, mineral occurrences, geochemistry and geochronology of the igneous rocks around Myitkyina area. There is no detail research on mineralogical, petrological and geochemical characteristics and geological map. So, the present research mainly focuses on petrography and geological map of the study area.

### **Methods of study**

The (50) representative rock samples were made by thin section. Detailed mineralogical characters, texture feature and other petrographical criteria of representative rock sample were systematically studied under petrographic microscope.

---

<sup>1</sup> Dr, Professor, Department of Geology, Kyaing Tong University

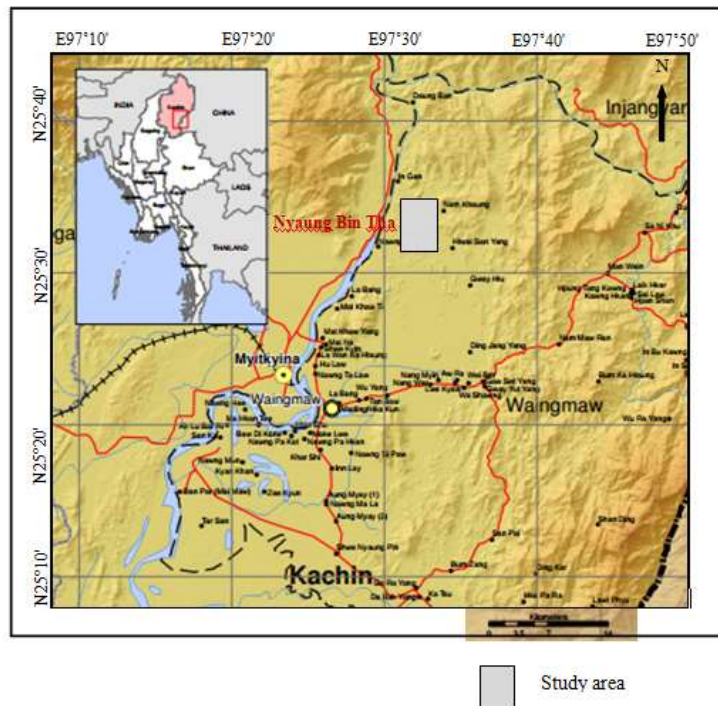


**Figure 1** Location map of the Nyaung Bin Tha area

### Geology of the study area

The present area lies between the Shan Plateau in the east and the Central Lowlands in the west. It is mountainous and rugged terrain and covered with fairly dense vegetation. The study area is mainly composed of igneous rocks including both plutonic and volcanic rocks. The plutonic rocks are peridotites, gabbro, granodiorite and dolerite. The volcanic rocks are basalt, andesite, dacite, rhyolite and volcanic tuff. Clegg (1941) regarded that peridotites, diorites and gabbro in the Katha and Myitkyina Districts associated with lava and tuffs as a result of Post Cretaceous to Early Eocene igneous activity. Using K/Ar dating method, UNDP project in which determination on hornblende from a pegmatite gabbro veins within a serpentine boulder at Ma-U Chaung area indicates  $158 \pm 20$  my which is Middle Jurassic (Mitchell *et.al*, 1979). The study area is a part of Tagaung-Myitkyina Belt of Upper Ayeyarwady Province. So the age of volcanic rocks such as dacite and rhyolite in the study area may be possibly Mesozoic to Tertiary (Mitchell *et al.*, 1978). Based on zircon U-Pb ages (ca. 173–171 Ma) are similar to ages previously reported for different lithologies (e.g., andesitic basalt, leucogabbro, and plagiogranite) of the Myitkyina ophiolite, i.e., 176–166 Ma (Yang *et al.*, 2012), and slightly older than the radiolaria age (i.e., Late Jurassic) of cherts at the confluence of the Mayhka and Malikha area was determined as Jurassic by Mg Mg (Maung *et al.*, 2014). Therefore, the Myitkyina ophiolite was formed during the Middle Jurassic (Liu *et al.*, 2016a). According to previous works and field observations, the rock sequences of the study area are shown in Table (1).

**Table 1 Rock sequences of the Nyaung Bin Tha area**

|                                          |   |               |                                         |
|------------------------------------------|---|---------------|-----------------------------------------|
| <b>Sedimentary Unit</b>                  |   |               |                                         |
| Alluvium                                 |   | Quaternary    |                                         |
| ^^^^^^^^^^^^^^^^^^^^^^^^^^^^^^^^^^^^^^^^ |   |               |                                         |
| <b>Igneous Unit</b>                      |   |               |                                         |
| Volcanic rocks                           | [ | Volcanic tuff | } Late Cretaceous<br>to<br>Early Eocene |
|                                          |   | Rhyolite      |                                         |
|                                          |   | Dacite        |                                         |
|                                          |   | Andesite      |                                         |
| Dyke rocks                               | [ | Basalt        | } Jurassic                              |
|                                          |   | Dolerite      |                                         |
| Plutonic rocks                           | [ | Granodiorite  | }                                       |
|                                          |   | Gabbro        |                                         |
|                                          |   | Peridotites   |                                         |

**Distribution of the Petrographic Units**

Peridotites are found in the eastern bank of the Ayeyarwady River. Gabbro can be observed in the northwestern part of the study area. Gabbro associated with volcanic tuff. Granodiorite can be found as a bold massive, predominant plutonic unit in the study area. Two-third of the study area is made up of granodiorite. Gold bearing quartz vein are found in granodiorite host rock. This unit can be found in the northern, eastern and southeastern part of the study area. Dolerite intruded as dyke into gabbro unit along the Nam Phu Hka Chaung sections. Dacite is the second most abundant unit in the study area and they are commonly exposed along the Pun Gre Hka Chaung. Basalt exposures are found along Nam Hkawng Hka Chaung section. Most of the basalt shows pillow structure piled one upon another and displays exfoliation. Xenoliths of granodiorite can be observed in the basalt body in the northern part of Nawng Mon village. So, basalt is younger than granodiorite. Rhyolite is well exposed in the northwestern part of the study area. Layerings of lava flow are common features of this rock unit. Good exposures are generally best seen at the stream section. The rest part of the study area is covered by alluvium. The geological map of the study area is shown in figure (2).

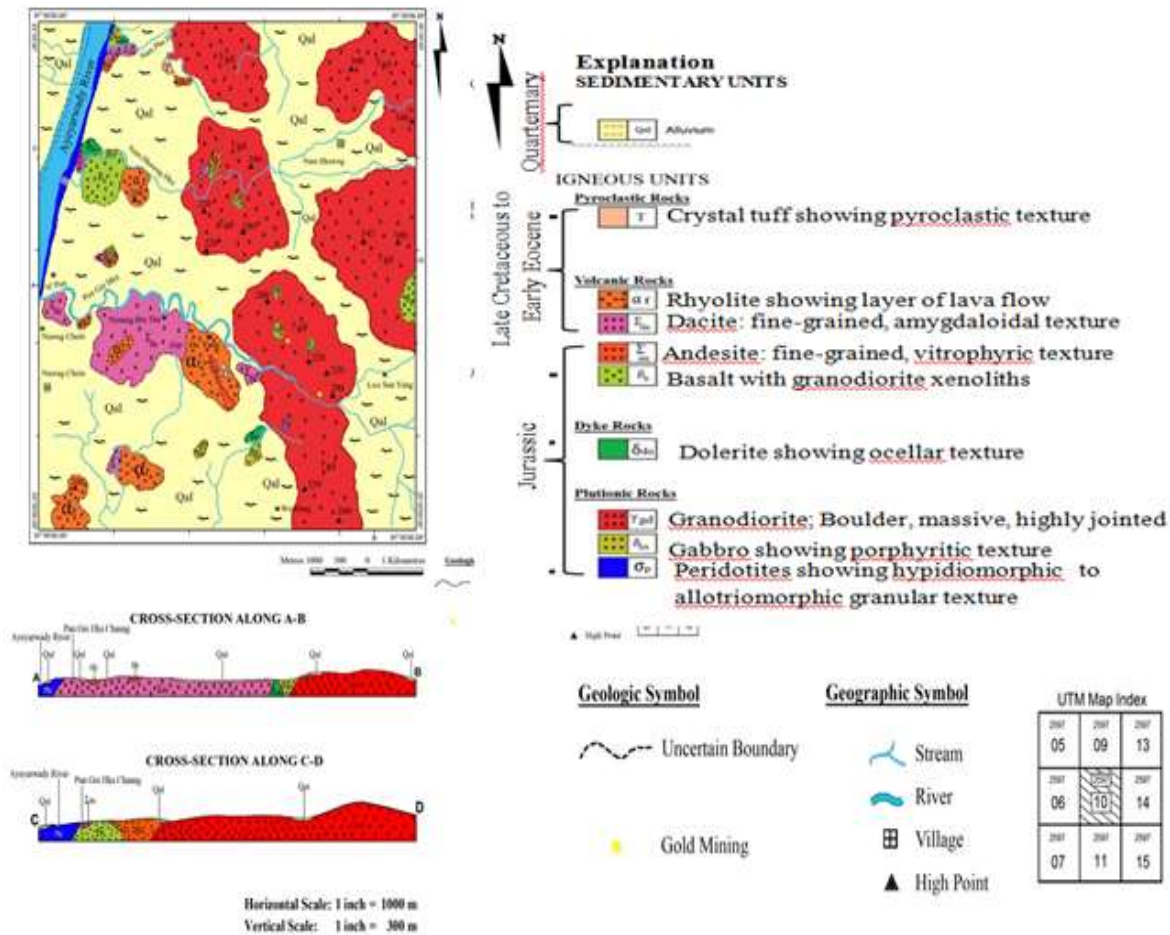


Figure 2 Geological map of the Nyaung Bin Tha area

## Petrography

### Plutonic Rocks

#### Peridotites

The rock is medium-grained, hypidiomorphic to allotriomorphic granular texture (Fig.3). The essential minerals are olivine (65%), orthopyroxene (11%) and clinopyroxene (9%) with minor amount of hornblende and biotite (10%). Chromite, iron ores and plagioclase (5%) are accessories minerals. Olivine is the chief constituent minerals in this rock. Olivine grains occur as granular form and average grain size is about 0.5 mm. It is also found as inclusion in enstatite. A few orthopyroxene occurs as subhedral to anhedral grains of more than 1mm in size. It shows lamella structure. Clinopyroxene occurs as grains and as short prismatic form. Chromite ore occurs as disseminated grains with varying sizes.

#### Gabbro

This rock is medium- to coarse- rocks with a hypidiomorphic granular texture. It essentially contains plagioclase (60%), pyroxene (25%), hornblende (10%) with minor amount of olivine (3%). Magnetite, apatite (2%) is present as accessories. Plagioclase occurs as subhedral to euhedral form and its size ranges from 1 mm to 3 mm. They commonly show polysynthetic twin, combination of Carlsbad and albite twin and display conspicuous zoning (Fig.4). Pyroxene occurs as large phenocryst shows sector-zoned and each sector displays oscillatory zoning (Fig.5). The

size ranges from 1 mm to 3 mm. Along the boundaries of some crystals, they are altered to chlorite. Hornblende occurs as subhedral to anhedral form and occasionally, typical hornblende cleavages are observed. Some hornblende is entirely enclosed in the plagioclase phenocryst. A few olivines interstitially replaces between plagioclase.

## **Granodiorite**

### **Hornblende-biotite granodiorite**

It is medium- to coarse-grained and shows hypidiomorphic granular texture. This rock is essentially composed of plagioclase (48%), orthoclase (20%), quartz (23%) with minor amount of hornblende and biotite (5%). Apatite, zircon and magnetite (2%) occur as accessories. Plagioclase is the most common mineral in this rock. The composition of plagioclase ranges (An<sub>11-17</sub>) albite to oligoclase. Plagioclase is mostly euhedral in form and coarser grain than others. Their grain size varies from 1.5 mm to 2 mm in length. Plagioclase is partly or completely altered to sericite or saussurite and some altered to epidote. Quartz and alkali feldspar are less abundant than plagioclase. Alkalifeldspar occurs as anhedral to subhedral grains and most of them are perthitic orthoclase. String perthite are also found (Fig.6). Quartz occurs as anhedral crystal and displayed consertal texture in quartz-rich portion (Fig.7). Two types of hornblende, consisting of the brown and green hornblende are found in the hornblende biotite granodiorite Hornblende occurs as long prismatic crystal, strong pleochroism from yellowish green to dark brown and the size range from 0.2 mm to 2 mm in length. Magnetite and quartz enclosed within the hornblende minerals, giving to the poikilitic texture (Fig.8). In some thin section, hornblende altered to chlorite (Fig.9). Biotite occurs as subhedral form and shows strong pleochroism from yellowish to dark brown. Their size ranges from 0.5 mm to 2 mm in length. Some biotite altered to chlorite along the cleavage plane. Olivine occur as anhedral to subhedral crystal, the maximum grain size reach up 0.5 mm. Marginal parts of the olivine altered to serpentine mineral (chrysotile) due to hydrothermal alteration (Fig.10).

### **Biotite granodiorite**

This rock is essentially composed of quartz (25%), plagioclase (50%), orthoclase (20%) and biotite (5%). Magnetite found as accessory minerals. The rock shows hypidiomorphic granular texture. Quartz appears mostly as anhedral crystals. The grain size ranges from 0.1mm to 0.5mm in diameter. Plagioclase displays subhedral to anhedral form. Some plagioclase crystal shows carlsbad twin or polysynthetic twinning. Orthoclase feldspar occurs as anhedral to subhedral and the grains size ranges from 0.1 mm to 0.5 mm. Biotite is the chief constituents minerals in this rock. Biotite occurs as subhedral, flaky form and their size ranges from 0.5 mm to 2 mm in length. It exhibits pleochroism from dark-reddish brown to light brown. In some thin section, partial replacement of hornblende by biotite is also observed (Fig.11). Magnetite and apatite are present. Magnetite totally inclusion in the cleave plane of the biotite flake.

### **Leucogranodiorite**

The leucogranodiorite occurs as light coloured, fine-grained rocks, consisting mainly of plagioclase (36%), orthoclase (30%), quartz (24%) with minor amount of biotite and hornblende (8%). Apatite, magnetite, chlorite (2%) occur as accessories. Quartz occurs in alternating bands of medium grained prismatic crystals, fine, and extremely fine mosaic textured quartz (indicating very rapid deposition), along with intervals of colloform chalcedony, which has now recrystallised to fine quartz (Fig.12). The intergrowth of quartz with plagioclase may be seen as myrmekitic texture in this rock (Fig.13). Orthoclase feldspar occurs as cloudy appearance. Hornblende occurs as brown

crystal. Plagioclase display subhedral to anhedral form and sometime prismatic form. In some thin section, it shows polysynthetic twinning is also observed. Biotite occurs as irregular flakes and magnetite occurs as inclusion in other minerals particularly in feldspar.

### Dolerite

It is composed essentially of olivine (5%), plagioclase (25%), augite (15%) hornblende (2%). Other fine-grained minerals also occur in the groundmass (53%). Dolerite shows ocellar texture (Fig.14). Each ocellus shows small spheroidal or ovoid form and olive-green colour of ocellus is olivine and shows zoning (the rim is more or less complete veneer of tiny magnetite crystals). The remainder of each ocellus comprises clear zeolites, turbid or very-fined grained zeolites. Kaersutite (black hornblende containing titanium) occurs as slender prisms, much more abundant than grains of augite and oxides. Plagioclase occurs as microlites in the fine-grained groundmass. The groundmass includes magnetite and other opaque minerals. Interstitial quartz and orthoclase are also observed in the matrix. Augite occurs in some thin section.

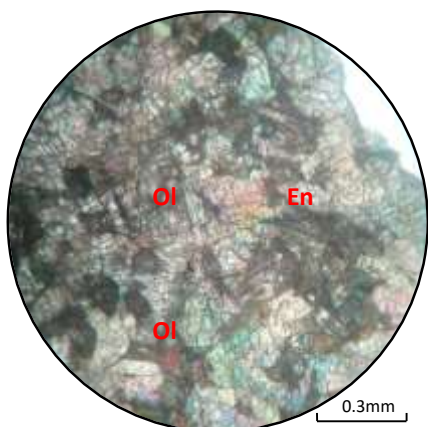


**Figure 3** Hypidiomorphic to allotriomorphic granular texture in peridotites, between XN



**Figure 4** Zoned plagioclase twinned on the Carlsbad law in gabbro, between XN

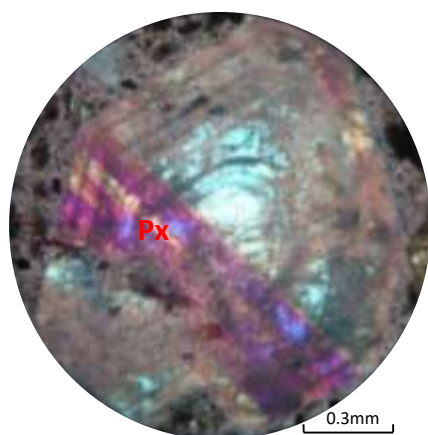


**Figure 5** Sector-zoned and each sector displays oscillatory zoning of pyroxene in gabbro, between XN

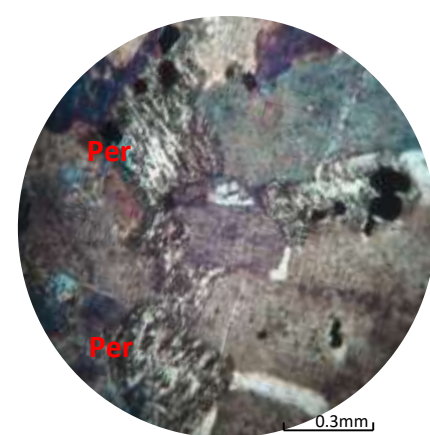


**Figure 6** String perthite in hornblende biotite granodiorite, between XN

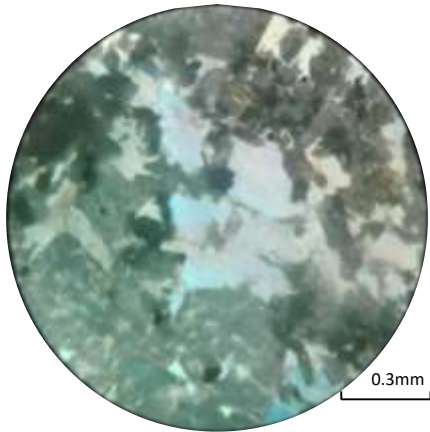


**Figure 7** Consertal texture in hornblende - biotite granodiorite, between XN



**Figure 8** Poikilitic texture of brown hornblende in the hornblende biotite granodiorite, between XN

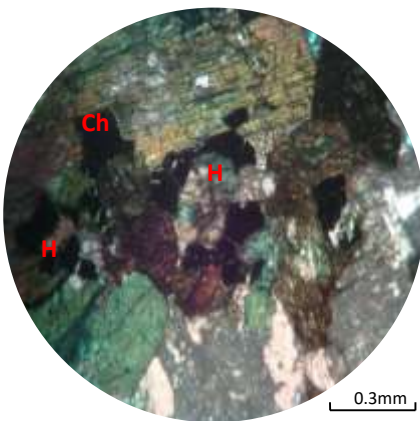


**Figure 9** Hornblende altered to chlorite in hornblende biotite granodiorite, between XN

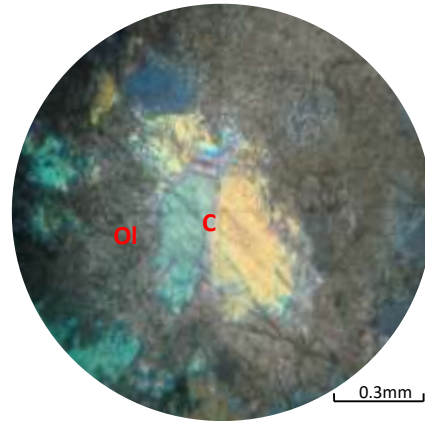


**Figure 10** Marginal parts of the olivine altered to serpentine mineral (chrysotile) in hornblende biotite granodiorite, between XN

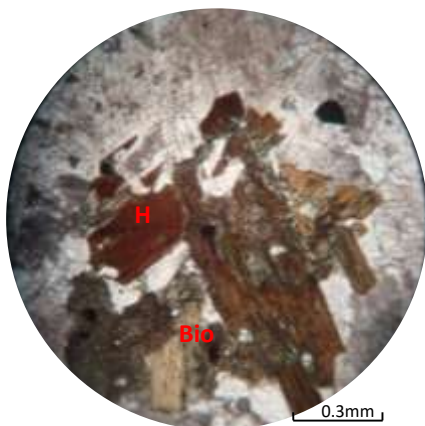


**Figure 11** Partial replacement of hornblende by biotite in biotite granodiorite, between XN

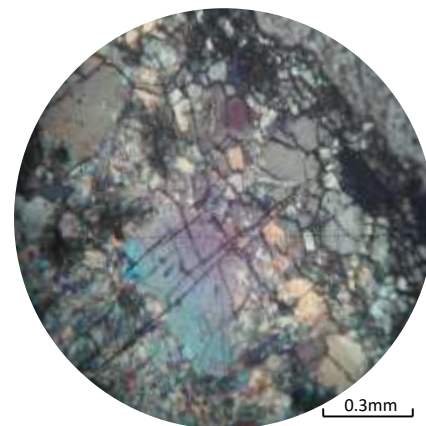


**Figure 12** Alternating bands of medium grained prismatic crystals, fine, and extremely fine mosaic textured quartz (indicating very rapid deposition), between XN

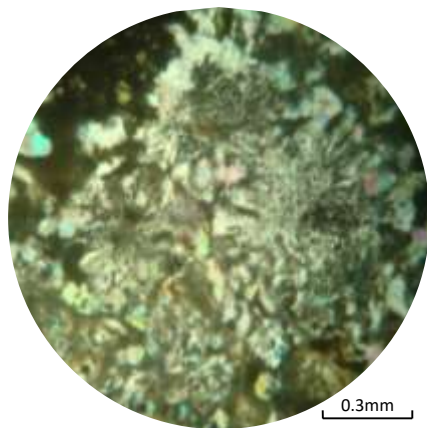


**Figure 13** Myrmekitic texture in leucogranodiorite, between XN

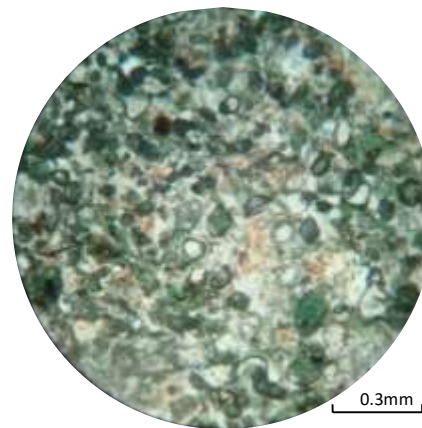


**Figure 14** Ocellar texture of dolerite, between XN

## Volcanic rocks

### Olivine basalt

The olivine basalt is essentially composed of plagioclase (55%), olivine (25%), pyroxene (15%) and minor amount of magnetite and apatite (5%). Phenocrysts of olivine, pyroxene are set in the groundmass. This rock display porphyritic textures. The groundmass is composed of plagioclase microlite with subordinate amount of granular olivine, pyroxene, magnetite, apatite and volcanic glass occurring as intergranular or interstitial matrix. Phenocrysts of olivine and pyroxene are of various sizes and they are fairly abundant. The main constituent mineral plagioclase is present as microlites and sometimes it is found as small amounts of phenocrysts. The matrix is chiefly composed of plagioclase microlites. Plagioclase shows sieve texture due to replacement of abundant inclusions (Fig.15). The grain size ranges from 0.1 mm to 0.3 mm. In some thin section, plagioclase feldspar shows conspicuous zoning are also noted. Some Olivine is also observed in two generations; as large phenocrysts and as small granules within the matrix. The former occurs as subhedral to euhedral prismatic form with the size ranges form 0.2 mm to 1.5 mm. Typical shape of olivine crystal shows irregular cracks and slightly alteration along cracks. In some thin section, olivine phenocrysts shows reaction rims of iddingsite (Fig.16). Pyroxene occurs as subhedral in form and their size ranges from 0.5 mm to 2.5 mm. Some pyroxene phenocrysts shows corona texture or keletic rim (Fig.17). In some thin section, resorbed crystal of pyroxene commonly have rounded corners or embayed (Fig.18). Granules of magnetite are mostly occupying interstitial spaces in the groundmass. Minute apatite are also observed in the groundmass.

### Xenoliths of granodiorite

This rocks exhibits holocrystalline, hypidiomorphic granular texture (Fig.19) and is composed essentially of plagioclase (45%), alkalifeldspar (25%), quartz (23%), biotite and hornblende (5%). Sphene, apatite, zircon and magnetite (2%) are constituted as accessories. Plagioclase is mostly euhedral in form and the size ranges from 0.5 mm to 1.3 mm. It displayed polysynthetic twinning. Some plagioclase altered to sericite. Orthoclase shows simple twin with subhedral form and the size ranges from 0.5 mm to 1 mm. Microcline occurs as minor amount and shows cross-hatch twinning. Quartz occurs as anhedral crystal, high  $\beta$  form and the maximum grain size exceed 0.5 mm. Hornblende occurs as brown colour, euhedral crystal. The grain size varies from 0.1 mm to 0.5 mm in length. Biotite occurs as brownish flakes and their size ranges from 0.1mm to 0.5 mm in length. Tiny sphene, zircon and magnetite are present as accessories.

## Andesite

This rock composed of plagioclase (50%), olivine (5%), pyroxene (3%) and hornblende (2%) with quartz, alkali-feldspar and dark glass (40%) in the groundmass. The rock varies in texture from intergranular to porphyritic. Plagioclase occurs as both phenocrysts and lath-shaped in the groundmass. Plagioclase phenocrysts are typically enclosed in a pilotaxitic groundmass of small plagioclase laths set in glass. Their grain size ranges from 0.5 mm to 2 mm. It exhibits well penetration twinning. Olivine occurs as anhedral granules occupying the space between feldspar laths. Pyroxene and hornblende are usually anhedral granules in the groundmass. Quartz, alkali-feldspar, magnetite are present in the groundmass in subordinate amounts. The inclusion such as mafic minerals, magnetite and glass are enclosed within plagioclase crystals.

## Dacite

Dacite are mainly composed of phenocrysts of plagioclase (20%), quartz (15%), orthoclase or sanidine (8%), pyroxene, hornblende or biotite (7%) and other fine-grained mineral in the groundmass (50%). Plagioclase ranges in composition from labradorite to oligoclase. The main constituent mineral plagioclase is present as microlites and sometimes it is found as small amount of phenocrysts. The matrix is chiefly composed of plagioclase microlites. Plagioclase phenocrysts are generally euhedral to subhedral in form ranging in size from 0.1 mm to 0.5 mm in diameter. Most of the plagioclase shows well penetration twinning. In some thin section, zeolite, quartz filled up in the vesicles and showing amygdaloidal texture (Fig.20). Biotite occurs as small flakes, brown to deep brown color. Its grain size is less than 0.1 mm in diameter. It is usually altered to chlorite. The groundmass is composed of microlites of plagioclase, orthoclase and quartz. Minor accessories minerals are pyrite and iron ores in this rock.

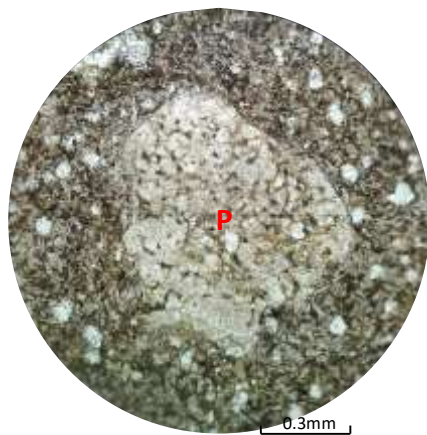


**Figure 15** Sieve texture in cumulo-phric cluster of plagioclase phenocryst in olivine basalt, between XN



**Figure 16** Alteration of olivine to "iddingsite" in olivine basalt, between XN

## Rhyolite

It is mainly composed of quartz (28%), orthoclase (20%) plagioclase (5%), biotite (3%) and other fine-grained minerals in the groundmass (44%). It shows hypocrySTALLINE texture. Quartz is usually present as small grains, suture contact and undulatory extinction. Orthoclase occurs as subhedral to anhedral grains and shows simple twin. Plagioclase feldspar occur as euhedral to subhedral crystal and cloudy appearance. Brown biotite may be present in lesser amount.

## Volcanic Tuff

The rock is composed of crystal of feldspar, small amount of quartz crystal, lithic fragments and volcanic glass in fine-grained matrix. It exhibits pyroclastic texture. The most common minerals are feldspar. Most of feldspar crystals show simple and polysynthetic twinning. Some of the lithic fragments contain opaque iron ore and abundant opaque volcanic glass. Quartz is accidental because it derived from surrounding rocks.

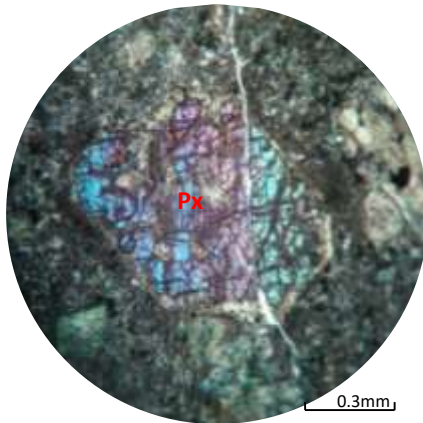


**Figure 17** Resorbed texture of pyroxene in olivine basalt, between XN

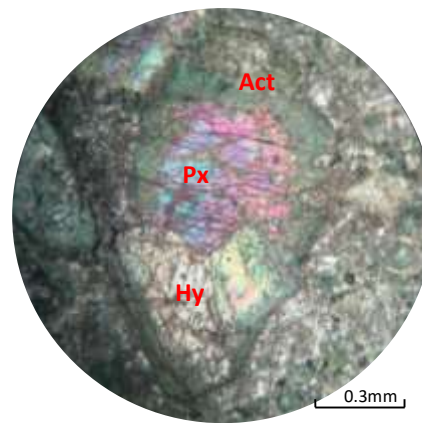


**Figure 18** Corona or kelyphitic rim of pyroxene in olivine basalt, between XN

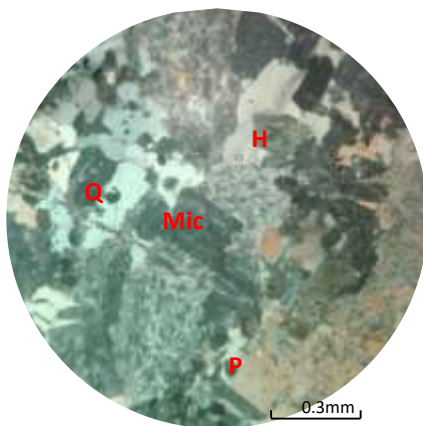


**Figure 19** Hypidiomorphic granular texture in xenoliths of microgranodiorite between XN

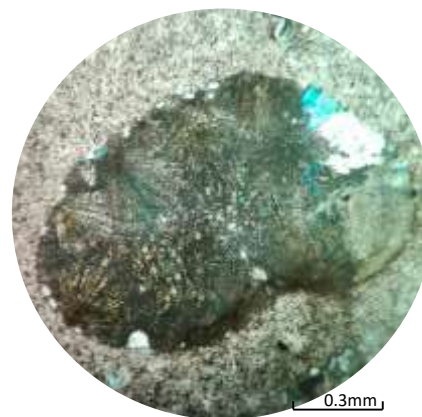


**Figure 20** Zeolite, quartz filled up in the vesicles, showing amygdaloidal texture in dacite, between XN

## Results

A geological map of the virgin area (Nyaung Bin Tha Area, Myitkyina District, Kachin State) was also attempted (Fig.2). According to the field observation and petrographic criteria, almost all plutonic rocks show medium to coarse-grained, hypidiomorphic granular texture. Porphyritic textures are also recognized in these rocks. Plagioclase feldspar shows conspicuous zoning and twinning. Pyroxene shows resorbed and embayed texture, coroner or keleptic rim. Myrmekites are regarded as the products of a subsolidus reaction. Concentric zoning represents magmatic differentiation processes within the magma. Being affected by the hydrothermal alterations (Chloritization, seritization, epidotization, zeolization and serpentization) it should be considered as a result of crystallization from wet magma. Gold bearing quartz vein are observed

in granodiorite host rock. Pyroxene and hornblende are most abundant in the study area. Thus, the sources of granodiorite rocks of the study area may be regarded as I-type nature.

### Discussion

According to previous works and field observations, the ages of the plutonic rocks and volcanic rocks (basalt and andesite) is regarded as Jurassic. The age of volcanic rocks (dacite, rhyolite and tuff) might be Late Cretaceous to Early Eocene.

### Conclusion

According to the field observation and petrographic criteria, almost all plutonic rocks show medium to coarse-grained, hypidiomorphic granular texture. Porphyritic textures are also recognized in these rocks. The presence of perthitic orthoclase in the hornblende-biotite granodiorite rocks suggest that these rocks are of subsolvus types and crystallized at the temperature of less than 700°C.

### Acknowledgement

I would like to express my appreciation to Dr. Myint Oo, Professor and Head of Geology Department, Myitkyina University, for his kind permission to carry out this research work.

### References

- Clegg, E.L.G., (1941), The geology of Burma Macmillan, London.
- Liu, C.Z., Chung, S.L., Wu, F.Y., Zhang, C., Xu, Y., Wang, J.G., Chen, Y., Guo, S., (2016a), Tethyan suturing in Southeast Asia: zircon U-Pb and Hf-O isotopic constraints from Myanmar ophiolites. *Geology* 44 (4), 311–314.
- Maung, M., Thu, A.N., and Suzuki, H., (2014), Latest Jurassic radiolarian fauna from the Chinghkran area, Myitkyina Township, Kachin State, northern Myanmar [abs.], in Win Swe, et al., eds., Thirteenth Regional Congress on Mineral and Energy Resources of Southeast Asia: GEOSEA Proceedings: Yangon, Myanmar, Myanmar Geosciences Society, p. 38–39.
- Mitchell, A.H.G., (1978), Phanerozoic plate boundaries in mainland SE Asia, the Himalayas and Tibet. *Jou. Geol. Soc. Lond.* Vol.116, P.323-334.
- Mitchell, A.H.G. *et.al.*, (1979), Geology and Exploration Geochemistry of part of the Northern and southern Chin Hills and Arakan Yoma, Western Burma. *Technical Report 4, UNDP, Rangon.*
- Nedelec A., Bouchez J. L., (2015), *Granites: Petrology, Structure, Geological Setting and Metallogeny*, Oxford University Press, ISBN 978-0-19-870561-1.
- Yang, J.S., Xu, Z.Q., Duan, X.D., Li, J., Xiong, F.H., Liu, Z., Cai, Z.H., and Li, H.Q., (2012), Discovery of a Jurassic SSZ ophiolite in the Myitkyina region of Myanmar [in Chinese with English abstract]: *Yanshi Xuebao*, v. 28, p.1710–1730.

# STUDY OF THE STRATIGRAPHY OF THE MARINE REPTILE FOSSIL BEARING LIMESTONE UNIT IN LASHIO AREA, NORTHERN SHAN STATE

Khaing Khaing San<sup>1</sup>, Soe Min Thant<sup>2</sup> & Zarni Swe<sup>3</sup>

## Abstract

The Triassic outcrops in northern Shan State have received relatively little study compared to correlative strata in the southern Shan State. Triassic section to the west of Lashio, northern Shan State encompasses the Late Permian to Middle Triassic Nwabangyi Dolomite Formation. The marine reptile bearing limestone is the sandwiched unit of the Nwabangyi Dolomite Formation. Two specimens of Pachypleurosaurs are the only identifiable fossil collected from this limestone unit. It can be divided into four main facies (in ascending order); sedimentary breccias, laminated limestone, thin to medium-bedded limestone and thin-bedded, limestone intercalated with siltstone and shale. The exact stratigraphic position of the CMLV-1 Specimen is not known because of quarrying in this locality. YDBGLV-4 specimen bearing beds are medium-bedded, grey to dark grey, fine- to medium-grained limestone unit lie between the thin-bedded and laminated limestone facies. This limestone unit apparently grades into the surrounding dolomites.

**Keywords:** Triassic, Lashio, marine reptile, limestone

## Introduction

The two specimens of Triassic marine reptile previously unrecorded from Myanmar were discovered in Lashio area, northern Shan State. Reptile and associated indeterminable scaly and bony fishes were occurred to the west of Lashio. This fossil-bearing limestone unit crops out in a mountain range, locally called Yebawhaung Kyauk-taung range, UTM map 2297-9; Lat 22°56'04", Long. 97°42'49" (Fig.1). This paper is mainly based on the stratigraphy, stratigraphic position and lithology of this limestone unit. Vertebrate fossils may help better constrain their ages. No adequate geological map of Lashio area exists, and this area also studied by MSc students from geology department of Mandalay University (2003) and geology department of Lashio University (2017) assigned Upper Permian to Middle Triassic Nwabangyi Dolomite Formation and Permian Plateau Limestone respectively. They gave, however, no paleontological evidence.

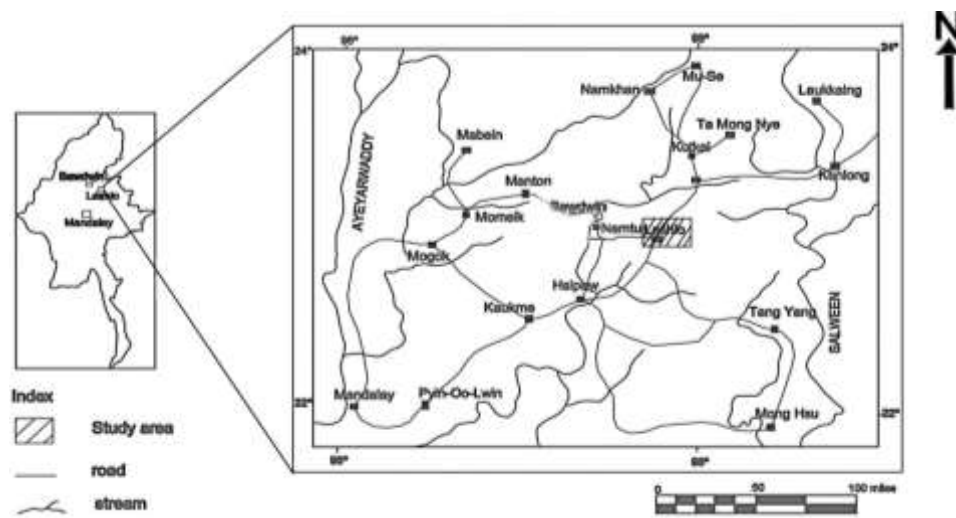


Figure 1 Location map of the study area.

<sup>1</sup> Dr, Professor, Department of Geology, Yadanabon University

<sup>2</sup> Lecturer, Department of Geology, Kyaukse University

<sup>3</sup> Dr, Associate Professor, Department of Geology, Shwebo University

### Regional geologic setting

Myanmar can be tectonically divided into four provinces. They are from east to west, (1) Shan-Tanintharyi Block, (2) Central Cenozoic Belt, (3) Western Fold Belt and (4) Rakhine Coastal Belt (Chhibber, 1934, Win Swe, 1972 and Maung Thein, 1973). MaungThein stated that the Shan-Tanintharyi Block contains Lashio Basin, Kalaw Basin and Myogyi-Pindaya Uplift. The present area is situated in the Shan-Tanintharyi Block of Lashio Basin which is lying in the northern part of the Shan Massif. The regional geologic setting of the Lashio and its environs is shown in (Fig.2).

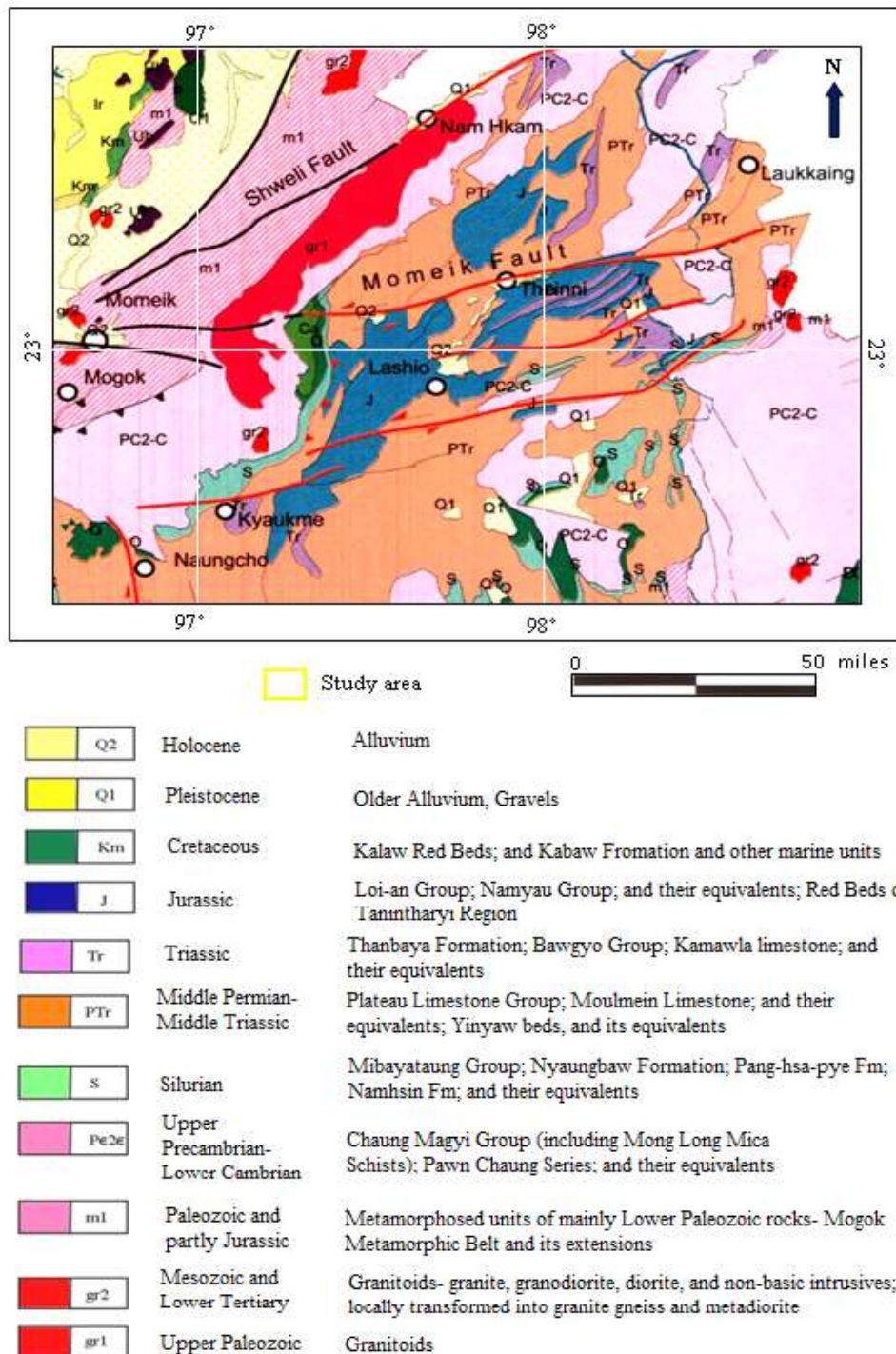


Figure 2 Regional geologic setting of the Lashio area. (Source: MGS, 2014)

## Previous Works

The fossil bearing limestone was previously mapped and designated as the Nwabangyi Dolomite Formation (Brönnimann et al., 1975) as Upper Permian to Middle Triassic based on the occurrence of foraminiferal association of *Glomospirella irregularis* in Kyaukme-Longtawkno area, northern Shan State. The occurrence of the lowermost Triassic (early Scythian) beds in northern Shan State was recorded by Sahni (1936) at Na-hkan, north of Lashio and west of Hsenwi. Ammonite fauna occur abundantly in the argillaceous limestones and shales that are intercalated in dolomite. He gave the name Na-hkan Beds, which is in need of revision. Locally, this area also studied by MSc students from geology department of Mandalay University (2003) and geology department of Lashio University (2017).

## Results and Discussion

### Lithostratigraphy of the reptile bearing limestone

The marine reptiles were found in rocks of the Lashio Basin, in the northern part of the Shan Massif, which is part of the Shan-Tanintharyi Block. The Lashio area is composed mainly of sedimentary rocks that date from the Middle Devonian to the Jurassic dolomitic limestone, dolomite, calcitic limestone, argillaceous limestone, siltstone, shale, sandstone and conglomerate. The fossil-bearing limestone is sandwiched between thin- to medium-bedded, light to dark grey, hard and compact limestone and red to purple, uniformly thin-bedded, siltstone and mudstone. This unit apparently grades into the surrounding dolomites. The stratigraphic measured section of the limestone unit is shown in (Fig. 3).

### Distribution

The units are generally striking NW-SE direction and well exposed at the mountain range, locally called the Yebawhaung Kyauk-taung range (UTM map 2297-9; 22°56'04" N, 97°42'49" E).

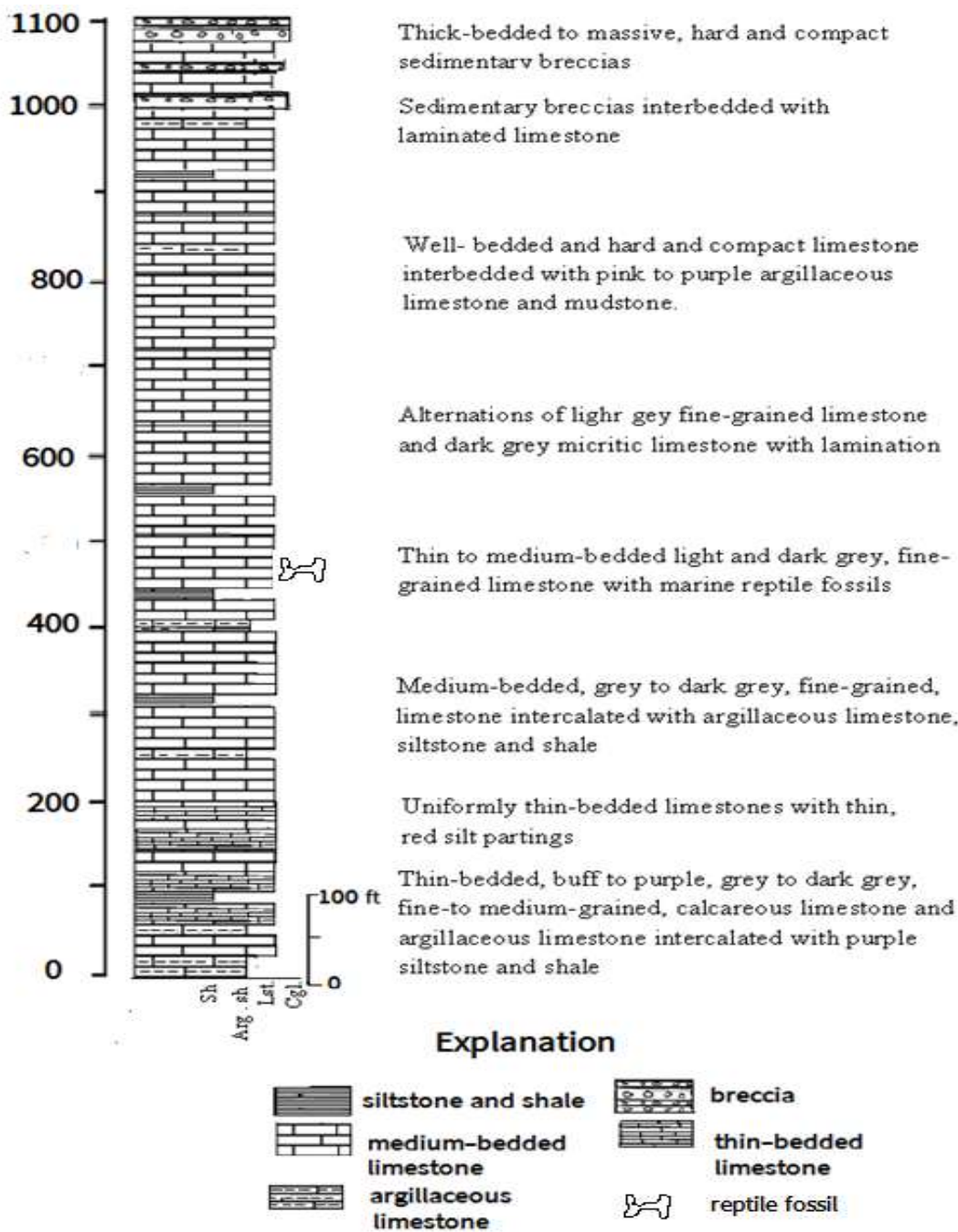


Figure 3 Stratigraphic measured section of the reptile bearing Limestone unit.

**Lithology**

In Yebaw-Haung Kyauktaung Quarry, the unit is consisted of thin- to medium-bedded, gery, purple and buff color and grey limestones, argillaceous limestone with lamination intercalated with siltstone and shale. The upper most part of the unit is overlain by medium- to thick-bedded sedimentary breccias. The stratigraphic succession of the unit in ascending order is as follows;

4. Sedimentary breccias – thick-bedded to massive, hard and compact forms 50 to 80 feet thick, interbedded with laminated limestone in the upper most of the unit (Figs. 20 & 21). The breccias consist of angular blocks or pebbles of various sizes of clasts such as laminated limestone,

calcareous siltstone, micritic limestone and dolomitic limestone which are sometimes flexed or contorted in the calcitic matrix (Fig. 22). It is polymitic breccias unit (Fig. 23).

3. Laminated limestone – Alternations of light grey fine-grained limestone and dark grey micritic limestone about 500 feet in thickness (Figs. 15&16). They show horizontal bedding, well-bedded and hard and compact character. They are interbedded with pink to purple argillaceous limestone and mudstone (Figs. 17&18). At the Quarry, minor amount of ore minerals (Lead-zinc) can be observed in argillaceous limestone. In some laminated limestone also gives a folded and contorted structure (Fig. 19). The surface of the formation is extremely irregular, lacking surface drainage and swallow-holes are common. Microscopically, it is sandy micrite and mainly composed of micrite, quartz, iron oxide mineral and others and micritic dolomitic limestones consist of laminated algae. The limestone is dominance of limemud, generally light in colour. The laminated micrites are probably of algal origin in a tidal flat environment.

2. Thin to medium-bedded limestone - Thin to medium-bedded, light and dark grey, fine-grained limestone, compact and occasionally criss-crossed structure with marine reptile fossils about 200- 300 feet in thickness (Figs. 8-12). This unit is rather hard and compact and Iron stained red colour in some parts of the bed (Figs. 13&14). Under the microscopic study, most of the limestones are micrite and pelmicrite composed of micrite, peloids and bioclasts.

1. Thin-bedded limestone - Thin-bedded (1-8 cm), buff to purple, grey to dark grey, fine-to medium-grained, hard and compact, calcareous limestone and argillaceous limestone intercalated with purple siltstone and shale about 200 feet in thickness. Uniformly thin-bedded limestones with thin, red silt partings are observed in this unit (Figs.4&5). Weathered surface shows yellowish brown, purple to light grey color whereas grey color on fresh surface (Figs. 6&7). Microscopically, these limestones are biomicrite and mainly composed of micrite, bioclasts (foraminiferal and thin-shelled bivalve) and iron oxide and ferruginous micrite composed of micrite, sparry calcite and iron oxide.

Thick carbonate sequence is mostly shallow marine water condition probably shelf environment.

### **Nature of contact**

In this area, the upper contact between the reptile bearing limestone unit and dolomitic limestone of Nwabangyi Dolomite Formation and the overlying Hsipaw Red Bed is faulted contact in the southern part of Sin Taung and occurs as unconformable contact in the eastern part of Sin Taung. It grades laterally into dolomite or dolomitic limestone. The lower contact of the unit is not clearly observed in this area due to covered soil which may be the conformable contact with the Plateau Limestone.

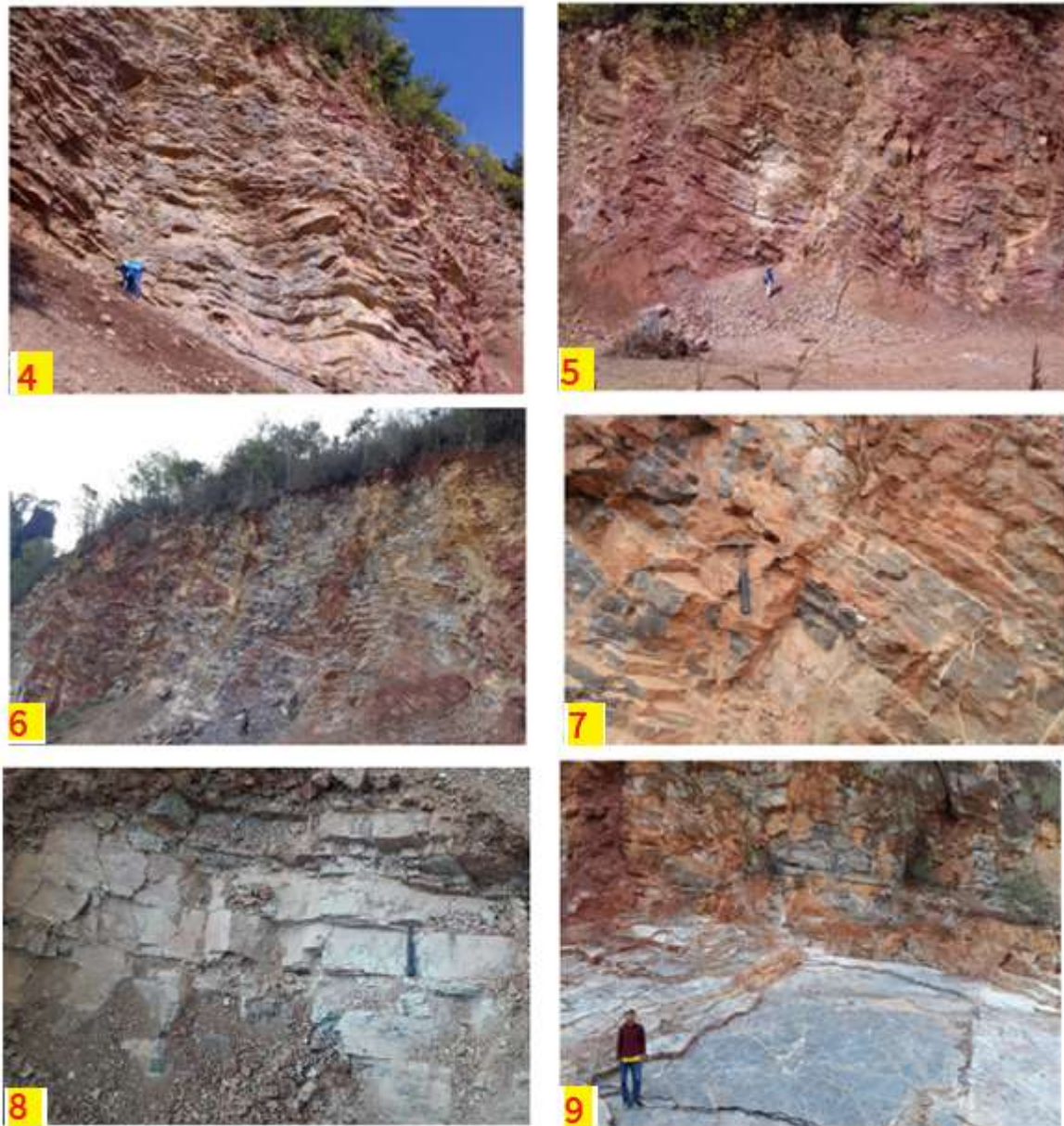


**Figure 4** Thin-bedded, grey to purple limestone intercalated with thinly bedded, argillaceous limestone in the lower most part of the unit. (N225552, E974258)

**Figure 5** Quarry site of thin-bedded limestone intercalated with purple limestone. (N225552, E974258)

**Figure 6** Thin-bedded, grey limestone intercalated with buff-colored argillaceous limestone. (N225606, E974303)

**Figure 7** Thin-bedded, grey limestone intercalated with purple siltstone and shale. (N225606, E974303)

**Figure 8** Medium-bedded, grey to dark grey, fine-grained limestone with marine reptile fossil in the middle part of the unit. (N225604, E974308)

**Figure 9** Medium-to thick-bedded, grey to purple, fine-grained limestone with secondary calcite veins. (N225604, E974305)



**Figure 10** Thin-bedded, grey, micritic limestone interbedded with purple mudstone at YebawHaung quarry near Namkhai village.

**Figure 11** Thin- to medium-bedded, grey limestone with iron stained red coloration on the bedding plane. (N225611, E974305)

**Figure 12** Medium-bedded, grey, micritic limestone in the middle part of the unit. (N225640, E974250)

**Figure 13** Thick-bedded, grey to purple, highly jointed limestone intercalated with purple siltstone and shale. (N225640, E974250)

**Figure 14** Medium-bedded, grey to purple, fine-grained limestone in the middle part of the unit. (N225640, E974250)

**Figure 15** Medium-bedded, light grey to grey, fine-grained laminated limestone in the middle part of the unit. (N225603, E974308)

**Figure 16** Close up view of Medium-bedded, light grey to grey, fine-grained laminated limestone in the middle part of the unit.



- Figure 17** Medium- to thick-bedded, grey, micritic limestone with parallel lamination in the middle part of the unit.
- Figure 18** Medium-bedded, grey to purple, highly jointed laminated limestone. (N225609, E974248)
- Figure 19** Medium-bedded, grey to purple, highly contorted and slightly folded, laminated limestone in the middle part of the unit. (N225604, E974249)
- Figure 20** Contact between the laminated limestone and sedimentary breccias. (N225512, E974245)
- Figure 21** Thick-bedded to massive, hard and compact, sedimentary breccia in the upper part of the unit. (N225512, E974245)
- Figure 22** Interbedded nature of laminated limestone and breccias in the upper part of the unit. (N225552, E974258)
- Figure 23** Sedimentary breccias with angular blocks or pebbles of various sizes of clasts such as laminated limestone, calcareous siltstone, micritic limestone and dolomitic limestone.

## Fauna and Age

The present limestone unit crops out in a mountain range. Khaing Khaing San et al. (2019) discovered the first Triassic vertebrate fossils (Pachypleurosaurs) from Yebaw-Haung Kyauktaung Quarry. Both specimens were found in a ferruginous, micritic limestone, associated with indeterminate fish bones and scales.

The fossil reptiles are embedded in ferruginous, micritic limestone layers sandwiched between the thin- to medium-bedded, light to dark grey, hard and compact limestone, red to purple, uniformly thin-bedded, siltstone and mudstone. Minor amount of ore (lead-zinc) mineralization can be observed in some parts of the bed. This limestone unit apparently grades into the surrounding dolomites. As these fossils are preserved by the replacement of iron for calcium, the detailed morphological structures are slightly obscured. In this unit, fossils are rare except the reptile and fish fauna.

This fossil indicates the Triassic age for the undolomitized part of the Nwabangyi Dolomite Formation. So, the age of this Formation has probably been regarded as Late Permian – Middle Triassic on the basis of stratigraphic position, lithologic character and faunal contact.

## Correlation

On the basis of the lithologic similarities and stratigraphic position, the reptile bearing unit of the present area can be correlated with the undolomitized part of Nwabangyi Dolomite Formation of the Southern Shan State (Garson et al, 1976).

## Discussion

La Touche (1913) first used the term Plateau Limestone of thick carbonate sequence in the Northern Shan State. He divided into the lower dolomitic part and upper calcitic part. Amos (1975) described the name Sha Dolomite Group and can be subdivide the two dolomitic units into the Maymyo Dolomite Formation and Nwabangyi Dolomite Formation. The calcitic part in the two dolomitic units is named as the Thitsipin Limestone Formation.

Garson et al. (1976) subdivided the Permo-Triassic unit of southern Shan State into three distinct Formations; the Thitsipin Limestone, the Nwabangyi Dolomite Formation and the Natteik Limestone Formation. He gave the Nwabangyi Dolomite Formation to a sequence of dolomitized carbonate rocks of Permian-Triassic age exposed in the vicinity of Nwabangyi village, Ye-ngan Township, Southern Shan State.

Garson et al. (1976) divided the brecciation escaped rocks of Nwabangyi Dolomite Formation into four main facies. They are from upper to lower-

4. Light and dark grey, fine-grained limestone facies
3. Sedimentary breccias facies
2. Laminated and turbiditic limestone facies
1. Thin-bedded foraminiferal limestone facies

In this study, Nwabangyi Dolomite Formation is used to describe a thick-bedded to massive, light grey to grey, highly brecciated dolomite and dolomitic limestone, thin- to medium-bedded, dark grey limestone, laminated argillaceous limestone and breccias.

The fossil-bearing limestone was previously mapped as belonging to the Nwabangyi Dolomite Formation (Garson et al. 1976), considered Late Permian to Middle Triassic in age based on the occurrence of the foraminiferan *Glomospirella irregularis* in the Kyaukme-Longtawkn area of northern Shan State (Brönnimann et al. 1975). This limestone has been correlated with the

Thigaungtaung Limestone (Early–Middle Triassic, Induan–Anisian) of southern Shan State (Amos 1975; Whittaker in Brönnimann et al. 1975; see also the recent review of the “Plateau Limestone” of southern Shan State by Win et al. 2015). Furthermore, Sahni (1936) compiled other records of lower-most Triassic units (Scythian, Induan–Olenekian) at Namhkam (north of Lashio and west of Hsenwi), to which he gave the informal name of the “Na-hkan Beds”. The detailed stratigraphy, correlations, and ages of these various units are in need of revision. Vertebrate fossils may help better constrain their ages.

### Conclusion

Garson et al. (1976) assigned the Nwabangyi Dolomite Formation as Late Permian to Middle Triassic based on the occurrence of foraminifera. Wolfart et al (1984) also described the youngest rocks of the Nwabangyi Dolomite are probably Anisian/Ladinian (Middle Triassic age) of the Northern Shan State. The dolomitized part of the Nwabangyi Dolomite Formation is mainly composed of thick-bedded to massive; light grey to grey, fine-grained, highly brecciated and highly jointed dolomite and dolomitic limestone. They are sandy to touché and have a granular texture. In the present study of the limestone unit, the Triassic index fossils of marine reptile (Pachypleurosaurs) have been found. Some micro-fossils and shell fragments have also been found in this unit under thin-section view. It grades laterally into dolomite or dolomitic limestone of the Nwabangyi Dolomite Formation and can be conclude that it is the undolomitized, sandwiched unit of Nwabangyi Dolomite Formation.

### Acknowledgements

We are grateful to Professor Dr. Aye Ko Aung (Retd.), Department of Geology, Dagon University for his constructive discussions, suggestions and comments. Thanks are also due to Daw Kathy Khaing, Assistant Lecturer and U Felika, Demonstrator, department of Geology, Lashio University and MSc geology students from department of geology, Lashio and Yadanabon Universities for their helping hands in the field works.

### References

- Amos, B.J. (1975). Stratigraphy of Some Upper Paleozoic and Mesozoic carbonate rocks of the eastern Highlands, Burma. *Newsl. Stratigr.*, 4(1): 49-70.
- Brönnimann, P, J.E. Whittaker, & L. Zennetti, (1975). Triassic foraminiferal biostratigraphy of the Kyaukme-Lonhtawkno area, Northern Shan State, Burma.- *Riv. Ital. Paleont.*, 81,1:1-30.
- Chhibber, H.L., (1934). *Geology of Burma*; London, Macmillan Co.Ltd., 538 p.
- Garson, M.S., B.J. Amos and A.H.G. Mitchell, (1976). The geology of the area around Nyaungga and Yengan, southern Shan State, Burma: *Overseas Mem. Inst. Geol. Sci.* No.2: 19-30.
- Khaing Khaing San, Nicholas C. Fraser, Davide Foffa, Olivier Rieppel, and Stephen L. Brusatte (2019) The first Triassic vertebrate fossils from Myanmar: Pachypleurosaurs in a marine limestone. *Acta Palaeontologica Polonica* 64 (2), 2019: 357-362.
- La Touche, T.H.D. DE, (1913). Geology of the Northern Shan States- *Mem. Geol. Surv. India*, 39, 2:1-379, 13 tap: Calcutta
- Maung Thein, (1973). A preliminary synthesis of the geological evolution of Burma with reference to the tectonic development of Southeast Asia. - *Geol. Soc. Malaysia, Bull.* 6:87-116, Kuala Lumpur.
- Myanmar Geoscience Society, (2014). Geological map of Myanmar, 1:2, 250,000.
- Sahni, M.R., (1936.) On the geological age of the Namyau, Liu-Wun and Napeng Geds and the certain other formations in Indo China. – *Rec. Geol. Surv, India*, 71, 1: 217-230.
- Win Swe, (1972). Strike-slip faulting in Central Belt of Burma., *Geol. Soc. Malaysia, Newsl.* (Reg. Conf. Geol. Southeast Asia), Abstr., No. 34:59, Kuala Lumpur.
- Win, Z., K.K. Shwe, and O.S. Yin, (2015). Sedimentary facies and biotic associations in the Permian–Triassic limestones on the Shan Plateau, Myanmar. *Geological Society of London, Memoirs* 48: 343–363.
- Wolfart, R., et al., (1984). Stratigraphy of the Western Shan Massif, *Burma.Geol. Jb.*, B.57, Hanover, 92pp

## **SOIL DEGRADATION ALONG YANGON-NAYPYIDAW HIGHWAY BETWEEN MILE POST 10 AND 40 IN MYANMAR**

Aung Kyaw Myat<sup>1</sup>, Day Wa Aung<sup>2</sup> and Hlaing Myo Nwe<sup>2</sup>

### **Abstract**

This research is carried out along Yangon-Naypyidaw Highway between Mile Post 10 and 40 to explore the degradation of soil especially caused by gully erosion. The study area covers along the road with Irrawaddy Formation, Older Alluvium (Lateritic soil) and Younger Alluvium. The top soil layer of study road segment is mainly composed of sand, silt, clay and little gravel of Older Alluvium. This layer consists of loosely consolidated, fine to medium grained silty sand with clay which possess 5-10 numbers of blow count as Standard Penetration Test. Moisture contents of top soil layer comprising cohesionless soil is mainly controlled to land degradation. There are many erosion processes along the study road because of the highly rainfall as well as deforestation. Land degradation is high potential during rainy season. The main causes of human-induced land degradation in this area are expansion of cropland and cutting for fire woods. Soil salinization caused by sodium and potassium elements composing in soil is also one of the main controlling factors for soil degradation in rainy season. Vegetation covered on gully floor is very important to protect soil degradation which can reduce surface erosion. Reforestation should also be made for soil stabilization. In some places, temporary physical structures such as gully reshaping, brushwood, sandbag, loose stone, gabion and arc-weir check-dams should be built to minimize gully erosion.

**Keywords:** Soil degradation, gully erosion, soil stabilization, Reforestation

### **Introduction**

Soil degradation is among serious prevailing issues in modern era. Soil erosion caused by runoff water is one of the most important land-degradation processes in the world. It is being caused due to natural and anthropogenic activities. The level of degradation depends on the degree of degradative processes; duration of usage of such degraded land and its management.

### **Location**

The study road starts at N 17°04' 00", E 96° 10' 02" and ends at N 17° 24' 46", E 96° 20' 32". This road is 18 km long from Yangon Township, Yangon Region to Phayargyi Township, Bago Region which is shown in Figure (1). This area is located at the southern part of Central Myanmar especially along the eastern part of Bago Yoma.

---

<sup>1</sup> Dr, Associate Professor, Department of Geology, University of Yangon (aungkyawmyat95@gmail.com)

<sup>2</sup> Dr, Professor and Head, Department of Geology, University of Yangon (dawaung.geol@gmail.com)

<sup>2</sup> Dr, Associate Professor, Department of Geology, Bago University (hmyonwe@gmail.com)

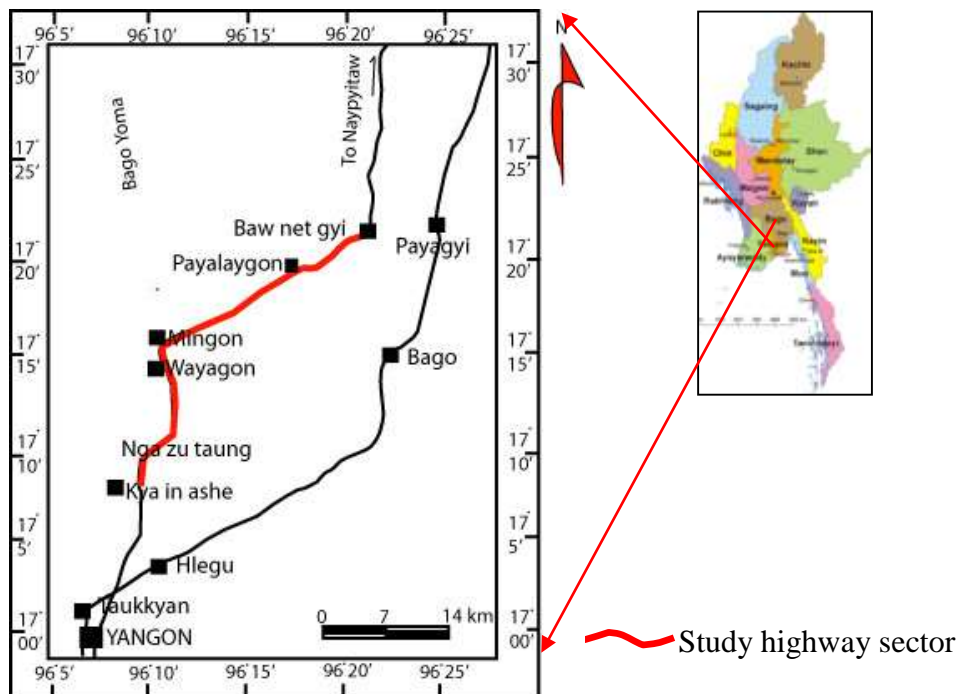


**Figure 1** Location map of the study area

### Regional Geologic Setting

The study area is located in Inner-Myanmar Tertiary Basin. This basin is divided into sub-basins with Tertiary sediments and uplift areas with older sediments and crystalline rocks, with block faulting and compressional folding of the basin filling. Among these, Bago Yoma is structurally an uplifted range in the Inner-Myanmar Tertiary Basin.

The study area is generally composed of Neogene clastic sedimentary rocks of Kyaukkok Formation (Early Miocene) and Obogon Formation (Middle Miocene), Irrawaddy Formation (Late Miocene to Pliocene), Older Alluvium (Pleistocene) and Younger Alluvium (Holocene). The study area along highway is mainly covered by Irrawaddy Formation, Older Alluvium and Younger Alluvium. Older Alluvium is composed of lateritic soil, silty sand and sandy silt mainly exposed along the road (Figure 2). Younger Alluvium is found as farms and stream sediments which is mainly composed of clayey silt and silty sand. The regional geology of the study area is described in Figure (3).



**Figure 2** Residual soil outcrop of Older Alluvium at mile post 15/4

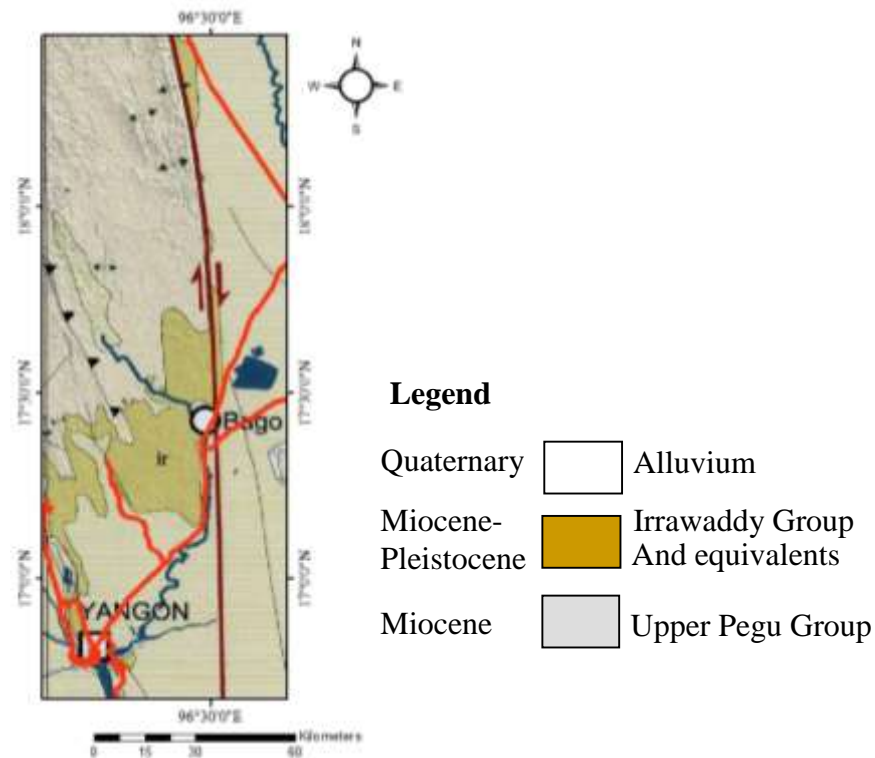


**Figure 3** Regional geological map of the study area (MGS, 2014)

### Aims and Objectives

The main aim of this research is to explore causes of land degradation by gully erosion and to find out suitable supporting system for that area. Moreover, the objectives of this study are as follows;

- To observe soil erosion along highway
- To explore the process of land degradation
- To identify the control of soil erosion along highway
- To select suitable soil stabilization method

### Methodology

Firstly, the literature surveys related to gully erosion and soil degradation such as Ravi and D'Odorico 2005, Pimentel and Burgess 2013 had been made by the authors who described. By using the (Garman 78) GPS, the waypoints are recorded in detail to plot on the google map.

Object-based segmentation and classification of bareland, vegetation and water bodies based on LANDSAT-8 satellite images acquired for the landcover changes of 2017 and 2020 along the road. Assessment of classification accuracy of the land-cover classes is used 600 randomly distributed control points by using field data and google earth images. Quantification of land-cover changes detection overlay-analysis and of net land-cover gains and losses using change cut and fill analysis.

Land erosion and measurement of the cutting slopes have also been made with Brunton compass and distance meter along the highway to measure the length and width of outcrops and

gullies. The velocity of water flowage was measured based on flowage meters per second along the gullies.

Geotechnical analysis for land degradation was made in accordance with the field investigation of American Society for Testing and Materials (ASTM D 1586-99/D 2487-98) and laboratory investigation of (ASTM D 2216, D 7263, D 422, D 3080-12).

Collecting soil samples had been made to explore the geochemical behaviors of soils especially salinity along highway. The collected soil samples were tested and analyzed by Atomic Absorption Spectrophotometer (AAS).

### Results and Discussions

Land degradation covers the various forms of soil degradation, adverse human impacts on water resources, deforestation, and lowering of the productive capacity of rangelands. This research is carried out based on the study of gully erosion by land cover changes, engineering geological aspects of soil, rainfall effect and geochemistry of soil.

#### Satellite Image Analysis

Land cover change was made on the application of object-based segmentation and classification techniques using 2017 and 2020 LANDSAT-8 satellite images for the road. It is characterized by a diverse landscape with two major landforms: plains and rolling hills. Rolling Hills cover 40 % of the total area. The land-cover maps produced for 2017 and 2020 are presented in Figure 8, 9 and 10. They show that the overall accuracies of the 2017 and 2020 land-cover maps were 75 % and 85 % respectively. Therefore, the achieved accuracies were considered to be acceptable for quantified change detection analyses.

The whole area of bareland, vegetation and water body areas was shown in Figure (4). According to classification of land cover changes, in 2017-2018, this area is composed of bareland (61.79%), vegetation cover (34.28%) and water body (3.93%). The bareland area changed 1598284.6 km<sup>2</sup> and unchanged area was 1065133.1 km<sup>2</sup>. The vegetation covered area also changed 772290.1 km<sup>2</sup> and unchanged area was 705219.2 km<sup>2</sup>. Besides, water body changes were found in 147247.3 km<sup>2</sup> and unchanged water bodies area was 22354.1 km<sup>2</sup>.

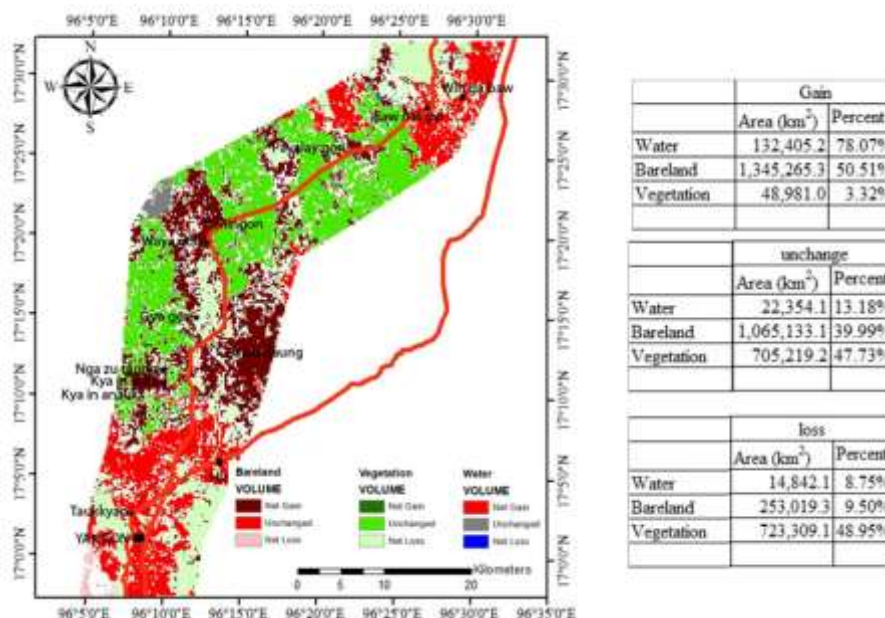


Figure 4 Land cover changes map of satellite imagery in 2017-2018

In 2018-2019, the total areas of bareland (88.89%), vegetation cover (5.81%) and water body (5.30%) were observed which is shown in Figure (5). The bareland area changed 3,164,200.1 km<sup>2</sup> and unchanged area was 667265.5 km<sup>2</sup>. The vegetation covered area also changed 140,304.2 km<sup>2</sup> and unchanged area was 667265.5 km<sup>2</sup>. Moreover, water body change occurred 203,361.5 km<sup>2</sup> and unchanged water body area was 25,143.2 km<sup>2</sup>.

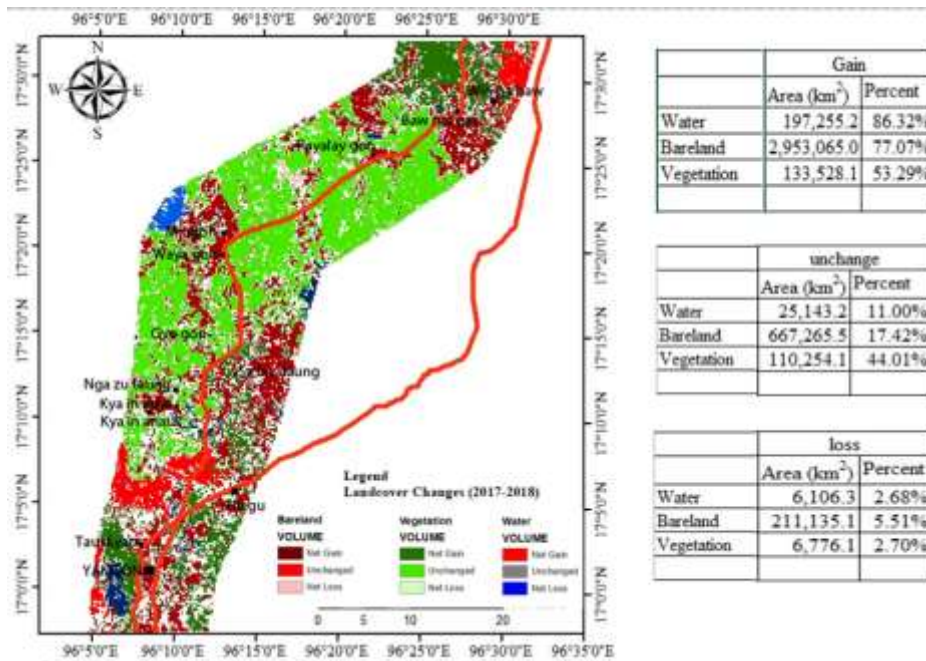


Figure 5 Land cover changes map of satellite imagery in 2018-2019

According to classification of land cover changes, in 2019-2020, this area is composed of bareland (84.03%), vegetation cover (15.34%) and water body (0.63%) which is shown in Figure (6). The bareland area changed 3,623,348.0 km<sup>2</sup> and unchanged area was 1,235.0 km<sup>2</sup>. The vegetation covered area also changed 340,945.2 km<sup>2</sup> and unchanged area was 320,157.1 km<sup>2</sup>. Besides, water body change was found in 26,213.2 km<sup>2</sup> and unchanged water bodies area was 1,100.1 km<sup>2</sup>.

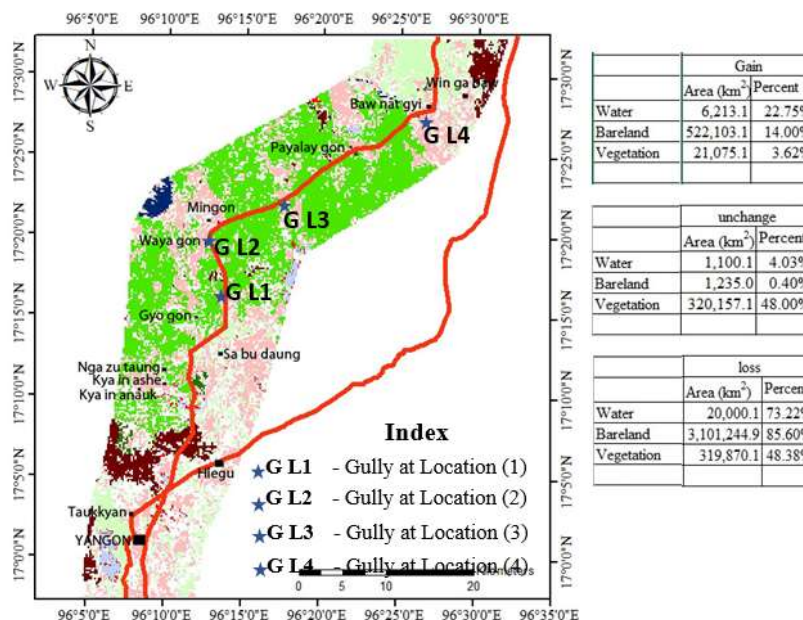


Figure 6 Land cover changes map of satellite imagery in 2019-2020

According to comparative study of land cover changes from 2017 through 2020, vegetation covered area gradually changed to bareland area in recent year. On the other hand, deforestation is most pronounced in this area.

### Case Study

There are many erosion processes along the road segment because of the high rainfall as well as deforestation. High potential land degradation is observed in the central part of the study road mainly occurred in rainy season. Some land degradations related to gully erosions are described in Table (1, 2, 3 & 4) and Figure (7, 8, 9 & 10). The main control of this erosion process is water flowage that the flowage velocity of the channels ranges from 0.25 to 0.7ms<sup>-1</sup> in raining time. Moreover, the estimate rates of sedimentation also range from 10 % to 25 % per liter in that time. According to field measurement, estimated surface eroded area of gully erosion can be calculated with  $A = bh + 2ls + lb$  and estimated eroded volume can also be calculated with  $V = \frac{1}{2} (bh)l$ .

**Table 1 Field measurements of gully erosion at location 1**

| Loc. 1  | Width (b) | Length (l) | Depth (h) | Slope of gully (s) | Eroded area         | Estimate volume     | Gully Material |
|---------|-----------|------------|-----------|--------------------|---------------------|---------------------|----------------|
| Gully A | 7 m       | 60 m       | 5 m       | 6.5 m              | 1235 m <sup>2</sup> | 1050 m <sup>3</sup> | Silty Sand     |
| Gully B | 12 m      | 70 m       | 7 m       | 9 m                | 2184 m <sup>2</sup> | 2940 m <sup>3</sup> | Silty Sand     |

**Table 2 Field measurements of gully erosion at location 2**

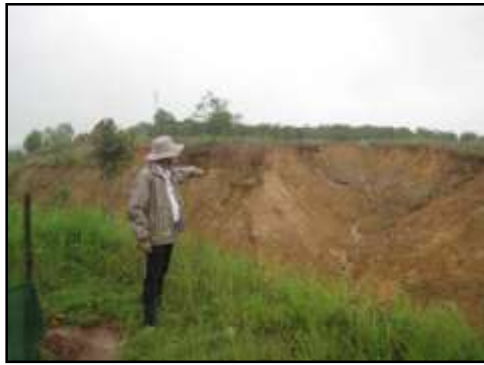
| Loc. 2  | Width (b) | Length (l) | Depth (h) | Slope of gully (s) | Eroded area        | Estimate volume    | Gully Material |
|---------|-----------|------------|-----------|--------------------|--------------------|--------------------|----------------|
| Gully A | 3 m       | 70 m       | 3 m       | 4 m                | 779 m <sup>2</sup> | 315 m <sup>3</sup> | Sandy Silt     |

**Table 3 Field measurements of gully erosion at location 3**

| Loc. 3  | Width (b) | Length (l) | Depth (h) | Slope of gully (s) | Eroded area         | Estimate volume     | Gully Material |
|---------|-----------|------------|-----------|--------------------|---------------------|---------------------|----------------|
| Gully A | 15 m      | 75 m       | 6 m       | 7.5 m              | 2340 m <sup>2</sup> | 2275 m <sup>3</sup> | Sandy Silt     |

**Table 4 Field measurements of gully erosion at location 4**

| Loc. 4  | Width (b) | Length (l) | Depth (h) | Slope of gully (s) | Eroded area        | Estimate volume    | Gully Material |
|---------|-----------|------------|-----------|--------------------|--------------------|--------------------|----------------|
| Gully A | 4 m       | 45 m       | 4 m       | 4.7 m              | 619 m <sup>2</sup> | 360 m <sup>3</sup> | Clayey Silt    |



(A)



(B)

**Figure 7** (A) Nature of gully erosion at Gully A (B) Recently eroded nature at Gully B



**Figure 8** Nature of gully erosion at Location 2



**Figure 9** Gully erosion caused by heavy rainfall at Location 3



**Figure 10** Gully erosion caused by heavy rainfall at Location 4

### Rainfall Data Analysis

According to rainfall data of (DMH) in Myanmar, rainfall is high in June and July (Figure 11). Highest rainfall occurs in August, 2019 and it is followed by the rainfall of June, 2015 and September, 2016.

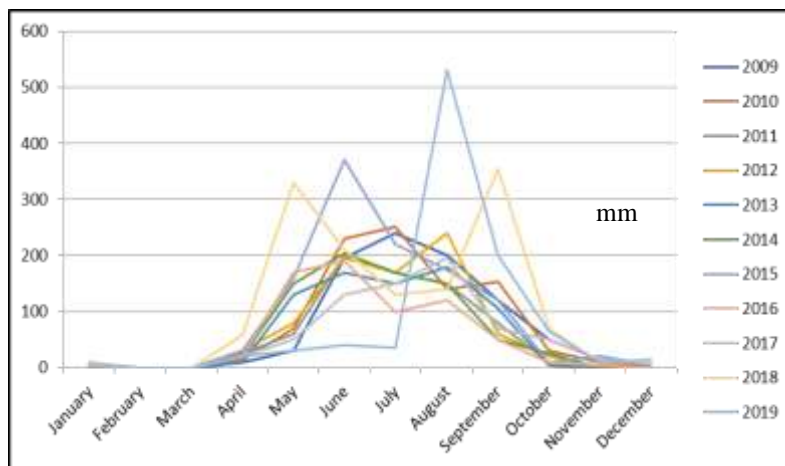


**Figure 11** Average rainfall data analysis of the study area

**Geotechnical Data Analysis**

On the basis of lithologic units, the research area of road segment is mostly composed of loosely consolidated sandstone intercalated with shale and clay of Irrawaddy Formation and laterite deposit of Older Alluvium and rarely found sand, silt, shale, clay and slope wash deposits of Younger Alluvium.

**Analysis from Standard Penetration Test Data**

The engineering geology of the research road is analyzed on the basis of geology and engineering behavior of soils. This investigation had been done based on the 12 boreholes especially along the road segment. Idealized cross-section of subsurface soil layer is described in Figure (12).

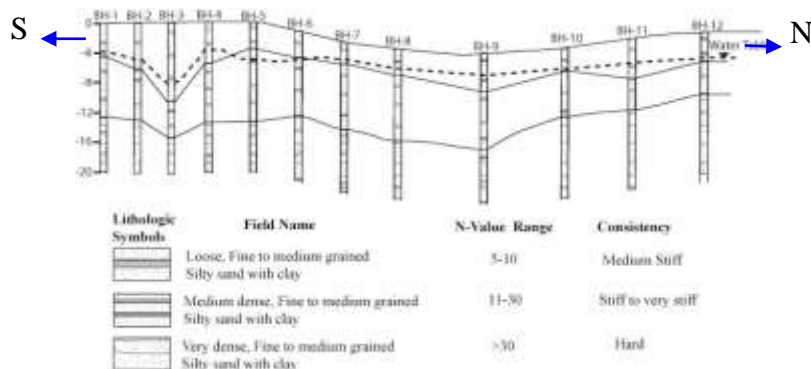


**Figure 12** Idealized cross-section of subsurface soil layers on borehole data

According to this study, subsurface soil layer can be classified basically as Top layer composed of loosely consolidated Silty sand, Middle layer made up of medium dense Silty sand and Lower layer composed of very dense Silty sand. Groundwater level contains in Top layer at 3-8 meter depth. Top layer has SPT N-value (5-10) and is composed of loosely consolidated soil layer. Hence, this layer can easily be eroded in external agents such as rain, stream and air.

**Grain Size Distribution Analysis**

According to the grain size distribution analysis, top soil layer of borehole 2, 5, 10, 11 and 12 is composed of poorly graded silty sand which is a cohesionless soil. It is not suitable for basement as well as for slope stability. Besides, it is also easily erodible in rainy season.

### ***Moisture Content Analysis***

Moisture content was used for determining the erosional resistance of top soil layer. These data were measured on two situations such as dry time and wet time or rainy time. According to this analysis, moisture contents of top soil layer have 13 to 28 % generally in normal condition. But in rainy time, moisture contents can contain to 32 to 38 % of total soil condition. This situation points out that the greater the water containing the soil, the more erosion can take place.

### ***Analysis from Direct Shear Test Data***

Direct shear test was conducted to determine the strength of soil of the area. The strength measurement parameters are cohesion (c) and angle of internal friction ( $\phi$ ) which is described in Table (5).

**Table 5 Results of direct shear test for top soil layer of each boreholes**

| <b>Borehole</b>                           | <b>1</b> | <b>2</b> | <b>3</b> | <b>4</b> | <b>5</b> | <b>6</b> | <b>7</b> | <b>8</b> | <b>9</b> | <b>10</b> | <b>12</b> |
|-------------------------------------------|----------|----------|----------|----------|----------|----------|----------|----------|----------|-----------|-----------|
| Cohesion (c)<br>KN/m <sup>2</sup>         | 0.0      | 0.0      | 0.0      | 13.0     | 18.0     | 9.8      | 13.7     | 13.5     | 0.0      | 16.8      | 9.8       |
| Internal<br>friction ( $\phi$ )<br>degree | 34.9     | 35.1     | 33.1     | 32.0     | 28.1     | 33.3     | 31.6     | 28.2     | 38.6     | 31.8      | 30.1      |

In this analysis, boreholes 1, 2, 3, and 9 show cohesionless soil condition that can be concluded that top soil layer of these borehole sites assumed as loosely consolidated and poorly graded soil condition.

### ***Engineering Properties of Soils***

The top soil layer of study area is mainly composed of sand, silt, clay and little gravel of Older Alluvium. This layer also consists of loosely consolidated, fine to medium grained silty sand with clay as field investigation of boreholes which possess 5-10 numbers of SPT blow count. According to Atterberg's Limit Test (ASTM D 4318), soils of top soil layer can be classified into three different types such as CL, ML and CL-ML. Moreover, moisture contents of top soil layer is different in normal condition and rainy time. This condition is a dangerous condition to erode the top soil where the lack of a ground improvement system prevailed. And the strength of top soil measured by Direct Shear Test indicated that some of top soil layer show cohesionless condition where land degradation processes such gully erosion and small landslides occur in these sites.

### **Soil Salinity Analysis on Geochemical Data**

The elements contained in rocks and minerals are released into the environment by both chemical and physical processes. The geochemical result for these four locations analyzed by AAS is shown in Table (6).

**Table 6 Element content in soil samples of location (1-4) (Unit – ppm)**

| No. | Location | As    | Mn  | Fe   | Na  | K   | Ca  | Mg  |
|-----|----------|-------|-----|------|-----|-----|-----|-----|
| 1   | 1        | ND    | 155 | 8320 | 165 | 365 | 210 | 190 |
| 2   | 2        | ND    | 185 | 8320 | 210 | 355 | 190 | 170 |
| 3   | 3        | 0.003 | 225 | 8150 | 210 | 295 | 275 | 160 |
| 4   | 4        | ND    | 230 | 8570 | 235 | 380 | 285 | 170 |

According to this result, iron is the main constituent element of soil in this area that has high strength in nature. Sodium, potassium and calcium contain 8-10% in total soils. These elements are soluble in water. Hence, in the rainy season, such elements are dissolve in rain water. In fact, erosion may take place more easily and also degrade the soil.

### Proposed Soil Stabilization Methods

It is essential that lands susceptible to gullying should be monitored regularly in early stages of gully formation. It is more suitable to prevent gullies from occurring than to attempt to control them once the erosion has started. Various authors from different countries described soil stabilization methods for gully protections. Among them, the following stabilization methods are suitable for this research area:

- (a) Promote revegetation of gully channels to reduce sediment transport capacity with reduction of the slope gradient
- (b) Maintain vegetation ground cover on gully features to reduce surface erosion
- (c) Some of places should be used with temporary physical structures such as gully reshaping, brushwood, sandbag, loose stone, gabion and arc-weir check-dams.

### Conclusions and Recommendations

Soil degradation is among serious prevailing issues in current time. This research is carried out along Yangon-Naypyidaw Highway between Mile Post 10 and 40. This highway does not meet international design, construction and safety standard has seen a spate of accidents since its opening in 2010.

The study road segment is mainly covered by Irrawaddy Formation, Older Alluvium (Lateritic soil) and Younger Alluvium. The construction materials are sand and gravel deposits, laterite, sandstone, granite and gneissic rocks in constructing this highway. Thin gravel beds of the Irrawaddian and Older Alluvium, lateritic soils in the Bago Yoma foot hills contain were also used as construction materials. Sandstone of the Peguan was used for the basement of highway.

There are many erosion processes along the studied highway segment due to high rainfall as well as deforestation. Gullies and sheetwash erosions are pronounced in four locations. Land degradation is potentially high in rainy season.

According to land cover changes of this area from 2017 through 2020, bareland area changes from 61.79 % to 84.03 %, vegetation covered area changes from 34.28% to 15.34% and water body area changes from 3.93 % to 0.63 %.

Moreover, top soil layer along studied road segment is mainly composed of sand, silt, clay and little gravel of Older Alluvium. Moisture contents of top soil layer is mainly changes in normal condition and rainy time which favours the severe erosion of top soil. Some of top soil layer show

cohesionless soil condition where land degradation processes such as gully erosion and small landslides occur in these sites.

According to geochemical analysis, soil salinization caused by sodium, potassium and calcium elements containing in soil may accelerate the erosion more easily in rainy season as one of the main control in degradation of soil.

Reforestation is one of the most effective method which can protect erosion of top soil. Some of places should be reinforced with suitable weirs.

### Acknowledgements

The authors are also thank to Dr. Myo Thant, Professor, Department of Geology, University of Yangon, for his advices to carry out this research.

The writers are also grateful to Dr. Tun Naing Zaw, Associate Professor of the Department of Geology, University of Yangon for his advices throughout the preparation of this research.

Finally, we would like to special thanks to U San Oo, Director of Future Soil Technics Co. Ltd., for his valuable geotechnical data of research area.

### References

- American Society for Testing and Materials, (1998). *Standard Practice for Classification of Soils for Engineering Purposes (Unified Soil Classification System)*, D 2487, West Conshohocken, PA 19428 Reprinted from the Annual Book of ASTM Standards, P. 1-11.
- American Society for Testing and Materials, (1999). *Standard Test Method for Penetration Test and Split-Barrel Sampling of Soils*, D1586, West Conshohocken, PA 19428 Reprinted from the Annual Book of ASTM Standards, P. 1-5.
- American Society for Testing and Materials, (2007). *Standard Test Method for Particle Size Analysis of Soils*, D422, West Conshohocken, PA 19428 Reprinted from the Annual Book of ASTM Standards, P. 1-8.
- American Society for Testing and Materials, (2009). *Standard Test Methods for Laboratory Determination of Density (Unit Weight) of Soil Specimens*, D 7263, West Conshohocken, PA 19428 Reprinted from the Annual Book of ASTM Standards, P. 1-7.
- American Society for Testing and Materials, (2010). *Standard Test Methods for Laboratory Determination of Water (Moisture) Content of Soil and Rock by Mass*, D2261, West Conshohocken, PA 19428 Reprinted from the Annual Book of ASTM Standards, P. 1-7.
- American Society for Testing and Materials, (2012). *Standard Practice for Direct Shear Test of Soils Under Consolidated Drained Condition*, D 3080, West Conshohocken, PA 19428 Reprinted from the Annual Book of ASTM Standards, P. 1-11. Pimentel and Burgess 2013, *Soil Erosion Threatens Food Production*, College of Agriculture and Life Sciences, Cornell University, USA, P. 443-463.
- Bieniawski, Z. T., (1989.) *Engineering Rock Mass Classifications*, John Wiley and Sons, New York, 251p.
- Pimentel and Burgess (2013), *Soil Erosion Threatens Food Production*, College of Agriculture and Life Sciences, Cornell University, USA, P. 443-463.
- Ravi, S., and P. D'Odorico (2005). A field-scale analysis of the dependence of wind erosion threshold velocity on air humidity, Department of Environmental Sciences, University of Virginia, Charlottesville, Virginia, USA, *Geophys. Res. Lett.*, Vol. 32, 4p.
- Sherwood, P., (1993). *Soil stabilization with cement and lime*. State of the Art Review. London: Transport Research Laboratory, HMSO.

# **ASSESSMENT OF SEISMIC SOIL LIQUEFACTION BASED ON SHEAR WAVE VELOCITY USING 2% AND 10% PROBABILITIES OF PGA VALUES WITH EARTHQUAKE MAGNITUDE-6.5 MW IN MANDALAY CITY**

Tun Tun Win<sup>1</sup>, Myo Thant<sup>2</sup>, Than Than Nu<sup>3</sup> Pyi Soe Thein<sup>4</sup>

## **Abstract**

Mandalay city is located on the eastern bank of Irrawaddy River and about 8 km east of seismically active Sagaing fault. By this fault, Mandalay region has been experienced by many destructive earthquakes. All liquefaction events in Myanmar were observed nearly water body as rivers. Due to these conditions, the liquefaction susceptibility is threatening the Mandalay city. Liquefaction triggering of soils were mainly calculated based on 55 shear wave velocity tests by using 1998 NCEER recommended of Liq.IT v.4.7.7.5 software. The liquefaction potential ( $P_L$ ) maps were developed by using overall liquefaction potential index ( $P_L$ ). The liquefaction potential ( $P_L$ ) maps by using PGA 2% probability should be considered for the construction of lifeline structures such as water pipe line, gas pipe line, transportation ways and telecommunication lines. The  $P_L$  maps using PGA 10% probability are appropriate for engineering construction of the various sorts of structures especially normal building. According to resulted data, the highly liquefied zones fall in the western parts of Aungmyaythazan and Chanayethazan townships. These  $P_L$  maps will help the structural designers or architects and city planners to check the vulnerability of the area against liquefaction. The present data will be very useful not only for seismic hazard mitigation programs but also for seismic safety plans.

**Keywords:** Mandalay city, shear wave velocity, peak ground acceleration (PGA), 1998 NCEER recommended method, liquefaction potential index ( $P_L$ )

## **Introduction**

Today, liquefaction is one of the most important topics for geotechnical earthquake engineers. Ground failures are commonly caused by liquefaction events during numerous devastating earthquakes all over the world. Its effects are mostly observed in near water bodies such as river, lake, bays and oceans. The study area, Mandalay city lies on the eastern bank of Irrawaddy River and about 8 km east of seismically active Sagaing fault. By historical records, Mandalay region had been impacted several times by strong to major earthquakes in the past. Moreover, liquefaction effects as sand boils were caused nearly Irrawaddy and Myitnge river in this region during Innwa earthquake (23<sup>rd</sup> March, 1839) and Thabeikkyin earthquake (11 Nov, 2012) (Chibber, 1934, Win Swe, 2013 and Myo Thant, 2013). By above factors, Mandalay City suffers threatening the seismic related hazard especially, liquefaction near future. Thus, liquefaction risk assessment should be carried out for the study area.

## **Site Investigations**

A total of 55 shallow boreholes and 197 microtremor points were commonly collected from various soil deposits at different locations in Mandalay city. Among them, only the best 55 shear wave velocity data nearly selected from 55 borehole points (Figure 1) were used for the evaluating soil liquefaction potential index of Mandalay city. The site investigations at 55 boreholes points of the Mandalay city were examined about  $\leq 30$  m depth of surface layer.

---

<sup>1</sup> Associate Professor, Department of Geology, Pang Long University

<sup>2</sup> Professor, Department of Geology, University of Yangon

<sup>3</sup> Professor, Department of Geology, University of Mandalay

<sup>4</sup> Associate Professor, Department of Geology, University of Mandalay

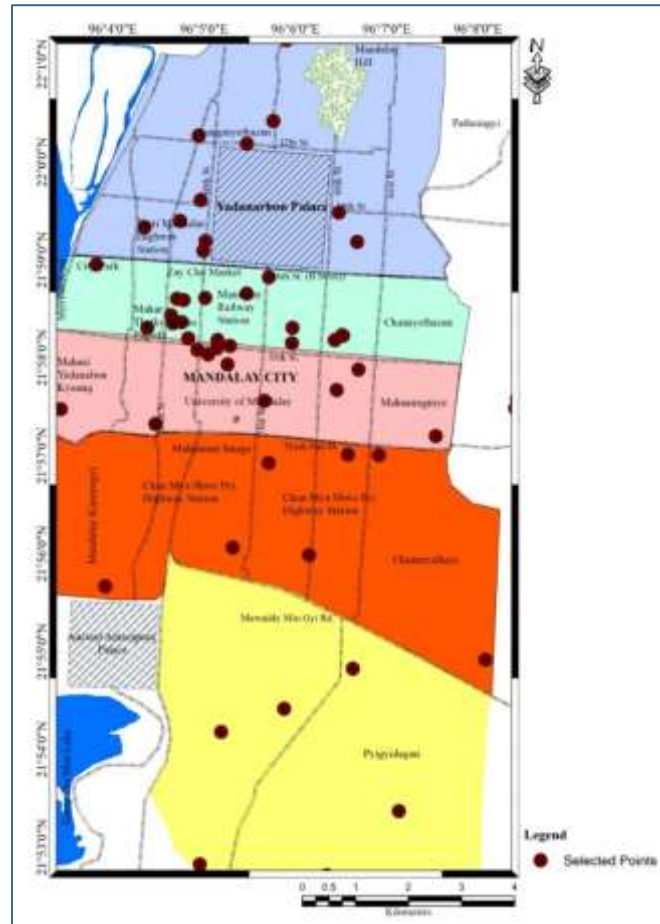


**Figure 1** Location map of the sites where liquefaction potential index assessment is carried out.

### Methodology

The main evaluation procedure in this research will be given to liquefaction potential analysis based on shear wave velocity to a depth of 30m ( $V_s^{30}$ ) value obtained from *HVSR* data. For the present research, the  $V_s$  values have been obtained from SMAR 6A3P microtremor test using inversion process. In this study, the calculation procedures for liquefaction potential analysis of soils have been used Liq.IT v. 4.7.7.5 software. For present research, the calculation procedure of Liq.IT v.4.7.7.5 software is commonly considered based on National Center for Earthquake Engineering Research (NCEER-1998). The depth to water table, shear wave velocity, earthquake magnitude and peak ground acceleration are essential for determining liquefaction potential index of the study area by using this software (Figure 2). The simplified procedure has to needs for calculating the cyclic stress ratio (CSR) and the cyclic resistance ratio (CRR) based on shear wave velocity. With the simplified methods, the liquefaction potential of soil is expressed as a factor of safety  $F_s$ , which is defined as the ratio of cyclic resistance ratio (CRR) over the cyclic stress ratio (CSR). The soil is said to be liquefied if  $F_s \leq 1$  and be non-liquefied if  $F_s > 1$ . It requires the calculation of three parameters; (i) the seismic demand on a soil layer, expressed as a cyclic stress ratio (CSR); (ii) stiffness of the soil, expressed as an overburden stress-corrected shear-wave velocity ( $V_{s1}$ ); and (iii) the resistance of the soil to liquefaction, expressed as a cyclic resistance ratio (CRR) at depth,  $z$  (Seed and Idriss, 1971). To be accurate data, all result data obtained from Liq.IT software were manually adjusted based on SPT and microtremor data. The summarized calculation methods are shown in Figure 3.

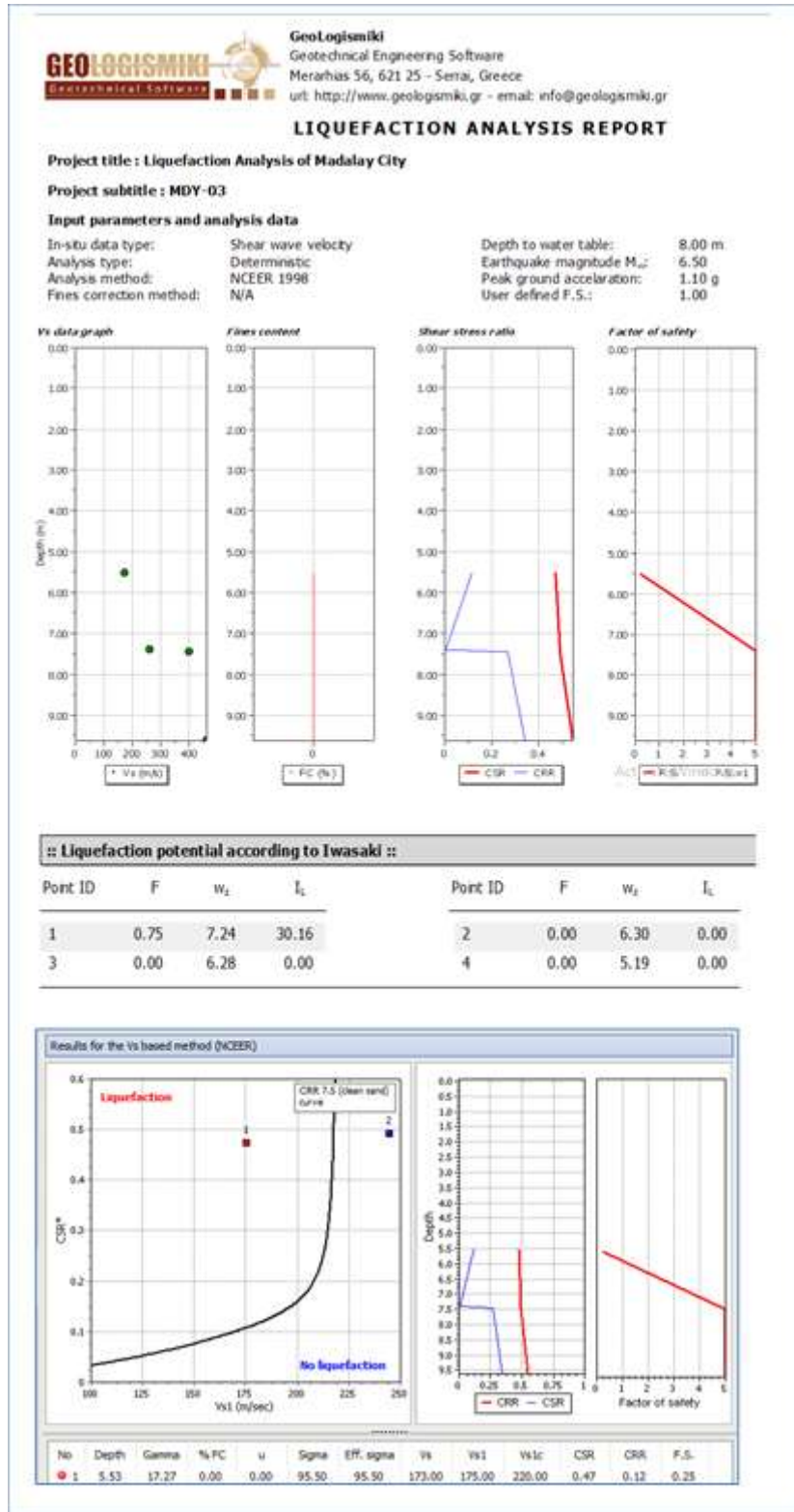
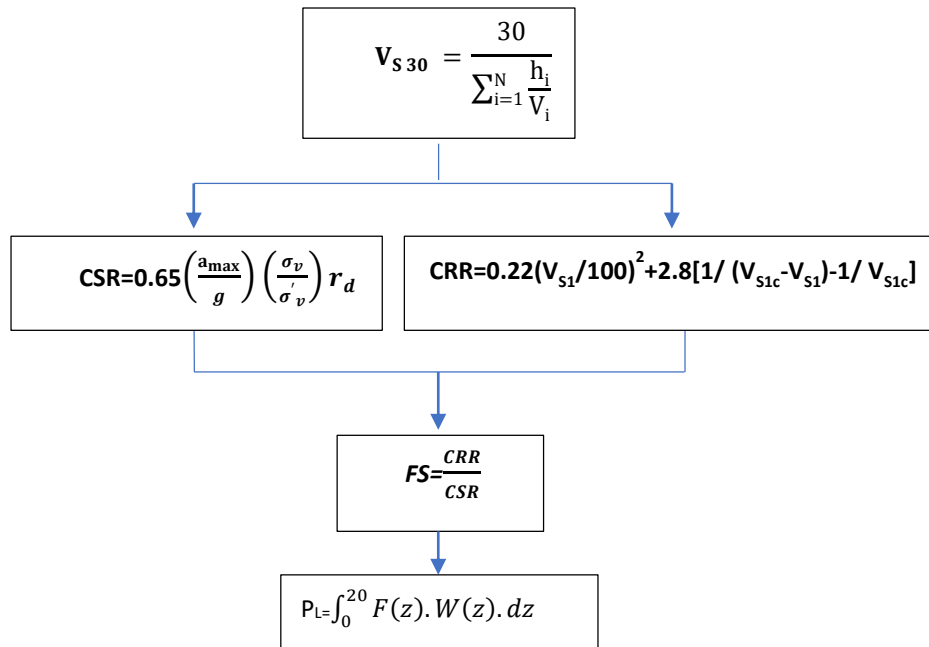


Figure 2 Example of Liq.IT v.4.7.7.5 soil liquefaction assessment software data at MD



**Figure 3** Flow chart of calculation procedure of  $P_L$  index

### Results and Discussion

Liquefaction assessment was performed by using 197 microtremor points compare with 55 boreholes but liquefaction susceptibility maps were established by using 55 shear wave velocity tests. Each point is subdivided into four layers for estimating  $P_L$  index. The variations of underground water depth in Mandalay city were defined by using ground water level in well log borehole data. Ground water levels were mostly found to vary from 0 to 20 m in the study area as shown in table (1). According to probabilistic seismic hazard map (Myo Thant 2013), various peak ground acceleration values as 0.7 – 1.4 g for 2% and 0.5 – 0.9 g for 10% with an scenario earthquake magnitude; Mw- 6.5 have already used for predicting liquefaction susceptibility of soils.

According to present resulted data, low velocities, shallow depth to water table ( $z$ ), high peak ground acceleration ( $a_{max}$ ) and earthquake magnitude (Mw) in soils lead to a higher liquefaction potential. The resulted data of liquefied layers in each site of the study area are shown in Table 1 for 2% and Table 2 for 10% PGA value. Liquefaction potential zones of the study area were designated based on Iwasaki (1984) namely as very low or not probable for  $P_L=0$ , low for  $0 < P_L < 5$ , moderate for  $5 < P_L < 15$  and high for  $15 < P_L < 25$  and very high  $P_L > 25$ . By these  $P_L$  value, it is occurred at very low or not probable liquefied area represent 45% of the whole area: low liquefied zone is < 23% of the study area; moderate liquefied zone is < 10%; high liquefied sites are < 12% of the area and very high liquefied points are < 10% of the study area. According to  $P_L$  resulted values, we should need to obey the following recommendations of Iwasaki (1984);

- For very low liquefaction susceptibility ( $P_L=0$ ), detail investigations on soil liquefaction aren't needed in general
- For low liquefaction susceptibility ( $0 < P_L < 5$ ), detail investigations on soil liquefaction are needed only for especially important structures.

- For moderate liquefaction susceptibility ( $5 < P_L < 15$ ), detail investigations for soil liquefaction are needed for important structures and countermeasures of soil liquefaction are needed in general.
- For high liquefaction susceptibility ( $15 < P_L < 25$ ), detail soil investigations are mandatory
- For very high liquefaction susceptibility ( $P_L > 25$ ), area should be avoided for developing structures

**Table 1 Detail resulted data of liquefied layers in each site of Mandalay City by using Mw 6.5 & PGA 2% probability.**

| Site No | Depth(m)<br>/Layer | Gamma | u     | Sigma  | Eff.<br>sigma | Vs     | Vs1    | Vs1c | CSR  | CRR  | FS          |
|---------|--------------------|-------|-------|--------|---------------|--------|--------|------|------|------|-------------|
| MDY-3   | 5.53/1             | 17.27 | 0.00  | 95.50  | 95.50         | 173    | 175    | 220  | 0.47 | 0.12 | <b>0.25</b> |
| MDY-4   | 5.19 / 1           | 17.68 | 0.00  | 91.76  | 91.76         | 200    | 204.35 | 220  | 0.45 | 0.26 | <b>0.57</b> |
| MDY-08  | 5.58 / 1           | 17.68 | 0.00  | 98.65  | 98.65         | 200    | 200.68 | 220  | 0.43 | 0.22 | <b>0.51</b> |
| MDY-10  | 5.19 / 1           | 17.68 | 0.00  | 91.76  | 91.76         | 200    | 204    | 220  | 0.45 | 0.26 | <b>0.57</b> |
| MDY-11  | 3.19 / 1           | 16.87 | 0.00  | 53.82  | 53.82         | 150    | 175.13 | 220  | 0.48 | 0.12 | <b>0.24</b> |
| MDY-19  | 5.53 / 1           | 17.27 | 0.00  | 95.50  | 95.50         | 173    | 175    | 220  | 0.48 | 0.12 | <b>0.25</b> |
| MDY-20  | 2.24 / 1           | 15.73 | 0.00  | 35.24  | 35.24         | 100    | 129.79 | 220  | 0.49 | 0.06 | <b>0.11</b> |
| MDY-21  | 2.00 / 1           | 16.24 | 0.00  | 32.48  | 32.48         | 120    | 158.96 | 220  | 0.47 | 0.09 | <b>0.19</b> |
|         | 6.00 / 2           | 17.68 | 0.00  | 103.20 | 103.20        | 200    | 198    | 220  | 0.45 | 0.20 | <b>0.44</b> |
| MDY-24  | 3,05 / 1           | 13.78 | 0.00  | 42.03  | 42.03         | 50     | 62.10  | 220  | 0.48 | 0.01 | <b>0.03</b> |
|         | 7.62 / 2           | 15.73 | 0.00  | 113.92 | 113.92        | 100    | 96.80  | 220  | 0.48 | 0.03 | <b>0.06</b> |
|         | 14.33 / 3          | 16.87 | 22.86 | 227.11 | 204.26        | 150    | 125.47 | 220  | 0.50 | 0.05 | <b>0.10</b> |
| MDY-25  | 5.24 / 1           | 15.73 | 0.00  | 82.43  | 82.43         | 100    | 104.95 | 220  | 0.56 | 0.04 | <b>0.07</b> |
|         | 8.05 / 2           | 16.87 | 0.49  | 129.83 | 129.34        | 150    | 140.66 | 220  | 0.58 | 0.07 | <b>0.12</b> |
| MDY-28  | 4.67 / 1           | 17.68 | 0.00  | 82.57  | 82.57         | 200    | 209.81 | 220  | 0.48 | 0.36 | <b>0.75</b> |
| MDY-29  | 6.10 / 1           | 16.24 | 0.00  | 99.06  | 99.06         | 120    | 120.28 | 220  | 0.47 | 0.05 | <b>0.10</b> |
| MDY-34  | 2.74 / 1           | 17.05 | 0.00  | 46.72  | 46.72         | 160    | 193.53 | 220  | 0.46 | 0.18 | <b>0.38</b> |
| MDY-36  | 6.10               | 17.61 | 0.00  | 107.42 | 107.42        | 195    | 191.54 | 220  | 0.48 | 0.17 | <b>0.35</b> |
| MDY-37  | 5.53/1             | 17.27 | 0.00  | 95.50  | 95.50         | 173    | 175    | 220  | 0.50 | 0.12 | <b>0.24</b> |
| MDY-40  | 5.19/1             | 16.87 | 0.00  | 87.56  | 87.56         | 150    | 155.07 | 220  | 0.56 | 0.08 | <b>0.14</b> |
|         | 9.05 / 2           | 17.68 | 0.00  | 10.30  | 155.80        | 145.50 | 200    | 220  | 0.63 | 0.13 | <b>0.21</b> |
| MDY-42  | 9.14 / 1           | 17.75 | 0.00  | 162.24 | 162.24        | 205    | 181.64 | 220  | 0.51 | 0.13 | <b>0.26</b> |
| MDY-44  | 3.96 / 1           | 16.87 | 0.00  | 66.81  | 66.81         | 150    | 165.92 | 220  | 0.48 | 0.10 | <b>0.21</b> |
| MDY-47  | 8.44 / 1           | 17.86 | 0.00  | 150.74 | 150.74        | 213.00 | 192.23 | 220  | 0.48 | 0.17 | <b>0.35</b> |
| MDY-48  | 2.19 / 1           | 16.87 | 0.00  | 36.95  | 36.95         | 150    | 192.40 | 220  | 0.53 | 0.17 | <b>0.32</b> |
| MDY-55  | 4.67 / 1           | 16.87 | 0.00  | 78.78  | 78.78         | 150    | 159.21 | 220  | 0.48 | 0.09 | <b>0.19</b> |

**Table 2 Detail resulted data of liquefied layers in each site of Mandalay City by using Mw 6.5 & PGA 10% probability**

| Site No | Depth(m)/<br>Layer | Gamma | u     | Sigma  | Eff.<br>sigma | Vs     | Vs1    | Vs1c | CSR  | CRR  | FS          |
|---------|--------------------|-------|-------|--------|---------------|--------|--------|------|------|------|-------------|
| MDY-3   | 5.53/1             | 17.27 | 0.00  | 95.50  | 95.50         | 173    | 175    | 220  | 0.35 | 0.12 | <b>0.34</b> |
| MDY-4   | 5.19 / 1           | 17.68 | 0.00  | 91.76  | 91.76         | 200    | 204.35 | 220  | 0.28 | 0.26 | <b>0.92</b> |
| MDY-08  | 5.58 /1            | 17.68 | 0.00  | 98.65  | 98.65         | 200    | 200.68 | 220  | 0.28 | 0.22 | <b>0.79</b> |
| MDY-10  | 5.19 /1            | 17.68 | 0.00  | 91.76  | 91.76         | 200    | 204    | 220  | 0.30 | 0.26 | <b>0.85</b> |
| MDY-11  | 3.19 /1            | 16.87 | 0.00  | 53.82  | 53.82         | 150    | 175.13 | 220  | 0.31 | 0.12 | <b>0.38</b> |
| MDY-19  | 5.53 /1            | 17.27 | 0.00  | 95.50  | 95.50         | 173    | 175    | 220  | 0.35 | 0.12 | <b>0.34</b> |
| MDY-20  | 2.24/ 1            | 15.73 | 0.00  | 35.24  | 35.24         | 100    | 129.79 | 220  | 0.33 | 0.06 | <b>0.17</b> |
| MDY-21  | 2.00 /1            | 16.24 | 0.00  | 32.48  | 32.48         | 120    | 158.96 | 220  | 0.31 | 0.09 | <b>0.29</b> |
|         | 6.00 /2            | 17.68 | 0.00  | 103.20 | 103.20        | 200    | 198    | 220  | 0.30 | 0.20 | <b>0.67</b> |
| MDY-24  | 3.05 /1            | 13.78 | 0.00  | 42.03  | 42.03         | 50     | 62.10  | 220  | 0.35 | 0.01 | <b>0.04</b> |
|         | 7.62 /2            | 15.73 | 0.00  | 113.92 | 113.92        | 100    | 96.80  | 220  | 0.35 | 0.03 | <b>0.09</b> |
|         | 14.33 /3           | 16.87 | 22.86 | 227.11 | 204.26        | 150    | 125.47 | 220  | 0.37 | 0.05 | <b>0.14</b> |
| MDY-25  | 5.24 /1            | 15.73 | 0.00  | 82.43  | 82.43         | 100    | 104.95 | 220  | 0.39 | 0.04 | <b>0.09</b> |
|         | 8.05 /2            | 16.87 | 0.49  | 129.83 | 129.34        | 150    | 140.66 | 220  | 0.40 | 0.07 | <b>0.16</b> |
| MDY-28  | 4.67 /1            | 17.68 | 0.00  | 82.57  | 82.57         | 200    | 209.81 | 220  | 0.33 | 0.36 | <b>1.10</b> |
| MDY-29  | 6.10 /1            | 16.24 | 0.00  | 99.06  | 99.06         | 120    | 120.28 | 220  | 0.32 | 0.05 | <b>0.15</b> |
| MDY-34  | 2.74 /1            | 17.05 | 0.00  | 46.72  | 46.72         | 160    | 193.53 | 220  | 0.31 | 0.18 | <b>0.57</b> |
| MDY-36  | 6.10               | 17.61 | 0.00  | 107.42 | 107.42        | 195    | 191.54 | 220  | 0.33 | 0.17 | <b>0.51</b> |
| MDY-37  | 5.53/1             | 17.27 | 0.00  | 95.50  | 95.50         | 173    | 175    | 220  | 0.35 | 0.12 | <b>0.34</b> |
| MDY-40  | 5.19/1             | 16.87 | 0.00  | 87.56  | 87.56         | 150    | 155.07 | 220  | 0.39 | 0.08 | <b>0.21</b> |
|         | 9.05 /2            | 17.68 | 0.00  | 10.30  | 155.80        | 145.50 | 200    | 220  | 0.44 | 0.13 | <b>0.31</b> |
| MDY-42  | 9.14 /1            | 17.75 | 0.00  | 162.24 | 162.24        | 205    | 181.64 | 220  | 0.35 | 0.13 | <b>0.38</b> |
| MDY-44  | 3.96 /1            | 16.87 | 0.00  | 66.81  | 66.81         | 150    | 165.92 | 220  | 0.33 | 0.10 | <b>0.30</b> |
| MDY-47  | 8.44 /1            | 17.86 | 0.00  | 150.74 | 150.74        | 213.00 | 192.23 | 220  | 0.32 | 0.17 | <b>0.53</b> |
| MDY-48  | 2.19 /1            | 16.87 | 0.00  | 36.95  | 36.95         | 150    | 192.40 | 220  | 0.38 | 0.17 | <b>0.45</b> |
| MDY-55  | 4.67 /1            | 16.87 | 0.00  | 78.78  | 78.78         | 150    | 159.21 | 220  | 0.33 | 0.09 | <b>0.27</b> |

### Development of Liquefaction Susceptibility Maps

For the study area, liquefaction susceptibility maps are created by means of GIS software using overall potential values ( $P_L$ ) of each point. These maps are evaluated for liquefaction susceptibility zones. The potential liquefaction hazard zone representing to five levels of liquefaction susceptibility such as very low, low, moderate, high and very high are shown in Figures (4 and 5). Each map represents different intensity values because of using different PGA values as shown in Table (1 & 2). The liquefaction potential ( $P_L$ ) maps by using PGA 2% probability should be considered for the construction of lifeline structures such as water pipe line, gas pipe line, transportation ways and telecommunication lines. The  $P_L$  maps using PGA 10% probability are appropriate for engineering construction of the various sorts of structures especially normal building. Most of the area falling  $P_L$  index  $> 25$  are more suffered the liquefaction susceptibility than other one.

Figure 4 represent liquefaction potential map of Mandalay City for PGA value of 10% probability in Mw-6.5. The maximum  $P_L$  index value of  $P_L$  map using 10% PGA value is 49.19. Figure 5 shows liquefaction potential map of the study area for PGA 2% probability of Mw-6.5. The highest  $P_L$  index value of  $P_L$  map using 2% PGA value is 51.09. By these maps, the very high representing red color and high (orange color) liquefied susceptible zones occurred at the western portions of Aungmyaythazan and Chanayethazan townships, and north western part of Mahaangmyay township. The very low or not probable potential liquefied area of Figure 4 is larger spaced than the area of Figure 5. Moderately liquefied zone represents yellow color.

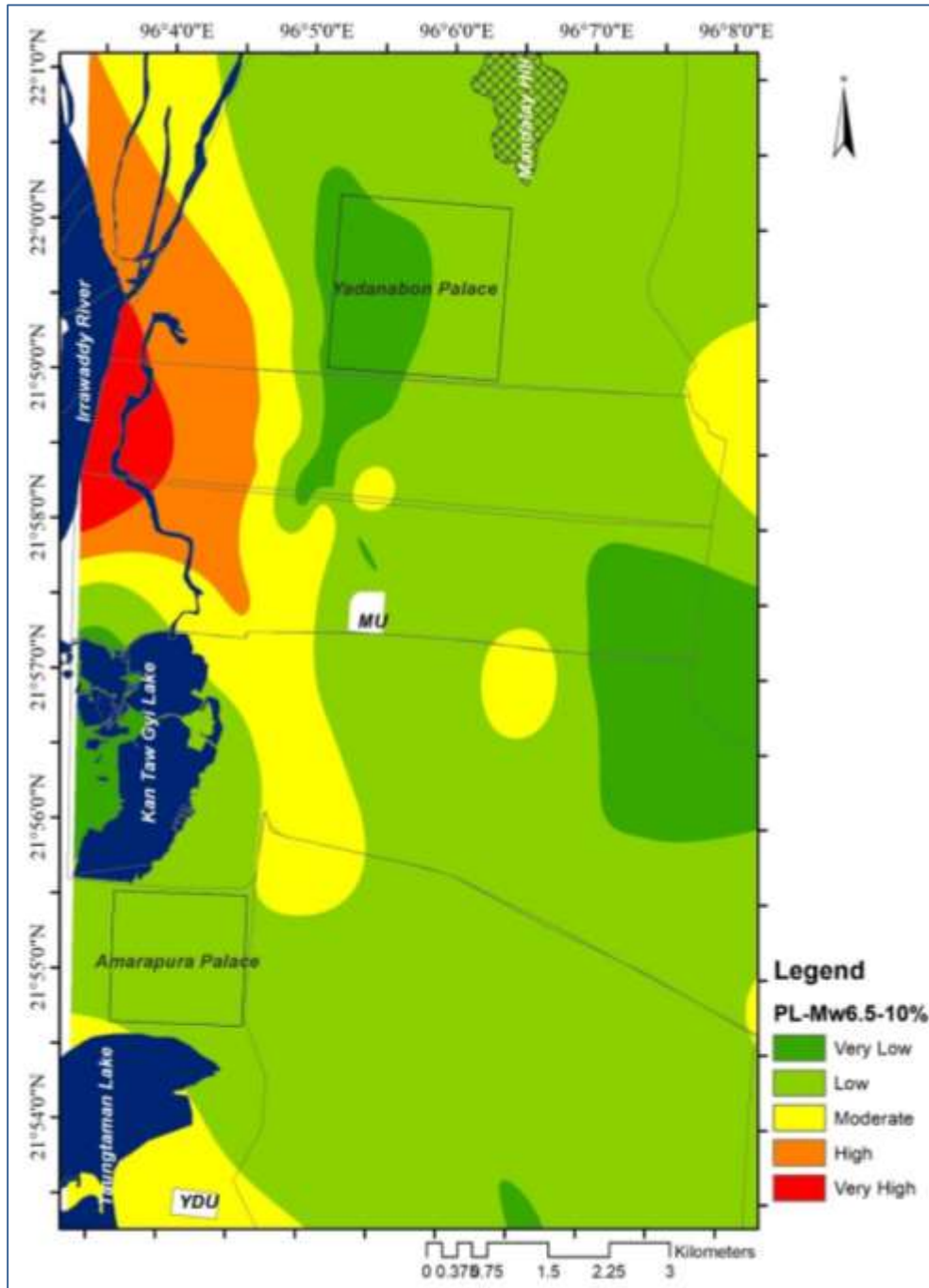


**Figure 4** Liquefaction potential map of Mandalay City using PGA10% probability and Mw-6.5

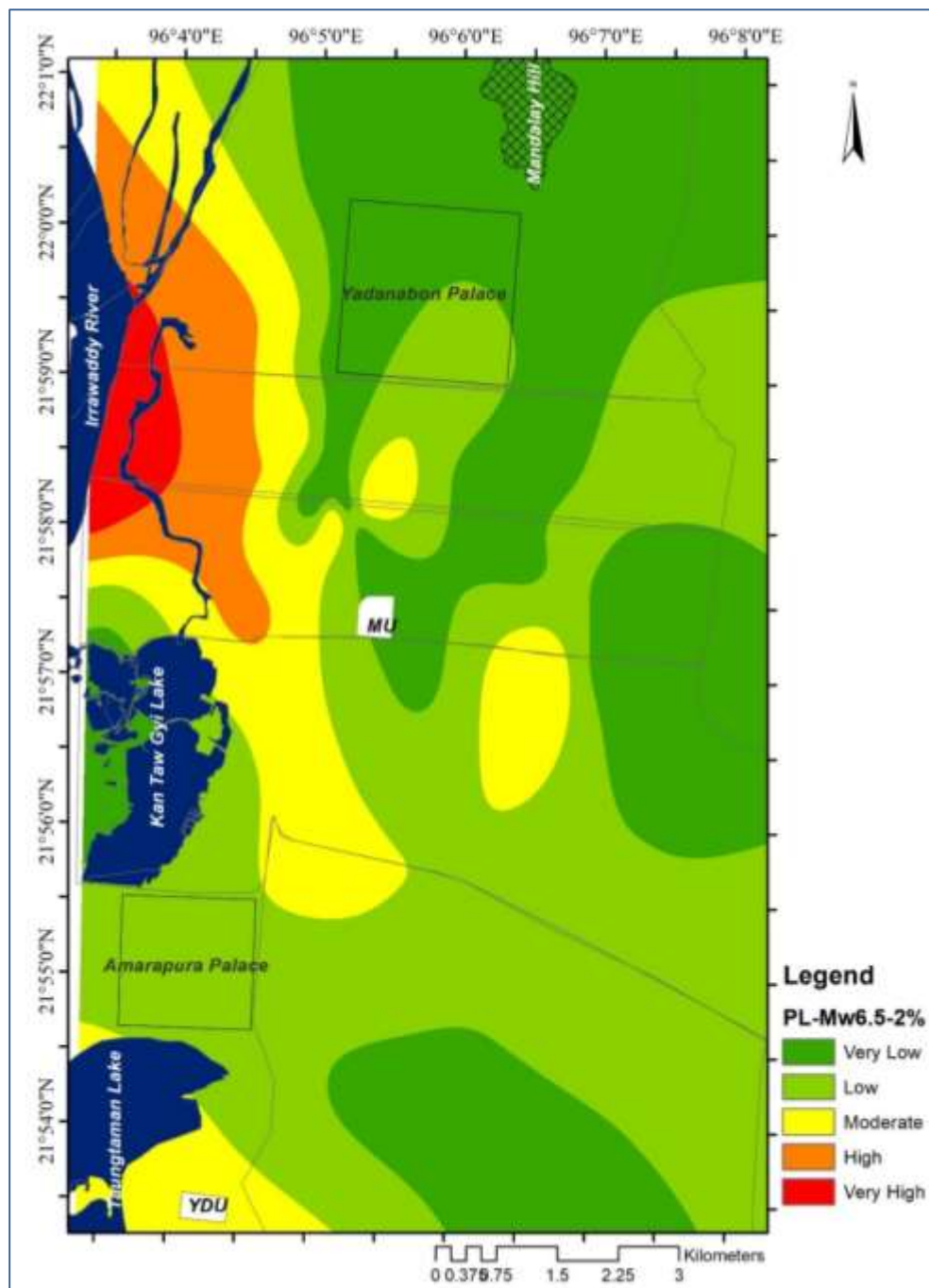


**Figure 5** Liquefaction potential map of Mandalay City using PGA 2% probability and Mw-6.5

### Conclusion

In this study, the liquefaction susceptibility of the study area had been calculated by using shear wave velocity, depth to water table and PGA value (2% & 10%) based on probabilistic seismic hazard assessment (PSHA). According to all resulted data, the high liquefaction susceptibility zone in the study area mainly lies under loose saturated soil, high thickness soil layer, low  $V_s$  value, shallow ground water depth and high PGA value. Exactly the northwestern portions of the study area fall under the very high liquefied zone due to representing maximum  $P_L$  index and low  $V_{s30}$  value. Thus, liquefaction susceptibility analysis is urgently needed for the study area in order to provide an effective mitigation plan for coming future earthquakes related hazards. The

produced  $P_L$  maps can be effectively used for development plans and risk management practices in the study area.

### Acknowledgements

We would like to express the heartfelt gratitude to Professor Hiroshi Kawase and Professor Junji Kiyono in Tokyo University, Japan for their constructive suggestion and supporting the machine to measure microtremor for various assessments in this research.

### References

- Bessason, B., and Erlingsson, S. (2011) Shear Wave Velocity in Surface Sediments, *JÖKULL No. 61, 2011*, <https://www.Research.gate.Net/publication/268384698>.
- CEN. (2004) EN 1998-1:2004, “Eurocode 8: Design of Structures for Earthquake Resistance – Part 1: General Rules, Seismic Actions and Rules for Buildings”, European Committee for Standardization.
- Chibber, H.L., 1934. The Geology of Burma, Macmilland. Com. & Limited, London, P538.
- Del Gaudio V, Wasowski J. (2013). Advances and Problems in Understanding the Seismic Response of Potentially Unstable Slopes, *Eng Geol* 122: 73-83.
- Dobery, R. et al. (2000) “New Site Coefficients and Site Classification System Used in Recent Building seismic Code Provisions, *Earthquake Spectra*, 16, pp. 41-67.
- Kawase, H., Francisco J. Sánchez-Sesma & Matsushima, S. (2011) “The Optimal Use of Horizontal-to-Vertical Spectral Ratios of Earthquake Motions for Velocity Inversions Based on Diffuse-Field Theory for Plane Waves”, *Bulletin of the Seismological Society of America*, Vol. 101, No. 5, pp. 2001–2014, doi: 10.1785/0120100263.
- Iwasaki, T., Tokida, K., and Arakawa, T. (1984) Simplified Procedures for Assessing Soil Liquefaction during Earthquakes. *Soil Dynamics and Earthquake Engineering*, v. 3(1), pp. 49–58.
- Myo Thant. (2013) Development of Seismic Microzonation Maps of Mandalay City, Mandalay Region, MES and MGS, Myanmar.
- Nakamura, Y. (1989) “A Method for Dynamic Characteristics Estimation of Subsurface using Microtremor on the Ground Surface,” *Quarterly Report of RTRI*, 30:1, 25-33.
- Seco e Pinto, P. S. (2002) “Eurocode 8 –Design Provisions for Geotechnical Structures”. Special Lecture, *3<sup>rd</sup> Croatian Soil Mechanics and Geotechnical Engineering Conference*.
- Soe Thura Tun & Ian M Watkinson (2017) The Sagaing Fault, Myanmar, Geological society London, Memoirs, Vol.48, Myanmar Geology, resources and Tectonics, Ch-19, pp. 413-441, <https://doi.org/10.1144/M48.19>.
- Win Swe (2013) “The Sagaing Fault of Myanmar: a brief overview, Geology of Sagaing Fault, in Commemoration of 9th Anniversary of MGS”, Myanmar Geosciences Society, Yangon, Myanmar, pp.1–20

## THE EXISTANCE OF HERCYNITE IN METAPELITES FROM MOGOK METAMORPHIC BELT

Wai Yan Lai Aung<sup>1</sup> and Thet Tin Nyunt<sup>2</sup>

### Abstract

Hercynite observed in the metapelitic rocks; sillimanite-garnet-biotite gneiss and felsic granulite rocks from Mogok and Momeik area. It is one of the spinel group minerals with the formula  $\text{FeAl}_2\text{O}_4$ . The present contribution provided and confirmed the presence of hercynite in pelitic rocks (gneiss and granulite) and pair essential assemblage of [Spinel (Hercynite)+Quartz] in Mogok Metamorphic Belt indicate that these rocks were experienced in/ developed under UHT metamorphism.

**Keywords:** Hercynite, Metapelitic, Granulite, Spinel, UHT metamorphism

### Introduction

**Hercynite** is one of the end-members of the spinel group in the spinel mineral series with the formula  $\text{FeAl}_2\text{O}_4$ . Chemical formula of common spinel is  $\text{MgAl}_2\text{O}_4$  and it is a Magnesium (Mg) spinel though hercynite is Iron (Fe) spinel. The Mg may be partially or fully replaced by Fe, Zn, and/or Mn. This leads to a mineral series with the formula  $(\text{Mg,Fe,Zn,Mn})\text{Al}_2\text{O}_4$ . It was first described in 1847 and its name originates from the Latin name for the Harz, Silva Hercynia, where the species was first found (Anthony, 1990), is a spinel of regular symmetry and normal cation distribution, but some disorder occurs in its structure. It consists of ferrous ( $\text{Fe}^{2+}$ ) ions and aluminium ions ( $\text{Al}^{3+}$ ), however some ferric ions ( $\text{Fe}^{3+}$ ) may be located in the structure of hercynite (Jastrzębska, 2015). General information of spinel mineral series is described in Table 1. Hercynite occurs in high-grade metamorphosed iron argillaceous sediments as well as in mafic and ultramafic igneous rocks (Anthony, 2001). The purpose of this paper is to provide and confirm the determination of metamorphic grade and facies and estimating *P-T* conditions of hercynite bearing pelitic rocks of Mogok Metamorphic Belt on the basis of mineral assemblages.

**Table 1 General information of the spinel mineral series (www.mineral.net)**

| The Spinel Mineral Series                                                                                                                                     |                             |
|---------------------------------------------------------------------------------------------------------------------------------------------------------------|-----------------------------|
| <b>Chemical Formula</b> : $\text{MgAl}_2\text{O}_4$                                                                                                           |                             |
| The Mg may be partially or fully replaced by Fe, Zn, and/or Mn. This leads to a mineral series with the formula $(\text{Mg,Fe,Zn,Mn})\text{Al}_2\text{O}_4$ . |                             |
| <b>The end-members of the Spinel group</b>                                                                                                                    |                             |
| <b>Spinel (or Magnesium Spinel)</b>                                                                                                                           | - $\text{MgAl}_2\text{O}_4$ |
| <b>Gahnite (Zinc Spinel)</b>                                                                                                                                  | - $\text{ZnAl}_2\text{O}_4$ |
| <b>Hercynite (Iron Spinel)</b>                                                                                                                                | - $\text{FeAl}_2\text{O}_4$ |
| <b>Galaxite (Manganese Spinel)</b>                                                                                                                            | - $\text{MnAl}_2\text{O}_4$ |
| <b>Composition</b> : Series of magnesium, iron, zinc, and/or manganese aluminum oxide.                                                                        |                             |

<sup>1</sup> Dr, Demonstrator, Department of Geology, University of Yangon (waiyanlaiaung@gmail.com)

<sup>2</sup> Dr, Director General, Department of Geological Survey and Mineral Exploration, Ministry of Natural Resources and Environmental Conservation

## Materials and Methods

Although spinels are widely distributed in nature, hercynite was analyzed by electron probe as a Fe Spinel and identified with the aid of petrological microscope. Minerals were analysed using the Electron Probe Micro Analyser (EPMA) Jeol, JXA 8200, equipped with SE- and a BSE-detector, 5 WDS crystal spectrometer and an EDS-analyser at Swiss Federal Institute of Technology (ETH) in Zurich, Switzerland. Operation conditions were: 15.0 kV applied accelerating voltage, 100  $\mu\text{m}$  beam size and 10 or 20 nA depending on the stability of the analyzed minerals under the electron beam. Hercynite bearing thin sections of different rock units exposed in the research area were analysed by means of polarizing microscope. Determination of metamorphic grade and facies and estimating *P-T* conditions of hercynite bearing pelitic rocks of Mogok Metamorphic rocks based on mineral assemblages and comparison is carried out on the literature and previous works of the area.

## Geology

The research area is situated within the northern part of Mogok Metamorphic Belt (MMB) of Searle and Haq, 1964 and Searle et. al., 2017. With reference to provided regional geological map (Myanmar Geosciences Society, 2014) (Fig. 1), rocks in the investigated area are categorized into medium-to-high grade metamorphic rock units and younger igneous intrusion. In metamorphic units, medium-to-high grade rocks consisting of marble, calc-silicate rocks, gneiss and granulite are exposed (Wai Yan Lai Aung, 2016) in the research area. Among them, hercynite can be noted from argillaceous pelitic rocks such as sillimanite-garnet-biotite $\pm$ ilmenite gneisses and felsic granulite. Location map is shown in (Fig. 2).

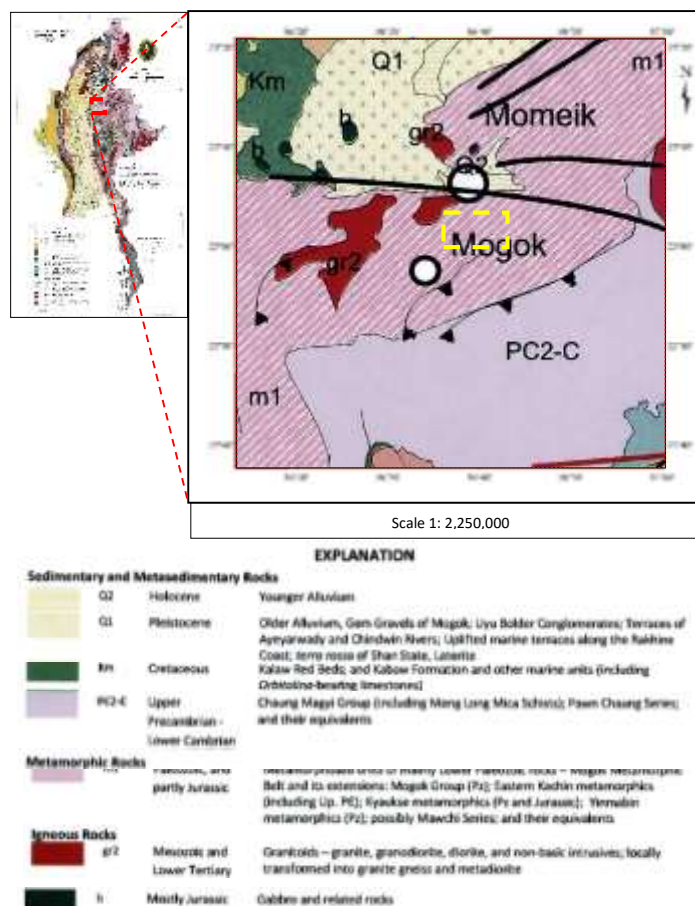


**Figure 1** Regional geological map of the research area and its environs (After Geological Map of Myanmar Geosciences Society, 2014).

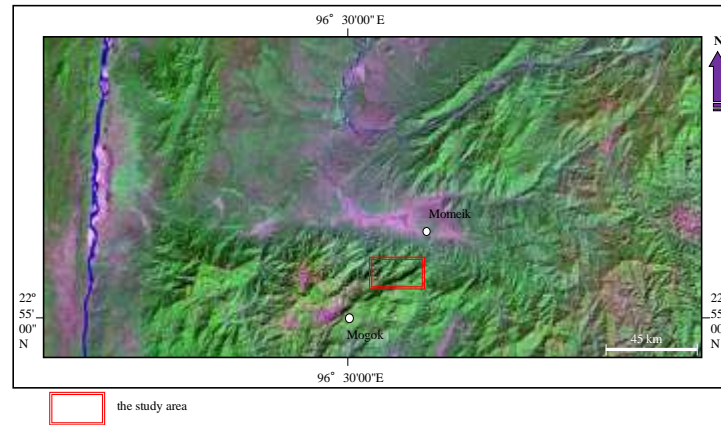


**Figure 2** Location map of the research and surrounding areas.

## Results

### Mineralogy

Hercynite is the predominant mineral of the sillimanite-garnet-biotite gneiss and felsic granulite units within the research area. In hand specimen, it is not distinct. Under the microscope, hercynite is characterized by its colour (greenish and black), medium- to coarse-grained subhedral to euhedral form, no cleavage and high relief in PPL. Isotropic nature is pronounced between XN (Kerr, 1977). In sillimanite-garnet-biotite gneiss, spinels (hercynite) show green and euhedral form (Fig. 3), which may probably formed by the releasing of alumina.

Mineral assemblages recognized in the sillimanite-garnet-biotite±ilmenite gneiss are (Fig. 4) :

Quartz + orthoclase + biotite + plagioclase + almandine + sillimanite + diopside + ilmenite + **spinel** + zircon + apatite + sphene + hypersthene

Quartz + orthoclase + plagioclase + biotite + almandine + sillimanite + ilmenite + **spinel**

Quartz + orthoclase + plagioclase + biotite + almandine + sillimanite + **spinel** + opaque + sphene

In some xenoblastic garnets, hercynites are observed as inclusions associated with small anhedral quartz grains, tabular biotite flakes and sillimanite as inclusions (Fig. 5)

Mineral assemblages of granulite rocks in the study area are:

orthopyroxene + alkali feldspar + biotite + plagioclase + chlorite + garnet + quartz + rutile + sapphirine + ilmenite + **hercynite** + sillimanite + zircon.

Hercynites, iron alumina spinels, are found as equant grains (Fig. 6). They show high relief, pale green under plane-polarized light and isotropic between cross nicols.

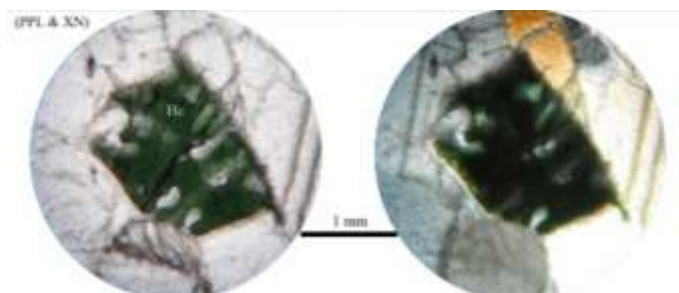


**Figure 3** Euhedral spinel (hercynite) in sillimanite-garnet-biotite gneiss

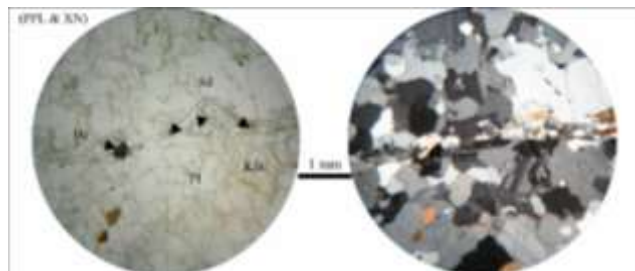


**Figure 4** Mineral assemblages of sillimanite, hercynite, quartz and feldspars in sillimanite-garnet-biotite-ilmenite gneiss

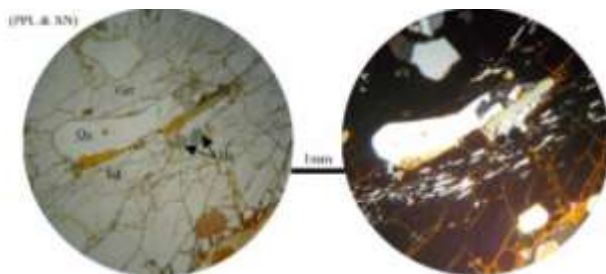


**Figure 5** Coarse-grained xenoblastic garnet with various inclusions (sillimanite trails, hercynite, quartz and biotite).

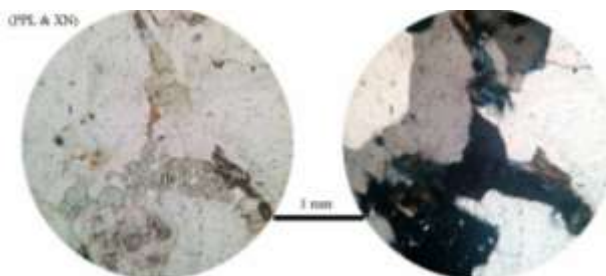


**Figure 6** Grains of hercynite in felsic granulite.

**Geochemistry**

Ilmenite and hercynite are diagnostic minerals of some acid granulitic assemblages. Electron microprobe analyses of spinel and ilmenite in sillimanite-garnet-biotite gneisses (Fig. 7) are shown in Table 2. Spinel in research area are ferroan aluminium spinel, hercynite. [Deer, Howie & Zussman, 1992](#), explained that the experimental investigation on the system  $FeAl_2O_4$  (hercynite) –  $Fe_3O_4$  (magnetite) shows there has complete solid solution above 858°C, but below this temperature, the two-phase region of exsolution widens with decreasing temperature. Hercynite forms complete solid solution with chromite and spinel but only limited solid solution with magnetite ([Rutley, 1991](#)). Hercynite of spinel series and ilmenite from the microprobe data are plotted as colourful dots on ternary diagrams of [Butler, 1998](#) (Fig. 8).

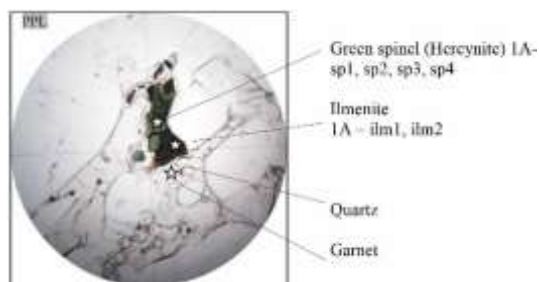


**Figure 7** Electron microprobe analyses of spinel and ilmenite in sillimanite-garnet-biotite gneisses

**Table 2 Analytical data of spinel and ilmenite in sillimanite-garnet- biotite gneiss**

| Name                                          | 1A-sp1 | 1A-sp2 | 1A-sp3 | 1A-sp4 | 1A-ilm1 | 1A-ilm2 |
|-----------------------------------------------|--------|--------|--------|--------|---------|---------|
| Symbol                                        | ●      | ●      | ●      | ●      | ●       | ●       |
| SiO <sub>2</sub>                              | 0.030  | 0.030  | 0.071  | 0.022  | 0.023   | 0.082   |
| TiO <sub>2</sub>                              | 0.093  | 0      | 19.300 | 0.154  | 46.410  | 43.740  |
| Cr <sub>2</sub> O <sub>3</sub>                | 0      | 0      | 0      | 0.552  | 0       | 0       |
| Al <sub>2</sub> O <sub>3</sub>                | 59.500 | 59.61  | 0.377  | 0      | 0.090   | 0.079   |
| Fe <sub>2</sub> O <sub>3</sub>                | 2.407  | 2.291  | 28.527 | 67.986 | 0       | 0       |
| FeO                                           | 27.844 | 27.648 | 46.879 | 30.992 | 50.120  | 52.600  |
| MnO                                           | 0.265  | 0.264  | 0.122  | 0.014  | 0.653   | 0.482   |
| NiO                                           | 0      | 0      | 0      | 0      | 0       | 0       |
| MgO                                           | 8.43   | 8.48   | 0.422  | 0.037  | 1.065   | 0.938   |
| CaO                                           | 0.039  | 0.008  | 0.002  | 0.019  | 0.010   | 0.024   |
| Na <sub>2</sub> O                             | 0      | 0      | 0.020  | 0.006  | 0       | 0       |
| K <sub>2</sub> O                              | 0.018  | 0.02   | 0.028  | 0.013  | 0.028   | 0.030   |
| Total                                         | 98.626 | 98.352 | 95.748 | 99.794 | 98.398  | 97.975  |
| FeAl <sub>2</sub> O <sub>4</sub> (Hercynite)  | 0.627  | 0.627  | 0.009  | 0      | -1.524  | -1.613  |
| MgAl <sub>2</sub> O <sub>4</sub> (Spinel)     | 0.338  | 0.343  | 0      | 0      | -0.058  | -0.051  |
| MnAl <sub>2</sub> O <sub>4</sub> (Galxite)    | 0.006  | 0.006  | 2.247  | 0      | -0.020  | -0.015  |
| FeFe <sub>2</sub> O <sub>4</sub> (Magnetite)  | 0.016  | 0.015  | 0.411  | 0.983  | 0       | 0       |
| MgFe <sub>2</sub> O <sub>4</sub> (Mg-Ferrite) | 0.009  | 0.008  | 0.007  | 0.002  | 0       | 0       |
| MnFe <sub>2</sub> O <sub>4</sub> (Jacobsite)  | 0      | 0      | 0.001  | 0      | 0       | 0       |

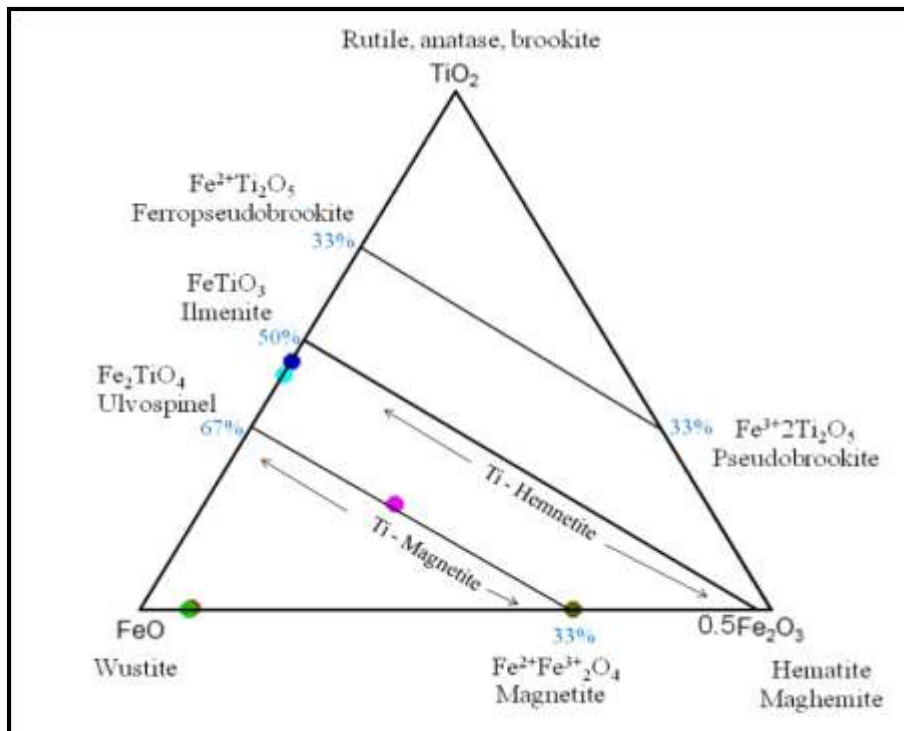


**Figure 8** The system FeO-Fe<sub>2</sub>O<sub>3</sub>-TiO<sub>2</sub> showing the major high-temperature solid solution series magnetite-ulvospinel, hematite-ilmenite, pseudobrookite-FeTi<sub>2</sub>O<sub>5</sub> plotted on a mol per cent basis (After Butler, 1998).

## Discussion

### Occurrences

Protolith of spinel-bearing rocks were clayey limestones and calcic limestones, which may become dolomitic limestone by metamorphism (Gübelin & Koivula, 2005). Spinel was formed both mafic igneous rock and metamorphic rock which found in carbonate series underwent high temperature amphibolite to lower granulite grade regional metamorphism (Malsy & Klemm, 2010). At Mogok, spinel was formed as a result of contact metamorphism or skarn metasomatism within regionally metamorphosed basement rocks where the presence of fluids played an important role (Iyer, 1953; Themelis, 2009), where, high temperature regional metamorphism and then larger - scale transformation of carbonate rocks, high mobilization and migration of many chemical elements and containing Al and Cr in the dynamothermal metamorphism of carbonate rocks (Kisin et al., 2016). Wai Yan Lai Aung, 2016, reported that, in Loi-Sau and its environs, sillimanite-garnet-biotite±ilmenite gneiss including spinel are high-grade gneiss and they are included in granulite facies. Moreover, she also contributed on granulite in Mogok and Momeik area.

In Mogok, Jedi spinel (Hot spinel) occurs as bright neon red spinel crystals and found in both Mogok Valley and the Namya area (Pardieu, 2014). Moreover, Man Sin Hot spinel in Mogok occurs as porphyroblast in marble and due to the presence of Cr (Thet Tin Nyunt and Phyu Phyu Win, 2018).

Ternary spinels in the system (Fe, Zn, Mg)  $Al_2O_4$  are apparently relatively common and widespread constituents of some metamorphic rocks in the amphibolite and granulite facies (Stoddard, 1979). High-grade metamorphic rocks of upper-amphibolite and granulite facies were reported in the Mogok metamorphic belt, central Myanmar (Yonemura et al., 2013; Maw Maw Win et al., and Wai Yan Lai Aung, 2016).

### *P-T* Condition

The temperature of spinel is about from 600°C and depending on the amount of magnesium which played an important factor during the genesis of spinel (Widmer, 2014). In Mogok Metamorphic Belt, Mitchell et. al., (2006) constrain that the K-feldsapr augen gneisses represents at  $4.9 \pm 1.7$  kbar and about 680 °C and Searle et. al., (2017) imply high-temperature sillimanite+muscovite metamorphism peak at  $4.9 \pm 1.7$  kbar and 680°C, and based on the result of EPMA. Yonemura et. al., (2013) found Grt-Opx granulite in the Mogok area, which was formed under pressure-temperature (*P-T*) conditions estimated as being 6.5-8.7 kbar and 800-950 °C with the aid of EPMA. Wai Yan Lai Aung and Maw Maw Win, et al., (2016) estimated petrologically and mineralogically that the metamorphic *P-T* conditions of pelitic gneisses in regional Mogok metamorphic belt with garnet-biotite-plagioclase-sillimanite-quartz assemblage and its peak metamorphic stage is 6–10 kbar and 780–850 °C. Ye Kyaw Thu, et al., (2016) reported a paragenesis with a spinel + quartz assemblage coexisting with Ti-rich biotite (up to 6.9 wt%  $TiO_2$ ) that formed under granulite facies conditions. They also suggest in (2017) that the *P-T* conditions of granulite facies paragenesis with Grt-Bt-Pl-Sil-Qtz and Grt+Crd+Sil+Bt+Qtz from the middle segment of the Mogok metamorphic belt is 6 – 7.9 kbar/ 800 – 860 °C and 6.5 kbar/ 820 °C, respectively. Wai Yan Lai Aung, (2017) calculated two occurrences of sillimanite-garnet-biotite gneiss with and without of pyroxene and hercynite minerals by using normalized composition of garnet, biotite and plagioclase from X-ray Fluorescence and Electron Microprobe analyses with Pseudosection and Perple\_X software. The *P-T* equilibration of hercynite bearing gneiss is higher than that of without; 6.5-9.3 kbar, 740-810 °C. In (2018), She also contributed the possible *P-T* condition of granulite rocks in Mogok and its environs, and the presence of spinel relics in sapphirine are shown in symplectitic intergrowths of the two minerals. Its development can be explained by the simple reaction: Spinel + Silica = Sapphirine (Deer, Howie & Zussman, 1992).

Schollenbruch, et al., (2010) investigated experimentally the stability of hercynite ( $\text{FeAl}_2\text{O}_4$ ) at high pressure and temperature between 7-24 GPa and 900-1700 °C. Hercynite breaks down to its constituent oxides at 7- 8.5 GPa and temperatures > 1000 °C. Zn-rich spinel is associated with quartz in the Al-rich metapelites of the Mashan complex, NE china and Al-rich metapelites from Mashan khondalite series are characterized by the assemblage Spl+Grt+Sil+Crd+Bt+Pl( $\text{An}_{72}$ )+Kfs+Quartz+graphite peak *P-T* condition is 820 °C and 8.0 kb (Guo, 2008). Spl + Qtz assemblage requires at least 840 °C (Bucher & Frey, 1994) and stated that hercynite spinel is present in metapelites with high  $X_{\text{Fe}}$  at 860 °C (Bucher, 2010). The rocks loose quartz between 620 °C (Mg-rich) and 670 °C (Fe-rich). At about 700 °C (at 600 °C), upper amphibolite facies, spinel appears at medium  $X_{\text{Fe}}$  in assemblages such as Spl + Grt + Crd. Spinel appears at a temperature 250 °C lower than in Qtz-saturated rocks. The assemblage Grt + Crd + Opx + Spl is characteristic for ultra-high grade metamorphism in Qtz-bearing rocks. In contrast, the temperature of Qtz-free rocks is as low as 700 °C. This shows that the pair Spl + Qtz is the essential assemblage for UHT metamorphism (Bucher, 2010). Hercynite from research area is associated with quartz and analysed by EPMA. Comparison of *P-T* analytical data and possible *P-T* condition in Mogok Metamorphic Belt (MMB) are shown in Table 3 and (Fig 9).

The spinels observed in the metapelitic rocks; sillimanite-garnet-biotite gneiss and felsic granulite of Mogok and Momeik area were identified as hercynite. A study of the chemical composition confirmed that it is iron aluminium spinel and the colour due to the Fe. In research area, hercynite bearing high-grade gneiss and felsic granulite indicate granulite facies and high-grade metamorphosed iron rich argillaceous sediments. The present study proved that hercynite in pelitic rocks (gneiss and granulite) and pair essential assemblage of [Spinel (Hercynite)+Quartz]] in Mogok Metamorphic Belt were experienced in/ developed under UHT metamorphism.

**Table 3 Comparison of *P-T* analytical condition and mineral assemblages in Mogok Metamorphic Belt (MMB)**

| Reference                | Rock Units of MMB                          | Analytical Methods       | Calculated mineral assemblages                | P / T                               |
|--------------------------|--------------------------------------------|--------------------------|-----------------------------------------------|-------------------------------------|
| Mitchell et al., 2006    | K-spar augen gneiss                        | EPMA                     | Bt-Sil-Pl-Kfs-Qtz                             | 4.9 ± 1.7 kbar/<br>& 680 °C         |
| Searle et al., 2007      | Sillimanite gneiss                         | EPMA                     | Sil-Mus                                       | 4.9 ± 1.7 kbar/<br>680 °C           |
| Yonemura et al., 2013    | Granulite                                  | EPMA                     | Grt-Opx                                       | 6.5 – 8.7 kbar/<br>800 – 950 °C     |
| Maw Maw Win et al., 2016 | Pelitic gneisses                           | Petrology/<br>Mineralogy | Grt-Bt-Pl-Sil-Qtz                             | 6 – 10 kbar/<br>780 – 850 °C        |
| Wai Yan Lai Aung, 2016   | Sillimanite-garnet-biotite-ilmenite gneiss | EPMA                     | Grt-Sil-Bt-Pl-Kfs-Qtz                         | 6.5 - 9.3 kbar/<br>740 - 810 °C     |
| Wai Yan Lai Aung, 2017   | Sillimanite-garnet-biotite gneiss          | EPMA                     | Grt-Sil-Bt-Pl-Kfs-Qtz                         | 6.2 - 8 kbar/<br>750 - 790 °C       |
| Ye Kyaw Thu et al., 2017 | Metasedimentary rocks                      | EPMA                     | Grt-Bt-Pl-Sil-Qtz                             | 6 – 7.9 kbar/<br>800 – 860 °C       |
| Ye Kyaw Thu et al., 2017 | Metasedimentary rocks                      | EPMA                     | Grt-Crd-Sil-Bt-Qtz                            | 6.5 kbar/<br>820 °C                 |
| Wai Yan Lai Aung, 2018   | Felsic granulite                           | Petrology/<br>Mineralogy | Opx-Grt-Bt-Rt-Sil-Plg-Kfs-Spr-Spl-Qtz-Zir-Ilm | <i>P-T</i> is greater than gneisses |
| Wai Yan Lai Aung, 2018   | Mafic granulite                            | Petrology/<br>Mineralogy | Cpx-Ca-Plg-Kfs-Qtz-Bt-Opx-Sp-Opq              | <i>P-T</i> is greater than gneisses |

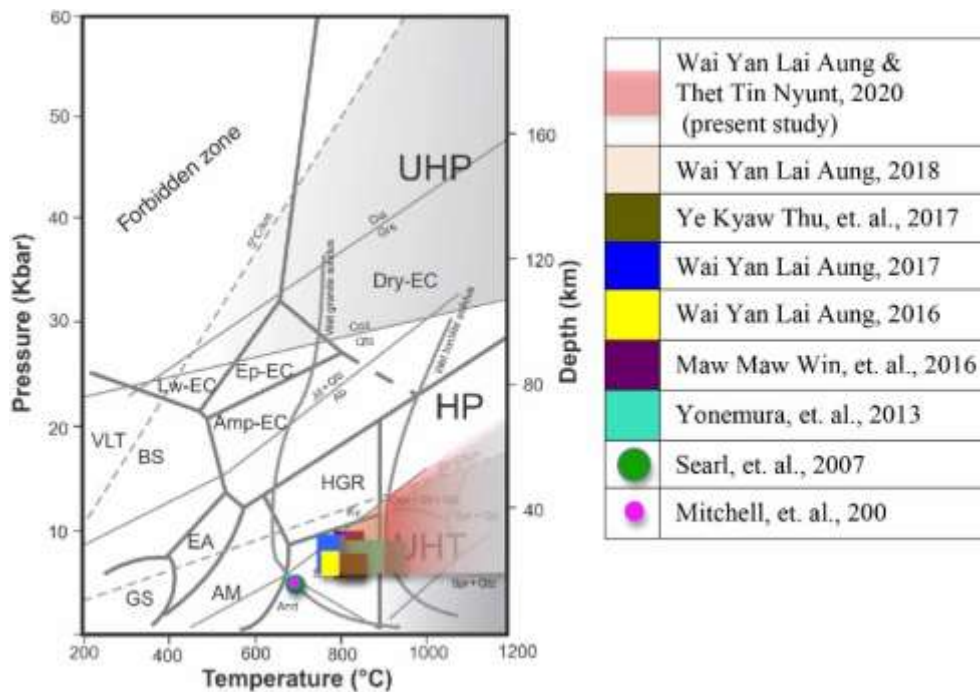


**Figure 9** *P-T* diagram showing the comparison of analytical data and possible *P-T* condition in Mogok Metamorphic Belt (After Liao et al., 1998, Harley, 1998, Okamoto and Maruyama, 1999, and Harley, 2004) UHP – ultrahigh pressure; UHT – ultrahigh temperature; VLT – very low temperature; AM – amphibolite; Amp-EC – amphibolite–eclogite; BS – blueschist; EA – epidote amphibolite; EC – eclogite; Ep-EC – epidote–eclogite; GR – granulite; GS – greenschist; HGR – high-grade granulite; Lw-EC – lawsonite–eclogite.

### Conclusion

The spinels observed in the metapelitic rocks; sillimanite–garnet–biotite gneiss and felsic granulite of Mogok and Momeik area were identified as hercynite. A study of the chemical composition confirmed that it is iron aluminium spinel and the colour due to the Fe. In research area, hercynite bearing high-grade gneiss and felsic granulite indicate granulite facies and high-grade metamorphosed iron rich argillaceous sediments. The present study proved that hercynite in pelitic rocks (gneiss and granulite) and pair essential assemblage of [Spinel (Hercynite)+Quartz] in Mogok Metamorphic Belt were experienced in/ developed under UHT metamorphism.

### Acknowledgements

The authors would like to express our sincere thanks to Dr. Day Wa Aung, Professor and Head, Department of Geology, University of Yangon for their permission to take this research. We would like to extend our sincere thanks to Prof. Hla Kyi, Part-time Professor, Applied Geology Department, University of Yangon, for his encouragement and advice. We would like to deeply grateful to Prof. Dr Christoph A. Heinrich and Prof. Dr Lucie Tajčmanová, Department of Earth Sciences, Institute of Geochemistry and Petrology, ETH Zurich for EPMA Analyses.

## References

- Anthony, J.W., (1990). *Handbook of mineralogy* (Vol. 4). Mineral Data Publishing.
- Anthony, J.W., Bideaux, R.A., Bladh, K.W. and Nichols, M.C., (2001). *Handbook of mineralogy*, Mineralogical Society of America. Chantilly, VA, pp.20151-1110.
- Bücher, K. and Frey, M., (1994.) *Petrogenesis of Metamorphic Rocks*, Springer-Verlag Berlin Heidelberg GmbH, pp.318.
- Bucher, K. and Grapes, R., (2011). *Petrogenesis of metamorphic rocks*. Springer Science & Business Media.
- Butler, C.J. and McCartney, D.G., (1998). An experimental study of phase transformations and a comparison with calculated phase equilibria in Ti–Al–Mn alloys. *Acta materialia*, 46(6), pp.1875-1886.
- Deer, W.A., Howie, R.A. and Zussman, J., (1992). *An introduction to the rock-forming minerals*, vol.696. London: Longman, pp.696.
- Guo, X., Takasu, A., Liu, Y. and Li, W., (2008). Petrological research of the high-T Al-rich pelitic rocks in the Mashan complex, NE China. In *Abstracts for Annual Meeting of Japan Association of Mineralogical Sciences 2008 Annual Meeting of Japan Association of Mineralogical Sciences* (pp. 65-65).
- Gübelin, E.J & Koivula, J.I., (2005). *Photoatlas of inclusions in Gemstones*, Opinio Verlag, Basel, vol.2, pp.829.
- Harley, S.L., (1998). On the occurrence and characterization of ultrahigh-temperature crustal metamorphism. *Geological Society, London, Special Publications*, 138(1), pp.81-107.
- Harley, S.L., (2004). Extending our understanding of ultrahigh temperature crustal metamorphism. *Journal of Mineralogical and Petrological Sciences*, 99(4), pp.140-158.
- Iyer, L.A.N., (1953). The geology and gem-stones of the Mogok Stone Tract, Burma. *Geological Survey of India Memoir*, 82, pp.100.
- Jastrzębska, I., Szczerba, J., Stoch, P., Błachowski, A., Ruebenbauer, K., Prorok, R. and Śnieżek, E., (2015). Crystal structure and Mössbauer study of FeAl<sub>2</sub>O<sub>4</sub>. *Nukleonika*, 60(1), pp.47-49.
- Kerr, P. F., (1977). *Optical Mineralogy*, 4<sup>th</sup> ed., Mc Graw-Hill, New York, pp.492.
- Kisin, A.Y, Murzin, V.V, Tomilina, A.V and Pritchyn, M.E., (2016). *Ruby- sapphire- spinel mineralization in marble of the middle and southern Urals: Geology, Mineralogy, and Genesis*, Pleiades Publishing, Ltd., vol.58, no.4, pp.385-402.
- Malsy, A. and Klemm, L., (2010). Distinction of gem spinels from the Himalayan mountain belt. *CHIMIA International Journal for Chemistry*, 64(10), pp.741-746.
- Myanmar Geosciences Society, (2014). Geological Map of Myanmar.
- Okamoto, K. and Maruyama, S., (1999.) The high-pressure synthesis of lawsonite in the MORB+H<sub>2</sub>O system. *American Mineralogist*, 84(3), pp.362-373.
- Pardieu, V., (2014). Hunting for “jedi” spinels in Mogok. *Gems & Gemology*, 50(1), pp.46-57.
- Rutley, (1991). *Element of Mineralogy*. 27<sup>th</sup> ed., revised by C.D.Gribble, pp.482.
- Schollenbruch, K., Woodland, A.B. and Frost, D.J., (2010). The stability of hercynite at high pressures and temperatures. *Physics and Chemistry of Minerals*, 37(3), pp.137-143.
- Searle, D. L. & Ba Than Haq, (1964). The Mogok Belt of Burma and its relationship to the Himalayan Orogeny. In *Int. Geol. Cong. India*, Twenty-Second Sec., India, Himalayan and Alpine Orogeny, Sec.11, pp.132-161.
- Searle, M.P., Morley, C.K., Waters, D.J., Gardiner, N.J., Htun, U.K., Nu, T.T. and Robb, L.J., (2017). Tectonic and metamorphic evolution of the Mogok Metamorphic and Jade Mines belts and ophiolitic terranes of Burma (Myanmar). *Geological Society, London, Memoirs*, 48(1), pp.261-293.
- Stoddard, A. and Osborn, J.F., (1979). Scheuermann's disease or spinal osteochondrosis: its frequency and relationship with spondylosis. *The Journal of Bone and Joint Surgery. British volume*, 61(1), pp.56-58.
- Themelis, T., (2008). *Gems & Mines of Mogôk: Fascinating Glimpses Into the Gemology, Geology and Gem Mining of Mogok, Myanmar (Burma)*. T. Themelis, pp.352.
- Thet Tin Nyunt and Phyu Phyu Win, (2018). The Chemical Characteristics of Man Sin Spinel, Mogok, *Journal of the MAAS, Myanmar*, Vo.XVI, No.5, pp.167-180.

- Thu, Y.K., Pa, W.P., Sagisaka, Y. and Iwahashi, N., (2016). Comparison of grapheme-to-phoneme conversion methods on a myanmar pronunciation dictionary. In *Proceedings of the 6th Workshop on South and Southeast Asian Natural Language Processing (WSSANLP2016)*, pp.11-22.
- Thu, Y.K., Enami, M., Kato, T. and Tsuboi, M., (2017). Granulite facies paragneisses from the middle segment of the Mogok metamorphic belt, central Myanmar. *Journal of Mineralogical and Petrological Sciences*, 112(1), pp.1-19.
- Wai Yan Lai Aung, (2016). *Mineralogy and Petrology of the Igneous and Metamorphic Rocks of the Mount Loi-Sau and Its Environs, Momeik Township, Shan State (North)*, (Doctoral dissertation, Ph.D, Thesis) Department of Geology, University of Yangon (Unpublished), pp.169.
- Wai Yan Lai Aung, (2017) Petrology, Phase Equilibria Modelling and *P-T* Conditions of High-Grade Gneiss from the Mount Loi-Sau and its Environs, Mogok Township, Mandalay Region and Momeik Township, Shan State (North), *Journal of the MAAS, Myanmar*, Vo.XV, No.5, pp.97-113.
- Wai Yan Lai Aung, (2018), Granulite and its *P-T* Condition of the Mount Loi-Sau and its Environs, Mogok Township, Mandalay Region and Momeik Township, Shan State (North), *Journal of the MAAS, Myanmar*, Vo.XVI, No.5, pp.131-150.
- Widmer, R., Malsy, A.K. and Armbruster, T., (2015). Effects of heat treatment on red gemstone spinel: single-crystal X-ray, Raman, and photoluminescence study. *Physics and chemistry of minerals*, 42(4), pp.251-260.
- Win, M.M., Enami, M. and Kato, T., (2016). Metamorphic conditions and CHIME monazite ages of Late Eocene to Late Oligocene high-temperature Mogok metamorphic rocks in central Myanmar. *Journal of Asian Earth Sciences*, 117, pp.304-316.
- Yonemura, K., Osanai, Y., Nakano, N., Adachi, T., Charusiri, P. and Zaw, T.N., (2013). EPMA U-Th-Pb monazite dating of metamorphic rocks from the Mogok Metamorphic Belt, central Myanmar. *Journal of Mineralogical and Petrological Sciences*, 108(3), pp.184-188.



## Methods of Study

Before going to the field literature and topographic maps were studied as a base. One-inch topographic map 84K/16 was used as a base map. As a result, the trend of outcrops, faults and folds are checked thoroughly and structural data was precisely plotted on it. In order to make the facies analysis and to construct the facies model of each unit, detail records of stratigraphic measurements were undertaken along Seikwa chaung in which the best rock units of Shwezettaw and Padaung Formations are well exposed for the purpose of facies analysis.

### General Statement

The Kangyigon - Chaungshe area is located in the eastern part of the Minbu Basin within the Centre Cenozoic Belt. It is essentially composed of the clastic sedimentary rock-units of the Cenozoic age, consisting of sandstone, clay, shale and conglomerate (in order of abundance). The rock-units of the area in ascending order are Shwezethaw formation (Early Oligocene) and Padaung formation (Middle Oligocene).

## Result

### Description of Facies

#### **Facies A (Thick-bedded to massive, grain supported conglomerate)**

Its lower contact is sharp, commonly flat and erosional. It consists of crowded gravelly clasts mainly intrabasinal arrangement along an erosional plane (Fig.2). The clasts mainly of pebble-size, the geometry of this facies is variable, so are internal organization, composition and thickness. They are chiefly composed of mud clasts, fossils, and shell fragments. This facies is well developed in the Shwezettaw and Padaung Formations. It may be interpreted as the base of distributary channel deposits or lag deposits (Reading, 1996).

#### **Facies B (Thick-bedded to massive, gritty sandstone)**

In this facies, sub rounded to rounded gravelly clasts in a sandy matrix are simple in composition, sorted and faintly imbricated (Fig.3). Its contact is commonly gradational. It is developed in the Shwezettaw and Padaung Formations and is assigned to have deposited in distributary mouth bar and channel fill.

#### **Facies C (Trough cross- stratified sandstone)**

It occurs as grouped trough-shaped cross-bedding sets (Fig.4). Its lower contact is sharp and erosional. It is assigned to have deposited in an upper flow regime (see also Reineck & Singh 1980) and in the distributary channel deposits and distributary mouth bar deposit of delta front environments (Reading, 1996).

#### **Facies D (Massive or crudely bedded sandstone, moderately sorted to sorted)**

The surface portion of the facies exhibits solution pits and holes due to the removal of concretions and numerous iron nodules (Fig.5) are remarkably recognized and is assigned to be deposited in the distributary channel and mouth bar of delta front environment influenced by fluvial sedimentation (Reineck & Singh (1980), Reading (1996) and Campbell (1967). This facies is clearly seen not only in the upper part of Pandaung Formation but also in the upper and lower sandstone members of Shwezettaw Formation.

### **Facies E (Planar cross-stratified sandstone)**

The contact is sharp, erosional. It is well developed in Shwezettaw Formation (Fig.6). This facies is gradually succeeded by horizontal stratified sandstone (Facies F) and may be assigned to have been formed in the distributary channel and distributary mouth bar deposits of delta front environment (Reading,1996 and Reineck & Singh, 1980), and channel fill deposits of the marsh and river channel deposit (Reineck & Singh, 1980).

### **Facies F (Horizontal-laminated sandstone)**

This facies is developed in fine to medium grained sandstone and it is characterized by the presence of horizontal laminations (Fig.7). The contact is sharp, either flat or slightly concave. This facies is also developed in Shwezettaw and Padaung Formations. It may be interpreted to have been formed in lower and upper flow regime (Reineck & Singh, 1980).

### **Facies G (Ripple-laminated sandstone and / or siltstone)**

They are formed in the upper part of the Shwezettaw Formation (Fig.8). They consist of alternating very thin beds of fine-sand, shale and siltstones. They belong to lower flow regime (Reineck & Singh, 1980) and may be assigned to have been deposited in subaqueous levees, distributary mouth bar deposits. The contacts are commonly sharp and non-erosional.

### **Facies H (Thin to medium bedded sandstone with wavy bedding)**

In this facies, mud and sandy layer alternate and form continuous layers. The contact is commonly gradational and erosional (Fig.9). The genesis of this facies requires conditions where the deposition and preservation of both sand and mud are possible (Reineck & Singh, 1980). The facies is commonly associated with Facies E, F and M and only found in Shwezettaw Formation. This facies may be assigned to have been deposited in environment of subaqueous levee deposits of delta.



**Figure 2** Facies (A) Intraformational conglomerate in Padaung Formation (N 21° 00' 23" E 94° 59' 42")

**Figure 3** Facies (B) Thick bedded to massive gritty sandstone in Padaung Formation (N 21° 00' 24" E 94° 59' 47")



**Figure 4** Facies (C) Trough cross-stratification in buff color massive sandstone of Shwezettaw Formation (Tin Aung Myint, 2001) (N 21° 02' 26" E 94 57' 51")

**Figure 5** Facies (D) Massive or crudely bedded sandstone in Shwezettaw Formation. (N 21° 00' 23" E 94° 59' 47")



**Figure 6** Facies (E) Large scale planar cross stratified sandstone in Shwezettaw Formation (N 21° 00' 24" E 94° 59' 47")

**Figure 7** Facies (F) Horizontal (or) parallel bedding in Padaung Formation (N21° 02' 32" E 94° 57' 52")

### **Facies I (Thick- bedded silty sandstone with lenticular bedding)**

In this facies, the ripples or sandstone lenses are discontinuous and sometimes isolated in nature both in vertical and horizontal directions (Fig.10). According to Reineck and Singh (1980), near the delta front environment, sediments are more silty and parallel and lenticular laminations are common. Thus, this facies is commonly associated with horizontal laminated Sandstone (Facies D). Therefore it should be assigned to the prodelta association (Reineck & Singh, 1980).

### **Facies J (Hard and compact sandstone)**

This facies is characterized by fine-to coarse-grained sandstone (Fig11). The contact is commonly sharp, flat and non-erosional. This facies is commonly associated with facies M, N, O and distributed in Padaung Formation. It may be interpreted as prodelta.

### **Facies K (Thin to thick bedded structureless sandstone)**

This facies consists of thin to thick bedded structureless sandstone and has 0.1 to 2 m in thickness (Fig.12). The contact is sharp and erosional. They are well-developed in Shwezettaw Formation. It is associated with Facies D,G,N,O. It may be assigned to be deposited in channel fill and distributary mouth bar deposit of delta.

**Facies L (Thin to medium bedded, sand, silt and clay or mud interbeds)**

In this facies, thin to medium bedded sand, silt and clay or mud are interbedded with different thickness (Fig.13) The contact is sharp and erosional. It is developed in Shwezettaw Padaung Formations. This facies may be assigned to be deposited in distributary mouth bar and prodelta.

**Facies M (Thin laminated silt and silt clay with thin-bedded sandstone)**

In this facies, internally laminated silt and silty clay are present (Fig.14). It is very common in all formations and it is variable in relationship with associated facies. It may be assigned to be deposited in the prodelta and distributary channel (see also Reineck and Singh, 1980). The contact is sharp and gradational.

**Facies N (Shale or silty shale with thin bedded sandstone)**

In this facies, internally laminated shale or silt shale are present (Fig.15). Its contact is sharp and gradational. It is also developed in Shwezettaw and Padaung Formations. This facies may also be interpreted to have been deposited in prodelta and distributary channel.

**Facies O (Massive clays and mudstone)**

This facies is characterized by fine grained sediments mainly clay and silty clay (Fig.16). They are commonly bluish grey to buff in color. They are usually friable and massive but sometimes show layering. The thickness ranges up to 25 m. Sometime they show homogeneous beds and are likely to be formed by organic process, inorganic process and grain flow (Reineck & Singh, 1980). The contact is commonly sharp and erosional. This facies may also be interpreted to have been deposited in prodelta, distributary channel and well drained swamps environment (Reineck and Singh, 1980 & Reading, 1996).

**Lithofacies Association**

At least 3- lithofacies associations can be established in the Paleogene sequence of the study area. They are delta plain (subaerial topset), delta front (subaqueous topset) and prodelta.

**Delta plain (subaerial topset) Association**

Delta plain (subaerial topset) deposits are marsh and river channel deposits (Reineck and Singh, 1980). In the present work, the association can be correlated with well-drained swamp deposit, channel fill and subaerial levee deposit of "The Swamp Deposits of the Atchafalaya Basin" proposed by Coleman (1965).



**Figure 8** Facies (G) Possible bifurcated ripple laminated sandstone of Shwezettaw Formation (N 21° 02' 56" E 94° 57' 36")

**Figure 9** Facies (H) Thin-to medium-bedded sandstone in Shwezettaw Formation. (N 21° 2' 51" E 94° 58' 03")



**Figure 10** Facies (I) Thick bedded silty sandstone with lenticular bedding in Padaung Formation. (N 21° 2' 26" E 94° 57' 51")

**Figure 11** Facies (J) Thin-to medium-bedded, hand and compact sandstone in Padaung Formation (N 21° 02' 20" E 94° 57' 52")



**Figure 12** Facies (K) Thin-to thick-bedded structure less sandstone in Shwezettaw Formation. (N 21° 02' 50" E 94° 58' 02")

**Figure 13** Facies (L) Thin-to medium-bedded sand, silt and clay (or) shale interbeds (upper and lower) in Shwezettaw Formation ( N 21° 00' 22" E 94° 59' 43")



**Figure 14** Facies (M) Thin laminated silt and silty clay with thin-bedded sandstone in Padaung Formation (N 21° 02' 50" E 94° 58' 03")

**Figure 15** Facies (N) Shale or silty shale with thin-bedded sandstone in middle Shwezettaw Formation (N 21° 02' 20" E 94° 57' 57")



**Figure 16** Facies (O) Massive clay sequence in Padaung Formation (N 21° 03' 02" E 94° 57' 55")

According to Reineck and Singh (1980), channel fill deposits are made up of coarser and poorly sorted sediments than the adjoining deposit. Deposition in the channel takes place by the migration of point bars and braid bars. This association represents sedimentation in stream channels that have been abandoned by a stream because of cut-off process or avulsions (Reineck & Singh, 1980). Moreover, various sizes of large-scale planar type cross-beddings are the most common features of this deposit. Thus, in the study area, channel fill deposit may be the combination of facies B, D, E, H and K because of the lack of lenticular bedding and parallel bedding.

Wood-chips, leaf imprints, structureless sandstone of facies K and planar cross-stratified sandstone of Facies E are only the indicators of channel fill deposit According to Reineck and Singh, (1980), subaerial levee deposit show current ripple and ripple beddings. Irregular lamination is very common. Unfortunately, current ripple is hardly to find in the area. However, common irregular lamination is horizontal laminated sandstone of facies (F) which are due to interference by grass roots in sedimentation (Reineck & Singh, 1980). Iron nodules and carbonate nodules are abundant. Thus Facies of D, E, F, K, L, M, N reveal that it is through to be assumed the subaerial levee deposit. This deposits are associated with channel fill deposit. Moreover, the calcium carbonate which is also concentrated along bedding and low organic matter is present in Facies O. Thus it is reasonable to say that those facies are thought to be assumed as well drained swamp deposits.

Therefore in general, most of the lower part of Shwezettaw Formation is subaerial topset deposit. In the Shwezettaw Formation, due to the present of gypsum deposits, this facies association is deposited in the arid climate.

In short subaerial topset association which is occurred at the lower part of the Shwezettaw Formation generally consist of thick-bedded to massive gritty sandstone, Facies B, massive or crudely bedded structureless sandstone, Facies D, planar cross-stratified sandstone. Facies E, thin to thick-bedded structureless sandstone. Facies K, sand/shale interbeds Facies L, thinly laminated silt and silty clay Facies M, shale or silty shale facies N, massive clays and mudstone Facies O.

In this respect, it is reasonable to conclude that during the progradation of delta, fluvial-influenced sedimentation had occurred in this sequence.

### **Delta front (subaqueous topset) Association**

In fact, subaqueous topset deposits are delta front deposits including channel deposits, natural levee deposits and flood basin deposits and, thus, these are accumulation almost entirely under the influence of fluvial processes. The most common sedimentary structures in the distributary channel deposit are cross-beddings, scour-and-fill structures and erosional surfaces. Intraformational deformation structures such as slump structures are commonly found (Reineck & Singh, 1980). Thus, this feature may be present in the thinly laminated silt and silty clay with thin bedded sandstone of (Facies L) in the area.

As the channel flume s out downstream, current direction become variable and current velocity is reduced. Thus, rate of deposition of sediments is increased. In the view, the significant coarse-grained facies such as A, D are thought to be considered as distributary channel. Another factor is that, the most common sedimentary structures like cross beddings, current ripples and erosional surfaces which are present in the study area are the best indicator of this deposit. In this respect, Facies of D,C, E, F, M & N may be distributary channel deposits.

Subaqueous levees are the submarine ridges broadening and shoaling of the channel. Locally combined current and wave action produce complex type of cross bedding (Reineck & Singh, 1980). The determination of planar cross-bedding (Facies, C) which angle is 30° points out the current actions. However, ripple-laminated sand or siltstone (Facies, F) is occurred, pointing

out the wave action as the presence of bifurcation. Thus, in the area both current and wave actions happened in subaqueous topset sequence. The distinct wavy bedding (Facies, H) occurred in the middle part of Shwezettaw Formation and burrows in (Facies, D, K, O) point out the characteristic features of subaqueous levees.

Distributary mouth bar is a sandy shoal formed near the seaward limit of the distributary channel. The role of sedimentation is exceptionally higher than in any gritty sandstone-Facies B are the distinctive features of this mouth bar. In short, the middle and upper part of Shwezettaw Formation and the upper sand capping of Padaung Formation belong to the subaqueous topset sequence.

In conclusion, the general accepting of subaqueous topset association includes conglomerate; Facies A, through cross-bedded; Facies E, horizontal laminated silty clay; Facies; M, silty shale; Facies N, and massive clay; Facies O.

### **Prodelta Association**

This facies association represents the region seaward of the delta front environment which is closely associated with the prograding delta system. This facies association is characterized by fine-grained muddy sediments of massive clay (Facies O), shale or silty shale (Facies N). This prodelta deposits are transitional into the shelf-mud deposit. Near the delta-front environments, the sediments are more silty and parallel and lenticular beddings are common. Thus, lenticular bedding (Facies I) and horizontal laminated sandstone (Facies F) are the belt examples for the prodelta association. Sediments show layering due to difference in both colour and grain size. This thinly laminated silt and clays are the most noticeable features in prodelta association.

Localized hard and compact sand of (Facies J) are occurred in it. It is overlain by the thin the medium bedded sand-silt and clay or mud interbed (Facies L), laminations are common. These are eventually represent by (Facies L, D, F). Thus, in prodelta environment, clays predominate and mostly colour layering predominates in it. Shell remains and wood fragments are also present. Thus, Facies of B, N and O are indicative of prodelta association.

### **Summary and Conclusion**

The Tertiary molassic sediments exposed in the Kangyigon Chaungshe area is covering about 19.5 square miles and situated between N 21° 2' to 21° 8' and E 94° 57' to 95° 0'. It falls in 84K/16 one inch topographic map. The area is mainly composed of sandstone, clay, shale and conglomerate in order of abundance. The stratigraphic succession in descending order is Padaung Formation and Shwezettaw Formation which are the age of Oligocene. On the whole, the petrographic characters of these formations are generally the same and fall within the same field of arkosic composition. Thus, only the stratigraphic characters and primary sedimentary structural assemblages can differentiate one formation to another. On the basis of its distinctive lithologic features including color, bedding, composition, texture, fossils and sedimentary structures, at least 15 lithofacies has been recognized in the study area. In the Paleogene sequence of the area, at least three lithofacies associations has been established, delta plain, delta front and prodelta. The former two are concerned with Shwezettaw Formation and the latter one combined with delta-front (Subaqueous topset) is responsible for Padaung Formation. According to the field evidences and facies model, the depositional environments for Shwezettaw and Padaung Formations are deltic environments.

## **Acknowledgements**

We acknowledge Rector Dr Aung Aung Min, Pro-rectors Dr Si Si Khin, Dr Tin Moe Thuza and Professor Dr Htay Win, Head of Geology Department, Yadanabon University for their encouragement and permission to accept this paper. Special thanks are extended to all members of the journal of the Myanmar Academy of Arts and Sciences for allowing us to publish the paper in journal. Thanks are also due to responsible personnel from village in the area for their hospitality and willing help during field trip.

## **References**

- Campbell, C.V., (1967), Lamina, Laminaset, bed and bed set, *sedimentology*.
- Colman, C.F., & Gayliano., (1965) *Ecological changes in a marine fresh water clay sequences*, Trans Gulf Coast Assoc. Geol. Soc. Ic.
- Reading , H. G (1996), *Sedimentary environments & facies* Oxford, Black Well Sci- Publications.
- Reineck, H.G., & Singh, I.B (1980), *Depositional environment*, New York, Springer, Verlag.
- Tin Aung Myint, (2001). Geology and Geomorphology of the Tawintaung Area, Pagan-Nyaung-U Township, Myanmar, Unpublished MSc Thesis, Department of Geology, University of Mandalay.

## PERISSODACTYLA FROM THE NEOGENE SEDIMENTS OF MYANMAR

Zin Maung Maung Thein<sup>1</sup>, Thaung Htike<sup>2</sup>, Maung Maung<sup>3</sup>

### Abstract

The order Perissodactyla contains three distinct families, Equidae, Rhinocerotidae, Tapiridae, distributing in the tropical forest of Asia, North and South America and Savana of Africa. Extant species of this order are a remnant of the well-diversified group which probably originated during the Paleocene or early Eocene in Indian subcontinent. In Myanmar, fossil remains of this lineage have been documented in the Neogene sediments of central Myanmar representing Chalicotheriidae (*Chalicotherium*, cf. *Nesterotherium* and two indeterminate genera) Rhinocerotidae (“*Diceratherium*”, *Brachypotherium*, *Rhinoceros*, *Dicerorhinus* and one indeterminate genus) and Equidae (*Hipparion* and *Equus*). In contrast to the present day arid condition in central Myanmar, the occurrences of the forest dwelling perissodactyla such as chalicotherids, *Dicerorhinus*, *Rhinoceros* indicates the existence of the considerable forested condition in central Myanmar. Stable isotope results of the *Hipparion* and *Brachypotherium* also suggest the dominance of closed environment in central Myanmar until the Pliocene. The expansion of grassland in central Myanmar is probably later than or different from that of Siwaliks of northern Pakistan due to occurrences of forest dwelling mammals in the Pliocene or later periods

**Keywords:** Chalicotheriidae, Equidae, Neogene, Paleoenvironment, Systematic Paleontology,

### Introduction

The order Perissodactyla, the odd-toed ungulates, contains at least 17 extant species belonging to three distinct families, Equidae (horses, zebras and asses), Rhinocerotidae (rhinoceros), and Tapiridae (tapirs). Most species of this order are now distributed in the tropical forest of Asia, North and South America and Savana of Africa. Extant species of perissodactyla are a remnant of the well-diversified group which probably originated during the Paleocene or early Eocene in Indian plate during its final drift toward Eurasia Continent in late Eocene and dispersed to India from Afro–Arabia or a contiguous area (Rose et al., 2014). Since then, this lineage became distributed in the Cenozoic of Europe, Asia, Africa and America. At the end of the Pleistocene, most species of this lineage became gradually extinct, now facing in the danger of extinction.

In Myanmar, fossil remains of Perissodactyla are recovered from the late Eocene Pondaung Formation and Neogene sediments of central Myanmar. The late Paleogene Pondaung Formation is well known for yielding at least 10 genera of archaic perissodactyla belonging to the families, Indolophidae, Deperetellidae, Amynodotidae, Brontotheriidae and Rhinocerotidae (Tsubamoto et al., 2006). In the Neogene sediments, remains of extant families, Rhinocerotidae and Equidae, and extinct family, Chalicotheriidae are discovered. However, the species diversity of this lineage as well as density of fossil finding is low compared to its counterparts, Artiodactyla and Proboscidea.

In the present work, we carry out the systematic paleontology of the newly discovered perissodactyla fossils from the Neogene sediments of central Myanmar and then elucidate the paleoecology of these extinct animals, implicating to the paleoenvironment of central Myanmar in the Neogene.

---

<sup>1</sup> Professor, Department of Geology, University of Mandalay

<sup>2</sup> Pro-rector, Department of Geology, University of Magway

<sup>3</sup> Pro-rector (Rtd.), Myingyan University

## Geological Setting

The terrestrial Neogene sediments are widely distributed along the Ayeyarwady and Chindwin Rivers in Central Myanmar Basin. This basin contains a series of pull-apart sub-basins, which were affected by the oblique subduction of the Indian oceanic Plate underneath the Myanmar micro-plate during early Eocene (Tankard et al., 1998; Naing Maw Than et al., 2017). In Myanmar, Neogene vertebrate fossils are mostly discovered from the Irrawaddy Formation of Salin Sub-basin (e.g. Colbert, 1935; Takai et al., 2006). Furthermore, Neogene vertebrate fossil were reported from the Khabo Formation of the northern most part of Bago Yoma sub-basin. This formation is characterized by fine- to medium-grained, cross-bedded to plane-bedded, yellow to buff sandstones, deposited under the tide dominated estuarine the tide dominated estuarine environment (Kyi Khin and Myitta, 1999; Myint Thein and Maung Maung, 2017). Towards the north of Bago Yoma sub-basin, the Khabo Formation becomes terrestrial and carries a rich assemblage of Middle Miocene mammalian fauna (Nwe New San, 2013; Myint Thein and Maung Maung, 2017).

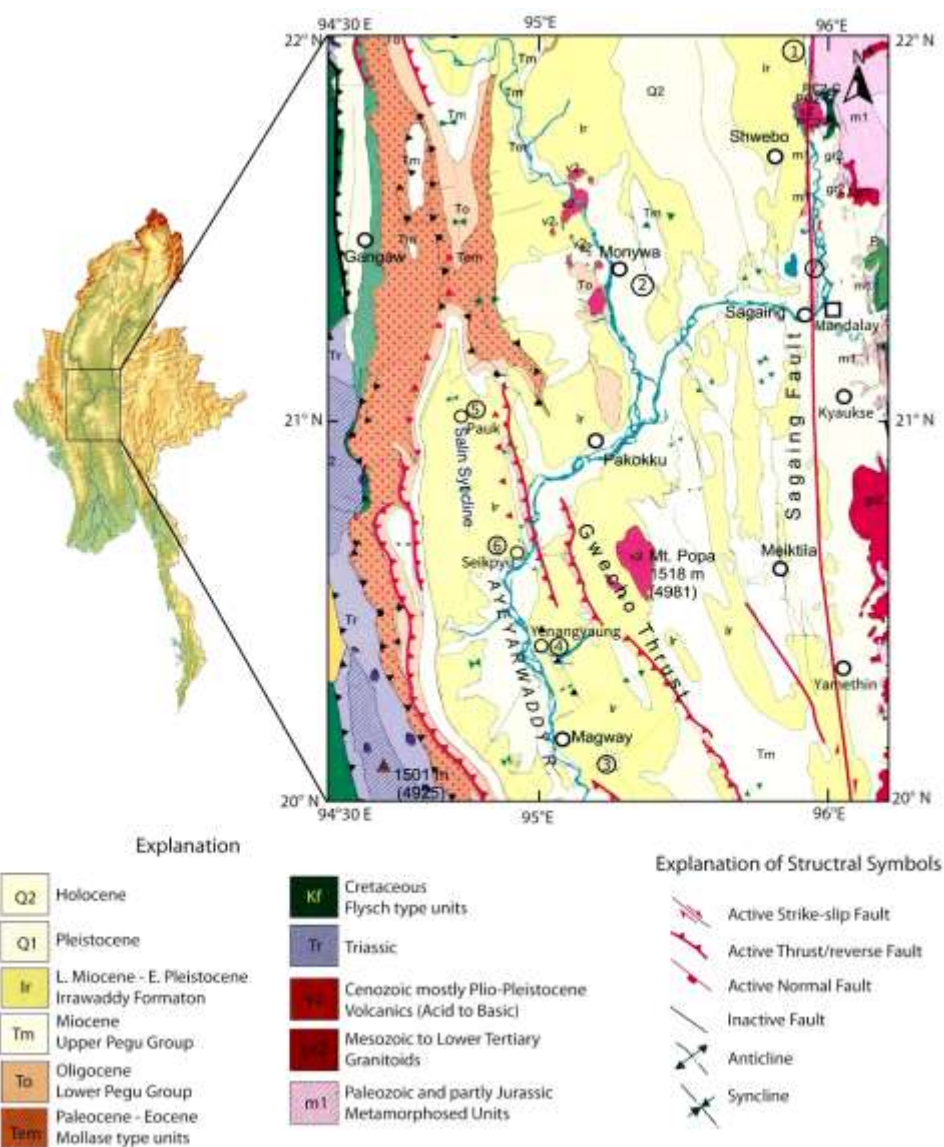


**Figure 1** Geological Map of Central Myanmar showing vertebrate bearing fossil localities (After the Geological Map of Myanmar Geosciences Society, 2014)

- ① = Chaungtha, late middle Miocene, ② = Thanbinkan, late middle Miocene, ③ = Yinseik, late Miocene, ④ = Yenangyaung, late Miocene, ⑤ = Chaingzauk, latest Miocene to early Pliocene, ⑥ = Gwebin, Pliocene, ⑦ = Mingun, early Pleistocene

## Materials and Methods

The specimens described here are housed in the National Museum, Yangon (NMMP-KU-IR), Geology Department of Mandalay University (MUDG-V), Geology Department of Magway University (Mgw-Ysk) and Zaykabar Museum, Yangon (MZKB-F). Dental morphology and distinct characteristics of fossil specimens were systematically studied and compared with available fossil specimens in the same phylogenetic group. Measurements of teeth were made with a digital caliper. All the measurements are given in mm. The taxonomy used in this paper follows that of Prothero and Schoch (1989). The terminology of anatomical designations and corresponding measurements generally follow the convention of Thenius (1989) (Fig. 2A, 4A & 6A).

## Systematic Paleontology

Order Perissodactyla Owen, 1848

Family Chalicotheriidae Gill, 1972

Subfamily Chalicotheriinae Gill, 1872

Gen. et sp. indet.

**Material:** Right maxillary fragment with M1/-M3/

**Horizon and Age:** Lower Irrawaddy Formation: Late Miocene

**Locality:** unknown, Pauk Township

**Description:** MZKB- F 011 can be assigned to the family Chalicotheriidae in having the W-shaped ectoloph with rhombic shape outline in upper molars. The teeth are brachyodont and M1/ is smaller than M2/ and M3/ and its occlusal surface on lingual side is broken.

The zygomatic arc is located at the level of M2/ and M3/. The teeth are moderately worn, indicating the remains of adult individual. Protocones in M2/ and M3/ are large and isolated consisting the rounded base and the conical top. In molars, there are V-shaped central valleys, closed to typical W-shaped ectoloph. The paracone is similar to the metacone, both reaching the midline of the tooth. According to its preserved dental characteristics, it will be difficult to assign a specific genera. Thus, it is preferable to assign it to indeterminate genus rather than specific assignment at present.

**Discussion:** Chalicotheriidae is an extinct clawed perissodactyls, documented from the Eocene to the Pleistocene, reaching its highest diversity in the Miocene of Asia, Europe, Africa and North America (Combs and Cote, 2010). To date, *Chalicotherium salinum*, cf. *Nestotherium* and two indeterminate genus are reported from the Neogene sediments of Myanmar (Tsubamoto et al., 2006; Chavasseau et al., 2010; Chit Sein, 2013).

The presence of chalicotheres in a fauna is usually assumed to be an indicator of the occurrence of trees and shrubs (Coombs and Cote, 2010). The microwear analysis on the teeth of this lineage suggests bark and twig feeding with considerable fruit consumption (Coombs and Semprebon, 2005). Stable isotope analysis on the tooth enamel of chalicotherids from Indian Subcontinent also suggests that they are forest dwelling browser (Nelson, 2007). Thus, discovery of this animal from the Irrawaddy Formation in Pauk area suggest the occurrence of forested condition in this area.

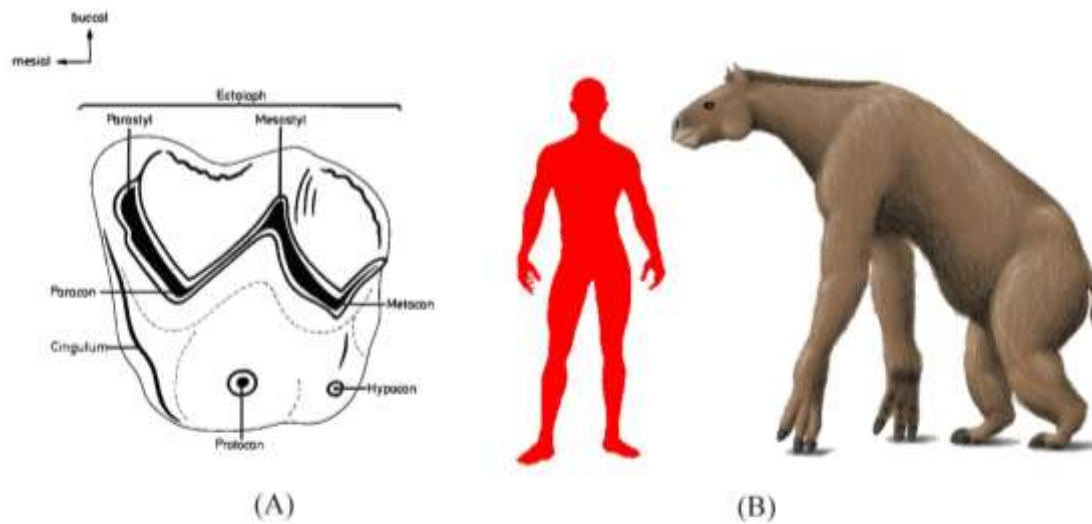


**Figure 2** A. Terminology of *Chalicotheriidae* upper molar (After Thennius, 2003),  
B. Reconstruction of *Chalicotheriidae* (Zapfe, 1979)

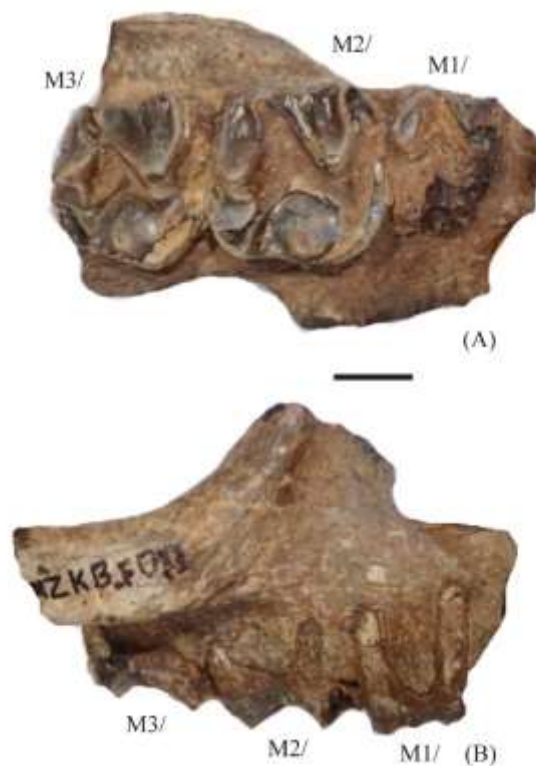


**Figure 3** *Chalicotheriidae*, MZKB- F 011, Right maxillary fragment with M1/-M3/: A. occlusal view, B. buccal view (Scale bar= 10 mm)

Family Rhinocerotidae Owen, 1845  
Subfamily Aceratheriinae Dollo, 1885  
Genus *Brachypotherium* Roger, 1904

*Brachyotherium perimense* Falconer and Cautley, 1847

**Materials:** MUDG-V 1011: Right mandibular fragment with M/1-M/3

**Horizon and Age:** Upper Part of Khabo Sandstone: Late Middle Miocene

**Locality:** Thanbinkan (21° 58' 35" N; 95° 21' 30" E), Monywa Township, Sagaing Division, Central Myanmar

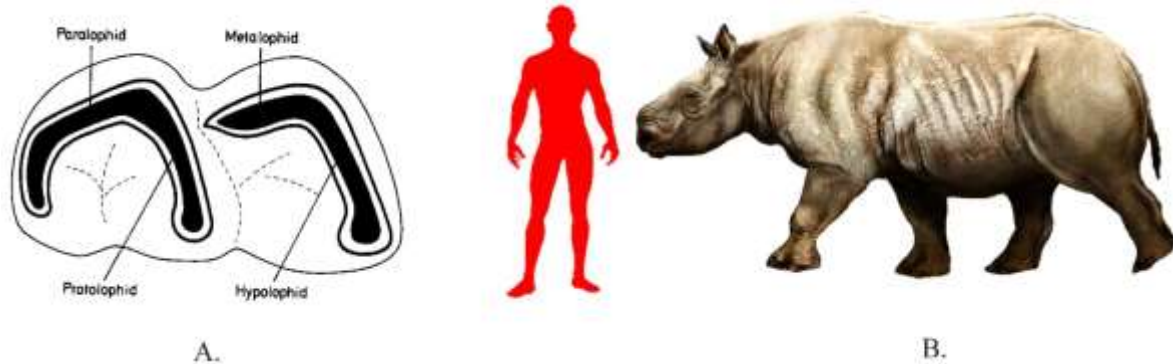


**Figure 4** A. Terminology of rhinoceros cheek teeth (after Thenius, 1989), B. Reconstruction of *Brachytherium* (www.memim.com)

**Description:** The mandible (MUDG-V 1011) is shallow with respect to height of the teeth (64 mm at level of M/1 and 70 mm at M/3), and is preserved from the level of M/1 to M/3. The teeth are moderately worn; the lingual groove is quite shallow and hypolophid is long; the posterior valley is deeper than the anterior one and show V shape in lingual view; the slanted posterior and anterior cingula are observed, although there is no posterior cingulum in M/3; the lingual cingulum is absent, but the labial cingulum is represented by the array of the small tubercle. On M/1 (Length=58.1 mm, Width=31.9 mm), anterior valley is unpreserved; trigonid and talonid are nearly same level due to the advanced wear stage; the talonid show the obtuse curve line. On M/2 (Length=54.2 mm, Width=32.1 mm), protocone is weak; the paralophid is short; the hypolophid is long and show smooth curve. M/3 (Length=56.2, Width=32.1) generally shows similar characteristic with M<sub>2</sub> although it is in early wear stage; lingual portion of hypolophid is broken; the posterior valley run down to the neck of the posterior root (Fig. 4).

**Discussion:** Rhinoceros fossils are common in the Neogene sediments of central Myanmar, representing four genera and eight species. (“*Diceratherium*” *naricum*, *Brachytherium perimense*, *Brachytherium fatehjangense*, *Rhinoceros sondaicus*, *Rhinoceros* sp.,

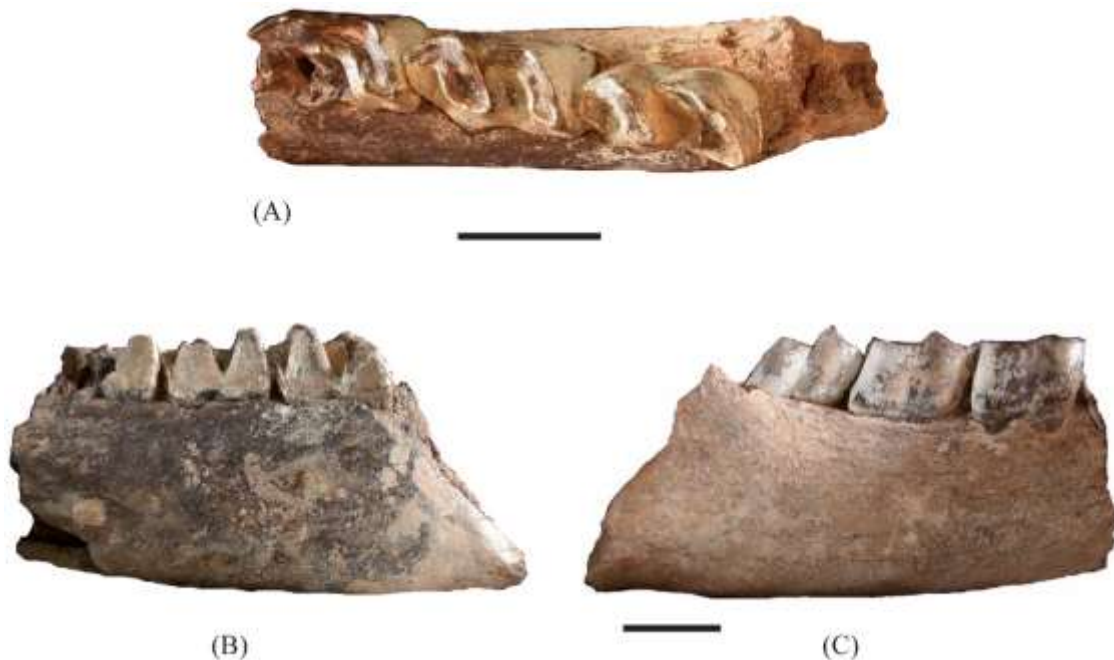


**Figure 5** *Brachytherium perimense*, MUDG-V-1011, Right mandibular fragment with M/1-M/3: A, occlusal view; B, lingual view; C, buccal view (Scale bar = 20 mm)

*Dicerorhinus gwebinensis*, *Dicerorhinus* cf. *sumatrensis*) and one indeterminate genus (Chavasseau et al., 2006; Zin-Maung-Maung-Thein et al., 2008, 2010). Among them, *Brachytherium* is a large, hornless rhinoceros and distributed in the Miocene of Old World, and survived until the late Pliocene in East Africa. Remains of this rhinoceros are recovered from middle to late Miocene localities in central Myanmar (Takai et al., 2006; Chavasseau et al., 2006; Zin-Maung-Maung-Thein et al., 2010). In the neighboring region of Myanmar, it has been discovered from the lower and middle Siwaliks of Indian subcontinent (Welcomme et al., 2001), from the early Miocene of China (Tong, 2001) and from the early late Miocene of Thailand (Chaimanee et al., 2004).

*B. perimense* is regarded as a hippo-like rhinoceros due to its morphological criteria, and might have spent a part of its daily life in water. The  $\delta^{13}\text{C}$  values of the tooth enamel of this animal from the middle Miocene Thanbinkan locality ranges between -13.3 to -10.1‰ suggesting it consumes  $\text{C}_3$  plants in the forest/woodland environment (Zin Maung Maung Thein et al., 2019).

Family Equidae Gray, 1821

Tribe Hipparionini Quinn, 1955

Genus *Hipparion* Christol, 1832

*Hipparion* sp.

**Materials:** Mgw-ysk-1: isolated right P4/

**Horizon and Age:** Lower Irrawaddy Formation, Late Miocene (~10.4 to 8.8 Ma)

**Locality:** Yinseik (20° 06' 13" N; 95° 07' 44" E), Magway Township

**Description:** The upper molar of *Hipparion* is characterized by hypsodont teeth with distinct oval shape protocone and the complicated enamel placcation on the prefossette and postfossette. However, it is usually difficult to assign isolated dentition of *Hipparion* to a proper species.

The specimen, Mgw-ysk-1 (Dimension: Length= 25.6 mm; Width= 26.3 mm; Height= 44.8 mm), is square shape outline. This specimen is still in the stage of moderate wear.

The protocone is sub-rounded and lingually slightly convex. The parastyle and metastyle are moderately developed and mesostyle is developed as a pillar. There are at least three plications on the posterior border of the prefossette and anterior border postfossette respectively.

**Discussion:** The earliest record of Equidae (horses) has been documented from the early Eocene of North America and Europe. In Myanmar, fossil record of the equidae is poor and two genera of fossil horses (*Hipparion antelopinum* and *Equus yunnanesis*) are known from the Neogene sediments of Myanmar (Colbert, 1938; Takai et al., 2006). The stable isotope study of the tooth enamel of *Hipparion* from Siwalik Group of Indian Subcontinent indicated that the equids around 9.1 Ma consumed a C3-dominated diet, then shifted to a C4-dominated diet in 8.1 Ma and finally adapted to a C4-dominated diet around 6 to 5 Ma (Quade et al., 1989; Cerling, 1993; Nelson, 2003). The enamel  $\delta^{13}\text{C}$  values of *Hipparion* (-12.1 to -9.9 ‰) from the late Miocene Irrawaddy sediments at Yinseit localities in Magway area indicate consumption of a large proportion of C<sub>3</sub> plants in their diet and suggest the existence of a rather dense canopy forest (Jaeger et al., 2010). Thus, the expansion of grassland in central Myanmar is probably later than or different from that of Siwaliks of northern Pakistan due to occurrences of forest dwelling mammals in the Pliocene or later periods.

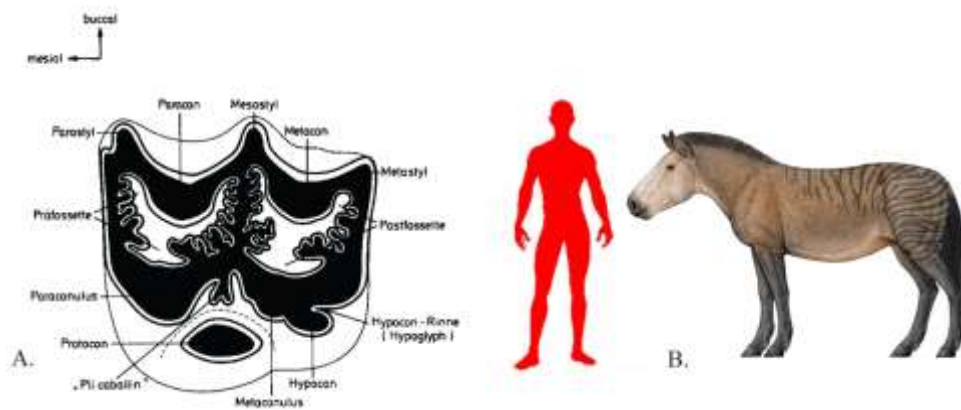


**Figure 6** A. Dental Terminology of *Hipparion* upper molar (After Thennius, 2003), B. Reconstruction of the extinct *Hipparion* (www.pinterest.com)



**Figure 7** *Hipparion*, Mgw-ysk-1, isolated right P4/: A, occlusal view; B. buccal view; C. lingual view (Scale bar= 10 mm)

## Summary and Conclusion

In Myanmar, fossil remains of the Order Perissodactyla have been documented in the Neogene sediments of central Myanmar representing Chalicotheriidae (*Chalicotherium*, cf. *Nesterotherium* and two indeterminate genera) Rhinocerotidae (“*Diceratherium*”, *Brachypotherium*, *Rhinoceros*, *Dicerorhinus* and one indeterminate genus) and Equidae (*Hipparion* and *Equus*). The occurrences of the forest dwelling perissodactyla such as chalicotherids, *Dicerorhinus*, *Rhinoceros* indicates the existence of the considerable forested condition in central Myanmar in the geological past. The presence of chalicotherids in a fauna is usually assumed to be an indicator of the occurrence of trees and shrubs. The  $\delta^{13}\text{C}$  values of the tooth enamel of the *Brachypotherium* from the middle Miocene Thanbinkan locality indicate that it consumes C<sub>3</sub> plants in the forest/woodland environment. The enamel  $\delta^{13}\text{C}$  values of *Hipparion* from the late Miocene Irrawaddy sediments at Yinseit and Yenangyaung suggest the predominance of forested condition in central Myanmar. The stable isotope study of the tooth enamel of *Hipparion* from Siwalik Group of Indian Subcontinent indicated that a decrease in forest habitation accompanied by an increase in open habitation in late Miocene (~8 Ma) (Nelson, 2003, 2007). However, the expansion of grassland in central Myanmar is probably later than or different from that of Siwaliks of northern Pakistan due to occurrences of forest dwelling mammals in the Pliocene or later periods.

## Acknowledgements

We foremost thank Dr Than Than Nu (Professor and Head, Department of Geology, University of Mandalay) for her enthusiasm and support for our research. We thank Masanaru Takai (Primate Research Institute, Kyoto University, Japan), Takehisa Tsubamoto (Department of Earth Sciences, Ehime University, Japan), Naoko Egi (Primate Research Institute, Kyoto University), Yuichiro Nishioka (Museum of Natural and Environmental History, Japan) for their help and support for fossil expedition in central Myanmar. We also thank U Khin Nyo (Curator, Zaykabar Museum, Yangon) for his permission to access the fossil collection of the museum. We thank faculty members of the Department of Geology, University of Mandalay for their kind help and assistance.

## References

- Chaimanee, Y., Suteethorn, V., Jintasakul, P., Vidthayanon, C., Marandat, B., Jaeger, J.-J. (2004). 2004. A new orangutan relative from the Late Miocene of Thailand. *Nature*, vol. 427, pp. 439–441.
- Chavasseau, O., Chaimanee, Y., Tun, Soe Thura, Soe, Aung Naing, Barry, C.J., Marand, B., Suder, J., Marivaux, L., Ducrocq, S., Jaeger, J.J. (2006) Chaungtha, a new middle Miocene mammal locality from the Irrawaddy Formation, Myanmar. *Journal of Asian Earth Sciences*, vol. 28, pp. 354-362.
- Chit Sein and Tin Thein (2013) A new record of Chalicotherium from the Irrawaddy Formation in Migyaungye Area, Magway Region. *Universities Research Journal*, vol. 6 (5), pp. 207-218.
- Colbert, E. H. (1935) Siwalik Mammals in the American Museum of Natural History. *Transaction of American Philosophical Society, New Series*, vol. 26, pp. 1- 401.
- Colbert, E.H. (1938) Fossil mammals from Burma in the American Museum of Natural History. *Bulletin of the American Museum of Natural History*, vol. 74, pp. 255-436.
- Cerling, T.E., Wang, Y., Quade, J. (1993). Expansion of C<sub>4</sub> ecosystem as an indicator of global ecological change in the late Miocene. *Nature*, vol. 361, pp. 344-345.
- Coombs, M. C., Semprebon, G. M. (2005) The diet of chalicotheres (Mammalia, Perissodactyla) as indicated by low magnification stereoscopic microwear analysis. *Journal of Vertebrate Paleontology* 25 (suppl. to no. 3): 47A.
- Combs, M., Cote, S. M. (2010) Chalicotheriidae. In *Cenozoic Mammals of Africa*, ed. Werdellin, L., and Sanders, W. J. University of California Press.
- Dollo, L. (1885) *Rhinoceros vivants et fossils. Revue des Questions Scientifiques*, vol. 17, pp. 293-299.
- Gloger, C.W.L. (1841) *Gemeinnutziges Hand- und Hilfsbuch der Naturgeschichte*. Aug. Schutz and Comp., Breslau.

- Kyi Khin and Myiita (1999) Marine transgression and regression in Miocene sequences of northern Pegu (Bago) Yoma, Central Myanmar. *Journal of Asian Earth Sciences*, vol. 17, pp. 369-393.
- Jaeger, J.J., Aung Naing Soe, Chavasseau, O., Coster, P., Emonet, E.-G. (2011) First Hominoid from the Late Miocene of the Irrawaddy Formation (Myanmar). *PLoS ONE*, 6, pp. 1-16.
- Myint Thein and Maung Maung (2017) The Eastern (Back –arc Basin) of Central Myanmar: the basement rock, lithostratigraphic units, paleocurrents, provenance and development history. Myanmar: Geology, Resources and Tectonics, In Barber, A.J., Khin Zaw, Crow, M. J. (Eds.). Geological Society, Memoir, 48.
- Naing Maw Than, Kyi Khin and Myint Thein (2017) Cretaceous Geology of Myanmar and Cenozoic geology in Central Myanmar Basin. Myanmar; Geology, Resources and tectonics, In Barber, A.J., Khin Zaw, Crow, M.J. (Eds). Geological Society, Memoir, 48.
- Nelson, S. V. (2003) *The Extinction of Sivapithecus*. Brill Academic Publishers, Inc. Boston.
- Nelson, S. V. (2007) Isotopic reconstructions of habitat change surrounding the extinction of Sivapithecus, a Miocene hominoid, in the Siwalik Group of Pakistan. *Palaeogeography, Paleoclimatology, Palaeoecology* vol. 243, pp. 204-222.
- Nwe Nwe San, (2013) Stratigraphy and Paleontology of the Middle Miocene-Pliocene Units in Thabinkan-Tigyon Area, Chau-U Township, Unpublished PhD thesis, Mandalay University.
- Owen, R. (1845) *Odontography*. Hippolyte Bailliere, London.
- Owen, R. (1848) *On the Archetype and Homologies of the Vertebrate Skeleton*. J. van Voorst, London.
- Prothero, D.R., Schoch, R.M. 1989. Classification of the Perissodactyla. 530-537. In Prothero, D.R., Schoch, R.M. (eds.), *The Evolution of Perissodactyls*. Oxford University Press, New York.
- Quade, J., Cerling, T.E., Bowman, J., 1989. Development of Asian monsoon revealed by marked ecological shift during the latest Miocene in northern Pakistan. *Nature*, vol. 342, pp. 163-165.
- Roger, O. (1904) Wirbelthierreste aus dem Obermiozan der bayerisch-schwabischen Hochebene. Bericht des naturwissenschaftlichen Vereines für Schwaben und Neuburg, vol. 36, pp. 1-22.
- Rose, D. K., Holbrook, T. D., Rana, R. S., Kumar, K., Jones, K. E., Ahrens, H. E., Missiaen, P., Sahni, A., Smith, T. (2014) Early Eocene fossils suggest that the mammalian order Perissodactyla originated in India. *Nature Communication*. 5:5570
- Takai, M., Saegusa, H., Thaug-Htike, Zin-Maung-Maung-Thein (2006) Neogene mammalian fauna in Myanmar. *Asian Paleoprimatology*, vol. 4, pp. 143-172
- Tankard, A.J., Balkwill, H.R., Mehra, A., Aung Din (1998) Tertiary wrench fault tectonics and sedimentation in the central basin of Burma. *American Association of Petroleum Geologists Bulletin*, vol. 78 (116)
- Tong, H., 2001: Rhinocerotids in China- systematics and material analysis. *Geobios*, vol. 34 (5), pp. 585–591.
- Thenius, E. (1989): Zähne und Gebiss der Säugetiere. *Handbuch der Zoologie*, v. 8, Mammalia, pt. 56. Walter De Gruyter, New York.
- Tsubamoto, T., Takai, M., Shigehara, N., Suzuki, H., Nishimura, T., Ugai, H., Maung Maung, Chit Sein, Soe Thura Tun, Aung Naing Soe, Aye Ko Aung, Tin Thein, Thaug Htike, Zin Maung Maung Thein, 2006. A summary of the Pondaung fossil expeditions. *Asian Paleontology*, vol. 4, pp. 1-66.
- Welcomme, J.-W., Benammi, M., Crochet, J.-V., Marivaux, L., Metais, G., Antoine, P.- O., Baloch, I. (2001) Himalayan Forelands: Palaeontological evidence for Oligocene detrital deposits in the Bugti Hills (Balochistan, Pakistan). *Geological Magazine*, vol. (138), pp. 397-405.
- Zapfe, H. 1979. *Chalicotherium grande* (Blainv.) aus der miozänen Spaltenfüllung von Neudorf an der March (Devinská Nová Ves), Tschechoslowakei. *Neue-Denkschriften des Naturhistorischen Museums in Wien* 2:1–282
- Zin-Maung-Maung-Thein, Masanaru, T., Tsubamoto, T., Thaug-Htike, Egi, N., Maung-Maung (2008) A new species of *Dicerorhinus* (Rhinocerotidae) from the Plio-Pleistocene of Myanmar. *Palaontology*, vol. 51 (6), pp. 1419–1433.
- Zin-Maung-Maung-Thein, Takai, M., Tsubamoto, T., Egi, N., Thaug-Htike, Nishimura, T., Maung-Maung, Zaw-Win (2010) A review of fossil rhinoceroses from the Neogene of Myanmar with description of new specimens from the Irrawaddy sediments. *Journal of Asian Earth Sciences*, vol. 37, pp. 105-206.
- Zin-Maung-Maung-Thein, Takai, M., Thaug Htike (2019) Paleocology of the Middle Miocene Mammals from central Myanmar: Evidence from the Stable Carbon and Oxygen Isotopes. *Second International Conference on Applied Earth Sciences in Myanmar and Neighboring Regions*, p. 55.

## **DETERMINATION OF SITE EFFECTS OF SOIL CONDITION ON SPT VALUES FOR GROUND MOTION IN YANGON BUSINESS CITY, MYANMAR**

Zaw Lin Kyaw<sup>1</sup>, May Thet Aye<sup>2</sup>, Myo Thant<sup>3</sup>,  
Khin Kyawt Kyawt Oo<sup>4</sup>, and Yan Naing Tun<sup>5</sup>

### **Abstract**

The influence of local geologic and soil conditions on the intensity of ground shaking and earthquake damage has been known for many years. Local site effects play an important role in earthquake resistant design and must be accounted for on case by case basis. The nature and distribution of earthquake damage is strongly influenced by the response of soils conditions. This response is controlled in large part by the mechanical properties of the soil. Yangon, also known as business city, is the former major capital city in Myanmar. Yangon area is fairly earthquake-prone as Myanmar itself lies in a major earthquake belt of the world. It is noticed that the soil conditions and soil factor are incorporated. This part of fair to good foundation soils lies on a north-south trending anticlinal ridge of Neogene formations. The flanks, covered by the alluvium, are mostly occupied by satellite towns where the period values range from 0.13 to 1.00 seconds and the magnification factors are 3.2 to 5.0. This research is purposed to determine the predominant periods and amplification factors of Yangon business city by utilizing the geological map of Yangon and transfer function method. Especially for ground motion, transfer function method and SPT of drilling sites are used to develop the site effects condition of Yangon business city.

**Keywords:** Ground motion, Periods, Magnification factors, Transfer function method and Yangon business city

### **Introduction**

Myanmar is located at the plate boundary between the Indian and Sunda plates. It is one of the most tectonically active regions in Southeast Asia. During the past several hundred years, numerous earthquakes occurred within this region, resulting from the on-going oblique convergence and extrusion processes between the Indian, Eurasian and Sunda plates (Wang, 2013). Most of the differential motion between these two plates in Myanmar is concentrated on the Sagaing Fault, which is a major north-striking, right-lateral fault that has a slip rate of approximately 18 mm/yr based on GPS data. Myanmar can be regarded as one of the highly seismicity countries due to its occurrence of the Alpide Earthquake Belt. Since several hundred years ago, Myanmar has already experienced many destructive major earthquakes with the magnitude > 7.0 (Mw). Yangon, the business largest city (Fig. 1), is one of the cities of Myanmar that low to medium seismicity based on the seismicity and the records of the previous considerably high magnitude earthquakes. The other significant earthquakes are Yangon earthquakes of September 10, 1927 and December 17, 1927. These events also resulted in a certain amount of damage in Yangon. All of these events and their consequences, and the rapid growth of population and various sorts of structures alarm to conduct the seismic hazard analysis for this region and the seismic hazard assessment was therefore performed applying the probabilistic way (Mg Thein, 2001).

---

<sup>1</sup> Dr, Associate Professor, Department of Geology, University of Yangon

<sup>2</sup> Dr, Associate Professor, Department of Geology, Maubin University

<sup>3</sup> Dr, Professor, Department of Geology, University of Yangon

<sup>4</sup> Assistant Lecturer, Department of Geology, University of Yangon

<sup>5</sup> Lecturer, Department of Geology, Meiktila University



**Figure 1** Location maps of the Yangon business region

### **Tectonic setting**

Myanmar spans a very complex and broad tectonic belt that accommodates the northward translation of the Indian Plate past the Sunda Plate (e.g., Socquet *et al.*, 2006). This motion is primarily expressed by right-lateral slip on the Sagaing Fault, which bisects Myanmar from south to north (Win Swe, 1970; Curray *et al.*, 1979; Le Dain *et al.*, 1984), and right-lateral oblique convergence across the northern Sunda megathrust beneath the western coast and adjacent Indo-Burman Ranges (Nielsen *et al.*, 2004; Socquet *et al.*, 2006).

Myanmar is currently experiencing strain partitioning between the Indian and Sunda plates. In the west the Indian plate is colliding obliquely with the Burma plate along the northern extension of the Sunda megathrust (Socquet *et al.*, 2006). In the east, relative motion between the Burma and Sunda plates occurs along the 1200 km long Sagaing fault. Farther south, this relative motion rifts the Andaman Sea Basin and bisects Sumatra along the 1900 km long Sumatran fault (Sieh and Natawidjaja, 2000) and West Andaman fault (Berglar *et al.*, 2010). Myanmar is located at the very active tectonic area which includes the Burma oblique subduction, the Sagaing strike slip fault system and the southern opening region (Fig. 2). The Burma microplate consists of the Andaman and Nicobar island chains, northern Sumatra, and the Andaman Ocean Basin. Surrounded by the Indian, Sunda, Australian and Eurasian plates, the Burma microplate is in a highly tectonically active region of the world. On the western flank lies the Sunda trench, where the Indian plate is subducting under the overriding Burma microplate. To the east lies the Sunda plate, and to the south lies the Australian plate. Yangon is tectonically bounded by the Indian-Burma plates, subduction in the west, Sagaing fault in the east, West BagoYoma fault in the north, Kyaykkyan fault in the northeast, and the Andaman rift zone in the south.

The earthquakes observed in the Andaman sea region are shallow focus earthquakes that show not only the normal fault mechanisms but also the strike-slip fault mechanisms. In and around Yangon Region, most of the earthquakes happened are shallow focus earthquakes, especially within about 250 km in radius. Most are related with Sagaing Fault, some corresponds to the blind faults located under Yangon Region and subduction zone of Indian and Burma Plate (Part of Eurasian Plate), and the Andaman Rift Zone. Moreover, some other faults whose geometry and other parameters are not well-known in and around this region also generated some earthquakes. Small numbers of intermediate and deep focus earthquakes can be seen in this region and those are caused by the subduction zone of Indian-Burma Plates (Mg Thein, 2001).

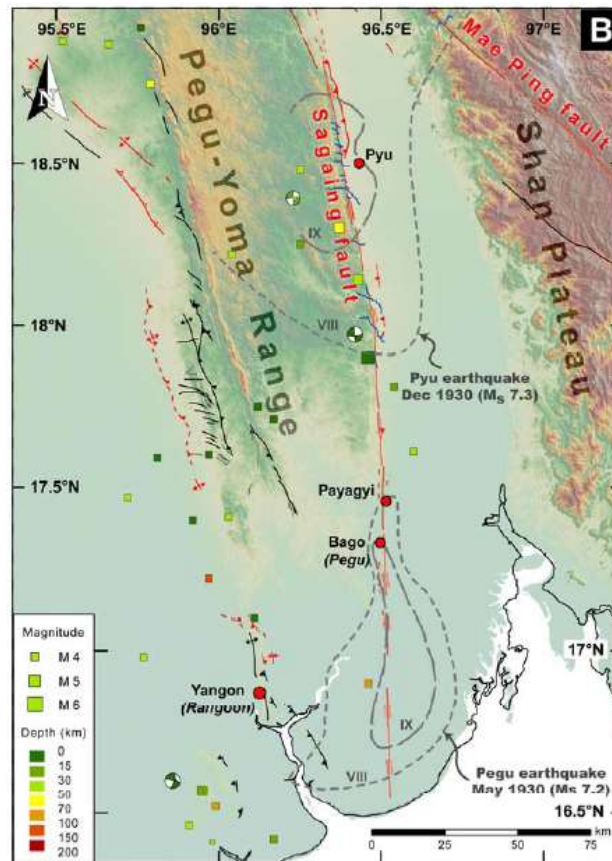


**Figure 2** Active tectonic framework and recent earthquake history around Yangon business city (Wang, 2013)

### Geology of Study Area

The Yangon area is underlain by alluvial deposits (Pleistocene to Recent), the non-marine fluvial sediments of Irrawaddy formation (Pliocene), and hard, massive sandstone of Pegu series (early-late Miocene). Alluvial deposits are composed of gravel, clay, silts, sands and laterite which lie upon the eroded surface of the Irrawaddy formation at 3 - 4.6 m above mean sea level (MSL). The rock type in Yangon is mainly soft rocks, which consist of sandstone, shale, limestones and conglomerate. The main geologic feature of the Yangon area is a low-lying anticlinal ridge that trends from north of Hlawga Lake to Shwe Dagon Pagoda hill for a distance of about 30 km. It is an elongated inlier of the Irrawaddy and Pegu beds surrounded by an alluvial plain. It is made up mainly Irrawaddy beds (Pliocene). Upper Pegu beds (Miocene) occupy only the northwestern part of the ridge. These Neogene rock units are folded into an elongated anticline. The low-lying ridge is flanked by Quaternary valley-filled deposits and alluvium in the west, and by the alluvium in the east (Fig. 3). In this area, the Irrawaddy Formation is subdivided by Wing Naing (1972) into two rock units. The lower unit (Arzarnigon sandrocks) mainly occurs in the northern part, and the upper unit (Danyingon clay) mainly occurs in the southern part. Because of the Monsoon climate, laterites and lateritic soil have been developed locally on these rocks, especially on the latter. The valley-filled deposits of gravels and sands with some clay bands occurs east of the Hlaing River. There is a minor fault trending approximately north-south. A small cross-fault is located north of Mingaladon, with downthrow on the southern side (Mg Thein, 2001).

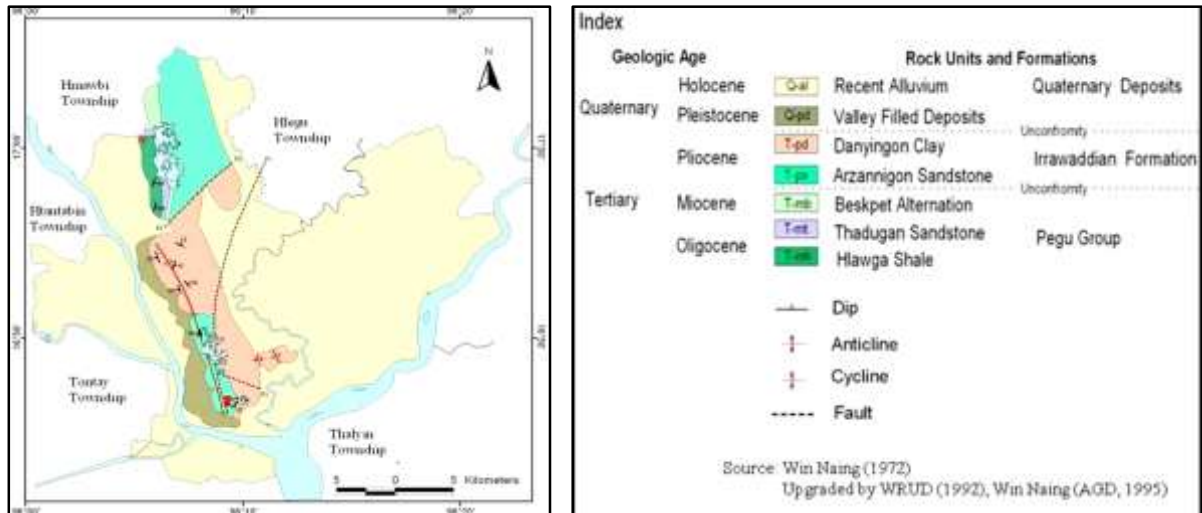


**Figure 3** Geological map of around Yangon Region (Win Naing, 1972)

### Historical Earthquakes

The Yangon Region is prone to natural disasters, including floods, storms, fires, earthquakes, and disease epidemics. Of all these natural disasters, floods, storms, and earthquakes are the most damaging in the Yangon Region. Among these natural disasters, all but earthquakes are able to receive early warnings for preparedness measures. The country itself is besieged by a series of faults, of which the Sagaing fault is the longest, trending north to south across the central part of the country.

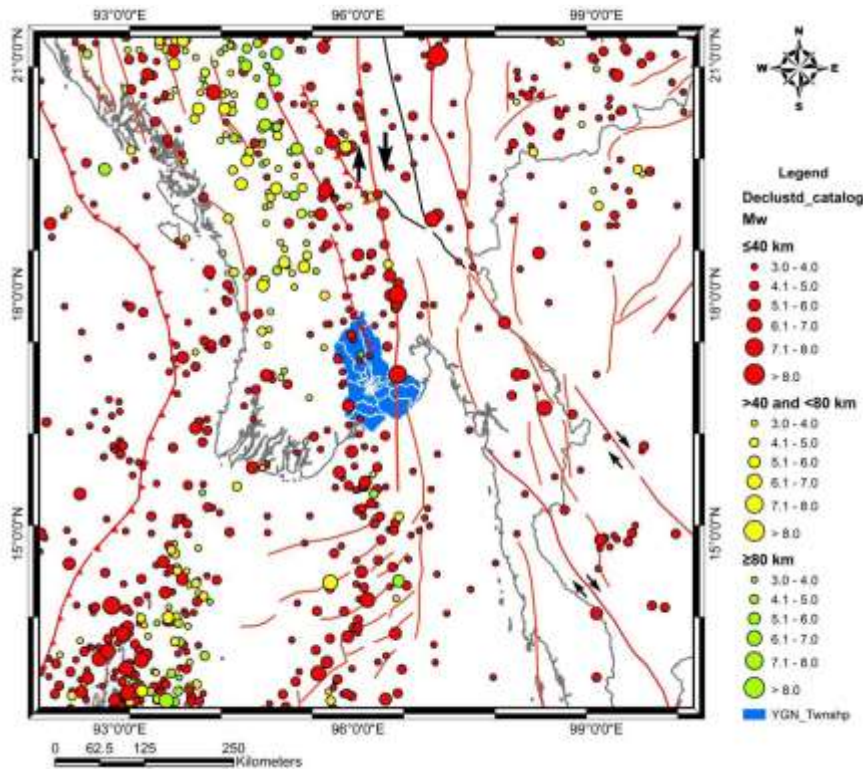


**Figure 4** The seismicity of Yangon region (Data Source – ANSS earthquake catalog, 1963 – 2012) (Myo Thant, *et. al.*, 2012)

Yangon City is about 30 kilometers west of the Sagaing fault. History suggests that earthquakes have had grim consequences on lives, social assets, and physical systems in the region. The Yangon area is fairly earthquake-prone as it lies just outside a major earthquake-hazard zone that lies along the southern segment of the Sagaing Fault. Historical sources recorded that during the 19<sup>th</sup> Century Yangon, then a mere provincial town, had felt five moderate shocks and five slight shocks which caused little damage to the wooden-frame houses in the town. Since 1900, there have been 14 recorded earthquakes in the Yangon area. These include ten slight shocks, three moderate shocks and only one fairly strong shock. The three moderate shocks with MMI VI-VII intensity, caused some damage, but no deaths. The fairly strong shock of 5<sup>th</sup> May 1930, however, caused considerable damage and some 50 deaths in the city, this earthquake did not originate in the Yangon region (Fig. 4). Actually, it was merely the shock of the very destructive Bago earthquake of the same date felt at 8:15 p.m. in Yangon. The epicenter lay on the Sagaing Fault about 30 km south of Bago where a very strong shock, it was felt as a fairly strong shock in Yangon even though the city was about 50 km away for the epicenter. The intensity was estimated to range for MMI VII to VIII, depending on the strength of the underlying soils (Mg Thein, 2001).

### Research Methodology

Local site conditions can profoundly influence all of the important characteristics; amplitude, frequency content, and duration of strong ground motion. The extent of their influence depends on the geometry and material properties of the subsurface materials, on site topography, and on the characteristics of the input motion. The nature of local site effects can be illustrated in several ways: by simple, theoretical ground response analyses, by measurements of actual surface and subsurface motions at the same site, and by measurements of ground surface motions from sites with different surface conditions (Kramer, 1996).

#### Multiple Reflections Analysis for SH-Wave

There are important theoretical reasons why ground surface motions should be influenced by local site conditions. At most sites the density and S-wave velocity of materials near the surface are smaller than at greater depths. The characteristics of local soil deposits can also influence the extent to which ground motion amplification will occur when the specific impedance is constant (Kramer, 1996). Transfer Function by (Ohta and Goto, 1976), It is noted that the shear wave velocity structures were calculated by using empirical equations, which mainly contributed on SPT values for comparative analysis:

$$V_{s30} = 62.48N^{0.218}H^{0.228}F \quad (1)$$

where  $V_{s30}$ =Shear wave velocity (m/s),  $N$ =N-value,  $H$ =Depth (m),  $F$ =Coefficient of soil type,  $F=1.000$  (Clay),  $F=1.073$  (Sand),  $F=1.199$  (Gravel)

$N$  is average number of blows in SPT. Besides, the soil classification is decided by using the results of site investigation of standard penetration testing at twelve bore holes. The average values of  $N$  are used for determining the soil classification on each site (Ohta and Goto, 1978). Table 1 displays the relationship of soil types and predominant periods of the ground and Table 2 shows the international building code (IBC, 2009). Then, the average  $T_G$ -values are determined for each layer of evaluated subsurface soil profile by using the following table (Okada, 1971):

**Table 1 The relationship of soil types and predominant periods of the ground (Okada, 1971)**

| Soil types     | Periods (s)          |
|----------------|----------------------|
| I Hard soil    | $T_G < 0.2$          |
| II Medium soil | $0.2 \leq T_G < 0.6$ |
| III soft soil  | $0.6 \leq T_G$       |

**Table 2 The International Building Code (IBC, 2009)**

| Site Class                     | $\bar{v}_s^{30}$            | SPT ( $\bar{N}$ ) |
|--------------------------------|-----------------------------|-------------------|
| E (Soft Soil)                  | < 600 ft/s (<175 m/s)       | < 15              |
| D (Medium Dense or Stiff Soil) | 600-1200 ft/s (175-350 m/s) | 15-50             |
| C (Dense Soil)                 | 1200-2500 ft/s (>350 m/s)   | >50               |

### Research Analysis

The soil classification is decided by using the results of site investigations of standard penetration testing at 22 boreholes in research area as shown in Fig. 5. The average values of  $N$  are used for determining the soil classification on each site. The average values of  $N$  until a depth of 30 m at the sites surrounding Yangon city vary from 10.00 to 86.00. The S-wave velocity structures which give such satisfactory results are at 22 drilling sites.

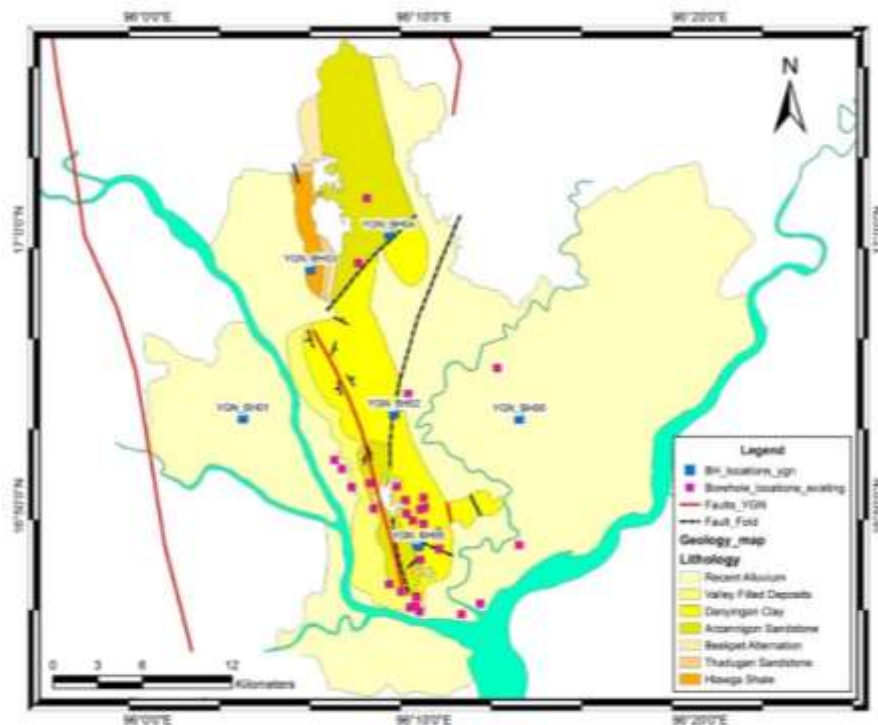


**Figure 5** Location map of the borehole sites in Yangon business city

Generally, the predominant periods of the transfer functions are more important and applicable for determination of S-wave velocity because it is more stable and well reflects to

sediment depth and S-wave velocity. It was received the realistic shear wave velocities and reliable thickness of soil layers and depths of lose sediment from these 22 drilling sites of S-wave velocity structures. The values of S-wave velocity from the 22 drilling sites were generally calculated between 170 and 360 m/s. Therefore, it is clearly found that it was utilized to take the S-wave velocity from the 22 drilling sites to calculate the predominant periods. Fig. 6 is shown as example of the magnification factors and period (sec) by using the transfer functions method in Yangon City.

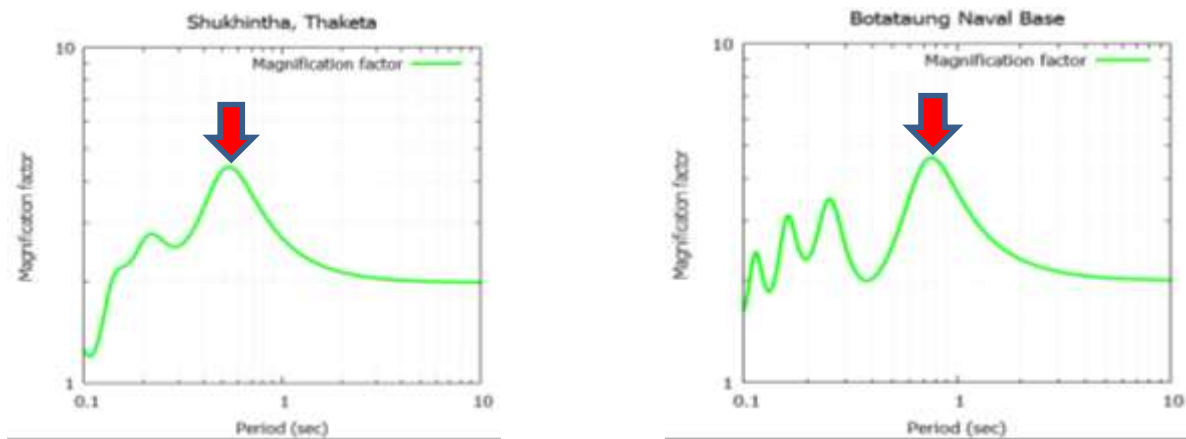


**Figure 6** Example of the magnification factors and period (sec) by using the transfer functions method in Yangon business city

**Table 3** The theoretical calculation of frequency, predominant periods and magnification factors of the transfer functions method

| No. | Name                                              | Depth (m) | Long    | Lat     | Freq (Hz) | Period (Sec) | MAX (MF) |
|-----|---------------------------------------------------|-----------|---------|---------|-----------|--------------|----------|
| 1   | Royal Hotel, Natmauk Road                         | 30        | 96.1275 | 16.8008 | 5.90      | 0.17         | 3.210    |
| 2   | Yangon Commercial Tower, Sule Pagoda Road         | 30        | 96.1586 | 16.7725 | 5.30      | 0.19         | 3.618    |
| 3   | Inya Lotus Lake Hotel, U Tun Nyein Road           | 30        | 96.1503 | 16.8453 | 8.00      | 0.13         | 4.575    |
| 4   | Institute of Foreign Language (I.F.L)             | 30        | 96.1414 | 16.8253 | 5.60      | 0.18         | 3.388    |
| 5   | Pansodan Street                                   | 30        | 96.1622 | 16.7789 | 5.10      | 0.20         | 3.518    |
| 6   | Garment Factory, Pyinmabin, Mingaladon            | 30        | 96.1322 | 17.0192 | 1.90      | 0.53         | 3.299    |
| 7   | Thaketa Shukhintha                                | 30        | 96.2006 | 16.7747 | 1.90      | 0.53         | 4.412    |
| 8   | State Lottery Building, 37th Street               | 30        | 96.1617 | 16.7736 | 2.00      | 0.50         | 3.496    |
| 9   | Bo Aung Kyaw Street, Zabyu Aung Construction Site | 30        | 96.1642 | 16.7697 | 1.70      | 0.59         | 3.384    |
| 10  | Ministry of Planning and Finance Office (Yankin)  | 30        | 96.16   | 16.8247 | 1.70      | 0.59         | 3.846    |
| 11  | Hlawga Substation (M.E.P.E)                       | 30        | 96.1269 | 16.9803 | 2.60      | 0.38         | 3.309    |
| 12  | Women Association, Dagon                          | 30        | 96.1531 | 16.7819 | 2.20      | 0.45         | 3.723    |
| 13  | Tamwe Natchaung                                   | 30        | 96.1756 | 16.8183 | 4.50      | 0.22         | 3.941    |
| 14  | Kandawgyi Hospital                                | 30        | 96.1644 | 16.8011 | 2.20      | 0.45         | 3.337    |
| 15  | Tamwe Market                                      | 30        | 96.1759 | 16.8077 | 1.60      | 0.63         | 4.706    |
| 16  | N0.2 Match Factory, Set San                       | 30        | 96.1561 | 16.8467 | 1.00      | 1.00         | 3.833    |
| 17  | GIC Factory, No.3 Highway, Mingaladon             | 30        | 96.16   | 16.778  | 1.50      | 0.67         | 4.043    |
| 18  | N. Okkalapa Hospital                              | 30        | 96.1573 | 16.901  | 1.50      | 0.67         | 4.434    |
| 19  | Dagon Myothit University                          | 30        | 96.2109 | 16.9169 | 1.30      | 0.77         | 4.766    |
| 20  | Botataung Naval Base                              | 30        | 96.1894 | 16.7683 | 1.30      | 0.77         | 4.637    |
| 21  | Sedona Hotel, Kabaaye Pagoda Road                 | 30        | 96.1561 | 16.829  | 1.50      | 0.67         | 4.428    |

The characteristics of seismic waves during earthquakes were mainly influenced by the local site conditions. The unconsolidated soil deposits tend to amplify certain frequencies of ground motion and extend the duration of the shaking which may cause further earthquake damage. According to the geological site conditions, the expected variation in the ground motion makes it necessary to perform a more detailed seismic hazard assessment as the research area. The nature and distribution of earthquake damage is strongly affected by the response of soils which is controlled in layers part by the mechanical properties of soil. Table (3) is displayed as the theoretical calculation of the frequency, predominant periods and magnification factors of the transfer functions method.

Based on the fundamental periods of the ground for each observation site, the hard soil has seen in Royal Hotel, Yangon Commercial Tower, Inya Lotus Lake Hotel, Institute of Foreign Language and Pansodan Street sites of Yangon business city because the smaller than 0.2 sec of the fundamental periods of the ground fine by the theoretical calculation. The recent alluvial and valley filled deposits sediments of the research area, the fundamental period identified from the S-wave velocity are mostly in the range of 0.22 - 0.63 sec, therefore these fundamental periods obtained may indicate the presence of generally medium sediments in the alluvial and valley filled deposits sediment of study areas. The NO. 2 Match Factory, GIC Factory, N. Okkalapa Hospital, Dagon Myothit University, Botataung Naval Base and Sedona Hotel sites are situated on the soft soils ( $0.6 \text{ sec} \leq T_G$ ) because these location sites are less than 0.6 sec in the study area (Fig. 7). Moreover, the magnification factors of Yangon city are between 3.00 and 5.00 (Fig. 8). The map of predominant periods and the map of magnification factors are very reliable for the site effects of ground motion in this research area.

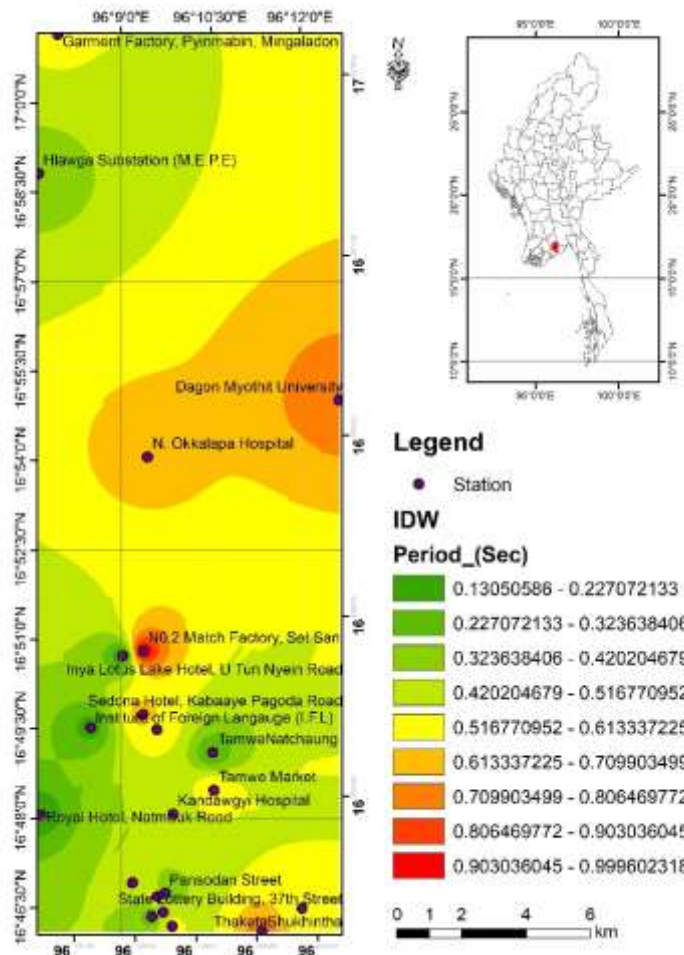


Figure 7 The predominant periods map of the research area

The results may confirm the suitability of using the S-wave velocity of transfer functions as a geophysical exploration tool in those structures with significant impedance contrast between sedimentary layers and the assume bedrock. Thus, the ground motion amplification due to medium soils, common in urban of Yangon city, is a major contributor to increasing damage and number of casualties.

Site Class is determined based on the average properties of the soil within 100 feet (30 meters) of the ground surface. Geotechnical engineers use a variety of parameters to characterize the engineering properties of these soils, including general soil classifications as to the type of soil, (e.g. hard rock, soft clay), the number of blows ( $N$ ) needed to drive a standard penetration tool 1 foot into the soil using a standard hammer, the velocity ( $V_s$ ) at which shear waves travel through the material as measured by on-site sonic and other tests, and the shear resistance of the soil ( $S_u$ ) as measured using standard laboratory test procedures.

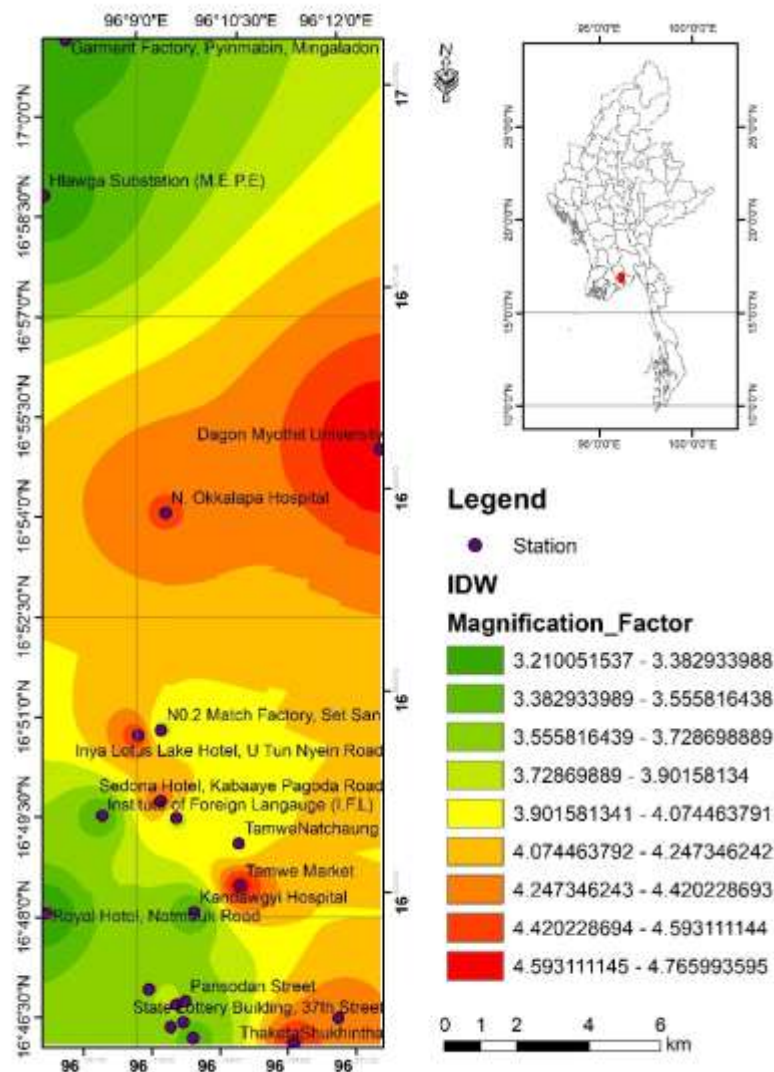


Figure 8 The magnification factors map of the research area

Based on this description, the  $V_{s30}$  contour show the site condition of Yangon business city and then can present the respective soil class of each portion of the city. The medium soil condition governed to the research area ( $175 \leq \bar{V}_s < 350$ ). The hard soil investigated the small region in the research area which are north and southwest of the studied area are ( $\geq 350$  m/s). That is why, it is verified that the research area is influenced the medium soil condition according to the

calculation of the Vs30 from the distribution of the 22 bore-hole sites. When the sites are located over the same structure, it can be assumed that the S-wave velocity is approximately constant from site to site. Inversely, if it can be assumed that in a certain region the surface layers have approximately a constant thickness, the dominant frequency at each point would be then related to an S-wave velocity and a map of surface velocities could be obtained. Therefore, the almost of the research area is also found the medium soil in the studied area.

### Conclusions

Yangon business city, known as largest city, is one of the cities of Myanmar that low to medium seismic region based on the seismicity and the records of the previous considerably high magnitude earthquakes. The main geologic feature of the Yangon area is a low-lying anticlinal ridge that trends from north of Hlawga Lake to Shwe Dagon Pagoda hill for a distance of about 30 km. For Yangon business city, it is verified that the research area is influenced the medium soil condition (170 m/s to 360 m/s) according to the calculation of the Vs30 from the distribution of the SPT values. Moreover, the magnification factors of Yangon city are between 3.00 and 5.00. The map of predominant periods and the map of magnification factors are very reliable for the site effects of ground motion in the research area. Thus, the ground motion amplification due to medium soils (0.22 - 0.63 sec), common in business Yangon city, is a major contributor to increasing damage and number of casualties in the future.

### Acknowledgment

We are indebted to Dr. Myo Thant, Professor, Department of Geology, University of Yangon, for his valuable suggestions and comments for this research. We would like to express our sincere gratitude to Dr Day Wa Aung, Professor and Head, Department of Geology, University of Yangon, for his encouragement and support throughout the present research and constructive suggestions.

### References

- Berglar, K., Gaedicke, C., Franke, D., Ladage, S., Klingelhoefer, F. & Djajadihardja, Y.S., (2010). Structural evolution and strike-slip tectonics off north-western Sumatra, *Tectonophysics*, Vol. 480, 1-4, 119-132, doi:10.1016/j.tecto.2009.10.003.
- Curry, J.R., D.G. Moore, L.A. Lawver, F.J. Emmel, R.W. Raitt, M. Henry & R. Kieckhefer, (1979). *Tectonics of the Andaman Sea and Burma*, Am. Assoc. Petrol. Geol. Mem., 29, 189–198.
- Kramer, S.L., (1996). *Geotechnical Earthquake Engineering*, ISBN 0-13-374943-6, 1996 by Printice-Hall, Inc. Pages: 653.
- Le Dain, A. Y., P. Tapponnier, and P. Molnar, (1984), Active faulting and tectonics of Burma and surrounding regions, *J. Geophys. Res.*, 89, 453–472.
- Mg Thein, (2001). Mitigation of earthquake hazards in Myanmar, *Journal of Myanmar Academy Tech.*, Vol. 1, no. 2, p. 124-134.
- Myo Thant, Nwai Le' Ngal, SoeThuraTun, Maung Thein, Win Swe, han Myint, (2012). Seismic Hazard Assessment For Myanmar, *Report to Myanmar Earthquake Committee and Myanmar Geoscience Society*, P58.
- Nielsen, C., et al., (2004). *From partial to full strain partitioning along the Indo-Burmese hyper-oblique subduction*, Mar. Geol., 209, 303–327, doi:10.1016/j.margeo.2004.05.001.
- Ohta, Y. and Goto, N., (1976). Estimation of S-wave velocity in Terms of Characteristic Indices of Soil, *Butsuri-Tankō*, Vol. 29, No. 4, pp. 34-41 (in Japanese).
- Ohta, Y. and Goto, N., (1978). Empirical shear wave velocity equations in terms of characteristic soil indexes, *Earthq. Eng. Struct. Dyn.*, 6:167-187.

- Okada, H., (1971). *A Seismic Refraction survey in Hachinohe City, Aomori Prefecture, Japan*, Faculty of Science, Hokkaido University, 26, 147-16.
- Socquet, A., C. Vigny, N. Chamot-Rooke, W. Simons, C. Rangin, and B. Ambrosius, (2006), India and Sunda plates motion and deformation along their boundary in Myanmar determined by GPS, *J. Geophys. Res.*, 111, B05406, doi:10.1029/2005JB003877.
- Sieh, K., and D. Natawidjaja (2000). Neotectonics of the Sumatran fault, Indonesia, *J. Geophys. Res.*, 105(B12), 28295–28326, doi:10.1029/2000JB900120.
- Wang, W., (2013). *Earthquake Geology of Myanmar*, Ph. D Dissertation, California Institute of Technology, Pages:317.
- Win Naing, (1972). *Geology and Groundwater Hydrology of Greater Rangoon*, M.Sc. Thesis, Department of Geology, University of Rangoon (unpublished).
- Win Swe, (1970), Rift-features at the Sagaing-Tagaung ridge, in *Proc. 5th Burma Research Congress*, Rangoon.

## **OBSERVATION OF LANDFORMS OF GRANITIC ROCKS IN PA NYIT BEACH IN LAUNGLON TOWNSHIP, TANINTHARYI REGION**

Su Su Khine<sup>1</sup>, Min Naing Soe<sup>2</sup>, Oo Tun win<sup>3</sup>

### **Abstract**

Many famous beaches are located at Dawei in Tanintharyi Region. Among them Pa Nyit Beach is situated in the westernmost part of Launglon Township. It is lying between Latitude 14°59'00"N to 15°02'30"N and Longitude 98°083'30"E to 98°05'30"E. It extends about 3.34 km from east to west and 5.85 km from north to south. The area covers about 19.52 square kilometers. In this area, the mountain ranges show the North-South trending. Regionally, three granite belts in the Dawei area are frontier range granite, central range granite and coastal range granite. The study area is located in the coastal range granite. Granitic rocks in the study area are hornblende biotite granodiorite, biotite granite, porphyritic biotite granite, microgranite and leucogranite. Aplite dykes and quartz and quartzofelspathic veins intruding into these rock units, especially biotite granite and microgranite. Both major and various minor landforms of granite are observed in the study area. Minor landforms are classified as weathering forms, tectonic forms and Structural forms. Observable weathering forms in the study area are blocks, boulders, exfoliation, pitting, sheet, flakes and spalls, polygonal cracks, gutter and grooves, pseudobedding and tafoni. Many of them are initiated in the surface. A-tent and orthogonal cracks are tectonic forms and they are formed by different ways of tectonic movements. Structural forms in this area are cleft, displaced blocks and split rocks, fault, joint, fracture and intrusive dykes and veins. Most of them are formed due to intrusive veins.

**Keywords:** Granitic, Landforms, Pa Nyit, Launglon, Weathering, Structural, Tectonic

### **Introduction**

Pa Nyit beach is situated in the westernmost part of Launglon Township in Tanintharyi Region. It is lying between Latitude 14°59'00"N to 15°02'30"N, Longitude 98°083'30"E to 98°05'30"E. It extends about 3.34 km from east to west and 5.85 km from north to south. The area covers about 19.52 square kilometers. (Fig 1.1) It is easily accessible by car in any season. Satellite image of the study area is shown in (Fig 1.2). Launglon area is regarded as coastal range. Many famous beaches are located along this coastal range. Almost all beaches have granitic rocks with many landforms.

---

<sup>1</sup> Dr, Professor and Head, Department of Geology, Dawei University

<sup>2</sup> Lecturer, Department of Geology, Dawei University

<sup>3</sup> Assiatant Lecturer, Department of Geology, Sittway University

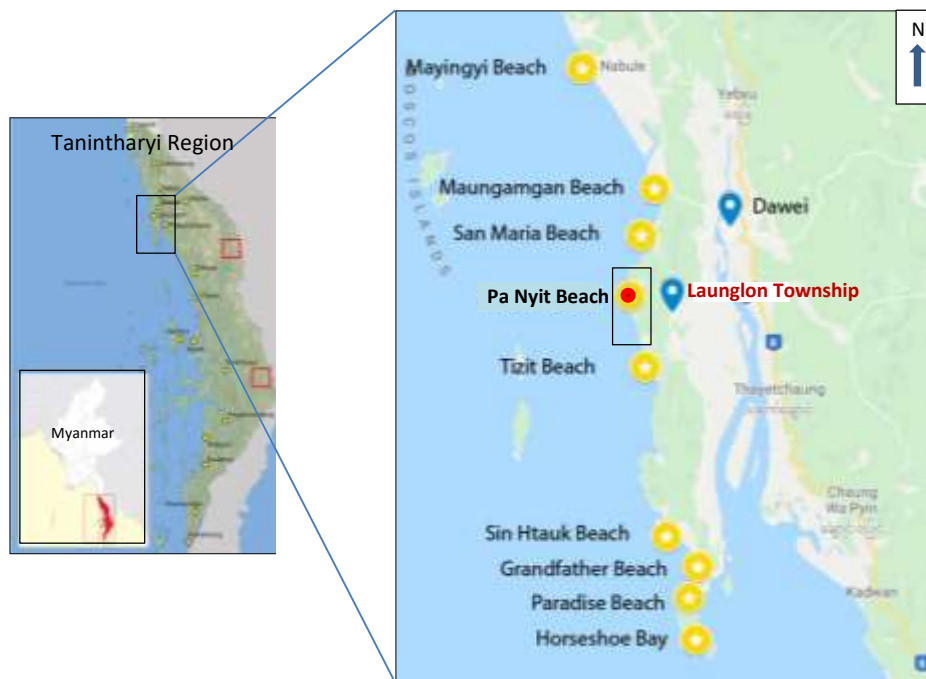


**Figure 1.1** Location Map of the study area

### 1.1 Purpose of Study

The purposes of the investigation are to study the rock units of the investigated area and to investigate landforms of granitic rocks exposed in the study area.

### 1.2 Methods of Study

Before conducting the field works, literature collection and studies of previous works were performed. Aerial photographs and the satellite image were also used as an aid to delineate the lithologic boundaries and the structures of the area. Field works including systematic sampling, measurement of geological structures were carried out by using tape and compass traverse method and GPS.

### Landforms of Granitic Rocks in Pa Nyit Beach

The study area is mainly composed of hornblende biotite granodiorite, biotite granite, porphyritic biotite granite, microgranite and leucogranite. Major and various minor granite landforms are observed in this area. Mainly three types of minor granite landforms in the study area are weathering forms, tectonic forms and structural forms. Interaction between bedrock and the atmosphere and hydrosphere, and especially meteoric and groundwater, leads to alteration of the rock and the formation of a regolith. Fresh granite is low in porosity and permeability, but is highly pervious by virtue of a connected series of orthogonal and sheet fractures. Granite is susceptible to weathering by moisture, leading to the formation of a regolith. The course and rate of weathering are influenced by the structure of the rock, including fractures, mineral composition, texture; especially size of the crystals and the physical, chemical and biotic nature of the invasive water. In this area, minor forms developed on granites are due primarily to weathering are blocks, boulders, exfoliation, plinths, pitting, sheet, flakes and spalls, polygonal cracks, gutter and grooves, pseudobedding and tafoni. Many of them are initiated in the surface. Tectonic forms contain A-tent, strain and rupture and orthogonal cracks. They are formed by different ways of

tectonic movements. Structural forms in this area are cleft, displaced blocks and split rocks, fault, joint, fracture and intrusive dykes and veins. Most of them are formed due to intrusive veins.



Northern part of Pa Nyit beach  
(Facing 350°)



Southern part of Pa Nyit beach  
(Facing 175°)

**Figure 1.2** Satellite image (Fig.a) and scenic view of the study area (Fig.b&c) (Latitude 14°59'00"N to 15°02'30"N and Longitude 98°03'30"E to 98°05'30"E)

## 2.1 Major Landforms

### 2.1.1 Slopes

Smooth gently inclined slope of coastal cliffs and moderately steep slope are mostly occurred in the study area. Flared slopes are also well represented on boulders but flared slopes not found in this area.

## 2.2 Minor Landforms

### 2.2.1 Weathering forms

Observable weathering forms in the study area are blocks, boulders, exfoliation, pitting, sheet, flakes and spalls, polygonal cracks, gutter and grooves, pseudobedding and tafoni. Many of them are initiated in the surface.

**Boulders and blocks** - Where steeply inclined fractures or foliation are closely spaced, penitent rocks are formed, and where orthogonal systems are developed, preferential weathering along fractures leads to essentially spheroidal corestones set in a matrix of grus. When exposed, the corestones become boulders. Subsurface weathering in well-jointed granite operates preferentially along the discontinuity planes and their intersections. The transformation of the hard bedrock into a decomposed and friable regolith (grus) progresses inwards from the joints towards the core of the compartments that they individualized.

Core stones are the hard residual blocks surrounded by soft grus located in weathering mantles. Their maximum sizes are determined by the joint spacing. They tend to become progressively smaller and more rounded as weathering proceeds and may have concentric weathering layers (spheroidal weathering). Corestones may be exposed at the surface when the soft residual mass is removed selectively by erosion. The resulting boulders may be left in place or may suffer some transport. Granite boulders may also form by weathering and erosion processes guided by jointing at the surface. The boulders may reach more than 30 m in length, although the modal dimension is typically close to 1m.

**Pitting** - Differential weathering at the crystal scale leads to feldspars and micas being altered to clays, leaving the quartz upstanding and giving a rough or pitted surface. Pitting is widely developed in granitic rocks on the coast here it may be the combination of high temperature, and alkaline waters (sea pray) together promote rapid differential weathering on exposed surfaces.

**Tafoni and hollow** - The tafoni are initiated at the weathering front, presumably as a result of especially intense subsurface moisture attack. Alveolar weathering is typical of fracture planes and the weathering front and represents an early stage of weathering. Miniature hollows may form on exposed surfaces but little is known of their origin. Tafoni undoubtedly evolve at the base of boulders and sheet structures, beginning with inverted saucers and enlarging upward into the mass as a result of salt crystallization, hence the occurrence of tafoni in arid and semiarid lands and some coastal areas.



**Figure 2.1** Chaotic mass of boulders and blocks of biotite granite which are fitted and polished ( $14^{\circ}59'27''\text{N}$  &  $98^{\circ}04'36''\text{E}$ )

**Figure 2.2** Well rounded boulder and different sizes (shingle) of biotite granite composed of released granite corestones ( $14^{\circ}59'32''\text{N}$  &  $98^{\circ}04'30''\text{E}$ )

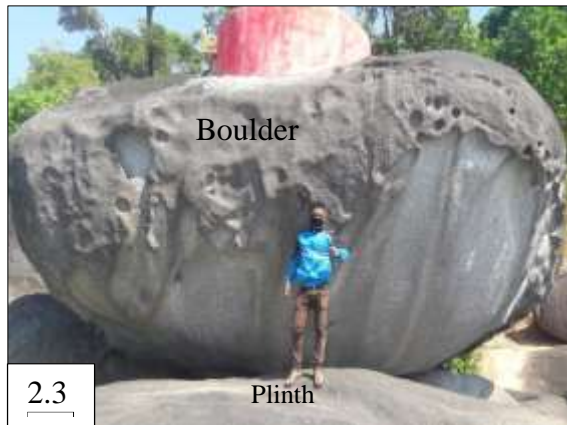


**Figure 2.3** Large boulders of porphyritic biotite granite and also show boulder and plinth (14°59'45"N & 98°04'55"E)



**Figure 2.4** Exfoliation features of biotite granite show concentric weathering layers, spheroidal weathering (15°00'36"N & 98°05'10"E)

**Sheet, Flakes and spalls** - Many exposed granite surfaces are covered, indeed essentially consist of a skin usually multilayered, of thin laminae, flakes or scale. Flakes are millimeters thick. Thicker lamellae, greater 1 cm thick, are referred to as spall plated. Both flakes and spall plates are associated with bush fires and other sources are ephemeral but intense heat.

**Polygonal crack** - Polygonal cracking affects spall plates on boulders and platforms and may be due to a surficial compressional stress caused by the accumulation of silica, iron oxide and manganese oxides either on exposed surfaces or at the weathering front. The cracks may be developed on as many as three successive small plates at any one site. Such patterns of cracks have been observed on corestones and on the recently exposed slopes and platforms.

**Gutters and Grooves** - After exposure, rudimentary gutters are deepened by running water. Abrasion is evidenced by the development of potholes. In some cases the gutters have become flask-shaped in cross section as a result of the undercutting of side walls by streams. Some gutters have exploited and follow fractures but that slope the prime determinant of the path follow by streams, and hence gutters, is demonstrated by the many places where the gutters leave fractures to follow the steepest local slope.

**Pseudobedding and foliation** - In some part of the world, the near surface granite is subdivided into thin slabs and attenuated lenses by fractures that run parallel or subparallel to the surface. Commonly known as Pseudobedding, it has been attributed to shear of the rock and preferential alteration along the foliation planes.



2.5



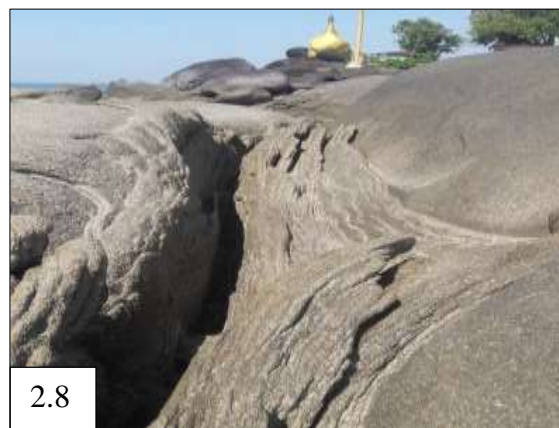
2.6

**Figure 2.5** Pits occur in porphyritic biotite granite (The pits show that the vertical face on which it is located was originally horizontal.) ( $15^{\circ}01'33''\text{N}$  to &  $98^{\circ}05'05''\text{E}$ )

**Figure 2.6** Tafoni in porphyritic biotite granite ( $14^{\circ}01'12''\text{N}$  &  $98^{\circ}04'55''\text{E}$ )



2.7



2.8

**Figure 2.7** Sheeted nature of biotite granite ( $14^{\circ}59'54''\text{N}$  &  $98^{\circ}04'42''\text{E}$ )

**Figure 2.8** Flakes and spalls occur in porphyritic biotite granite ( $14^{\circ}59'39''\text{N}$  &  $98^{\circ}04'50''\text{E}$ )



2.9



2.10

**Figure 2.9** Polygonal crack occur in biotite granite ( $15^{\circ}01'08''\text{N}$  &  $98^{\circ}01'33''$ )

**Figure 2.10** Gutters and Grooves occur in biotite granite ( $14^{\circ}59'37''\text{N}$  &  $98^{\circ}04'23''\text{E}$ )



**Figure 2.11** Kluftkarren on a vertical wall occur in biotite granite (15°02'08"N & 98°05'41"E)

**Figure 2.12** Pseudobedding in porphyritic biotite granite (15°01'28"N & 98°04'48"E)

### 2.2.2 Tectonic forms

Tectonic forms contain A-tent and orthogonal cracks. They are formed by different ways of tectonic movements.

**A-tent** - Tectonic processes are responsible for a small but notable suite of landforms in granite. A tent or pop-ups cannot in reason be attributed either to insolation or to erosional offloading. They involve a permanent expansion, are consistently oriented in a given area and, in some instances, have been induced by detonation of explosives. They could be due to weathering but, as they involve a small expansion, may be incomplete or incipient A-tents.

**Orthogonal crack** - At first sight, some patterns of cracks seem comparable to polygonal cracking, but they are orthogonal rather than pentagonal or hexagonal and give rise to chocolate blocks or tablets. They commonly occur on several parallel planes at the same site. The orthogonal cracks are interpreted as due to shearing stress on surfaces that tough during dislocation. Orthogonal cracking is also developed on the extended crests of domical structures.



**Figure 2.13** A –tent occur in porphyritic biotite granite (15°02'15"N & 98°04'52"E)

**Figure 2.14** Orthogornal crack occur in microgranite (15°02'25"N & 98°04'10"E)

### 2.2.3 Structural forms

Structural forms in this area are cleft, displaced blocks and split rocks, fault, joint, fracture and intrusive dykes and veins. Most of them are formed due to crystal strain and intrusive veins.

**Cleft** - Exploitation of vertical fractures leads to clefts or slots. Such exploitation of fractures and veins can, of course, take place either at the weathering front or after exposure, some depresses, some raised, depending on the relative resistance of material injected into the fractures during deformation.

**Displaced blocks and split rocks** - The rounded or subrounded mass of a boulder rests on the base on only a small part of the whole surface. Rounded blocks and boulders include secondary partings, gravity causes unsupported sections to fall apart, in displaced blocks or split rocks, depending on whether the two parts remain in situ or whether they tumble downslope.



2.15



2.16

**Figure 2.15** Klufftkarren or clint and grike in porphyritic biotite granite. Clefts (grikes) about 15 cm deep ( $14^{\circ}59'34''\text{N}$  &  $98^{\circ}04'34''\text{E}$ )

**Figure 2.16** Displaced blocks and split rocks occur in biotite granite ( $15^{\circ}02'10''\text{N}$  &  $98^{\circ}04'55''\text{E}$ )



2.17



2.18

**Figure 2.17** Sub-rounded block with secondary fracture in biotite granite ( $15^{\circ}02'09''\text{N}$  &  $98^{\circ}04'53''\text{E}$ )

**Figure 2.18** Vertical joint observed in microgranite ( $14^{\circ}59'35''\text{N}$  &  $98^{\circ}04'31''\text{E}$ )

**Fault and Joint and fracture** – Most of faults in this area are minor and which are recognized by displacement of dykes and veins. Secondary fractures and flexures are generally associated with minor faults. Joints observed in the study area shrinkage and sheet joints. Shrinkage joints are caused by tensional forces set up in rock body as a result of cooling. Sheet joint is a set of joints may develop which are more or less parallel to the surface of the ground. They probably arise as a result of the unloading of the rock mass when a cover is eroded away.

**Intrusive dykes and veins** - Numerous dykes and veins are found in this area. Many are weathered more rapidly than the host rock and some are still level with biotite granite surface.



**Figure 2.19** Aplite veins intruding into porphyritic biotite granite (14°59'21"N & 98°04'46"E)

**Figure 2.20** Intruding aplite vein is cut and displaced by microfault and also occur large fractures near the vein (15°02'13"N & 98°05'10"E)

**Figure 2.21** Intruding aplite vein is apart and move down due to microfault (14°59'23"N & 98°04'49"E)

## Discussion

In Pa Nyit beach, many of the landforms developed on granite, both major and minor are related to the characteristics of the rock, the composition of the penetrating water and the relative amounts of weathering and erosion. Tectonic factors are significant in a suite of forms due to the release of compressive stress. Granite outcrops will acknowledge that many curves, flakes, cracks and hollows occur in this area. Minor granite forms originate in a variety of ways, many are due to weathering, some are initiated at the weathering front, others on exposed surfaces; some evolve in response to structural weakness, others on intrinsically homogeneous surfaces; some develop and diversify after exposure, others are destroyed; some are structural and others tectonic.

## Results and Conclusions

Many famous beaches are located along this coastal range. Almost all beaches have granitic rocks with many landforms. Most of granitic forms, major and minor, reflect the structure of the rock developed over eons of time from the stage of intrusion onwards. Some climatic influence on the distribution of some minor weathering forms. Many of weathering landforms are initiated in the surface and at the weathering front. Tectonic landforms are formed by different ways of tectonic movements. Most of structural landforms are formed due to crystal strain and intrusive veins. The relief developed on granite rocks may be of exogenous and endogenous origin.

Exogenous processes are directly related to the climate and contribute to the exposure of the granite rock. Flared slope do not occur in the study area but moderately steep slope occur only in this beach. In addition, it is clear that several well known minor granite forms are convergent, for they originate at different sites and evolve in different ways.

### **Acknowledgements**

I am greatly indebted to Acting Rector Dr Theingi Shwe in Dawei University and Dr Cho Cho Myint (Pro-Rector in Dawei University) for the permission to study my research area.

I am grateful to Dr Khin Aung Than, (Pro-Rector in Dagon University Rtd) for his kind help, given valuable advice and discussion during my research.

### **References**

- Bander, F., (1989). Geology of Burma. *Gebuder Borntraeger, Berlin, Stuttgart*, 278 p.
- Migon, P. (2006) Granite Landscapes of the world. Oxford University Press.
- Streckeisen, A. L. (1974). Classification and nomenclature of Plutonic rocks. *Geol. Rundschau*, 63, 773-786.
- Twindale, C.R. (1982) Granite Landforms. Elsevier, Amsterdam. 372pp
- Twindale, C.R. Vidal Romani, J.R. (2005) Landforms and Geology of Granite Terrains. Balkema, Leiden. 352pp
- Twindale, C.R. (1971) Structural Landforms. Australian National University Press, 247 pp
- Winter, (2001). An Introduction to Igneous and Metamorphic Petrology. *Prentice Hall*.

## **POTENTIAL LANDSLIDES ON WEATHERED GRANITIC ROCKS ALONG THE MYITKYINA-KANPETII CAR ROAD, KACHIN STATE**

Me Me Aung<sup>1</sup>

### **Abstract**

The Myitkyina-Kanpetii car road connects mainly Myitkyina-Waingmaw-Sadon-Kanpetii to China. It is about 80miles (96km) long that runs in east-west direction. Myanmar-China Border Gate is linked by this road consequently it transports goods for Kachin State so the economy of local people depends on it. During the rainy season, landslides often occurred along this road so local people encounter transportation and economic difficulties. This road is constructed on granitic batholiths thus two-third of the area is covered with granitic rocks. Based on field data, petrographic result and previous paper records, weathered granitic rocks are classified into two profile types: Type-A (without core-stones) and Type-B (with core-stones). Both types induce rockfalls and rock slope failures especially wedge failure and circular failure. We can deduce two potential landslides places for the study area. The first one is between the Bum Taung (N 25° 22' 54.8" and E 97° 44' 7.7") and Sadon village (N 25° 23' and E 97° 53' 12.1"). Another is between the Laphi village (N 25° 25' 30" and E 97° 59' 20") to Wai Mo village (N 25° 24' 30" and E 98° 03'). The main facts to induce landslides are a period of high rainfall, increase pore water pressure and reduce soil cohesion, steep slope nature, road construction across the slope, deforestation, lack proper drainage system, and need effective retaining wall.

**Keywords:** landslides, weathered granitic rocks, pore water pressure, soil cohesion

### **Introduction**

The Myitkyina-Kanpetii car road situates within the eastern part of the Kachin State. It is the union road which connects mainly Myitkyina-Waingmaw-Sadon-Kanpetii to southwestern border of China. It is about 80miles (96km) long from Myitkyina to Kanpeti that runs in east-west direction. It is situated between Latitude 25°21' to 25°25' N and Longitude 97°25' to 98°07' E in UTM maps (2597-7, 11, 15 & 2598-03). Location map of the study area is shown in figure (1). Annual rain fall rate of Kachin State is 78inches. The road is constructed on granitic batholiths so bedrock types are mainly granite, granodiorite and metamorphic rocks with minor amount of basic and ultrabasic igneous rock. Two-third of the area is covered with weathered granitic rocks. Granitic rocks of the study area are mainly composed of plagioclase feldspar, alkali feldspar, biotite, muscovite, quartz and hornblende with accessory iron oxides minerals.

The primary of landslides occurrence and potential regions are mountainous areas especially Eastern Highland and Western Ranges of Myanmar. The Myitkyina-Kanpetii car road falls within Eastern Highland. Myanmar-China Border Gate at Kanpetii adjacent to China border is connected by this road which is one of the entry gates to China. As a result, it is the main transportation route for goods so the economy of local people depends on it. During the rainy season, road site is rather difficult to access due to landslide often, consequently local people encountered transportation and economic difficulties. If we know potential landslides area, we can prevent it. Therefore, we should do many researches not only for landslides but also for prevention methods of landslides. Most of the people think that granitic rocks are not associated with landslides but huge and numerous slides have occurred in some granitic areas (Durgin, 1977). Granitic rocks are commonly weathered to as deep as 10-30 meters, and innumerable slides in weathered granites have been documented in tropical and humid regions, resulting in great numbers of casualties (Chigira, 2011).

---

<sup>1</sup> Dr., Professor, Geology Department, Myitkyina University, memeaung@umkn.edu.mm

Many researchers have been done some research about petrology and mineralogy for Kachin State. But well known research about landslides and its prevention methods for the study area and its environs have not been yet. Therefore, this research work aimed to describe the potential landslides for the study area and to know how to prevent it.

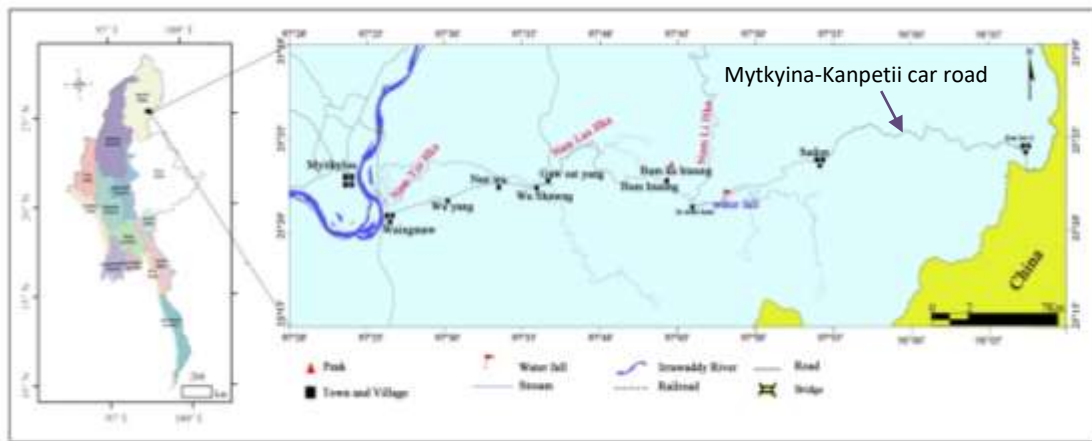


**Figure 1** Location map of the study area.

### Purposes and Method of Study

The main objectives of the study area are (1) to classify profile types of weathered granitic rocks, (2) to explain the relation of weathered granitic rocks and landslides, (3) to prepare sketch map for potential landslides area, and (3) to describe how to prevent it.

**For field method**, the UTM maps (2597-7, 11, 15 & 2598-03) are used as base map. The representative samples were collected to cut thin sections. Lithologic contacts and structural trends were measured by aiding Brunton transit and checked with the landsat images. The locations of the outcrops and potential landslide places were recorded by GPS navigator. The field data are plotted on Google Earth and UTM map linked with GPS data to illustrate the distribution of rock units and potential landslide places.

**For laboratory work**, the rock specimens collected from the field were prepared to more than (40) thin sections to examine the constituent minerals and rock types. The petrographic analysis is based on thin sections by using petrological microscope. Modal compositions were estimated not only in thin sections but also in hand-specimens. Soil genesis has been examined using field data, petrographic criteria and mineralogy of source rock. For the chemical data, major and minor oxides composition of rocks was determined by X-ray fluorescence method which was made at Mandalay University Research Centre.

### Previous Work

The Mytkyina-Kanpetii car road is built on granitic batholiths and metamorphic rocks. Landslides often occurred along this road during the every rainy season. But many researches about landslides have been done conducted for the study area. Rhodes (1968) compared the landslides in granitic rock to ten other lithologies in humid tropical New Guinea. He found that silicic igneous rocks had the most landslides per unit area. Roddick, 1974 classified four transition stage of weathering granite: fresh rock (maximum of 15% weathered material), corestones (15 to 85% weathered rock enclosing remnants of fresh rock), decomposed granitoid (85 to 100% weathered disintegrated rock that can be broken down into granules), and saprolite (fine-grained residual rock

that generally has an upper lateritic layer). A typical weathering profile of granite in subtropical climate consists of decomposed granite with core stones in the lower part and saprolite in the upper part (Ruxton & Berry, 1957). In the profile of weathered granite, the core stones are formed by spheroidal weathering (Ollier, 1967). If decomposed granite is removed from core stones, tors are left (Linton, 1955). Durgin (1977) pointed out that shallow landslides or debris avalanches occur preferentially in decomposed, weakly weathered granitic areas. In 1985, Komoo mentioned that although the characteristics of weathering profiles differ from place to place, two most common types of profiles are with and without core-stones. Granitic rocks are recognized to be very susceptible to weathering and are induced to landslides except the granites of North America and north Europe. These granites are not generally associated with landslides because most of the weathered granites on these continents have been eroded by glaciations (Chigira, 2011). Smooth-surfaced granite can reduce the effective friction angle with the overlying material. Besides, water flows through the thin permeable zone above the fresh bedrock, producing pore-water pressures and seepage forces during rainstorms. (O'Lough-lin, 1972; Swanston, 1967).

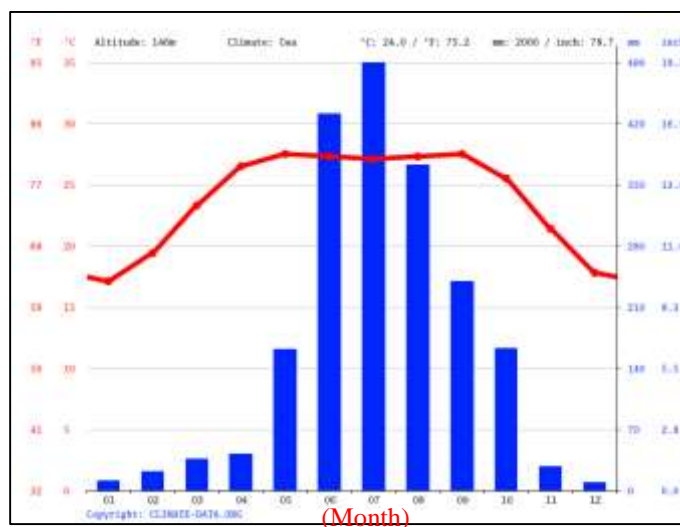
### Rock types and their distribution

The Myitkyina-Kanpetii car road is constructed on granitic batholiths and metamorphic rocks. According to field data combined with thin section result and chemical data, the igneous rocks comprise in the study area are pegmatite, hornblende granite, granodiorite, diorite, dolerite, basalt, gabbro and peridotite. Metamorphic rocks include metaigneous (orthogranite, orthogranodiorite and amphibolite) and metasedimentary (slate, schist, biotite gneiss, migmatite). Exposure of granitoids especially granite and granodiorite are exposed along the road especially at GPS references (from Latitude 25°22' to 25°24' N and Longitude 97°41' to 97°47' E) and (from Latitude 25°23' to 25°26' N and Longitude 97°50' to 98°05' E). These granitoids are intruded into metamorphic, and have complex texture, i.e., transform from granitic to granodioritic composition within a batholith. Almost all of the igneous and metamorphic rocks of the study area possess highly jointed nature. They exhibit batholiths to semi-circular bodies with exfoliation nature. The core stones from weathered granitoids are formed by spheroidal weathering of granite.

The rock distribution along the road site is calculated by aiding field data combined with petrographic data. In relation to this result, the extent outcrop of hornblende granite with granodiorite is 40 to 60 %, diorite is 2%, dolerite is 5 to 15%, peridotite 1 to 2%, metagranite is 20 to 35%, metapelite is 5 to 20%, and sedimentary rock is 1 to 3%, of the overall abundance. These results point out two-third of the areas is covered by weathered granitic rocks and soil. Granitic rocks of the study area are mainly composed of plagioclase feldspar, alkali feldspar, biotite, muscovite, quartz and hornblende with accessory iron oxides minerals.

These batholiths were built on continental arc which associated with subduction zones; therefore, it possesses complex structure and rugged topography. Zhang, J.E. et. al., 2018 stated that the igneous rocks especially peridotite, andesite, hornblende gabbro, diorite, granodiorite and plagiogranite, from Eastern Kachin State possess arc geochemical signatures and ages of 177–166 Ma. Eastern Kachin State has long-term tectonic history so the rocks from the study area encountered long-termed physical and chemical weathering which caused the physical appearance and properties of granitic rock change as weathering progresses. According to field data joint with petrographic data, biotite is a particularly active agent in the weathering process and it expands to form hydro-biotite that helps disintegrate the rock into grus. The feldspars break down by hydrolysis and hydration into clays and colloids, which may migrate from the rock. Muscovite and quartz grains weather slowly and usually form the skeleton of saprolite. Saprolite is a fine-grained residual rock that generally has an upper lateritic layer.

The topography of the study area is very different from east to west, i.e., eastern part has high relief (within 1200m to 2100m height) with rugged terrain, the centre part has medium to high relief (between 600-1100m height) and the western part has low relief with soil cover and. Steep slope and landslides are more common in eastern part than centre part. Annual rain fall rate of Kachin State is 78 inches (Fig.2).



(Source:CLIMATE-DATA.ORG)

**Figure 2** Annual rainfall and Temperature of Myitkyina Area.

The Myitkyina-Kanpetii car road through from Myitkyina to Waingmaw-Bum Taung-In Want Kaung-Sadon-Lu Kyi-Laphi-Waw Chon- Shan Ji-Wai Mo and Kanpetii. During the rainy season, landslides often occurred along this road: e.g., Landslides due to rainstorms in Wai Mo village (N 25° 24' 30" and E 98° 03') in 25<sup>th</sup> June 2019; and Rocks falls (size -100ft\_30ft\_20ft) between mile stone (105/106) km, and circular failure (size -100ft\_30ft\_20ft) between mile stone (105/106) km around the Waw Chon village group (N 25° 26' and E 98° 01' 30") especially between 105km and 108km in 19<sup>th</sup> July 2020 (source:21<sup>st</sup> July 2020 Myanmar Alinn Daily).

During the rainy season, small to deep landslide frequently occurred in two places. The first one is between the In Want Kaung village (N 25° 21' 35.2" and E 97° 45' 27.1") and the Sadon village (N 25° 23' and E 97° 53' 12.1"), and their height range is within 600m to 1200m. The second is between the Waw Chon village (N 25° 26' and E 98° 01' 30") and the Wai Mo village (N 25° 24' 30" and E 98° 03') and their height reached up to 2000m. These villages are built on fresh and decomposed granotoids and metamorphic especially metapelites and metagranitoids. Weathered granite soil has its own unique physical and chemical properties so it can cause easy weathering and particle breakage. Therefore, the susceptibility of landslides of the study area relies on slope angles of hill, soil cohesion, pore water pressure and a period of rainfall.

## Result from Field data

### Characteristic Profile Types of Weathered Granitic Rocks

Based on the field data, petrographic criteria and chemical data together with previous paper records, the weathering of granitic rocks from the study area can be classified into two profile types: Type (A) and Type (B). Both types of profiles are induced to landslides.

**Type-A** (without core-stones) contains three characteristic features: (1) fresh rock, (2) decomposed granitoid, and (3) thick layer of residual soil (Fig. 3). Type-A profile is recognized in the field by presence of a very thick layer of residual soil and completely weathered material. Besides, the soil-

rock boundary between the overlain soil material and slightly weathered fresh rocks is very sharp. Some weathering profile can have a thickness of up to 21m (70ft). Both shallow and deep landslides are caused on Type-A profile.



**Figure 3** Type-A Profile: (1) fresh rock (N 25° 24' 32.2" and E 97° 58' 01.5"), (2) decomposed granitoid (N 25° 22' 25.2" and E 97° 44' 57.3"), and (3) residual soil (N 25° 23' 46.2" and E 97° 38' 40.5").

**Type-B** (with core-stones) is especially found in granitic rocks with exfoliation texture and with highly jointed nature. This profile type includes (1) fresh rock, (2) core-stones, (3) decomposed granitoid, and (4) saprolite (Fig. 4). The core stones are formed by spheroidal weathering of granite and their size ranges from few centimeters to meters in diameter (Fig. 5). This profile type is easily noticed in the field by the presence of core stones (Fig.5). Besides, highly to moderately weathered materials contain core stones of various sizes.

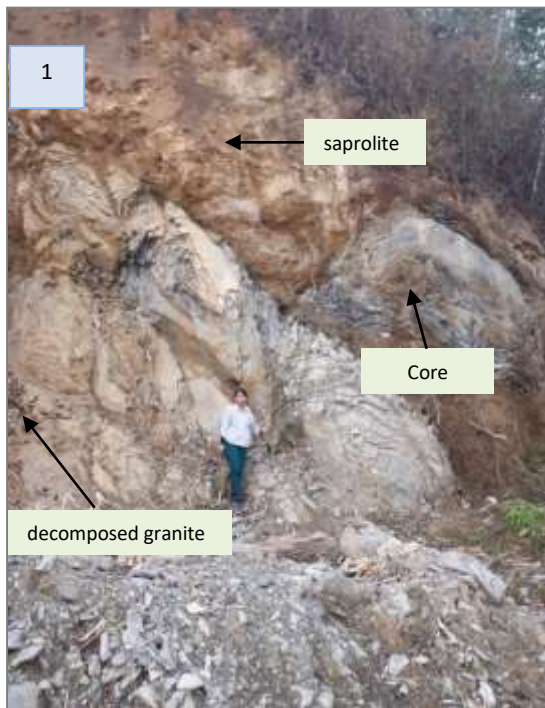


**Figure 4** Core stone, decomposed granite and saprolite formed by spheroidal weathering of granite. (N 25° 24' 25.2" and E 97° 54' 56.1")

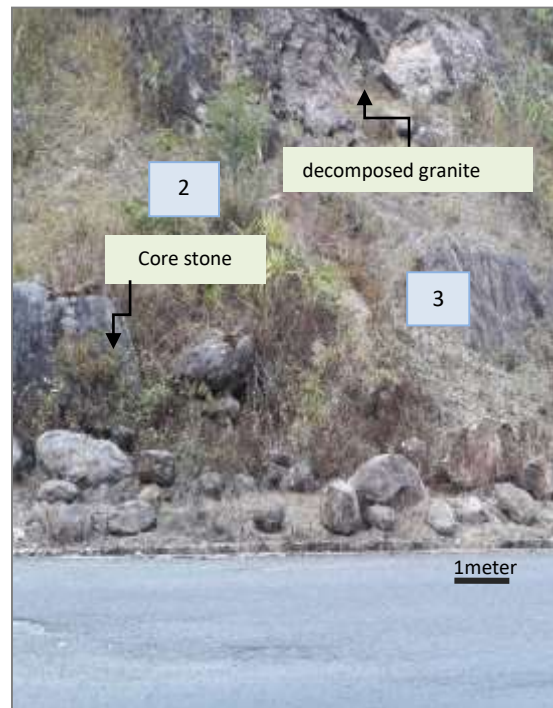


**Figure 5** Various size of core stones fall at the side of the road. (N 25° 24' 35.2" and E 97° 53' 22.8")

The failure originated in **fresh granite** if having fracture and highly jointed nature. The susceptibility of fresh bedrock to rockfalls and rockslides depends upon the angle of shearing

resistance of the jointed rock, the effective cohesion, and pore water pressure. As weathering progresses, decomposed granite forms along the joint planes and decreases the effective cohesion while increasing the void ratio. Rockfall especially debris flow and wedge failure may occur in fresh granite.

When the weathered zone developed, outward from the joints and isolates blocks or boulders of fresh rock to form **corestones** and which may roll down slopes during rainy periods, causing extensive damage. Rockfalls have been formed by presence of corestones. It consists of a large rock mass that falls off a steep slope, generating a stream of fast-moving debris.

During the stage of **decomposed granitoids**, granular disintegration takes place, and crystals become increasingly detached from each other. At this stage, biotite and feldspar weather first, to form microfractures and pores. The degree of saturation of the decomposed granite is important factor to safety. Saturated decomposed granite has essentially no cohesion when saturation reaches 100%, the apparent cohesion is zero, and pore-water pressures may cause failure. The weathering front in granitoids is abrupt, and water can be perched above the fresh impermeable bedrock. Subsurface water drains through the decomposed granitoid above the fresher rock. Rainstorms usually bring on the failures that produce rockfalls. The most widespread slide problems have been reported at granitoid decomposes stage (Matsuo, 1968; Durgin 1977). Rockfall (Fig.6) and rock slope failure may be occurred on granitoid decomposes areas.

**Saprolite** is the final stage of weathering results and shows brownish colour overlain by a red lateritic layer. Residual granitoid consists mainly of quartz, muscovite, and kaolinite. Although the presence of overburden pressures, the void ratio increases the pore spaces to decrease as the rock compresses. If tension cracks form at the head of failure plane where the soil will collapse, there is forming a failure (Fig.7). Durgin (1977) described a slope failure characteristic of saprolite is the slump or rotational slide. The rupture surface is no longer controlled by a fresh rock boundary as in earlier stages, but forms a circular failure surface. Rock slope failures especially circular failure may be formed at this stage.

Both types of profiles are found in the study area and these types induced rockfalls and rock slope failures especially wedge failure and circular failure.



**Figure 6** Rockfall site at the side of the road.  
(N 25° 21' 35.8" and E 97° 45' 30.1")



**Figure 7** Forming tension cracks indicate to occur circular failure.  
(N 25° 21' 35.2" and E 97° 45' 27.1")

### Potential Landslides areas

The Myitkyina-Kanpetii car road through from Myitkyina to Waingmaw-Bum Taung-In Want Kaung-Sadon-Lu Kyi-Laphi-Waw Chon- Shan Ji-Wai Mo and Kanpetii. During the rainy season, landslides often occurred along this road. Therefore, this road often meets block of transportations and goods due to landslides within the rainy season every year.

According to the field data combined with petrographic criteria and previous causes records; we can estimate two potential landslides places for the study area as follows;

1. The first place is between the Bum Taung (N 25° 22' 54.8" and E 97° 44' 7.7") and Sadon village (N 25° 23' and E 97° 53' 12.1").
2. The second is between the Laphi village (N 25° 25' 30" and E 97° 59' 20") to Wai Mo village (N 25° 24' 30" and E 98° 03').

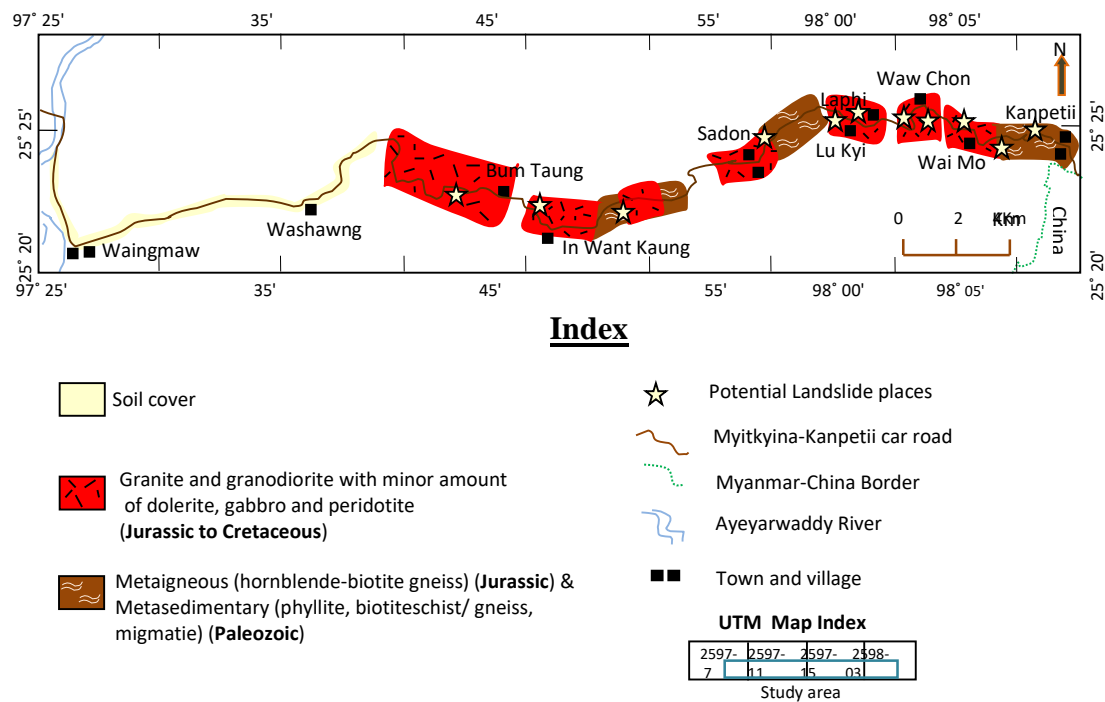


**Figure 8** Sketch Map for potential Landslides places and granitic rocks distribution of the study area. (Modified after Me Me Aung, 2019a and Yar Zar Aung, 2019)

### Causes of Landslides

Two characteristic profile types can recognize in the field are Type-A (without core- stones) and Type-B (with core-stones). Both types of profiles are common on weathered granitoids, and induced to landslides.

According to their profile types, and previous landslides records, two types of landslides can be recognized for the study area; (1) rockfalls, and (2) rock slope failure especially circular failure and wedge failure. Circular failure occurs on loose soil while wedge failure occurs on highly jointed granite and metamorphic rocks.

The main causes of landslides for the study area are (1) a period of high rainfall, (2) increasing pore water pressure and reduce soil cohesion, (3) steep slope nature, (4) road cutting along the slope, (5) deforestation, (6) lack of proper drainage system, and (7) require effective retaining walls.

The rockfalls are related to road construction across the slope, steep slope nature and a period of very high rainfall. Both rockfalls and rock slope failure depend on increasing pore water pressure and reduce soil cohesion. Soil reduces its cohesion because of water contents exceeds optimum moisture contents of the soil, oversaturated soils especially clayey soil loses their cohesiveness. Slope stability mainly depends on the cohesion of soil so-called shear strength.

Steep slope of soil that is slope of the hill is more than the angle of impose of soil, the angle of impose should not exceed the frictional angle ( $\phi$ ) of soil and infiltration of water into the soil that reach transition zone (i.e, Saprolite) and the water acts as a lubricant between hard rock and overlying weathered soil. The water in Saprolite becomes more pore water pressure and this pressure kick off the overlying soil. Also water added to the soil become heavier the existing soil and gravitational force exerted to the soil pull down the soil to downhill.

Smith (1970) stated the Mohr-Coulomb failure criterion which represents the linear envelope that is obtained from a plot of the shear strength of a material versus the applied normal stress. This relation is expressed as:

$$T = c + \sigma \tan \phi$$

Where T = Shear strength of the soil or rock

c = Cohesion of soil or rock

$\phi$  = internal frictional angle of soil or rock

If water invasion to the soil, the basic formula becomes as:

$$T = c + \sigma \tan \phi - \mu$$

Where  $\mu$  = pore water pressure of soil or rock

So, it is clearly seen how water is important to the slope stability and causes of landslides. The more the pore water pressure contents effects the less the stability of the slopes.

Tree roots growing in the decomposed granitoid help stabilize the slope. At some sites, rainstorms have triggered failures a few years after road building and clear cutting of forests. The large, deep-seated failures involved rotational sliding and slumping. The tree roots probably had no stabilizing effect on deep slides. In addition, woodland soils have infiltration capacities that conduct rainfall to the subsurface rather than surface run-off.

Retaining walls are used to bound soils between two different elevations. Weep holes in retaining walls must be sized adequately to overcome surface tension and they allow water to escape from behind the wall. Although retaining walls have been constructed along the road of the study area, need to repair more effective style, i.e., need adequate size weep holes to drain water. (Fig.9)



**Figure 9** Retaining walls, which have been constructed by granitoids, along the Mtitkyina-Kanpetii car road; (a) weep holes (b) wall without weep holes (c) damaged wall.

## Discussion

Weathered soil, which have been formed by final stage of weathering results, and thick residual soil, may slides as circular failure or plane failure and combination of both. To prevent weathered soil landslide, it need to reduce the overburden weight and to draw out the infiltration water into the soil. So bench cutting the slope or gentle slope may reduce the weight of the soil. To draw out the infiltration water, installation of weep holes should be properly put in. Sometimes construction of retaining walls and installation of the weep holes are more effective to prevent landslides. Good drainage system is needed to prevent infiltration of rain water into the soil and it can reduce the pore water pressure of the soil.

Hills with weathered granitoids outcrop having steep slope can cause rockfalls and rock slope failure especially as wedge failure due to its highly jointed nature. To retain the strength of the jointed granitic rocks, rock bolts or anchors should be installed. Besides, forests on hillslope reduce the surface runoff and vegetation cover prevents erosion of the soil slope. The roots of the trees hold on the weathered soil firmly. Trees on hillslope reduce the surface runoff. So planting trees not only reduce the soil erosions but also the dwindling of pore water pressure.

## Conclusions

The Myitkyina-Kanpetii car road connects from Myitkyina to Waingmaw-Bum Taung-In Want Kaung-Sadon-Lu Kyi-Laphi-Waw Chon- Shan Ji-Wai Mo and Kanpetii. Two characteristic profile types can distinguish in the field are Type-A (without core- stones) and Type-B (with core-stones). Both types of profiles are common on weathered granitoids, and induced to landslides. Two types of landslides can be found along the route are (1) rockfalls, and (2) rock slope failure especially circular failure and wedge failure. Circular failure occurs on loose soil while wedge failure occurs on highly jointed granite and metamorphic rocks.

In accordance with the field data combined with petrographic criteria and previous causes records; we can guess two potential landslides places for the study area as follows;

1. The first one is between the Bum Taung (N 25° 22' 54.8" and E 97° 44' 7.7") and Sadon village (N 25° 23' and E 97° 53' 12.1").
2. The second is between the Laphi village (N 25° 25' 30" and E 97° 59' 20") to Wai Mo village (N 25° 24' 30" and E 98° 03').

The main causes of landslides for the study area are (1) a period of high rainfall, (2) increasing pore water pressure and reduce soil cohesion, (3) steep slope nature, (4) road cutting along the slope, (5) deforestation, (6) lack of proper drainage system, and (7) require more effective retaining walls.

The engineering properties of granitic rock change as weathering continues. Granitoids break down progressively from massive blocks to a deep layer of clay-size particles. Each stage of weathering is susceptible to specific landslides hazards. If the stage of weathering is identified at a site, it will provide clues to the engineering properties of the material and help the engineering geologist predict the slope-stability hazards of proposed actions. This research work is only based on field data and petrographic criteria to estimate potential landslides areas. Therefore, many researchers should do several geological and geotechnical research works especially soil mechanics and rock mechanics for this area.

## Acknowledgement

We express our thanks to Rector Dr Aung Win, Pro-rectors Dr Aye Aye Ko of Myitkyina University and Professor and head Dr Myint Oo, Geology Department of Myitkyina University for providing necessary resources.

## References

- Chigira, M. Chigira M., Mohamad Z., Sian L.C. & Komoo I. (1999). Landslides in weathered granitic rocks in Japan and Malaysia. *Bulletin of the Geological Society of Malaysia* 57 (2011) 1 – 6.
- Durgin, P.B. (1977). Landslides and the weathering of granitic rocks. *Geol. Soc. Am., Rev. in Engng. Geol.*, 3, 127-131.
- Komoo, I., (1985). Engineering properties of weathered rock profiles in Peninsular Malaysia. Proc. 8th Southeast Asian Geotechnical Conference, Kuala Lumpur, Malaysia, 3.81-3.3.86.
- Linton, D.L., (1955). The problem of tors. *Geog. Jour.*, 121, 470-486.
- Matsuo, S. Nishida, K., and Yamashita, S., (1968). Weathering of the granite soils and its influence on the stability of slope: *Kyoto Univ. Fac. Eng. Mem.*, v. 30, pt. 2, p. 85-93.
- Me Me Aung (2019a). Outcrop nature and types of Igneous and Metamorphic Rocks exposed around the road section from Maingna to Sadon Waterfall, Waingmaw Township, Kachin State (Departmental Research)
- Ollier, C., (1967). Spheroidal weathering, exfoliation and constant volume alteration. *Z. Geomorph.*, 11, 103-108
- O'Loughlin, C. L., (1972), An investigation of the stability of the steep land forest soils in the Coast Mountains, southwest British Columbia [Ph.D. dissert.]: Vancouver, Univ. British Columbia, 147 p.
- Rhodes, D. C., (1968), Landsliding in the mountainous humid tropics: A statistical analysis of landmass denudation in New Guinea: Office of Naval Research, Geography Branch, Tech. Rept. 4, 77 p.
- Roddick, J. A., (1974). Circum-Pacific plutonism-Foreword: *Pacific Geology*, v. 8, p. i-ii.
- Ruxton, B. P., and Berry, L., (1957). Weathering of granite and associated erosional features in Hong Kong: *Geol. Soc. America Bull.*, v. 68, p. 1263-1291.
- Swanston, D. N., (1967), Soil-water piezometry in a southeast Alaska landslide area: U.S. Dept. Agriculture Forest Service Research Note PNW-68, 17 p.
- Smith, M. J., (1970). *Soil Mechanics: 2<sup>nd</sup> ed.*, The English Language Societh and Macdoland and Evans Ltd.
- Yar Zar Aung (2019). Geology of the Waw Chon Area, Waingmaw Township, Kachin State. p.14. (M.Sc Thesis)
- Zhang, J.E., Xiao, W. J., Windley, B. F., Wakabayashie, J., Cai F. L., Seing, K., Wua, H., Soe Naing, S., (2018). Multiple alternating forearc- and backarc-ward migration of magmatism in the Indo-Myanmar Orogenic Belt since the Jurassic: Documentation of the orogenic architecture of eastern Neotethys in SE Asia. *Earth-Science Reviews* 185 (2018) 704–731

## **HYDROCARBON POTENTIAL OF CRETACEOUS TETHYAN REALM IN MYANMAR**

Than Than Thwe<sup>1</sup> and Thura Oo<sup>2</sup>

### **Abstract**

Occurrence of organic matters in the Cretaceous marine fossiliferous limestones, viz., Thauungpwet Taung limestones exposed at the Second Defiles of Ayeyarwady River and Paungchaung limestones exposed at the eastern foothill of Mt. Victoria are studied. The identified fossil assemblages indicate that the paleobiogeographic locations of the two units were in the northern Tethys Sea during Cretaceous. Both lithofacies and biofacies analysis reveal that the light bluish grey limestones (Thauungpwet Taung Formation) were deposited in an opened lagoonal basin in the shallow marine shelf underlain by the well-oxygenated subsoils and later, the organic matters accumulated in the limestones were eventually replaced by calcites during diagenesis. The dark brownish grey limestones (Paungchaung Limestone Formation) were deposited as distal carbonate ramps in deeper sea with euxinic floor and later enriched with organic matters due to the worldwide oceanic anoxic event (OAE) which is indicated by the high ratio of smaller planktic foraminifers and dinoflagellates to the smaller benthic foraminifers, and occurrence of iron sulphide (pyrite) in the chambers of planktons' test. In addition, the planktic foraminiferal biostratigraphic zones recognized in the Paungchaung limestones indicate a coincidence with the mid-Cenomanian OAE which caused a large accumulation of organic carbon across the Tethyan realms. It is contrasted, that above two types of limestones have different amount of organic matters though a global event provided similar euxinic condition. Therefore, it can be regarded that the geometry of individual basin was major controlling factor to the physiochemical condition of each basin. Present study evidenced that Paungchaung limestones with high organic matters were accumulated during the mid-Cenomanian OAE occurred across the Tethys Sea. Indeed, these limestones underlie the Tertiary clastic sequences of Central Myanmar which are being drilled for the hydrocarbon industries.

**Keywords:** Cenomanian, organic matters, oceanic anoxic events,

### **Introduction**

Mesozoic rocks deposited in the Tethyan realm are very interested for their hydrocarbon potential as source rocks for the oil and gas exploration. It was noted that Tethyan realm provides about 70 per cent of the world petroleum reserves. Therefore, paleodepositional configuration of the Tethyan realm has been prepared to understand the controlling parameters for the accumulation of organic carbon. With reference to that integrated works, a microfacies analysis and paleodepositional synthesis is carried out with comparative study on the Myanmar Mesozoic rocks with those prolific units reported from the other Tethyan realm.

Most of the hydrocarbon source rocks are marine sedimentary rocks, e.g., limestone and shale, which are rich in primary organic matters. Both organic carbon and inorganic carbon are accumulated in the marine sediments. The organic matters derived from the terrestrial sources and also from the marine sources are deposited and then changed into the organic carbon during the diagenesis.

During Cretaceous, marine sediments with high organic carbon content were deposited widely in the Tethyan Sea as well as in the epi-continental seas of Boreal region. The depositional basins were formed in a variety of paleo-bathymetric configuration. The widespread and synchronous occurrence of these organic carbon-rich deposits in various basins with different geometry indicates that organic carbon accumulation is not strictly controlled by the basin

---

<sup>1</sup> Professor, Department of Geology, East Yangon University

<sup>2</sup> Rector, Monywa University

geometry but much provided by a worldwide mechanism, certainly, Oceanic Anoxic Events (OAEs) (Gambacorta *et al.*, 2016).

### **Objectives of the present research**

During Cretaceous, there were three salient events, of which tremendous accumulation of organic matters in the marine carbonate and shale. These three events were known as (OAE 1) occurred in the Early Albian, (MCE) occurred at mid-Cenomanian and (OAE2) began near to the end of Cenomanian. In Myanmar, marine fossiliferous limestones with Albian-Cenomanian fossils are found in the northern and western Myanmar and hence, those limestones are re-examined for present research with following objectives;

- (i) lithofacies and biofacies analysis done for the regional correlation of studied Myanmar limestones with those of the Tethyan realm,
- (ii) paleo-depositional synthesis carried out to decipher the controlling factors on the accumulation of organic matters in the limestones.

### **Study areas and the methods of study**

In Myanmar, the Cretaceous Tethyan realms are recognized by the presence of globally distributed smaller planktic foraminifers, nannofossils, and dinoflagellates which were boomed in the Tethys Sea. Profuse numbers of these zooplanktons and phytoplanktons are observed in the limestones exposed along the Tagaung-Myitkyina track, in the Jade-mines area, in the Pinlebu-Banmauk area, and at the eastern foothills of Mt. Victoria. Among them, fossiliferous limestones of Thauungpwet Taung Formation exposed at the Second Defile of Ayeyarwady River (study area 1 in Figure 1), and Paungchaung Limestone Formation near Saw (study area 2 in Figure 1) were re-visited and re-examined in year 2017 and 2019. Both megascopic and microscopic analyses of lithofacies and biofacies were done and some rock-samples are being processed for the TOC analysis.

### **Cretaceous Tethyan marine sediments in Myanmar**

During Cretaceous the Shan-Thai Block is a particular domain which was amalgamated into the Indochina Block of Eurasia Plate. The succeeding oceanic part behind the Shan-Thai Blocks became a shallow marine shelf for the deposition of fossiliferous Cretaceous limestones and later it was amalgamated into the foregoing Shan-Thai Block. The oceanic fragment underlying the present western Myanmar, west of the East Kachin ranges and Shan Plateau, was evolved as Burma Block after Cretaceous.

During Triassic and Jurassic, the posterior margin of the Shan-Thai Block was passive continental margin and accommodated for the deposition of mudstone-dominated turbidites (i.e., Shweminbon Formation and its homotaxial) and volcanoclastic silici-clastics (i.e., Loi-an Formation and its homotaxial). The block was regarded to be in the tropical Tethys Sea as suggested by the fauna and the occurrence of red-beds (i.e., Kalaw and Hsipaw red beds).

The proto-Burma Block comprising with ophiolitic basement (i.e., Ngapyawdaw Chaung Formation and its homotaxial) and overlying Thauungpwet Taung limestones, Namakauk limestones, Paungchaung limestones, Kyigone/Kabaw shales and Falam turbidites was developed as a narrow shallow marine shelf in the northern tropical (arid) Tethys Sea as shown in Figure 2. Therefore, present studied limestones were deposited in the northern Tethys Sea and observed foraminifers analogues to the affinities of western Tethyan realms described from the Tibet, Alps, Spain, Zagros (Iran). By contrast, Myanmar Cretaceous foraminiferal assemblages are different to

the assemblages described from the India's east coast and Tunisia, which were southern Tethyan realms (Thura Oo, 2000).

The northern Tethyan realm in Myanmar are recognized by the presence of globally distributed planktic foraminifers, nannofossils, and dinoflagellates which were boomed in the Tethys Sea. Profuse numbers of zooplankton and phytoplankton assemblages leading by the Albian and Cenomanian foraminiferal index species and zone species are observed in two limestone successions exposed at study area 1 and 2, respectively.

### **Thaungpwet Taung limestones**

Albian-Cenomanian limestones exposed at the Second Defiles are thinly laminated to poorly bedded light bluish grey bioclastic and micritic limestones (lime mudstone-wackestone-packstone-grainstone-floatstone) (Figure 3) (Than Than Thwe and Thura Oo, 2020). Intense diagenesis and tectonic deformation are observed. The comprising mega-fossils are; gastropods, bivalves, bryozoans and Scleractinian corals. The foraminiferal assemblages represent *Orbitolina concava* Biozone and *Hedbergella planispira* Biozone (Thura Oo, 2000). Both carbonate lithofacies and biofacies analyses indicate that majority of the limestones are proximal carbonate ramps, deposited in an open lagoonal shelf. Rich population of larger and smaller benthic foraminifers with other bottom dwelling organisms, viz., bivalves, gastropods, corals, bryozoans and algae indicate a well-oxygenated subsoil and bottom water. Presence of nannofossils and dinoflagellates also suggests well-access to the opened sea and nutrient-rich basin-water-circulation (Than Than Thwe, 2010, 2011).

Though, the limestones are fossiliferous, original organic matters, such as, shells, tests and algal mat, were totally replaced by the calcite, and the chambers were filled with sparry calcite and lime-mud. Therefore, most of the organic matters accumulated in the sediments were already transformed during the diagenesis. In addition, some lime-mud or micrite were replaced by the sparry calcite and plant-derived organic matters were already decayed, too. No salient organic matters were observed in thin-sections of the limestones (Figure 3).

### **Paungchaung limestones**

Albian-Cenomanian limestones exposed in the Paung-nge stream in Saw Township are well bedded dark brownish grey bioclastic and micritic limestones (lime mudstone-wackestone) intercalated with thin dark grey calcareous mudstone and fine-grained sandstone (Figure 4) (Than Than Thwe and Thura Oo, 2020). Moderate diagenesis and tectonic deformation are observed. The biotas contained in the limestones are planktic foraminifers and dinoflagellates with minor radiolarians. The planktic foraminiferal assemblages represent *Hedbergella planispira* Biozone together with occurrence of *H. delrioensis*, *Rotalipora* spp. *Textularia* spp. (Thura Oo, 2000). Both carbonate lithofacies and biofacies indicate that the limestones are distal carbonate ramps, deposited on a slope with minor as well as intermittent muddy turbidity currents. No larger benthic foraminifers have been found in present study. Therefore, the subsoil might be less-oxygenated and unfavourable for the bottom dwellings. However, presence of smaller planktic foraminifers and dinoflagellates suggests opened sea and nutrient-rich upper water.

Though, most of the shells and tests of the foraminifers were replaced by the calcite, the chambers of the tiny tests were filled with pyrites. In addition, most of the organic matters accumulated in the sediments were preserved and found as dark brown amorphous organic matters in thin-sections. The controlling factors on the depositional paleo-environmental might prohibit the bottom oxygenation and bottom habitats by prevailing a euxinic condition.

### Findings and Concluding Remarks

The identified fossil assemblages in the limestones indicate that the depositional environment of the two units were in the northern Tethys Sea during mid-Cretaceous. Both lithofacies and biofacies analyses of the limestones reveal that the Thauungpwet Taung Formation was deposited in an opened shallow marine shelf with lagoonal condition which was underlain by the well-oxygenated subsoils. Therefore, the organic matters accumulated in the limestones were eventually replaced by calcites during diagenesis.

The Paungchaung Limestone Formation was deposited as distal carbonate ramps in deeper sea with euxinic floor. At the same time, it was considered that the arid and warm climate with high  $p\text{CO}_2$  provided from the volcanisms prevailed highly productive and nutrient-enrich upper water while deeper water on the base of the continental slope and abyssal plain condition were reducing and anoxic caused large accumulation and preservation of organic matters. This worldwide OAE is indicated by the high ratio of smaller planktic foraminifers and dinoflagellates to the benthic foraminifers, and the occurrence of iron sulphide (pyrite) in the micron-sized chambers of planktic foraminifers' test.

In addition, among the Albian-Cenomanian planktic foraminiferal biostratigraphic zones, the *Hedbergella planispira* Zone was well-recognized in the Thauungpwet taung limestone and Paungchaung limestones. In the western Tethyan realm, the occurrence of mid-Cenomanian OAE (MCE) overlapped with this biozone.

It is noted that both limestones have similar stratigraphic position and were deposited in northern Tethyan realm, physiochemical condition of the bottom-waters which was largely controlled by the basin geometry caused oxidizing condition to the shallow shelf while a worldwide anoxic condition of the sea was occurred. Therefore, it is contrasted, that above two types of limestones have different amount of organic matters though a global event provided similar euxinic condition. Therefore, it can be regarded that the geometry of individual basin was major controlling factor to the physiochemical condition of each basin.

Organic carbon-rich sediments were developed worldwide in pelagic sedimentary sequences of Early and mid-Cretaceous Tethys, oceanic plateaus, basins, continental margins and shelf. They were deposited in a variety of paleodepositional and basin geometry. The widespread occurrences of these large accumulation in short interval of Cretaceous were regarded to be a product of Cretaceous OAEs but there were modification prevailed by the local basin geometry. In addition,

Based on the study of the Mesozoic rocks exposed along the east, northeast, north and western margin of the Cenozoic Basin of Myanmar, the oil and gas producing reservoirs are underlain by the Cretaceous fossiliferous marine sediments and ophiolitic basement (Thura Oo, 2000). Therefore, these Cretaceous limestones are being paid much attention for the source rocks identification as well as origin and migration of the hydrocarbon.

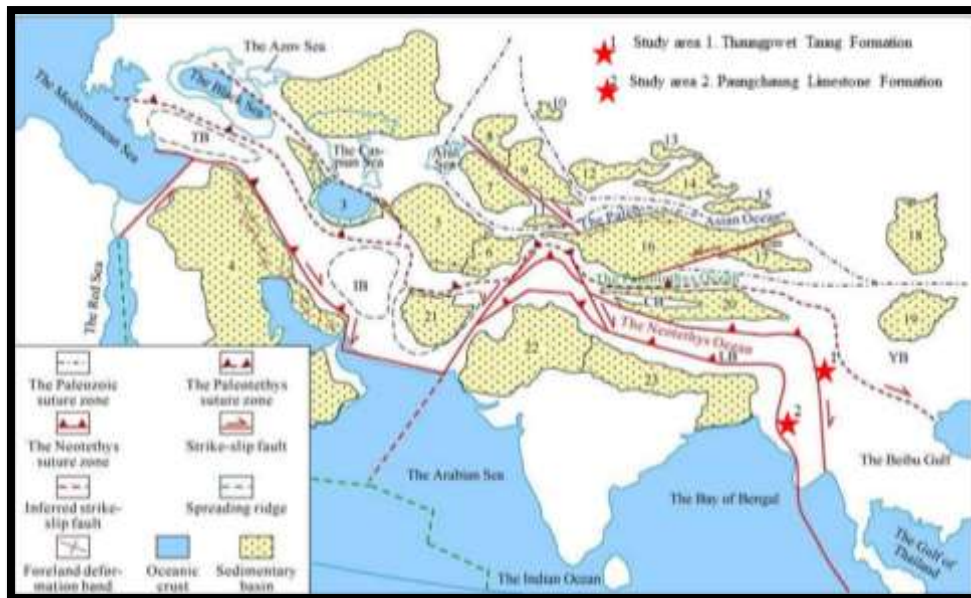


**Figure 1** Locations of the present study areas (red stars) demarcated on the Map of the modern spatial distribution of the Tethys structure domains (Chengzao *et al.*, 2018).

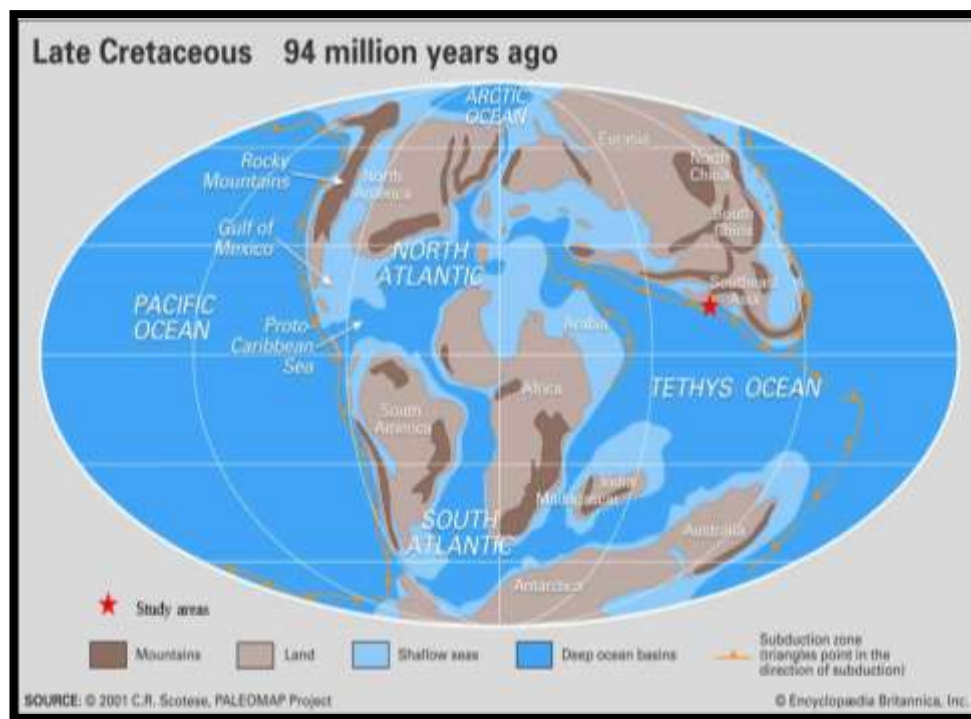


**Figure 2** Showing the study areas on the reconstructed paleogeographic map of the Earth for Late Cretaceous to recognize their position in Tethys Ocean.

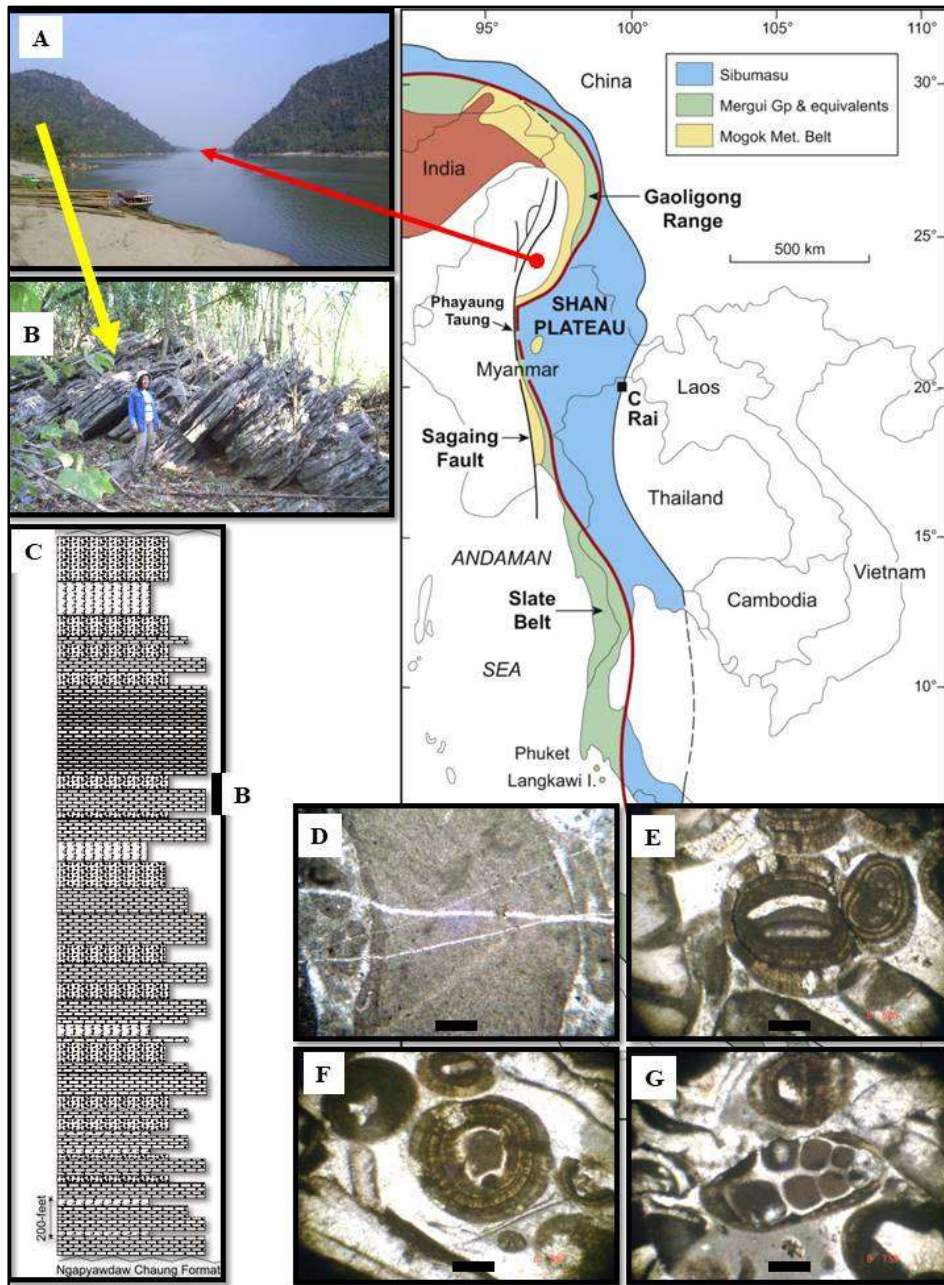


**Figure 3** Thaukpwet taung limestones exposed at the Second Defile of Ayeyarwady River. The inserted tectonic domain map (Mitchell, 2018) is used to show the location of sampled limestones. (A) The Defile. (B) The thin-bedded bioclastic floatstone-grainstone-rudstone. (C) The measured lithostratigraphic column of the Formation at the defile, the stratigraphic position of the outcrop (B) is indicated. (D-G) Microphotographs showing the biotas including organic carbon are already replaced by the calcite. All scale-bars are 0.1 mm in length.

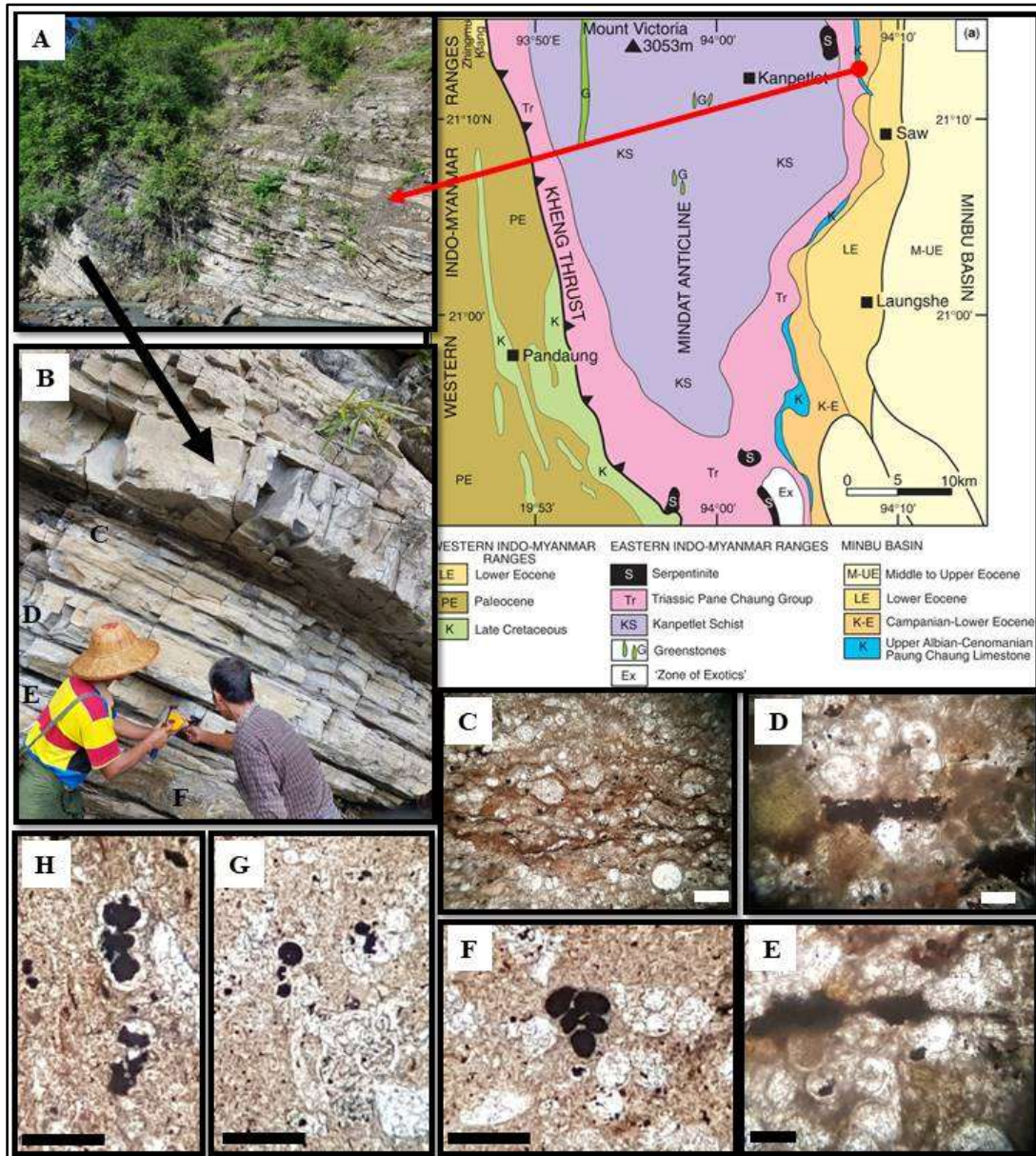


**Figure 4** Paungchaung limestones. The inserted geological map of southern Mt. Victoria (Mitchell, 2018) is used to show the location of sampled Paungchaung Limestone Formation, well-bedded limestones intercalated with thin calcareous mudstones and fine-grained sandstone, exposed on the northern cliff of Paung-nge stream. (B) The outcrop of thin-bedded bioclastic wackestones. (C-E) Microphotographs showing organic-rich laminations and amorphous organic matter. (F-H) Microphotographs showing pyrite-filled chambers of foraminifers' tests. All scale-bars are 0.1 mm in length.

## Acknowledgment

It is acknowledged those authority concerned of the Zinbon village, Shwe ku Township and Anyakadin village, Saw Township for the accommodation and security provided for us during our research field trips.

## References

- Chengzao, JIA, ZOU Caineng and *et al.*, (2018) Significant progress of continental petroleum geological theory in basins of Central and Western China, *PETROL. EXPLOR. DEVELOP.*, vol. 45, p. 573-588.
- Gambacorta, G., R. Bersezio, H. Wlissert and E. Erba (2016) Onset and demise of Cretaceous oceanic anoxic events: The coupling of surface and bottom oceanic processes in two pelagic basins of the western Tethys. *Paleoceanography*, vol. 31, p. 732-757.
- Mitchell, A.H.G. (2018) *Geological Belts, Plate Boundaries, and Mineral Deposits in Myanmar*. Elsevier, 509 pp.
- Than Than Thwe, (2010). *Lithofacies and biofacies analysis of the Thaungpwet Taung Formation, Second Defile of Ayeyarwady River, Myanmar*. Ph. D. Thesis, University of Yangon (unpublished)
- Than Than Thwe, (2011). Paleodepositional Environment of the Thaungpwet Taung Formation, Second Defile of Ayeyarwady River. *Universities Research Journal*, vol. 4.
- Thura Oo, (2000). *A biostratigraphic synthesis on the Cretaceous Foraminifers in Myanmar*. Ph. D Dissertation, University of Yangon (unpublished)
- Thura Oo and Than Than Thwe, (2020) Reinvestigation on the Cretaceous marine lithostratigraphic units of Myanmar. *University Research Journal*, vol. 11, 2, pp 268-281.

# **PETROLOGICAL SIGNIFICANCE ON GRANITOID ROCKS EXPOSED IN MYA YEIK- TA YAW GYIN AREA, MONYWA-SALINGYI SEGMENT OF WESTERN MYANMAR ARC**

Teza Kyaw<sup>1</sup>, Htay Maung<sup>2</sup>, Pyae Phyo Han<sup>3</sup>

## **Abstract**

The present area is situated in the Monywa-Salingyi segment of Western Myanmar Arc that is composed of diverse igneous rocks during early Cretaceous to Quaternary age. Although the plutonic rocks having mafic to felsic composition are exposed, the present research emphasize only on granite and granophyre as granitoid rocks. Mineralogically, these granitoid rocks are mainly composed of quartz, orthoclase, plagioclase, hornblende, and biotite. The textures of granitoid rocks indicate in terms of volatile rich composition, highly differentiate and magma mixing condition of magma. Moreover, the mineral composition and textures strongly supports to interpret I-type, calc-alkaline magma. Petrochemically, these rocks belong to the calc-alkaline suite and I-type granitoid. In addition, they can also be interpreted as the subduction related volcanic arc. Thus granitoid rocks were probably formed in an arc setting during subduction of Neo-Tethyan oceanic lithosphere.

**Keywords:** Western Myanmar arc, Monywa-Salingyi Segment, granitoid rocks, calc-alkaline, Neo-Tethyan

## **Introduction**

Myanmar is situated at the eastern margin India-Asia collision that is characterized by the existence of 1200 km long Sagaing Fault (Lee *et al.*, 2016). The western Myanmar geological province comprises all of Myanmar west of the Mogok Metamorphic Belt (MMB) that were formed with the Himalayan orogeny during Mesozoic to Cenozoic (Mitchell *et al.*, 2012; Shi *et al.*, 2014). Moreover, there are two principal Neo-Tethyan related magmatic belts in Myanmar: the Western Myanmar Arc (WMA) of western Myanmar, and the Mogok-Mandalay-Mergui Belt found in central and southern Myanmar (Gardiner *et al.*, 2015). The WMA was widely considered as the Andean-type continental arc formed along the South Asian margin during the Neo-Tethyan oceanic subduction (United Nations, 1979; Bender, 1983; Mitchell *et al.*, 2012; Wang *et al.*, 2014; Lin *et al.*, 2019). These rocks in the WMA can be correlated with (1) Cretaceous–Paleogene granitoids of the Gangdese batholith (Barley and Pickard, 2003; Gardiner *et al.*, 2015; United Nations, 1979; Mitchell *et al.*, 2012), and (2) a series of Miocene-Quaternary volcanoes along the Andaman–Sunda (Sumatra)–Banda subduction system in southeast Asia (Hutchison, 1989).

The WMA, located in the central part of the Burma terrane, is a N-S trending magmatic belt delineated by the Banmauk-Wuntho Batholith in the north, and the Monywa-Salingyi Segment in the south that intruded the Basement Complex (Figure 1) (Barber, 1936; Mitchell *et al.*, 2012). In the Salingyi segment including present area, amphibolites, gabbros, diabases, and pillow basalts (Barber, 1936; United Nations, 1979) are interpreted as part of an ophiolite, overlying mica-schists, gneisses and pegmatites occurring in small inliers beneath conglomerates of similar materials (Mitchell, 1993).

The Chindwin Basin including present area lies west of the WMA, and is regarded as the forearc basin of the WMA (Wandrey, 2006 in Wang *et al.*, 2014). Moreover, the Chindwin Basin was filled by the upper Cretaceous-Eocene shallow marine or deltaic clastic rocks and carbonates, and the unconformably overlying Neogene fluvial sediments (Bender, 1983).

---

<sup>1</sup> Associate Professor, Department of Geology, Monywa University

<sup>2</sup> Lecturer, Department of Geology, Monywa University

<sup>3</sup> Lecturer, Department of Geology, Monywa University

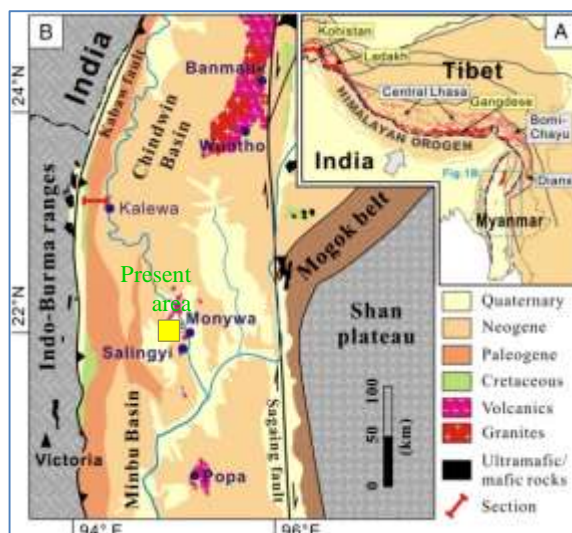


**Figure 1** A: Simplified tectonic map of the Tibetan plateau and adjacent regions, B: Geological Map of northern Myanmar. Western Myanmar Arc is delineated by the Banmauk - Wuntho - Monywa - Poba magmatic belt (Wang *et al.*, 2014)

This research emphasizes petrographical data and petrochemical data of the granitoid rocks in the area, and all results can examine the petrogenesis and tectonic implications to better understand the magmatic evolution of the part of WMA. Because the granitoid rocks are important to deduce the origin, evolution, and geodynamics condition due to the main component of continental crust (Barbarin, 1999). This research also postulates the findings of oceanic plate fragments to ensure the island arc setting.

### Method of Investigation

Detailed field work was carried out in order to perform the geologic mapping at 1: 50,000 scale of UTM map, and geological map of United Nations (1979). The field observations were carried out along car-road, cart-tracts, food-paths, and quarries where good exposures are appeared. 30 samples were collected for petrography and 6 representative samples of different plutonic rocks were selected for geochemical analysis of major elements.

The 30 thin sections are examined by using polarizing microscope for mineral identification according to Kerr (1959), for mineral composition according to William *et al.*, (1982) and for textural analysis according to Winter (2014). The whole rock geochemical analyses were performed at Department of Chemistry, Monywa University by using XRF (X-ray Fluorescence). From these major oxides, the classification of rocks according to Cox *et al.*, (1979) for plutonic rocks; identification of magma series according to Ivrine and Bragar (1971), Pearce *et al.* (1984), Chappel and White (2001), Frost *et al.* (2001); and then possible tectonic settings are interpreted.

### Lithologic Units

The study area is mainly composed of igneous rocks forming as intrusive and extrusive. These igneous rocks are the southern part of WMA that have been formed from the Mesozoic to Quaternary. Moreover, the basement of the study area was recognized as Monywa-Salingyi Volcanics and Crystalline Complex for green rock, diorite intruding the green rock, and granophyre of middle Cretaceous (Barber, 1936; Bender, 1983; Min Aung, 1994). The present research subdivided this basement complex into Ophiolitic rocks with limestone and chert, siliceous

mudstones, Yinbochaung Granite and Granophyre as Granitoid Rocks (Figure 2). In addition, Tertiary and Quaternary volcanic rocks are extruded contemporaneously with Magyigon Formation of Miocene-Pliocene age.

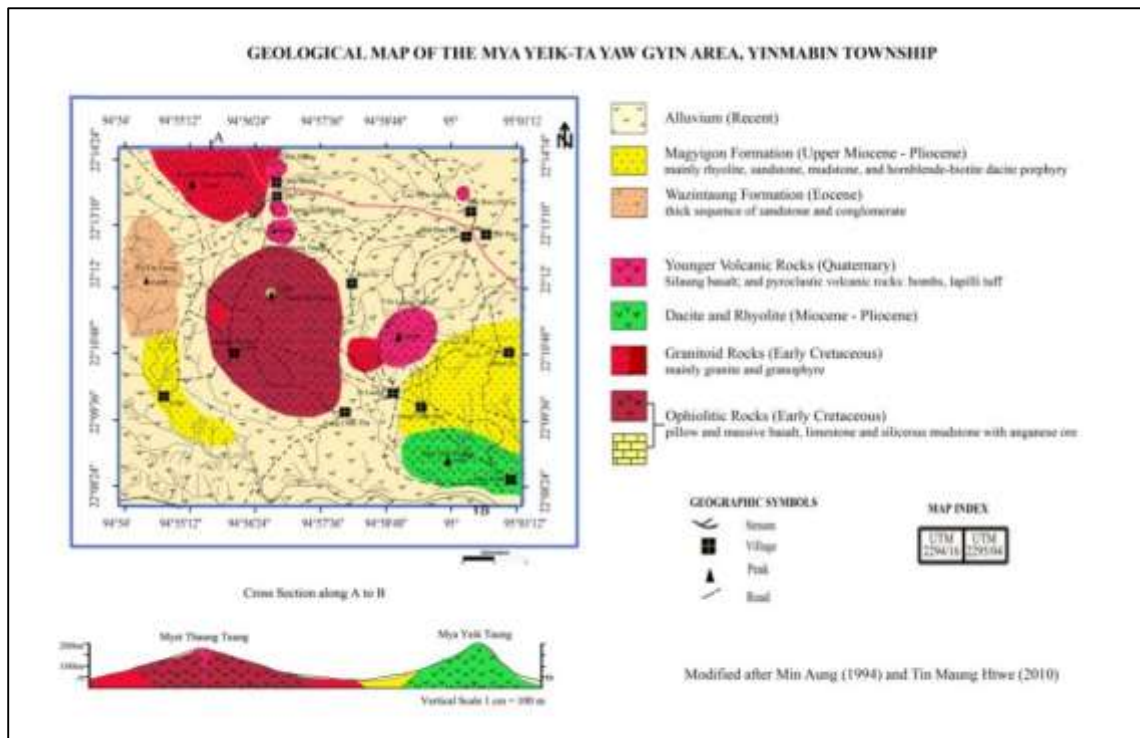


**Figure 2** Geological Map of the study area

### Ophiolitic Rocks

Basaltic rock units are exposed in the stream just west of Ta Yaw Gyin village, west of Kan Su village and vicinity of Taungbu Taung. The volcanic rocks are exposed as massive with bed like jointing and as pillow structures (Figure 3). These rocks mostly display green color and constitute mainly of olivine, pyroxene and plagioclase which are more or less altered. Some rocks are very fine-grained as basalt whereas some are medium-grained size as dolerite. These basaltic rocks were intruded by quartz veins at the margin of this unit in which zeolite and actinolite minerals were found. Diorite was also intruded these volcanics at the Powin taung (Min Aung, 1994). Some residual manganese ores are also found in this unit (Figure 4).

In addition, these units are overlain by the medium-to thick-bedded micritic limestone unit in which chert nodule are also noted (Figure 5 and 6). This limestone may be deposited during or after Early Cretaceous in age due to stratigraphic position. Moreover, the siliceous mudstones are also intercalated within the limestone units (Figure 7). Fossil evidences have not been yielded from limestone whereas some radiolarians have been found in the siliceous mudstone.

This unit is equivalent to those in the Mawgyi Volcanics in the Wuntho-Banmauk arc segment to the north (Mitchell, 2017). Mawgyi Volcanics were also intruded by the early Upper Cretaceous Kanzachaung Batholith and small diorite stocks of pre-Upper Cretaceous (United Nations, 1979). Moreover, the age of diorite at Salingyi had a zircon U-Pb age of  $105.3 \pm 1.7$  Ma (Mitchell *et al.*, 2012), K/Ar determinations from hornblende ages on diorites of  $106 \pm 7$  Ma (United Nation, 1979). By the stratigraphic relationship with southern and northern continuation of Salingyi and Mawgyi Volcanics along the WMA, this unit can be assumed as Upper Cretaceous in age.

## Granitoid Rocks

### Yinbochaung Granite

This unit is well exposed along the Yinbochaung and at Kyauk Sabyone Taung that intruded the ophiolitic rocks. They have dark-grey on weather surface and little pinkish to white color on fresh surface (Figure 8). They are composed mainly of coarse-grained quartz, plagioclase, orthoclase and biotite with xenoliths of basalt (Figure 9). Some granite rocks along the road of Monywa-Alaungdawkathapha and at Kyauk Sabyone Taung are highly weathered and are only remained quartz grains.

### Granophyre

Granophyres are exposed on a small hill southwest of Silaung Taung that form as NNE striking dyke with about 300 feet wide (Figure 10). The granophyre intruded the volcanic rocks of the ophiolitic rocks at the northwest of Myayeik taung. They are composed of coarse-grained quartz, feldspar and accicular form of amphibole minerals (Figure 11). The granophyre was assigned as the part of the Yinbochaung Granite because it also intruded the ophiolitic rocks.

The granite in the study area is compositionally and texturally similar to that of Baingdaung granite in Salingyi-Shinmataung Area (United Nations, 1979). A K/Ar radiometric determination on a biotite concentrate from the granite at the Salingyi yielded an age of  $103 \pm 4$  m.y., indicating a probable age of intrusion of late Upper Cretaceous (United Nations, 1979). Moreover, the granites from the Wuntho-Banmauk Segment assigned the oldest age as  $98 \pm 1$  at Wuntho and  $103 \pm 1$  Ma based on the U-Th-Pb (Lin *et al.*, 2019). It can be recognized that granitoid rocks were intruded during Upper Cretaceous.



**Figure 3** Basalt showing pillow structure exposed at the east of Taungbu Taung (N 22°12' 1" and E 94° 56' 39")



**Figure 4** Residual manganese ore exposed at the east of Taungbu Taung (N 22°12' 1" and E 94° 56' 39")



**Figure 5** Limestone with karst features exposed at the east of Taungbu Taung (N 22°12'7" and E 94°56'43")



**Figure 6** Chert layer and nodules in limestone exposed at the east of Taungbu Taung (N 22°12'7" and E 94°56'43")



**Figure 7** Intercalated siliceous mudstone exposed at the east of Taungbu Taung (N 22°12' 1" and E 94° 56' 39")



**Figure 8** Granites with joints exposed at Yinbochaung (N 22°14'6"and E 94°56'16")



**Figure 9** Xenolith of basalt in granite exposed at Yinbochaung (N 22° 14'6"and E 94°56'16")



**Figure 10** Dyke like nature of granophyre exposed just southwest of Silaung Taung (N 22°11'1" and E 94°58' 17")



**Figure 11** Accicular amphibole minerals in granophyre exposed just southwest of Silaung Taung (N 22°11'1" and E 94°58'17")

### Mineralogical an Textural Significance

#### Yinbochaung Granite

This rock is mainly composed of quartz (20-40%), orthoclase (10-20%), plagioclase (10-20%), hornblende (~10%), biotite (10%) and microcline (3-5%) showing hypidiomorphic to allotriomorphic texture (Figure 12 and 13). The hornblende minerals are suggested as I-type granitoid (Chappel and White, 1992; Winter, 2014) as well as amphibole-rich calc-alkaline granitoid (ACG) (Barbarin, 1999). Quartz minerals are mostly anhedral forms and show wavy extinction that fill interstitial spaces between other minerals. The multiple twinned plagioclases with interstitial quartz and orthoclase (Figure 12) that is the characteristic feature of calc-alkaline granodioritic plutonic rock (Wilson, 2007).

In addition, cross-hatched twinned microclines are also included in granites (Figure 14) which occurred in most differentiated stage of the volatile-rich conditions (Wilson, 2007). Moreover, the euhedral plagioclase contain within the orthoclase (Figure 15). A mineral is included only in the core areas of another mineral indicate the strongest evidence for one mineral ceasing to crystallize before the other forms (Winter, 2014).

Quartz and feldspar intergrowth show myrmekitic texture that appear to have grown from the plagioclase–K-feldspar boundary into the K-feldspar (Figure 16). As the plagioclase replaces the K-feldspar, SiO<sub>2</sub> is released (the anorthite component of plagioclase contains less SiO<sub>2</sub> than the K-feldspar), thereby producing the quartz (Winter, 2014). Myrmekite commonly forms during cooling of granitic rocks (Winter, 2014; Collins and Collins, 2013).

Alkali feldspars are present as orthoclase, albite and microcline. Plagioclase crystals are subhedral to euhedral in shape that show zoning (Figure 17). These zoning are formed when a mineral change in composition as it grows during cooling (Gill, 2010). This irregular compositional change may indicate magma mixing, unstable crystallization or both (Aslan, 2005).

### Granophyre

They are composed of quartz (20-45%), plagioclase (30-50%), hornblende (~7%), orthoclase (3-10%) and biotite (~3%) minerals (Figure 18). The intergrowth texture of quartz minerals and alkali feldspar displaying a granophyric texture (Figure 19) is possibly reflecting eutectic crystallization of the final residual melt, shows cunei form and rod-like form (Winter, 2014). In addition, if the H<sub>2</sub>O is suddenly lost, the melting point will rise quickly, resulting in undercooling (even at a constant temperature) and rapid simultaneous crystallization of the alkali feldspar and quartz (Winter, 2014). Moreover, Granophyric intergrowths are formed from the highly differentiated of the most volatile-rich magmas (Wilson, 2007).

### Petrochemical Significance

The major, minor and trace elements of the granitoid rocks are described in Table (1). The granitoid rocks in the study area belong to the granite clan of subalkaline field based on the total alkalis and silica content (Figure 20) (Cox *et al.*, 1979). In the AFM diagram of the (Na<sub>2</sub>O+K<sub>2</sub>O), FeO and MgO, subalkaline series of granites and granophyres fall in the field of calc-alkaline (Figure 21) (Irvine and Baragar, 1971 in Rollinson, 1993). Calc-alkaline magmas are essentially restricted to subduction related plate tectonic processes (Winter, 2014).

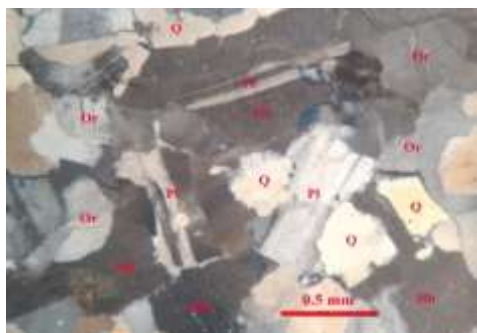


**Figure 12** Granite composed of quartz (Q), plagioclase (Pl), orthoclase (Or), hornblende (Hb) showing allotriomorphic texture (XN, 4x)



**Figure 13** Hornblende minerals with two sets of cleavage in granite (XN, 4x)



**Figure 14** Cross-hatched twin microcline in granite (XN, 4x)

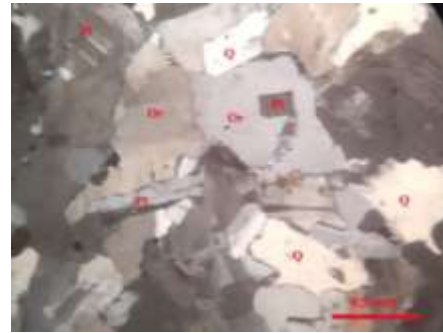


**Figure 15** Euhedral plagioclase within the orthoclase in granite (XN, 4x)

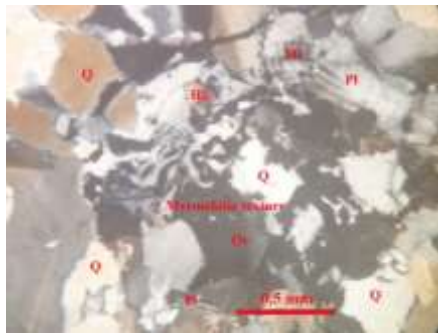


**Figure 16** Quartz and feldspar intergrowth of myrmekitic texture and interstitial quartz grain (Q) in granite (XN, 4x)



**Figure 17** Zoning and twinning plagioclase in granite (XN, 4x)



**Figure 18** Granophyre composed of quartz (Q), orthoclase (Or), hornblende (Hb) and plagioclase (Pl) (XN, 4x)



**Figure 19** Quartz and alkali feldspar showing granophyric texture in granophyre (XN, 4x)

To classify the I-type and S-type granitoid, when plotted on the ACF ( $Al_2O_3-Na_2O+K_2O$ , CaO, and  $FeO+MgO$ ) diagram on the basis of major oxides, it is found that these plutonic rocks fall in the I-type field (Figure 22) (Chappell and White, 1992).

Frost *et al.* (2001) had classified according the geochemical data for granitoids based on Fe-number ratio of the rock to classify the ‘ferroan’ (Tholeiitic) and ‘magnesian’ (Calc-alkaline); based on modified alkali-lime index (MALI); and is based on aluminum saturation index (ASI). The samples fall within the slightly ferroan field except one sample of granite; and within calcic to alkali-calcic field. The granophyres fall within metaluminous whereas the granite within slightly peraluminous field (Figure 23) that also indicates the I-type granitoid (Winter, 2014).

The granitoid rocks are further discriminated by using trace element Rb, Y, and Nb according to Pearce *et al.* (1984). Most of the samples fall within the volcanic arc granite (VAG) except one sample based on Rb-(Y+Nb) as well as fall within the volcanic arc granite and collision granite (VAG+syn-COLG) except one sample based on Nb-Y(Figure 24).

**Table 1 Major, minor, and trace element contents of the granitoid rocks**

| Sample No                      | 3-a         | 3-a1        | 3-a2        | 5-g                | 5-g1               | 5-g2               |
|--------------------------------|-------------|-------------|-------------|--------------------|--------------------|--------------------|
| Rock types                     | Granite     | Granite     | Granite     | Granophyre         | Granophyre         | Granophyre         |
| Localities                     | Yinbochaung | Yinbochaung | Yinbochaung | S of Silaung Taung | S of Silaung Taung | S of Silaung Taung |
| Major oxides (wt%)             |             |             |             |                    |                    |                    |
| SiO <sub>2</sub>               | 71.885      | 76.267      | 80.821      | 70.368             | 69.071             | 71.59              |
| TiO                            | 0.142       | 0.045       | 0.113       | 0.338              | 0.345              | 0.39               |
| Al <sub>2</sub> O <sub>3</sub> | 16.564      | 14.278      | 11.285      | 15.654             | 15.982             | 14.937             |
| Fe <sub>2</sub> O <sub>3</sub> | 0.942       | 0.209       | 0.689       | 2.062              | 2.234              | 1.892              |
| MnO                            | 0.027       | 0.01        | 0.018       | 0.082              | 0.088              | 0.076              |
| MgO                            | 0.114       | 0.064       | 0.177       | 0.39               | 0.357              | 0.307              |
| CaO                            | 3.046       | 2.312       | 1.963       | 3.158              | 3.763              | 3.221              |
| Na <sub>2</sub> O              | 5.457       | 4.871       | 3.686       | 7.043              | 7.096              | 6.535              |
| K <sub>2</sub> O               | 1.547       | 1.089       | 1.041       | 0.427              | 0.552              | 0.565              |
| P <sub>2</sub> O <sub>5</sub>  | 0.034       | 0.017       | 0.071       | 0.219              | 0.229              | 0.22               |
| Trace element (ppm)            |             |             |             |                    |                    |                    |
| Cr                             | 62          | 48          | 34          | 246                | 109                | 164                |
| Rb                             | 37          | 37          | 37          | 9                  | 9                  | 9                  |
| Sr                             | 135         | 85          | 76          | 186                | 211                | 186                |
| Y                              | 31          | 24          | 24          | 24                 | 39                 | 31                 |
| Zr                             | 7           | 30          | 52          | 74                 | 74                 | 104                |
| Nb                             | 7           | 0           | 0           | 252                | 7                  | 7                  |
| La                             | 563         | 205         | 384         | 759                | 699                | 716                |
| Ce                             | 627         | 90          | 293         | 488                | 757                | 676                |
| Hf                             | 93          | 263         | 68          | 93                 | 161                | 68                 |
| Ta                             | 229         | 205         | 139         | 221                | 270                | 197                |

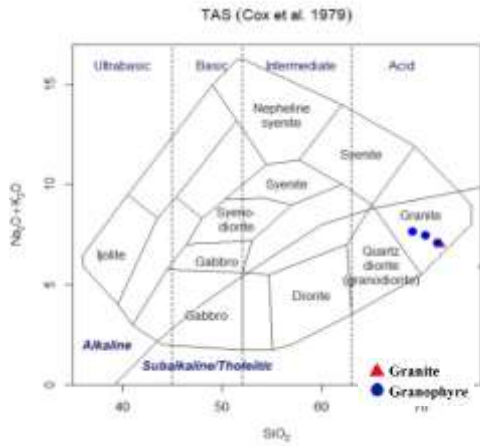


**Figure 20** The chemical classification of plutonic rocks based on total alkalis ( $\text{Na}_2\text{O}+\text{K}_2\text{O}$ ) and silica ( $\text{SiO}_2$ ) (Cox *et al.*, 1979) (Drawing from GCDkit 5)

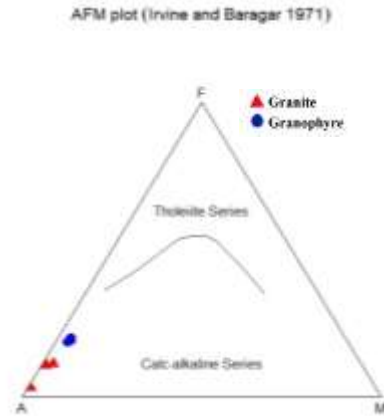


**Figure 21** AFM diagram for plutonic rocks of the study area showing the discrimination between tholeiitic and calc-alkaline suite (Irvine and Bragar, 1971) (Drawing from GCDkit 5)

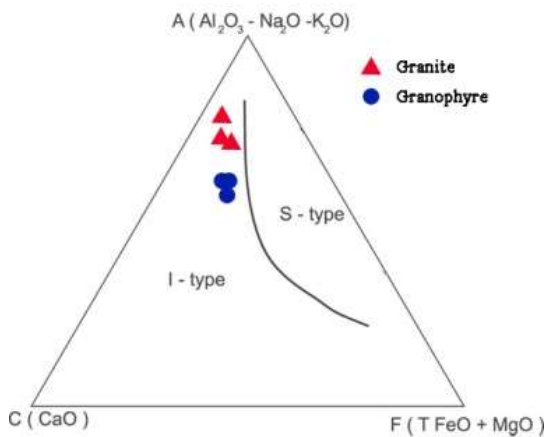


**Figure 22** ACF diagram for the granite rock of the study area compared with the typical I-type and S-type (Chappel and White, 2001)

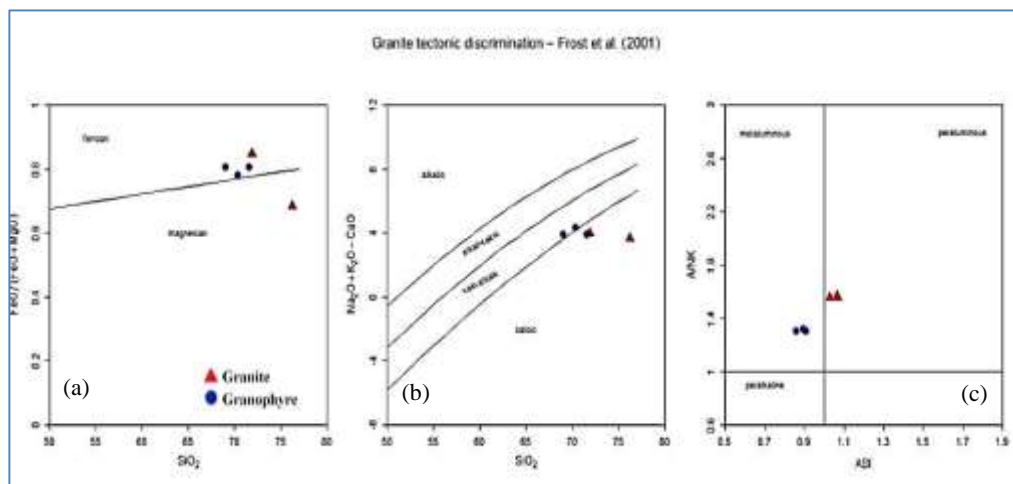


**Figure 23** Granite tectonic discrimination (Frost *et al.*, 2001)

- (a) Fe-number [ $\text{FeO}/(\text{FeO} + \text{MgO})$ ]
- (b) Modified alkali-lime index (MALI) ( $\text{SiO}_2$  vs  $\text{Na}_2\text{O} + \text{K}_2\text{O} - \text{CaO}$ )
- (c) Aluminum saturation index (ASI)

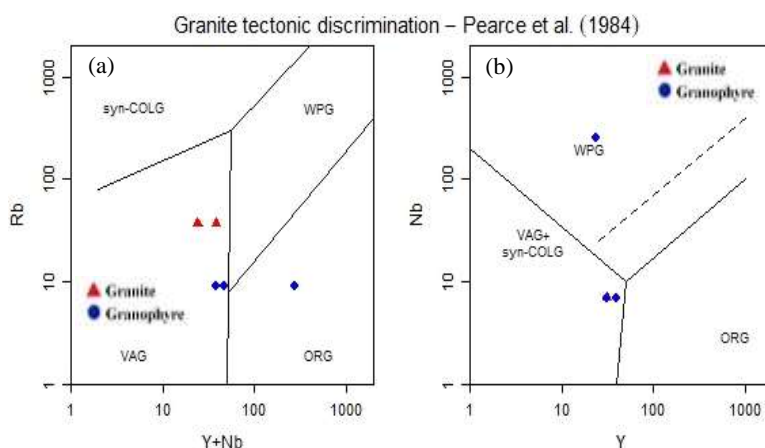


**Figure 24** Granite tectonic discrimination (Pearce *et al.*, 1984) (a) Rb vs (Y+Nb) (b) Nb vs Y

## Discussion

The granitoid rocks are examined systematically by using field occurrence, mineralogical and textural parameters, and geochemical parameters. From the field relationship, the basalt xenoliths are found in the granitoid rocks that indicate the granitoid rocks intruded the ophiolitic rocks.

All these rocks are mainly composed of quartz, plagioclase, orthoclase, hornblende and biotite in which hornblende is the indicator of I-type granitoid (Chappell and White, 1992; Winter, 2014) and amphibole-rich calc-alkaline granitoid (ACG) (Barbarin, 1999).

The presence of interstitial quartz and orthoclase, and microcline suggest the highly differentiated volatile rich calc-alkaline magma. The granophyric textures in all granophyres also indicate the highly differentiated volatile rich magma. Moreover, euhedral plagioclase within the orthoclase provides the temperature condition and changes of magma composition. In addition, zoning plagioclases suggests that the changing of composition of magma as magma mixing or unstable crystallization during cooling of magma.

All the granitoid rocks fall within the granite field based on the total alkalis and silica content as well as calc-alkaline field according to  $(\text{Na}_2\text{O}+\text{K}_2\text{O})$ , FeO and MgO. Moreover, these samples also belong to calcic to calc-alkalic based on the modified alkali-lime index. This geochemical data supports the petrographical result to identify calc-alkaline magma.

Considering I-type or S-type, all samples belong to I-type according to ACF diagram. In addition, these samples fall within the metaluminous and weakly peraluminous of aluminum saturation index which also suggest the I-type character (Winter, 2014).

The paleotectonic environment of these granitoids is interpreted as volcanic arc granite (VAG) from the trace elements Rb, Y, and Nb. Moreover, the low Nb contents (<11 ppm) is a characteristic of the arc setting above subduction zone (Pearce *et al.*, 1984). In addition, the VAG can vary in setting from oceanic to continental and in composition from tholeiitic through calc-alkaline to shoshonitic (Peccerillo & Taylor, 1976 in Pearce *et al.*, 1984).

The following facts can be pointed out with the regional tectonics along WMA,

- (1) The basaltic rocks of the ophiolitic rocks can be correlated with the Mawgyi Volcanics along the northern continuation of WMA due to the occurrences of pillow basalts with local

limestone. Moreover, these basaltic rocks were extruded in deep marine environments (United Nations, 1979; Mitchell, 2017).

- (2) Moreover, the age of ophiolites from igneous rocks and chert throughout Myanmar indicated Middle Jurassic-Early Cretaceous (Liu *et al.*, 2016; Teza Kyaw *et al.*, 2019; Suzuki *et al.*, 2020; Tin Tin Naing *et al.*, 2020). Thus, Tethyan ocean was existed in the Western Myanmar during that time.
- (3) The granitoid rocks also intruded the basaltic rocks in the present area. Most of the intrusions along WMA were hosted by the Pre-Albian Mawgyi Volcanics (Mitchell, 2017).
- (4) The WMA is the N-S trending magmatic-volcanic arc with numerous mafic-felsic plutons. In addition, ACG is also the characteristic plutons of the subduction related volcanic arcs that form vast batholiths, elongate parallel to the trench (Barbarin, 1999).
- (5) Moreover, the Cretaceous mafic-felsic magmatism along WMA was generated during subduction of the Neo-Tethyan oceanic lithosphere (Mitchell *et al.*, 2012; Li *et al.*, 2020)

It can be concluded that the granitoid rocks in the present area were intruded from the calc-alkaline, I-type magma at volcanic arcs during subduction of the Neo-Tethyan oceanic lithosphere.

### Acknowledgements

We are grateful to Rector Dr Thura Oo, Monywa University for their permission. We are greatly indebted to our Professors Dr. Zaw Myint Ni (Head) and Dr. Myat Khaing, Department of Geology, Monywa University, for their permission to conduct this research and valuable suggestions. Finally, we also thanks to our colleague in the Department of Geology, Monywa University, for their supporting everything in this research.

### References

- Aslan, Z., (2005). Petrography and Petrology of the Calc-Alkaline Sarihan Granitoid (NE Turkey): An Example of Magma Mingling and Mixing, *Turkish J. Earth Sci.*, vol.14, pp.185-207.
- Barbarin, B., (1999). A review of the relationships between granitoid types, their origins and their geodynamic environments, *Lithos*, 46, pp.605-626.
- Barber, C. T., (1936). The Intrusive and Extrusive Rocks of the Salinyi Uplands and Linzagyat, *Memoir of the Geological Survey of India*.
- Barley, M. E., Pickard, A. L., Khin Zaw, Rak, P., Doyle, M. G., (2003). Jurassic to Miocene magmatism and metamorphism in the Mogok metamorphic belt and the India-Eurassia collision in Myanmar, *Tectonics*, vol. 22, No. 3, 1019, TC001398.
- Bender, F., (1983). *Geology of Burma*, Gebruder Brontraeger, Berlin.
- Chappell, B.W. and White, A.J.R., (1992). I and S-type granites in the Lachlan Fold Belt. Transactions of the Royal Society of Edinburgh: *Earth Sciences* 83, 1-26.
- Chappell, B.W., and White, A.J.R., (2001). Two Contrasting Granite Types: 25 years later, *Australian Journal of Earth Sciences*, vol. 48, pp. 489-499.
- Collins, L. G. and Collins, B. J., (2013). Origin of myrmekite as it relates to K-, Na-, and Ca-metasomatism and the metasomatic origin of some granite masses where myrmekite occurs, [www.csun.edu/~vcgeo005/Nr56Metaso.pdf](http://www.csun.edu/~vcgeo005/Nr56Metaso.pdf).
- Cox, K. G., Bell, J. D. and Pankhurst, R. J., (1979). *The interpretation of igneous rocks*. Boston, George Allen and Unwin London.
- Frost, B.R., Barnes, C.G., Collins, W.J., Arculus, R.J., Ellis, D.J., Frost, C.D., (2001). A Geochemical Classification for Granitic Rocks, *Journal of Petrology*, V.42, No.11, p.2033-2048.
- Gardiner, N.J., Searle, M.P., Robb, L.J., Morley, C.K., (2015). Neo-Tethyan magmatism and metallogeny in Myanmar-An Andean analogue?, *Journal of Asian Earth Sciences*, vol. 106, p.197-215.
- Gill, R., (2010). *Igneous Rocks and Process: A Practical Guide*, Wiley-Blackwell, A John Wiley & Sons, Ltd., Publication, U. K.

- Hutchison., C. S., (1989). *Geological Evolution of South-East Asia*, 2<sup>nd</sup> ed., Art Printing Works Sdm. Bhd., Malaysia.
- Irvine, T. N., and Baragar, W. R. A., (1971). A guide to the chemical classification of the volcanic rocks, *Canada Journal of Earth Science*, Vol. 8, pp 523-548.
- Kerr, P.F., (1959). *Optical Mineralogy*, 3<sup>rd</sup> Edition, McGraw-Hill Book Company Inc., New York.
- Lee, H.Y., Chung, S.L., Yang, H.M., (2016). Late Cenozoic volcanism in central Myanmar: Geochemical characteristics and geodynamic significance, *Lithos*, 245, pp. 174-190.
- Li, J.X., Fan, W.M., Zhang, L.Y., Peng, T.P., Sun, Y.L., Ding, L., Cai, F.L., Kyaing Sein, (2020). Prolonged Neo-Tethyan magmatic arc in Myanmar: evidence from geochemistry and Sr-Nd-Hf isotopes of Cretaceous mafic-felsic intrusions in the Banmauk-Kawlin area, *International Journal of Earth Sciences*, <https://doi.org/10.1007/s00531-020-01824-w>.
- Lin, T.H., Mitchell, A.H.G., Chung, S.L., Tan, X.B., Tang, J.T., Thura Oo, Wu, F.U., (2019). Two parallel magmatic belts with contrasting isotopic characteristics from southern Tibet to Myanmar: zircon U-Pb and Hf isotopic constraints, *Journal of the Geological Society*, London, vol. 176, pp. 574-584.
- Liu, C.Z., Chung, S.L., Wu, F.Y., Zhang, C. Xu, Y., Wang, J.G., Chen, Y., (2016). Tethyan suturing in Southeast Asia: Zircon U-Pb and Hf-O isotopic constraints from Myanmar ophiolites. *Geology*, Geological Society of America, 44, pp.311–314.
- Min Aung, (1994). Geology of the Powintaung-Silaung area, Yinmabin Township, *M. Sc. Thesis*, University of Mandalay, unpub.
- Mitchell, A. H. G., (1993). Cretaceous-Cenozoic tectonic events in the western Myanmar (Burma) – Assam region in *Journal of the Geological Society of London*, vol. 150, p. 1089-1102.
- Mitchell, A., Chung, S. L., Thura Oo, Lin, T. S., Hung, C. H., (2012.) Zircon U-Pb ages in Myanmar: Magmatic-metamorphic events and the closure of a neo-Tethys ocean?, *Journal of Asian Earth Sciences*, Vol. 56, pp. 1-23.
- Mitchell, A., (2017). *Geological Belts, Plate Boundaries, and Mineral Deposits in Myanmar*, Elsevier Inc., United States.
- Pearce, J.A., Harris, N.B.W., Tindle, A.G., (1984). Trace element discrimination diagrams for the tectonic interpretation of granitic rocks, *Journal of Petrology*, vol. 25, part-4, pp. 956-983.
- Rollinson, H. R., (1993). *Using Geochemical Data: Evaluation, Presentation, Interpretation*, Longman, P. 352.
- Shi, G.H., Lei, W.Y., He, H.Y., Nok Ng, Y., Liu, Y., Liu, Y.X., Yuan, Y., Kang, Z.J., Xie, G., (2014). Superimposed tectono-metamorphic episodes of Jurassic and Eocene age in the jadeite uplift, Myanmar, as revealed by <sup>40</sup>Ar/<sup>39</sup>Ar dating. *Gondwana Research*. 26, pp. 464–474.
- Suzuki, H., La Ja, Maung Maung, Aung Kyaw Thin, Kuwahara, K., (2020). The first report on Early Cretaceous Radiolaria from Myanmar, *Paleontological Research*, 24, pp. 103-112.
- Teza Kyaw, Maung Maung, Suzuki, H., (2019). Upper Jurassic Radiolarians from Bedded Chert of Tagaung Area in Tagaung-Myitkyina Belt, *Myanmar, 3<sup>rd</sup> International Conference on Substantial Scientific Collaborations of Ocean & Earth Sciences*, Conference Proceeding, pp. 27-33.
- Tin Tin Naing, Robinson, S., Searle, M., Henderson, G., Millar, I., (2020). Age, Depositional History and Tectonics of the Indo-Burman Ranges, *Geomyanmar 2020 International Congress Plus IGCP 668 & IGCP 679*, Oral Presentation.
- United Nations, (1979.) Geology and Exploration Geochemistry of the Salingyi-Shinmataung Area, Central Burma, *Technical report 5*, New York.
- Wang, J. C., Wu, F. Y., Tan, X. C., Liu, C. Z., (2014.) Magmatic evolution of the Western Myanmar Arc documented by U-Pb and Hf isotopes in detrital zircon, *Tectonophysics*, 612-613 (2014), p. 97-105.
- Williams, H., Turner, F. J., Gilbert, C. M., (1982). *An Introduction to the Study of Rocks in Thin Sections*, 2<sup>nd</sup> Edition, W. H. Freeman and Company, New York.
- Wilson, M., (2007). *Igneous Petrogenesis: A Global Tectonic Approach*, Springer, Netherlands.
- Winter, J. D., (2014.) *An Introduction to Igneous and Metamorphic Petrology*, Prentice-Hall Inc., Upper Saddle River, New Jersey.

# TECTONIC SETTING AND PROVENANCES OF PANE CHAUNG FORMATION EXPOSED AT THE EASTERN PART OF INDO-MYANMAR RANGE, WEST MYANMAR

Tint Swe Myint<sup>1\*</sup>, Khin Su Su Shwe<sup>2</sup>, Zam Khan Mang<sup>3</sup>

## Abstract

The Pane Chaung Formation exposes at the eastern part of the Indo-Myanmar Range. It overlies on the Kanpetlet Schist and underlies by ophiolites. The present study intends to petrography and whole rock geochemistry for tectonic and provenances of this formation. Thirty samples of sandstone were collected from Kalay-Tiddim Road, Webula Section and Gangaw Section along the eastern Indo-Myanmar Range that were made thin sections for petrographic study. Sixteen sandstones samples were collected for whole-rock major and minor oxide analyses. This formation consists predominantly of turbidite sandstones, graywacke, mudstone and shale. Graywacke, sandstone and shale interbedded units are dominant. The *Halobia* sp. is found at the Kalay-Tiddim Road that indicated the Triassic depositional age and deep water condition of salted Tethys Sea. The sandstones are composed of a detrital framework of angular to subangular, poorly sorted sand-sized grains associated with high matrix. The petrographic characters show the lithic wacke or greywacke. In the chemical composition, the  $\text{SiO}_2/\text{Al}_2\text{O}_3$  ratio ranges from 1.97 – 7.943 and  $\text{Al}_2\text{O}_3/\text{SiO}_2$  also ranges from 0.163-0.559. The  $\text{Na}_2\text{O}/\text{K}_2\text{O}$  ratio range from 1.01- 23.09 and  $\text{K}_2\text{O}/\text{Na}_2\text{O}$  range 0.228-2.619. The geochemical characters indicate that the sandstones are wacke to greywackes. These chemical data show the tectonic environment of active continental margin to oceanic island arc. Their source rocks indicated by chemical data are acid to basic igneous rocks. So, these turbidite sandstones may be deposited at trench near the collision-subduction boundary of southern Asian margin during the closing events of Meso-Tethys at Triassic Period.

**Keywords:** Pane Chaung Formation, Turbidite, *Halobia* sp., active continental margin, provenances

## Introduction

The Pane Chaung Formation exposes at the eastern part of the Indo-Myanmar Range that separate the western trough and Indo-Myanmar Range (Fig.1). These Pane Chaung Formation and Kanpetlet Schist were assumed as continental fragments (Mitchell, 1993; Yao *et al.*, 2017).

The Pane Chaung Formation was deposited over the southern margin of Southeast Asia during the Late Triassic that confirmed by Asian-affinity Cr-spinel and Permo-Triassic detrital zircon ages (Sevastjanova *et al.*, 2015). On the other hand, Permian-Triassic zircons in its sandstones were derived from West Papua along the northern Australian shelf (Metcalf, 1996; Cai *et al.*, 2016). This formation deposited in Carnian-Norian derived from the multi-sources at the submarine fan along northern margin of Australia (Yao *et al.*, 2017). Upper Triassic turbidites in Central Tethyan Himalaya, western Myanmar (Pane Chaung Formation) and Australia were sourced from India continent and Australia, respectively (Liu *et al.*, 2020). In this study, petrographical and whole rock geochemical data from sandstones of Pane Chaung Formation were interpreted for tectonic setting, source rocks and provenance.

## Regional Geologic Setting

Myanmar consists of the Eastern Highland, Central Basin, and Indo-Burman Ranges from east to west. The Eastern Highland or Shan Plateau is part of Sibumasu terrane (Metcalf, 2011). This terrane consists of Precambrian to Late Mesozoic carbonate and clastic sedimentary rocks

---

<sup>1</sup> Dr, Associate Professor, Geology Department, Kalay University, tintswemyint.geol@gmail.com\*Correspondence,

<sup>2</sup> Lecturer, Geology Department, Kalay University

<sup>3</sup> Assistant Lecturer, Geology Department, Kalay University

(Oo *et al.*, 2002) At the Shan Scarp Zone, the Mogok metamorphic belt separates the Eastern Highland and Central low land Basin. Magmatic rocks were intruded in metamorphic rocks and sedimentary rocks that called Eastern Granitoid Belt. Sagaing Fault divides the Sebumasu from West Myanmar Block (Win Swe, 1980). The West Myanmar Block (West Burma) composes of Central Low Land and Indo-Myanmar Ranges (Fig. 1).

The Central Low Land was subdivided into three parts: (1) the central magmatic arc, (2) the western forearc basin, and (3) eastern backarc basin. Forearc strata exposed in the western basin consist of Late Cretaceous to Pliocene sediments (Khin and Myitta, 1990). Eastern backarc strata are Early Eocene to Pliocene. The central magmatic arc consists of Late Cretaceous tholeiitic to calc-alkaline rocks and Cenozoic potassic rocks (Bender, 1983), generated during subduction of oceanic lithosphere and upwelling of asthenospheric material, respectively.

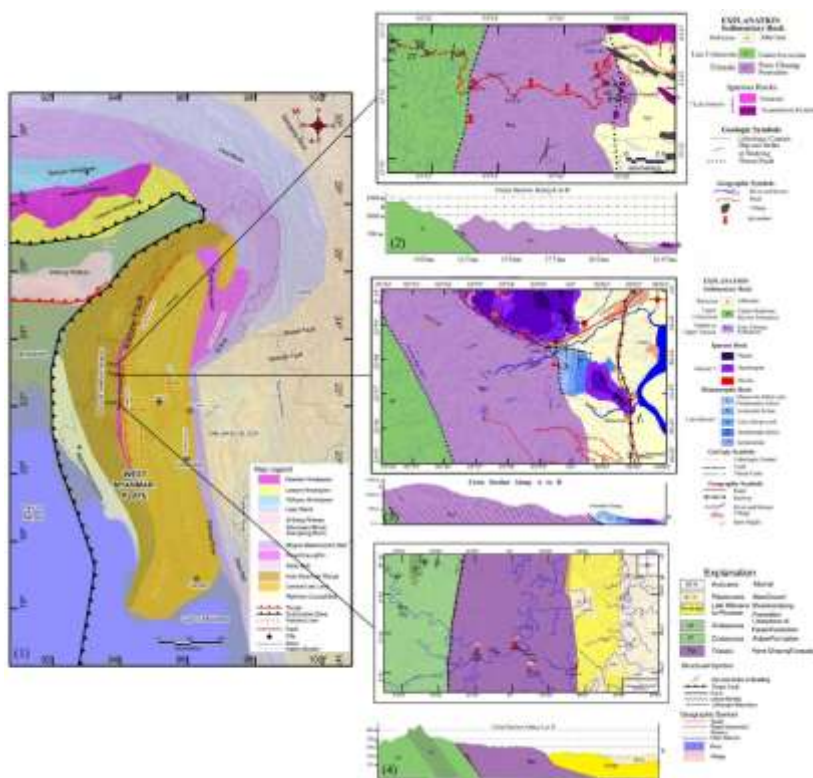


**Figure 1** Regional geological map showing major terranes, terrane boundaries and geological units in Myanmar and eastern Himalayan regions (After Robinson *et al.* 2014)

**Figure 2** Geological Map of Kalay-Tiddim Road Section

**Figure 3** Geological Map of the Webula Area (After Tint Swe Myint, 2015)

**Figure 4** Geological map of the Gangaw Area.

From east to west, the Indo-Burman Ranges include: (1) Cretaceous ophiolitic rocks, (2) the Triassic Pane Chaung Formation and Kanpetlet Schist, (3) Cretaceous Falam Formation, and (4) Cenozoic flysch and molasse (Bannert *et al.*, 2011; Liu *et al.*, 2016). The Pane Chaung Formation and Kanpetlet Schists flank at the eastern part of Indo-Myanmar Range (Fig. 1) and comprised turbidite sandstone and shale (Tint Swe Myint, 2015). Sandstone and shale contain *Halobia* fossils, indicating deposition in Late Triassic (Myint Lwin Thein, 1970, Bannert *et al.*, 2011). Falam Formation consists of mudstone, turbiditic sandstones and limestone containing Late Cretaceous foraminifera (Bannert *et al.*, 2011). Overlying Paleocene Chungsung Formation consist of mudstone, limestone with nammulites and minor sandstone with trace fossils (Tint Swe Myint, 2019). Atop this is the Kennedy Formation which contains phytodetritus fossils (Bannert *et al.*, 2011).

## Analytical Methods

Thirty samples of sandstone were collected and made thin sections for petrographic study. The petrographic texture, grain size, grain morphology were studied under microscope. Six samples from Kalay-Tiddim Road, five samples from Webula Section and another five from Gangaw Section were choose for whole-rock major and minor oxide analyses. Major and minor element oxides were measured by X-ray fluorescence spectrometry (XRF) at the laboratory of Defense Service and Technology Academy (DSTA) of Pyinoolwin, Mandalay University Research Center and Monywa University Research Centre. The major and minor oxides were used to classify the sandstone and to define the tectonic setting and provenance.

## Results

### Stratigraphy and Lithology

The Pane Chaung Formation exposes along the Panmon chaung and Zi chaung in Webula Section (Fig. 2), Kalay- Tiddim Road (Fig. 3) and Gangaw Area (Fig. 4). This formation consists predominantly of monotonous succession of turbidite sandstone and graywacke, mudstone and shale. The graywackes are fine- to medium-grained, hard and compact, light gray color when fresh and buff color when weathered.

Sandstones are commonly massive or weakly graded beds up to 2 m thick. They are mostly medium to thick bedded, many crossed quartz veins (Fig. 5a), highly jointed and intercalated with mudstones and shale. Minor fold and contorted fold are well dominant. Graywacke, sandstone and shale interbedded units (Fig. 5.b) are exposed 1.5 km west of Panmon village in Webula Section. The shales are dark grey to black, compact, well laminated and highly deformed feature (Fig. 5c). Medium- bedded sandstone outcrop is found along the road section (Fig. 5d). Buff colour sandstone and shale interbedded unit dominant (Fig. 5e). The beds are steeply dipping. This formation overlies the Kanpetlet metamorphics and underlies the Ophiolitic rocks and Falam Formation. According to the load cast on the bedding planes (Fig. 5f), the beds may be overturned beds. The trace fossils found in sandstone near Yazagy (Fig. 5g). The Halobia fossils are found at the Kalay-Tiddim Road (Fig. 5h) that proved the Triassic depositional age.

### Petrography

The sandstones of the Pane Chaung Formation are composed of a detrital framework of angular to subangular sand-sized grains associated with chemical cement and matrix (Fig. 6). The framework made up of grains supported 55 to 65 % of the rock, made up of quartz, feldspar, micas, rock fragments and other heavy minerals. The average grain size varies from 0.03 mm to 0.2 mm in diameter. They have poor sorting. Quartz grains are found as sub-angular to sub-rounded, grain size range from 0.05 to 0.25 mm and poor sorting. It is the most common mineral and composed of 30 – 50 percent of the total detrital grains (Figs. 6a, b & c). They are coated by iron oxide in some grains. Feldspar comprises 10 to 24 percent of the detrital sediment. They are plagioclase feldspar and a few orthoclase. Their sizes are less than 0.04 mm, sub-angular to sub-rounded and poor sorting. Plagioclase feldspar shows polysynthetic twin, albite twin and the other are untwined feldspar (Figs. 6a, b, c & d). Muscovite comprises about 2 to 4 percent of the total detrital grains. It can be found as green colour as euhedral flake.



**Figure 5** Field photographs of the Pane Chaung Formation. (a) Quartz vein cross-cutting in sandstone, (b) sandstone and shale interbedded deformed beds, (c) oolitic black shale, (d) medium-bedded sandstone, (e) buff colour sandstone and shale interbedded unit, (f) load cast, (g) trace fossil in sandstone and (h) *Halobia* fossil in black shale

Approximately 1 to 2 percent of the detrital fraction is made up of heavy minerals, mostly zircon, apatite and other opaque minerals. Quartzite, chert, phyllite, schist, slate and volcanic fragments constitute 25 to 46 percent of the detrital framework. Quartzite, chert and volcanic fragments are more abundant. The matrix constitutes approximately 30%. These petrographic characters show the sandstone of lithic wacke or greywacke (Fig. 3).

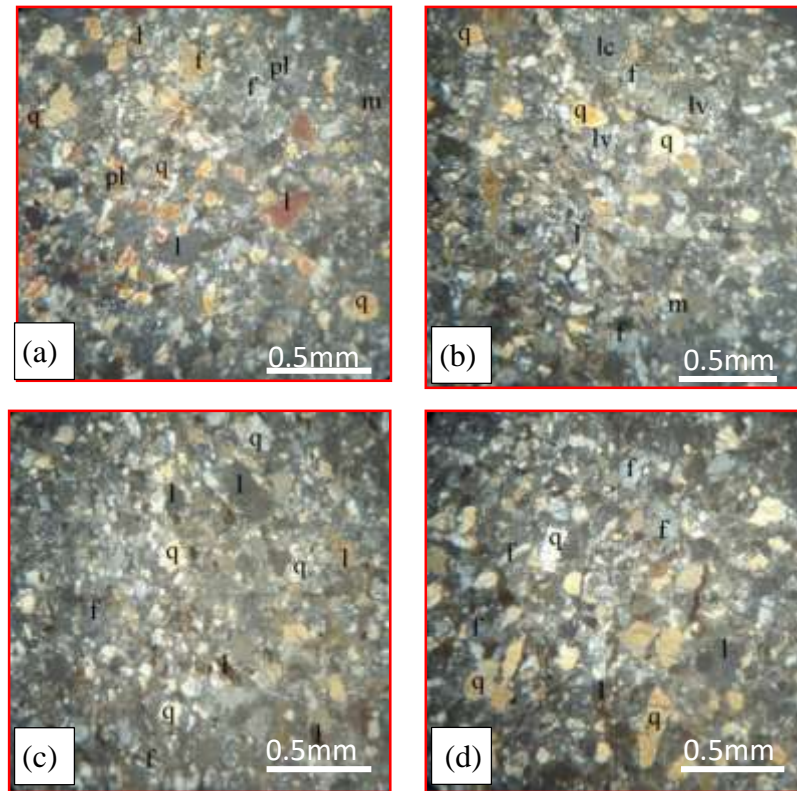


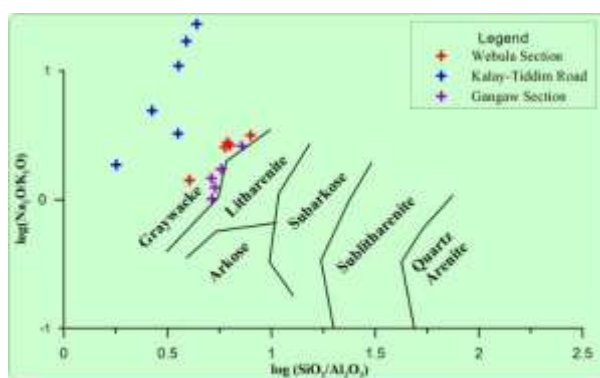
**Figure 6** Petrography of sandstones (a) irregular crack in angular fragment of quartz, feldspar, (b) mica, volcanic & quartz fragments, (c) poorly sorted and (d) angular fragment of quartz

### Whole-rock geochemistry

Sixteen sandstone samples were collected from three different localities and analyzed by XRF for whole rock geochemical data. The chemical compositions of these sandstones are shown in Table (1). The  $\text{SiO}_2/\text{Al}_2\text{O}_3$  (1.97 – 7.943),  $\text{Al}_2\text{O}_3/\text{SiO}_2$  (0.163-0.559),  $\text{Na}_2\text{O}/\text{K}_2\text{O}$  (1.01- 23.09) and  $\text{K}_2\text{O}/\text{Na}_2\text{O}$  (0.228-2.619) values keys for classification and tectonic setting, respectively. The  $\log (\text{SiO}_2/\text{Al}_2\text{O}_3)$  vs.  $\log (\text{Na}_2\text{O}/\text{K}_2\text{O})$  (Roser & Korsch 1986) diagram show geywackes (Fig. 7a). In the  $\text{Na}_2\text{O}$  vs  $\text{K}_2\text{O}$  variation diagram, their compositions are fairly high, the study samples fall in the quartz intermediate to quartz poor region (Fig. 7b). The  $\text{SiO}_2/\text{Al}_2\text{O}_3$  vs.  $\text{Na}_2\text{O}/\text{K}_2\text{O}$  diagram expresses quartz-rich greywacke to greywacke type (Fig. 8). In this diagram,  $\text{Na}_2\text{O}/\text{K}_2\text{O}$  values are fairly low and range in wacke-greywacke field. Therefore, sandstones of the Pane Chaung Formation are graywacke or wackestone.

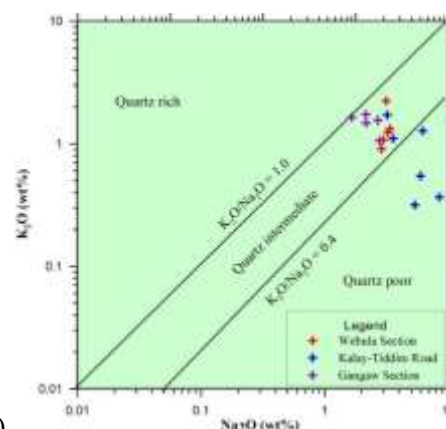
**Table 1 Whole rock geochemical data of the sandstone samples**

| Area                           | Webula Section |             |             |             |             | Kalay-Tiddim Road |            |             |             |             |             | Gangaw Section |             |             |              |             |
|--------------------------------|----------------|-------------|-------------|-------------|-------------|-------------------|------------|-------------|-------------|-------------|-------------|----------------|-------------|-------------|--------------|-------------|
|                                | Sp.No.         | 1           | 10          | 14          | 107         | 128               | 1          | 2           | 14          | 51          | 52          | 98             | 5           | 6           | 10           | 13          |
| Na <sub>2</sub> O              | 3.37           | 3.25        | 3.15        | 2.98        | 2.88        | 3.58              | 5.96       | 5.37        | 6.23        | 8.45        | 3.2         | 2.69           | 2.17        | 2.16        | 1.66         | 2.78        |
| MgO                            | 1.60           | 2.32        | 1.15        | 0.80        | 0.69        | 1.58              | 3.8        | 4.36        | 1.58        | 0.97        | 3.18        | 0.80           | 1.28        | 0.78        | 1.41         | 0.86        |
| Al <sub>2</sub> O <sub>3</sub> | 12.2           | 11.5        | 17.5        | 12.0        | 10.1        | 18.4              | 18.9       | 17.2        | 24.1        | 16.4        | 31.5        | 13.0           | 13.3        | 13.6        | 13.6         | 10.7        |
| SiO <sub>2</sub>               | 72.9           | 72.6        | 70.6        | 73.7        | 80.2        | 65.3              | 67.6       | 66.9        | 64.2        | 71.8        | 56.4        | 74.6           | 69.5        | 72.9        | 70.7         | 76.8        |
| P <sub>2</sub> O <sub>5</sub>  | 0.12           | 0.25        | 0.10        | 0.13        | 0.09        | 0.11              | 0.09       | 0.13        | 0.13        | 0.15        | 0.17        | 0.17           | 0.21        | 0.16        | 0.15         | 0.18        |
| K <sub>2</sub> O               | 1.32           | 1.23        | 2.23        | 1.07        | 0.91        | 1.1               | 0.54       | 0.32        | 0.27        | 0.37        | 0.72        | 1.56           | 1.48        | 1.73        | 1.64         | 1.06        |
| CaO                            | 2.53           | 1.25        | 0.20        | 0.14        | 1.39        | 6.95              | 0.58       | 2.88        | 0.17        | 0.11        | 0.17        | 2.06           | 3.04        | 3.24        | 1.49         | 2.88        |
| TiO <sub>2</sub>               | 0.47           | 0.45        | 0.53        | 0.61        | 0.40        | 0.28              | 0.14       | 0.23        | 0.33        | 0.22        | 0.50        | 0.58           | 0.44        | 0.54        | 0.47         | 0.42        |
| MnO                            | 0.14           | 0.12        | 0.00        | 0.02        | 0.04        | 0.13              | 0.05       | 0.06        | 0.0         | 0.02        | 0.04        | 0.08           | 0.19        | 0.05        | 0.21         | 0.13        |
| Cr <sub>2</sub> O <sub>3</sub> | 0.03           | 0.00        | 0.02        | 0.00        | 0.04        | 0.02              | 0.02       | 0.05        | 0.0         | 0.0         | 0.03        | 0.01           | 0.02        | 0.02        | 0.01         | 0.01        |
| Fe <sub>2</sub> O <sub>3</sub> | 1.13           | 1.03        | 1.16        | 1.17        | 1.04        | 0.77              | 0.76       | 0.7         | 0.61        | 0.48        | 0.99        | 0.98           | 2.23        | 1.12        | 2.38         | 1.01        |
| FeO                            | 2.37           | 2.17        | 2.43        | 2.46        | 2.18        | 1.61              | 1.6        | 1.47        | 1.3         | 1.0         | 2.07        | 2.05           | 4.69        | 2.36        | 7.15         | 3.04        |
| CoO                            | 0.00           | 0.01        | 0.00        | 0.01        | 0.00        | 0.00              | 0.00       | 0.00        | 0.00        | 0.00        | 0.00        | 0.00           | 0.00        | 0.00        | 0.00         | 0.00        |
| NiO                            | 0.00           | 0.02        | 0.00        | 0.00        | 0.00        | 0.00              | 0.01       | 0.01        | 0.00        | 0.00        | 0.00        | 0.00           | 0.00        | 0.00        | 0.00         | 0.00        |
| SO <sub>3</sub>                | 0.00           | 0.05        | 0.00        | 0.00        | 0.00        | 0.00              | 0.00       | 0.00        | 0.00        | 0.00        | 0.00        | 0.00           | 0.00        | 0.00        | 0.00         | 0.00        |
| SrO                            | 0.01           | 0.01        | 0.01        | 0.01        | 0.01        | 0.05              | 0.00       | 0.01        | 0.01        | 0.00        | 0.01        | 0.01           | 0.02        | 0.01        | 0.02         | 0.02        |
| ZrO <sub>2</sub>               | 0.04           | 0.04        | 0.03        | 0.08        | 0.05        | 0.02              | 0.01       | 0.02        | 0.03        | 0.02        | 0.01        | 0.05           | 0.03        | 0.05        | 0.03         | 0.04        |
| Rb <sub>2</sub> O              | 0.01           | 0.01        | 0.01        | 0.00        | 0.01        | 0.00              | 0.00       | 0.00        | 0.00        | 0.00        | 0.00        | 0.01           | 0.01        | 0.01        | 0.01         | 0.02        |
| <b>Total</b>                   | <b>98.2</b>    | <b>96.2</b> | <b>99.1</b> | <b>95.0</b> | <b>99.9</b> | <b>99.9</b>       | <b>100</b> | <b>99.7</b> | <b>98.9</b> | <b>99.9</b> | <b>98.9</b> | <b>98.7</b>    | <b>98.6</b> | <b>98.7</b> | <b>100.9</b> | <b>99.9</b> |



(a)

The classification of terrigenous sandstones using  $\log(\text{Na}_2\text{O}/\text{K}_2\text{O})$  vs  $\log(\text{SiO}_2/\text{Al}_2\text{O}_3)$  from Pettijohn *et al.* (1972) with the boundaries redrawn by Harren (1988)



(b)

**Figure 7** Classification diagram of terrigenous sandstones using  $\log(\text{Na}_2\text{O}/\text{K}_2\text{O})$  vs.  $\log(\text{SiO}_2/\text{Al}_2\text{O}_3)$  from Pettijohn *et al.* (1975) with the boundaries that show the greywacke type of Pane Chaung Formation sandstone. (b)  $\text{Na}_2\text{O}$  vs.  $\text{K}_2\text{O}$  diagram for determination of quartz dominant sandstone that show quartz intermediate sandstone of Pane Chaung Formation

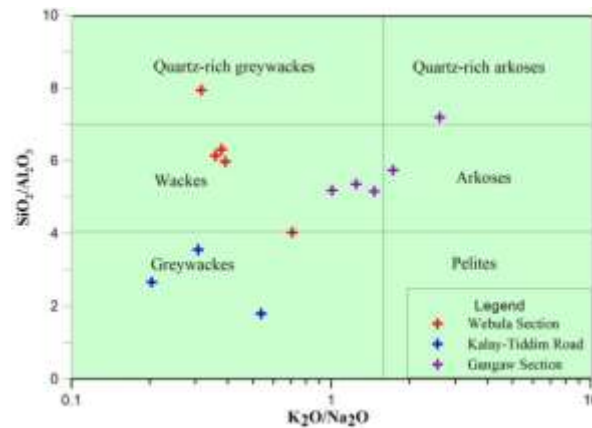


**Figure 8** K<sub>2</sub>O/Na<sub>2</sub>O vs SiO<sub>2</sub>/Al<sub>2</sub>O<sub>3</sub> scatter diagram of sandstone (after Pettijohn, 1975). Most of the studied samples fall in the wacke-greywacke fields.

## Discussion

### Tectonic Setting

Sandstone samples were plotted on the Fe<sub>2</sub>O<sub>3</sub>+MgO vs TiO<sub>2</sub>, Al<sub>2</sub>O<sub>3</sub>/SiO<sub>2</sub>, K<sub>2</sub>O/Na<sub>2</sub>O and Al<sub>2</sub>O<sub>3</sub>/(CaO+Na<sub>2</sub>O) diagrams (Fig. 9). The studied samples fall around the passive margin and active continental margin fields. In the SiO<sub>2</sub> vs K<sub>2</sub>O/Na<sub>2</sub>O diagram, most of the sandstone samples of the study area fall in the active continental margin and island arc (Fig. 10). In Na<sub>2</sub>O/K<sub>2</sub>O vs SiO<sub>2</sub>/Al<sub>2</sub>O<sub>3</sub> diagram, all Webula sandstones fall in active continental margin and two samples of Gangaw Section and one of Kalay-Tiddim Road are fall (Fig. 11). Sp. No. 5 & 15 of Gangaw sandstones are high SiO<sub>2</sub> and fall in the passive margin. The rest samples fall in active continental margin and island arc.

### Provenances

The Pane Chaung Formation sandstones have uniform K/Rb ratios that lie close to a typical differentiated magmatic suite or main trend with a ratio of 230 (Fig. 12) (Shaw, 1968). So, Pane Chaung Formation sandstones are more similar to values of sediments derived from felsic-intermediate source rocks to basic igneous rocks.

Major oxides data of sandstones fall in the field of felsic igneous provenance, intermediate igneous provenance to basic igneous provenance. Only one sample from Webula Section fall in quartzose sedimentary provenance. In the second diagram, the study sandstone samples fall in the intermediate to basic igneous provenances. The halobia-daonella fossils evidence in black shale indicates the salt water condition of Tethys Sea. Moreover, the maximum age was assigned as Late Triassic from these fossil evidences. Therefore, the sandstones of Pane Chaung Formation deposited under the marine condition when tectonic setting was active continental margin. Base on abundant of Permian-Triassic zircons, the Pane Chaung are most probably derived from the SE Asia tin belt granitoids (Sevastjanova *et al.*, 2015). The Triassic turbidite possibly Pane Chaung Formation was deposited on the southern margin of Asia, which was identified with the Shan-Thai foreland (Mitchell, 1993).

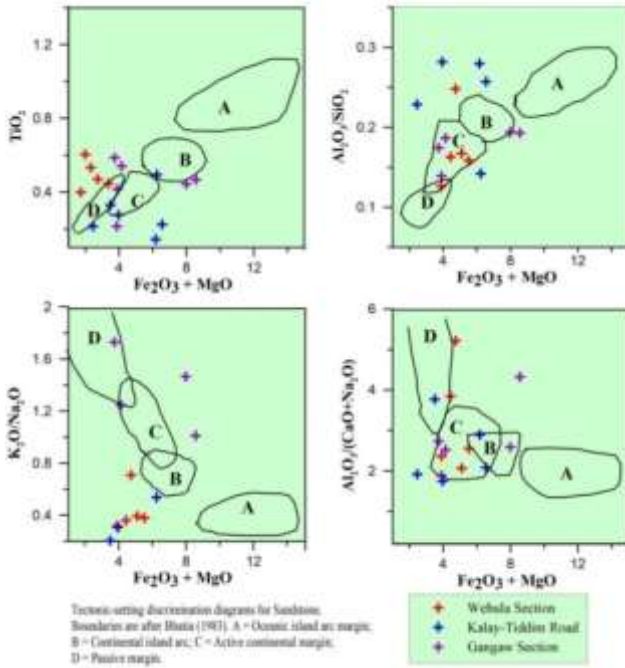


**Figure 9** Sandstones of the studied samples plotted in tectonic discrimination diagram for sandstones base upon  $Fe_2O_3+MgO$  vs  $TiO_2$ ,  $Al_2O_3/SiO_2$ ,  $K_2O/Na_2O$  and  $Al_2O_3/(CaO+Na_2O)$  diagrams, boundaries after Bhatia (1983)

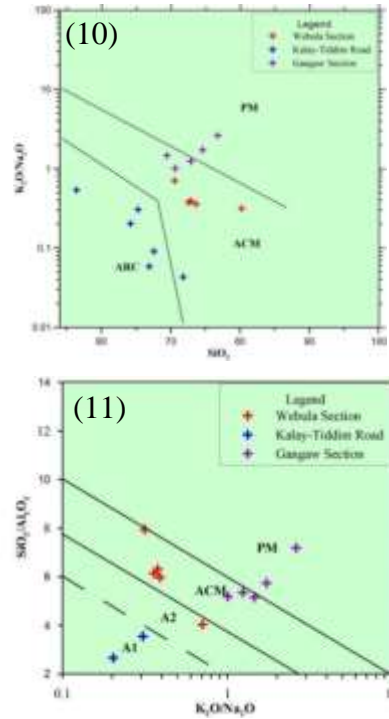


**Figure 10** Tectonic setting of the sandstone of the Pane Chaung Formation

**Figure 11**  $K_2O/Na_2O$  vs  $SiO_2/Al_2O_3$  diagram of Roser and Korsch (1986)

PM, passive continental margin; ACM, active continental margin, ARC, island arc

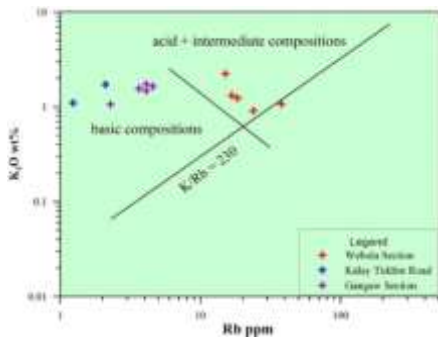


**Figure 12**  $K_2O$  and Rb content in the Pane Chaung Formation sandstones indicate acid + inermeciate composition (main trend of Shaw, 1968).

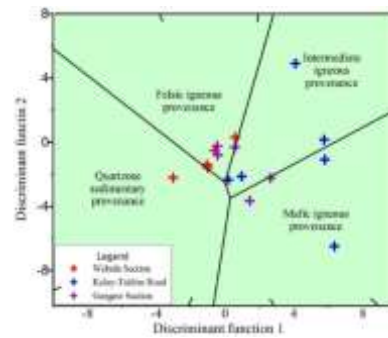


**Figure 13** Studied sandstones were plotted on the discriminant function diagram (Roser and Korsch, 1988) sandstone-mudstone suites for provenance using discriminant function 1 and 2

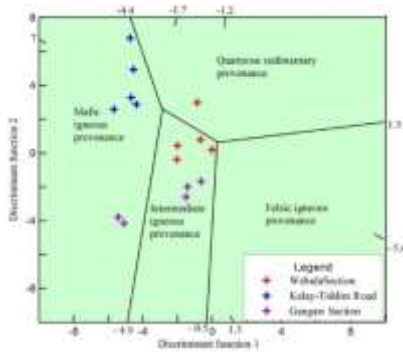


**Figure 14** Provenance determination plot of discriminant functions F1 and F2 for the sandstones from the Pane Chaung Formation. Fields are after Roser and Korsch (1988)

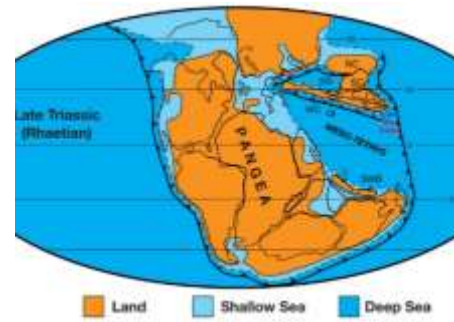


**Figure 15** Paleogeographic reconstructions of the Tethyan region for the Late Triassic West Burma showing relative position of the East and SE Asian terranes, land and sea. (After Metcalfe, 2011)

SE Asia was built largely from continental fragments that separated from Gondwana and have amalgamated from the Paleozoic onwards (Fig. 15). The West Sumatra, East Malaya, Indochina and West Burma blocks rifted and separated from Gondwana opening the Paleo-Tethys in the Devonian and formed a composite terrane ‘Cathaysia land’ (Metcalfe, 2011). It was supported with the occurrence of Permian fusulinids Cathaysian type from Karmine in the northern part of the West Burma Block (Thura Oo, 2002).

### Conclusions

South East Asia is composed of continental fragments derived from the Gondwana super-continent by rifting during Paleozoic and Mesozoic. The present studies of lithology, petrography and whole-rock geochemical data indicate the following points:

1. Petrographically, sandstones contain poorly sorted, angular to subangular, low sphericity more poly quartz, less amount of feldspar and abundant of lithic fragment. The matrix contents are range in wacke composition.
2. The geochemical data indicates active continental margin, continental arc to island arc. The provenances study indicates the source of acid to basic igneous provenances.
3. The halobia-daonella species in black shales deposited at deep water condition of salt Tethyan Sea. The turbidity currents cannot carry the low sphericity and high matrix sediment for long distances. So, these turbidite sandstones may be deposited at trench near the collision-subduction boundary of southern Asian margin during the closing events of Meso-Tethys at Triassic Period.

### Acknowledgements

I am sincerely thankful to Dr Yin Yin Latt, Professor and Head of Geology Department, Kalay University, for her force to carry out this research paper and for lab facilities assistant. My special thanks are extended to all colleagues from the Department of Geology, Kalay University who participated in field trips throughout the preparation of this work and gave much assistance in various ways. Moreover, this paper partly intended to U Salai Thakap Lian, Lecturer of Geology Department, for remembrance to him.

## References

- Bannert, D., A. Sang Lyen, & Than Htay (2011), The Geology of the Indoburman Ranges in Myanmar. *Geologisches Jahrbuch, Reihe B, Regionale Geologie Ausland, Heft 101*, 1-100.
- Bender, F., (1983), *Geology of Burma*, Gebruder Brontraeger, Berlin.
- Bhatia (1983), Plate tectonics and geochemical composition of sandstones, *J. Geol.* 91, 611-627.
- Cai, F., L. Ding, , A. K. Laskowski, P. Kapp, H. Wang, Q. Xu, L. Zhang, (2016), Late Triassic paleogeographic reconstruction along the Neo-Tethyan Ocean margins, southern Tibet. *Earth Planet. Sci. Lett.* 435, 105-114.
- Metcalf, I. (1996), Gondwanaland dispersion, Asian accretion and evolution of eastern Tethys. *Aust. J. Earth Sci.* 43, 605-623.
- Metcalf, I. (2011), Paleozoic–Mesozoic history of SE Asia, The SE Asian Gateway: History and Tectonics of the Australia–Asia Collision. *Geological Society, London, Special Publications*, 355, 7–35.
- Mitchell, A. H. G. (1993), Cretaceous Cenozoic Tectonic Events in the Western Myanmar (Burma) Asian Regions, *Journal of Geological Society, London, vol. 150*; pp. 1084 – 1102
- Myint Lwin Thein (1970), On the Occurrence of Daonella Facies from the Upper Chindwin Area, Western Burma. *Union of Burma Journal. Sic. Tech.* 3(2), 277 – 282.
- Oo, T., T. Hlaing, N. Htay, (2002), Permian of Myanmar. *J. Asian Earth Sci.* 20, 683-689.
- Pettijohn, F. J. (1975), *Sedimentary rocks*, third edition: New York, Harper & Row, 628 p.
- Robinson, R.A.J., C.A. Brezina, (2014), Large rivers and orogens: the evolution of the Yarlung Tsangpo-Irrawaddy System and the eastern Himalayan syntaxis. *Gondwana Research*, 26, 112–121
- Roser, B.P. & R.J. Korsch, (1986), Provenance signatures of sandstone-mudstone suites determined using discriminant function analysis of major element data. *Chemical Geology*, 67, 119–139.
- Sevastjanova, I., R. Hall, M. Rittner, S.M.T.L. Paw, T.T. Naiang, D.H. Alderton, G. Confort, (2015), Myanmar and Asia united, Australia left behind long ago. *Gondwana Res* 32, 24-40.
- Shaw, D. M. (1968), A review of K–Rb fractionation trends by covariance analysis. *Geochim. Cosmochim. Acta* 32, 573–602.
- Tint Swe Myint (2015), Petrology and Mineralization of the Natchaung – Webula Area, Kalay and Falam Townships, unpublished PhD Dissertation, Geology Department, Mandalay University.
- Tint Swe Myint, (2019). Paleontological Evidences from the Chunsung Formation Exposed in Northern Chin Hill, Myanmar. *Proceeding of The Third Myanmar Conference on Earth Sciences (MNCES)*, 224-235.
- Win Swe (1980), Tectonic Evolution of the Western Ranges of Burma in *Contribution to Burmese Geology*, vol.1, no.1, Department of Geology Survey & Mineral Exploration, Rangoon.
- Yao, W., L. Ding, F. Cai, H. Wang, Q. Xu, and Than Zaw, (2017), Origin and tectonic evolution of upper Triassic Turbidites in Indo-Burman ranges, West Myanmar, *Tectonophysics* 721, 90-105.

# **EVOLUTION OF TIDE-DOMINATED ESTUARINE FACIES SYSTEM IN THE OLIGOCENE OKHMINTAUNG FORMATION OF THE MYASAGAING-SHWEMAUNGZUN AREA, THE MINBU SUB-BASIN, CENTRAL MYANMAR**

Naing Htun Lin<sup>1</sup>, Maung Maung<sup>2</sup>, Nyan Min Naing<sup>3</sup>, Hlaing Hlaing Win<sup>4</sup>

## **Abstract**

The data obtained from the Oligocene Okhmintaung Formation in the Myasagaing-Shwemaungzun Area, the Minbu Sub-Basin, central Myanmar are observed, and then used to establish the depositional processes and environments, and to reconstruct depositional model of the research area. A total of fourteen lithofacies are recognized, and grouped into four facies associations: tidal channel, tidal sand bar, tidal flat and transgressive shelf. Based on studies of the facies and facies associations, the lower part of the Okhmintaung Formation may mainly be deposited in tide-dominated estuarine system, which consist of a combination of tidal channel, tidal sand bar and tidal flat facies associations, and then followed by marine transgressive, resulting in deposition of alternating of transgressive shelf and tidal flat sequences in the upper part of the Okhmintaung Formation.

**Keywords:** Oligocene, Okhmintaung Formation, Minbu Sub-Basin, tide-dominated estuarine system

## **Introduction**

The research area is situated in the southern part of the Minbu Sub-Basin, lying between north latitudes (19°35'05" to 19°24') and east longitudes (95°10' to 95°03') and covering by one inch topographic maps of 85M/2 and 85M/3 (Figure 1A). It is located on the western bank of the Ayeyarwaddy River, and is bounded by Shwemaungzun Village of Sinbaungwe Township in the north and Myasagaing Village of Thayet Township in the south, Magway Region of Myanmar.

The mollassic clastic sedimentary rocks of the Oligocene-Miocene units of Pegu Group are mainly exposed in the research area (Theobald, 1973). The Pegu Group is distinctly marine portion in the south with the exception of the uppermost beds, while in the north it exhibits continental facies. The Pegu Group has been given much attention due to its presence of oil-bearing horizons. Accordingly, the Okhmintaung Formation of lower Pegu Group (Late Oligocene) has been selected for this research to recognize the detailed lithofacies types together with their distribution and to interpret the depositional environment through the lithofacies analysis (Figure 1B). This result allow to provide new insights on the purpose of a reconstructing depositional model of the Okhmintaung Formation, which help to understand the sedimentary characteristics of ancient depositional system and to estimate the prospective regions for hydrocarbon accumulations.

---

<sup>1</sup> Lecturer, Department of Engineering Geology, Defence Services Technological Academy

<sup>2</sup> Principal of the Myingyan Degree College

<sup>3</sup> Lecturer, Department of Geology, Magway University

<sup>4</sup> Lecturer, Department of Geology, Yadanabon University

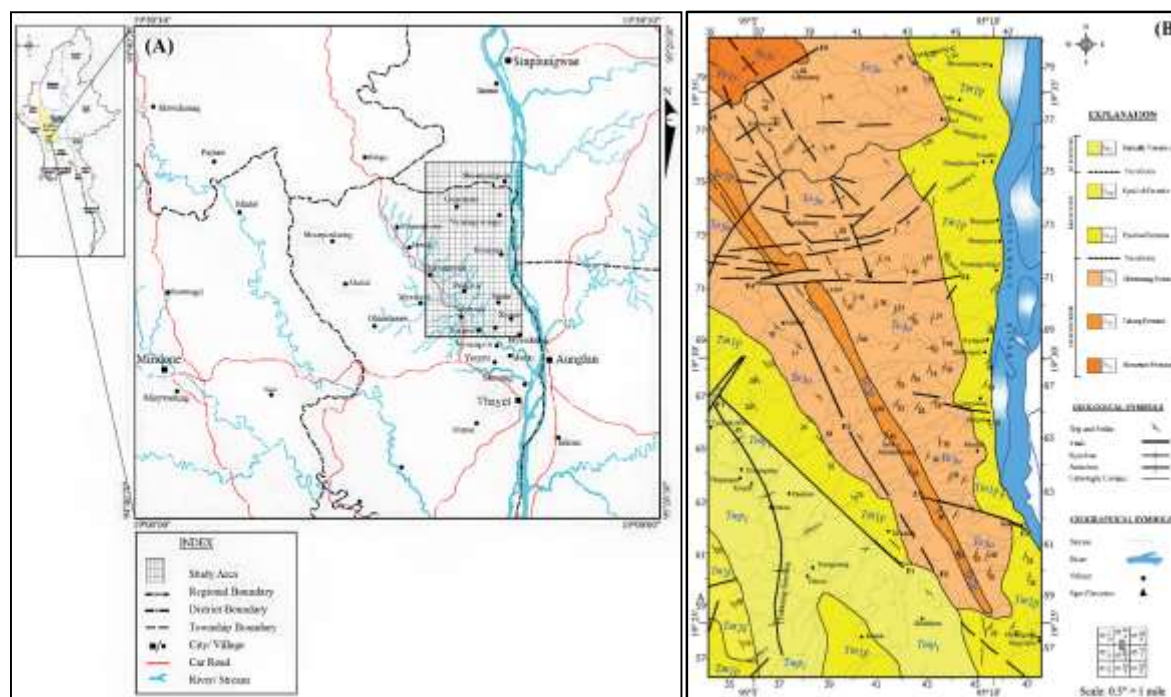


**Figure 1** (A) Location map of the research area with the inset showing map of Myanmar and (B) Geological Map modified After M.O.G.E (1980).

### Methods of Study

The traverses especially along the streams, rolling hills and road cuts are made by many measurements. While measuring along the traverses with tape measure, compass and GPS (Global Positioning System), one vertical section was profiled and logged in detail Kadin Chaung section in the western part of Sinthe Village. Recorded observations during field work include lithology, the degree of sorting of grains based on Compton (1962), grain size scale for sedimentary rocks based on the revised Udden-Wentworth scale (Blair and Mcpherson, 1999), sedimentary structures using the cross-bedding scale (Collinson, et al., 2006), trace and body fossil contents, and the mapping of discontinuity surfaces. The sedimentological information was graphically transformed into detailed textural graphic logs (Tucker, 1996). A modified lithofacies classification scheme from (Miall, 1977; 1978; 1985; 2006) was used in this study.

### Facies Association and Interpretation

In the research area, fourteen lithofacies can be recognized for the Okhmintaung Formation (Table 1), and can be grouped into four facies associations: (1) tidal channel, (2) tidal sand bar, (3) tidal flat and (4) transgressive shelf.

#### Facies Association 1: Tidal Channel

In the inner part of the estuary where the river channel is influenced by tidal processes, the low-gradient channel commonly adopts a meandering form (Dalrymple et al., 1978). The outer part of a tide-dominated estuary is the zone of strongest tidal currents, which transport and deposit both fluviially derived sediment and material brought from the sea. In supratidal zone, the currents will be strong enough to cause local scouring and to move both sand and gravel. Bioclastic debris of facies A is common among the gravelly detritus deposited as a lag on the channel floor (Reinson, 1992).

The tidal effects mean that there are considerable fluctuations in the strength of the flow during different stages of the tidal cycle: when a strong ebb tide and the river act together, the combined current may transport sand, but a strong flood tide may completely counteract the river flow, resulting in standing water, which allows deposition from suspension. The deposits in the point bar consist of more than one grain size, in this case alternating layers of sand and mud (Reineck and Singh, 1980). This style of point-bar stratification has been called ‘inclined heterolithic stratification’ (IHS) (Thomas et al., 1987) and named as facies L in this research. Trough cross-bedding (facies G) and ripple mark (facies D) in sandstones may serve as channel deposits.

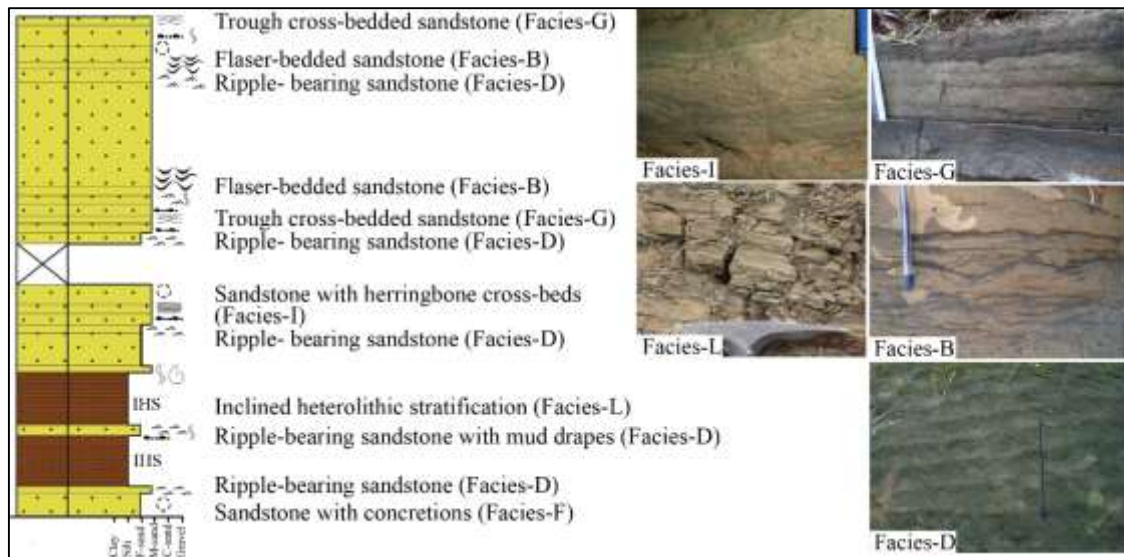


**Figure 2** Idealized sequence of tidal channel facies association and outcrop photographs of trough cross-bedded sandstone (Facies-G), flaser-bedded sandstone (Facies-B), ripple-bearing sandstone (Facies-D), sandstone with herringbone cross-beds (Facies-I) and inclined heterolithic stratification (Facies-L).

**Table 1 Lithofacies scheme for the Okhmintaung Formation exposed in the Myasagaing-Shwemaungzun area**

| Lithofacies Code | Lithofacies Name                            | Grain size       | Bed Thickness (cm) | Sedimentary Structure      | Boundary           | Interpretation                                                           |
|------------------|---------------------------------------------|------------------|--------------------|----------------------------|--------------------|--------------------------------------------------------------------------|
| A                | Intraformational conglomerate               | Pebble           | 30                 | Lack of internal structure | Sharp              | Marginal marine to estuarine                                             |
| B                | Medium bedded sandstone with flaser bedding | Medium sand      | 45                 | Flaser bedding             | Sharp              | Delta, tidal flat                                                        |
| C                | Planar-cross bedded sandstone               | Medium sand      | 53                 | Planar-type cross bedding  | Sharp, erosional   | Tidal sandbar, channel bar                                               |
| D                | Ripple-bearing sandstone                    | Medium sand      | 40                 | Wave ripple                | Sharp              | Offshore, channel-shoal, transition zone in delta, tidal flat, estuarine |
| E                | Fossiliferous sandstone                     | Fine-medium sand | 18                 | Lack of internal structure | Sharp, gradational | Lower shore face deposit                                                 |

| Lithofacies Code | Lithofacies Name                                                                                                                 | Grain size              | Bed Thickness (cm) | Sedimentary Structure                        | Boundary           | Interpretation                                                         |
|------------------|----------------------------------------------------------------------------------------------------------------------------------|-------------------------|--------------------|----------------------------------------------|--------------------|------------------------------------------------------------------------|
| F                |  Sandstone with spherical shaped concretion     | Fine-medium sand        | 197                | Sandstone concretion (6 to 10cm in diameter) | Sharp              | Beach ridge develops on marshy regions                                 |
| G                |  Trough type cross-bedded sandstone             | Fine-medium sand        | 10                 | Small scale cross stratification             | Gradational        | Aeolian deposits, fluvial, tidal fat                                   |
| H                |  Sandstone with mud clasts                      | Fine sand               | 215                | Lack of internal structure                   | Sharp, gradational | Sand flat, upper flow regime                                           |
| I                |  Sandstone with herring- bone cross bedding     | Fine sand               | 70                 | Herring-bone cross bedding                   | Gradational        | Tidal channel                                                          |
| J                |  Medium bedded sandstone with wavy bedding      | Fine sand               | 649                | Wavy bedding                                 | Sharp, gradational | Shore face, tidal flat, tidal channel and delta                        |
| K                |  Thick bedded sandstone with lenticular bedding | Mud, fine sand          | 195                | Lenticular bedding                           | Sharp              | Subtidal-intertidal zone, tidal flat                                   |
| L                |  Inclined heterolithic stratification (IHS)    | Mud, silt, fine sand    | 720                | IHS                                          | Sharp, gradational | Deltaic channels, estuarine channel bar in mixed tidal-fluvial channel |
| M                |  Sand-shale interbed                          | Shale, fine-medium sand | 1177               | Sandstone & shale interbed                   | Gradational        | Tidal flat                                                             |
| N                |  Concretionary mudstone                       | Mud                     | 120                | Concretionary mudstone                       | Gradational        | Inner to mid shelf                                                     |

### Facies Association 2: Tidal Sand Bar

Tidal sand bar facies association make up almost entirely of sandstone with planar-cross bedded (facies C), mud drapes (facies H) and inclined heterolithic stratification (IHS) (facies L) and grade upward into horizontally laminated sandstone with a minor percentage of siltstone and shale. Bed-bases are sharp with scours and in some places, load structures. This facies association mostly occupy the middle part of the Okhmintaung Formation and is directly associated with tidal flat and tidal channel facies associations.

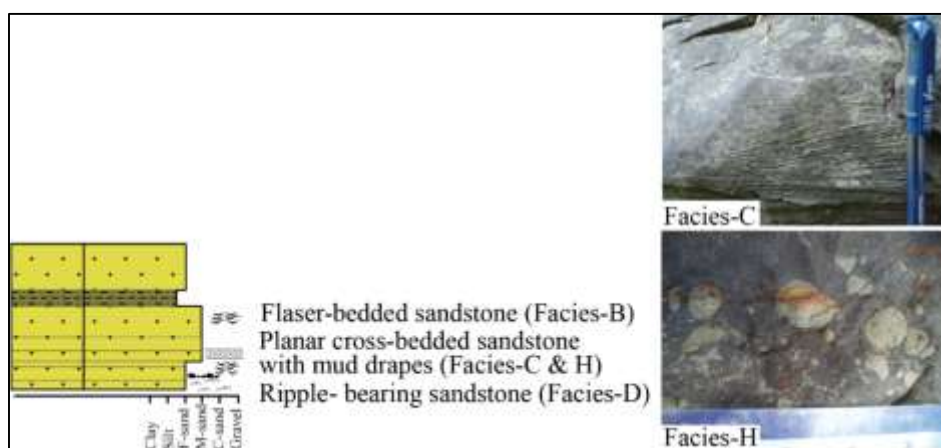


**Figure 3** Idealized sequence of tidal sand bar facies association and outcrop photographs of planar cross-bedded sandstone (Facies-C) and mud clasts in sandstone (Facies-H).

**Facies Association 3: Tidal Flat**

Tidal flats develop along the gently dipping sea coasts with marked tidal rhythms, where enough sediment is available and strong wave action is not present (Reineck and Singh, 1980). The main part of the tidal flat is located between intertidal zones. Primary sedimentary structures for tidal flat deposits include lenticular (facies K), wavy (facies J) and flaser bedding (facies B). This facies association is divided into three main parts: (1) sand flat, (2) mixed flat and (3) mud flat. Planar cross-bedded sandstone (facies C), sandstone with herring-bone cross bedding (facies I), medium bedded sandstone with wavy bedding (facies J) and thick bedded sandstone with lenticular bedding (facies K) may be sand flat deposits. Medium bedded sandstone with flaser and wavy beddings (facies B and J), thick bedded sandstone with lenticular bedding (facies K), and sand-shale interbed (facies M) may be assigned as the mixed flat deposit. Massive or crudely bedded mudstone with concretionary may be assigned to be deposited in the mud flat. Tidal flat facies associations are generally topped by transgressive shelf facies association, and underlain by tidal channel facies association.

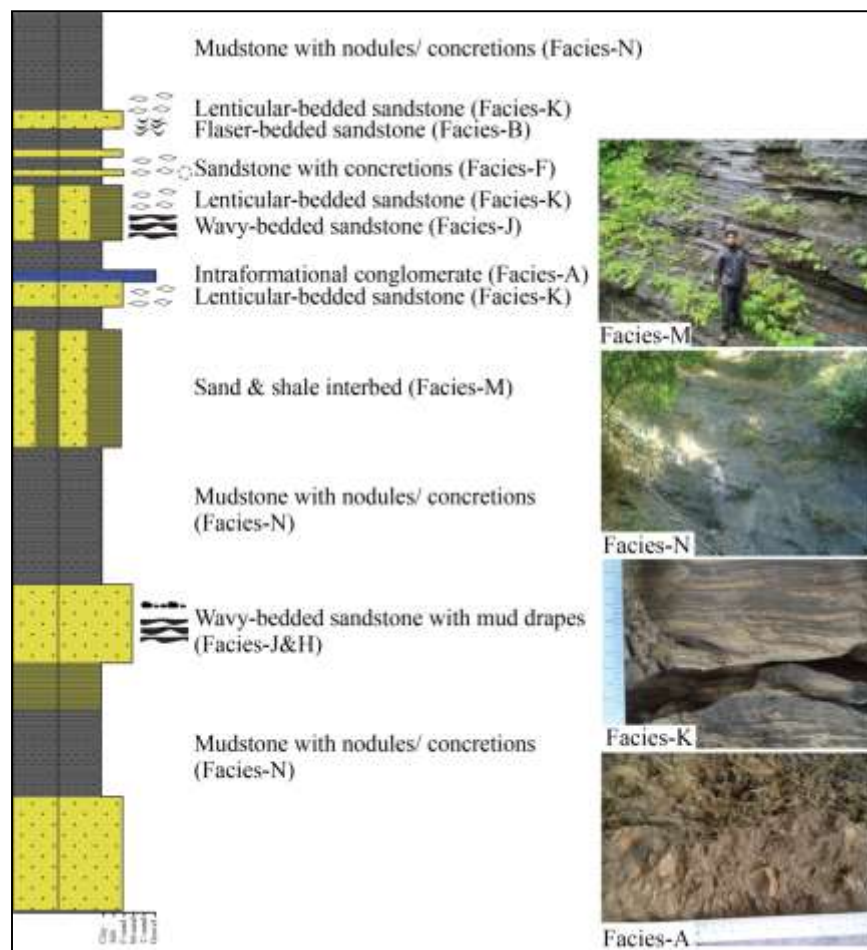


**Figure 4** Idealized sequence of tidal flat facies association and outcrop photographs of sand & shale interbed (Facies-M), mudstone with nodules/ concretions (Facies-N), lenticular-bedded sandstone (Facies-K) and intraformational conglomerate (Facies-A).

**Facies Association 4: Transgressive Shelf**

The continental shelf is submerged under an area from the shore line down, to about 200m, where the gentle slope of the continental shelf changes into the steep slopes of the continental slope (Reineck and Singh, 1980). Mud deposits can be found on the near shore shelf with small amount

of coarse silt layers. The degree of bioturbation of shelf mud can be highly variable and bioturbation structures are abundant. A thin shell layer sometimes is present, pointing to intermittent erosion, that lead to concentration of shells as lag. Sediments are homogenous-looking clay, shelly clay, and shell layers. The major source of shell mud sediments is the suspension load of rivers, which by passes the coastal region and is deposited on the shelf (Reineck and Singh, 1980).

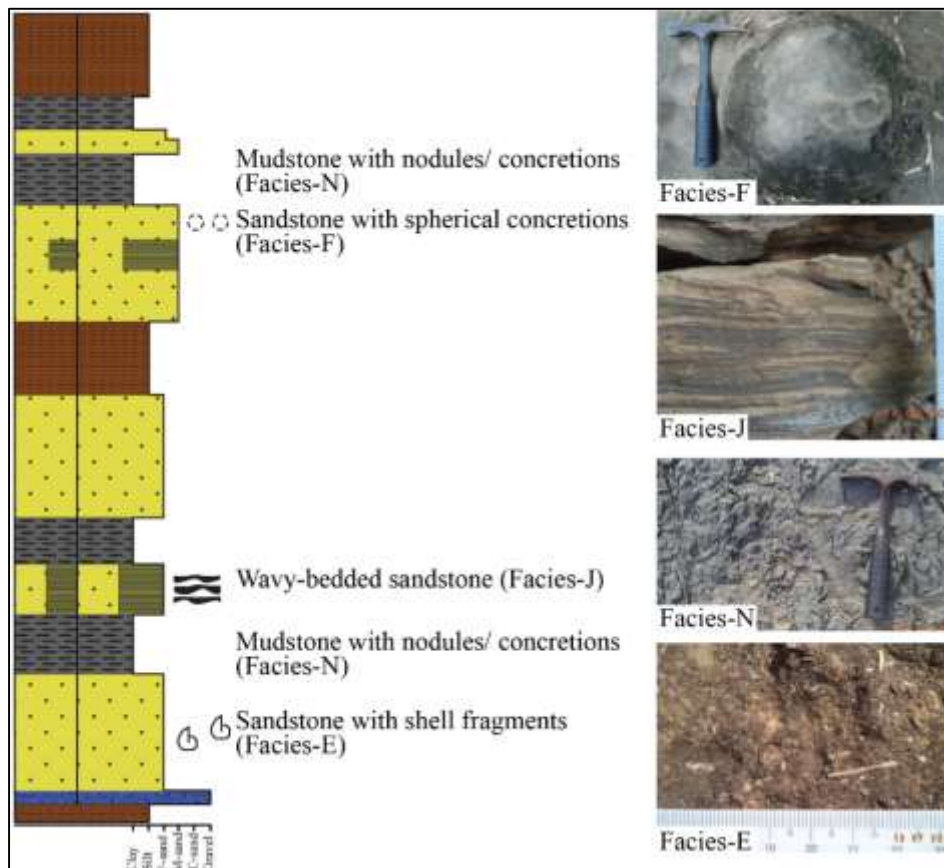


**Figure 5** Idealized sequence of transgressive shelf facies association and outcrop photographs of sandstone with concretions (Facies-F), sandstone with wavy bedding (Facies-J), mudstone with nodules/ concretions (Facies-N) and sandstone with shell fragments (Facies-E).

The combination of reddish brown to greenish brown colored, fine grained sandstones with shell fragments and burrows (facies E) and bluish grey colored, concretionary mudstone (Facies N) represent into transgressive shelf marine facies association. This facies association is associated with tidal-flat deposits of estuarine system.

### Discussion of the Depositional System

The Tertiary sediments recorded a history of infilling of the forearc basin (Minbu Sub-Basin) by marine sediments from the south and non- marine deposits from the north. The process was interrupted by marine transgressions and regressions, resulting in intertonguing of continental and marine units (Stamp, 1922; Chhibber, 1934). Depositional environment of the research area may be interpreted on the basis of the textures, sedimentary structures, fossils, and lithologic associations of sedimentary rocks on the scale of an outcrop.

Evidence for tidal conditions include mud drapes (facies H), and herringbone cross-stratification (facies I). The mud drapes form as the current slows down when the tide turns.

Subtidal zone make up of channel and sand bar sediments. Bioturbation is very weak, as the rate of sedimentation is very high in the tidal channel. The tidal channel show mud drapes and inclined heterolithic stratification. The channel bottoms of the larger tidal channels are mostly sandy, enriched in shells (facies E). Evidence for tidal bar conditions in sand beds include planar-cross bedded (facies C), mud drapes (facies H), and herringbone cross-stratification (facies I). Herringbone cross-bedding is relatively uncommon because the ebb and flood tidal flows tend to follow different pathways, with the flood tide going up one side of the estuary and the ebb tide following a different route down the other side.

The tidal flat is located in intertidal zone where sediments have been deposited by tides or rivers. The primary sedimentary structures which were formed under tide flat condition include mega-ripple (facies D), small amount of herringbone cross bedding (facies I), small scale cross bedding (facies G) on the sand flat, flaser (facies B), wavy (facies J), and lenticular beddings (facies K) on the mixed flat. Mud and silt layers with concretion (facies N) rich in organic material are typically in muddy tidal flat deposits.

Transgressive shelf succession is typically mudstone, often organic-rich with thin, wave-rippled sand beds (Boggs 2006). Sandstone with shells or shell fragments (facies E) and bioturbated muds (facies N) indicate the influence of shallow marine clastic system. Summing up the above factors, lower part of the Okhmintaung Formation may be deposited in the tide-dominated estuarine environment which consist of tidal channels, tidal sand bars, and tidal flats, and followed by deposition of transgressive shelf system in the upper part of the formation.

### Conclusion

Fourteen distinguishable lithofacies frameworks can be established, and can be grouped into four facies associations, comprising tidal channel, tidal sand bar, tidal flat and transgressive shelf. The facies architectures reveal that the evolution of the Okhmintaung Formation is mainly related to the Oligocene sea-level rise. At the early depositional stage of the Oligocene transgression, tide-dominated estuarine system occurs as the basal units at the lower part of the Okhmintaung Formation. At the late depositional stage of the Okhmintaung Formation, significant marine transgression takes places and it shifts in facies depositions from tide dominated estuarine to a transgressive shelf sequences in the upper Okhmintaung Formation. As a result of the factors mentioned above, the Oligocene Okhmintaung Formation may have deposited in tide-dominated transgressive estuarine system (Figure 6).

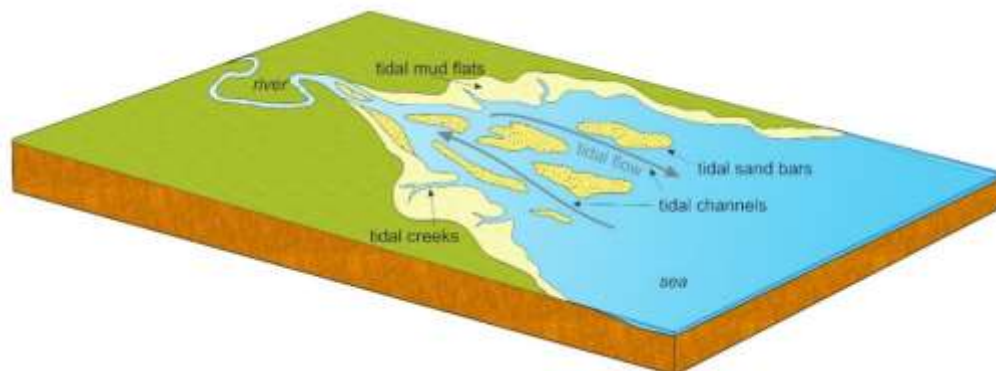


**Figure 6** Depositional model of the research area showing tide-dominated estuarine facies system (Nichols, 2009).

## Acknowledgements

We would like to express our deep gratitude to Prof. Dr. Khin San, Head of Department of Geology, Magway University, for her encouragement and great attention throughout this research. We would like to express our very great appreciation U Aye Ko, U Hlaing Win Htun and Daw Ei Ei Win, Lecturers and colleagues at Geology Department of Magway University and Daw Chaw Su Hlaing, Lecturer at Geology Department of West Yangon University for their generous supports in the preparation of this research. Finally, our special thanks are extended to local people of Ywathitkyi, Sinthe and Myasagaing Villages, Sinbaungwe and Thayet Townships, for their valuable helps and facilities during fieldworks.

## References

- Blair, T.C., and McPherson, J.G., (1999). Grain-size and textural classification of coarse sedimentary particles. *Journal of Sedimentary Research* 69(1), 6-19.
- Boggs, S., (2006). *Principles of Sedimentology and Stratigraphy*. 4<sup>th</sup> Edition. Pearson Prentice Hall, Upper Saddle River, NJ.
- Chhibber, H.L., (1934). *The geology of Burma*. Macmillan London.
- Collinson, J., Mountney, N., and Thompson, D., (2006). *Sedimentary Structures*, Terra Publishing, 3<sup>rd</sup> Edition, 292 pp.
- Compton, R.R., (1962). *Manual of field Geology*. John Wiley & Sons, New York.
- Dalrymple, R. W., Knight, R.J., and Lambiase, J. J. (1978). Bedforms and their hydraulic stability relationships in a tidal environment, Bay of Fundy, Canada. *Nature* 275, 100-4
- Miall, A.D., (1977). A review of the braided river depositional environment. *Earth Sci. Rev.*, 13, 1-62.
- Miall, A.D., (1978). Lithofacies types and vertical profile models in braided river deposits; a summary. In: *Fluvial Sediementology* (Eds. Miall, A.D.). Can. Soc. Petrol. Geol. Mem. Soc., 597–604.
- Miall, A.D., (1985). Architectural-element analysis: a new method of facies analysis applied to fluvial deposits. *Earth Sci. Rev.* 22, 261–308.
- Miall, A.D., (2006). *The Geology of Fluvial Deposits*. Springer-Verlag, Berlin. 4<sup>th</sup> Edition. 191 pp.
- Nichols, G., (2009). *Sedimentology and Stratigraphy*, 2<sup>nd</sup> Edition. United Kingdom, p 279-287.
- Reineck, H.E. and Singh, I.B., (1980). *Deposition Sedimentary Environments*. Springer-Verlag, Newyork.
- Reinson, G.E., (1992). Transgressive barrier island and estuarine systems. In: *Facies Models: Response to Sea level Change* (Eds. Walker, R.G and James, N.P.). Geological Association of Canada, St Johns, Newfoundland; 179-194.
- Stamp, L.D., (1922). An outline of the Tertiary geology of Burma. *Geol-Map*, vol-59
- Theobald, W., (1973). The Geology of Pegu. *Mem. Geol. Surv. India*, 10.2.
- Thomas, R.G., Smith, D.G., Wood, J.M., Visser, J., CalverleyRange, E.A. and Koster, E.H., (1987). Inclined heterolithic stratification–terminology, description, interpretation and significance. *Sedimentary Geology*, 53, 123-179.
- Tucker, M.E., (1996). *Sedimentary Rocks in the Field*. Wiley, Chichester, 2<sup>nd</sup> Edition, 153 pp

## PETROGRAPHY AND GEOCHEMISTRY OF CALC-SILICATE ROCKS EXPOSED IN KANTHA-AUNGTHARYA AREA, THABEIKKYIN TOWNSHIP, MANDALAY REGION

May Thet Aye<sup>1</sup>, Myo Min Tun<sup>2</sup>, Zaw Lin Kyaw<sup>3</sup>, Yan Naing Tun<sup>4</sup> and Min Aung<sup>4</sup>

### Abstract

The research area, Kantha-Aungtharya area, lies in Thabeikkyin Township, Mandalay Region. The study area falls within the Mogok Metamorphic Belt, lying between Sagaing fault and Shan scarp. It is located about 6.5 km east of Thabeikkyin and 122 km north of Mandalay. Metasedimentary such as marbles and calc-silicate rocks and igneous rock (such as biotite microgranite) units are prominent in this study area. The relatively high Al<sub>2</sub>O<sub>3</sub> and fairly high values of Fe<sup>3+</sup> and Fe<sup>2+</sup> in the calc-silicate rock could be due to (a) impurities containing iron in the sedimentary environment and (b) diffusion of ions from the igneous body. The original material from which the calc-silicates can be formed may be impure dolomitic limestone, marls and limestone.

**Keywords:** Petrography, Geochemistry, XRF, Calc-silicate Rocks and Kantha-Aungtharya area.

### Introduction

Myanmar is situated in an area of complex plate tectonic setting. As a result of plate tectonic evolution, the country has been divided from west to east into four major geotectonic units, the Arakan Coastal Zone, Indo-Burma Range, Inner-Burma Basin and Sino-Burma Ranges, forming the north-south elongated structures. The research area is located in Thabeikkyin Township, Mandalay Region. The main rock units exposed in this area are metamorphic and igneous rocks. The study area is mainly composed of diopside marble interbedded with calc-silicate rocks and marbles, and biotite microgranite. Several gold worksites of the primary gold deposit are situated in the research area. Based on the lithologic characters and mineralogy as well as associated features of metamorphic rock unit, it is apparent that the existence of gold deposits will be encouraging in the area and can probably be explored as primary deposits.

Various workers (geologists) have studied the Mogok Metamorphic Belt of Myanmar. They mentioned their views with respect to geology, metamorphism and tectonism involving in this metamorphic belt. La Touche (1913) described the principal rock types of the area in the Memoir of the Northern Shan State. The term 'Mogok Gneiss' was first introduced. Clegg (1941) suggested that the rocks are considered to be metamorphosed Paleozoic and Mesozoic rock units. He published a geological report for northern Thabeikkyin area and east Ayeyarwaddy. Searle and Haq (1964) described that the Mogok Series comprises stratigraphic groups ranging from Precambrian to Upper Paleozoic. The metamorphism must have been occurred during post Paleozoic and related to the Himalayan Orogeny. Ali Akbar Khan (1985) reported that the metasedimentary rocks were intruded by Tertiary igneous rocks on the geology of Wabyudaung-Ondan area. Myint Naing (1987) studied the geology of Chaunggyi-Zayetkwin area, Thabeikkyin Township. He stated that Lower to Upper Paleozoic metasedimentary rocks were intruded by Late Cretaceous to Paleocene igneous rocks. Myint Lwin Thein *et al.*, (1990) studied the main rock units of the Mogok-Thabeikkyin-Singu-Madaya area. He described the stratigraphic consideration on marble as well as other metamorphic rock units and associated igneous rocks. Zaw Win Ko (1997) also studied the geology of Kwinthonze-Onzon area. Bertrand *et al.*, (1999; 2001 and 2003)

---

<sup>1</sup> Dr, Associate Professor, Department of Geology, Maubin University

<sup>2</sup> Dr, Associate Professor, Department of Geology, Kyaukse University

<sup>3</sup> Dr, Associate Professor, Department of Geology, University of Yangon

<sup>4</sup> Lecturer, Department of Geology, Meiktila University

<sup>5</sup> Dr, Pro-rector (Ret), Maubin University

proposed the Oligocene to Mid-Miocene age of metamorphic rocks of the Mogok Belt. Myo Thant (2002) studied the geology and ore deposits of Kwinthonze-Leikkya area, Thabeikkyin Township. Tin Aung Myint (2009) studied precious and base-metal mineralization in the Chaunggyi-Kandaung-Kwinthonze area, just south of the research area. Zar Oo San (2010) also studied the petrology and genetic aspects of gem minerals in the Kyetsaung Taung-Kyaukkyi area, Thabeikkyin Township. This area lies to the south of the study area. Zaw Win (2015) contributed the petrology and gold mineralization of the Kyaukbalu-Donwe area of Thabeikkyin Township.

### Location, Size and Accessibility

The Kantha-Aungharya area lies in Thabeikkyin Township, Mandalay Region. It is located about 6.4 km (4 miles) east of Thabeikkyin and 122 km (76 miles) north of Mandalay. The area is bounded between the coordinates of North Latitude  $22^{\circ} 51' 15''$  to  $22^{\circ} 58' 00''$  and the East Longitude  $96^{\circ} 01' 00''$  to  $96^{\circ} 06' 00''$  in one-inch topographic maps of 93 B/1. The areal extent is about 8 km (5 miles) from North to South and 8 km (5 miles) from East to West, covering approximately of 64 square kilometers. The study area is easily accessible via motorcar throughout the year. The location map of the research area is shown in Figure 1.

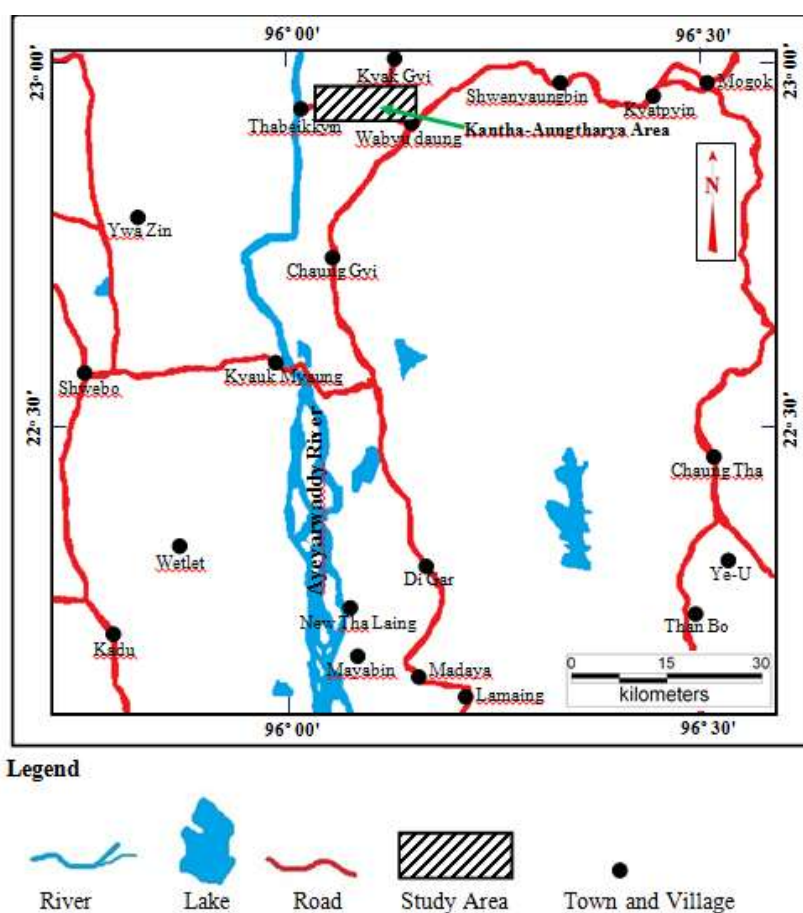


**Figure 1** Location map of the study area, Thabeikkyin Township, Mandalay, Region.

### Physiography

Geomorphologically, the study area lies on the western border of the Eastern Highlands. Lowland (plain) and rolling hills are common in the research area. The eastern and northern parts are high in relief that gradually lower down towards the west and south. The eastern part is higher than any other parts in the research area and the highest point is about 397m (1304 ft). This part

contains massive NE-SW trending ridges covered by dense forest. Late Paleozoic to Mesozoic metasedimentary rock units (mostly marbles) occur in the southern and western part of the research area. Middle Miocene igneous rock Unit (microgranite) is exposed largely in the northern part of the research area. Marble units are also encountered in this part. The interbeds of marbles and calc-silicate rocks are observed in the eastern part of the area. These rock units are sometimes intruded by the microgranite. Marbles are widely exposed where biotite microgranites are limited in occurrence in the study area. Generally, the drainage pattern of the area shows dendritic nature (Figure 2). Gway Pin Hmaw Chaung is the main stream in the study area. It flows from east to west through the northern part of the research area. The So Gyi Chaung joins the Gway Pin Hmaw Chaung in the northern part of the research area. The So Gyi Chaung runs through the middle part of the study area in south to northwest direction. Finally, Gway Pin Hmaw Chaung flows into the Ayeyarwaddy River. The research area has a subtropical climate and gets fairly high rainfall.

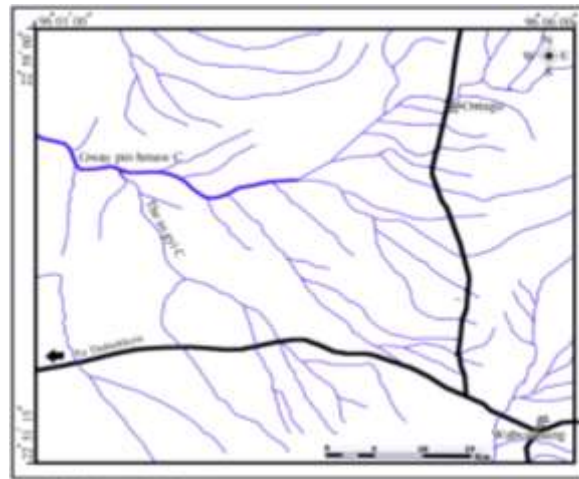


**Figure 2** The drainage map of the research area

### Purposes of Research

- 1) To identify the petrological characteristics of the Calc-silicate rocks unit and their distributions in the study area
- 2) To investigate the geochemical signatures and suggest the paragenesis of these rocks.

### Methods of Study

- 1) The research methods mainly include two parts: detailed field investigation and laboratory works.
- 2) The GPS and Brunton compass are used to locate the lithologic contact and collect rock samples.
- 3) The major and trace elemental composition of rocks and mineralized rocks and veins was analyzed by X-Ray Fluorescence (XRF) under pressed pellets using a RIGAKU RIX-3100 (Series VR 25006) X-ray Fluorescence spectrometer. The LOI (loss of ignition) data were measured at 1000°C for all samples to be analyzed by XRF. XRF analyses were carried out at the laboratory of Economic Geology, Department of Earth Resources Engineering, Kyushu University.

## Petrography

### Nature of exposure and distribution

Calc-silicate rocks are widespread in the research area. Good exposures of these rocks are located north of Chan-tha village (N 22° 53' 04.5" and E 96° 04' 47.4"). They usually form distinctive ridges striking parallel to the east-west foliation. Generally, they are medium- to coarse-grained, well-banded meta-sediment with distinct mineralogical layering (Figure 3a). Layering varies in thickness between 2mm and 2cm.

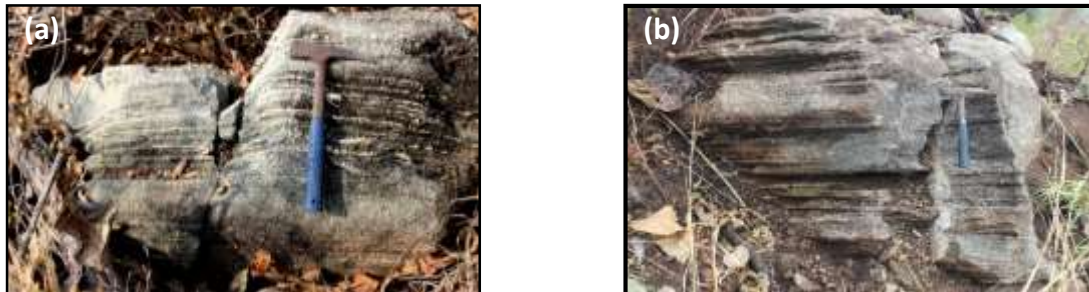


**Figure 3** (a) The banded calc-silicate rock showing distinctive quartz-rich layers (white) and diopside rich layers (green) and (b) typical rib and furrow structures of calc-silicate rock

In outcrop, the calcium-rich layers are often more deeply weathered leaving the more resistant silica layers to stand out. By the differential weathering rib and furrow structure are also observed on weathered surface (Figure 3b). The calc-silicate layers dip steeply 70-85 degree to the north-northwest and show evidence of multiple deformations with small folds striking east-west (Figure 4).



**Figure 4** The calc-silicate rock showing drag folds as the evidence of plastic deformations.

Diopside grains are anhedral to subhedral and rounded. The grain size ranges from 0.2 mm to 1.5 mm in diameter. Diopside porphyroblasts are seen along the mosaic of quartz and calcite grains. The relief is high, pale green and greenish pink in thin section. They are randomly oriented (Figures 5a & b).

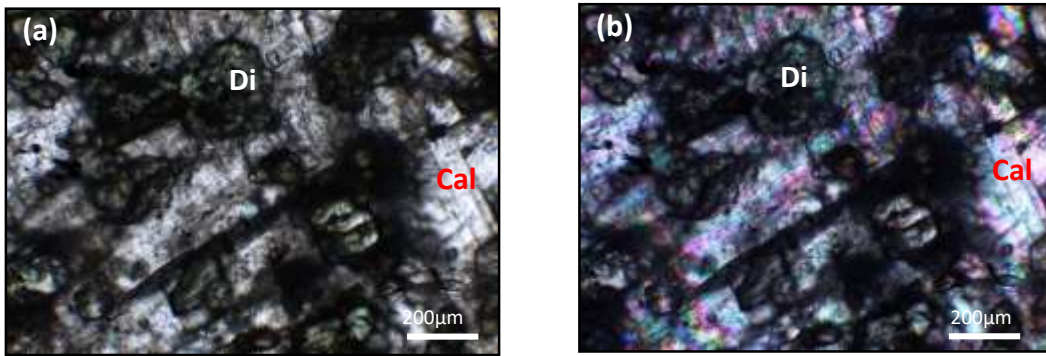


**Figure 5** Photomicrograph showing randomly oriented diopside grains (a) under PPL (b) under XN. Di=Diopside and Cal= Calcite

Calcite appears as xenoblastic to idioblastic grains. They can be easily recognizable under microscope. Most calcite grains reach up to 2mm in diameter.

Sphene is greyish brown in color. It shows very high relief. Color and pleochroism are more distinct. Lozenge-shaped sphene occurs as idioblastic grains (Figures 6a & b). It occurs at the contact of diopside.

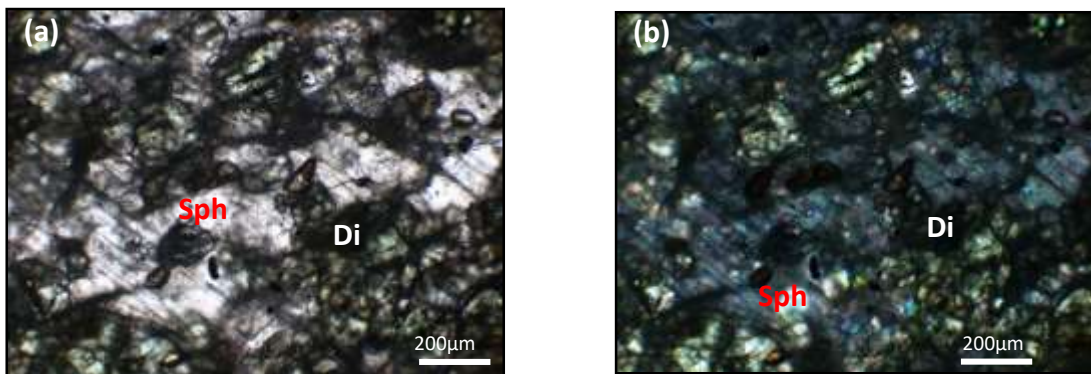


**Figure 6** Photomicrograph showing disseminated granules of sphene in calc-silicate rock (a) under PPL (b) under XN. Di=Diopside, Sph=Sphene

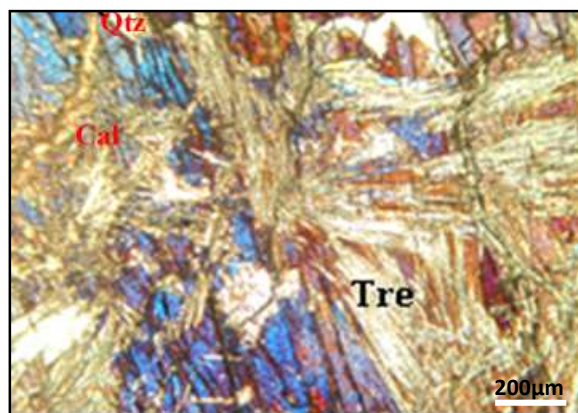


**Figure 7** Photomicrograph showing fibrous aggregate of tremolite in calc-silicate rock, (Under XN), Tre = Tremolite, Cal = Calcite and Qtz = Quartz

Tremolite is observed as an accessory mineral. Tremolite laths are sub-idioblastic. It shows moderate to high relief. It is colorless in thin section. Darker color and stronger pleochroism are associated with higher iron content (William, 2013). Tremolite shows up to the middle second

order white interference color. It occurs as the acicular pattern. It forms fibrous aggregates (Figure 7).

### Geochemistry of Calc-Silicate Rocks

Calc-silicate rocks owe their origin mainly from contact metamorphism when magma intrudes into colder region and the adjacent rocks are heated. If the heat content of the magma is high, there will be a temperature rise in the bordering country rocks lasting long enough to cause mineral reactions to start and proceed to completion.

The following minerals were identified in thin section calcite, quartz, tremolite, garnet, diopside, forsterite and iron oxide. Representative samples of calc-silicate rock were selected and prepared for geochemical analysis, using X-ray fluorescence (XRF).

In rock samples of the study area, SiO<sub>2</sub> occupies (46.61%) a significant proportion of the rock. This high proportion is not unrelated to the high immobility of the Si<sup>4+</sup> ion. CaO is the second most abundant element (23.15%) from the result of analysis. This abundance is to be expected since Ca<sup>2+</sup> ion is very mobile and goes into reaction easily. The relatively high Al<sub>2</sub>O<sub>3</sub> (14.12%) may be due to the mobility of an Al<sup>3+</sup> ion. Al<sup>3+</sup> ion may have migrated from the acid igneous rocks which metamorphose the carbonates. Due to diffusion and metasomatism, the ions have transferred into the carbonate. The low content of magnesium (3.05%) may have resulted also from leaching of the dolomitic limestone. TiO<sub>2</sub> value (<1%) is quite low. The low value should be expected due to the limited or small abundance of Ti-bearing minerals in the rock. Fairly high values of Fe<sup>3+</sup> and Fe<sup>2+</sup> in the rock could be possibly due to (a) impurities containing iron in the sedimentary environment and (b) diffusion of ions possibly come from the igneous body. The presence of high oxygen fugacity in the environment may have resulted in the oxidation of the Fe ions.

The original material from which the calc-silicates can be formed may be impure dolomitic limestone, marls and limestone. However, these carbonates can be found deposited under the same environment. Generally, limestone and dolomite are very common in fresh water lake or marine environments.

Experiment has shown that Tremolite is mainly stable at temperatures below 400°C at the fluid pressure of 2 kilobars (Helmut, *et al.*, 1976; Shaw, 1960; Knorring, 1958). Tremolite + Calcite + Quartz will not be stable at temperatures greater than 400°C. Diopside + Calcite + Quartz are stable at temperature higher than 400°C and fluid pressure of about 2 kilobars. Therefore, for calc-silicate minerals, it may be concluded that they are direct result of contact metamorphism of impure siliceous dolomitic limestone in the study area.

### Conclusions

Based on the available data from field investigation and resultant data from the analyses, the following conclusions are summarized:

The Kantha-Aungtharya area lies in Thabeikkyin Township, Mandalay Region. It is located about 6.5 km east of Thabeikkyin and 122 km north of Mandalay. The research area falls within the Mogok Metamorphic Belt. Metasedimentary rocks such as marbles and calc-silicate rocks and igneous rock (such as biotite microgranite) units are prominent in this study area. Calc-silicate rocks owe their origin mainly to contact metamorphism when magma intrudes into colder region, the adjacent rocks are heated. The relatively high Al<sub>2</sub>O<sub>3</sub> may be due to the mobility of a Al<sup>3+</sup> ion. Al<sup>3+</sup> ion may have migrated from the acid igneous rocks which metamorphose the carbonates. Fairly high values of Fe<sup>3+</sup> and Fe<sup>2+</sup> in the calc-silicate rock could be due to (a) impurities containing iron in the sedimentary environment and (b) diffusion of ions from the igneous body. respectively

Calc-silicate minerals, it may be concluded that they are direct result of contact metamorphism of impure siliceous dolomitic limestone in the study area.

### Acknowledgements

We would like to express our sincere gratitude to Dr Than Than Nu, Professor and Head, Department of Geology, University of Mandalay, for her encouragement and support throughout the present research and constructive suggestions.

### References

- Ali Akbar Khan, (1985). Geology of Wabyudaung-Ondan area, Thabeikkyin Township, *M.Sc Thesis*, University of Mandalay (Unpublished).
- Bertrand, G., C. Rangin, H. Maluski, Tin Aung Han, Myint Thein, Ohn Myint, Win Maw, and San Lwin, 1999, 2001 and 2003. Cenozoic metamorphism along the Shan Scarp (Myanmar): Evidence for ductile shear along the Sagaing fault or the northward migration of the eastern Himalaya syntaxis? *Geophys. Res. Lett.*, 26, 915-918.
- Clegg, E. L. G., (1941). The Cretaceous and Associated Rocks of Burma. *Mem. of the Geol. Surv. India. V. 74*, pp 1-101.
- Helmut, G.F Winkler (1976). *Petrogenesis of Metamorphic rocks*. Springer-Verlag.334 pages. A. H. Brownflow, "Geochemistry (2nd ed.)," Prentice Hall, 1996, pp. 350-351.
- Knorring O.V, (1958); The mineral Parageresis and metamorphic status of Garnet-horblende, Pyroxene-Scapolite genesis from Ghana. *Mineral Magazine* 31, 846-859.
- La Touche, T.H.D., (1913). Geology of the Northern Shan State; *Mem. Geol. Surv. India, vol.39*, p.1-379.
- Myint Naing, (1987). Geology of Chaunggyi-Zayetkwin Area, Thabeikkyin Township, *M.Sc Thesis*, University of Mandalay (Unpublished).
- Myint Lwin Thein, Ohn Myint, Sun Kyi and Hpone Nyunt Win, (1990). *Geology and stratigraphy of the metamorphosed early Paleozoic rocks of the Mogok-Thabeikkyin-Singu-Madaya areas*. Unpublished staff report, No. 98, A.G.D., Y.U.
- Myo Thant, (2002). Geology and Ore Deposits of Kwinthonze-Leikkya Area, *M.Sc Thesis*, Thabeikkyin Township, University of Mandalay (Unpublished).
- Searle, D.L and Ba Than Haq, (1964). The Mogok Belt of Burma and its relationship to the Himalayan Orogeny, *Proc. Int. Geol. Cong., IGCP 22nd session part XI*, 132-161.
- Shaw, D.M (1960.) *The Geochemistry of scapolite-part 1*. Previous and general mineralogy part 11. Trace elements, Petrology and general Petrology 1 218-285.
- Tin Aung Myint, (2009). Precious and Base Metal Mineralization in Singu and Thabeikkyin Townships; A Genetic Approach, *Ph.D Dissertation*, University of Mandalay, (Unpublished).
- William, D.N., (2013). *Introduction to Optical Mineralogy*, 4th edition, Oxford University Press, Inc, New York and Oxford.
- Zar Oo San, (2010). Petrology and Genetic Aspects of Gem Minerals in the Kyetsaung Taung-Kyaukkyi Area, Thabeikkyin Township, *Ph.D Dissertation*, University of Mandalay, (Unpublished).
- Zaw Win, (2015). Petrology and Economic Significance of the Igneous Rocks Exposed in Pinlebu-Banmauk Area, Sagaing Division, *Ph.D Dissertation*, University of Mandalay, (Unpublished).
- Zaw Win Ko, (1997). The Geology of Kwinthonze-Onzon Area, Thabeikkyin Township, *M.Sc Thesis*, University of Mandalay, (Unpublished).

## REPTILIAN REMAINS OF IRRAWADDY FORMATION IN YINSEIK AREA, MAGWAY REGION

Khaing Myat Thwin<sup>1</sup>, Zin Maung Maung Thein<sup>2</sup>

### Abstract

Yinseik area occupies Obogon Formation (Middle Miocene) and Irrawaddy Formation (Late Miocene to Early Pleistocene). The dominant lithology of Obogon Formation is an alternation of yellowish brown- to buff-colored, fine to medium-grained, thin-bedded sandstone and light gray to bluish gray clay and shale with fine- to medium-grained sandstone. Irrawaddy Formation is mainly composed of thick bedded to massive, medium to coarse-grained, light gray to light brown, concretionary sandstone with cross stratification in the lower part and massive, medium to coarse-grained, light gray to yellowish brown, gritty to pebbly, incoherent sandstone interbedding with siltstone in upper part. The sediments of Irrawaddy Formation in research area yields the fossilized remains of primate (*Khoratpithecus* sp), carnivores, Anthracothere (*Merycopotamus* sp.), tragulid, wild boar (*Tetraconodon* sp. and *Propotamochoerus* sp.), bovids, rhinoceros (*Rhinoceros* sp.), horse (*Hipparion* sp.), elephant (*Stegolophodon* sp.) and crocodile (*Gavialis* sp.) which occur in the sediments of Irrawaddy Formation. The present faunal assemblage suggests the existence of forest/woodland adapted animals in Yinseik area in the geological past. Occurrence of crocodile (*Gavialis* sp.) and extinct river shark (*Glyphis* sp.) in this area supports the presence of riverine environment. Present day's environmental conditions in Central Myanmar are characterized by a subtropical semi-arid climate especially in most parts of Mandalay and Magway Regions. The vegetation of this region is dominated by open shrub lands and grasslands. Therefore, the occurrence of forest dwelling mammals in present area contributes to the implication that the Late Miocene paleoenvironment of Yinseik area was drastically different from the present day's conditions in central Myanmar.

**Keywords:** Irrawaddy Formation, *Gavialis* sp., Paleoenvironment.

### Introduction

Myanmar has a lot of vertebrate fossils existing Mesozoic and Cenozoic Strata especially Pondaung Formation (Late Eocene) and Irrawaddy Formation (Late Miocene to Early Pleistocene). These fossils are very important in exploring paleoclimate, paleoenvironment, paleoecology and paleontology. The present research is mainly conducted on crocodile's remains in the sediments of Irrawaddy Formation.

Yinseik area is situated about 20 km south of Magway Township, lying on the eastern side of Ayeyarwaddy River (Fig 1). Therefore, it is easily accessible throughout the year. The research area is 12 kilometers long in north-south direction and 12 kilometers wide in east-west direction, covering an area of 144 square kilometers of flat plain and low-lying rolling hill.

---

<sup>1</sup> Assistant Lecturer, Department of Geology, University of Yangon

<sup>2</sup> Dr., Associate Professor, Department of Geology, University of Mandalay

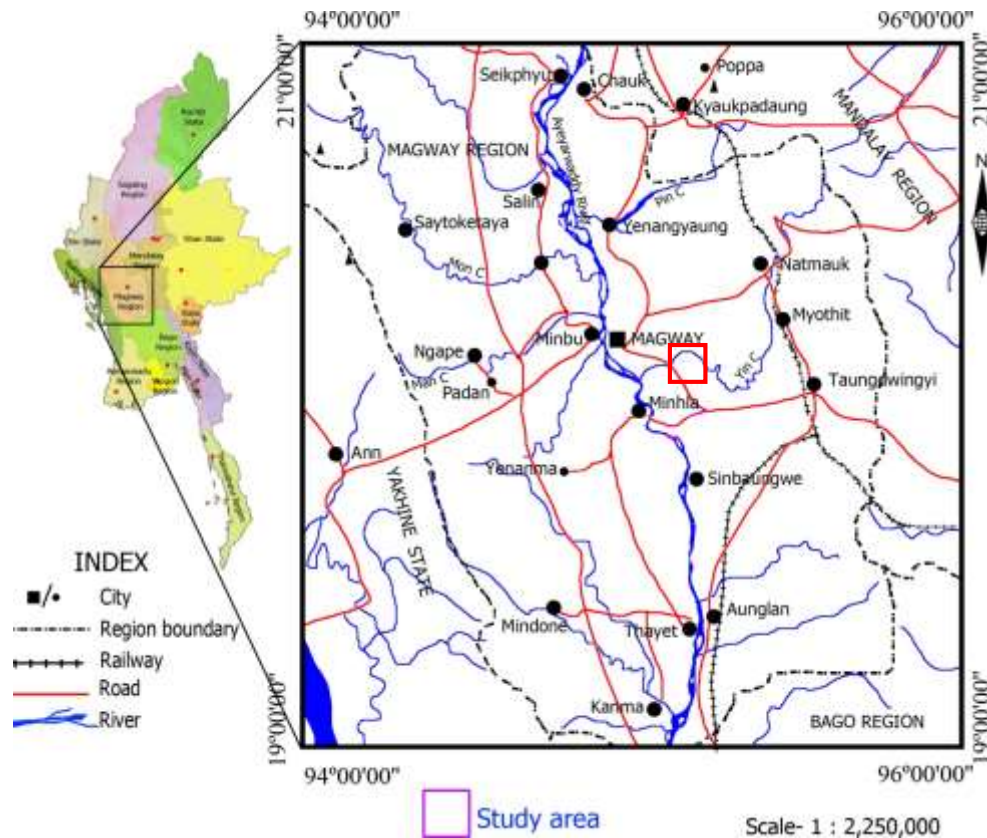


**Figure 1** Location map of Yinseik area, Magway Township

The research area is mainly composed of clastic sediments which is dissected and eroded by Yin Chaung (Yin stream) and its tributaries. The largest stream is Yin Chaung which passes through the area from east to west. The most prominent drainage patterns of the area are dendritic, trellis and rectangular (Figure 2). Yin Chaung, flows from east to west and then joined with the Ayeyarwaddy River in the west of the research area.

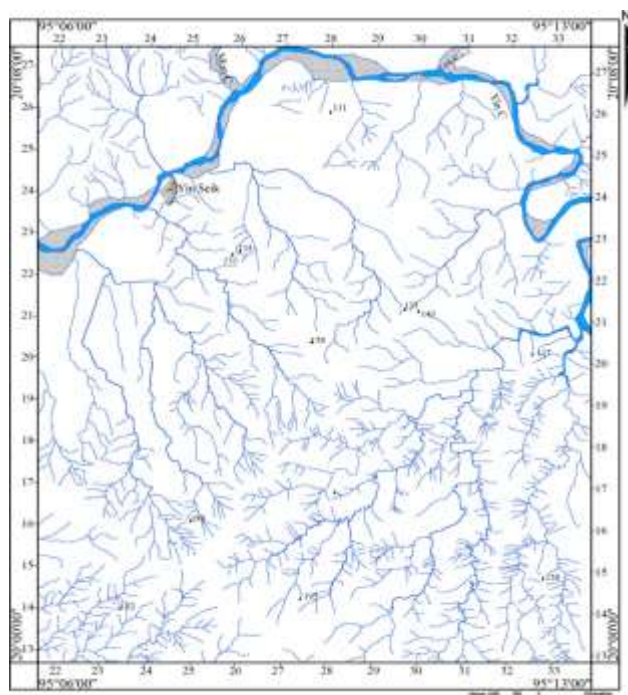


**Figure 2** Drainage Pattern of Yinseik area, Magway Township

## **Aims and Objectives**

The main aim of this research is to explore systematic paleontology and paleoecology based on *Gavialis* sp. of Irrawaddy Formation. The research has been carried out with the followings:

- (1) To prepare the geological map
- (2) To describe the systematic paleontology of *Gavialis* sp.
- (3) To evaluate the paleoecology of research area

## **Methodology**

The UTM topographic map 1:50000 and satellite images are used for the location, linear structure and topography, general structural elements and regional structures.

The dips and strike of the beds, joints, folds and faults were studied and measured in the field by using Brunton Compass. The certain location of outcrops is attained by GPS navigator and checked by bearing and intersection methods. The diagnostic fossils were collected, properly marked and carefully packed for detailed investigation.

## **Stratigraphy**

In the area, the rock sequence is composed mainly of upper Cenozoic clastic sediments. The stratigraphic succession of the area is constituted of Upper Pegu Group and Irrawaddy Formation. The lithologies are dominated by sandstone, shale and clay, and conglomerate. The regional tectonic setting and lithostratigraphic characteristics indicate the molasse nature of these sediments.

The sedimentary rocks in the area are subdivided into two formations based on the lithologic and faunal characteristics. They are

- (2) Irrawaddy Formation (Late Miocene to Early Pleistocene)
- (1) Obogon Formation (Middle Miocene)

The abundance of fossil woods is the distinguishing characteristic for Irrawaddy Formation. Furthermore, the remains of terrestrial and aquatic vertebrates are recovered from the sediments of this formation.

### **Obogon Formation**

It is composed of alternations of mottled, blue gray clay with fine- to medium-grained sandstone. In the area, Obogon Formation occurs as inlier, surrounded by younger Irrawaddy Formation. However, the outcrop of Obogon Formation has been limited or poorly exposed and good exposures are found along the southern bank of Yin Chaung and Pagoda Hill (Phayagon) in Ondwe Village. The lower boundary of Obogon Formation with underlying Kyaukkok Formation is not observed in the area. The contact with overlying Irrawaddy Formation is indicated by gradual lithologic changes from fine grained, thin bedded sandstone to yellowish brown, massive pebbly

sandstone of Irrawaddy Formation. According to the lithology, stratigraphy and faunal assemblage, Obogon Formation of Yinseik area may belong to the Middle Miocene in age.



**Figure 3** Light gray clay at the lower part of Obogon Formation



**Figure 4** Fossiliferous hard sandstone band intercalated with buff colored, poorly indurated sandstone of Obogon Formation  
(Loc: 20°06'43" N; 95°08'31" E)

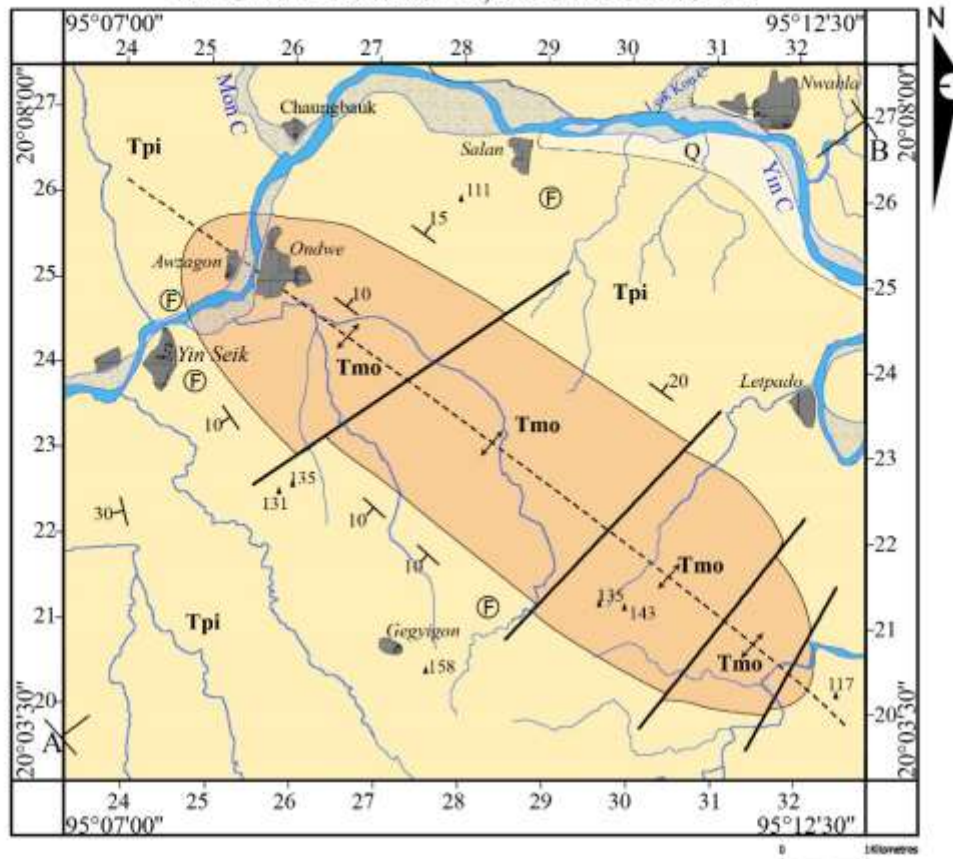
### Irrawaddy Formation

Irrawaddy Formation is characterized by the abundance of fossil wood and yielding of vertebrate fossils. Irrawaddy Formation is widely exposed on both north eastern and south western flanks of Ondwe Uplift as the low lying where the dips gently dipping to north east and south west respectively. Good exposure of this formation can be observed along the road section of Magway-Taungdwin road and in the vicinity of Yin Chaung bridge. Irrawaddy Formation unconformably overlies Obogon Formation in the area. The middle to late Pleistocene River Terraces deposits unconformably overlie on this formation. Several genera of vertebrates (Primate, Carnivora, Perissodactyla and Artiodactyla) have been documented from Irrawaddy Formation exposed in Yinseik area (Jaegear et al., 2011). This faunal assemblage generally suggests Late Miocene age for the sediments of Irrawaddy Formation.

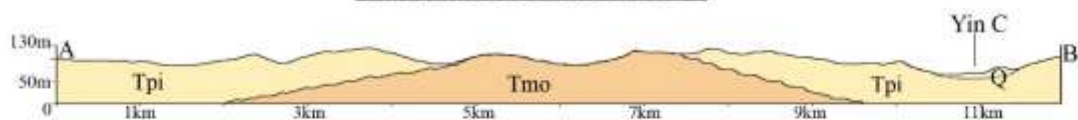


**Figure 5** Left. Medium to thick bedded, horizontally laminated, concretionary sandstone & Right. Large scale planar type cross bedding in medium to thick bedded sandstone of Irrawaddy Formation  
(Loc: 20°06' 38" N; 95°08'40" E)

**GEOLOGICAL MAP OF THE YINSEIK AREA,  
MAGWAY TOWNSHIP, MAGWAY REGION**



**CROSS SECTION ALONG A - B**



**EXPLANATION**

| AGE                              | SYMBOL | FORMATION           | LITHOLOGY                                                                                               |
|----------------------------------|--------|---------------------|---------------------------------------------------------------------------------------------------------|
| PLEISTOCENE                      | Q      | Alluvium            |                                                                                                         |
| EARLY PLEISTOCENE                | Tpi    | Irrawaddy Formation | Light grey-to whitish, massive, friable micaceous sandstone with subordinate massive clay to silty clay |
| ~ ~ ~ ~ ~ Unconformity ~ ~ ~ ~ ~ |        |                     |                                                                                                         |
| MIDDLE MIOCENE                   | Tmo    | Obogon Formation    | Yellowish brown-to buff coloured, fine to medium-grained, thin-bedded sandstone                         |

| GEOGRAPHICAL SYMBOLS |  | GEOLOGICAL SYMBOLS |  |
|----------------------|--|--------------------|--|
| Stream               |  | Dip and Strike     |  |
| Village              |  | Lithologic Contact |  |
| Spot high            |  | Fault              |  |
|                      |  | Fossil locality    |  |
|                      |  | Anticlinal axis    |  |

## Vertebrate Paleontology

Vertebrate fossils from Irrawaddy Formation exposed in Yinseik area have been poorly known although geological survey had been taken place due to its hydrocarbon prospect in this area. Bender (1983) reported the dental remains of *Stegolophodon* from the Irrawaddy Formation. Chavasseau (2009) reported the remains of extinct perissodactyla (Chalicotheriidae) from the Irrawaddian sediments of present area. Jaeger et al., (2011) described the discovery of hominoid (*Khoratpithcus* sp.) and other vertebrate remains from Irrawaddy Formation exposed in Yinseik area.

To date, 13 families and 16 genera of vertebrate fossils have been documented from the Yinseik area (Table 1). However, due to the fragmentary nature of the specimens, it is difficult to indentify some specimens to appropriate genus or species level. Thus, these specimens are referred to genus and species indeterminate (gen et sp. indet.) or conferred genus. The present work carried out the systematic paleontology of crocodile remains recovered from Yinseik area.

The recovered specimens include gnathic materials as well as skeletal materials. The taxonomic assignments to generic/species level are based mainly on the dento-gnathic materials which are the most reliable for taxonomic comparison. All fossil materials used in this work are deposited in University of Magway. Taxonomic system mainly follows those of Carrol (1998) and Mc Kenna and Bell (1997).

**Institutional Abbreviation.** MGW-YSK, Magway University-Yinseik

**Table 1** Vertebrate Fossils from Irrawaddy Formation of Yinseik area, Magway Township (after Jaeger et al., 2011), \* represents the specimens studied in present work

|                                                                                                                                                                                                                                                                                                                                                                                                                                                                                                                                                                                                                         |                                                                                                                                                                                                                                                                                                                                                                                                                            |
|-------------------------------------------------------------------------------------------------------------------------------------------------------------------------------------------------------------------------------------------------------------------------------------------------------------------------------------------------------------------------------------------------------------------------------------------------------------------------------------------------------------------------------------------------------------------------------------------------------------------------|----------------------------------------------------------------------------------------------------------------------------------------------------------------------------------------------------------------------------------------------------------------------------------------------------------------------------------------------------------------------------------------------------------------------------|
| <p><b>PRIMATE</b></p> <p><b>Hominidae</b></p> <p><i>Khoratpithcus ayeyarwadyensis</i></p> <p><b>PROBOSCIDEA</b></p> <p><b>Stegodontidae</b></p> <p><i>Stegolophodon</i> sp.</p> <p><b>ARTIODACTYLA</b></p> <p><b>Suidae</b></p> <p><i>Tetraconodon minor</i></p> <p>cf. Hippopotamodon sivalense</p> <p>Propotamocheorus hysudricus</p> <p><b>Palaeochoeridae</b></p> <p><i>Schizochoerus</i> sp.</p> <p><b>Tragulidae</b></p> <p>Gen. et sp. indet. (medium-sized)</p> <p><b>Bovidae</b></p> <p>Antilopini indet.</p> <p>Gen. et sp. indet.</p> <p><b>Anthracotheriidae</b></p> <p><i>Merycopotamus medioximus</i></p> | <p><b>CARNIVORA</b></p> <p>Gen. et sp. indet.</p> <p><b>PERISSODACTYLA</b></p> <p><b>Rhinocerotidae</b></p> <p>cf. <i>Rhinoceros</i></p> <p><b>Equidae</b></p> <p><i>Hipparion</i> sp.</p> <p><b>Chalicotheriidae</b></p> <p>Gen. et sp. indet.</p> <p><b>CARCHARHINIFORME</b></p> <p><b>Carcharhinidae</b></p> <p><i>Glyphis pagoda</i></p> <p><b>CROCODILIA</b></p> <p><b>Gavialidae</b></p> <p>*<i>Gavialis</i> sp.</p> |
|-------------------------------------------------------------------------------------------------------------------------------------------------------------------------------------------------------------------------------------------------------------------------------------------------------------------------------------------------------------------------------------------------------------------------------------------------------------------------------------------------------------------------------------------------------------------------------------------------------------------------|----------------------------------------------------------------------------------------------------------------------------------------------------------------------------------------------------------------------------------------------------------------------------------------------------------------------------------------------------------------------------------------------------------------------------|

## Systematic Paleontology

Order Crocrodilia Gmelin 1789  
 Superfamily Gavialoidea Hay 1930  
 Family Gavialidae Hay 1930  
 Genus Gavialis Opper 1811  
*Gavialis* sp.

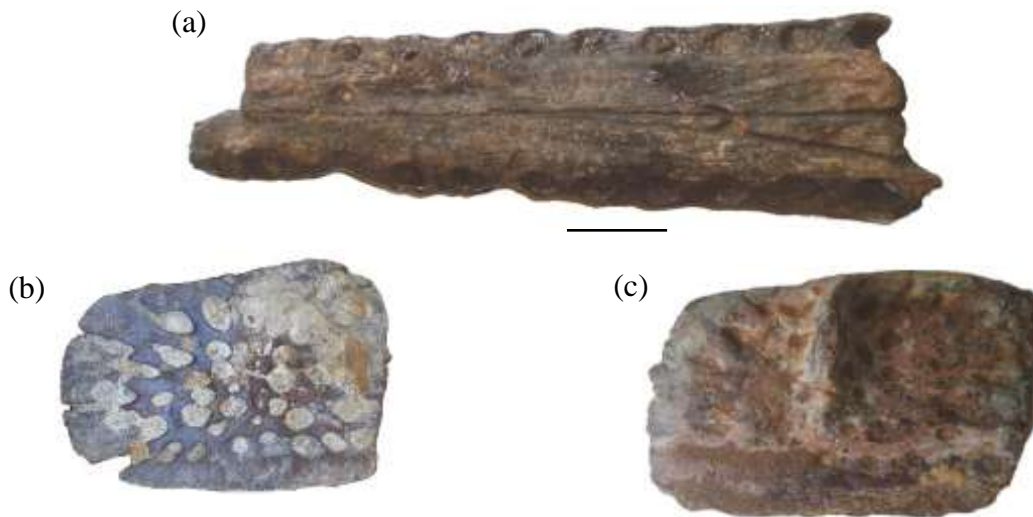


**Figure 6** *Gavialis* sp. (a) MGW-YSK 1, mandibular fragment (b) MGW-YSK 2, bony plate, Osteoderm (c) MGW-YSK 3, bony plate, Osteoderm

**Material:** MGW-YSK 4, mandibular fragment

**Locality:** southwest of Salan Village (20° 07' 30" N, 99° 09' 58" E)

**Horizon and Age:** Lower Irrawaddy Formation, Late Miocene

**Description:** The **mandibles (MGW-YSK 1)** show longitudinal furrows on the ventral surface. The morphology of the dentary reflects that of maxilla in being flat and tubular along most of its length and then spatulate in its anterior portion, comprising the first two alveoli. The anterior most region of the dentary is not preserved. For most of its length, the dentary is perfectly straight. The present fragmentary dentary contains 20 to possibly 22 alveoli, as suggested by the presence of a rugose bony infilling within the last alveolus.

**Osteoderms (MGW-YSK 2 & YSK 3)** are square and the majorities of them are rectangular, being wider than long (Fig 6) and flat to slightly convex. They are relatively thin and bear only a few relatively large pits on their dorsal surface. A short median keel is present on the dorsal surface, which does not spread anteriorly or posteriorly. The edges of these osteoderms are irregular, bearing small spiny outgrowths possibly indicating the presence of a suture. The ventral surface shows striae for epaxial muscle attachments as well as one or two relatively large foramina per osteoderm.

**Comment:** The genus *Gavialis* comprises a single living species, *G. gangeticus* which today is restricted to the riverbanks of Bangladesh, India, Nepal and West Pakistan. The global wild gharial population is estimated at fewer than 235 individuals, which are threatened by loss of riverine habitat, depletion of fish resources, and entanglement in fishing nets. As the population has declined drastically in the past 70 years, this genus is listed as Critically Endangered on the IUCN

Red List. It is characterized by its extremely long, thin jaws, which are regarded as an adaptation to a primarily piscivorous diet (fish eating). The oldest fossil material allegedly referable to this genus has been recovered from the Miocene of Pakistan. *Gavialis* is abundant in continental Pleistocene deposits of the Indo-Pakistani region. The genus was also reported from the Pleistocene of Java, Myanmar and Thailand.

### Paleoecology

From the Yinseik area, remains of the primate (*Khoratpithecus* sp.), carnivores, Anthracothere (*Merycopotamus* sp.), tragulid, wild boar (*Tetraconodon* sp. and *Propotamochoerus* sp.), bovids, rhinoceros (*Rhinoceros* sp.), horse (*Hipparion* sp.), elephant (*Stegolophodon* sp.) and crocodile (*Gavialis* sp.) occur in the sediments of Irrawaddy Formation. Among these animals, *Khoratpithecus* is a close relative of extant ape, Orangutan, and is as an arboreal whereas carnivores, tragulids, anthracotheres, wild boar, bovids, rhinoceros and elephant are terrestrial mammals. The tragulids, wild boars, rhinoceroses and elephants might have been the habitants of forest/woodland as their living counterparts whereas the bovids might have roamed in the open grass land or on rolling hills as cattle of the present day.

The anthracotheres have long been considered to have habits and habitats similar with hippopotamus (Kron and Manning, 1998) and are likely to be a dependent of riverine environment. The crocodile might have preferred in the swamps or in the streams/rivers as present day's crocodiles do. The abundance of forest/woodland adapted animals in Yinseik area indicates the dominance of forested condition rather than grassland for these animals. Thus, these animals probably lived in the forest/woodland associated with riverine environment. The evidence for forested habitats in the present area by the early Late Miocene is further reinforced by the stable isotope analyses on extinct horse (*Hipparion*) teeth from the Yinseik area. These specimens yielded highly depleted  $\delta^{18}\text{O}$  and  $\delta^{13}\text{C}$  values suggesting the existence of closed and humid habitat in present area (Jaeger et al., 2010).

Present day environmental conditions in Central Myanmar are characterized by a subtropical semi-arid climate especially in most parts of Mandalay and Magway Region. The vegetation of this region is dominated by open shrub lands and grasslands. Therefore, the occurrence of forest dwelling mammals in research area contributes to the implication that the Late Miocene paleoenvironment of the Yinseik area was drastically different from the present day's conditions in Central Myanmar.

### Acknowledgement

The authors would like to express his gratitude towards Professor Dr. Phoe Kaung, Rector of University of Yangon for permission to carry out this research work.

The writers would also like to thank to Professor Dr. Day Wa Aung, Head of Geology Department, University of Yangon for his valuable guidance and great encouragement through the doing of the research.

### References

- Aung Khin and Kyaw Win, (1969). Geology and hydrocarbon prospects of the Burma Tertiary Geosyncline, Union of Burma. *Journal of Science and Technology*, 2 (1), 52-73.
- Bender, F., (1983); *Geology of Burma*: Gerbruder Borntrae Borntraeger, Berlin Stuttgart, 293 p.
- Chhibber, H.L., (1934); *Geology of Burma*, London, MacMillan, 538 p.
- Carroll, R.L., (1988). *Vertebrate Paleontology and Evolution*. Freeman, New York. pp. 1-698.

- Lepper, G.W., (1933). Geology of the oil-bearing regions of the Chindwin-Irrawaddy valley of Burma and Assam-Arakan: *Proc. World Petroleum Congress, vol.1.*
- Maung Thein, (1973). A preliminary Synthesis of the geological evolution of Burma with reference to the tectonic development of Southeast Asia. *Geological Society of Malaysia, Bulletin*, **6**, 87–116.
- Noetling, F. (1885) The development and subdivision of the Tertiary System in Burma. *Record of Geological Survey of India* 28, p. 59-86.
- Nyein Chan, (2011). Geological Structure of Myingun- Than Bo Area, Magway Township, Unpublished MSc Thesis, Magway University.
- Pascoe, E. H., (1912). The Oil field of Burma. *Mem. Geological Survey of India*, v.1, pt.1.p. 101-123.
- Ridd, M. F. and Racey, A. (2015). Onshore petroleum geology of Myanmar: Central Burma Depression. *Petroleum Geology of Myanmar*. Geological Society, London, *Memoirs*, 45, 21–50.
- Shimada, K., Egi, N., Tsubamoto, T., Maung Maung, Thaung Htike, Zin Maung Maung Thein, Nishioka, Y., Sonoda, T., Takai, M. (2016). The extinct river shark *Glyphis pagoda* from the Miocene of Myanmar and a review of the fossil record of the genus *Glyphis* (Carcharhiniformes: Carcharhinidae). *Zootaxa* 4161 (2): 237–251
- Stamp, L.D. (1922). An outline of Tertiary Geology of Burma. *Geological Magazine*, **59**, 481–501.
- Theobald, W., (1873.)The Geology of Pegu. *Memoir of Geological Survey of India*, 10.P. 198-359.
- Tucker., M.E. (2003). *Sedimentary Rocks in the Field*. John Wiley & Sons Ltd., West Sussex, 234 pp.

# **A STUDY ON EVOLUTION OF POROSITY IN SANDSTONE RESERVOIRS OF OKHMINTAUNG FORMATION BETWEEN NGAPE AND YENAMA AREA, MAGWAY REGION**

Naw Chel Phaw<sup>1</sup>, Day Wa Aung<sup>2</sup>, Tun Naing Zaw<sup>3</sup>

## **Abstract**

The area under investigation lies in Ngape Township, western part of Minbu, Magway Region. In the study area, the Cretaceous to Pliocene Formations are exposed. The main structure of the study area is monocline. The present research aimed to conduct reservoir potential of Okhmintaung Formation. Stratigraphically, the Okhmintaung Formation (Late Oligocene) is mainly made up of thin- to medium-bedded sandstone with bluish gray shale. Petrographically, the sandstone of Okhmintaung Formation is arkose and lithic arkose. By the facies analysis, in Okhmintaung Formation, from top to bottom, Thick- bedded to massive sandstone facies, sand with gypsum intercalation facies, bioturbated sandstone facies, nodular gray shale facies, and sand-shale alternation facies were observed. By the petrographic texture, porosity, and diagenetic features enhancing or destroying the potential porosity of the sand body are also started in Okhmintaung Formation. Some of the sand bodies do not favor the potential of good reservoir because of the size, textural features and diagenetic imprints. Some of the reservoir cannot regard as medium potential due to the petrographic fabric forming lesser potential. By studying the diagenetic features, some of the Okhmintaung sandstone possesses pore-filling clays and very thin grain coating. These authigenesis can destroy reservoir potential and cannot regard as medium potential due to the petrographic fabric forming lesser potential. The textural features suggest that Okhmintaung sandstones are fair reservoir.

**Keywords:** Porosity, Permeability, reservoir potential, authigenic mineral.

## **Introduction**

The area is located between latitudes 19°46'00"N to 20°04'00" N, and longitudes 94°25'00" E to 94°40'00" E, covering approximately 9.3 miles (15km) in width and 24.8 miles (40 km) in length. It is situated in the western flank of Salin syncline and also situated between Padan to the south and Yenamma to the north, Figure (1). There are two major streams which generally flow from west to east and locally named Mann Chaung in the northern part and Sabwet Chaung in the southern part. These streams flow into the Ayeyarwaddy River. Generally, pattern of the main streams and its tributaries are mainly developed parallel to the regional strike, and tectonic structure such as faults and fractures. The topography of the eastern region is characterized by flat lying and the mountainous rugged terrains in the western margin, trending NNW-SSE direction.

---

<sup>1</sup> Lecturer, Department of Geology, Bago University

<sup>2</sup> Professor and Head , Department of Geology, University of Yangon

<sup>3</sup> Associate Professor, Department of Geology, University of Yangon

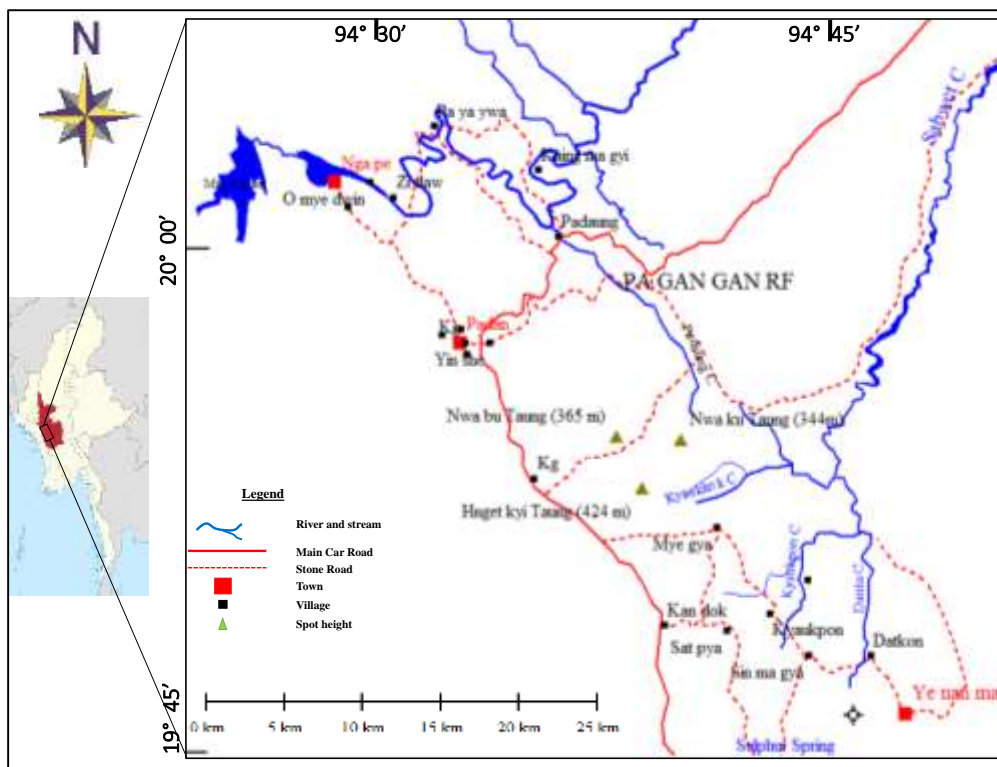


**Figure 1** Location map of the study area

### Regional Geologic Setting

The study area consists of the following formations and the lithostratigraphic correlation. This research mainly focused on the Oligocene Formations such as Shwezettaw Formation, Padaung Formation, and Okhmintaung Formation.

The general structural trends of the study area is NNW-SSE in direction. Attitude of the rock unit of the Shwezettaw Formation is about (45°) with NE dipping. The rock unit of Padaung Formation is about (30°) attitude and (45°) direction. The attitude of the rock unit of Okhmintaung Formation is average in (30°/050°). All of the beds of formations are nearly NE in directions.

Major fold is a broad monoclinial syncline. Present study area is the western part of Salin Syncline. In the western part of the study area, steep dips towards the east in dip amount of 45° to 60°. In the eastern part of the study area, become gradually shallow to the east towards the Minbu syncline, 20° to 15°. In the southern part of the study area, dip amount of the monocline gradually decrease from 30° to 10°. Monocline is cut-cross by a series of E-W trending cross faults, more abundant in distribution and longer in length to the south of the study area.

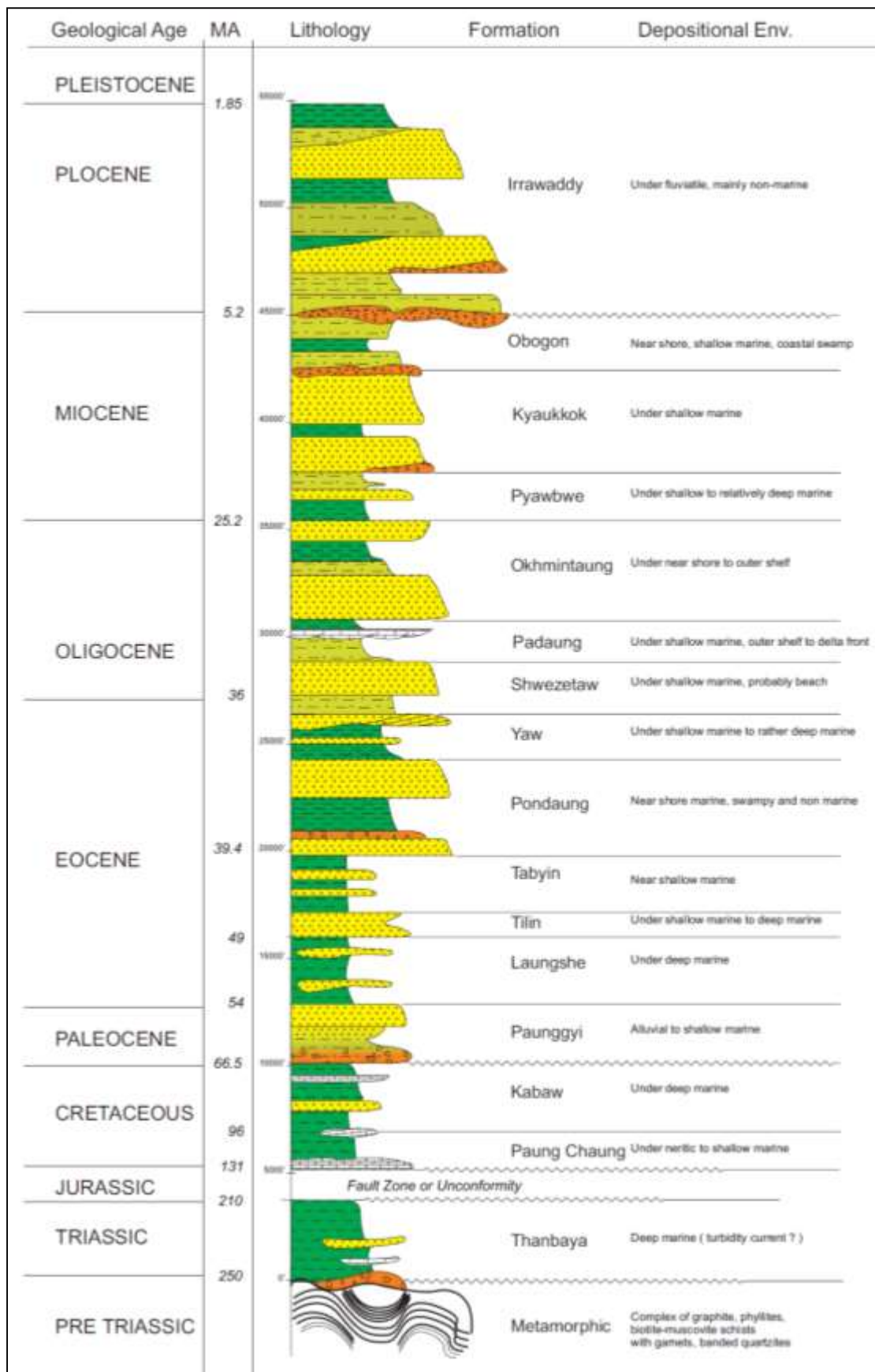
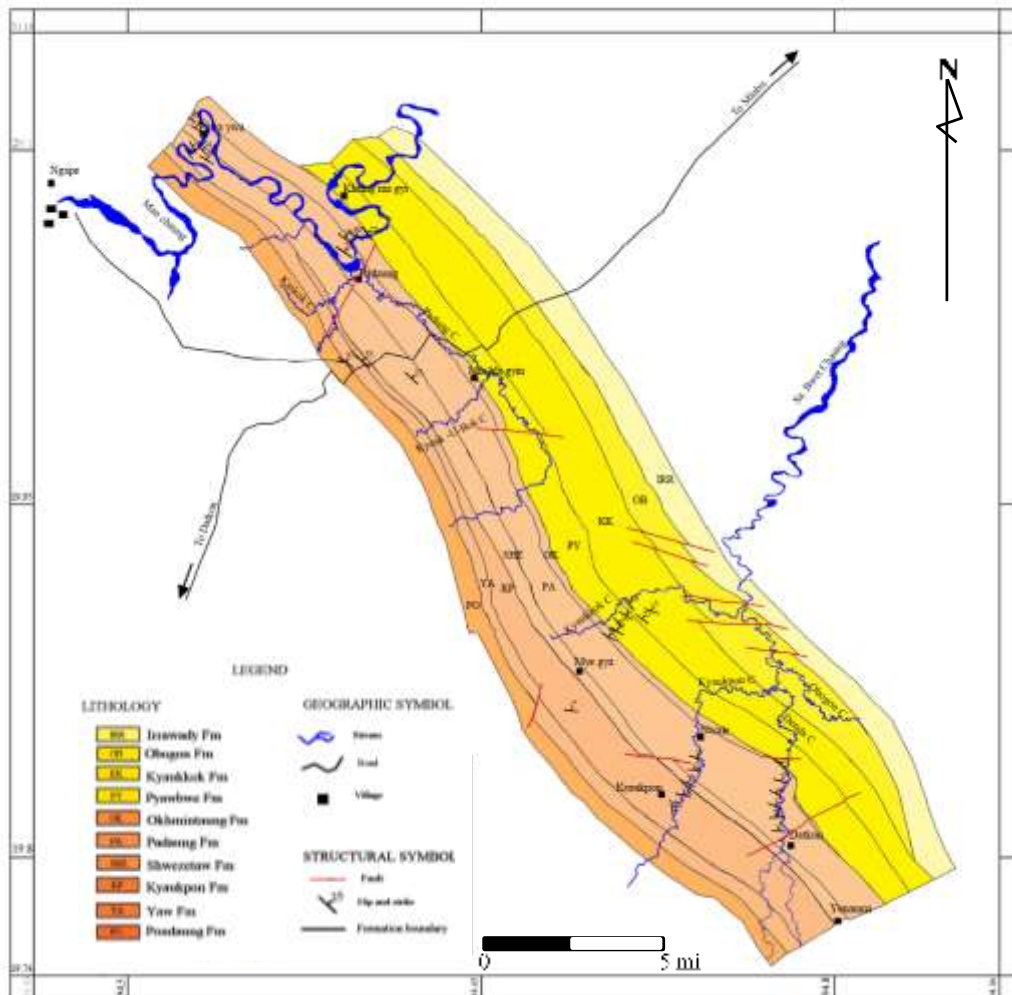


Figure 2 Regional stratigraphic succession of the Minbu Basin (Than Htut, 2008)



**Figure 3** Geological map of the study area (Based on M.O.C, 1982)

### **Effect of Texture on Sandstone Reservoir of Okhmintaung Formation**

#### **Relationship between porosity, permeability, and grain shape**

The grain shape of Okhmintaung sandstones are angular to sub-angular with sub sphericity. Figure (4). Fraser (1935) inferred that porosity might decrease with sphericity because spherical grains may be more tightly packed than subspherical ones.

#### **Relationship between porosity, permeability, and grain size**

Okhmintaung sandstones mainly comprise average on 60% to 80% of detrital grains, and 20% to 30% of cement. The minimum grain sizes are ranging from (0.08 mm to 0.12mm) and the maximum grain sizes are (0.16mm to 0.38mm) in diameter. Therefore the general grain sizes of the Okhmintaung sandstones are very fine- to medium-grained. Figure (5).

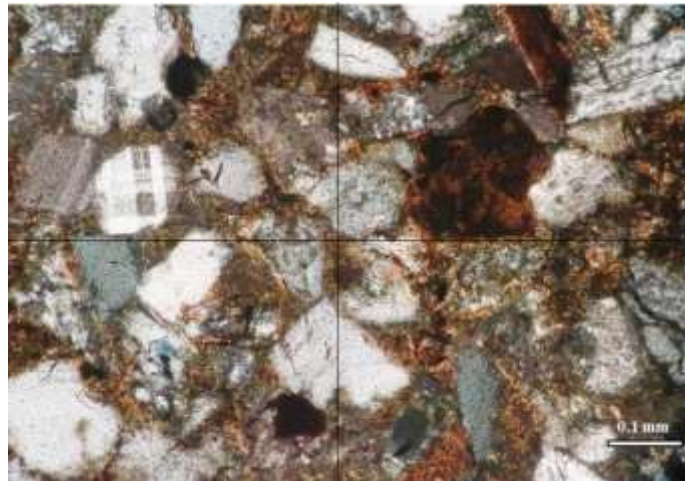


**Figure 4** Photomicrograph showing sub-angular to sub-rounded with high sphericity of Padaung sandstone (Between X.N)

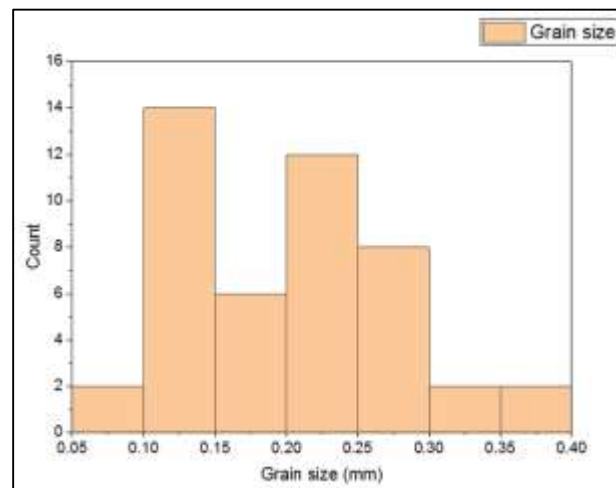


**Figure 5** Average grain size of Okhminatung sandstones

**Relationship between porosity, permeability, and grain sorting**

According to the result of the petrographic study, the grains of the Okhmintaung sandstones are moderate to well sorted by comparing with the effects of sorting and grain size on porosity and permeability (After Beard and Wely, 1973, Nagtegaal, 1978, and Simpson, 1995). Therefore, the porosity of the Okhmintaung sandstones may be fair to good. Figure (6). The average porosity and permeability of Okhmintaung sandstones are shown in figure (7).

**Relationship between porosity, permeability, and grain packing**

According to the result of the petrographic study, the grain packing of Okhmintaung sandstones is loose packing (cubic packing). It means that the porosity of the sandstone may be good. Figure (8).

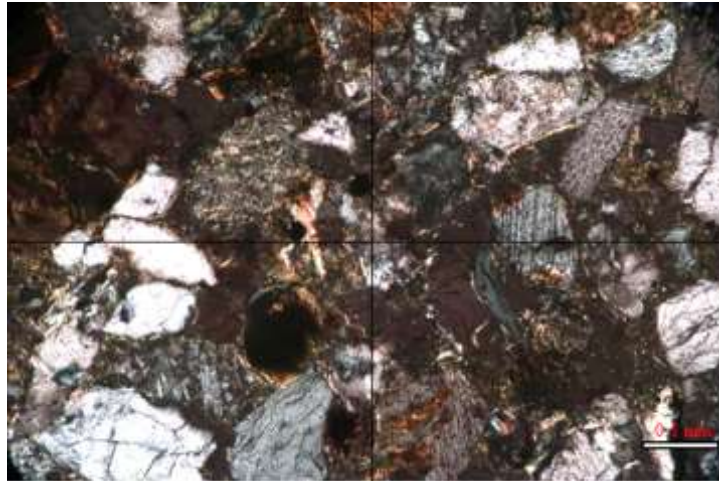


**Figure 6** Photomicrograph showing moderate to well sorted sandstone of Okhminatung Formation

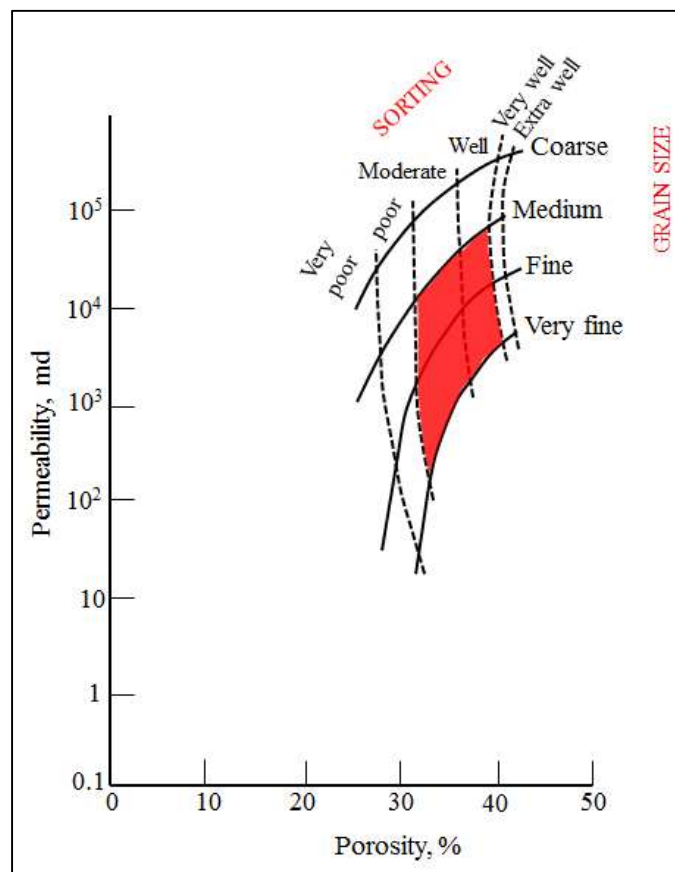


**Figure 7** Graph of porosity against permeability of Okhmintaung Formation showing their relationship with grain size and sorting for uncemented sands. (After Beard and Weyl, 1973; Nagtegaal, 1978)

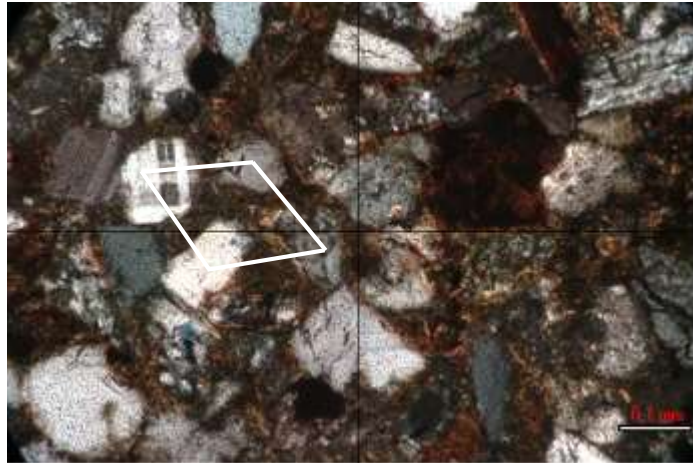


**Figure 8** Photomicrograph showing the tight packing (rhombohedral packing) of Padaung sandstone

**Effects of diagenesis on sandstone reservoirs of Okhmintaung Formation**

The effects of diagenesis on sandstone reservoirs include the destruction of porosity by compaction and cementation, and the enhancement of porosity by solution.

**Porosity loss by cementation of Okhmintaung Formation**

Calcite is one of the most common cement in the sandstones of Okhmintaung Formation. It generally occurs as calcite crystals, which, as they grow from pore to pore, may form a poikilitic fabric of crystals enclosing many sand grains. Grain boundaries are corroded, suggesting that some replacement has occurred. Calcite also occur infilling pores and microfractures.

Pore linings are occurred by clay coating deposited on the surface of detrital grains and the absence at points of grain to grain contact. The individual clay particle or aggregates commonly exhibit a preferred orientation normal to or parallel to the detrital grain surface (Wilson and Pittman, 1977).

According to the study of cementation in the Okhmintaung sandstone, minor pore-filling cements include chlorite and pyrite. Some feldspar grains are partially replaced by illite. Therefore, the Okhmintaung sandstones may have fair porosity but with anomalously may low permeability. Because of clay floccules have migrated to pore throats and then been cemented by pore-lining diagenetic chlorite and illite.

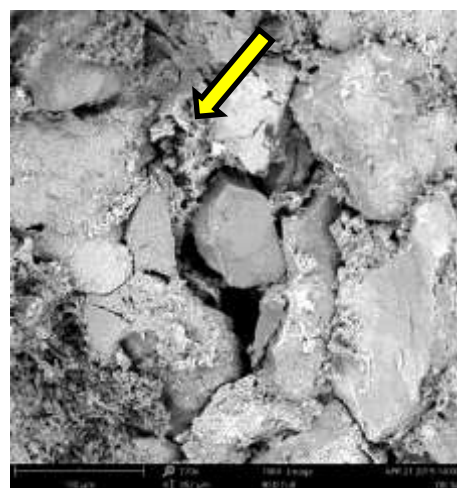


**Figure 9** SEM image showing the kaolinite clay mineral fill the pore spaces (K)

**Figure 10** SEM image showing the grains are coated by early clay mineral (arrow)

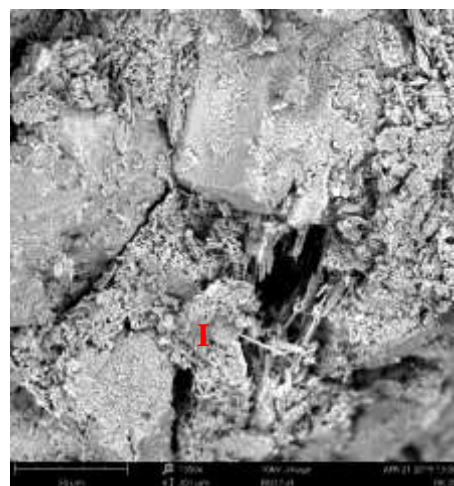
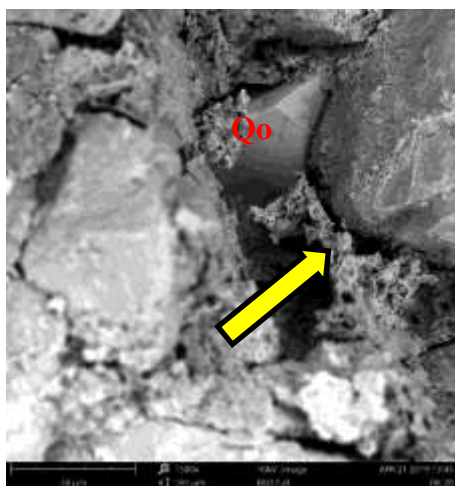


**Figure 11** SEM image showing clay mineral occurs as a selective grain-replacive mineral and is also attached to grain surfaces and fill the pore, and quartz grain has the secondary overgrowth (Qo).

**Figure 12** SEM image showing the clay mineral illite (I) fill the pore space

**Porosity and Permeability Analysis by Digital Image Analysis (DIA) of Okhmintaung Formation**

**Massive sandstone body (total 15 m thick)**

The pore spaces of massive sandstone body are represented mainly by intergranular porosity, intragranular porosity, and connected porosity. The pore quality is controlled by the effects of compaction, and relative amounts or cements and matrix. Figure (13), and (14). The values of porosity and permeability by DIA method is shown in table (1).

**Table 1 Porosity and permeability value of massive sandstone, OK20 by the DIA method**

| No   | Pore Diametre (µm) | Interconnected Porosity (%) | Total Porosity (%) | Permeability (µm <sup>2</sup> ) | Permeability (md) |
|------|--------------------|-----------------------------|--------------------|---------------------------------|-------------------|
| OK20 | 40.90822387        | 3.217                       | 19.001             | 1.68237316                      | 1.70E+02          |

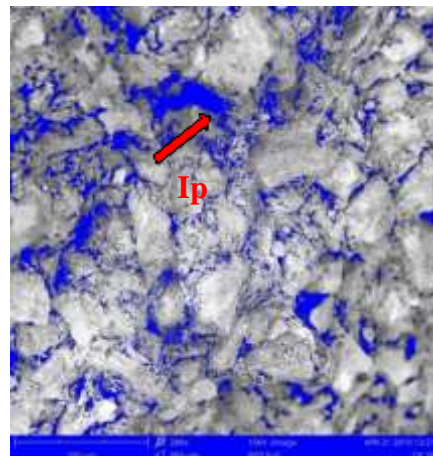
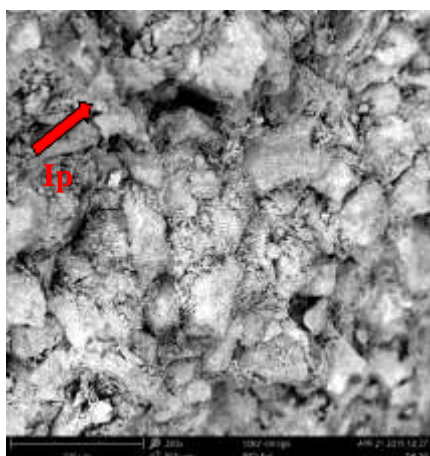


**Figure 13** SEM image showing intergranular pore space (Ip) before image analysis

**Figure 14** SEM image showing intergranular pore space (Ip) after image analysis

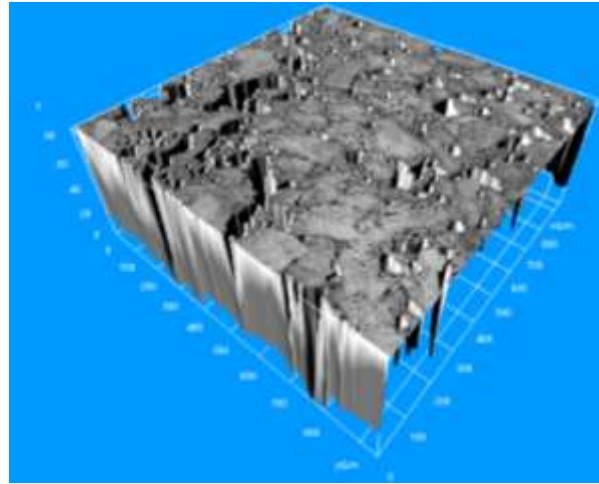


**Figure 15** 3D image showing the pore network structure of massive sandstone, OK20 to calculate the permeability

**Thick-bedded to massive sandstone body (about 20 m thick)**

The pore spaces of thick-bedded to massive sandstone body are represented mainly by intergranular porosity, intragranular porosity, and connected porosity. In the case of this study, the former unstable grains have dissolved at a late diagenetic stage creating secondary pores. The pore quality is controlled by the effects of compaction, and relative amounts or cements and matrix. Figure (16), and figure (17). The values of porosity and permeability by DIA method is shown in table (2).

**Table 2** Porosity and permeability value of thick-bedded to massive sandstone, OK21 by the DIA method

| No   | Pore Diametre (µm) | Interconnected Porosity (%) | Total Porosity (%) | Permeability (µm <sup>2</sup> ) | Permeability (md) |
|------|--------------------|-----------------------------|--------------------|---------------------------------|-------------------|
| OK21 | 35.601877          | 8.34                        | 21.824             | 3.30340532                      | 3.35E+03          |

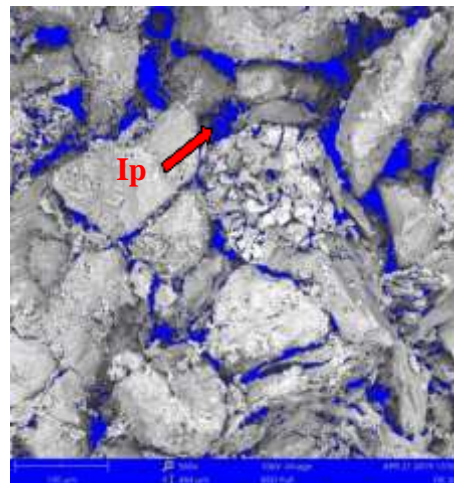
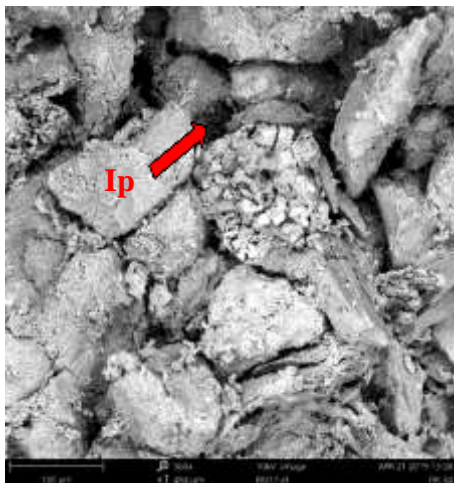


**Figure 16** SEM image showing intergranular pore space (Ip) before image analysis

**Figure 17** SEM image showing intergranular pore space (Ip) after image analysis

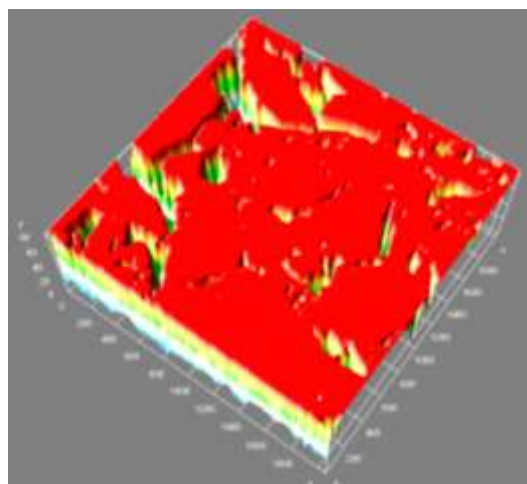


**Figure 18** 3D image showing the pore network structure of thick-bedded to massive sandstone, OK21 to calculate the permeability

### Porosity and permeability of Okhmintaung Formation

**Table 3** Summary of porosity and permeability of Oligocene strata

| No    | Pore Diametre (μm) | Interconnected Porosity (%) | Total Porosity (%) | Permeability (μm <sup>2</sup> ) | Permeability (md) |
|-------|--------------------|-----------------------------|--------------------|---------------------------------|-------------------|
| OK21  | 35.601877          | 8.34                        | 21.824             | 3.303405315                     | 3.35E+03          |
| OK20  | 40.90822387        | 3.217                       | 19.001             | 1.682373158                     | 1.70E+02          |
| PD19A | 48.3184411         | 3.252                       | 13.371             | 2.372610166                     | 2.40E+03          |
| PD19  | 18.93317673        | 3.45                        | 17.791             | 0.386470273                     | 3.92E+02          |
| PD18  | 51.77055799        | 3.953                       | 15.517             | 3.310873043                     | 3.35E+03          |
| SZT16 | 11.19279206        | 6.79                        | 13.212             | 0.265825517                     | 2.69E+02          |
| SZT15 | 134.9259999        | 9.565                       | 26.307             | 54.41595887                     | 5.51E+04          |
| SZT12 | 55.21516738        | 10.953                      | 30.571             | 10.43517882                     | 1.06E+04          |
| SZT6  | 92.34526735        | 13.747                      | 33.849             | 36.63424456                     | 3.71E+04          |

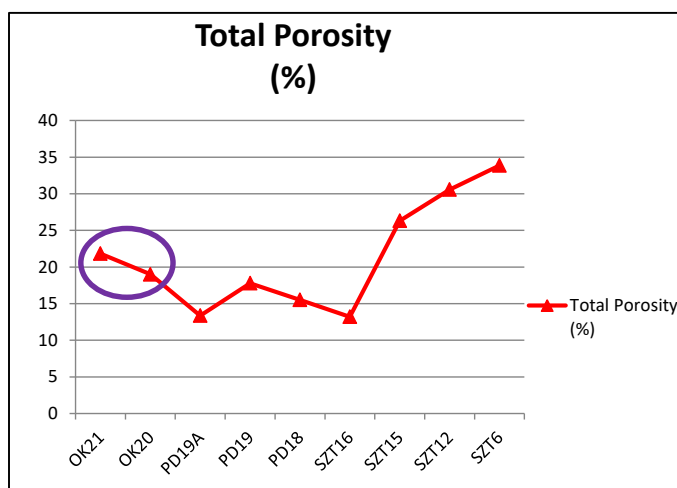


**Figure 19** Showing the total porosity of sandstone from the Oligocene strata

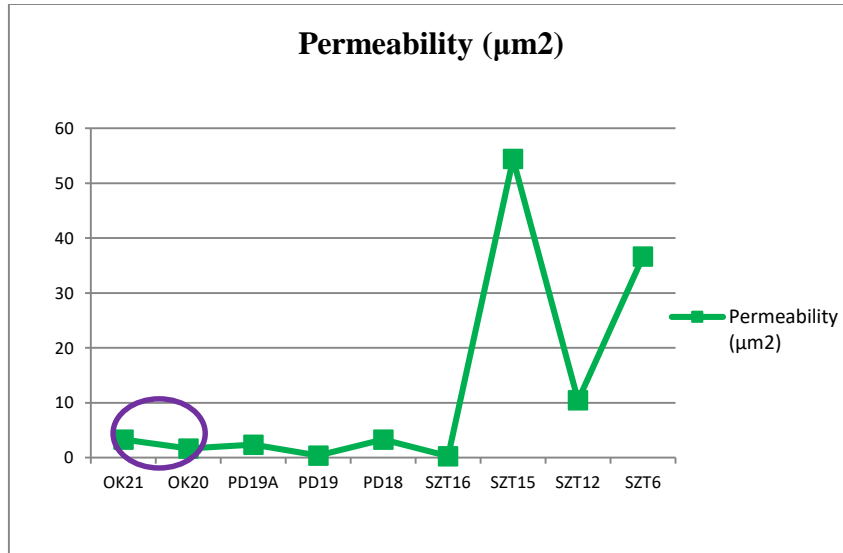


**Figure 20** Showing the permeability of sandstone from the Oligocene strata

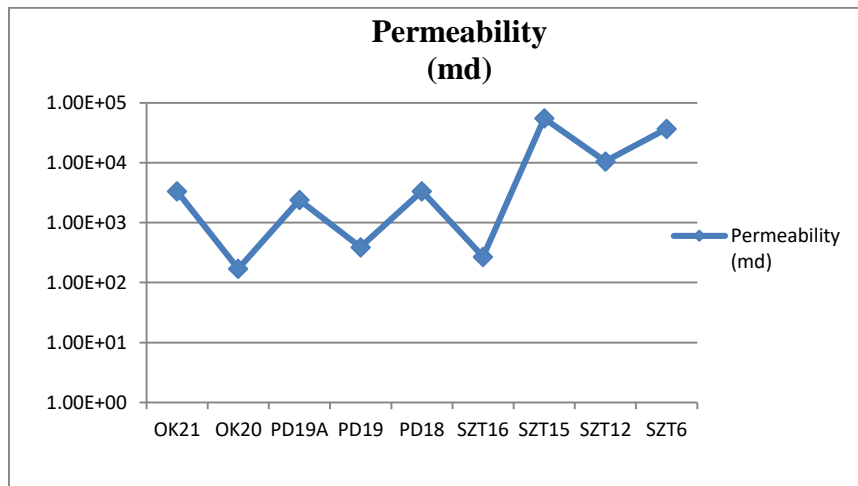


**Figure 21** Showing the permeability of sandstone from the Oligocene strata

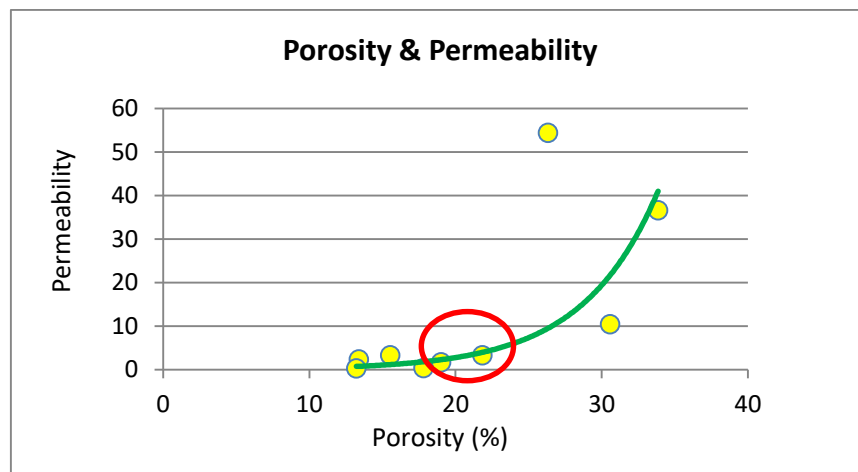


**Figure 22** Relationship between porosity and permeability of sandstone from the Oligocene strata

## Summary and Conclusions

By the petrographic texture, porosity, and diagenetic features enhancing or destroying the potential porosity of the sand body are also started. Some of the sand bodies do not favor the potential of good reservoir because of the size, textural features and diagenetic imprints. Some of the reservoir cannot be regarded as medium potential due to the petrographic fabric forming lesser potential.

By studying the diagenetic features, some of the Okhmintaung sandstone possesses pore-filling clays and very thin grain coating. These authigenesis can destroy reservoir potential and cannot be regarded as medium potential due to the petrographic fabric forming lesser potential. The textural features suggest that Okhmintaung sandstones are fair reservoir.

## Acknowledgements

The authors are greatly indebted to Dr Aye Aye Tun (Rector, Bago University) for her kind permission to undertake this research and we would like to express our gratitude to Dr Khin Maung Hla, Professor and Head of Department of Geology, Bago University for the permission to study the present research area. We are also deeply grateful to U Than Htut, Chief Research Officer (Retd.), Myanmar Oil and Gas Enterprise, for his kind help, give valuable advice and discussion.

## References

- Atkins, J.E., and McBride, E.F., (1992). Porosity and packing of Holocene river, dune, and beach sands: American Association of Petroleum Geologists Bulletin. V. 76. P. 339-355.
- Beard D.C., and Weyl P.K., (1973). Influence of texture on porosity and permeability in unconsolidated sand. AAPG Bull 57:349-369.
- Bender, F., (1983), *Geology of Burma*: Gebruder Borntraeger, Berlin-Stuttgart, Stuttgart, Germany, 293 pp.
- Chilingar, G.V., (1964). Relationship between porosity, permeability and grain size distribution of sands and sandstones. In: Van Straaten, L.M.J.U. (Ed), *Deltaic and Shallow Marine Deposits*. Elsevier, Amsterdam, pp. 71-75.
- Datta, D., et al., (2016). Determination of porosity of rock samples from photomicrographs using image. 2016 IEEE 6th International Conference on Advanced Computing, p. 320-325.
- Bentz, D. P., and Martys, N. S., (2007). A Stokes Permeability Solver for Three-Dimensional Porous Media, NISTIR 7416, p.1-117.
- Debabrata, D., and Sharmila, S., (2016). Determination of Porosity of Rock Samples from Photomicrographs Using Image Analysis, (2016) IEEE 6th International Conference on Advanced Computing (IACC).
- Edgar Berrezueta, E., et al., (2015). Pore network quantification of sandstones under experimental CO<sub>2</sub> injection using image analysis. *computers & Geosciences* 77 (2015) 97–110.
- Fraser, H.J., and Gratton, L.C., (1935). Systematic packing of spheres with particular relations to porosity and permeability. *J Geol* 1935; November-December: 785-909.
- Wilson, M. D., and Pittman, E. D., (1977) Authigenic clays in sandstones: Recognition and influence on reservoir properties and paleoenvironmental analysis, *Jornal of sedimentary petrology*, Vol. 47, No.1, P.3-31.

## **PETROLOGICAL STUDY OF METAMORPHIC ROCKS EXPOSED IN CHAUNGZON AREA, CHAUNGZON TOWNSHIP, MON STATE**

Tint Tint Tun<sup>1</sup>, Khin Maung Hla<sup>2</sup>, Mya Moe Khaing<sup>3</sup>,  
Hlaing Myo Nwe<sup>4</sup>, Min Han Nyein<sup>5</sup>

### **Abstract**

The study area occupies the Chaungzon Township, Mon State. It is situated between Latitude 16° 15' 00" to 16° 30' 00" N and Longitude 97° 30' 00" to 97° 35' 00" E, one-inch topographic map No.94H/11. It covers approximately 6.56 km<sup>2</sup>. It is located in the western part of Shan-Tanintharyi block. The area was composed of low to medium grade metamorphic rocks which were intruded by igneous rocks. The metamorphic rocks are garnet-biotite gneiss, graphite-sillimanite-mica schist and calc-silicate rock, quartz-sericite schist and quartzite, banded quartzite and mica schist, micaceous quartzite and quartzite and slate, phyllite and quartzite interbedded. Slaty, phyllitic, schistose, gneissose and granoblastic texture are observed in the area. Mineralogical and textural features indicate that all metamorphic rocks had undergone regional and contact metamorphisms. In general, the grade of metamorphism increases from east to west. On the basis of the mineral assemblages, the metamorphic rocks are greenschist facies, amphibolite facies and hornblende hornfels facies. The relative age of metamorphic rocks was probably Post Carboniferous.

**Keywords:** regional and contact metamorphism, greenschist facies, amphibolite facies, hornblende hornfels facies and Post Carboniferous

### **Introduction**

#### **Location and Size**

The study area situated Chaungzon area, Chaungzon Township, Mon State. It is bounded by Latitude 16 ° 17' 00" – 16° 23' 30" N and Longitude 97 ° 30' 00" – 97 ° 34' 00" E, and vertical grid 08 to 16 and horizontal grid 74 to 96 in one-inch topographic map index of 94 H/11 (Figure 1). This area is about 10.4 km long in north-south direction and 6.4 km wide in east-west direction. It covers about 66.56 km<sup>2</sup>.

#### **Methods of Study**

Rock samples from each rock unit were collected at all locations where the lithology of rock units changed. Under the microscope, 50 thin sections of different rock units were examined to interpret petrography and petrogenesis of rock units.

#### **Purposes of study**

The purposes of this study area are as follows:

1. To describe detailed geological map of the area
2. To study the petrography of the rock units
3. To interpret types of metamorphism and petrogenesis of rock units

---

<sup>1</sup> Assistant Lecturer, Department of Geology, Bago University, tintintun26@gmail.com.

<sup>2</sup> Dr, Professor and Head, Department of Geology, Bago University, drkhinmghla23@gmail.com.

<sup>3</sup> Dr, Associate Professor, Department of Geology, Bago University, myamoekhainggeol@gmail.com.

<sup>4</sup> Dr, Associate Professor, Department of Geology, Bago University, hmyonwe@gmail.com.

<sup>5</sup> Assistant Lecturer, Department of Geology, Bago University, minhannyein817@gmail.com.

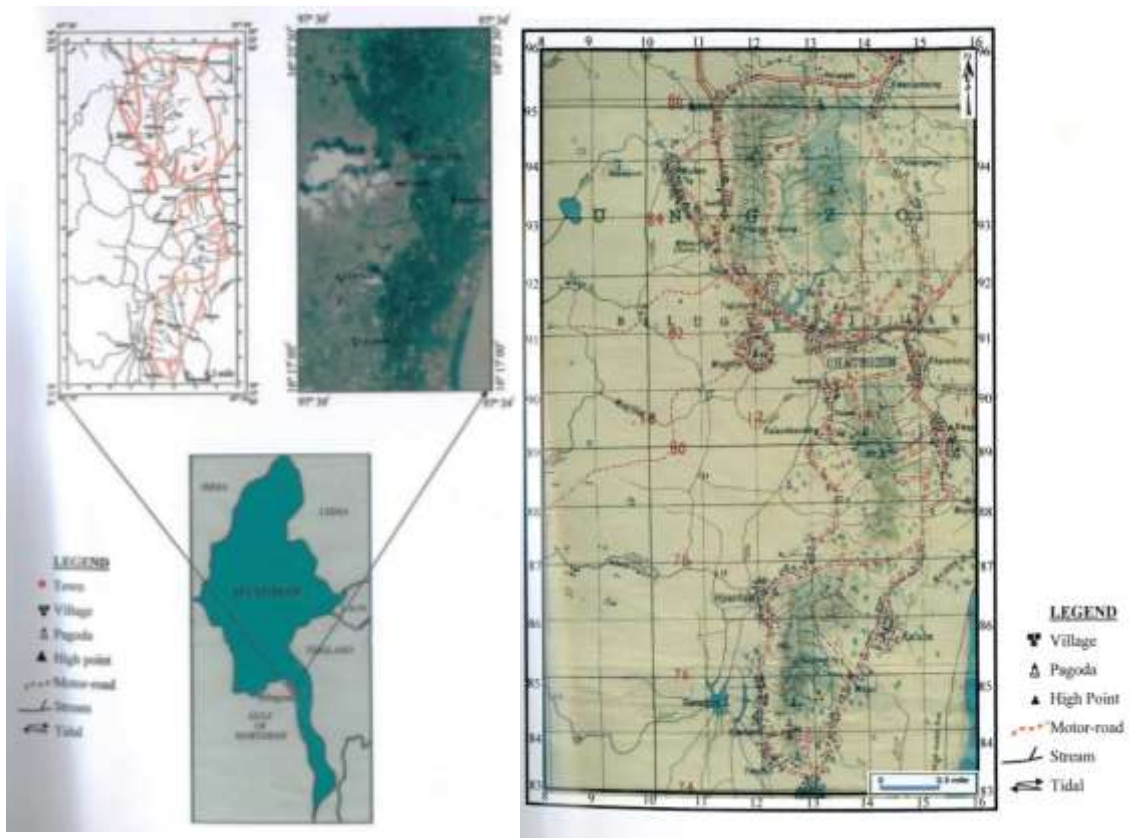


**Figure 1** Location and Topographic maps of the study area

### Rock Sequence

The rock sequence of the area has six major metamorphic rocks, (Table 1). Most of the rock units exposed along the stream sections, ranges, at the hills and foot-paths. These rocks are mapped in the geological map (Figure 2).

**Table (1) Rock sequence of the study area**

Alluvium -Holocene

Laterite and lateritic soil

-Pleistocene

#### Metamorphic Rocks

- (6) Slate, phyllite and quartzite interbedded
- (5) Micaceous quartzite and quartzite
- (4) Banded quartzite and mica schist
- (3) Quartz-sericite schist and quartzite
- (2) Graphite-sillimanite-mica schist and calc-silicate rock
- (1) Garnet-biotite gneiss

Probably  
Silurian to  
Carboniferous

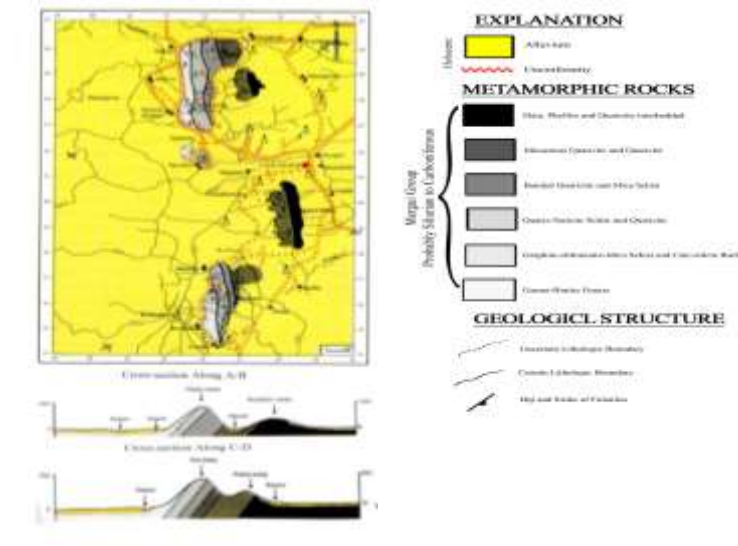


**Figure 2** Geological map of the study area

**Petrography of Metamorphic rocks**

The area is mainly composed of metamorphic rocks. Metamorphic rocks are divided into six units. The classification is mainly based on textural structural criteria and laboratory work including petrographic analysis for precise determination of mineral assemblages.

**(1) Garnet-biotite gneiss**

**Megascopic Nature**

Garnet-biotite gneiss exposed at the western part of Nat taung, especially Kadon village (Loc. 116764) (Figure 3). This rock is well foliated, hard and compact. It shows medium to coarse-grained and gneissose texture. Both banded and augen textures are observed in the outcrop.

**Microscopic Nature**

These rocks show gneissose, banded texture under the microscope. It is mainly composed of quartz, orthoclase, biotite and minute flakes of muscovite and almandine. Orthoclase is subhedral form. Inclusions of small quartz, biotite and apatite are present in orthoclase (Figure 4). String perthites are found in this rock (Figure 5). Microcline occurs as porphyroblasts which are cloudy and grey in color (Figure 6) and almandine garnet (Figure 7 and 8).



**Figure 3** West dipping outcrop nature of garnet-biotite gneiss at the gneiss quarry in Kadon village (Loc. 116764)

**Figure 4** Inclusions of small quartz, biotite and apatite in orthoclase of garnet-biotite gneiss (Loc. 116764, between X.N)

**Figure 5** String perthite in garnet-biotite gneiss (Loc. 116764, between X.N)

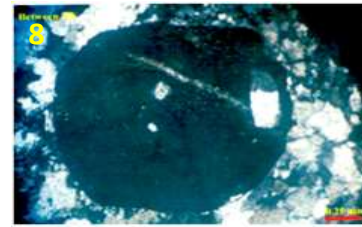
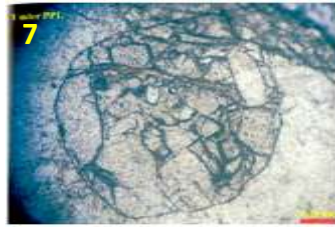
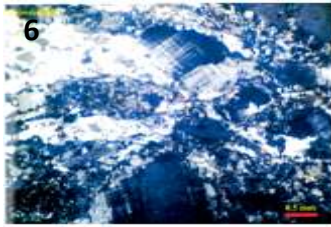


**Figure 6** Microcline with cross-hatched twinning in garnet-biotite gneiss (Loc. 116764, between X.N)

**Figure 7** Subhedral almandine garnet in garnet-biotite gneiss (Loc. 129753, under PPL)

**Figure 8** Almandine garnet crystal in garnet-biotite gneiss (Loc. 129753, between X.N)

## (2) Graphite-sillimanite-mica schist and calc-silicate rock

### Megascopic Nature

Graphite-sillimanite-mica schist occurred along the Nat taung and Gin Eit Monastery (Loc. 124749) (Figure 9). Calc-silicate rock exposed at the stream sections of Nat taung (Loc. 125761). Ridges and furrows are occurred in this rock (Figure 10).



**Figure 9** Outcrop nature of graphite-sillimanite-mica schist, Gin Eit Monastery (Loc. 124749)

**Figure 10** Ridge and furrow features of calc-silicate rock along the stream sections near the Nat taung (Loc. 125761)

### Microscopic Nature

Graphite-sillimanite-mica schist is medium to coarse-grained and schistose texture. The chief minerals are biotite, muscovite, graphite, sillimanite and tourmaline. Mica appears as elongated alignment of flaky minerals (Figure 11). Sillimanites are found as pale yellow color, acicular form and fibrous form. Calc-silicate rock shows medium-grained, granoblastic texture. Diopside and tremolite minerals occur as in this rock (Figure 12). Basal section of diopside show distinct pyroxene cleavage under the microscope.

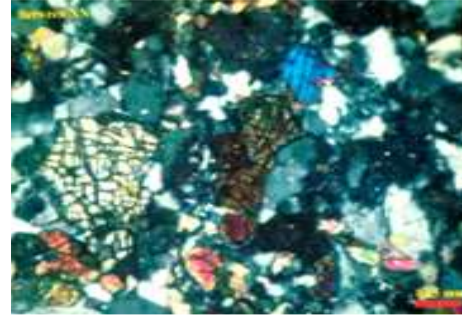


**Figure 11** Muscovite (Mus), tourmaline (Tur) and accicular sillimanite (Sil) in graphite-sillimanite-mica schist (Loc. 124749, between X.N)

**Figure 12** Anhedral basal section of diopside (Di) and subhedral tremolite (Tr) in calc-silicate rock (Loc. 125761, between X.N)

**(3) Quartz-sericite schist and quartzite**

**Megascopic Nature**

The exposures of quartz-sericite schist are found near the Paingkada village (Loc. 121863), Thetke taung (Loc. 116835) and at the middle part of Nat taung (Loc. 126760) (Figure 13). Light grey color on fresh surfaces and yellowish color on weathered surfaces. Quartzite is alternately occurred within quartz-sericite schist. It is found as massive exposures but in some places it occurs as thick bedded and highly jointed nature (Loc. 125761). It is whitish grey color on fresh surfaces and grey color on weathered surfaces (Figure 14).

**Microscopic Nature**

Quartz-sericite schist is mainly composed of quartz, sericite and mica under the microscope. Some muscovite flakes and sericite streaks are showing parallel alignment along the foliation planes. Some muscovite is altered to sericite (Figure 15). Quartzite is fine to medium-grained and mainly composed of granular quartz grains. Quartz shows anhedral grains, flattened grain boundaries and suture contact. Muscovite patches are observed between the quartz grains. Crystal aggregates of zircon are found in this unit (Figure 16).



**Figure 13** Highly weathered and moderately jointed outcrop nature of quartz-sericite schist of at the middle part of Nat taung (Loc. 126760)

**Figure 14** Highly jointed outcrop nature of quartzite at the middle part of Nat tuang (Loc. 125761)

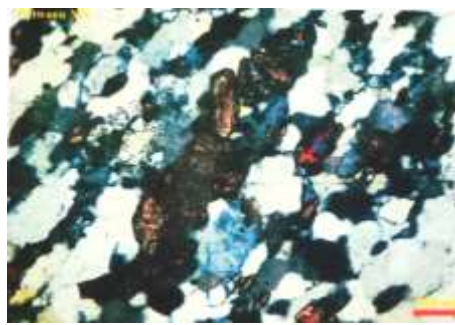
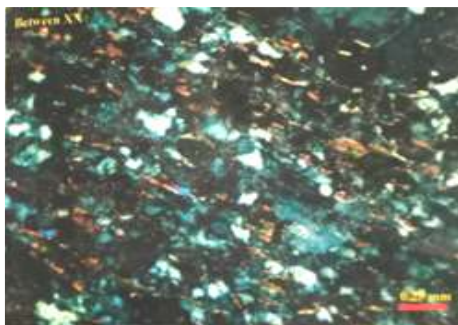


**Figure 15** Parallel alignments of sericite and muscovite in quartz-sericite schist (Loc. 126760, between X.N)

**Figure 16** Zircon crystal (Zrn) aggregates in quartzite (Loc. 125761, between X.N)

#### (4) Banded quartzite and mica schist

##### Megascopic Nature

Banded quartzite exposed at the eastern part of Nattaung (Loc. 128757). It shows light grey color on fresh surfaces and grey color to weathered surfaces. It is fine to medium-grained, hard and compact with distinct banding character. The characteristic features of banding are well developed. Sometimes quartzofeldspathic veins are intruded in this banded quartzite (Figure 17). Mica-schist is found along the Nattaung range (Loc. 129768). Quartz veins are found in this unit. It is medium-grained and schistose texture. Light grey color on fresh surfaces and yellowish to grey color on weathered surfaces (figure 18).

##### Microscopic Nature

Banded quartzite is fine to medium-grained and mainly composed of quartz 95% and other accessories about 5%. It shows granoblastic texture and slightly foliated texture due to the elongation of quartz grains which show wavy extinction (Figure 19).

Under the microscopic, mica schist is mainly composed of quartz, feldspar, biotite, muscovite and sericite minerals. Quartz grains are elongated and parallel alignments which showed ribbon-shaped. Biotite appears as parallel orientation and lies along the foliation (Figure 20).



**Figure 17** Quartzofeldspathic vein intruded in banded quartzite at the eastern part of Nat taung (Loc. 128757)

**Figure 18** Quartz vein intruded into the foliation planes of mica schist, C<sub>1t</sub><sup>4</sup> unit along the Nat taung range (Loc. 129768)

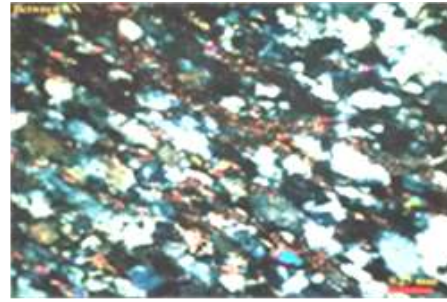


**Figure 19** Slightly foliated texture due to the elongation of quartz grains in banded quartzite (Loc. 128757, between X.N)

**Figure 20** Parallel orientation of flattened mica flakes in schist (Loc. 129768 between X.N)

### (5) Micaceous quartzite and quartzite

#### Megascopic Nature

Exposures of micaceous quartzite occur at the middle part of Kyaikkwe taung Pagoda (Loc. 141794) and its vicinity. It is mainly composed of quartz. The outcrop natures are brecciated and highly jointed (Figure 21). It also shows faintly foliation. Quartzite can be seen at the slope of Kyaikke taung (Loc. 143794). It is more hard and compact than micaceous quartzite. Brownish grey on weathered surfaces and light grey on fresh surfaces can be seen. It is mainly composed of quartz (Figure 22).

#### Microscopic Nature

Micaceous quartzite shows fine to medium-grained, granoblastic texture. It contains quartz and minor biotite, muscovite and chlorite. Quartz occurs as subhedral, granular and some are elongated crystals. They are sub-parallel to each other in orientation. Flatten and elongated quartz crystals exhibit foliation (Figure 23). Most of the quartz showing undulatory extinction indicates that it had structural strain effect. Quartzite is fine to medium-grained and mainly composed of granoblastic quartz grains. Quartz occurs as anhedral grains interlocking and also shows suture contact. Some quartz crystal show wavy extinction. Small amount of plagioclase and muscovite, epidote and sericite patches are observed between quartz grains (Figure 24).



**Figure 21** Highly weathered and faintly foliated outcrop nature of micaceous quartzite at the middle part of Kyaikkwe taung Pagoda (Loc. 141794)

**Figure 22** Outcrop of quartzite at the slope of the Kyaikkaw taung (Loc. 143794)

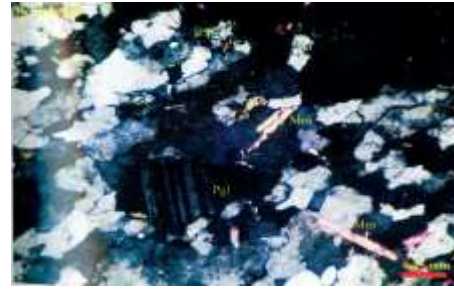


**Figure 23** Sub-parallel orientation of stretched and flattened quartz grain boundaries in micaceous quartzite (Loc. 141794 between X.N)

**Figure 24** Plagioclase (Pgl), muscovite (Mus) and epidote (Ep) in quartzite (Loc. 143794, between X.N)

## (6) Slate, phyllite and quartzite interbedded

### Megascopic Nature

Exposure of slate can be seen at the eastern part of Kyaikkwe taung (Loc. 143796). Slate is fine-grained, dark grey color on fresh surfaces and brownish grey color on weathered surfaces. It is an indurated and argillaceous rock. It is highly weathered and moderately jointed. Carbonaceous minerals also contain in this slate. It is fairly hard and smooth and compact (Figure 25). Phyllite occurred at the Mayan Monastery near the Kyaikkwe taung (Loc. 145790). Phyllite is a fine-grained rock. The phyllitic texture and sheen is well observed on the surface. Some phyllites are more compact and indistinct foliation (Figure 26). It is brownish grey color on fresh surfaces and yellowish grey color on weathered surfaces. Exposure of quartzite can be seen along the eastern part of Kyaikkwe taung (Loc. 140785). The weathered surface color is buff to grey and light grey on the fresh surface (Figure 27).



**Figure 25** Exposure nature of slate at the eastern part of Kyaikkwe taung (Loc. 143796)

**Figure 26** Outcrop nature of phyllite at the Mayan Monastery near the Kyaikkwe taung (Loc. 145790)

**Figure 27** Outcrop nature of quartzite along the eastern part of Kyaikkwe taung (Loc. 140785)

### Microscopic Nature

Under polarizing microscopic, the slate always shows the parallel orientation of both mica and quartz mineral (Figure 28). The major mineral assemblages observed quartz (white patches), biotite (dark brown patches), and muscovite (milky gray patches) with occasional chlorite. The accessory constituents are iron ore and other opaque mineral. Phyllite shows fine-grained phyllitic texture with parallel orientation of mica flakes and quartz grains as shown (Figure 29). It is mainly composed of quartz, biotite, muscovite and chlorite. Minor constituents are opaque minerals. Muscovite occurs as scaly aggregated crystals. Elongated quartz grains sandwiched between mica

bands and quartz showed wavy extinction. Microscopic nature of quartzite shows fine to medium-grained, granoblastic texture. Quartz shows wavy extinction and little amount of feldspar is present. Alternate banding of fine-grained and coarse-grained quartz crystals can be seen (Figure 30).



**Figure 28** Parallel orientation of quartz and mica flakes in slate (Loc. 143796, between X.N)

**Figure 29** Elongated quartz grains sandwiched between mica bands in phyllite (Loc. 145790, between X.N)

**Figure 30** Wavy extinction and suture contact of quartz grains in quartzite (Loc. 140785, between X.N)

### Types of Metamorphism

In general, grade of metamorphism increases gradually from east to west. Slate, phyllite, quartzite, schist, graphite-sillimanite-mica schist, garnet-biotite gneiss and quartzite are the product of regional metamorphism. Some graphite-sillimanite-mica schist suffered local contact metamorphism.

### Metamorphic Facies

The metamorphic facies classification, nomenclature and defining mineral assemblages used in this study are mainly based on Winter (2010). Based on the mineral assemblages, the metamorphic rocks of the study area were formed under the greenschist facies, amphibolite facies to hornblende hornfels facies. The mineral assemblages are graphically represented by ACF and AKF diagrams (Figure 31-a, b, c, d).

**Table 2 Mineral assemblages of greenschist facies**

| 1.Greenschist facies                  |                             |
|---------------------------------------|-----------------------------|
| Mineral assemblages                   | Pelitic and Psammatic rocks |
| 1.Quartz+muscovite+biotite+chlorite   | Slate, Phyllite             |
| 2.Quartz+plagioclase+sericite+epidote | Quartzite                   |
| 3. Quartz+muscovite+biotite+chlorite  | Banded quartzite            |
| 4.Quartz+orthoclase+biotite+epidote   | Micaceous quartzite         |

**Table 3 Mineral assemblages of amphibolite facies**

| <b>2.Amphibolite facies</b>                                          |                                    |
|----------------------------------------------------------------------|------------------------------------|
| <b>Mineral assemblages</b>                                           | <b>Pelitic and Psammatic rocks</b> |
| 1. Quartz+muscovite+biotite+sercite+ orthoclase                      | Quartz-sericite schist             |
| 2. Muscovite+biotite+tourmaline+plagioclase +quartz+almandine garnet | Mica schist                        |
| 3. Biotite+muscovite+microcline+orthoclase +quartz                   | Garnet-biotite gneiss              |
| 4. Orthoclase+plagioclase+biotite+ quartz+almandine garnet           | Garnet-biotite gneiss              |
| 5 .Biotite+muscovite+sillimanite+ tourmaline+ quartz                 | Graphite-sillimanite-mica schist   |
| 6. Muscovite+quartz+orthoclase+graphite +tourmaline                  | Graphite-sillimanite-mica schist   |
|                                                                      | Calcareous rocks                   |
| 7. Quartz+tremolite+diopside+muscovite                               | Calc-silicate rocks                |
| 8. Quartz+diopside+plagioclase+calcite                               | Calc-silicate rocks                |

**Table 4 Mineral assemblages of hornblende hornfels facies**

| <b>Hornblende hornfels facies</b>                                          |                                  |
|----------------------------------------------------------------------------|----------------------------------|
| <b>Mineral assemblages</b>                                                 | <b>Pelitic rock</b>              |
| 1. Muscovite+sillimanite+graphite+orthoclase +almandine garnet+ tourmaline | Graphite-sillimanite-mica schist |
| 2. Quartz+muscovite+almandine garnet +orthoclase                           | Graphite-sillimanite-mica schist |

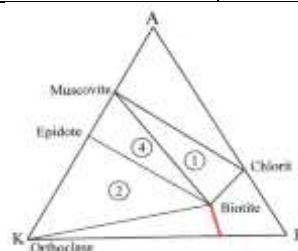


**Figure (31-a) AKF diagram showing the mineral assemblages of greenschist facies**

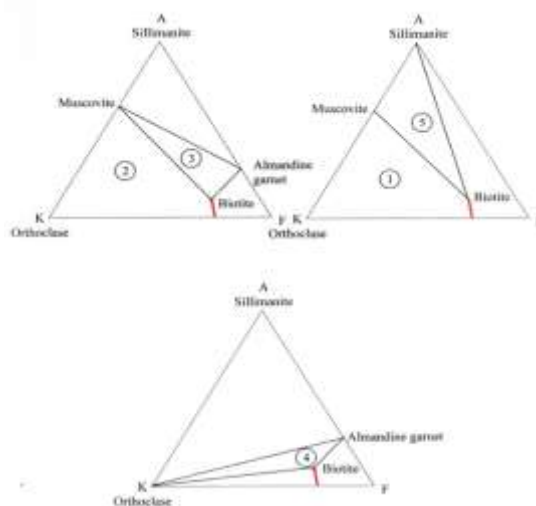


**Figure (31-b) AFK diagrams showing the mineral assemblages of amphibolite facies.**

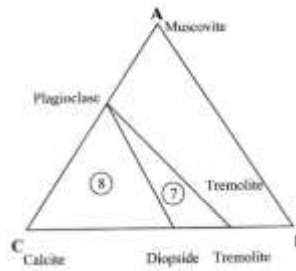


Figure (31-c) ACF diagram showing the mineral assemblages of amphibolite facies

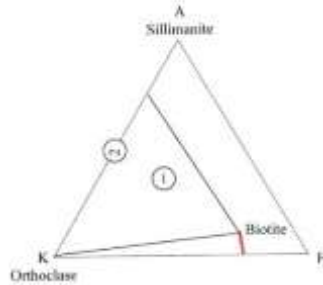


Figure (31-d) AKF diagram showing the mineral assemblages of hornblende hornfels facies

**Estimation of P-T condition**

According to (Winter, 2010), the estimate P-T condition of metamorphism in the area may be between 250°C to 680°C and pressure about 2 kb to 5 kb. The probable P-T condition of metamorphic rocks (figure 32).

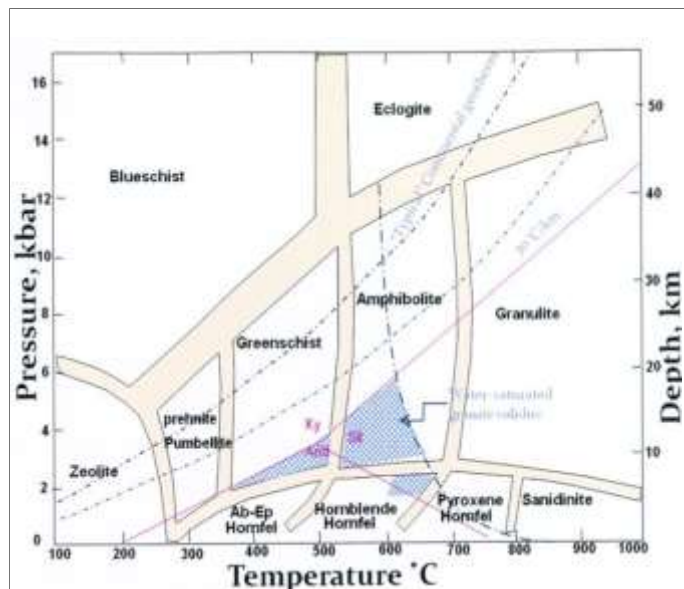


Figure 32 P-T range of greenschist facies, amphibolite facies and hornblende hornfels facies (after Winter, 2010)

**Time of metamorphism**

Mergui Group, Taungnyo Formation and Martaban beds are in the same composite series, which is assigned Silurian to Carboniferous based on the fossil evidence. Moulmein Limestone

(Premian age) overlying unconformably Taungnyo Formation was not metamorphosed. As mentioned earlier, the metamorphic rocks of this area most probably belong to the Mergui Series. Thus the main phase of regional metamorphism in the area was probably Post Carboniferous.

### **Conclusion**

The research area is situated in Chaungzon Township, Mon State and covers about 66.56 km<sup>2</sup>. The metamorphic rocks are gneiss, schist, calc-silicate rock, quartzite, phyllite and slate in the area. The area has been subjected to regional metamorphism. The grade of metamorphism increases from east to west. Regional metamorphism is most widespread in garnet-biotite gneiss, mica schist, calc-silicate rock, quartz-sericite schist, quartzite, phyllite and slate. According to the mineral assemblages, greenschist facies and amphibolite facies are noted in the area. Overprinting of contact metamorphism also took place. The effect of contact metamorphism is found in graphite-sillimanite mica schist where minerals belonging to hornblende hornfels facies. The estimate of P-T condition of metamorphism may be between 250°C to 680°C and pressure about 2kb to 5kb. The rocks of this area most probably belong to the Mergui Group. Thus, the main phase of regional metamorphism in the area was probably Post Carboniferous.

### **Acknowledgement**

I wish to express my sincere thanks to Dr Khin Maung Hla, Professor and Head and Dr Mya Moe Khaing, Associate Professor, Department of Geology, Bago University for their helpful suggestions. I am deeply indebted to U Soe Htay, Lecturer, Department of Geology, Mawlamyine University for his kind suggestion and discussion during research work.

### **References**

- Aye Thaug, (1991): Geology of Bilugyun, M.Sc Thesis University of Yangon.
- Hyndman, D.W., (1972): Petrology of Igneous and metamorphic rock, New York, Mac Graw Hall Book Co. Ltd.
- Turner, F.J., (1968): Metamorphic Petrology, New York, Mac Graw Hall Book Co. Ltd.
- Winkler, (1979): Petrogenesis of metamorphic Rocks, 5<sup>th</sup> Edition. Prentice Hall New York.

# **DEFORMATION CHARACTERS ALONG THE SAGAING FAULT ZONE BETWEEN INDAW AND SINGU TOWNSHIP, CENTRAL MYANMAR**

Khin Maung Hla<sup>1</sup>, Mya Moe Khaing<sup>2</sup>, Hlaing Myo Nwe<sup>3</sup>,  
Min Han Nyein<sup>4</sup>, Tint Tint Tun<sup>5</sup>

## **Abstract**

The study area is situated along the dextral Sagaing Fault zone, about 208 km long, between Indaw Township in Sagaing Region and Singu Township in Mandalay Region, in central Myanmar. It is demarcated by Latitude 22° 30' N to 24° 20' N and Longitude 95° 50' E to 96° 10' E. In this area, on the basis of the right stepover (releasing step) pattern; the Sagaing Fault can be subdivided into two segments – the northern Indaw-Peinnegon segment (52 km+) and the southern Peinnegon-Singu segment (156 km). There are four types of structural deformation which are determined from both the mesoscopic and microscopic characters of the oriented samples. These are ductile extensional deformation, brittle-ductile extensional deformation, semibrittle extensional deformation, and brittle extensional deformation. The former three types are especially present in the metamorphic rocks exposed between Chaunggyi and Thabeikkyin, and Katha. The brittle extensional deformation is especially present in the sandstones and conglomerates of Male Formation, Irrawaddy sandstones and Singu basalt along the southern and northern parts of the Sagaing Fault zone in the area. Rock units of the study area show distinctive structural deformation characters related to the progressive deformation processes due to the dextral shearing of the Sagaing Fault.

**Keywords:** Sagaing Fault zone, Indaw-Peinnegon segment, Peinnegon-Singusegment, structural deformation and progressive deformation processes

## **Introduction**

### **Location**

The study area is situated between Indaw and Singu Townships, Sagaing and Mandalay Regions, in central Myanmar. The area is demarcated by Latitude 22° 30' N to 24° 20' N and Longitude 95° 50' E to 96° 10' E (Figure 1).

### **Objective**

The study of the structural deformation along the Sagaing Fault zone is focused as the principal objective.

### **Method of study**

The topographic maps, satellite images and aerial photographs are used for preliminary work. This is supported by later field observations and microscopic investigations in order to get the structural deformation in the study area.

---

<sup>1</sup> Dr, Professor and Head, Department of Geology, Bago University, drkhinmghla23@gmail.com

<sup>2</sup> Dr, Associate Professor, Department of Geology, Bago University

<sup>3</sup> Dr, Associate Professor, Department of Geology, Bago University

<sup>4</sup> Assistant Lecturer, Department of Geology, Bago University

<sup>5</sup> Assistant Lecturer, Department of Geology, Bago University

## Segmentation of Sagaing Fault

On the basis of the right stepover (releasing step) pattern, Sagaing Fault in the study area can be subdivided into two structural segments (Figure 2). These are as follows:

Northern segment: (Indaw-Peinnegon segment, between lat.  $24^{\circ} 00'$  and  $24^{\circ} 20' N$ ).

Southern segment: (Peinnegon-Singu segment, between lat.  $22^{\circ} 30'$  and  $24^{\circ} 00' N$ ).

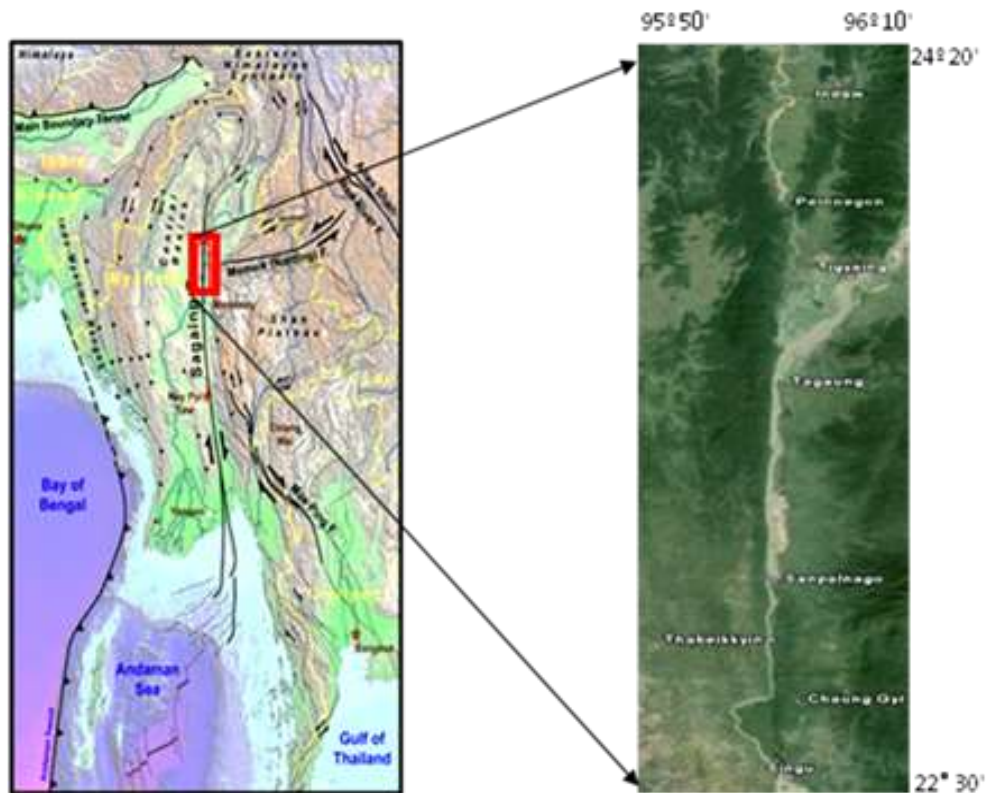


**Figure 1** Location map of the study area.

## Deformation Characters

Rock units of the study area show distinctive structural characters related to the progressive deformation processes along the Sagaing Fault. These evidences are studied in mesoscopic structures from outcrop investigations and microscopic textures from petrographic examination. On the basis of these studies, structural deformation in the study area can be classified as ductile extensional deformation, brittle-ductile extensional deformation, semibrittle extensional deformation and brittle extensional deformation.

## Field Evidence of Structural Deformation

### (1) Ductile extensional deformation

The mesoscopic characters of ductile deformation consist of foliation and stretching mineral lineation. Evidences for ductile deformation in Thabeikkyin area are represented by foliation and fold which are observed in hornblend-biotite schist of Mogok metamorphics (Figure 3a, b). In Chaunggyi, mylonite and gneiss of Mogok metamorphics are evidences of ductile deformation (Figure 3c, d).

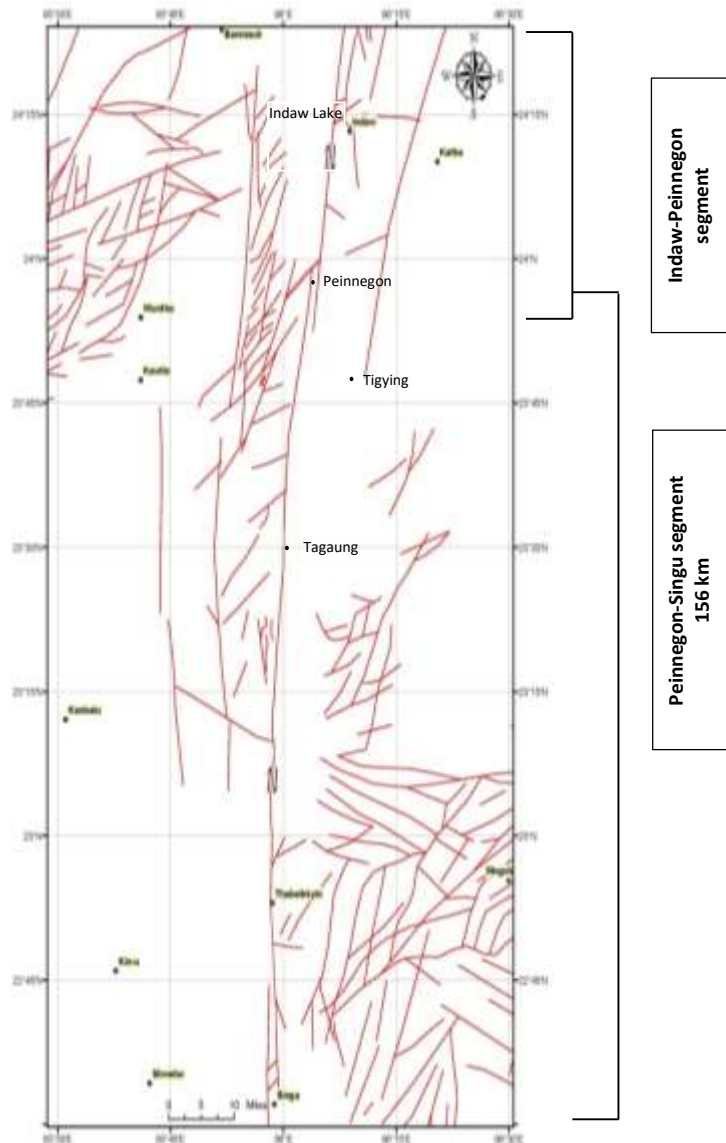


**Figure 2** Two structural segments of the Sagaing Fault in the study area.

### (2) Brittle- ductile extensional deformation

Rock deformation is dominated by both brittle and ductile mechanisms. Many brittle-ductile deformations contain boudins, rock fragments, and porphyroclasts of the more brittle minerals and rock types, all floating in a tectonite matrix of more easily deformed minerals and rocks. Cataclasite in thabeikkyin area and blastomylonite in Chaunggyi area are evidences for brittle-ductile extensional deformation (Figure 4a, b).

### (3) Semibrittle extensional deformation

It is dominated by brittle deformation mechanisms (fracturing and cataclastic flow), but some ductile aspects are well remarkable. *En echelon* veins, *en echelon* joints and *en echelon* stylolites are evidences of this deformation. Evidence for this deformation in Chaunggyi is represented by *en echelon* quartz veins which are observed in gneiss of Mogok metamorphics (Figure 5).

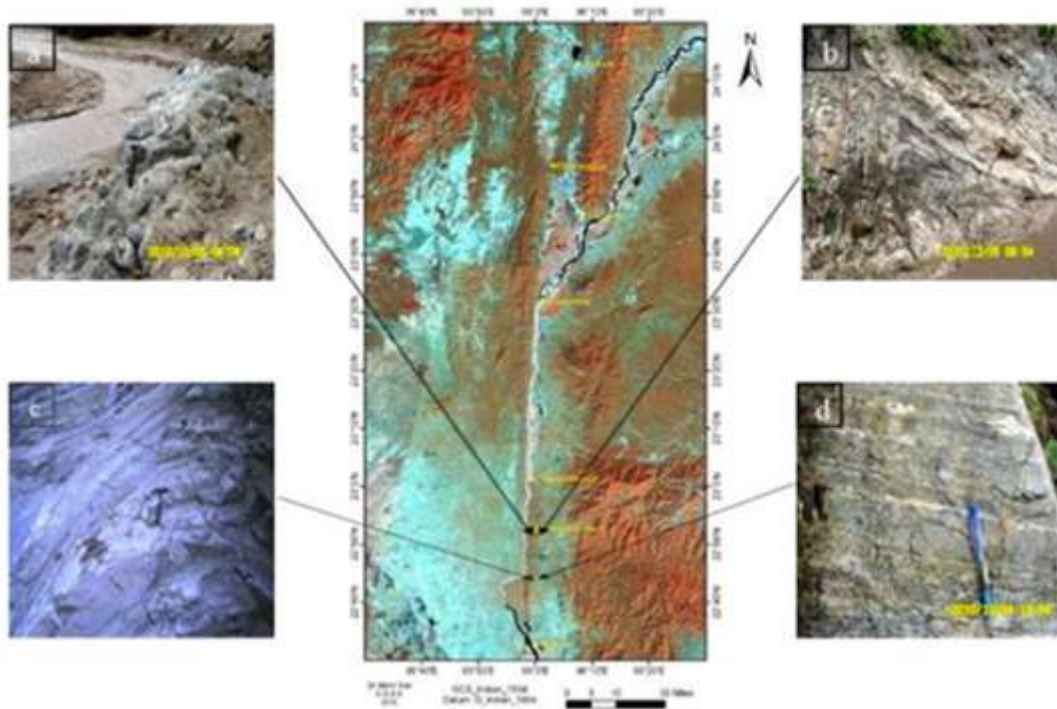


**Figure 3** Ductile extensional deformation character. (a) foliation in hornblend-biotite schist of Mogok metamorphics in Thabeikgyin area, (b) fold in hornblend-biotite schist of Mogok metamorphics in Thabeikgyin area, (c) mylonite in Chaunggyi area, and (d) gneiss of Mogok metamorphics in Chaunggyi area.

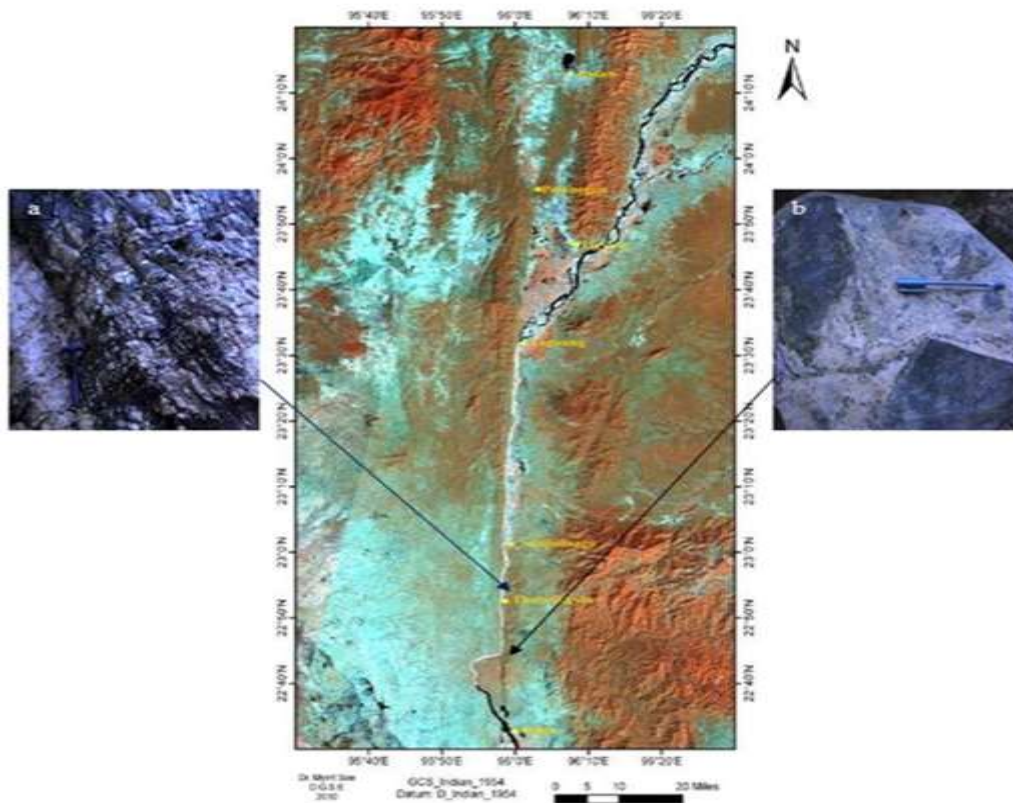


**Figure 4** Brittle-ductile extensional deformation character. (a) Cataclasite in Thabeikgyin area and (b) blastomylonite in Chaunggyi area.

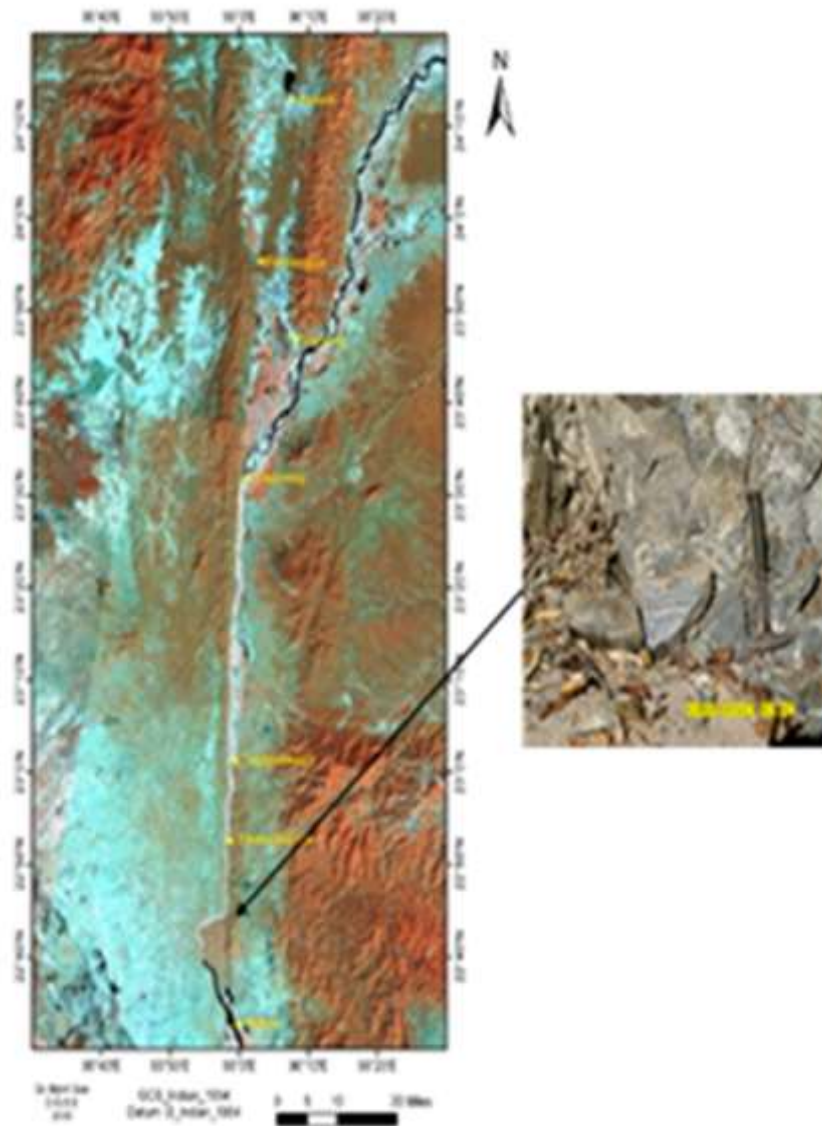


**Figure 5** Semibrittle extensional deformation character. (a) En echelon quartz veins in gneiss of Mogok metamorphics in Chaunggyi area.

#### **(4) Brittle extensional deformation**

Brittle extensional deformation operates in the shallow part of the earth crust generally within the 5-10 km level of the earth surface, where deformation is dominated by brittle mechanisms, such as fracturing and brecciation. In the study area, brittle shear planes, fault gouge and breccias are evidences for this deformation (Figure 6). Evidences for this deformation in Thetkeyyin area (Indaw) are mainly represented by brittle shear plane and fault gouge which are observed in sandstone of Irrawaddy Formation (Figure 6a, b). In Peinnegon area, brittle shear planes are observed in sandstone of Male Formation (Figure 6c, d). In the northwestern part of Zethaung area, normal fault plane is observed in limestone unit (Figure 6e). In Thabeikkyin area, normal fault plane is observed in calc-silicate rock of Mogok metamorphics (Figure 6f). Evidences for this deformation in Singu area are mainly represented by shear fault plane, fault gouge and fault breccias are observed in Singu olivine basalt (Figure 6g-j).

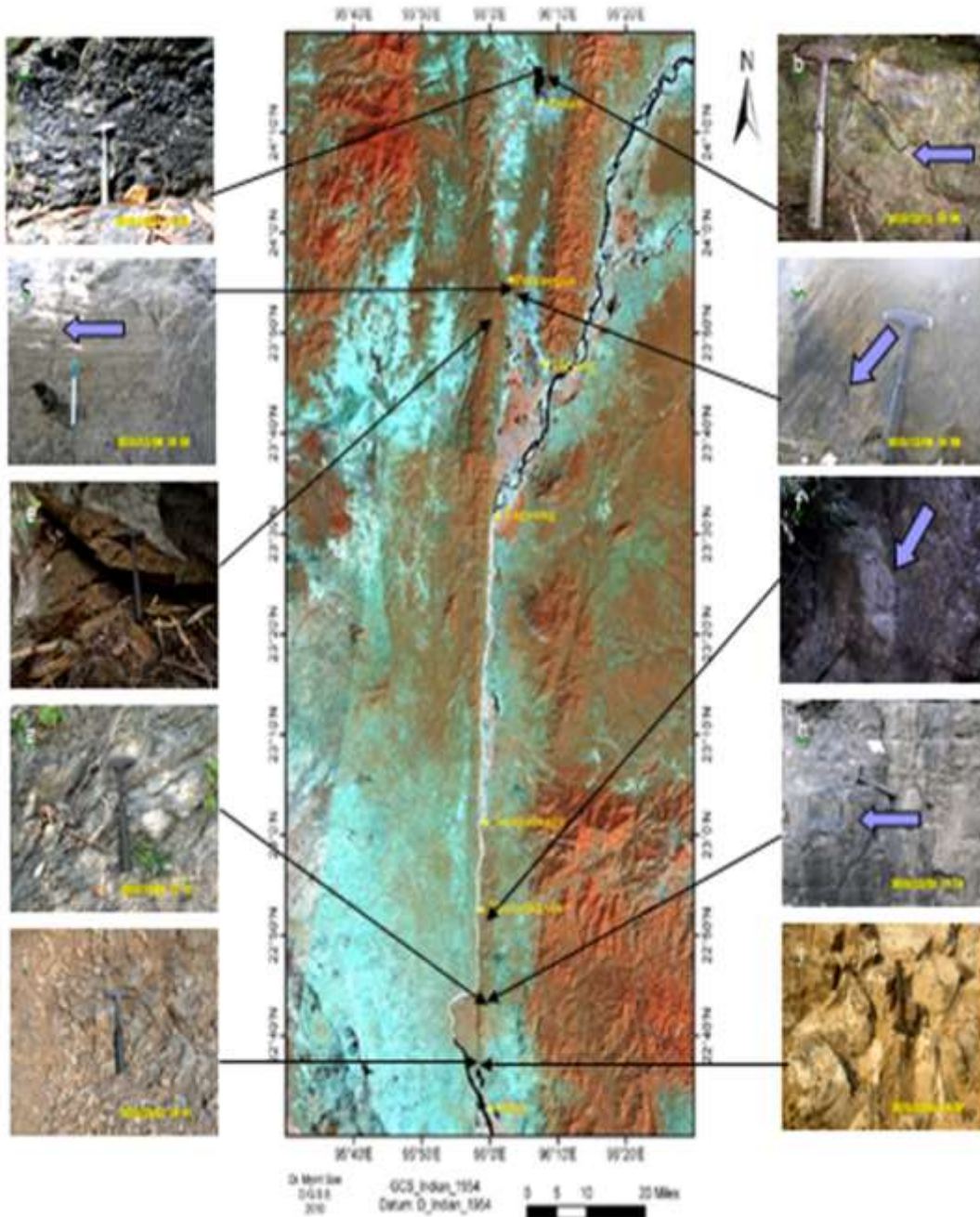


**Figure 6** Brittle extensional deformation character. (a) Fault gouge in sandstone of Irrawaddy Formation in Thetkeyin area (Indaw), (b) Dextral strike-slip fault plane in sandstone of Irrawaddy Formation in Thetkeyin area (Indaw), (c) Dextral strike-slip fault plane in sandstone of Male Formation in Peinngon area, (d) Oblique normal strike-slip fault plane in sandstone of Male Formation in Peinngon area, (e) Normal fault plane in limestone in Zethaung area, (f) Normal fault plane in calc-silicate rock of Mogok metamorphics in Thabeikkyin area, (g) Fault gouge in Singu olivine basalt in Singu area, (h) Dextral strike-slip fault plane in Singu olivine basalt in Singu area, (i) Fault breccias in Singu olivine basalt in Singu area and (j) Fault breccias in Singu olivine basalt in Singu area.

## Microscopic Evidence of Structural Deformation

### (1) Ductile extensional deformation

Microscopic characters of ductile extensional deformation are composed of deformation twin, undulose extinction, sub-grain development and grain-boundary migration.

Deformation twins are formed by crystal growth during structural deformation. Conjugate set of deformation twin is observed in calcite crystals of marble of Mogok metamorphics (Figure 7). The occurrence of deformation twinning suggests extensive recrystallization process involving grain-boundary migration and intercrystalline slip as the dominant mechanism during ductile shear deformation (Barker, 1998).

Undulose extinction is a strain shadow effect. It is formed by deformation or distortion of crystal lattice. It is observed in quartz of quartz schist of Mogok metamorphics (Figure 8). It represents the process of intracrystal dislocation, and intracrystalline deformation during ductile shearing.

In quartz schist of Katha metamorphics, ductile deformation can be represented sub-grain development (Figure 9). It is observed at crystal boundary. It is one of the dynamic recrystallization processes in ductile deformation (Davis and Renolds, 1996).

Grain-boundary migration shows irregular, serrated grain boundaries (Figure 10). It caused boundary-migration recrystallization. The controlling factors are temperature, lattice-orientation and minor constituents or impurities within the aggregate of grains (Barker, 1998).

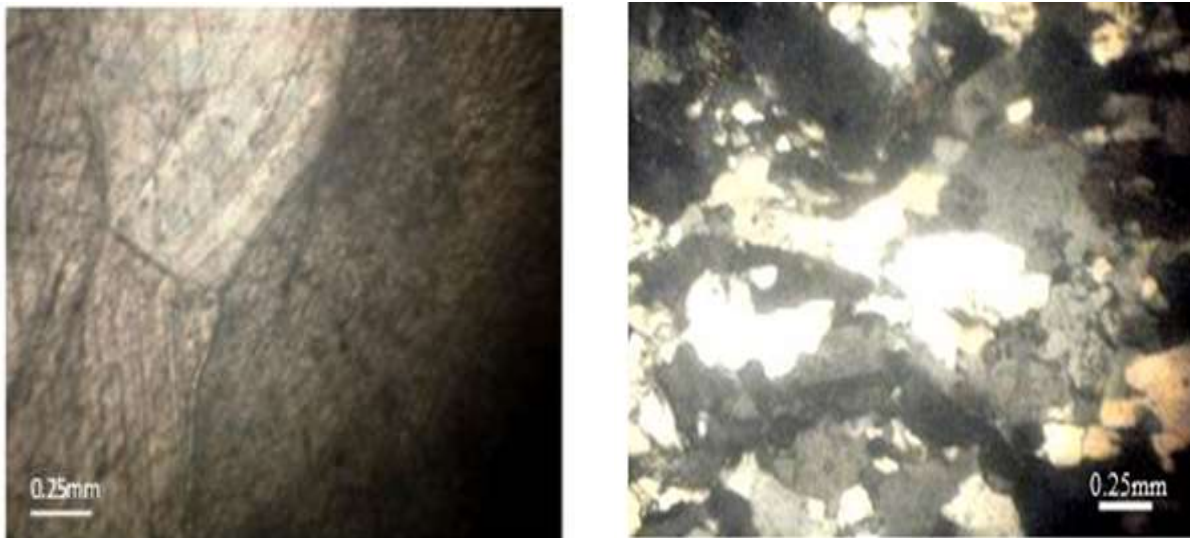


**Figure 7** Conjugate set of deformation twin in marble of Mogok metamorphics. Loc. 22° 52. 178' N and 95° 59. 203' E, between XN.

**Figure 8** Undulose extinction of quartz in quartz schist of Mogok metamorphics. Loc. 22° 44. 085' N and 95° 59. 256' E, between XN.

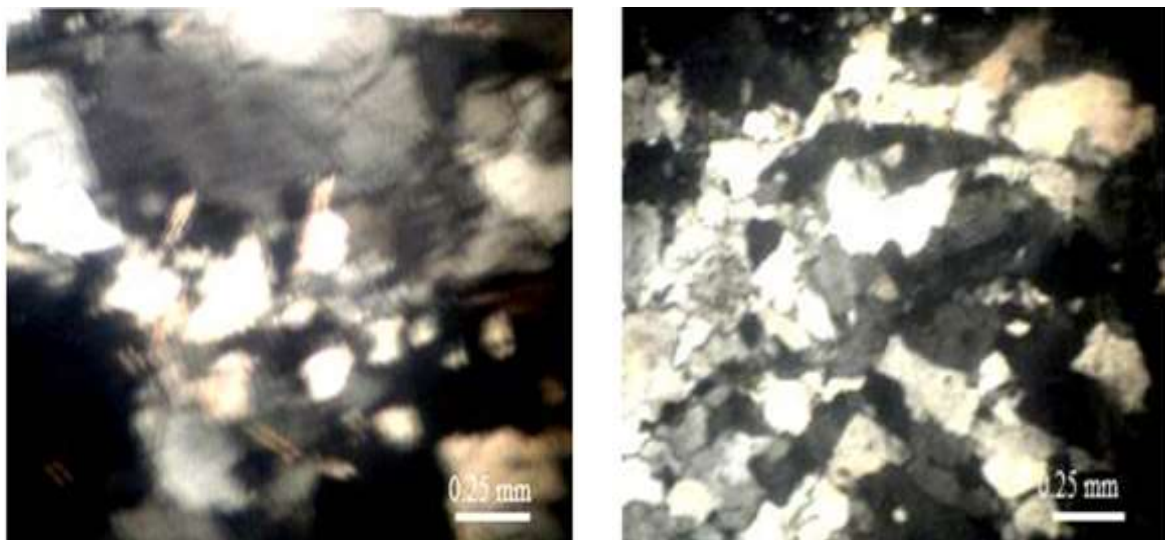


**Figure 9** Sub-grain development in quartz schist of Katha metamorphics. Loc. 23° 45. 550' N and 96° 09. 102' E, between XN.

**Figure10** Grain-boundary migration in quartz schist of Mogok metamorphics). Loc. 22° 44. 085' N and 95° 59. 430' E, between XN.

## (2) Brittle-ductile extensional deformation

Microscopic characters of brittle-ductile deformation are well recorded in gneiss of the Mogok metamorphics. In gneiss, this deformation is expressed by grain fragmentation which associated with stretching quartz and sweeping undulatory extinction (Figure 11).



**Figure 11** Grain fragmentation associated with stretching quartz and undulatory extinction in gneiss of Mogok metamorphics. Loc. 22° 53. 700' N and 95° 59.612' E, between XN.

## (3) Semibrittle extensional deformation

Microscopic characters of semibrittle extensional deformation are well documented within the marble and limestone. Calcite crystals in marble of Mogok metamorphics show small scale dislocation in calcite twins (Figure 12). Conjugate set of calcite veins in limestone reflects the semibrittle deformation (Figure 13).

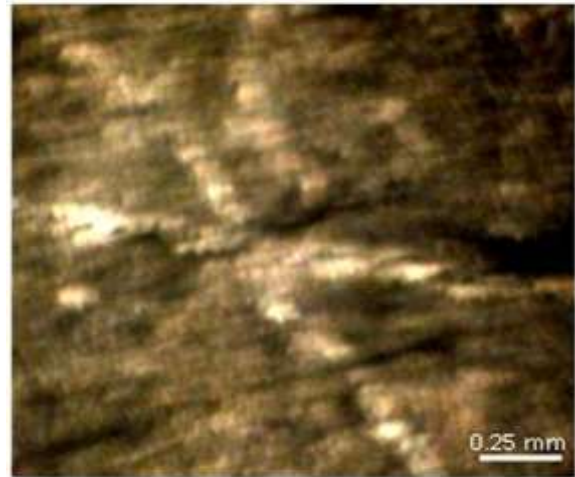
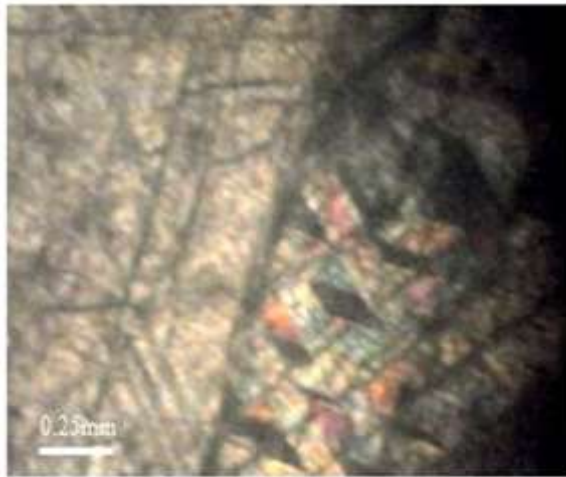


**Figure 12** Small scale dislocation of calcite twins in marble (Mogok metamorphics). Loc. 22° 52. 142' N and 95° 59. 265' E, between XN.

**Figure 13** Conjugate set of calcite veins in limestone. Loc. 23° 51.342' N and 96° 05.021'E, between XN.

#### **(4) Brittle extensional deformation**

Microscopic characters of this deformation are fracturing of olivine in Singu olivine basalt, grain fragmentation in conglomerate and microbrecciation in sandstone of Male Formation (Figure 14, 15, 16).

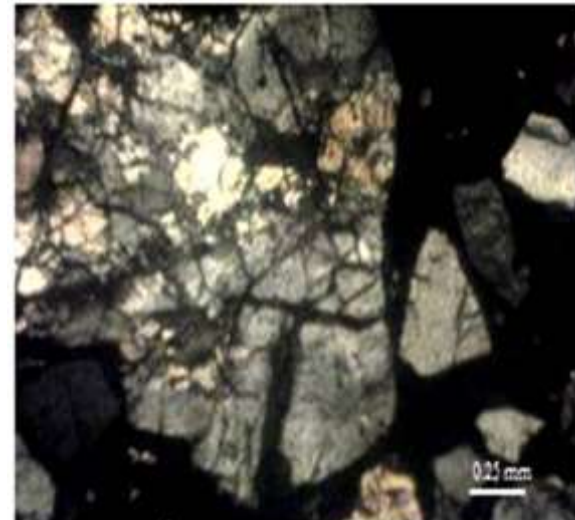


**Figure 14** Fracturing of olivine in Singu olivine basalt. Loc. 22°40.135'N and 95° 58.990'E, between XN.

**Figure 15** Grain fragmentation in conglomerate (Male Formation). Loc. 23° 05. 435' N and 95° 59.501' E, between XN.

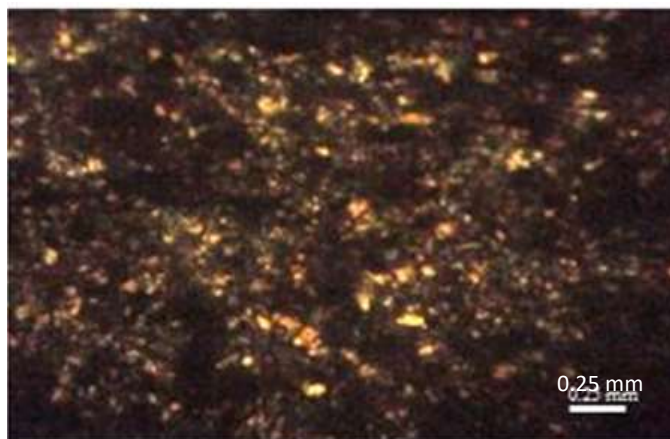


**Figure 16** Microbrecciation in sandstone (Male Formation). Loc.  $23^{\circ} 55.728'N$  and  $96^{\circ} 02.693'E$ , between XN.

### Conclusion

There are four types of structural deformation which are determined from both the mesoscopic and microscopic characters of the oriented samples from eleven different localities along or near the Sagaing Fault zone in the study area. These are ductile extensional deformation, brittle-ductile extensional deformation, semibrittle extensional deformation and brittle extensional deformation. The former three types are especially present in the metamorphic rock types exposed between Chaunggyi and Thabeikkyin, and Katha. The brittle extensional deformation is especially present in the sandstones and conglomerates of Male Formation, Irrawaddy sandstones and Singu basalt along the southern and northern parts of the Sagaing Fault zone in the area. Rock units of the study area show distinctive structural deformation characters related to the progressive deformation processes along dextral shearing of the Sagaing fault. Brittle deformation forms in the shallow parts of the crust, generally within 5-10 km of the Earth's surface. Ductile deformation is formed by shearing under ductile condition, generally in the middle to lower crust and in the asthenosphere. Brittle versus ductile character may change along a shear zone as it encounters rocks of contrasting mechanical properties. Some rock types affected by the shear zone may respond brittly, whereas others respond by ductile flow. In other cases, a shear zone may operate under progressively changing physical condition, from ductile to brittle. Alternatively, a shear zone may be reactivated under physical condition totally different from those under which it first formed. All these situations can produce a shear zone that is neither strictly brittle nor strictly ductile.

### Acknowledgements

I would like to express my sincere gratitude to Professor Dr Day Wa Aung, Head of the Department of Geology, University of Yangon, and Dr Maung Thein, Former President of the Myanmar Geosciences Society, for their supervision, guidance, critical reading of the manuscript and offering many valuable suggestions throughout the course of this study.

I wish to express my special thank to Dr Win Naing, Rector (Rtd), Dagon University, Dr Myint Thein, Rector (Rtd), University of Education, Sagaing, and Dr Win Swe, Former President of the Myanmar Geosciences Society, for their kind supervision, critical reading of the manuscript, and offering many valuable suggestions.

### References

- Barker, A.J. (1998): Introduction to metamorphic textures and microstructures. 2<sup>nd</sup> Ed., Stanley Thornes (Publishers) Ltd.
- Davis, G.H., and S.J. Reynolds, (1996): Structural geology of rocks and regions. 2<sup>nd</sup> Ed., John Wiley and Sons Inc.

## **GEOCHEMICAL PROPERTIES OF LATERITE AND LATERITIZATION PROCESSES IN HPA-AN TOWNSHIP, KAYIN STATE**

Hlaing Myo Nwe<sup>1</sup>, Aung Kyaw Myat<sup>2</sup>, Khin Maung Hla<sup>3</sup> & Mya Moe Khaing<sup>3</sup>

### **Abstract**

The present research is carried out laterite and lateritic soils of the Hpa-an Township, Kayin State. In this area, Taungnyo Formation (Carboniferous to Early Permian), Moulmein Limestone (Middle to Late Permian) are exposed covering with older alluvium (Pleistocene) and younger alluvium (Holocene). Laterite altered from all kind of rocks such as igneous, sedimentary and metamorphic rocks. Geochemical analysis of lateritic soil samples is tested with EDXRF to differentiate the laterite type and lateritization processes. Geochemical study of laterite in Hpa-an area suggest that it is made up of within 24% - 64% of SiO<sub>2</sub>, between 16 % and 50 % of Fe<sub>2</sub>O<sub>3</sub>, from 13 % to 27 % of Al<sub>2</sub>O<sub>3</sub>. Others oxides such as K<sub>2</sub>O, MnO and CaO are composed of small amount. Trace elements are shown that S, Sr, Cr, V, Zr Cu, Zn, Y, Nb and Rb. The identification and analysis of laterites were made by Molar Ratio of laterite which is based on the ratios of sesquioxides (Fe<sub>2</sub>O<sub>3</sub> + Al<sub>2</sub>O<sub>3</sub>) to silica (SiO<sub>2</sub>). Molar ratio less than 1.33 is true laterite, between 1.33 and 2 is lateritic soil and greater than 2 is non-lateritic soil. Ternary Diagram is used to explore degree of lateritization. Four stages of alteration are recognized in lateritization process: (i) kaolinitization, (ii) weak lateritization, (iii) moderate lateritization and (iv) strong lateritization. Based on the results, Taunggalay and Myaing-gale areas have less than 1.33 in Molar ratio and moderate lateritization. Vicinity of Hpa-an and Ya-The Byan Taung display between 1.33 and 2 in Molar ratio. These areas pronounced lateritic soil and lied in weak lateritization zone. Southern parts of the study area show greater than 2 in Molar ration where it is non-lateritic soil zone and kaolinization stage.

**Keywords:** Sesquioxides, lateritization, Molar ratio

### **Introduction**

The term 'laterite' was originally applied to Fe-rich material in Kerala (India) by Buchanan (1807). It was sufficiently consolidated to be cut into building blocks, which hardened on exposure. McFarlane (1976) adopted the definition of Sivarajasingham et al. (1962 "laterites are highly weathered material, depleted in alkalis and alkaline earths, composed principally of secondary oxides and oxyhydroxides of iron (goethite, hematite, maghemite) and hydroxides of aluminium (gibbsite). These oxides may incorporate other minerals including clays and other secondary minerals (kaolinite, anatase), resistant primary minerals (quartz, zircon) and weather able primary minerals (ilmenite, muscovite). Laterite was the product of alteration or weathering of an original rock.

Laterite is suitable as a base, subbase and select course for a medium traffic road or airfield. Besides, lateritization is economically most important for the formation of iron and nickel ore deposits.

The present research was investigated in the laterite and lateritic soils of the Hpa-an Township, Kayin State. The research area is bounded between North Latitude 16°44' to 16°58' and East Longitude 97°31' to 97°43' as shown in (Figure.1). This area can be easily accessible by car, train and various kinds of vehicle.

---

<sup>1</sup> Dr, Associate Professor, Department of Geology, Bago University (hmyonwe@gmail.com)

<sup>2</sup> Dr, Associate Professor, Department of Geology, University of Yangon (aungkyawmyat95@gmail.com)

<sup>3</sup> Dr, Professor and Head, Department of Geology, Bago University

<sup>4</sup> Dr, Associate Professor, Department of Geology, Bago University (myamoekhainggeol@gmail.com)

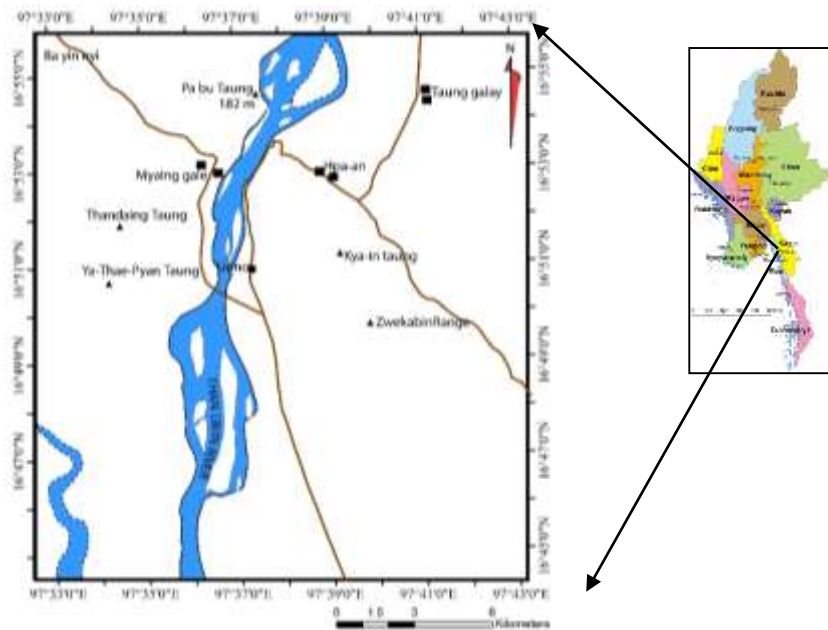


**Figure 1** Location Map of the research area.

### Geology of the research area

The rocks of Taungnyo Formation (Carboniferous to Early Permian), Moulmein Limestone (Middle to Late Permian), Older Alluvium (Pleistocene) and Younger Alluvium (Holocene) covered in the study area. The rocks of the Taungnyo Formation are exposed at the northern part of the Zwekabin Range and southern part of the Hpa-an area. The rocks are mainly composed of clastic units; thin bedded, whitish grey to pinkish colored siltstone, partly light grey to dark grey siltstone intercalated with thinly laminated shale, partly fine grained nodular sandstone.

Moulmein Limestone is mostly composed at the Zwekabin Range with gentle dipping. The other isolated hills with karst topography are also composed of Moulmein Limestone. The rocks consist of medium to thick bedded, light grey to grey colored micritic limestone, dolomitic limestone and brecciated limestone. Most of the flat plain along the western and eastern part of research area are covered by reddish brown to yellowish brown colored, thick lateritic soil. Besides, light grey to yellowish grey colored silty soils of younger alluvium expose along the central part of this area, especially Thanlwin River.

In northern part of Kya-in Taung, two layers of soil occur. Upper part is composed of recent soil that is overlain on the lateritic soil. This layer shows yellowish brown colour, medium to coarse grained soils with minute iron concentration (Figure.2 & 3). In the western part of Kya-in Taung, lateritic soil also occurs as yellowish brown colour with iron and aluminium oxides which is shown in (Figure.4 & 5). In the north western part of Zwekabin Range, reddish brown colour lateritic soil with iron concretions occurs as shown in (Figure.6) and also reddish brown colour lateritic soil occurs in northern part of Ye-thae-pyan Cave (Figure. 7). Laterite is more compacted and indurated in the Taunggaly and Myaing-gale areas (Figure. 8 & 9). They show red to reddish brown colour and wormlike appearance in one quarry, which one produce for local used. Samples are collected by using random method in the study area. Totally 18 laterite and lateritic soil samples are collected in the research area (Figure. 10).



**Figure 2** Lateritic soil profile at the northern part of Kya-in Taung



**Figure 3** Lateritic soil altered from bed rock at the northern part of Kya-in Taung



**Figure 4** Lateritic soil profile at the western part of Kya-in Taung



**Figure 5** Lateritic soil altered from bed rock at the western part of Kya-in Taung



**Figure 6** Partially indurated lateritic soil at the north-western part of Zweekabin Range



**Figure 7** Lateritic soil exposure at the northern part of Ye-thae-pyan Cave



**Figure 8** Indurated laterite outcrop at Myaing-gale area



**Figure 9** Laterite exposure at Taunggalay area

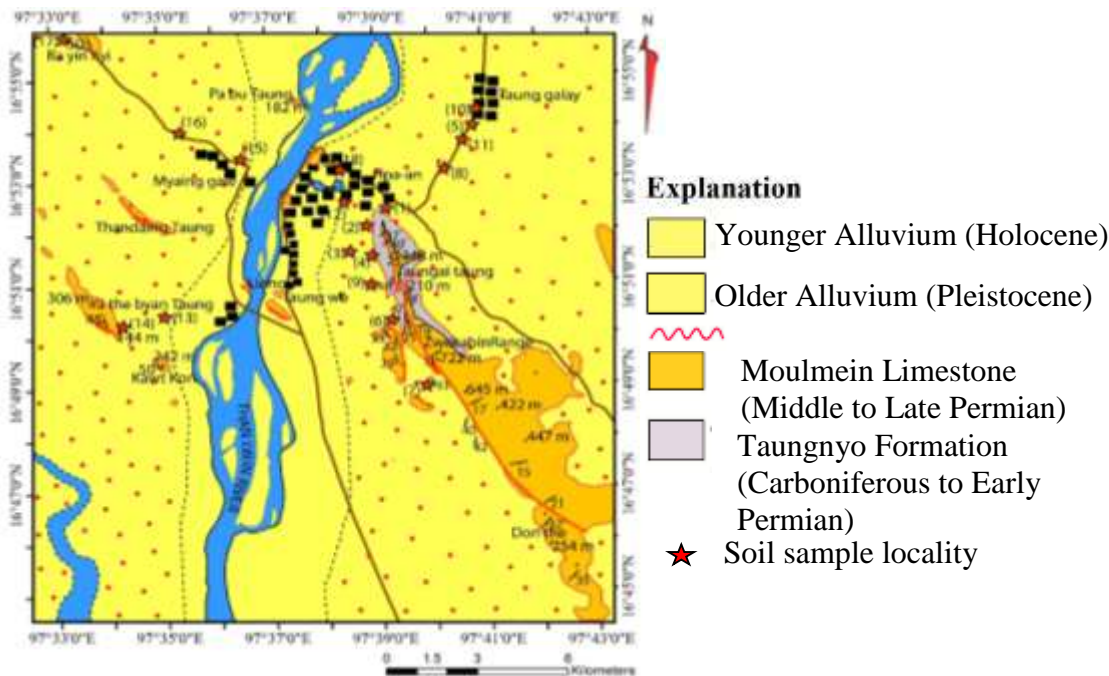


**Figure 10** Geology Map showing soil sample localities of the research area

### Aims and Objectives

This research aims to explore lateritization processes of the area analyzing on geochemical properties of laterite. Moreover, the main objectives are as follows;

- To observe the geology of the study area
- To analyze the geochemical properties of the laterite in research areas
- To identify the type of laterite
- To estimate degree of lateritization processes of this area

### Methodology

It has studied a collection of all available geological data and geochemical data. Topographic map interpretation is plotted on the UTM map no. 1697-9, 10, 13 and 14 of Survey Department (Ministry of Forestry). Samples collections are made by using the GPS methods to get the distribution of lateritic soil samples. And then, all of soil samples are tested with EDXRF as the laboratory work to know the containing element in soils.

The identification and analysis of laterites were made by using Molar Ratio of Person, B.S (1970) which is based on the ratios of sesquioxides ( $\text{Fe}_2\text{O}_3 + \text{Al}_2\text{O}_3$ ) to silica ( $\text{SiO}_2$ ).

Diagram of Schellmann (1982, 1986) is used to explore degree of lateritization. This method is a useful, quantitative approach to the classification of laterite and it compares the extent of chemical alteration of a weathering product within the profile to the composition of the parent rock in order to define 'the degree of lateritization'. Of crucial significance, it is the fact that the scheme recognizes the importance of the nature of the protolith upon the composition of the weathering product. Using a  $\text{SiO}_2$ ,  $\text{Fe}_2\text{O}_3$  and  $\text{Al}_2\text{O}_3$  ternary diagram, four stages of alteration are recognized in lateritization process: (i) kaolinitization, (ii) weak lateritization, (iii) moderate

lateritization, and (iv) strong lateritization. Moreover, laterites distribution map of the area are built based on the above data.

## Results and Discussions

### Geochemistry of laterite in study area

Geochemical study of laterite in Hpa-an area is made up of (7) major oxides and (10) trace elements. Most of the samples, SiO<sub>2</sub> is highest amount, the second is Fe<sub>2</sub>O<sub>3</sub>, the third is Al<sub>2</sub>O<sub>3</sub> and the fourth highest is TiO<sub>2</sub>. Variation of these four major oxides is shown in (Figure.11). SiO<sub>2</sub> is influence within 24% - 64% of the area. Fe<sub>2</sub>O<sub>3</sub> contain between 16 % and 50 % in all soils. Moreover, Al<sub>2</sub>O<sub>3</sub> also contain from 13 % to 27 %. Others oxides such as K<sub>2</sub>O, MnO and CaO are composed of small amount in all samples. Among the (10) trace elements, S is highest amount (83 ppm), but S doesn't contain in some sample. Sr, V and Cu occurred in all samples. Nb is least amount in all samples. The chemical results of lateritic soils from the Hpa-an area were analyzed by the result of EDXRF are shown in Table (1 and 2).

**Table 1 Major oxide and trace elements of location (1-9)**

|                                | Major Oxides (wt%)   |       |       |       |       |       |       |       |       |
|--------------------------------|----------------------|-------|-------|-------|-------|-------|-------|-------|-------|
|                                | 1                    | 2     | 3     | 4     | 5     | 6     | 7     | 8     | 9     |
| SiO <sub>2</sub>               | 43.14                | 56.30 | 43.24 | 37.79 | 24.20 | 40.26 | 57.03 | 55.39 | 42.95 |
| Fe <sub>2</sub> O <sub>3</sub> | 28.13                | 16.10 | 29.37 | 34.62 | 50.02 | 36.21 | 23.28 | 26.12 | 30.08 |
| Al <sub>2</sub> O <sub>3</sub> | 19.73                | 19.04 | 20.28 | 20.99 | 20.55 | 18.59 | 13.99 | 15.04 | 17.97 |
| TiO <sub>2</sub>               | 2.66                 | 2.78  | 2.84  | 2.52  | 1.72  | 2.03  | 1.22  | 1.42  | 2.02  |
| K <sub>2</sub> O               | 4.79                 | 5.02  | 3.36  | 3.10  | 2.61  | 2.09  | 1.43  | 0.89  | 3.88  |
| CaO                            | 0.82                 | 0.00  | 0.00  | 0.00  | 0.00  | 0.30  | 2.26  | 0.30  | 1.81  |
| MnO                            | 0.14                 | 0.10  | 0.05  | 0.08  | 0.07  | 0.07  | 0.56  | 0.13  | 0.44  |
|                                | 99.41                | 99.34 | 99.14 | 99.11 | 99.16 | 99.55 | 99.77 | 99.29 | 99.16 |
|                                | Trace Elements (ppm) |       |       |       |       |       |       |       |       |
|                                | 1                    | 2     | 3     | 4     | 5     | 6     | 7     | 8     | 9     |
| S                              | 0                    | 0     | 50    | 73    | 83    | 52    | 0     | 69    | 73    |
| Sr                             | 6                    | 8     | 4     | 8     | 14    | 5     | 10    | 6     | 7     |
| Cr                             | 5                    | 0     | 7     | 8     | 9     | 10    | 0     | 7     | 5     |
| V                              | 10                   | 8     | 11    | 12    | 9     | 1     | 7     | 7     | 9     |
| Zr                             | 37                   | 67    | 38    | 28    | 8     | 0     | 7     | 0     | 27    |
| Cu                             | 6                    | 4     | 6     | 7     | 6     | 6     | 1     | 1     | 5     |
| Zn                             | 8                    | 0     | 7     | 0     | 0     | 0     | 7     | 8     | 5     |
| Y                              | 5                    | 4     | 5     | 4     | 0     | 3     | 0     | 4     | 4     |
| Nb                             | 2                    | 0     | 0     | 0     | 0     | 0     | 0     | 0     | 0     |
| Rb                             | 6                    | 8     | 5     | 0     | 0     | 0     | 2     | 0     | 0     |

**Table 2 Major oxide and trace elements of location (10-18)**

| Major Oxides (wt%)             |       |       |       |       |       |       |       |       |       |
|--------------------------------|-------|-------|-------|-------|-------|-------|-------|-------|-------|
|                                | 10    | 11    | 12    | 13    | 14    | 15    | 16    | 17    | 18    |
| SiO <sub>2</sub>               | 25.12 | 46.82 | 63.63 | 37.43 | 39.96 | 32.47 | 23.85 | 23.74 | 53.28 |
| Fe <sub>2</sub> O <sub>3</sub> | 40.33 | 26.80 | 19.24 | 32.39 | 30.23 | 37.60 | 41.78 | 40.92 | 27.71 |
| Al <sub>2</sub> O <sub>3</sub> | 25.27 | 17.93 | 12.96 | 23.00 | 21.94 | 22.90 | 25.61 | 26.93 | 15.57 |
| TiO <sub>2</sub>               | 2.50  | 2.30  | 0.95  | 2.42  | 2.71  | 3.01  | 4.50  | 3.61  | 1.29  |
| K <sub>2</sub> O               | 5.59  | 3.03  | 0.98  | 3.86  | 4.01  | 2.72  | 2.37  | 3.68  | 1.09  |
| CaO                            | 0.80  | 1.95  | 0.92  | 0.50  | 1.00  | 0.41  | 0.46  | 0.50  | 0.61  |
| MnO                            | 0.22  | 0.27  | 0.32  | 0.29  | 0.11  | 0.17  | 0.40  | 0.17  | 0.11  |
|                                | 99.83 | 99.10 | 98.99 | 99.89 | 99.96 | 99.29 | 98.81 | 99.55 | 99.66 |
| Trace Elements (ppm)           |       |       |       |       |       |       |       |       |       |
|                                | 10    | 11    | 12    | 13    | 14    | 15    | 16    | 17    | 18    |
| S                              | 51    | 60    | 88    | 0     | 55    | 0     | 39    | 44    | 50    |
| Sr                             | 9     | 5     | 53    | 3     | 4     | 8     | 6     | 4     | 6     |
| Cr                             | 7     | 8     | 9     | 6     | 7     | 7     | 6     | 8     | 6     |
| V                              | 14    | 8     | 5     | 11    | 14    | 14    | 18    | 15    | 5     |
| Zr                             | 29    | 40    | 7     | 43    | 49    | 49    | 65    | 44    | 0     |
| Cu                             | 8     | 7     | 5     | 8     | 7     | 7     | 10    | 8     | 1     |
| Zn                             | 11    | 12    | 9     | 6     | 7     | 6     | 8     | 6     | 0     |
| Y                              | 6     | 5     | 4     | 5     | 4     | 5     | 6     | 5     | 0     |
| Nb                             | 2     | 0     | 0     | 0     | 0     | 0     | 4     | 0     | 0     |
| Rb                             | 0     | 2     | 0     | 4     | 10    | 0     | 0     | 0     | 0     |

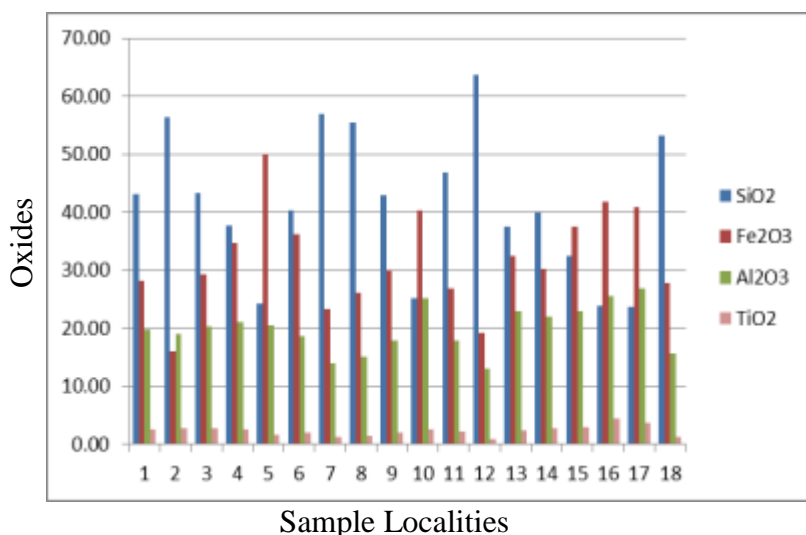


**Figure 11** Four major oxides in laterite of the study area

**Identification of Laterite**

In the research area, based on composition of SiO<sub>2</sub>, Fe<sub>2</sub>O<sub>3</sub> and Al<sub>2</sub>O<sub>3</sub> use to calculate according to Molar ratio for dividing laterite type. This equation is based on the ratios of sesquioxides (Fe<sub>2</sub>O<sub>3</sub> + Al<sub>2</sub>O<sub>3</sub>) to silica (SiO<sub>2</sub>), types of laterite can be identified. The silica/sesquioxide molar ratios were computed using the following equation.

$$\text{Silica/Sesquioxide Molar Ratio} = \frac{\% \text{SiO}_2 / \text{Mol.Wt of SiO}_2}{\% \text{Al}_2\text{O}_3 / \text{Mol.Wt of Al}_2\text{O}_3 + \% \text{Fe}_2\text{O}_3 / \text{Mol.Wt of Fe}_2\text{O}_3}$$

Molar mass of Si = 28.0g

Molar mass of O = 16.0g

Molar mass of Al = 27.0g

Molar mass of Fe = 56.0g

Molar weight of SiO<sub>2</sub> = 28 + (16 x 2) = 60.0g

Molar weight of Al<sub>2</sub>O<sub>3</sub> = (27.0 x 2) + (16 x 3) = 102.0g

Molar weight of Fe<sub>2</sub>O<sub>3</sub> = (56.0 x 2) + (16.0 x 3) = 160.0g

Ratio less than 1.33 is true laterite, between 1.33 and 2.0 indicate lateritic soils while those greater than 2.0 indicate non-lateritic soils (Person, B.S., 1970). Laterites can also be identified based on the value of sesquioxide ratio (Table.3).

**Table 3 Identification of laterites based on value of sesquioxides ratio (Person, B. S, 1970)**

| Name               | Sesquioxides ratio |
|--------------------|--------------------|
| True Laterite      | < 1.33             |
| Lateritic soil     | 1.33-2             |
| Non-Lateritic soil | > 2                |

In the research area, the percentage of each of the three essential constituents must be related to a total of 100 when applying this means of identification. And then plot the results in triangular diagram (Figure.12). Laterite samples 5, 10, 15, 16 and 17 fall in laterite zone. In this zone, the contents of Al<sub>2</sub>O<sub>3</sub> and Fe<sub>2</sub>O<sub>3</sub> increase and SiO<sub>2</sub> content decreases. In lateritic soil zone, SiO<sub>2</sub> content is more than, and also Al<sub>2</sub>O<sub>3</sub> and Fe<sub>2</sub>O<sub>3</sub> are lower than the laterite zone. In this zone, samples no.1, 3, 4, 6, 9, 13 and 14 lie. Samples no.11 and 18 falls on line of lateritic soil. Samples no.2, 7, 8 and 12 fall in non-lateritic zone; these samples contain mainly the quartz than other zone. So, SiO<sub>2</sub> percent is higher than other samples.

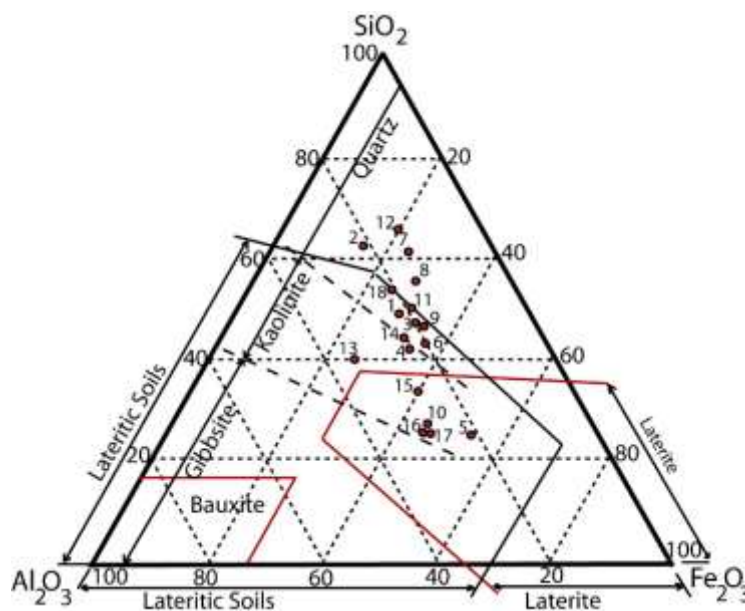


**Figure 12** Identification of Laterite in study area based on Molar Ratio (Lukens, 1964)

### Classification of laterite in study area

Ternary diagram is used to estimate the degree of lateritization in the study area. This diagram is also based on  $\text{SiO}_2$ ,  $\text{Fe}_2\text{O}_3$  and  $\text{Al}_2\text{O}_3$  percentage and four stages of alteration are classified as lateritization processes: (i) kaolinization, (ii) weak lateritization, (iii) moderate lateritization, and (iv) strong lateritization (Schellmann, 1982). The relative positions of these stages on the ternary diagram vary according to the chemical composition of the protolith. Accordingly, the Schellmann scheme is useful for determining the degree of alteration of laterites.

In the study area, sample no. 2, 7 and 12 lie in kaolinization stage. Sample no.1, 3, 4, 6, 8, 9, 11, 13, 14 and 18 fall in weak lateritization stage. Five samples fall in moderate lateritization stage. They are sample no. 5, 10, 15, 16 and 17. (Figure.13)

According to two diagrams, laterites around the Taunggalay area and Myaing-gale areas are true laterite. They are moderate lateritization. Hence, they are more indurated than other areas. Small laterite quarries occurred in Taunggalay area for local uses. Laterites are also used as building stone. Results of other samples show weak lateritization zone. The results of molar ratio are between 1.33 and 2. Hence, lateritic soil of these areas is used for subbase of road construction. Non-lateritic soils greater than 2 (molar ratio) are considered as earlier stage of actual lateritization (kaolinization). Real laterite has suffered a stronger transformation than merely kaolinized rocks.

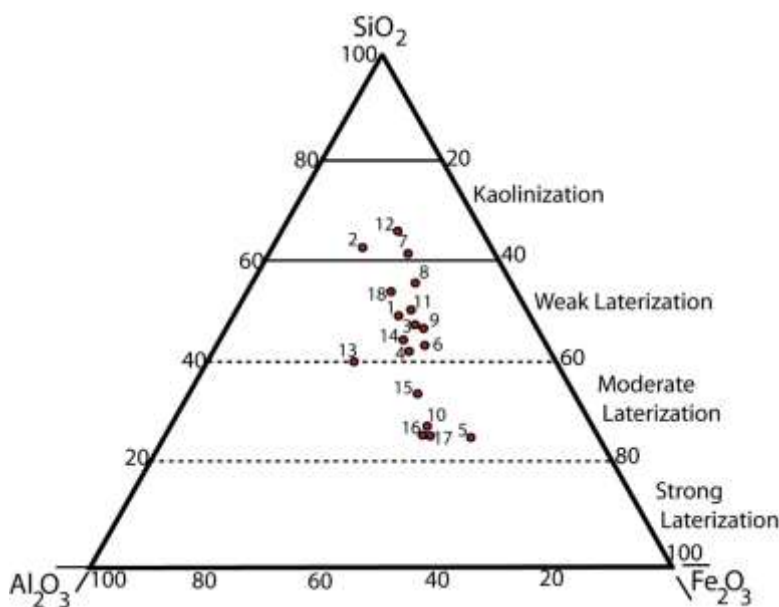


**Figure 13** Ternary diagram to estimate lateritization processes

### Distribution of Laterite and Lateritic Soil

The laterite distribution map is based on the above two diagrams (Figure.14). This map has been constructed on molar ratio. Northern part of the study area composed of true laterite. The middle part of this area shows lateritic soil and southern part is covered with non-lateritic soil. The degree of weathering typically diminishes with depth. Laterite profiles consist of a progression from unaltered protolith at the base, up through increasingly altered parent rock (or saprolite), iron enriched zones (mottled zone), and culminating at the top as an iron-rich laterite duricrust (Widdowson, M 2009).

The southern parts of the study area are near the host rock, so this area can be altered from bed rock containing with unaltered bed rock in a soft matrix. Middle part is first stage of weakly-lateritised zone in which some primary lithological characteristics remain. Iron percent are higher than non-lateritic soil. Northern part of the area is more iron segregation and vermiform textures where lies in moderately lateritized zone. Hence, true laterite is found in northern part of study area especially in the Taunggalay and Myaing-gale areas.

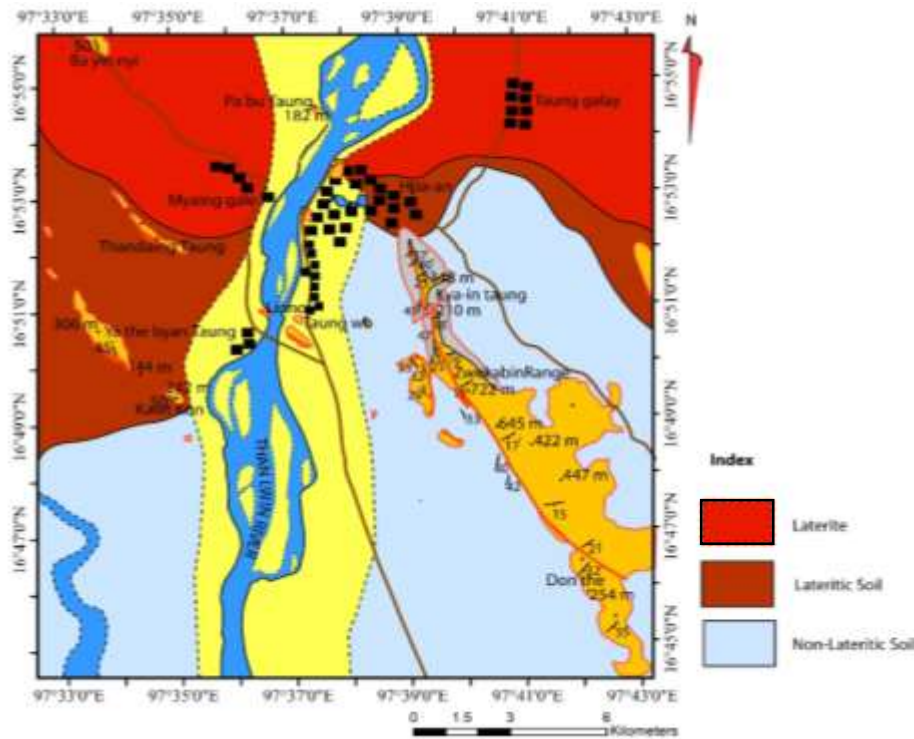


**Figure 14** Laterite and lateritic soil distribution map of the research area.

### Conclusion

The present research is carried out the laterite and lateritic soils of the Hpa-an Township, Kayin State. The rocks are composed of Taungnyo Formation (Carboniferous to Early Permian), Moulmein Limestone (Middle to Late Permian), Older Alluvium (Pleistocene) and Younger Alluvium (Holocene). Most of the flat plain along the western and eastern part of research area are covered by reddish brown to yellowish brown colored, thick lateritic soil. Laterite is more compacted and indurated, red to reddish brown colour in the Taunggalay and Myaing-gale areas.

Geochemical study of laterite in Hpa-an area is made up of (7) major oxides and (10) trace elements. Most of the samples, SiO<sub>2</sub> is highest amount, the second is Fe<sub>2</sub>O<sub>3</sub>, the third is Al<sub>2</sub>O<sub>3</sub> and the fourth highest is TiO<sub>2</sub> as EDXRF results.

Based on Lukens Diagram, samples 5, 10, 15, 16 and 17 fall in laterite zone where the contents of Al<sub>2</sub>O<sub>3</sub> and Fe<sub>2</sub>O<sub>3</sub> increase and SiO<sub>2</sub> content decreases. Samples no.1, 3, 4, 6, 9, 13 and 14 lie in lateritic soil zone in which SiO<sub>2</sub> content is more than, and also Al<sub>2</sub>O<sub>3</sub> and Fe<sub>2</sub>O<sub>3</sub> are lower than the laterite zone. Samples no.11 and 18 falls on line of lateritic soil. The last zone is non-lateritic zone. Samples no.2, 7, 8 and 12 fall in this zone where this zone contains more clay minerals than other zone. Hence, SiO<sub>2</sub> percent is higher than other samples.

According to Ternary diagram, laterites in Taunggalay area and Myaing-gale areas can be moderate lateritization. Hence, the laterites in this area are more indurated than other areas. . In Taunggalay area, geochemical properties of laterite have SiO<sub>2</sub> (23-24%), Fe<sub>2</sub>O<sub>3</sub> (40-50%) and Al<sub>2</sub>O<sub>3</sub> (20-25%). These laterites are used as building stone and it is also suitable for base and subbase for a medium traffic road. Small laterite quarries occurred in Taunggalay area for local uses. Results of other samples show weak lateritization zone. Lateritic soils are well suited for rubber tree plantations, fruit growing and horticulture.

Moreover, molar ratio is between 1.33 and 2. Non-lateritic soils greater than 2 (molar ratio) are considered as earlier stage of actual lateritization (kaolinization). So, it can be concluded that this area can be affected by moderate lateritization and weak lateritization.

### Acknowledgements

I express my immense sense to gratitude to Dr. Aye Aye Tun, Rector of Bago University for her permission to this research. And also I am greatly indebted to Dr. Yin Yin Than, Pro-rector of Bago University for her encouragement to submit this paper.

I am sincere thanks to Dr.Than Than Oo, Pro-rector of Magway University for her precious suggestions and guidance during this research.

I am grateful to Dr.Tin May Tun, Professor, Department of Geology, Bago University for her encouragement to this paper.

Finally, I also thanks to all my colleagues and my family for their support, either morally or financially.

### References

- Buchanan, F.A., (1807). *The journey from Madras through the countries of Mysore, Kanara and Malabar*, East India Co., London, 2, P. 440-441.
- Lukens, J.E., (1964). *Chemicals Properties of Tropical Soils*, Cornell University of Unpublished Report.
- McFarlane, M.J., (1976). *Laterite and Landscape*. Academic Press, London.
- Person, B.S., (1970). *Laterite; Genesis, Location, Use*. Plenum Press. New York-London. PP. 103.
- Schellmann, W., (1982). *Eine neue Laterite definition*. Geologische Jahrbuch D58, P. 31-47.
- Schellmann, W., (1986). *A new definition of laterite*. In: Banerji, P.K. (Ed.) Lateritisation processes. Memoir of the Geological Survey of India, 120, 1-7.
- Sivarajasingham,S, et al., (1962). *Laterite*. Advances in Agronomy 14: P. 1- 60.
- Widdowson, M., (2009). *Evolution of Laterite in Goa, A Geological Perspective*. Editors: Antonio Mascarenhas and Glenn Kalavampara, Geological Society of Goa, P. 35-68

## **CHEMICAL ANALYSIS OF THE GROUNDWATER IN MAYANGONE TOWNSHIO, YANGON REGION**

Min Han Nyein<sup>1</sup>, Khin Maung Hla<sup>2</sup>, Mya Moe Khine<sup>3</sup>,  
Khaing Khaing Thet Lwin<sup>4</sup>, Tint Tint Tun<sup>5</sup>

### **Abstract**

The research area, Mayangone Township is situated on the Shwedagon-Mingaladon ridge. The topography of the research area is slight moderate rolling plain and it gently slope towards the west. This area is about 62.49 square kilometer. The research area is underlain by Recent to Pleistocene age valley fill deposit and Pliocene age Arzarnigon sand rocks. Arzarnigon sand rocks are medium to coarse-grained sand rocks, and sometime gritty. The sources of water supply are water from tube well and reservoir (Gyobyu reservoir). The main aquifer in western part is valley filled deposit and in the middle part it is Arzarnigon sand rock. The yield of valley filled deposit is 2000 to 4000 gallons per hour. pH is mostly about 7.77. TDS is 380 ppm. Total salinity is low and electrical conductivity (E.C) is always not more than 280  $\mu$  mho/cm. Iron content rising up to 6 ppm, is encountered. The concentration of chloride ion is widely distributed in most of the water of the studied region and the amount present in groundwater is relative higher than other anions. The results analyzed by KURLOV'S method and PIPER method can classified the water types. Groundwater is classified on the basic of total dissolved solid (T.D.S). According to WHO Drinking Water Standard, the groundwater of the research area is suitable for the drinking water.

**Keywords:** pH, TDS, groundwater, KURLOV's method and PIPER method

### **Introduction**

The research area is lying at 20 to 60 feet above sea level. Population of Yangon City is dense. It lies on the bank of the Yangon River in the delta of the Irrawaddy. The main city area is situated between the Hlaing and Rangoon River on the west and the Pazundaung creek on the east at the southern extremity of a long narrow spur of the Bago Yoma.

### **Location and Size**

Mayangone Township is situated in the northern part of the Yangon City. The research area lies at North Latitude 16° 49' 00" to 16°54' 30"and East Longitude 96° 5' 3" to 96° 11' 00". The area coverage is about 62.49 km<sup>2</sup>(figure 1). The map index of the research area is 94 D/1 of one inch topographic map of Myanmar Survey Department.

### **Purpose of Research**

The purpose of research includes the following:

- (1) To obtain groundwater that is truly representative of the geologic formation.
- (2) To investigate the chemical quality of the water.
- (3) To research the characteristics of aquifer based on aquifer function.

---

<sup>1</sup> Assistant Lecturer, Department of Geology, Bago University, minhannyein817@gmail.com

<sup>2</sup> Dr, Professor & Head, Department of Geology, Bago University, drkhinmghla23@gmail.com

<sup>3</sup> Dr, Associate Professor, Department of Geology, Bago University, myamoekhainggeol@gmail.com

<sup>4</sup> Dr, Associate Professor, Department of Geology, Pathein University

<sup>5</sup> Assistant Lecturer, Department of Geology, Bago University

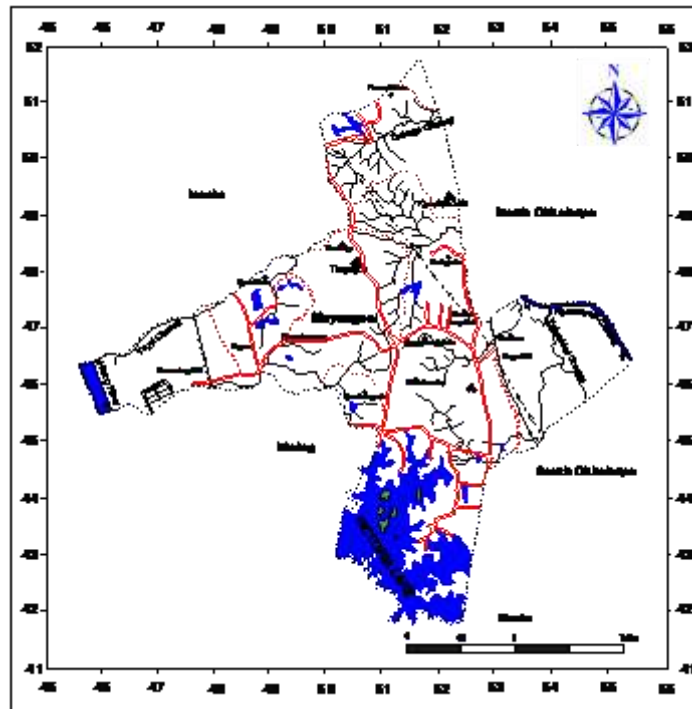


**Figure 1** Location map of the research area

### Methods of Study

Before commencement of the field work, the author visits to exit wells gathering of available data, such as relevant, topographic maps, meteorological data, pumping test data, recovery test data, well design and chemical data of groundwater in research area. These collected data are examined systematically and then they are reviewed and analyzed in the Water Resources Utilization Department. During the field, the measurements of water level, well depth, the position of wells by G.P.S are made. The step includes contouring of chemical analysis data and piezometric level setting up subsurface diagram of potential aquifers and presentation of chemical data using surfer version 8 computer processing programmed.

### Topography

The topography of the area is marked by the presence of Shwedagon-Mingaladon Ridge, a north-south trending anticline. The research area is located at the southern end of the Pegu Yoma anticline where Miocene to Pliocene rocks crop out. The highest point of this range is central part of the area, which is Junction area (8), with an elevation of between 30-60 feet above sea level. The research area is bounded by Insein Township, Hlaing Township, North Okkalarpa and South Okkalarpa at the north and east respectively and Kamaryut Township. The research area is sloping to the gently east and westwards. The eastern and western parts of the research area are the tidal affected area.

### Drainage

Tidal action also takes place in the stream channel in the eastern and western part of the area. (e.g. Hlaing River and Ngamoeyeik Chaung). The water from the upper part of the research area drains the left and right side of the ridges and which into the Hlaing River and Ngamoeyeik Chaung River. The drainage pattern of the area is coarse dendritic or tree-like pattern (figure 2). Drainage pattern is important because the part of the drainage pattern indicate changes in under groundwater condition, type of rock and geologic structure.

### Climate

The research area remains with the perimeter of tropical monsoon climate. Climate condition can be categorized into two seasons, the wet and the dry. Between mid October and mid May is a dry period known as inter monsoonal period when there are no monsoon winds. Yangon receives most of its rain during this season which usually last till October. The research area has a high mean temperature range of 30.4°C (figure 4a). It receives more than 559.6 mm of rain per annum. Annual mean evaporation is 3.647 mm per day (figure 4b) and annual rainfall is 92.3% of (figure 4c) at Kaba-Aye station. When the temperature is high; there is more evaporation and transpiration which reduces the amount of water in the river. The records of the Kaba-Aye meteorological station for the average monthly rainfall, temperature, evaporation and humidity during the period of 1999 to 2008 are shown in (figure 4d).

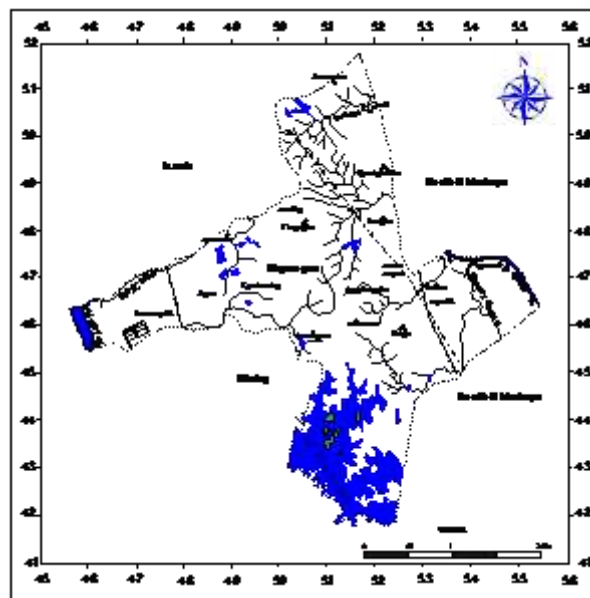


Figure 2 Drainage map of research area

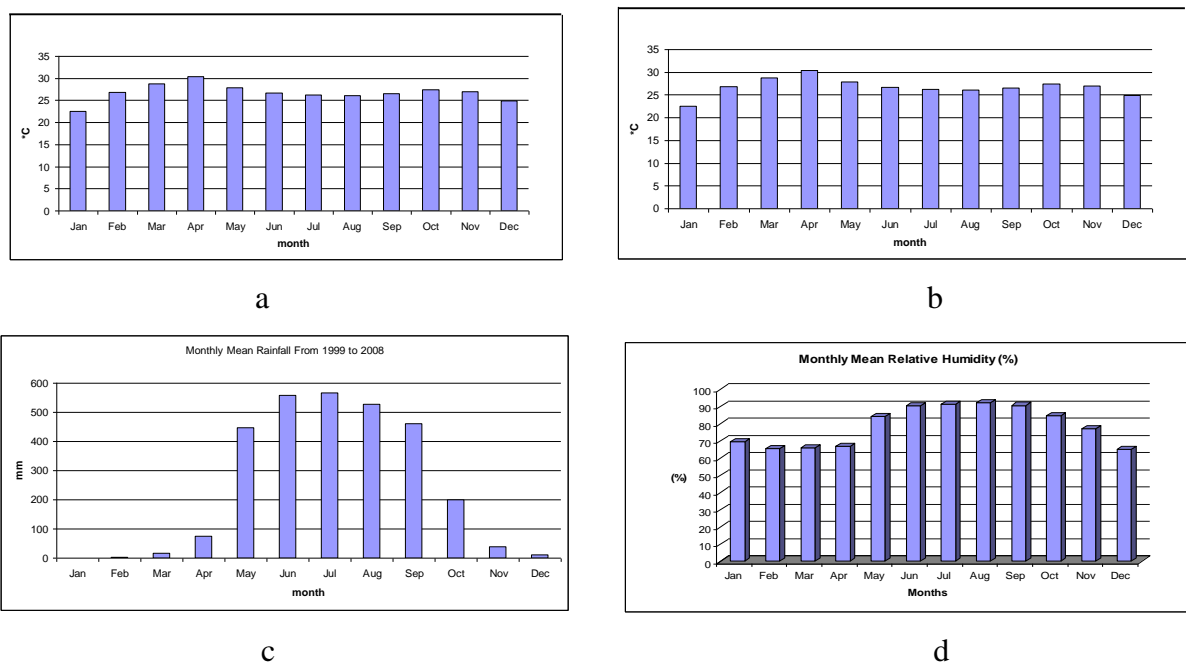


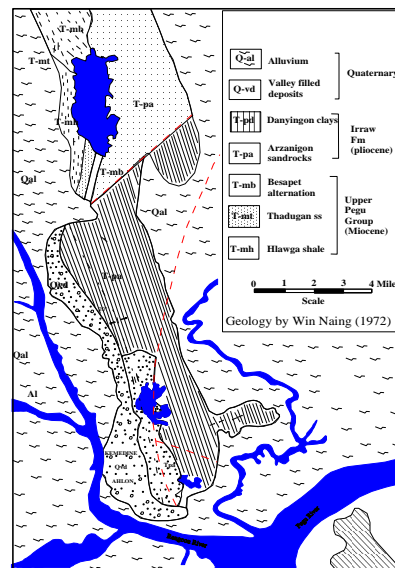
Figure 4 Climate condition of the research area a. mean temperature, b. mean evaporation, c. mean annual rainfall and d. mean humidity

## Regional Geologic Setting

Yangon and its environs are underlain by thick Tertiary deposits and Quaternary deposits are shown in figure (5).

### Pegu Group

Marine sandstones and shale of Oligocene (?) and Miocene age belong to Pegu Group. Hlawga shale of this group mainly consists of bluish grey silty shale and very fine-grained micaceous sand rock. Thadugan sandstone compose of bluish grey to brownish grey, fine to medium-grained, micaceous and argillaceous sandstone with ferruginous bands on the bedding planes. Besapet alternation is characterized by interbedded sequences of medium to very fine-grained, loosely cemented sandstone and shale. (Kyaw Tun , 1996).



After Win Naing (1972)

**Figure 5** Geological Map of Yangon City

### Irrawaddy Formation

The continental and marginal marine deposits of Pliocene belong to Irrawaddy Formation. It consists of massive, fine to medium-grained yellowish to yellowish brown micaceous sand rocks, sandy silt and shale. Shale is predominant at the upper horizon and sand beds are found at the middle and lower part. Iron rich hard bands of yellowish to red dish coloured are intercalated as inter layer. (Win Naing, 1972) This deposit composed of fine to coarse sand and gravel with yellowish coloured sometime clays lenses may interrupt the consistency of these beds. The alluvium deposit mainly consists of yellowish grey, bluish grey, brownish grey colored silts and clays. It may be about 50 feet thick. There is variation according to depositional environments.

### Geological Structure

Yangon City Area constitutes ridge and low-land lying south Pegu Yoma between Sittaung delta in the east and Irrawaddy delta in the west. Regionally, the inclination of the eastern part is low angle or less than 30 degree. (Win Naing, 1972). En-echelon folding system of Yangon City is found as Hlawga Anticline, Yangon –Mingalardon Anticline, Thingangyun-Thanlyin Anticline and Twante Anticlines trending toward the south direction that is towards the Gulf of Mattaban. (Win Naing 1972). Three sets of faults are being identified in Yangon City area. Mingalardon Fault

and Danyingone Fault are found in the research area. Mingalardon Fault is the largest fault which is trending in NE-SW direction and the fault plane is estimated to be dipping southeast direction and downthrown to be at the eastern side. Another Transverse Fault divides two rock units of Irrawaddy formation and Pegu Group. (Win Naing, 1972)

## **Hydrogeologic Characteristics of Research**

### **Collection of Data**

One inch topographic map was used in collection of the water samples of the area under investigation. The collected samples were analyzed at Health Department. Tube-wells data were collected from the Water Resources and Utilization Department (W.R.U.D) and Ministry of Agriculture and Irrigation Department. Data of chemical analyzes of water samples were obtain from Health Department of Yangon City Development Committee (Y.C.D.C). The southern part of Mayangone area includes Inya Lake. There are two main types of lithology, i.e. there are Arzarnigon sand rocks and Danyingone clay, Irrawaddian Formation and in some places valley filled deposits. According to lithologic logs the water bearing horizons consist of yellow and blue coloured sand, sand with clay and gravel. According to well logs data the aquifer type is confined type. The depth of aquifer is ranging from 19 to 70ft from the ground surface.

### **Irrawaddy Aquifer**

The distribution of the Irrawaddy aquifer blankets the whole research area. This formation includes two lithologic units: (i) Arzarnigon sand rocks and (ii) Danyingone clays. The valley-filled deposits and alluvium are found in eastern and western part of the research area. Arzarnigon sand rocks are overlain by Danyingone clays. According to well-log data from (W.R.U.D), Danyingone clays are found at the depth between 45ft and 200ft. The total area of distribution of the Danyingone clays approximately of the research area covered in middle portion.

Irrawaddian rocks mainly composed of siltstone, clay, shale and sandstone which generally dipping towards the east and the south with a very low angle. Arzarnigon sand rocks are made up of fine to coarse sand and sand with clay. Yield of the tube-wells vary from place to place is depending on the well's size, thickness of aquifer, well's design and well's development. The Danyingone clay unit is impervious and capable to produce small amount of water. The wells at the east of Shwedagon-Mingaladon ridge are shallow depths of 120 feet - 200 feet wells. In the northern part of the research area, the depth reaches up to 530 feet. The water bearing horizon of Irrawaddy Formation is encountered at the depth ranging between 60 feet and 530 feet. In the research area, well no. T5 with the depth yields 4000 gallons per hour from the depth 200ft. The well no. T 7 with the depth of about 530 feet which yield 500 gallons per hour.

## **Chemical Composition of Groundwater**

The collected samples are analyzed at the Health Department of Y.C.D.C for the cations and anions and TDS, EC, pH, total alkalinity and total hardness.

### **Classification by KURLOV'S Method**

The Kurlov's formula is written by using ionic concentrations that are expressed in milliequivalent percent (meq/l). The highest amount of ion is expressed first and lesser ion in second and so on. The anions are written above the line and cations are written below the line. The degree of mineralization (m) is placed in front of the format while pH, temperature, Fe<sup>++</sup> etc., is placed behind. Based on Kurlov's Method, the chemical classification of groundwater types in the research area shows are 1.Chloride Bicarbonate -Magnesium-Calcium, 2.Chloride Sodium,

3.Chloride -Calcium -Sodium, 4.Chloride Sodium, 5.Sulphate Bicarbonate-Chloride-Calcium,6.Chloride Sodium-Calcium, 7.Chloride Bicarbonate-Sodium, 8.Chloride Magnesium-Calcium, 9.Chloride Calcium-Magnesium, 10.Chloride Sulphate-Calcium-Sodium, 11.Chloride Bicarbonate-Magnesium-Sodium, 12.Chloride Magnesium-Sodium, 13.Chloride Calcium, 14.Chloride Bicarbonate-Calcium, 15.Chloride Bicarbonate-Sodium-Calcium, 16.Chloride Sulphate-Sodium and 17.Chloride Sulphate- Sodium-Calcium

The water samples classified by KURLOV'S Method for Mayangone area describe as follow

|                 |                                                                            |                                        |
|-----------------|----------------------------------------------------------------------------|----------------------------------------|
| T <sub>1</sub>  | $M 0.1 \frac{Cl_{59}HCO^3_{25}SO^4_{20}}{Na_{2.4}Ca_{38}Mg_{57}Fe_{1.24}}$ | Chloride Bicarbonate Magnesium-Calcium |
| T <sub>2</sub>  | $M 0.14 \frac{Cl_{65}HCO^3_{22}SO^4_{13}}{Na_{58}Ca_{12}Mg_{24}Fe_5}$      | Chloride Sodium                        |
| T <sub>3</sub>  | $M 0.38 \frac{Cl_{73}HCO^3_{18}SO^4_{13}}{Ca_{45}Na_{39}Mg_{15}Fe_1}$      | Chloride -Calcium -Sodium              |
| T <sub>4</sub>  | $M 1.36 \frac{Cl_{89}SO^4_{10}HCO^3_{0.9}}{Na_{72}Mg_{19}Ca_7Fe_2}$        | Chloride Sodium                        |
| T <sub>5</sub>  | $M 0.17 \frac{SO^4_{37}HCO^3_{33}Cl_{30}}{MG_{49}Ca_{32}Na_{16}Fe_3}$      | Sulphate Bicarbonate-Chloride-Calcium  |
| T <sub>6</sub>  | $M 0.13 \frac{Cl_{67}HCO^3_{18}SO^4_{15}}{Na_{46}Ca_{32}Mg_{20}Fe_1}$      | Chloride Sodium-Calcium                |
| T <sub>7</sub>  | $M 0.16 \frac{Cl_{51}HCO^3_{30}SO^4_{15}}{Na_{40}Ca_{23}Mg_{20}Fe_7}$      | Chloride Bicarbonate-Sodium            |
| T <sub>8</sub>  | $M 0.19 \frac{Cl_{64}HCO^3_{19}SO^4_{17}}{Mg_{49}Ca_{39}Fe_{8.9}Na_{1.6}}$ | Chloride Magnesium- Calcium            |
| T <sub>9</sub>  | $M 0.14 \frac{Cl_{70}HCO^3_{15}SO^4_{24}}{Ca_{32}Mg_{37}Na_{23}Fe_{7.5}}$  | Chloride Calcium-Magnesium             |
| T <sub>10</sub> | $M 0.13 \frac{Cl_{49}SO^4_{25}HCO^4_{25}}{Ca_{62}Na_{28}Mg_{22}Fe_2}$      | Chloride Sulphate-Calcium-Sodium       |
| T <sub>11</sub> | $M 0.05 \frac{Cl_{53}HCO^3_{26}SO^4_{19}}{Mg_{46}Na_{29}Ca_{14}Fe_{9.7}}$  | Chloride Bicarbonate-Magnesium-Sodium  |
| T <sub>12</sub> | $M 0.14 \frac{Cl_{61}SO^4_{24}HCO^3_{14}}{Mg_{48}Ca_{44}Na_6Fe_2}$         | Chloride Magnesium-Calcium             |
| T <sub>13</sub> | $M 0.04 \frac{Cl_{59}SO^4_{21}HCO^3_{19}}{Mg_{37}Na_{28}Ca_{19}Fe_{17}}$   | Chloride Magnesium-Sodium              |
| T <sub>14</sub> | $M 0.18 \frac{Cl_{57}SO^4_{22}HCO^3_{20}}{Ca_{57}Mg_{32}Na_{12}}$          | Chloride Calcium- Magnesium            |
| T <sub>15</sub> | $M 0.11 \frac{Cl_{71}HCO^3_{20}SO^4_9}{Ca_{78}Mg_{12}Na_9Fe_1}$            | Chloride Calcium                       |
| T <sub>16</sub> | $M 0.06 \frac{Cl_{56}HCO^3_{33}SO^4_{10}}{Ca_{72}Mg_{13}Na_4}$             | Chloride Bicarbonate-Calcium           |
| T <sub>17</sub> | $M 0.12 \frac{Cl_{47}HCO^3_{17}SO^4_8}{Ca_{50}Na_{29}Mg_{18}Fe_3}$         | Chloride Calcium-Sodium                |
| T <sub>18</sub> | $M 0.17 \frac{Cl_{62}HCO^3_{26}SO^4_{12}}{Na_{48}Ca_{33}Mg_{16}Fe_2}$      | Chloride Bicarbonate-Sodium-Calcium    |
| T <sub>19</sub> | $M 0.15 \frac{Cl_{58}SO^4_{32}HCO^3_{20}}{Na_{42}Mg_{28}Ca_{24}Fe_6}$      | Chloride Sulphate-Sodium               |
| T <sub>20</sub> | $M 0.23 \frac{Cl_{60}SO^4_{40}}{Na_{55}Ca_{35}Mg_9}$                       | Chloride Sulphate- Sodium-Calcium      |

### Classification of Piper Diagram

This method is proposed by Piper (1944) and by Hill (1940). This method of tri linear diagram is widely use to depict chemical data and show the relative concentrations of the major cations ( $\text{Ca}^{+2}$ ,  $\text{Mg}^{++}$  and  $\text{K}^+$ ) and anions ( $\text{CO}_3^-$ ,  $\text{HCO}_3^-$ ,  $\text{Cl}^-$  and  $\text{SO}_4^-$ ). Cations are plotted on the left triangle and anions on the right triangle. Piper diagram are show in figure (5). Kurlov’s method and Piper method are compared the result of the research area in groundwater types, which in table (1).

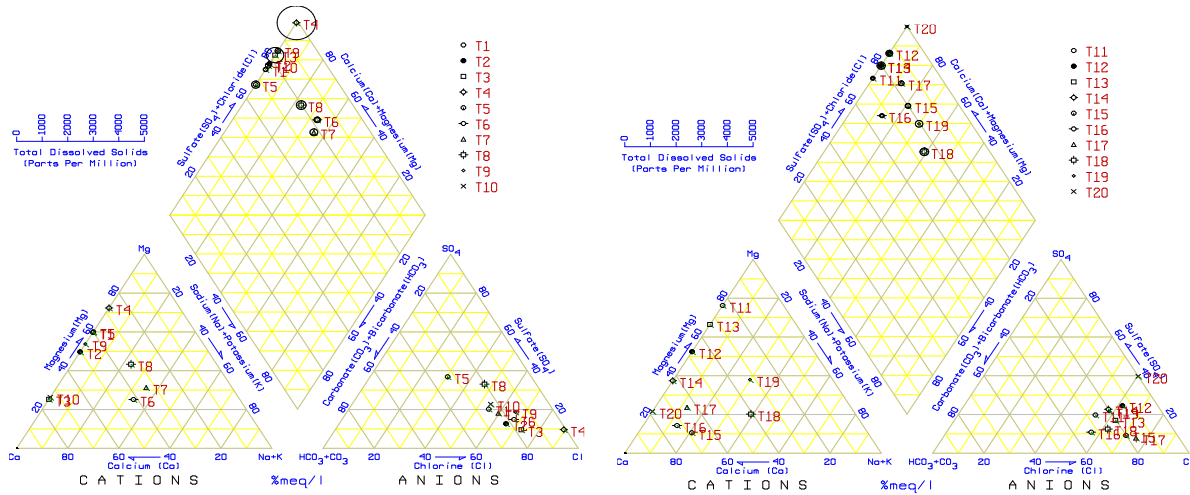


Figure 5 Classification of the Piper diagram

Table 1 Compares ion with Kurlov’s method and Piper Method

| Tube Well No.   | Kurlov’s Method                           | Piper Method                              |
|-----------------|-------------------------------------------|-------------------------------------------|
| T <sub>1</sub>  | Cl HCO <sub>3</sub> Mg Ca                 | Ca Mg Cl                                  |
| T <sub>2</sub>  | Cl Na                                     | Ca Mg Cl                                  |
| T <sub>3</sub>  | Cl Ca Na                                  | Ca Cl                                     |
| T <sub>4</sub>  | Cl Na                                     | Mg Cl                                     |
| T <sub>5</sub>  | SO <sub>4</sub> HCO <sub>3</sub> Cl Mg Ca | Ca Mg HCO <sub>3</sub> Cl SO <sub>4</sub> |
| T <sub>6</sub>  | Cl Na Ca                                  | Ca Mg Na Cl                               |
| T <sub>7</sub>  | Cl HCO <sub>3</sub> Na                    | Ca Mg Na Cl                               |
| T <sub>8</sub>  | Mg Ca                                     | Ca Mg Na SO <sub>4</sub> Cl               |
| T <sub>9</sub>  | Cl Ca Mg                                  | Ca Mg Cl                                  |
| T <sub>10</sub> | Cl SO <sub>4</sub> HCO <sub>3</sub> Ca Na | Ca HCO <sub>3</sub> Cl                    |
| T <sub>11</sub> | Cl HCO <sub>3</sub> Mg Na                 | Mg HCO <sub>3</sub> Cl                    |
| T <sub>12</sub> | Cl Mg Ca                                  | Ca Mg Cl                                  |
| T <sub>13</sub> | Cl Mg Na                                  | Mg Cl                                     |
| T <sub>14</sub> | Cl Ca Mg                                  | Ca HCO <sub>3</sub> Cl                    |
| T <sub>15</sub> | Cl Ca                                     | Ca Cl                                     |
| T <sub>16</sub> | Cl HCO <sub>3</sub> Ca                    | Ca HCO <sub>3</sub> Cl                    |
| T <sub>17</sub> | Cl Ca Na                                  | Ca Cl                                     |
| T <sub>18</sub> | Cl HCO <sub>3</sub> Na Ca                 | Ca Na Cl                                  |
| T <sub>19</sub> | Cl Na Mg                                  | Ca Mg Na Cl                               |
| T <sub>20</sub> | Cl SO <sub>4</sub> Na Ca                  | Ca Cl                                     |

## Chemical Analysis

Chemical Analysis is important to specify the actual characteristic of groundwater. Determination of pH, total dissolved solids, T.D.S, electric conductivity E.C, dissolved cations of  $\text{Na}^+$ ,  $\text{K}^+$ ,  $\text{Ca}^{++}$ ,  $\text{Mg}^{++}$  and  $\text{Fe}^{++}$  and dissolved anions of  $\text{CO}_3^-$ ,  $\text{HCO}_3^-$ ,  $\text{Cl}^-$  and  $\text{SO}_4^-$  are made in the laboratory.

The pH values of groundwater show that all the water collected and analyzed are “potable water” because pH values fall in the range of 6.64 to 7.77 and the average pH value is 6.61. Total dissolved solids or salinity have been determined by TDS meter within 25°C to 30°C of room temperature. Total dissolved solid values fall in fresh water quality rang that is not more than 1000 ppm. The groundwater is fresh water according to K.A Gorrell classification. But of T.D.S of (T-4) is found to contain noticed that ranges 1360 mg/l. The E.C water is required to evaluate because it is very useful in accessing total salinity and concentrations of some of the major cations and anions. Correlation will be made between specific conductance, total dissolved solids, cations and anions. The result of the analysis of water samples fall in the range of from 40  $\mu$  mho/cm to 2100  $\mu$ mho/cm.

### Major Cations

Cations, which commonly contained in tube-wells including iron  $\text{Fe}^{++}$  cations have been determined. Common cations are calcium  $\text{Ca}^{++}$ , Magnesium  $\text{Mg}^{++}$ , Sodium  $\text{Na}^+$  and Potassium  $\text{K}^+$ . Calcium ion concentration in groundwater of the research area falls in the range of 3.20 to 58.51 mg/l. The tube well T-3 is 58.51 ppm which displays a little bit rises in Calcium concentration than other tube-wells. Magnesium ion is very useful parameter in groundwater quality determination. In the research area, the value of Magnesium concentration is between 1.14 and 16.32 ppm. The concentration of Sodium ion in this studied area does not too differ from the remaining cations. The value of Sodium concentration is ranging from 1 to 29 ppm. Generally, the iron concentration in the research area is in the range of 0.3 to 6 mg/l. The value of iron concentration of tube well T<sub>10</sub> reaches up to 6 ppm

### Major Anions

Anions are playing a vital role in quality determination of groundwater. Only major anions of Carbonate ( $\text{CO}_3^-$ ), Bicarbonate ( $\text{HCO}_3^-$ ), Sulphate ( $\text{SO}_4^-$ ) and Chloride ( $\text{Cl}^-$ ) ions should be taken into account. In the studied area, there is no Carbonate concentration according to the analyzed result from the water sample of the research area. In all water samples from tube-wells in Irrawaddy aquifer Bicarbonate concentration is generally in the range of 8 to 70 ppm. Especially, the tube-well no. T<sub>3</sub> rises up to 70 ppm. The concentration of sulphate ion present is Irrawaddy aquifer usually shows the range between 3 and 48.96 mg/l. Moreover, the tube-wells no. T<sub>9</sub> is 48.96 ppm. The concentration of Chloride ion is widely distributed in most of the water of the studied region and the amount present in groundwater in relatively higher than other anions. Its concentration value is falling within the amount of 10 to 169 ppm. Chloride concentration of the tube wells no. T<sub>3</sub> is 169 ppm.

## Drinking Water

Most of the people use drinking water and domestic water from the tube-wells. The standard proposed by WHO standard guideline for the drinking water is shown in compares with the obtained value of groundwater analysis from Mayangone Area. According to this table, generally the quality of groundwater is suitable to drink but T-4 is the brackish water is shown in table (2).

**Table 2 WHO standard guideline for the drinking water in research area**

| Characteristics            | Guideline value |                     | The rang obtained from groundwater | Remark                              |
|----------------------------|-----------------|---------------------|------------------------------------|-------------------------------------|
|                            | Desirable       | Max Permissible     |                                    |                                     |
| Calcium                    | 75 mg/l         | 200 mg/l            | 3.2-58.51 mg/l                     | Good                                |
| Magnesium                  | 30 mg/l         | 150 mg/l            | 0.8-43.2 mg/l                      | Potable                             |
| Sodium                     | 0- mg/l         | 200 mg/l            | 0 –19 mg/l                         | Good                                |
| Potassium                  | 0- mg/l         | 200 mg/l            | 0 –5 mg/l                          | Good                                |
| Sulphate                   | 0- mg/l         | 400 mg/l            | 5.76 – 48.9 mg/l                   | Potable                             |
| Chloride                   | 200 mg/l        | 600 mg/l            | 14 –590 mg/l                       | Rather                              |
| Iron                       | 0.5 mg/l        | 1.5 mg/l            | 0 – 8 mg/l                         | Poor ,T <sub>4</sub>                |
| TDS                        | 0- mg/l         | 1000 mg/l           | 65 – 1360 mg/l                     | But T <sub>4</sub> Brackish         |
| PH                         | 6.5 mg/l        | 9.2 mg/l            | 6.64 – 7.77                        | Potable                             |
| Hardness CaCO <sub>3</sub> | 0- mg/l         | 500 mg/l            | 15 –248 mg/l                       | Rather                              |
| Colour turbidity           | 5               | 20                  | -                                  | Nil                                 |
| Zinc                       | 5 mg/l          |                     | -                                  | Nil                                 |
| EC                         | 0- micro mho/cm | 1500 micro mhos/ cm | 0 – 2100 micro mhos/cm             | Good water, But T <sub>4</sub> poor |

### Conclusion

The research area is underlain by Recent to Pleistocene age valley-filled deposits and Pliocene age Arzarnigon sand rocks. The valley-filled deposits are yellow to red, fine to coarse sand, gravel, yellow to red of lateritic soil and yellowish clay. The yield of valley filled deposit is 2000 to 4000 gallons per hour for 8 inches diameter well and the depth of water bearing horizon is ranging from 40 to 90 ft. The yield of Arzarnigon sand rocks is up to 3000 gallons per hour for 4 inches diameter well and the depth of water bearing horizon is ranging from 230 ft to 270 ft. The concentration of hydrogen ion (pH) is between 6.64 and 7.77. Mostly, total dissolved solids are always less than 380 ppm in the research area. Total salinity is low and electrical conductivity (E.C) is not more than 280  $\mu$  mho/cm. The concentration of Chloride ion is widely distributed in most of the water of the studied region and the amount present in groundwater relative higher than other anions. The analyzed results are classified by KURLOV'S method and PIPER method to indication the water types of groundwater of the research area. According to result of the chemical analysis data, the groundwater in Mayangone Township can be used for drinking water and domestic water.

### Acknowledgement

I would like to express my most profound thanks to Professor and Head Dr. Khin Maung Hla, Department of Geology, Bago University, for his permission and valuable suggestions.

I wish to express his sincere thanks and gratitude to my supervisor Dr. Maung Thin, Retired Rector, Dagon University, for his supervision guidance, critical reading of the manuscript and offering many valuable suggestions throughout the course of the study.

### **References**

- Leiscenster,P,(1959)**, “The Geology and Underground Water of Rangoon with Special Reference to Tube Wells, Rangoon”. Government Printing and Stationary, 78PP.
- Maung Thin, Dr, (1995)** “Some Urban Geological Aspects of Yangon Area” Unpuboished country Paper read at the Seminar on Environment and Urban Geology for sustainable Development of Fast Growing Cities.
- Maung Maung, (1996)** “Urban Geology of Western Yangon Area”. Unpublished M.Sc. (Thesis) University of Yangon.
- Win Naing, (1972)**, “The Hydrogeology of Greater Rangoon Area” Unpublished M.Sc. (Thesis), University of Yangon.
- Win Naing, (1996)**, “Urban Geology of Eeastern Yangon Area”. Unpublished M.Sc. (Thesis), University of Yangon.

## **A NEW LIGHT ON DEVELOPMENT AND EVOLUTION OF MANN ANTICLINE EAST FLANK OF SALIN BASIN**

Tin Myint Oo<sup>1</sup>, Myat Thuzar Soe<sup>2</sup>, Lai Lai Min<sup>3</sup>, and Lynn Myint<sup>4</sup>

### **Abstract**

The Mann anticline occupies the northern part of the NNW-SSE trending first line of anticline structures known as Minbu-Htaukshabin-Tagaing-Chaungtha structural line which develops on the east flank of Salin Basin. It expresses on surface as an elongated, asymmetrical north plunging fault related anticline where Irrawaddian, Kyaukkok, Pyawbwe, Okhmintaung and Padaung formations as core were exposed and the northern plunging area of which is mainly covered by alluvium and Irrawaddians. Present study revisited the interpretations of gravity and dense seismic data and well to well correlations, as a result proposes a new light on the development and evolution of Mann anticline. From the gravity data it can be assumed that the northward plunge continues in the subsurface up to the latitude 20° 18' about 8 miles from outcrop area; the anticline is intersected by two longitudinal faults, one on the western and the other on the east limb, and there exist a E-W transverse fault at latitude 20° 15'. The seismic images of the anticline suggest that Mann anticline is a strike slip fault related inversion anticline of positive flower shape bounded by west hading high angle fault zone on the east limb and syn-inversion antithetic faults on the west. The anticline is broad with gentle flanks in the north and the core of the anticline nose narrows to the south with steepening flanks. The structural analysis of the seismic data led to the conclusion that two phases of structuration took place in Minbu area. The first phase was E-W compression in Late Oligocene and formed proto Mann anticline with a NNW-SSE trending oblique longitudinal normal fault along the crestal portion. The second phase is the dextral strike slip faulting initiated from Pliocene and continues to recent which caused inversion of the existing structures resulted in current positive flower shape configuration of Mann anticline. Over 600 wells were drilled on the Mann anticline to date and the well to well correlations confirmed existence of cross and oblique normal faults and longitudinal reverse faults which have effective sealing potential and compartmentalizing the anticline into numerous oil pools. The Sabwet Chaung indicated by gravity low anomaly is a zone of high angle conjugate normal faults dipping towards each other and separated Mann anticline from Htaukshabin Anticline. It may possibly has an active strike slip component and forming a passage through which the clay intermingled with water and gas seeps to the surface as small mud volcanoes at Nagapwet Taung.

**Keywords:** seismic, attribute

### **Introduction**

The Mann anticline is located in the Minbu District, Magway Region, between latitude 18° 10' to 18° 18' and longitudes 94° 45' to 95° 0', covering about 10 square miles (6400 acres). The Mon Chaung is the northern boundary and the Sabwet Chaung is the southern boundary. (Figure - 1) The area north of latitude 18° 14' is a flat plain with average elevation of 140 ft above sea level covered by alluvium. The area between latitudes 18° 14' and 18° 10' is a fairly rugged terrain with average elevation of 250 ft covered by Miocene to Oligocene rocks.

---

<sup>1</sup> Dr, Associate professor, Geology Department, Mandalay University, E-mail: tinmyintoo12@gmail.com

<sup>2</sup> Dr, Professor, Applied Geology Department, University of Yangon

<sup>3</sup> Dr, Associate professor, Applied Geology Department, University of Yangon

<sup>4</sup> President Myanmar Association of Petroleum Geologist

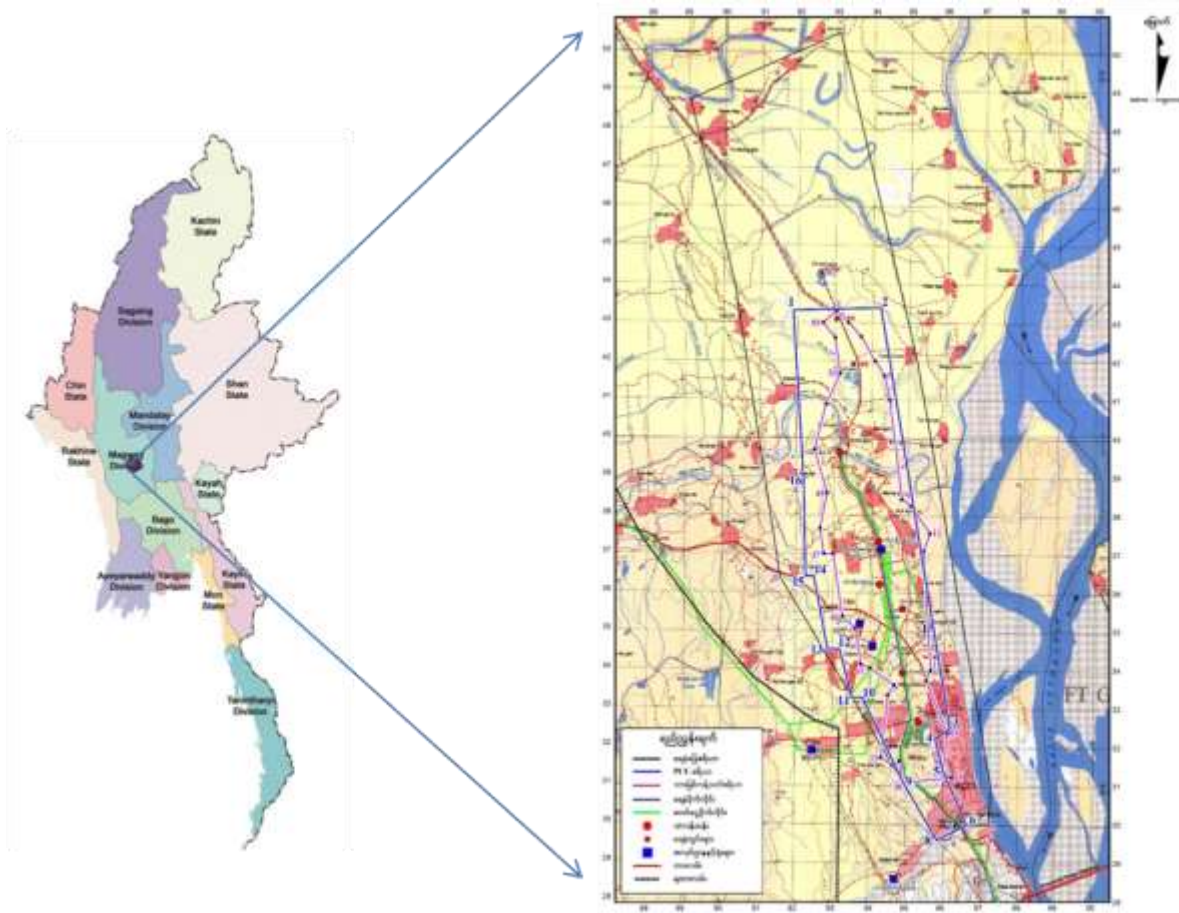


**Figure 1** Location map of Mann anticline

**Geological Interpretation**

The Mann anticline occupies northern crestal area and northern plunging area of the Minbu anticline. The Minbu anticline is an asymmetrical, elongated anticline continuing from the Tagaing-Chaungtha structural trend through Peppi, Palanyon, and Htaukshabin to Minbu with the NNW-SSE trend. The Minbu-Taggaing- Chaungtha anticlinal structure trend is the first line of structure reference to the Salin Syncline developed on the east flank of Salin Basin (figure-2). The Sabwet Chaung fault located at the latitude 18° 10' divided Minbu anticline into two anticlines namely Mann anticline and Htaukshabin anticline.

Mann anticline is a broad-crested, asymmetric, cross and crest ally faulted anticline bound to the east by the west hading thrust. The dips are as high as 70° on the west flank and rarely exceed 30° on the east flank. The nose of the anticline and most of the crestal area have dips in the range 10° -15°. Geological map of the Mann anticline is shown in figure(2).

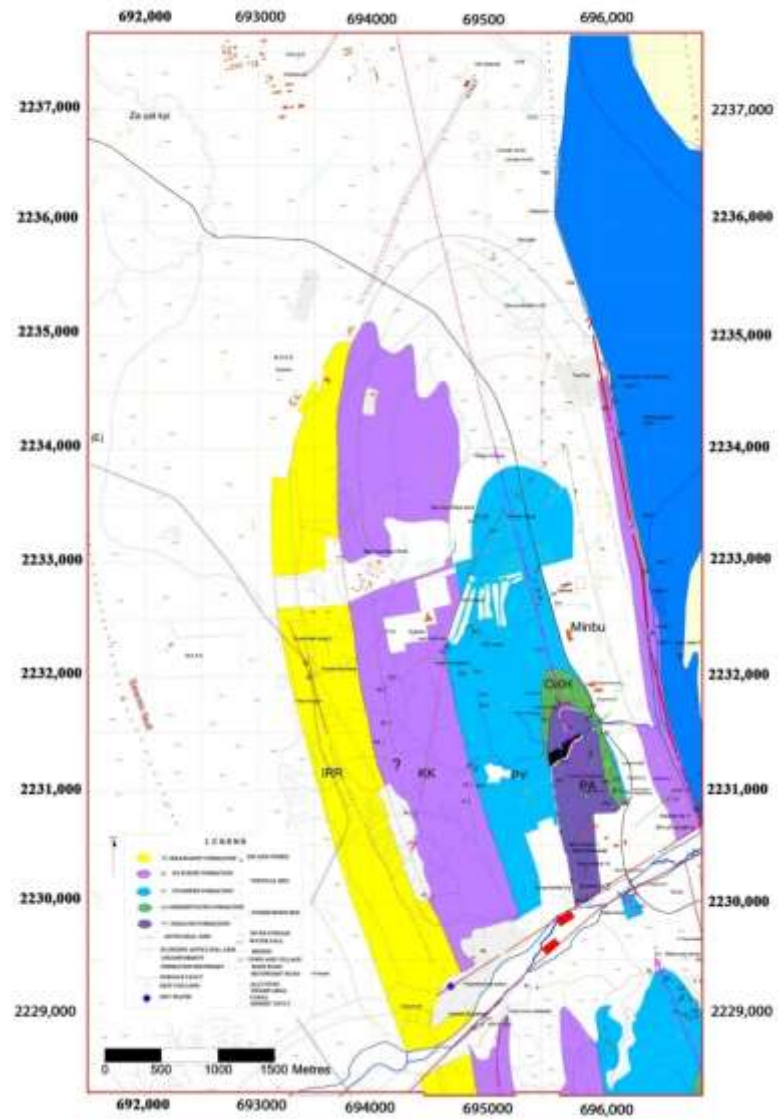


**Figure 2** Geological map of Mann anticline(source: MPRL E&P )

The tectonic map of the east flank of Salin basin including Minbu anticline is display in figure 3.

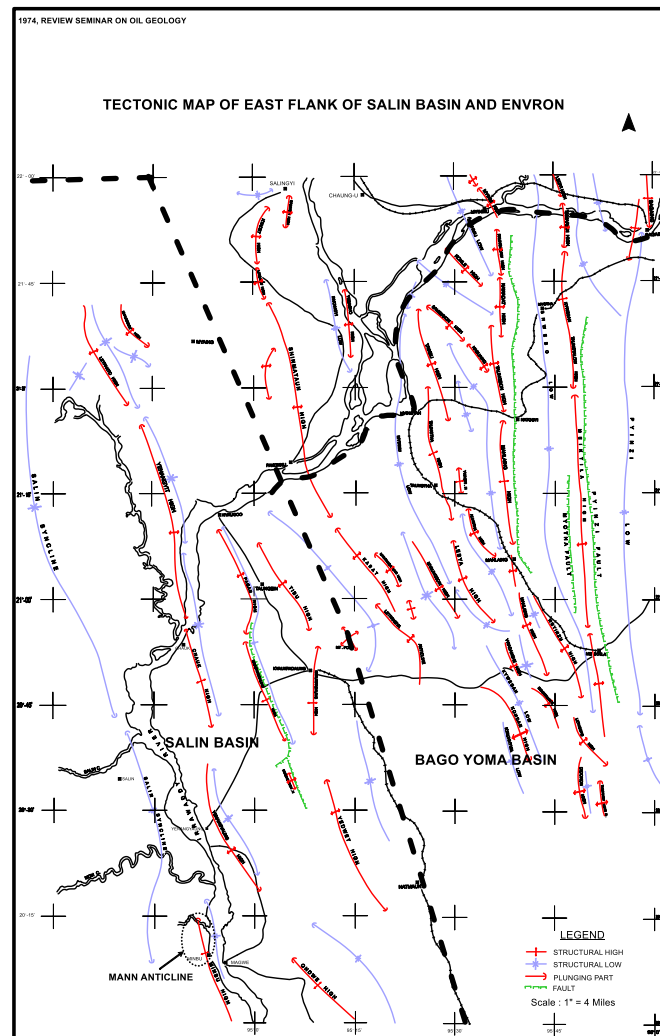


**Figure 3** Tectonic map of east flank of Salin Basin.(source : POI, 1966)

### Gravity Interpretation

In 1966, a detailed gravity survey using Worden Gravity meter 753 was conducted by the People's Oil Industry (POI) in the northern Minbu area covering an area of 64 square miles with a total of 171 gravity stations composing of two N-S lines and thirteen E-W lines. The gravity anomalies have a general NNW-SSE trend and three gravity low zones are separated by two gravity high zones (Minbu High and Paukkon High). Bouguer gravity profile indicate that gravity value increase towards the east, culminating over the Minbu gravity high and decrease toward the east of Minbu. (Figure 4 )

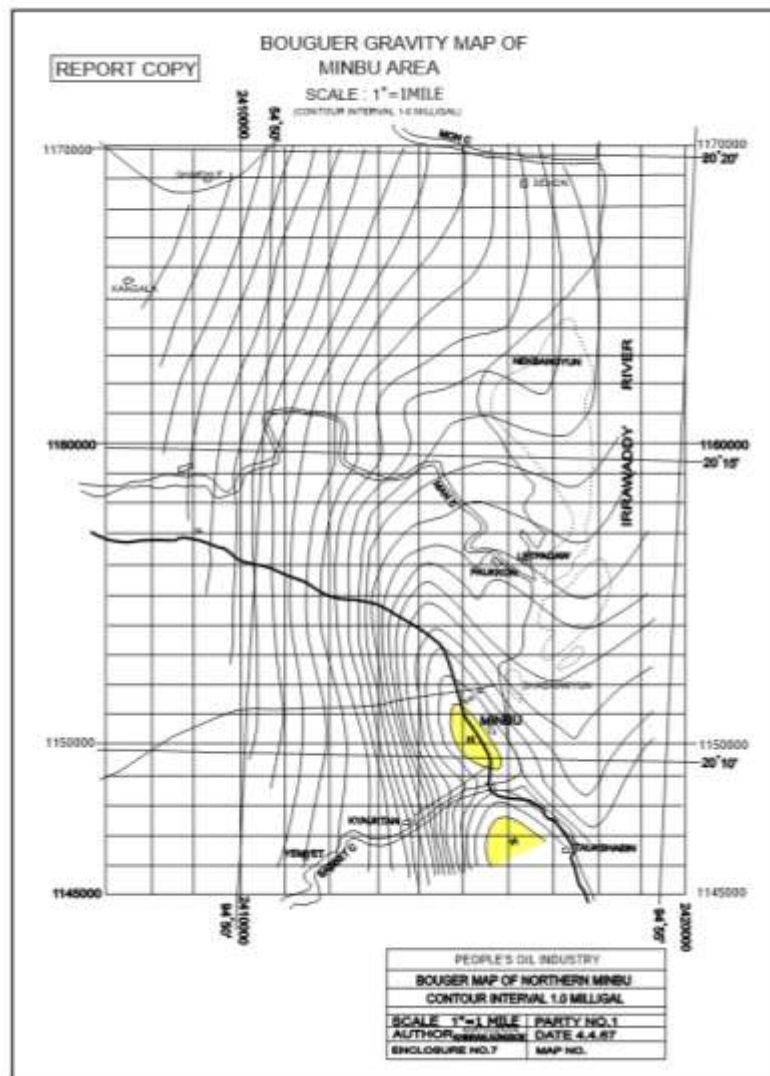


**Figure 4** Bouguer gravity map of Mann Anticline (source : People's Oil Industry, 1966)

The residual gravity profile shows that with the gentle gradient of 1 milligal/ mile the profile steepens abruptly at the middle part of the western side to 3 milligal/ mile up to highest part of at Minbu. Then the profile decreases again with a gradient of 2.2 milligal/mile and formed a minor culmination at the middle part of the eastern side at Paukkon high. And decreases again with same gradient to the eastern boundary of the survey area.

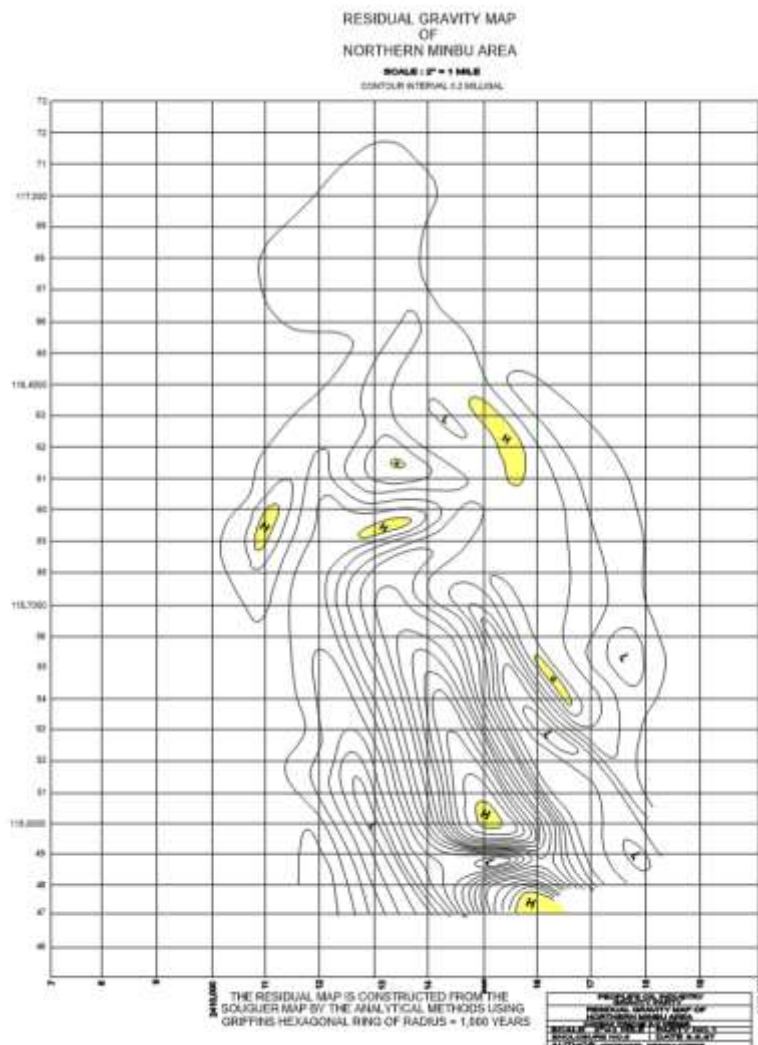


**Figure 5** Residual gravity map of northern Minbu area. ( Source: People’s Oil Industry, 1966)

From the result of the gravity survey, two anticlinal structures are recognised i.e., Mann Anticline and Paukkon Anticline. From the gravity profiles, the western flank of the Mann anticline is found to be more gentle than the east flank. The contours forming closures at the north of Minbu indicate that the northward plunge is still continues in the subsurface up to the latitude  $20^{\circ} 18'$  (about 8 miles further north of Shwelinban field). Two longitudinal faults are assumed to intersect the structure, one on the western and the other on the eastern limb. The fault zone on the eastern limb can possibly be occupied by a series of faults as assumed from the steep gradient in the bouguer map.

Two probable transverse faults are considered to exist also, the southern one at latitude  $20^{\circ} 10'$  coinciding with the course of Sabwet chaung indicated by the gravity contours forming a saddle, and the northern fault at the latitude  $20^{\circ} 15'$  suggested by the east west trending gravity low areas separating the high zone into two parts in residual map. The fault zone at Sabwet Chaung may possibly formed a passage through which the clay intermingled with water and gas escapes to the surface.

## New Interpretation

In the regional tectonic sense, the Salin Basin is a forearc sub-basin of the Central Myanmar Tertiary Belt and experienced two phases of deformation. The first phase is east-west compression which took place in upper Oligocene. The second phase is an inversion phase (transpressional deformation) induced by dextral strike slip movement of the Sagaing and Kabaw faults which initiated in early Pliocene and continues to Recent.

Since the Mann anticline is a northernmost part of the Minbu-Tagaing-Chungtha line of anticlinal structures which is a first line of structure developed on the east flank of Salin Basin, it had undergone above said two phases of structurations. The present day configuration of Mann anticline is an inversion anticline bounded by west hading reverse fault zone on the east flank and east hading antithetic fault on the west flank. (major fault in previous interpretation in figure-6)

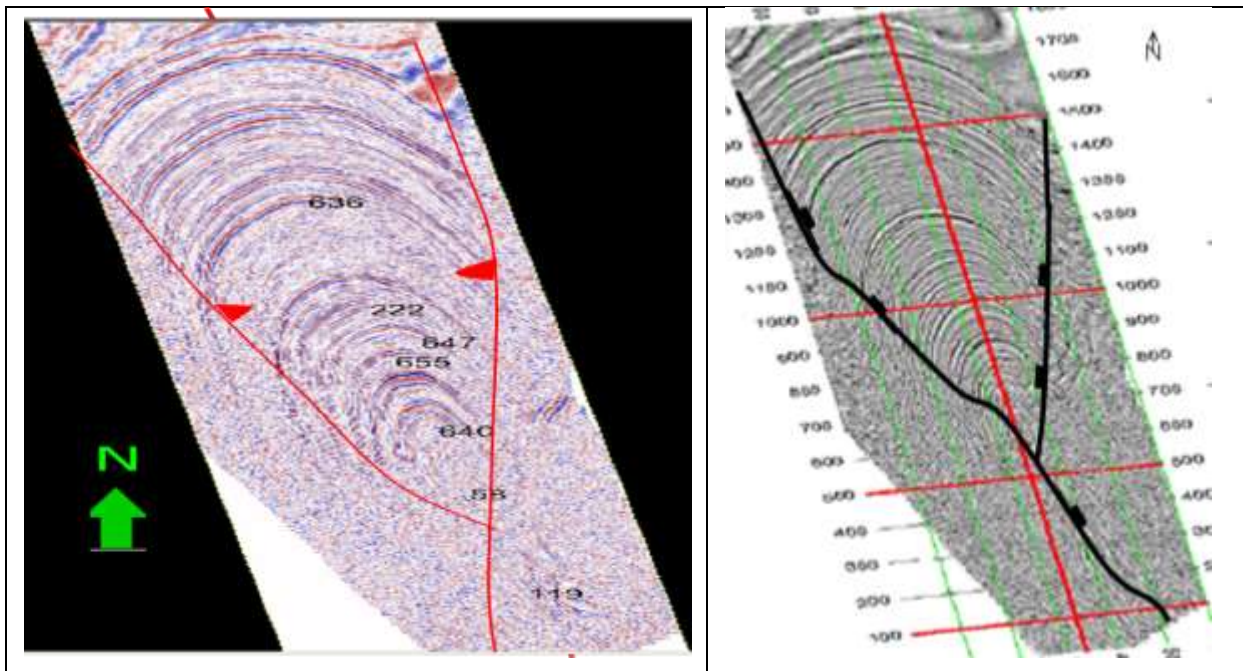


**Figure 6** Time slice section of Mann inversion anticline forming a positive flower shape.(Modified from MPRL E&P,2009)

## Development and Evolution of Mann Anticline

The integrated structural analysis using surface geology, gravity, well logs and seismic data shed the new light on development and evolution of the Mann anticline as follows:

1. The cyclic deposition of coarse grained and fine grained sediments took place from Paleocene to late Oligocene (Kabaw, Paungyi, Laungshe, Tilin, Tabyin, Pondaung, Yaw, Shwezetaung, Padaung and Lr. Okhmintaung formations), on the Mesozoic acoustic basement in the Salin Basin including Mann area.

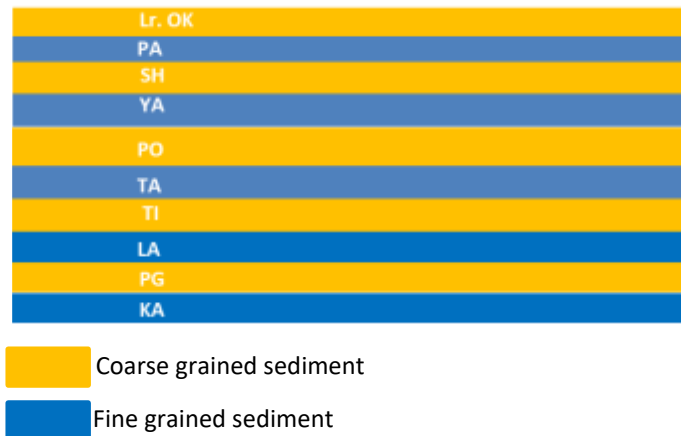


**Figure 7** Cyclic sedimentation of coarse and fine grained sediments in Salin Basin from Paleocene to upper Oligocene

2. During late Oligocene, the collision of India plate and Burma plate created east-west compression and formed proto Mann anticline. The subsequent tensional movement created NNW-SSE oblique longitudinal normal fault near the crestal part on the east flank .

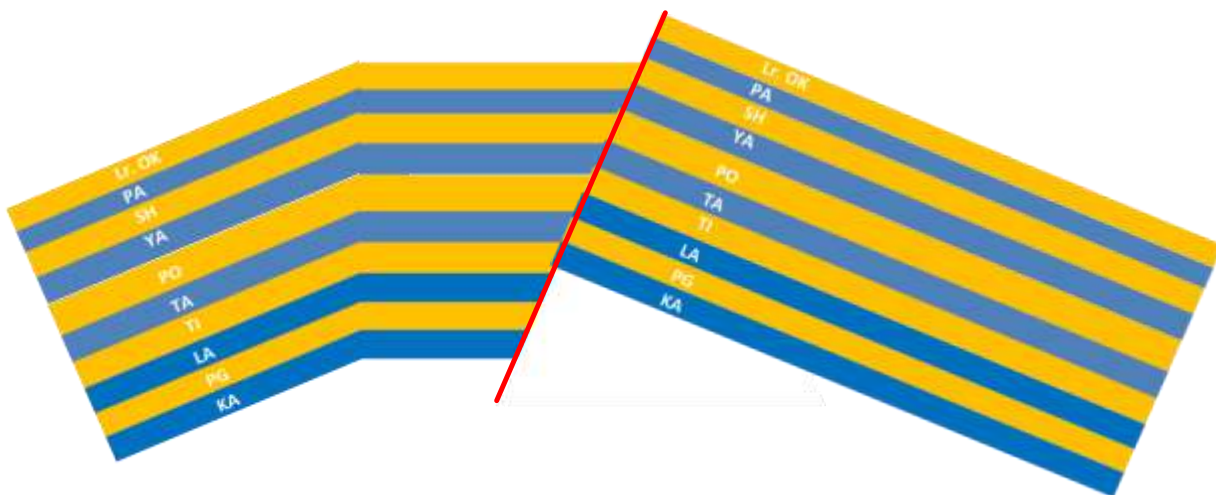


**Figure 8** Proto Mann Anticline with longitudinal normal fault in upper Oligocene time.

3. The Salin Basin subsided again and continued cyclic sedimentation from late Oligocene to upper Miocene (Pyawebwe, Kyaukkok, Obogon formations).
4. The terrestrial sediments ( Irrawaddian Fm) were deposited from upper Miocene to Pliocene.

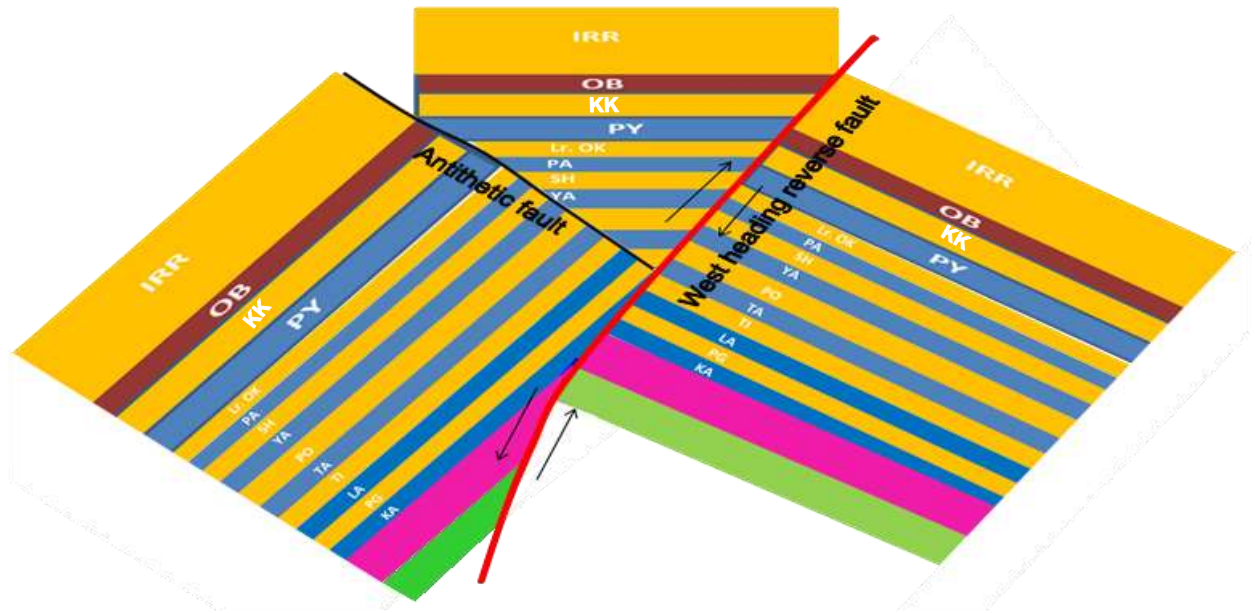


**Figure 9** Inversion of Mann Anticline during Pliocene to recent.

- 5 The inversion of the existing structures in Salin Basin initiated in early Pliocene and continues to recent. The present day structural configuration of Mann anticline is a result of this inversion phase. The evidence of inversion anticline is that the west heading reverse fault becomes normal fault in the deeper part. (Figure 14 & 15)

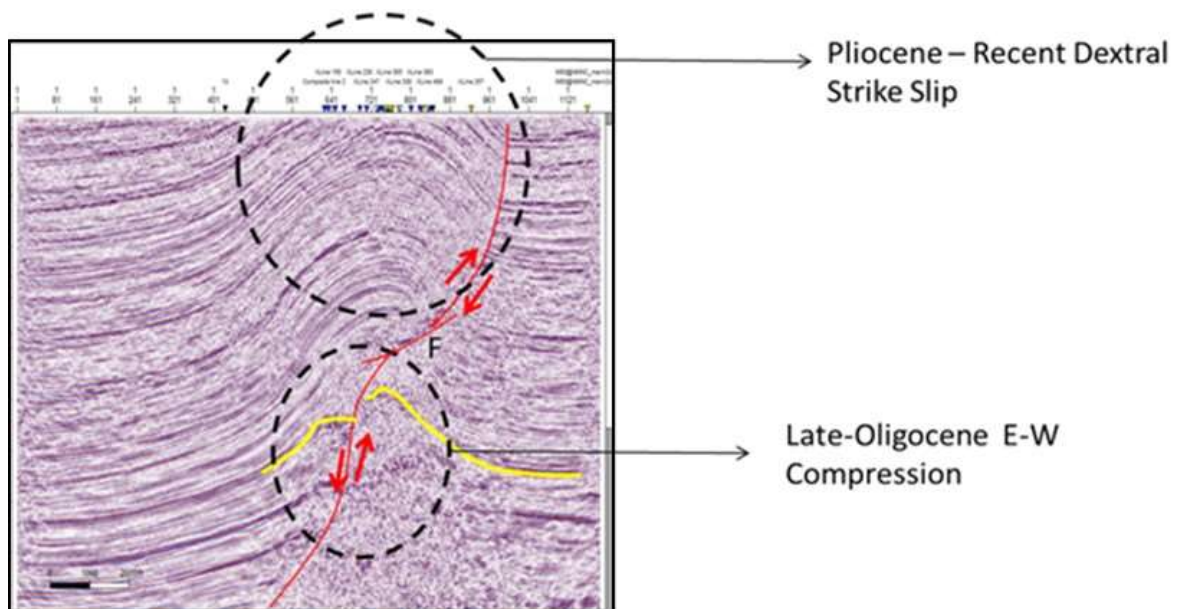


**Figure 10** Structure evolution of Mann Anticline. (modified from MPRL E&P )

### Conclusion

The 3D seismic images of the northern part of Mann anticline clearly indicate that Mann anticline is an positive flower shape inversion anticline. In the southern part it becomes tight and complex due to development of many syn-inversion antithetic faults. The present day oblique longitudinal normal fault “B” which rooted to basement as per gravity data interpretation strongly support the idea on formation of NNW-SSE longitudinal normal fault ( west heading major reverse

fault of present day) in proto-Mann anticline. The mud volcanoes in the southern part especially at Nagapwet Taung are formed by the seepages of clay intermingled with water and gas along the fractures which may possibly caused by active strike slip movement. Further high resolution 4D seismic survey or 4C seismic survey will improve understanding on structural geology of Mann anticline and the whole basin.

### **Acknowledgements**

We wish to express my special thanks to Professor Dr. Day Wa Aung Professor and Head, Department of Geology, and University of Yangon, U Lynn Myint President, Myanmar Association of Petroleum Geologist (MAPG) and MPRL E&P for their advices, comments and great encouragement. This paper could not be completed without the helpful hands and willing help from all staff members from Geology Department, University of Yangon.

### **References**

- Htut, T., and T. Wynn, (1979), Geology of Chaungtha area: MyanmaOil Corporation Report, T. Ht. 7, T. Wy. 2.
- Lawn, N., (1986), Report on Ondwe structure: Myanma OilCorporation Report N.L. (13).
- Lawn, N., and A. Nyunt, (1979), Geological report on Yedwet struc-ture: Myanma Oil Corporation Report N.L.2, A.N.5.
- Lofting, M. J. W., (1964), Prospects and oil potential of the Yinaingstructure: Myanma Oil Corporation Report M.J.W.L.8.
- Soe, K., and T. Myint, (1976), Geological report on Gwegyo-Ngashandaung-Nyaunggon areas: Myanma Oil CorporationReport K.S.2.T.Mt.2.
- Tun, P., (1972), Geology of Tagaing Structure: Myanma OilCorporation Report P.T. (5).
- Unpublished report of Ministry of Oil and Gas (MOGE) (1966).
- Unpublished report of MPRL E&P.(2009).

## MIDDLE SHELF ZONE FORAMINIFERAS OCCURRED IN THE SEDIMENTS OF NORTHERN PART OF THE ANDAMAN SEA

Ko Yi Hla<sup>1</sup>, Day Wa Aung<sup>2</sup>, Tun Tun Zaw<sup>3</sup>

### Abstract

The sample collection sites are located in the northern part of the Andaman sea. Ayeyarwady continental shelf is a part of Andaman Sea. There are five zones of Ayeyarwady continental shelf are recognized; Near shore zone, Inner shelf zone, Middle shelf zone, Outer shelf zone and Upper slope zone. Very low to high diversity of twenty four foraminiferal species are found in the Middle shelf zone environment. Faunal distribution and population are different in the study area and distinct genera of foraminiferas are observed in specific condition. It is noteworthy that faunal diversity and species diversity are encountered in different areas. By studying of the foraminiferas, *Osangularia bengalensis* species are dominant in the Middle shelf zone environment.

**Keywords:** Ayeyarwady continental shelf, Middle shelf zone, foraminifera, *Osangularia bengalensis*.

### Introduction

#### Location and size of the study area

The study area is located in northern Andaman Sea. It is bounded by latitudes 13° 25' N and 15° 40' N and longitudes 93° 15' E and 97° 45' E, occupying the south and southwest oceanic area of Myanmar. The area extends N-S in 225 km and E-W in 450 km respectively. The area extent of study area is approximately 101250 km<sup>2</sup>. The study area is bounded by southern part of Ayeyarwady delta and Gulf of Martaban, and western part of Tanintharyi coast. Therefore, the area occupies the oceanic area around the Myanmar coast of northern Andaman Sea. The location map and sample collection sites of the study area are shown in figure (1).

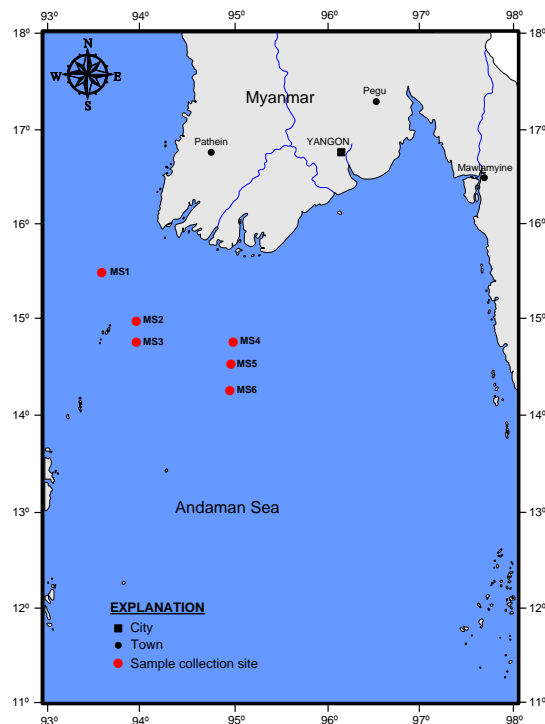


**Figure 1** Location map of the study area with sample collection sites.

<sup>1</sup> Dr, Professor, Department of Geology, Mawlamyine University

<sup>2</sup> Dr, Professor and Head, Department of Geology, University of Yangon

<sup>3</sup> Dr, Associate Professor, Department of Geology, Mawlamyine University

## Materials and methods of study

### Data Source

The 125 specimens of surface-sediment were collected during the India-Myanmar joint Oceanographic research programme in April - May 2002. The located specimens were acquired from the stations along the geophysical line (Fig.1). The research is mainly focused on (10) specimens of the area.

### Field method

In April-May 2002, India and Myanmar have organized a joint multidisciplinary oceanographic cruise to study oceanographic and geological aspects of the northern Andaman Sea of Myanmar waters, particularly in the Bay of Bengal, off the Rakhine coast, in the Ayeyarwady continental shelf area, including the Gulf of Martaban, and off the Taninthayi coast and offshore. The acquired specimens were carefully packed, labeled and stored in a cold storage to minimize the decaying. The spacing between sampling stations are generally 25 km.

### Laboratory Method

The dried samples were dissolved in a quarter of gallons of water containing a little amount washing soda (soda ash) and a small amount of detergent. The samples were left for a day. The samples were completely disintegrated after a day. The samples soaked with water were washed over the sieve with the opening size of mesh 200, and dried in an aluminum bowl under the temperature of 60°C, especially within an electric oven. The dried samples are called "Residues". The dried sieving of the residue was done over brass sieves with the openings of mesh 30, 60, 90 and 100. The fractions obtained by dry sieving were examined under a binocular microscope. The foraminiferal specimens were extracted and picked up by means of soft sable hair brush with a size of 0.00. The foraminiferal specimens were identified with the literatures and manuals by Cushman (1959), Le Roy (1941, 1944, 1964), Bermudez (1949), Grahan and Militante (1959), Postuma (1971), Barker (1960), Cushman, Told and Bronnimanr (1957), and finally Loeblich and Tappen (1985). A detailed description of each species was taxonomically made with revelant taxonomic references. The distribution of each species was determined in terms of frequency symbols, such as VR for very rare occurrence (1 specimen), R for rare occurrence (2-5 specimens), C for common occurrence (6-10 specimens) and A for abundant occurrence (11-15 specimens) and F for flooded occurrence (> 15 specimens).

## The Study of Recent Foraminifera

### Distribution of Foraminiferal Species

There is a very large continental shelf, which is situated due south of the Ayeyarwady Delta Division, according to the figure by Curry (*et al*, 2003). No classification of the marine has been defined based on bathymetry as yet. The author is to follow the classification of marine environments established and defined by Hedgpeth (1957), Tipsword (*et al*, 1966) (Fig. 2), and Ingle (1980) (Fig. 3) from the model of the Gulf of Mexico. Accordingly, the seafloor from the low tide to 20 meters of depth is termed as "Inner shelf" ( Inner Neritic), the depth between 20 meters and 100 meters is called Middle shelf and the depth between 100 meters and 200 meters is the area of continental shelf, i.e Outer shelf (Outer Neritic). The depth beyond 200 meters to 500 meters is named as Upper slope (Upper Bathyal). By the occurrence of distinct species, there are (5) marine zones, which are nearly fitted with the depth zones, as adopted by Hedgpeth (1957), Tipsword (1966), and Ingle (1950) (Table 1).

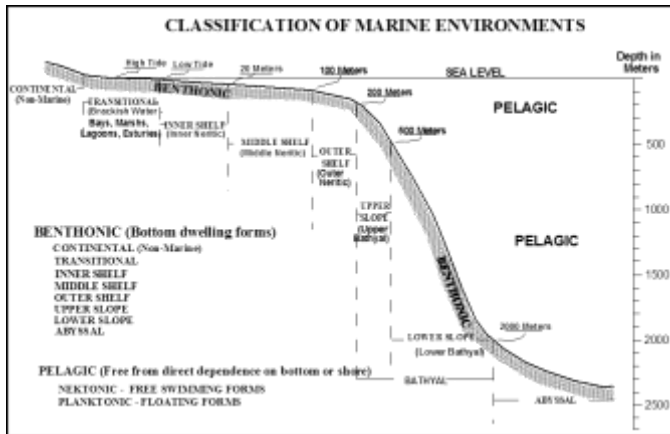
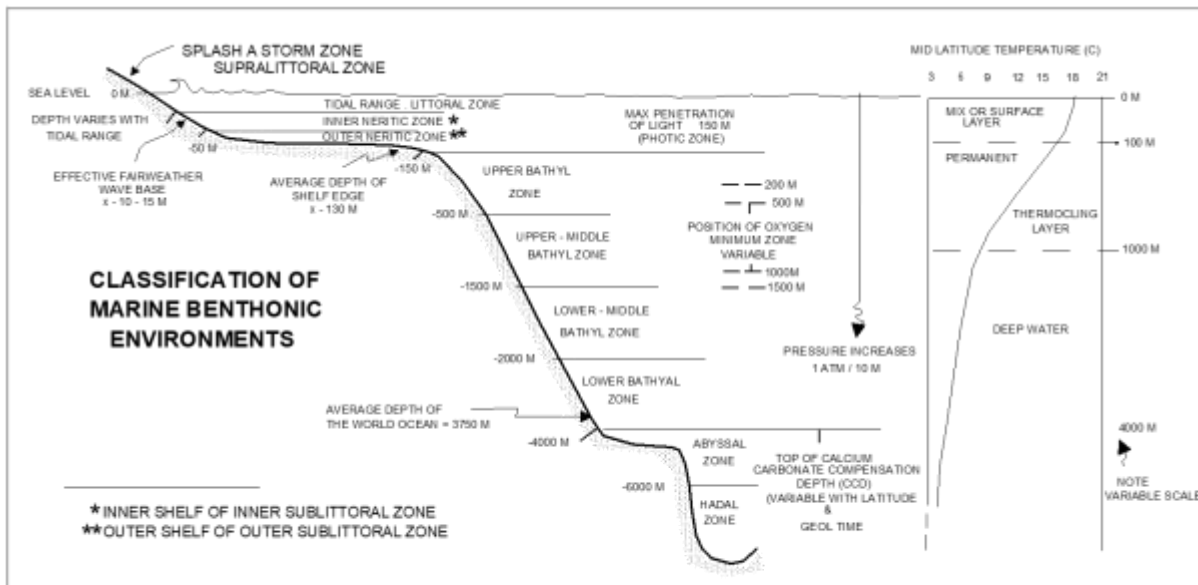


**Table 1** The classification of the Ayeyarwady continental shelf and slope

| Names             | Depths            |
|-------------------|-------------------|
| Near shore zone   | 16-25 meters      |
| Inner shelf zone  | 27-32 meters      |
| Middle shelf zone | 50-90 meters      |
| Outer shelf zone  | beyond 105 meters |
| Upper slope zone  | 290-600 meters    |

**Figure 2** Geographic zonation of Gulf of Mexico (After H.L. Tipsword et al., 1966)



Classification of benthonic marine environments in terms of depth and positions of critical oceanographic boundaries of transitional zones in the modern world ocean. Note that water depths are given in meters. This classification is a modification of that presented by Hedgpeth (1957): from Ingle (1975a).

**Figure 3** Bathymetric zonation of environments (After J.C. Ingle, 1980)

### Middle shelf zone

The middle shelf zone is in the middle part of the main shelf. The inner shelf is in the north, and the outer shelf is in the south. Therefore, this zone is characterized by more numbers of total numbers of species, as shown by the specific diversity, which ranges from 35 to 43 (i.e from sample no. 28 to 27 or from sample no. 90, 33, 34). The depths range from 50 meters to 90 meters. There are 24 foraminiferal species, which have been recorded only from the middle shelf. *Sigmolopsis schlumbergeri* and *Globorotalia menardii cultrata* are very rare in population. Abundant species are *Rotalia annectens*, *Globorotalia tumida tumida*, *Pulleniatina obliquiloculina*, *Osangularia bengalensis*, *Globigerinodes quadrilobatus*, and *Hastigerina siphonifera*. *Globorotalia tumida tumida* are flooded occurrence in the study area. The diversity of foraminiferas species are ranges from very rare to abundant in the middle shelf zone environment (Figs. 4 to 9).

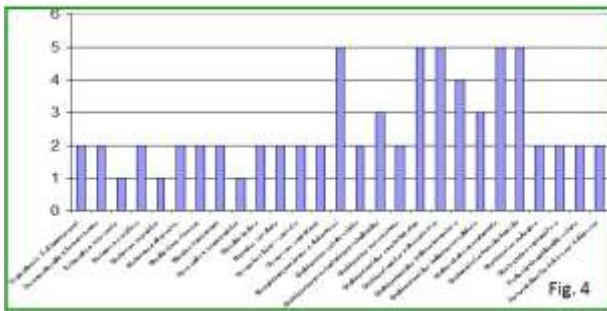


Figure 4 High diversity of foraminifers in MS1

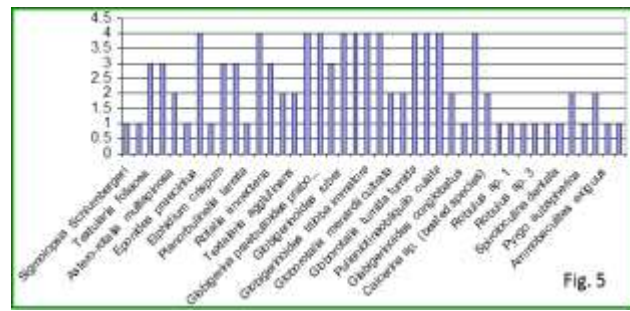


Figure 5 Very high diversity of foraminifers in MS 3

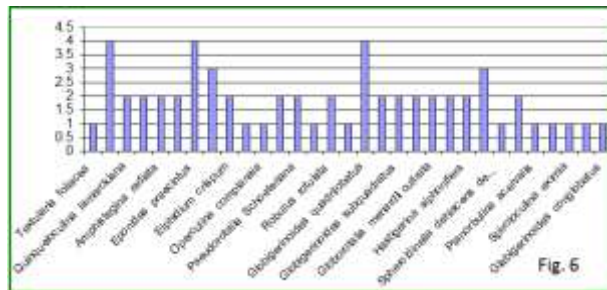


Figure 6 Very high diversity of foraminifers in MS2

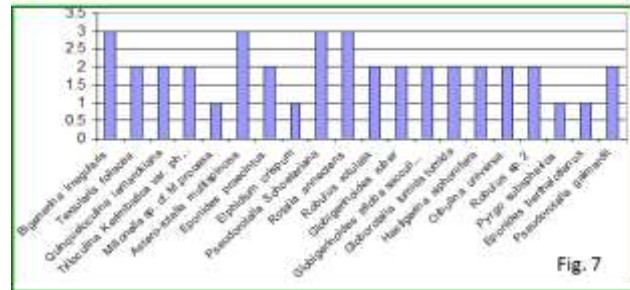


Figure 7 High diversity of foraminifers in MS 4

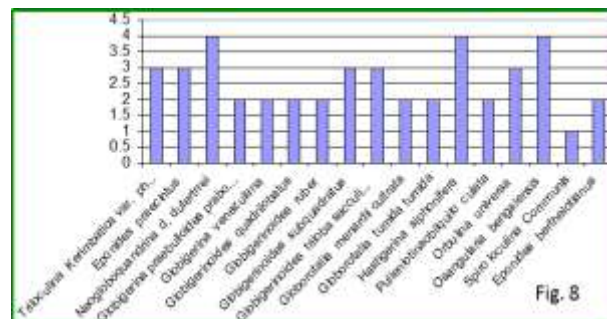


Figure 8 High diversity of foraminifers in MS 6

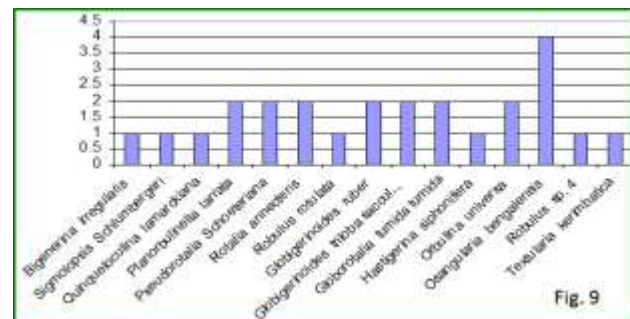


Figure 9 High diversity of foraminifers in MS 5

**Systematic Description**

*Bigenerina irregularis* Phleger & Parker  
*Bigerina irregularis* Phleger and Parker, -Bandy,  
 1954 p.135, pl.29, fig. 8-9

Test very small, chambers arranged biserially initially, later chamber rounded, uniserially; wall arenaceous, coarse grains: sutures, distinct, depressed. horizontally; aperture, a little rounded opening, terminal in position. Dimension is 0.25 mm in length and 0.10 mm in width. This species has been recorded from MS 4 and 5, where it occurs from very rare to commonly.

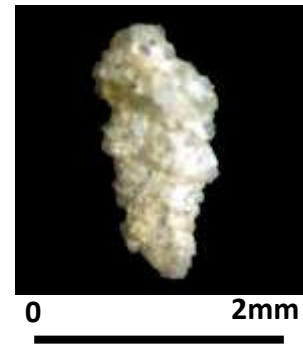


0 2mm

***Textularia foliacea***, Heron-Allen-Earland

*Textularia foliacea*, Heron-Allen-Earland Graham & Militante, 1959, p.28, pl.2, figs. 4a-b

Test free, medium to small, about three times as long as broad, the apical end pointed, the test becoming wider and wider in the apertural end, periphery slightly rectangular, angular and sharp, slightly truncate on both sides of the test, chambers arranged biserially throughout; wall arenaceous with coarse grains; suture distinct, wide and depressed; aperture slight slit, narrow at the base of the last chamber. Dimension is 0.75 mm in length and 0.45 mm in width. This species has been recorded from MS 2, 3 and 4, where it occurs very



***Sigmoilina schlumbergeri*** (Silverstri)

*Sigmoilina schumbergeri* (Silverstri)-Barker, 1960 p.16, pl.8 fig. 1

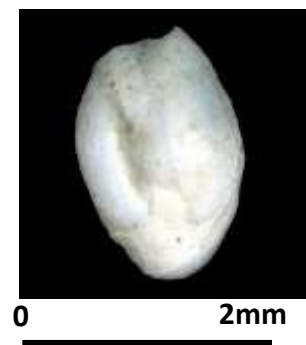
Test small to medium in size, flattened shape, chambers arranged following the Spiroloculina type, ie, at angle of Quinqueloculine like finally spiroloculine type, wall typically arenaceous, with fine and medium grains, periphery rounded, thin; suture, distinct nearly in final chamber arrangement; aperture like spiroloculina type with phialine type, bottle shape with defined lip. Dimension is 0.25 mm in length and 0.14 mm in width. This species has been recorded from MS 1 and 3, where it occurs rarely to very rarely. Preservation is fairly good.



***Quinqueloculina lamarckiana*** d' Orbigny

*Quinqueloculina lamarckiana* d' Orbigny Todd & Bronnimann, 1957, p.27, pl.3, figs. 12 a-b

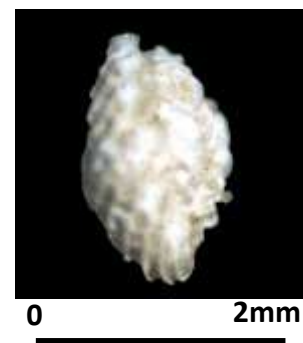
Test free, small to medium, nearly as broad as long, test section nearly triangular, the angles subacute, not carinate, chambers distinct, arranged in a quinqueline type; wall calcareous smooth and shining; aperture end of two chamber slightly extended forming an elliptical neck without defined lip, but a narrow elongate tooth. Dimension is 0.55 mm in length and 0.50 mm in width. This species has a wide distribution, occurring in MS 1, 2, 3, 4 and 5, from rarely to commonly.



***Triloculina kerimbatica*** Heron Allen & Earland var. *reticulostrata*.

*Triloculina kerimbatica* Philippinensis Cushman var.3 Graham & Militante, p.55, pl.8, figs. 13

Test free, small to medium in size, oblong shaped, as long as broad, generally triangular in test section, chambers arranged in typically quinqueloculine type, periphery subrounded, with strong, deep strips, and ribs all around the chambers; wall calcareous, porcellaneous milky; suture, indistinct; aperture with a narrow neck, and a tooth. Dimension is 0.65 mm in length and 0.55 mm in width. This species has been recorded from MS 2, 5 and 6, where it occurs rare to commonly.



***Pyrgo subspherica*** d'Orbigny

*Pyrgo subspherica* d'Orbigny, - Le Roy,  
1964, p. 21, pl.12, figs. 34-35

Test small, spherical shape, with carina, strongly inflated into a ball like test, chambers, spherical, arranged biserially, wall calcareous, porcellaneous, vitreous, shiny, with a strong sharp carina; suture distinct between two chambers, all of which inflated like a ball; aperture, an elongated, curved, bent opening with a bifid tooth. Dimension is 0.25 mm in length and width. This species has been recorded from MS 2 and 4, where it occurs very rarely in the main shelf.

***Robulus rotulatus*** (Lamarck) = sp.1

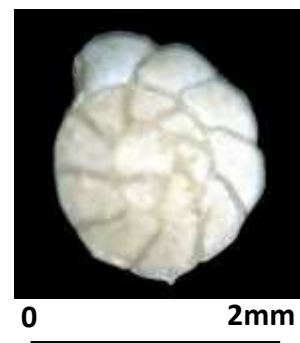
*Robulus rotulatus* (Lamarck) Bermudez,  
1949 p.130, pl. 8, figs. 3-4

Test free, small to medium in size, chamber shape lenticulate, compressed from the periphery side, and inflated in the umbo-centre, about 5-6 chambers, plamspirally coiled, involute, periphery subacute, without a keel, wall calcareous, hyaline, shining suture curved, and slightly bent towards earlier chambers, with a small umbo, which is slightly rounded with shell material; aperture, peripheral, radiate. Dimension is 0.40 mm in length and 0.38 mm in width. This species has been recorded from MS 2, 4 and 5, where it occurs rarely to very rarely in the main shelf.

***Rotalia annectens*** Parker & Jones

*Ammonia annetens* (Parker & Jones)-Huang,  
1964 p. 50, pl. 21, fig. 3, figs. 1-3, Text fig. 3

Test free, small to large, biconvex, chambers distinct 16 to 17 in number, arranged trochospirally, with a low height, size increasing gradually and added, wall calcareous, smooth, and ornamented with cannas, sutures distinct, raised or devoted, sometimes beaded, limbate, ventrally, limbate, periphery slightly lobulate, acute and carinate, aperture interiomarginal, placed between the periphery and umbilicus, without any spines. Dimension is 0.50 mm in length and 0.37 mm in width. This species has been widely distribution, recorded from MS 3, 4 and 5 in the Main Shelf.

***Pseudorotalia schroeteriana schroeteriana*** (Parker & Jones)

*Pseudorotalia schroeteriana scliroeteriana* (Parker & Jones),  
Huang, 1964, 10(1), p. 60, pl. 1, fig. 12

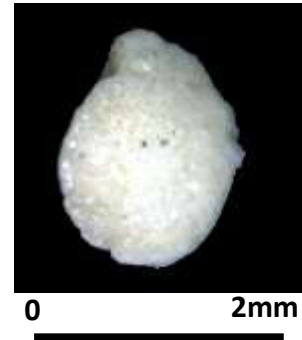
Test free, small to medium, some large, dorsal side flat, and ventral side very curved, chambers about 18 coiled trochospirally with a very high, 12 chambers in the last whorl periphery very acute, with thin keel, wall calcareous, hyaline, vitreous, rough; suture, strongly raised and beaded on the dorsal side, some fused in the earlier chambers, suture on ventral side strongly limbate pores or keels arranged on both sides of limbate suture, umbilical plug forms a rounded ball like beads 8 in number; aperture a slit, interiomarginal, between the periphery and umbilicus. Dimension is 0.82 mm in length and 0.80 mm in width. This species has a wide distribution, recorded from the sample MS 2, 3, 4 and 5, where it occurs very rarely to abundantly.



***Osangularia bengalensis*** d' Orbigny

*Osangularia bengalensis* d' Orbigny-Le Roy,  
1964, p. 38, pl. 9, figs. 32-33

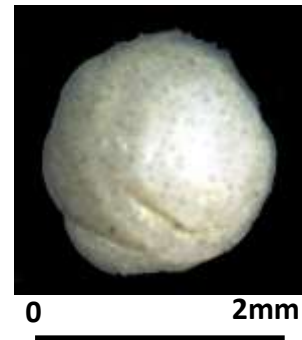
Test free, small to medium in size, dorsal side slightly flat or slightly convex, ventral side convex to slightly conical, chambers, distinct, thick, 12-15 chamber coiled in a trochospirally, with a low spire, 8 chambers in the last whorls, periphery thick, forming a thick carina, wall calcareous, porcellaneous in most of specimens with full and crowded small beads all over the dorsal side; suture, distinct, sometimes, flush with surface: aperture a narrow slit, at the base of the last chamber. Dimension is 0.62 mm in length and 0.59 mm in width. This species has a wide distribution, recorded from MS 2, 5 and 6, where it occurs very abundantly in the main shelf.



***Eponides berthelotiana*** d' Orbigny

*Eponides berthelotiana* d' Orbigny-Barker.  
1960, p. 218, pl. 105, figs.1, Le Roy, 1944, p. 39, pl. 2, figs. 15-17.

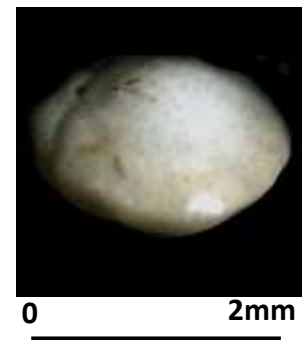
Test free, small ventral flat ad dorsal side typically conical, 20 chambers, distinct, arranged trochospirally with a high spire, 8 chambers in the last whorl, periphery, sub-acute, wall calcareous, porcellaneous, sometimes shiny; suture, very thick, depressed, on the dorsal side, sometimes, thick, and ventral side thick, straight, radiate from the umbilical centre, aperture at the base of the last chamber. Dimension is 0.35 mm in length and 0.30 mm in width. This species has been recorded from MS 3, 4 and 6 in the main shelf, where it occurs fairly rare.



***Eponides praecintus*** (Karrer)

*Eponides praecintus* (Karrer)- Le Roy, 1944  
p. 34, pl. 2, figs. 31-33

Test free, small to medium in size, biconvex, ventrally and dorsally nearly flat, ventrally conical or convex, chambers numerous 12 to 14m in number, arranged trochospirally with a low height periphery sub-acute, not rounded; wall calcareous coarsely perforate flush with surface, suture slightly limbate dorsally curved back to earlier ones, spiral suture distinct, raised, quite visible aperture a slit at the base of the last chamber, with a medium sized umbilical plug, which is smooth and rounded. Dimension is 0.68 mm in length and 0.65 mm in width. This species has a wide distribution, recorded from MS 2, 3, 4 and 6, where it occurs rare to abundantly.



***Asterorotalia multispinosa*** (Namura)

*Asterorotalia multispinosa* (Namura)-Huang,  
1964, p. 58, pl. 2, fig. 4

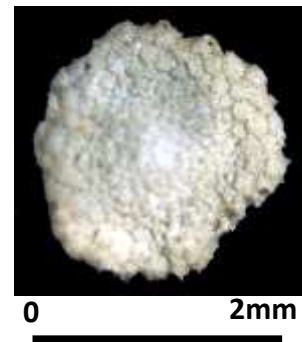
Test free, small to medium, chambers distinct, about 11 to 15 chambers arranged trochospirally with a low height, periphery very acute, bearing short spines from each last chambers, the shape is rounded, not in triangular shapes; wall calcareous, smooth hyaline, shiny, suture distinct, depressed on dorsal side limbate on the ventral sides; aperture, interiomarginal, umbilical. Dimension is 0.50 mm in length and 0.45 mm in width. This species has been recorded from MS 2 and 4, where it occurs rare to commonly.



***Planorbulinella larvata* (Parker & Jones)**

*Planorbulinella larvata* (Parker & Jones) Graham & Militante, 1959, p. 118, pl. 19, figs. 17a-b

Test free, small to medium in size, disc-shaped, rounded, with a lobulate periphery formed by interspaces between the chambers of the last formed whorl and whose surface are wholly covered with beaded like cells, surrounded regularly a thick periphery, wall rough with assorted materials; surface around the periphery, aperture, not seen. Dimension is 0.30 mm in length and 0.28 mm in width. This species has been recorded from MS 2, 3 and 5, where it occurs rare to very rarely.

***Orbulina universa* d' Orbigny**

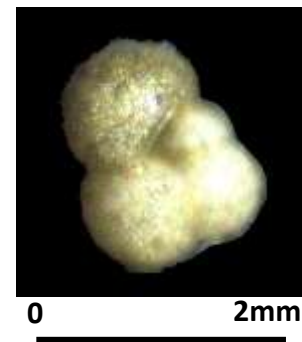
*Orbulina universa* d' Orbigny-Blow, 1959, p. 200, pl. 13, fig. 5

Test free, spherical, and composed of single chamber, primary developed from *Globigerinoides triloba*, from stage to *Orbulina universa*; aperture are over the all surface; well calcareous, perforate, radial in structure. Dimension is 0.55 mm in diameter. It has a wide distribution recorded from MS 2, 3, 4, 5 and 6, where it is occurring rarely to commonly.

***Globigerina preabulloides preabulloides*. Blow**

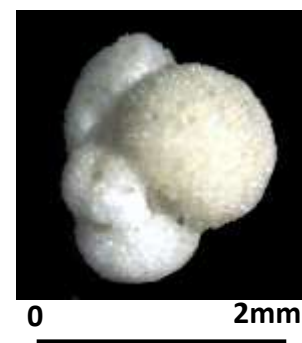
*Globigerina preabulloides preabulloides*. Blow Bolli and Saunders, 1985, p. 198, figs. 13-14a-c

Text free, typically trochospiral, of 2½ whorls, a chambers in the last whorl, chambers are spherical, to radial in structure; wall calcareous, finely perforate, and pitted periphery strongly lobulate; suture depressed, radial; aperture semicircular, a large opening, interior marginal, umbilical. Dimension is 0.30 mm in diameter and 0.25 mm in minimum. This species has been recorded from MS 1, 3 and 6, where it occurs rare to abundantly.

***Globigerinodes triloba sacculifera* (Brady)**

*Globigerinodes triloba sacculifera* (Brady) Bolli, 1957, p.113, pl.25, figs. 5a-c; Bolli & Saunders, 1985, p. 196, Figs. 16a-b

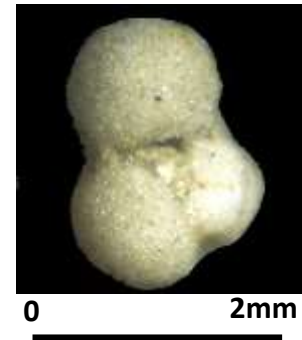
Test free, large, typically trochospirally, chambers, distinct, earlier chambers slightly globular, to ovate; later slightly elongate about 10 to 12 coiled into two whorls trochospirally, 4 chambers, in the last whorl, the last chamber larger, sac like shaped, surface perforate and pitted; wall calcareous, primary aperture, on arched, umbilical, supplementary apertures, placed between the last three chambers, sutural in position. Maximum diameter is 0.60 mm and minimum is 0.45 mm. This species have a very wide distribution, recorded from MS 1 to 6, where it occurs rare to commonly in the main shelf.



***Globigerinodes quadrilobatus*** d'Orbigny

*Globigerinodes quadrilobatus* d'Orbigny-Bolli and Saunders, 1985, p. 193, fig. 20-17

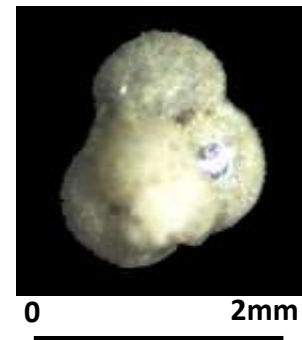
Test free, medium to large typically trochospirally globular, chamber globular, slightly ovate, 10 to 12 chambers arranged trochospirally 4 the chambers in the last whorl, lobulate; wall calcareous, perforate, and pitted; suture radial on both dorsal and ventral side, the primary aperture an arched opening interiomarginal, umbilical, supplementary aperture slightly wide placed between three last chambers. Maximum diameter is 0.50 mm and minimum is 0.49 mm. This species has very wide distribution, recorded from MS 2, 3, 4, 5 and 6, where it occurs rare to abundantly.



***Globigerinodes rubra*** d'Orbigny

*Globigerinodes rubra* d'Orbigny Bolli, 1957, p.113 pl.25, figs 9a-c; Bolli and Saunders, 1985, p. 192, figs. 20-1-2

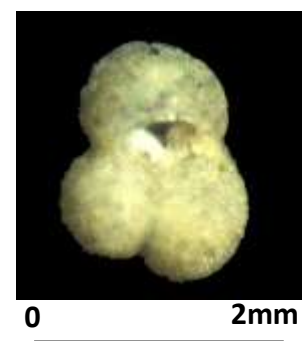
Test free, small to medium in size, typically trochospiral chambers globular to ovate, about 10 arranged in a very high trochospiral of 2½ whorls, the last whorl contains three chambers; wall calcareous, finely perforate, smooth, sometimes surface hispid; suture distinct, depressed, and radial, primary aperture opening to umbilicus, smaller supplementary apertures on the spiral side, one or more apertures confined to the chambers and two other near chambers. Maximum diameter is 0.70 mm and minimum is 0.35 mm. This species has a very wide distribution, recorded from MS 2, 3, 4, 5 and 6, where it occurs rare to abundantly.



***Globigerinodes subquadratus*** Bronnimann

*Globigerinodes subquadratus* Bronnimann, Bolli & Saunders, 1985, p. 192, fig. 20-6

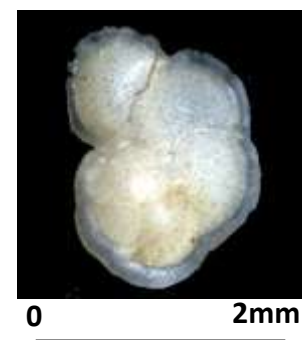
Test free, small in size, typically trochospiral, globular chambers, about 10 arranged in a tightly trochogural, only three chambers in the last whorl, wall calcareous, smooth, very finely perforate, suture distinct, radial, one primary aperture, a rounded opening placed at the junction of the last chamber and other penultimate chambers, supplementary aperture, not distinct. Dimension is 0.28 mm in maximum and 0.20 mm in minimum diameter. This species has been recorded from MS 2, 3, 4 and 6, where it occurs commonly to abundantly in the main shelf area.



***Globorotalia tumida tumida*** (Brady)

*Globorotalia tumida tumida* (Brady)- Bolli & Saunders, 1985, p. 227, figs. 33.8; 34-11-13

Test free, medium to large, biconvex, compared with its ancestral form *G. merotumida* and *G. plesiotumida*. *G. tumida tumida* is still more biconvexly coiled, tumid and its walls and peripheral keel more robust. In equatorial view, the taxon is more elongate. All base features as well test size are subject to considerable conditions. Dimension is 2.95 mm in length and 1.50 mm in width. This species is a deeper marine species, widely recorded from MS 1 to 6, where it occurs flooded in the main shelf.



***Globorotalia menardii cultrata* d'Orbigny**

*Globorotalia menardii cultrata* d'Orbigny- Bolli & Saunders, 1985, p. 226, figs. 23.3, 34.10.

Test free, very trochospiral, biconvex, compressed, equatorial periphery lobulate, axial periphery acute with a pronounced keel, wall finely perforate, surface of the earlier chambers slightly rugose, near shoulders, later ones smooth; chambers strongly compressed, arranged into 3 holes, the five to seven chambers to the last whorl, increase regularly in size; sutures dorsal curved and ventrally, radial to slightly curved, depressed umbilicus fairly wide open, shallow; aperture interiomarginal, extraumbilical, a low slit bordered by distinct lip. Dimension is 0.80 mm in length and 0.70mm in width. This species has wide distribution recorded from MS 2, 3 and 6, where it occurs rarely.

***Pulleniatina obliquiloculina* Parker & Jones,**

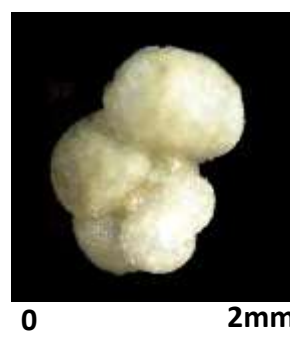
*Pulleniatina obliquiloculina* Parker & Jones, Bolli, 1957, p. 33, pl. 4, figs. 3-5

Text free, typically trochospiral to streptospiral, early chambers arranged like *Glonigerima* with open umbilicus, later chambers completely enveloping the entire umbilical side of the previous open umbilicus and thus even appear involutely coiled, wall calcareous, perforate, radiate in structure; aperture interiomarginal in the young, a broad umbilical area, in the adult a broad low extraumbilical and at the base of the final enveeping chamber bordered above by a thickened lip, but not directly open into the earlier umbilicus, because of the streptospiral plan of growth. Dimension is 0.35 mm in maximum and 0.30 in minimum diameter. This species has been recorded from MS 1, 2, 3 and 6, where it occurs rare to abundantly in the shelf.

***Hastigerina siphonifera* d'Orbigny**

*Hastigerina siphonifera* d'Orbigny Banner & Blow, 1960, p. 20, pl. text., figs. 2a-e  
Bolli & Saunders 1985, p. 251, fig. 42, 1a-3b.

Test free, typically planispirally, totally evolute, chamber distinct, completely in a planispiral coil, chambers increasing in size and added; the last chamber embraces earlier chambers; wall calcareous, perforate, or hispid; suture depressed, radial in structure; aperture a large opening interiomarginal, peripheral. Maximum diameter is 0.55 mm and minimum is 0.45mm. This species has a wide distribution, recorded from MS 1 to 6 in the shelf area.



### Summary and Conclusion

The study area located in the northern part of Adman Sea; bounded by latitudes 13° 25' N and 15° 40' N and longitudes 93° 15' E and 97° 45' E occupies the south and southwest oceanic area of Myanmar. The area extent is approximately 101250 km<sup>2</sup>. In the present study, the sedimentological studies and foraminifera aspects was focused in various ways. 125 specimens of surface sediments were collected from the India-Myanmar joint oceanographic research

programme. Ayeyawady continental shelf is part of an area of a complex geological setting in Andman basin, located in the south of Ayeyawady delta surrounded by land area in north and east. Ayeyawady continental shelf has a tidal range between 4m-7m is located in tropical climate and the Ayeyawady, Thanlwin and Sittaung rivers flow into the study area. A total of 6 specimens were systematically studied for microfaunal aspects. Owing to the distribution of different sediments in the studied area, water depth, turbidity, influence the distribution of fauna. By the ecology, the conspicuous scenario is that faunal distribution is mainly governed by the types of sediments where they lived and bathymetry which they need for flourished. In the present study, the faunal distribution and population are somewhat different in localities. Some fauna cannot be occurred in some area, whereas some lived in a specific region which favoured the dominance of distinct genera. It is a noteworthy that faunal population and species diversity occurred in different areas. Moreover, in some localities the species diversity is very low, which is thought to be stressed areas, where the fauna accept the specific conditions to live. Besides, some depth assemblages brought by current circulation should be differentiating with living fauna. By the occurrence of biospecies the high diversity of foraminifera is also occurred in the western part of the study area. This means that on the open continental shelf which is far from the influence of near shore physiographic and geographic barrier (Imbrie and Newell, 1904). The low species diversity encountered in the Gulf of Martaban is quite different from high species diversity of western area. Moreover western part of the area bounded by clear water is thought to be favoured the occurrence of highly diverse biospecies than the turbid martaban gulf area.

### Acknowledgement

We wish to express our thanks to Dr Aung Myat Kyaw Sein, Rector of Mawlamyine University, and Dr San San Aye, Pro-Rector of Mawlamyine University, for their kind permission to undertake this research work. Thanks are also extended to Dr Yin Yin Aye, Professor and Head of Geology Department, Mawlamyine University, for her kind permission and valuable advices.

### References

- Bandy, O.L. (1953) Ecology and Paleontology of California Foraminiferal. Part I. *Jour. Pal.* 27, p-161-182
- Bandy, O.L. (1960) Ecology of Foraminifera in the northern Gulf of Mexico. *United States. Geol.Surv. Prof. paper.* 274.G p. 197-204.
- Blow, W.H (1969) Late Middle Eocene to Recent planktonic Foraminifera Biostratigraphy. *First International Planktonic Congerence*, p.199-422, pl. 1-54.
- Bolli, H.and Saunders, J.B, (1985) Oligocene to Holocene low latitude Planktonic Foraminifera. Chapter 6. *Plankton Stratigraphy*, p.155-262. Cambridge University Press.
- Chit Saing, (2007) A study of deeper marine Recent Foraminifera, Bay of Bengal, off the Rakhine Coast, *Jour. Myanma. Acad. Arts & Science*, 5 (1), p 1-26.
- Cushman, J.A, Foraminifera, Their classification and Economic Use. Cambridge University Press 478 p.
- Grahamm, J.J and Militante, P.J, (1959) Recent Foraminifera from Puerto Galera areas, Northern Mindoro, Philippines, *Geological science*, Stanford University 6(2) 132 p.
- Huang, H. 1964 Rotalia Group of the Upper Cenozoic of Taiwan. *Micropal.* 10(1), p.45-62.
- Ingle, I.C, (1980) Cenozoic Paleobathymetry and depositional History of selected sequences within the southern California Continental borderland *Cushman. Found. Foram. Res.* Special publication No. 19, p. 163-195.
- Le Roy, L.W (1944) Miocene Foraminifera from Sumatra and Java, Netherland, East Indies. *Colorado School. Mines. Quart.* 39 (3) p.1-113.
- Noetling, F. (1902) Fauna of the Miocene Beds of Burma: *Paleontologia Ind. Men* 3., p. 1379.

- Phleger F.B, and Parker, F.L, (1952). Ecology of Foraminiferal Distribution, *Geol, Soc: Amer. Memoir*. No. 46, pl 1-68.
- Postuma, J.A, (1971) Manual of Planktonic Foraminifera. The Elseuoir Publishing Company, NewYork, pl 1-397.
- Theingi Kyaw and Chit Saing, (2001) Distribution of Recent Foraminifera from The Ayeyawady Delta Shelf. A paper presented in student family Day Ceremony. p 1-20.
- Tipsword, E.L., Setzer, F.M, and Smith, (1966) Interpretation of depositional Environments in the Gulf Coast Petroleum Exploration from Paleoecology and related stratigraphy. *Trans. Gulf. Coast. Assoc. Geol. Soc.* vol. 16, Haustan, U.S.A.
- Todd, R, and Bronnimann, P. (1957). Recent Foraminifera and Thecamoebina from the Eastern Gulf of Paria. Cushman, *Found. Foram. Res. Special publicaton No.3*, p 1-30.